

HIGH-RESOLUTION SEQUENCE STRATIGRAPHY
AND RESERVOIR CHARACTERIZATION OF MID-
CONTINENT MISSISSIPPIAN CARBONATES IN
NORTH-CENTRAL OKLAHOMA AND SOUTH
CENTRAL KANSAS

By

LARA JAECKEL

Bachelor of Science in Geology

George Mason University

Fairfax, VA

2010

Submitted to the Faculty of the
Graduate College of the
Oklahoma State University
in partial fulfillment of
the requirements for
the Degree of
MASTER OF SCIENCE
July, 2016

HIGH-RESOLUTION SEQUENCE STRATIGRAPHY
AND RESERVOIR CHARACTERIZATION OF MID-
CONTINENT MISSISSIPPIAN CARBONATES IN NORTH-
CENTRAL OKLAHOMA AND SOUTH CENTRAL KANSAS

Thesis Approved:

Dr. G. Michael Grammer

Thesis Advisor

Dr. James Puckette

Dr. Jay Gregg

ACKNOWLEDGEMENTS

First, I would like to thank my advisor, Dr. Michael Grammer, for his guidance and assistance throughout my research. I will always be asking “so what?” in everything I do and I am extremely grateful for the carbonate knowledge! Thank you to Boone Pickens School of Geology for the opportunity and, specifically, the Skinner, Patrick and Sharrie Ely and Alumni Graduate Fellowships and the Mississippian Lime Consortium for making it possible to conduct this research. Thank you to my committee members, Dr. Jim Puckette and Dr. Jay Gregg for their insight regarding my research.

I would also like to thank my colleagues in the “Carbonate Clan” for their willingness to discuss academic questions, share knowledge, and collaborate. Being a part of the “Carbonate Clan” and working with the group enriched my experience at Boone Pickens School of Geology.

Lastly, I owe infinite thanks to my husband/soulmate, Tony, and my family (close friends included, along with pets, especially my cat, Tully... yes, I went there!). Without their support, encouragement, and love, I would not have pursued this dream to fulfillment. I am truly blessed to have such wonderful people in my life who were there for me every step of this journey and I can never thank them enough!

Name: LARA JAECKEL

Date of Degree: JULY, 2016

Title of Study: HIGH-RESOLUTION SEQUENCE STRATIGRAPHY AND
RESERVOIR CHARACTERIZATION OF MID-CONTINENT
MISSISSIPPIAN CARBONATES IN NORTH-CENTRAL OKLAHOMA
AND SOUTH CENTRAL KANSAS

Major Field: GEOLOGY

Abstract:

Mid-Continent Mississippian carbonates, known informally as the “Mississippian Lime”, constitute unconventional carbonate reservoirs (low porosity and/or low permeability) with significant hydrocarbons (2+ BBO). The “Mississippian Lime” is aerially extensive (spanning hundreds of miles across Arkansas, Missouri, Oklahoma and Kansas) and represents a dynamic set of carbonate depositional systems. The reservoirs are heterogeneous and the current limited understanding of the depositional system makes the prediction of lateral facies distribution difficult.

Facies identified from core and thin section analysis from north-central Oklahoma and south central Kansas indicates that deposition of the “Mississippian Lime” most likely occurred within a regionally pervasive, distally-steepened carbonate ramp environment. Results from the Oklahoma cores (Albus 1-34H and Bann 1-14) indicate that overall shoaling-upward packages are characterized by dolomitized mudstones (Oklahoma Facies 1, porosity range 4.5 – 10.9%, permeability range 0.002 – 0.011 mD) at the base that progress into higher energy grainstones (Oklahoma Facies 4, porosity range 5.4 – 14.3%, permeability range 0.0003 – 3.06 mD) at the top, some of which are associated with subaerial exposure features (porosity range 9.2 – 22.6%, permeability range 0.022 – 100 mD). Results from the Kansas core (Trophy Farms 32-34-16 1H) also exhibited shoaling-upward packages, starting with skeletal wackestones (Kansas Facies 1, porosity 0.7%, permeability 0.0001 mD) at the base and progressing into crinoidal grainstones (Kansas Facies 4, porosity range 0.6 – 7.3%, permeability range 0.0001 – 3.9 mD) at the top. Moldic, vuggy and interparticle porosity represent the most common pore types observed in thin section and hand sample for all three cores.

The sequence stratigraphic hierarchy of the “Mississippian Lime” in these cores display a threefold hierarchy that can be defined as probable 3rd order sequences containing high-frequency 4th order sequences and probable 5th order cycles, which were formed due to variations in eustatic and relative sea level. Reservoir development within the “Mississippian Lime” appears to be controlled by the 3rd order sequences as the primary reservoir facies for all three cores are related to the regressive phase of the interpreted 3rd order sequences. In the Oklahoma cores, the reservoir facies is compartmentalized through intercalation of cemented grainstone and impermeable mudstone layers. In the Kansas core, the reservoir facies appears compartmentalized by impermeable wackestone intervals. Employing an integrated approach utilizing core and wireline log analysis to identify facies and to interpret depositional environments for the associated regional facies distribution, combined with the development of a sequence stratigraphic framework to enhance chronostratigraphic correlation provides a means to better understand and predict the reservoir distribution and lateral and vertical variability in these “Mississippian Lime” reservoirs.

TABLE OF CONTENTS

TABLE OF CONTENTS.....	v
LIST OF TABLES.....	viii
LIST OF FIGURES.....	ix
CHAPTER I.....	1
INTRODUCTION.....	1
PLAY HISTORY.....	1
OBJECTIVES AND PRIMARY GOALS OF STUDY.....	3
HYPOTHESES.....	4
FUNDAMENTAL QUESTIONS.....	5
GEOLOGICAL BACKGROUND.....	7
STRUCTURAL AND TECTONIC HISTORY.....	7
PALEOGEOGRAPHY AND CLIMATE.....	10
SEA LEVEL.....	11
DATA AND METHODS.....	12
CORE WORK.....	15
PETROGRAPHIC ANALYSIS.....	16
SEQUENCE STRATIGRAPHIC FRAMEWORK.....	17
X-RAY DIFFRACTION (XRD).....	17
WIRELINE LOGS.....	18
LIMITATIONS.....	19
CHAPTER II.....	21
HIGH-RESOLUTION SEQUENCE STRATIGRAPHY AND RESERVOIR CHARACTERIZATION OF MID-CONTINENT MISSISSIPPIAN CARBONATES IN NORTH-CENTRAL OKLAHOMA AND SOUTH CENTRAL KANSAS.....	21
INTRODUCTION.....	21
SEQUENCE STRATIGRAPHY.....	23
MILANKOVITCH CYCLES.....	25
REGIONAL STRATIGRAPHY AND GENERALIZED DEPOSITIONAL FABRICS AND ENVIRONMENTAL INTERPRETATIONS.....	26
FACIES ASSOCIATIONS.....	32
OKLAHOMA FACIES 1: DOLOMITIZED MUDSTONE.....	38

OKLAHOMA FACIES 2: BURROWED WACKESTONE TO PACKSTONE	40
OKLAHOMA FACIES 3: BIOTURBATED PACKSTONE.....	42
OKLAHOMA FACIES 4: SKELETAL PACKSTONE TO GRAINSTONE.....	44
KANSAS FACIES 1: SKELETAL PACKSTONE TO WACKESTONE	46
KANSAS FACIES 2: BRYOZOAN GRAINSTONE TO PACKSTONE	48
KANSAS FACIES 3: CRINOIDAL GRAINSTONE TO PACKSTONE A.....	50
KANSAS FACIES 4: CRINOIDAL GRAINSTONE TO PACKSTONE B.....	51
OKLAHOMA AND KANSAS EXPOSURE INTERVAL	53
SEQUENCE STRATIGRAPHIC FRAMEWORK/ INTERPRETATION	58
IDEALIZED FACIES SUCCESSION: OKLAHOMA AND KANSAS	64
SEQUENCE STRATIGRAPHIC HIERARCHY	65
“THIRD” ORDER SEQUENCES	66
“FOURTH” ORDER HIGH- FREQUENCY SEQUENCES	66
HIGHER-FREQUENCY CYCLES.....	67
WIRELINE LOG CORRELATION.....	69
GAMMA – RAY	69
DENSITY AND NEUTRON POROSITY	70
RESISTIVITY	72
CHAPTER III	74
DISCUSSION.....	74
RESULTS/SEQUENCE STRATIGRAPHIC ARCHITECTURE AND REGIONAL CORRELATION	74
SUBSURFACE CROSS SECTIONS	77
RESERVOIR CONSIDERATIONS.....	93
FACIES.....	93
DOMINANT PORE TYPE.....	96
SEQUENCES	98
TRANSGRESSIVE VERSUS REGRESSIVE PHASE	101
TRANSGRESSIVE VERSUS REGRESSIVE PHASE BY SEQUENCE.....	104
PREDICTION CAPABILITIES.....	113
CONTROLS ON RESERVOIR DEVELOPMENT	114
CHAPTER IV	115
SUMMARY AND CONCLUSIONS	115

REFERENCES	118
APPENDICES	124
APPENDIX A	125
WRITTEN CORE DESCRIPTIONS	129
SEQUENCE STRATIGRAPHIC FRAMEWORK SUMMARY	143
APPENDIX B	145
GRAPPHICAL CORE DESCRIPTIONS	145
APPENDIX C	150
WHOLE CORE PHOTOGRAPHS	150
CORE #1: WHITE LIGHT (BANN 1-14)	152
CORE #1: UV LIGHT (BANN 1-14)	168
CORE #2: WHITE LIGHT (ALBUS 1-34H)	184
CORE #2: UV LIGHT (ALBUS 1-34H)	194
CORE #3: WHITE LIGHT (TROPHY FARMS 32-34-16H)	204
CORE #3: UV LIGHT (TROPHY FARMS 32-34-16H)	223
APPENDIX D	241
THIN SECTION PHOTOMICROGRAPHS	241
OKLAHOMA FACIES	243
Facies 1	244
Facies 2	245
Facies 3	255
Facies 4	280
Exposure	290
KANSAS FACIES	309
Facies 1	310
Facies 2	312
Facies 3	328
Facies 4	336

LIST OF TABLES

Table	Page
Table 1: List of Wells/Cores Used in this Study.....	7
Table 2A: Oklahoma Facies Characteristics.....	34
Table 2B: Oklahoma Facies Characteristics.....	35
Table 3A: Kansas Facies Charateristics.....	36
Table 3B: Kansas Facies Charateristics.....	Error! Bookmark not defined. 37
Table 4: Summary of Porosity/Permeability by 3rd Order Sequence for Oklahoma Cores	101
Table 5: Summary of Porosity/Permeability by 3rd Order Sequence for Kansas Core.	101
Table 6: Summary of Oklahoma Reservoir Characteristics	112
Table 7: Summary of Kansas Reservoir Characteristics.....	112
Table 8: Rock-Color Chart.....	126
Table 9: Bioturbation Index	127
Table 10: Fracture Numbers Per Foot.....	128

LIST OF FIGURES

Figure	Page
Figure 1: General Paleo-Depositional Model of the Mid-Continent during the Early Mississippian.....	2
Figure 2: “Mississippian Lime” Play Map.....	3
Figure 3: Study Area and Core Location Map.....	6
Figure 4: Map of Oklahoma and Kansas Structural Features	8
Figure 5: Paleogeographic Map of the Late Mississippian (325 Ma).....	11
Figure 6: Global Sea Level and Onlap Curves for the Carboniferous Period	12
Figure 7: Dunham Classification of Carbonate Rocks	14
Figure 8: Choquette and Pray Classification of Porosity Types	15
Figure 9: Idealized Depositional Sequence Model for a Carbonate Ramp.....	24
Figure 10: Relationship between Milankovitch Orbital Patterns.....	25
Figure 11: Milankovitch Cycle Hierarchy Chart	26
Figure 12: Stratigraphic Nomenclature for Kansas, Oklahoma, Missouri and Arkansas .	28
Figure 13: Conceptual Facies Mosaics on a Distally-Steepened Carbonate Ramp	31
Figure 14: Core Photographs and Thin Section Photomicrographs of Oklahoma Facies 1	39
Figure 15: Core Photographs and Thin Section Photomicrographs of Oklahoma Facies 2	41
Figure 16: Core Photographs and Thin Section Photomicrographs of Oklahoma Facies 3	43
Figure 17: Core Photographs and Thin Section Photomicrographs of Oklahoma Facies 4	45
Figure 18: Core Photographs and Thin Section Photomicrographs of Kansas Facies 1 ..	47
Figure 19: Core Photographs and Thin Section Photomicrographs of Kansas Facies 2 ..	49
Figure 20: Core Photographs and Thin Section Photomicrographs of Kansas Facies 3 ..	51

Figure 21: Core Photographs and Thin Section Photomicrographs of Kansas Facies 4 ..	52
Figure 22: Core Photographs and Thin Section Photomicrographs of Exposure Interval	55
Figure 23: Cross Section Diagram of a Distally-Steepened Carbonate Ramp	58
Figure 24: Sequence Stratigraphic Framework and Idealized Facies Succession Previous Study	59
Figure 25: Sequence Stratigraphic Framework Previous Study	61
Figure 26: Idealized Facies Succession Previous Study	62
Figure 27: Wireline Log Correlation Previous Study	63
Figure 28: Idealized Facies Succession This Study	65
Figure 29: Sequence Stratigraphic Hierarchy This Study.....	68
Figure 30: Sequence Stratigraphic Hierarchy and Borehole Measured Gamma-Ray and Density-Neutron Porosity	71
Figure 31: Sequence Stratigraphic Hierarchy and Borehole Measured Gamma-Ray and Deep Resistivity	73
Figure 32: Location Map of Subsurface Cross Section Lines	76
Figure 33: Comparison of Lithostratigraphic and Chronostratigraphic Subsurface Cross Section Correlations.....	79
Figure 34A: Equidistant Scaled Subsurface Cross Section A to A'	81
Figure 34B: Actual Distance Scaled Subsurface Cross Section A to A'	81
Figure 34C: Cropped Version of Equidistant Scaled Subsurface Cross Section A to A'	813
Figure 34D: Cropped Actual Distance Scaled Subsurface Cross Section A to A'	814
Figure 35A: Equidistant Scaled Interpretation 1 of Dip-Oriented Subsurface Cross Section B to B'	85
Figure 35B: Actual Distance Scaled of Interpretation 1 Dip-Oriented Subsurface Cross Section B to B'	857
Figure 36A: Equidistant Scaled of Interpretation 2 Dip-Oriented Subsurface Cross Section B to B'	88

Figure 36B: Actual Distance Scaled of Interpretation 2 Dip-Oriented Subsurface Cross Section B to B'	90
Figure 37A: Equidistant Scaled Subsurface Cross Section C to C'	91
Figure 37B: Actual Distance Scaled Version of Subsurface Cross Section C to C'	91
Figure 37C: Cropped Version of Actual Distance Scaled Subsurface Cross Section C to C'	913
Figure 38: Cross-Plot of Whole Core Porosity and Permeability by Depositional Facies	95
Figure 39: Cross-Plots of Whole Core Porosity and Permeability by Dominant Pore Type and Depositional Facies	97
Figure 40: Cross-Plots of Whole Core Porosity and Permeability by 3 rd Order Sequence Number	100
Figure 41: Cross-Plot of Whole Core Porosity and Permeability by Transgressive/Regressive Phase	103
Figure 42: Cross-Plot of Whole Core Porosity and Permeability by Transgressive/Regressive Phase of Each 3 rd Order Sequence Compared to Dominant Pore Type for Oklahoma Cores.....	105
Figure 43: Cross-Plot of Whole Core Porosity and Permeability by Transgressive/Regressive Phase of Each 3 rd Order Sequence Compared to Dominant Pore Type for Kansas Core.....	107
Figure 44: Cross-Plot of Whole Core Porosity and Permeability by Transgressive/Regressive Phase of Each 3 rd Order Sequence Compared to Reservoir Facies for Oklahoma Cores.....	109
Figure 45: Cross-Plot of Whole Core Porosity and Permeability by Transgressive/Regressive Phase of Each 3 rd Order Sequence Compared to Reservoir Facies for Kansas Core	110
Figure 46: Application of Wireline Log Correlation Tied to Depositional Facies	113

CHAPTER I

INTRODUCTION

PLAY HISTORY

Mississippian-aged carbonates were deposited across the Burlington Shelf in portions of New Mexico, Colorado, Nebraska, Iowa, Illinois, Texas, Kansas, Oklahoma, and Arkansas (Lane and DeKyser, 1980) (Figure 1). The “Mississippian Lime”, an informal name used in the oil and gas industry to describe multiple zones in the predominantly carbonate units of Mississippian age, is an unconventional, shallow (3,000 – 6,000ft/915 – 1828m) hydrocarbon producing play targeted in northern Oklahoma and southern Kansas with low well costs (\$3-4 million), making this an appealing unconventional reservoir (Montgomery et al., 1998) that has produced several billion barrels of oil (Figure 2). Unconventional reservoirs by definition require stimulation, such as hydraulic fracturing, for economic hydrocarbon production (Roundtree et al., 2010) and are characterized by low porosity and/or permeability that inhibit conventional buoyancy-driven hydrocarbon migration. Initial discoveries in this play occurred in the 1920s and 1930s, with an increase of vertical drilling activity in the 1940s and 1950s (Montgomery et al., 1998). Horizontal drilling activity rejuvenated this play in the 2000s but has since slowed due to variable production caused by reservoir heterogeneity.

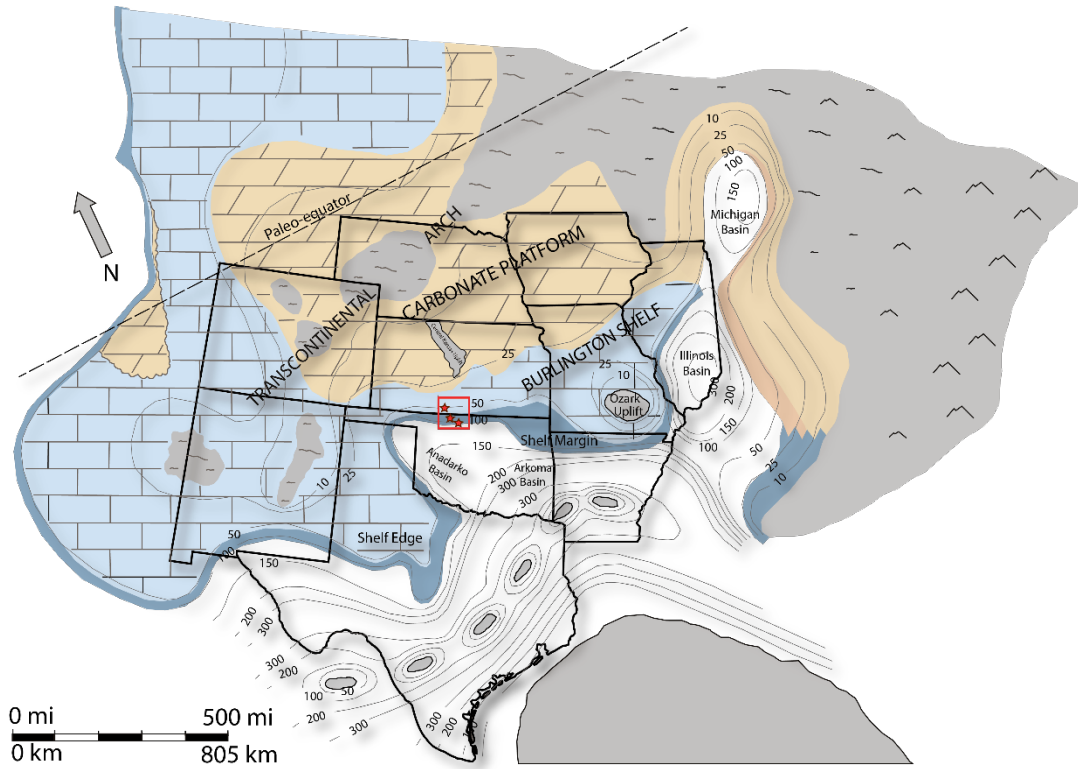


Figure 1: General paleo-depositional model of the Mid-Continent representative of the Early Mississippian (Tournaisian) time with study area outlined in red box and core locations represented by red stars. Modified from Gutschick and Sandberg (1983) and Chaplin (2010).

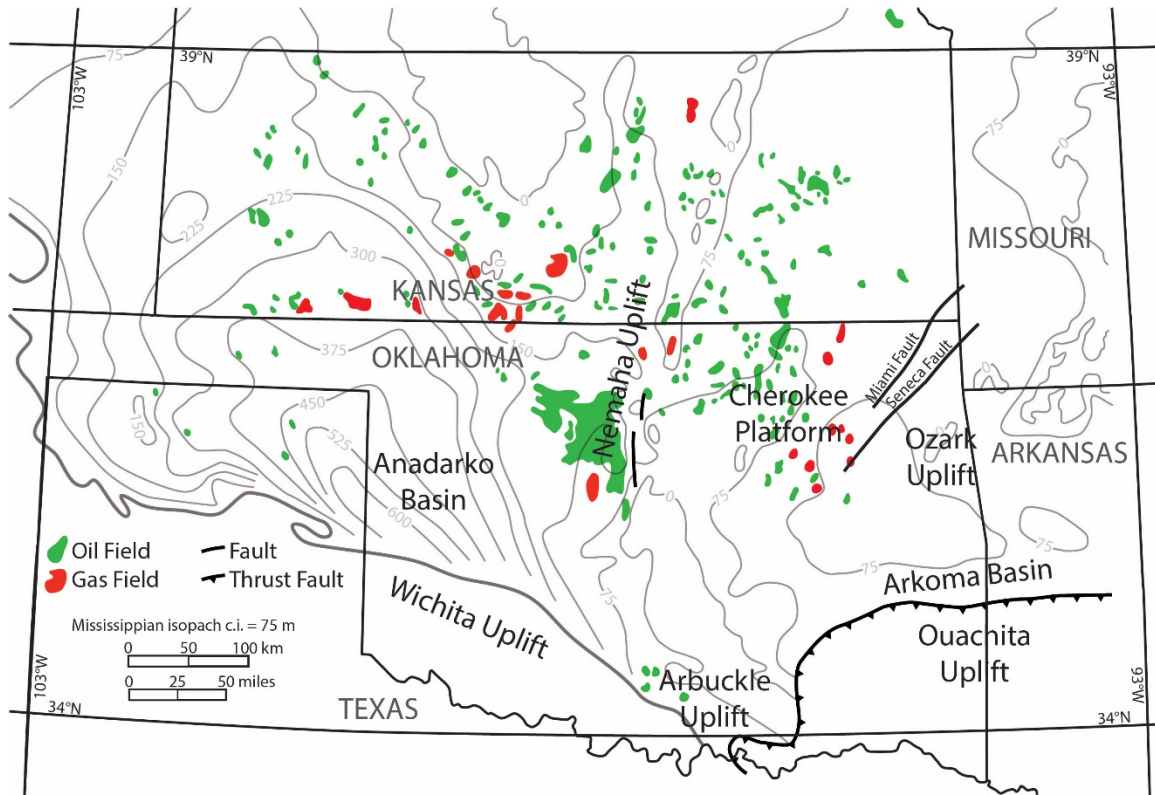


Figure 2: “Mississippian Lime” play map (vertical production) showing the distribution of oil (green) and gas (red) fields across Oklahoma and Kansas. Thickness of post Woodford and pre-Chester Mississippian rocks are shown in gray and is contoured at 250ft (76.2m) intervals. Thickness of the Mississippian section reaches a maximum of 2000ft (610m) in western Oklahoma and is not present in the Wichita Uplift or the Ouachita Uplift in southern Oklahoma. Thickness reaches a maximum of 1000ft (304.8m) in south western Kansas and is absent in northern Kansas. Modified from Harris (1987).

OBJECTIVES AND PRIMARY GOALS OF STUDY

The primary objective of this thesis is to identify sequence stratigraphic controls affecting the reservoir architecture of the “Mississippian Lime” in north-central Oklahoma and south central Kansas. The primary goals are to: 1) define the sequence stratigraphic hierarchy by identifying a vertical facies stacking pattern through core and thin section analysis in Woods County, Oklahoma and Comanche County, Kansas; 2) evaluate the variations in pore systems and related porosity and permeability within the identified sequences that control the reservoir development to lead towards greater predictability of reservoir units; and 3) compare and contrast the facies types and

sequence stratigraphic framework between cores in a more proximal regional setting in northern Oklahoma and southern Kansas, with recent studies on the Mississippian in more distal positions further south.

Utilizing a sequence stratigraphic approach provides an enhanced understanding of the vertical and lateral continuity of the facies and allows for better prediction of reservoir-quality facies in the subsurface. The strength of sequence stratigraphy lies in its potential to predict facies within a chronostratigraphically constrained framework of unconformity-bound depositional sequences. This methodology provides an enhanced predictability of sedimentary packages, including sediment type, probable reservoir or source potential, and the geometry, lateral and vertical continuity of strata across a sedimentary basin (Handford and Loucks, 1993; Grammer et al., 2004).

This study will build on previous work done in the Mid-Continent (Childress, 2015; Childress and Grammer, 2015; Flinton, 2016; Price, 2014; Price and Grammer, 2015; LeBlanc, 2015) to establish a regional sequence stratigraphic framework for a portion of the “Mississippian Lime” in north-central Oklahoma and south central Kansas, west of the Nemaha Uplift. Using three representative wells in the play area, a regional sequence stratigraphic framework should provide insight on facies architecture, fabrics, textures, and compositions associated with subsurface reservoir and non-reservoir facies.

HYPOTHESES

The overarching hypothesis of this investigation is that the observable sequence stratigraphic hierarchy within the Mid-Continent “Mississippian Lime” in more proximal locations of the basin compared to previous work consists of regular and predictable

sequences with facies mosaics and associated depositional environments that are consistent with studies conducted in relatively more distal areas of the Mid-Continent “Mississippian Lime”.

The specific hypotheses of this research are: 1) There are predictable and definitive facies mosaics (i.e. proximal versus distal) and associated stacking patterns in the “Mississippian Lime” diagnostic of deposition on a distally-steepened ramp; 2) These facies stacking patterns can be correlated to 3rd order (1 – 3 Ma) sea level changes, and possibly with higher frequency 4th order (100 – 400 ky) sea level changes, that likely control the heterogeneity of the “Mississippian Lime” reservoirs; and 3) The facies stacking pattern in southern Kansas will likely vary from the stacking pattern present in northern Oklahoma due to a more proximal depositional setting present in Kansas. These hypotheses aim to address the fundamental questions needed to achieve a better understanding of, and predictability for, the lateral heterogeneity in the “Mississippian Lime” reservoirs.

FUNDAMENTAL QUESTIONS

This study utilized three cores within the “Mississippian Lime” play, located in Woods County, Oklahoma and Comanche County, Kansas to address the primary objectives and hypotheses listed above (Figure 3, Table 1). With the well-established global pattern of eustatic sea level variations present in the Mississippian (Haq and Schutter, 2008), and the hypersensitivity of the carbonate factory to sea level changes (Read, 1995), this study addresses the following questions:

1. Are the facies and the corresponding depositional model in the northern (more proximal) part of the basin comparable to previous regional studies further south (more distal)?
2. Are the reservoir and non-reservoir facies present in these cores similar to corresponding reservoir types found elsewhere in the basin?
3. Are repetitive vertical stacking patterns identifiable in core and/or logs as observed elsewhere in the basin, and if so, how do they compare to those found in recent studies further south?
4. Is there an identifiable sequence stratigraphic hierarchy, and if so, is this comparable to what is observed in more distal portions of the basin?
5. Are reservoir intervals predictable based upon facies and/or sequence stratigraphic framework?

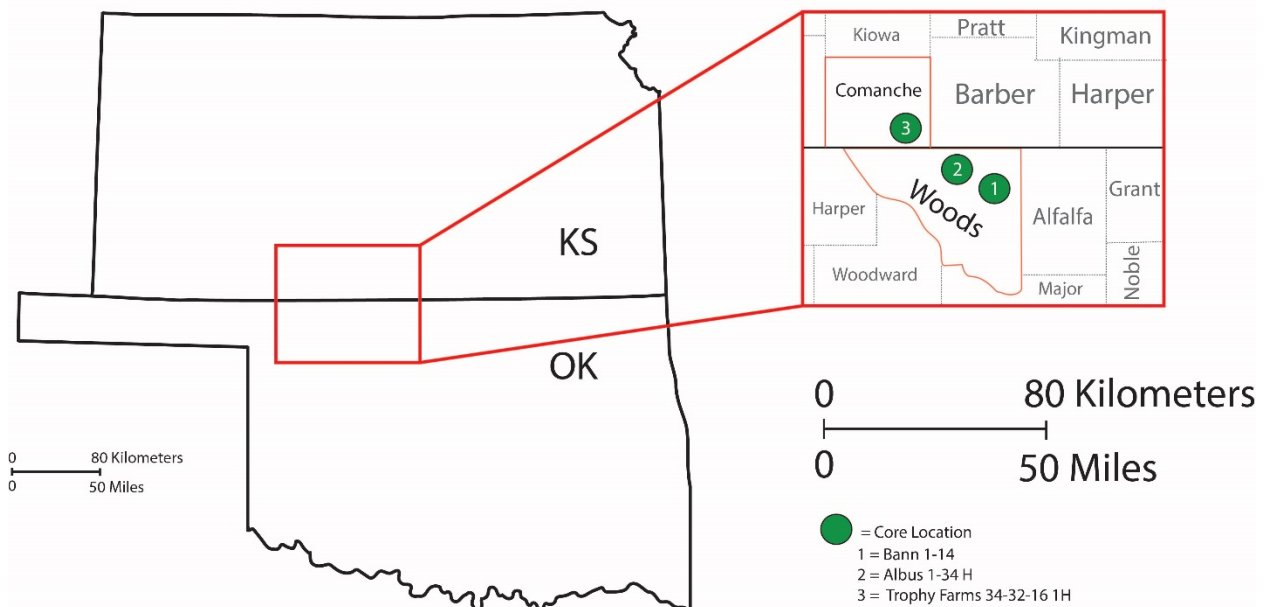


Figure 3: Core locations represented by green dots, with Woods County, OK and Comanche County, KS outlined in the red box.

Lease Name	Well Number	Core Footage	Location	Operator	County
Bann	1-14	5205' – 5355'	SEC 14-28N-14W	Chesapeake Energy	Woods, OK
Albus	1-34	5110' – 5201.1'	SEC 34-29N-15W	Chesapeake Energy	Woods, OK
Trophy Farms	32-34-16 1	5260' – 5456.9'	SEC 32-34S-16W	Chesapeake Energy	Comanche, KS

Table 1: Location and associated core footage for the three cores utilized in this study.

GEOLOGICAL BACKGROUND

STRUCTURAL AND TECTONIC HISTORY

The study area is located in north-central Oklahoma and south central Kansas on the Anadarko Shelf in Woods County, Oklahoma and Comanche County, Kansas. Structural features bordering the study area are the Nemaha Uplift, also known as the Nemaha Ridge, and the Cherokee Platform to the east, the Anadarko Basin to south, the Cimarron Arch and Hugoton Embayment to the west, and the Central Kansas Uplift and Sedgwick Basin to the north (Chaplin, 2012; Northcutt and Campbell, 1996). The timing of the structural activity and resulting paleo-topographic and bathymetric highs and lows in the study area is important to understand because of the potential effects on reservoir distribution, as facies distribution is strongly influenced by current regimes and overall energy levels within the depositional system. Figure 4 illustrates the approximate orientation of these structural features in relation to Woods County and Comanche County.

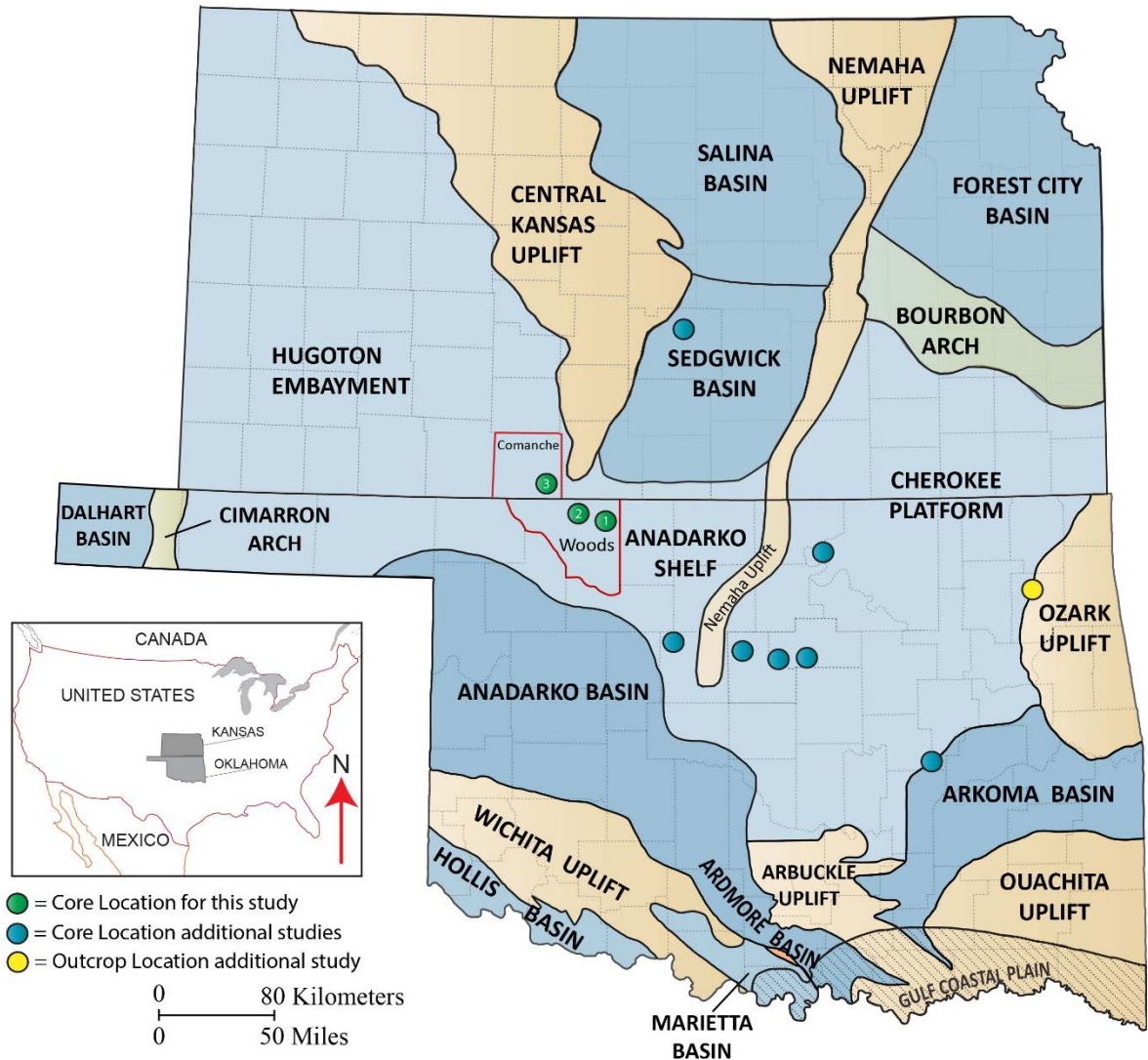


Figure 4: Map of Oklahoma and Kansas showing major structural features and the location of cores in Woods County, OK and Comanche County, KS (outlined in red) represented by green dots. Core locations from additional recent studies in Oklahoma and Kansas are represented by blue dots, and outcrop study areas represented by the yellow dot. Note the Central Kansas Uplift to the north and Nemaha Uplift to the east. Geologic platforms are light blue, basins in dark blue, uplift features in orange and arches in light green. Modified from Chaplin (2010) and Northcutt and Campbell (1996).

During the Early (~359 Ma) and Middle (~345 Ma) Mississippian, the Mid-Continent was relatively inactive in terms of tectonic activity and structural deformation compared to the eastern and western margins of the North American Craton (Gutschick and Sandberg, 1983). Mississippian-aged carbonates were deposited on the Burlington Shelf in portions

of New Mexico, Colorado, Nebraska, Iowa, Illinois, Texas, Kansas, Oklahoma, and Arkansas (Gutschick and Sandberg, 1983; Lane, 1978). The depositional strike of the system is roughly east-west, with shallower water settings occurring to the northwest and deeper water settings to the southeast (Gutschick and Sandberg, 1983). The Mid-Continent ramp/shelf setting is bounded to the north and northwest by the Transcontinental Arch, to the east by the Ozark Uplift, and to the south by Anadarko and Arkoma Basins in southern Oklahoma.

The major tectonic structure in north-central Oklahoma created during the Late Mississippian (~326 Ma) to Early Pennsylvanian was the Nemaha Uplift (Chaplin, 2010). The Nemaha Uplift is a series of northeast- to north-south-trending faults extending ~900 mi (1448km) northward from central Oklahoma across eastern Kansas and southeastern Nebraska into Iowa, Wisconsin, and Minnesota. In Oklahoma and Kansas, the Nemaha Uplift consists of a number of small crustal blocks (horst and graben fault-block pattern) that were uplifted and eroded in Late Mississippian and Early Pennsylvanian (Chaplin, 2010), which may have affected the deposition and aerial distribution of the “Mississippian Lime”. The Nemaha Uplift was generated by three regional compressional events related to the Appalachian and Rocky Mountain orogenies and caused regional reverse faulting in Oklahoma, Kansas and Nebraska (Gay, 2003).

The second major tectonic structure pertinent to this study is the Central Kansas Uplift in south central Kansas. The Central Kansas Uplift is a broad complex structural high found only in the subsurface that trends northwest to southeast across central Kansas (Evans and Newell, 2013). The timing of the development of the Central Kansas Uplift is speculative because extensive uplift and erosion in Early Pennsylvanian time removed most or all of

the older Paleozoic rocks surrounding central Kansas (Adkison, 1972). Both the Nemaha Uplift and the Central Kansas Uplift are thought to be manifestations of the Ouachita orogeny on the shelf margin during the Late Mississippian to Early Pennsylvanian, and serve to define the five basins in Kansas (Anderson and Hedke, 1995).

PALEOGEOGRAPHY AND CLIMATE

During the Mississippian, much of North America was covered by a shallow epicontinental sea (Figure 5) (Gutschick and Sandberg, 1983). Oklahoma and Kansas were located approximately 20 – 30° south of the paleoequator within tropical to subtropical belts where Mississippian carbonate sediments were deposited in a series of transgressive and regressive events (Evans and Newell, 2013). The Mississippian was a transitional period between greenhouse (Devonian) and icehouse conditions (Pennsylvanian and Permian).

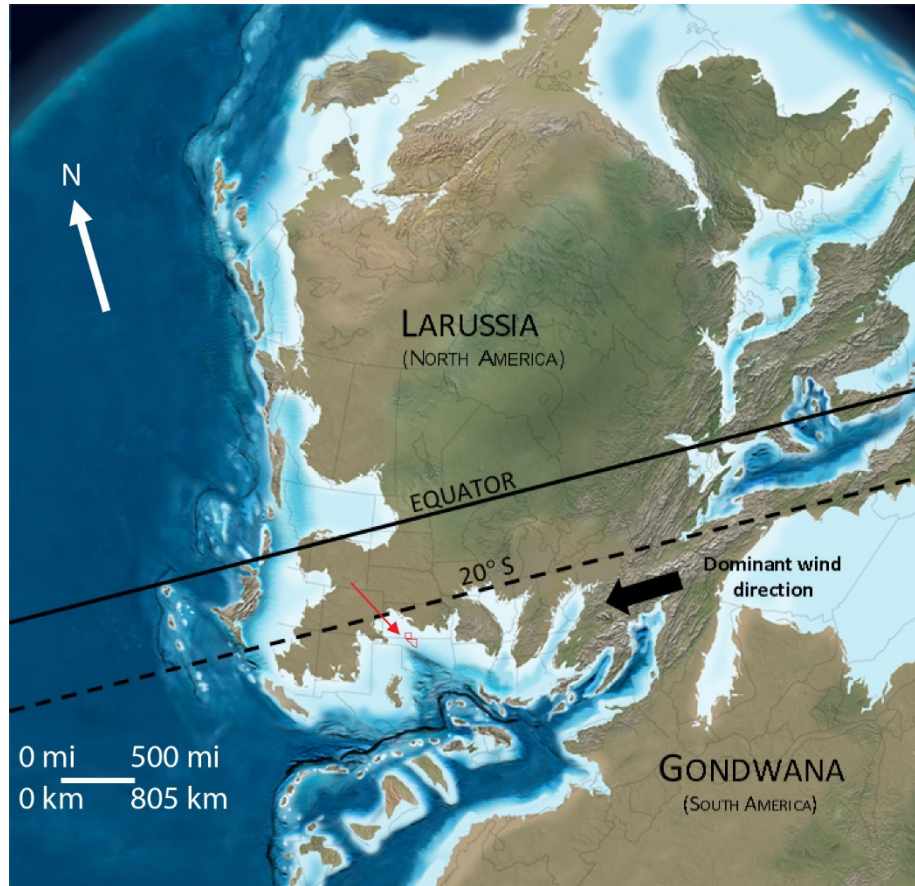


Figure 5: Late Mississippian (325 Ma) paleogeography. Study area (outlined in red and red arrow) is located about 20-30° south of the paleo-equator. Deeper water is darker blue, shallower water is lighter blue. More land exposure is present during the late Mississippian compared to the earlier Mississippian. Deposition of sediments occurred in a shallow marine setting, but the exposure of more terrestrial surfaces could have influenced the distribution of facies. The dominant paleo wind direction is interpreted to be from the west-northwest (Mazzullo et al., 2009). Modified from Blakey (2014).

SEA LEVEL

Long term (first order) Mississippian eustatic sea level was positioned between 50 – 100m above present day sea level (Figure 6) and represents about 40 million years from the Kinderhookian to the Chesterian (Haq and Schutter, 2008). Previous work on the Lower to Middle Mississippian of the Mid-Continent tied depositional trends related to global fluctuation in sea level on the order of one to six million years (3rd order resolution) (Haq and Schutter, 2008). Haq and Schutter recognize 21 transgressive and regressive cycles throughout the Lower to Middle Mississippian period. Several workers (Westphal et al.,

2004; Elrick and Read, 1991) have interpreted higher-frequency 4th and 5th order cycles within the Mississippian, supporting the potential control that high-frequency cyclicity has on the stratigraphic hierarchy observed within the “Mississippian Lime”.

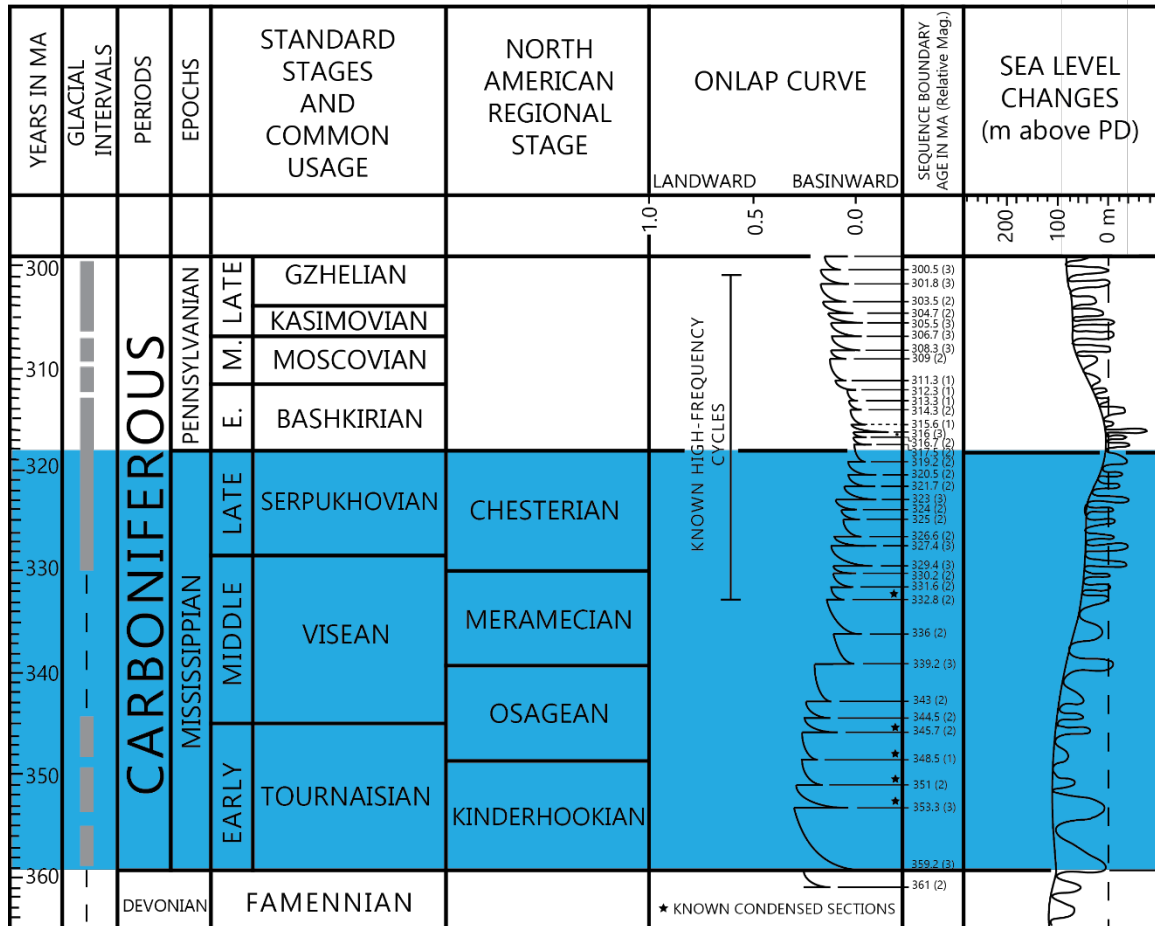


Figure 6: Diagram illustrating Carboniferous sea level change and onlap curve patterns. Known glacial intervals are denoted by gray bars to the right of the numerical time scale displaying the transition between greenhouse (Devonian) and icehouse (Pennsylvanian) times. The Mississippian (shaded in blue) is marked by “known high-frequency cycles” in the onlap curve column, along with long term (2nd order) and short term (suspected 3rd order) sea level changes relative to present day (PD) sea level. Numbers 1 to 3 adjacent to the sequence boundary age represent a semi quantitative measure of the relative magnitude of base level change (1= minor, <25m, 2= medium, 25-75m, 3=major, >75m). Modified from Haq and Schutter (2008).

DATA AND METHODS

A fundamental step in evaluating carbonate depositional systems is to construct a sequence stratigraphic framework based on facies relationships and stratal relationships.

Sequence stratigraphy is defined as a stratigraphic method that uses unconformities (sequence boundaries) and their correlative conformities to package sedimentary successions into spatially and temporally constrained sequences. The strength of sequence stratigraphy lies in its potential to predict the lateral and vertical distribution of facies within a chronostratigraphically constrained framework of unconformity-bound depositional sequences (Handford and Loucks, 1993), whereas lithostratigraphy fails to encompass this crucial step. Facies within a carbonate depositional system are defined by environments of deposition through the identification of similar fauna, textures, ichnofacies and sedimentary structures. An idealized facies stacking pattern correlates the identified facies to respective transgressive and regressive areas of the sea level curve based on likely water conditions (energy regimes and quality) and available accommodation space. Stacking pattern analysis is an important technique in hydrocarbon recovery and exploitation because the correlation of these units helps develop an accurate model of reservoir distribution when core and well logs are commonly the only data available (Lehrmann and Goldhammer, 1999). Understanding the mechanisms that control the distribution of carbonate cyclicity enhances the predictability of the lateral and vertical continuity and distribution of non-reservoir and reservoir facies (Eberli and Grammer, 2010). Using high-resolution sequence stratigraphy to assess the control on reservoir quality, this study addresses the lateral and vertical heterogeneity of the “Mississippian Lime” in north-central Oklahoma and south central Kansas.

This study utilized the integrated reservoir characterization approach as proposed by Grammer et al. (2004), starting with core descriptions (Refer to Table 1, Figure 3 for core locations) using the Dunham (1962) and Choquette and Pray (1970) classification

schemes (Figures 7 and 8), thin section analysis and wireline log data as described in the following sections.

DEPOSITIONAL TEXTURE RECOGNIZABLE					DEPOSITIONAL TEXTURE NOT RECOGNIZABLE
Components not bound together during deposition				Components bound together during deposition	CRYSTALLINE CARBONATE
Contains carbonate mud (clay/fine silt) (< 30 μm)		Lacks mud and is grain-supported	Grain-supported		
Mud-supported				MUDSTONE	
Less than 10% grains	More than 10% grains	PACKSTONE	GRAINSTONE		

Figure 7: The Dunham (1962) carbonate classification scheme study utilized in this study for describing textures in cores. Modified from Scholle and Ulmer-Scholle (2003).

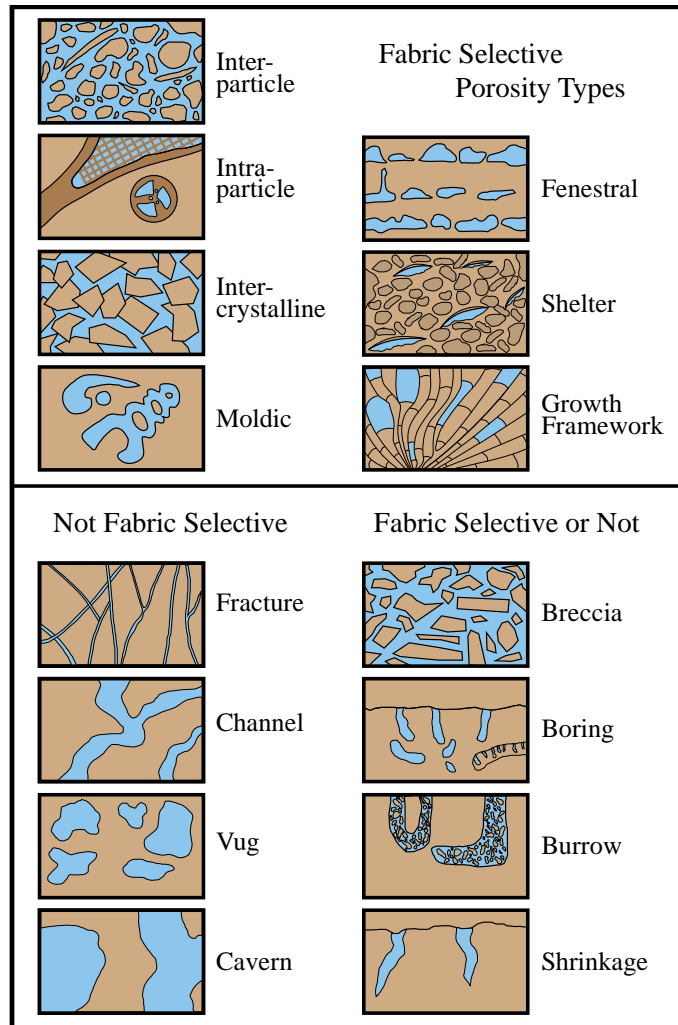


Figure 8: Choquette and Pray's (1970) representation of different fabric selective and not fabric selective pore systems that occur in carbonates. Modified from Scholle and Ulmer-Scholle (2003).

CORE WORK

Subsurface investigation is a critical component to understanding the reservoir architecture present in the "Mississippian Lime". Three cores (441.06 total linear feet) provided by Chesapeake Energy were described in this study (refer to Table 1). These cores were selected to analyze the facies mosaics present west of the Nemaha Uplift along with the availability of wireline log suites. Core #1 is 7 miles (11.3km) from Core #2 and Core #3 is 17 miles (27.3km) from Core #2. Previous subsurface studies focused on cores to the

east and south of the Nemaha Uplift and these cores provide insight on subsurface facies in a relatively proximal position compared to previous studies.

Analysis of the core included documentation of facies, visible pore types, sedimentary structures and fossil content. The facies analysis was then utilized to develop a model for the depositional environment, to identify high-frequency cycles and sequences, and to establish reservoir heterogeneities. Clay rich intervals or potential flooding surfaces, exposure horizons and a dramatic shift from relatively deeper water facies to relatively shallower water facies (or vice versa) observed in core were utilized to distinguish high-frequency cyclicity (i.e. cycle boundaries). Observations (see Appendix A) are presented using a core description log modified in Adobe Illustrator (See Appendix B).

PETROGRAPHIC ANALYSIS

A total of 210 thin sections were collected by Chesapeake Energy from the three cores to enable the identification of key facies types and pore systems. Thin sections provide crucial information for quantifying grain size, pore types, fossil content and textural classification that cannot be accurately described in hand sample due to the fine-grained nature and microscopic variabilities within these units. All thin sections were stained with alizarin red for calcite and impregnated with blue dyed epoxy to facilitate identification of open pores. A majority of the thin sections were made from the same plugs from which porosity (NCS) and permeability (Klinkenberg) values were available (measured at Omni Laboratories). Klinkenberg values were used as this correction factor (Asquith and Krygowski, 2004) provides a more accurate permeability value in tight (low porosity and/or permeability) reservoirs. Porosity was estimated using standard visual estimation charts for the remaining thin sections. Porosity and permeability data was utilized to

describe reservoir and non-reservoir facies to provide insight for patterns that were present among the facies. Grain size and allochem content were estimated using standard visual estimation charts. Grain size variations can indicate proximal or distal deposition relative to the basin or changes in environmental setting due to sea level change. Mineralogical identification within the facies aided in the prediction of porosity enhancement or occlusion. Fossil content provided evidence for similarities of depositional environment.

SEQUENCE STRATIGRAPHIC FRAMEWORK

Sequence stratigraphic principles and related Milankovitch driven high-frequency cycles were used in this study for defining a sequence stratigraphic hierarchy. Once the transgressive and regressive cycles were established, these were correlated to wireline logs. Specifically, the sequences and cycles were correlated to borehole gamma-ray logs first, to neutron and density porosity logs second and finally to resistivity curves. The correlation of the sequences and cycles to wireline log signatures allowed for better prediction of reservoir facies distribution and subsurface mapping away from the study area.

X-RAY DIFFRACTION (XRD)

X-ray diffraction (XRD) is an analytical technique that provides percentages of crystalline material, primarily for calcite, dolomite, quartz, feldspars and clay. Chesapeake Energy retrieved 120 core plugs from the three whole core sections for bulk whole rock mineralogy XRD analysis. An approximation of clay content was estimated from the bulk XRD data, however oriented mounts for clays were not utilized in the bulk analysis. XRD data was primarily used in this study to enhance interpretations of depositional environment by identifying potential trends in depositional cycles (i.e. clay content increasing at the base of a transgressive phase or an increase in quartz content in the

regressive phase that can occur as reciprocal sedimentation in a mixed system). Additionally, the XRD data provided the mineralogical abundances of the facies identified from each core.

WIRELINE LOGS

Chesapeake Energy provided gamma-ray, caliper, neutron porosity, density porosity and medium and deep resistivity open hole logs acquired with the three cores in this study. An additional 79 gamma-ray and resistivity image logs were provided by Chesapeake Energy to construct regional subsurface cross sections. Gamma-ray (GR) measures the natural radioactivity from K, Th, and U found in clay minerals commonly associated with shales and mudrocks. GR usually increases with clay content and is principally used to distinguish sand and shale lithologies. Caliper logs measure the borehole diameter and fluctuations in the borehole diameter can indicate filtercake build up (a qualitative indication of a zone with permeability) or a washout (bore hole conditions that can negatively affect the tool contact with the bore hole walls). Caliper logs verify if high measurements from wireline logs are accurate or due to a washout. Neutron porosity logs measure the hydrogen concentration in a formation and density porosity logs measures the amount of returning GR particles affected by the density of electrons in formation. Density and neutron porosity logs combined provide an estimate of porosity and if there is a gas or liquid bearing zone. Resistivity curves can qualitatively indicate permeable zones and hydrocarbon versus water bearing zones. Asquith and Krygowski (2004) provide a more comprehensive overview of these wireline logging tools.

Wireline logs measure the physical attributes of the formation in the borehole environment but they cannot provide the fundamental rock properties of grain size,

sedimentary structures and texture. “Ground truthing” the open hole logs to the core is essential for facies interpretation and correlation (Grammer et al., 2004). Facies observed in the core were tied to the wireline log signatures to aid in the prediction of sequence distribution where core and thin section data was not available. Nearby wells were then correlated to the “ground truthed” logs using gamma-ray and resistivity logs.

LIMITATIONS

Using three cores, this study defined a high-resolution sequence stratigraphic framework to enhance previous sequence stratigraphic models of the “Mississippian Lime”. The cores provided in this study are not a complete Mississippian section because they do not extend down to the Woodford Shale (Late Devonian – Early Mississippian). However, the Pennsylvanian unconformity contact is present in all three cores. This unconformity was used as a datum to correlate the Oklahoma sequence stratigraphic framework from Core #1 to Core #2. The wireline logs for Core #1 and Core #3 provided for this study extended down to the Woodford Shale but the wireline logs for Core #2 did not. In order to flatten the subsurface correlations on the Woodford Shale, the top of the Woodford Shale was estimated for Core #2 based on nearby (1 – 1.2 mi/1.6 – 1.9km) well log signatures. The age of the cores is known to be Mississippian but lack of biostratigraphic control precludes identification of age even at the 3rd order (1-3 million years) scale. Conodont biostratigraphy can provide a relatively high-resolution age constraint (approximately one million years, Boardman et al., 2013), in the Mississippian, however no conodont biostratigraphic data is available for these cores. Knowing the absolute age of the cores would constrain the sea level fluctuations for the study area and provide a more accurate sequence stratigraphic framework. However, there is a distinct

hierarchy of cyclicity observed in the cores and will be labeled as probable 3rd, 4th and 5th order (largest to smallest) to convey this observation.

One limitation with the high-resolution sequence stratigraphic method is defining the higher frequency sequences and cycles (possible 4th and 5th order). These high-frequency sequence and cycles can be ambiguous and lack a consistent definition among sedimentologists and stratigraphers (Catuneanu et al., 2009), making them seem highly subjective. For this study, a high-frequency cycle was defined based on the repeating stacking pattern and associated sequence boundaries (i.e. exposure horizons and clay-rich intervals) observed in core and wireline log signatures, without reference to a particular temporal duration.

Another limitation for this study is the distance of the cores from each other, which are 7 miles (11.2km) to 17 miles (27.6km) apart. Core #3 has more proximal facies associations than Core #1 and #2 and has a different facies stacking pattern. This aspect provided a unique insight from previous studies conducted for a more proximal representation of facies and the dynamic system changes in a proximal setting.

CHAPTER II

HIGH-RESOLUTION SEQUENCE STRATIGRAPHY AND RESERVOIR CHARACTERIZATION OF MID-CONTINENT MISSISSIPPIAN CARBONATES IN NORTH-CENTRAL OKLAHOMA AND SOUTH CENTRAL KANSAS

INTRODUCTION

Carbonate depositional systems are sensitive to sea level fluctuations due to base level changes that affect the productivity of the carbonate factory (Read, 1995) and can also affect the geometry of the system. Understanding the depositional geometry with associated facies mosaics is crucial in predicting facies distribution laterally and vertically. Recent subsurface analysis and outcrop work (Childress, 2015; Price, 2014; Price and Grammer, 2015; LeBlanc, 2015) proposed that deposition of the “Mississippian Lime” occurred on a distally steepened ramp. A ramp is a sloping surface connecting two levels, with no break in slope (Ahr, 1973). The surface of a ramp is gently sloping (generally less than 1°), with gradients that vary on the order of a few meters/ kilometers. Near-shore facies of ramps exhibit wave agitated grainier facies and pass offshore into deeper water, muddier facies (Tucker and Wright, 1990). Ramps are typically comprised of clastic carbonate grains and mud, forming in both temperate and tropical seas (Handford and Loucks, 1993). The break in distally steepened ramps occurs many kilometers seaward of high-energy shoals rather than at the seaward margin of a high energy rim. Facies on a distally steepened ramp include deep ramp wackestones/mudstones, slumps, breccias and turbidites (Read, 1995), such as those seen in recent work within the Mississippian Mid-Continent outcrop studies (Childress, 2015).

Ramps display lateral facies patterns where grainstones and packstones are landward facies and the sediments become increasingly muddier seaward (Ahr, 1973).

Shallow water carbonate depositional systems, such as the system in the Mississippian of the Mid-Continent, display a facies mosaic that can be correlated to sea level variations. Eustatic and relative sea level changes are driven by allogenic processes that operate on a basin wide or global scale, such as global tectonics and glacial ice volume, and autogenic process that operate locally, such as sedimentation rates and subsidence (Read, 1995; Plint et al., 1992; Kerans and Tinker, 1997). The amplitude of glacially-driven eustatic sea level fluctuation and overall ocean water temperature is directly related to the amount of ice volume present on earth. During times of continental glaciation, or icehouse conditions, the amplitude of sea level changes are large (up to 100m/328ft) (Read, 1995). Greenhouse times are characterized by less ice volume compared to icehouse conditions and sea level fluctuations are small (commonly with amplitudes less than 10m/32.8ft) (Read, 1995). During icehouse conditions, a rapid decrease in global ice volume can cause quick transgressions while slower glaciation can cause relatively gradual regressions (Read, 1995). Since the Mississippian is a transitional period between greenhouse conditions in the Devonian and icehouse conditions in the Pennsylvanian and Permian, sea level could have fluctuated up to 100m/328ft. In a shallow (less than 30m/98ft), low angle carbonate ramp system, 100m/328ft sea level changes can cause a drastic lateral migration of facies and the drowning or exposure of the carbonate factory.

Sea level fluctuations occurring at frequencies of approximately 1 to 5 million years are typically responsible for deposition of sequences tens to hundreds of meters thick.

These sequences are generally referred to as lower frequency or 3rd order sequences (Read, 1995). Superimposed within 3rd order sequences, 4th and 5th high-frequency sequences and cycles occur as a result of sea level fluctuation on the order of 20 to 400 thousand years driven by climate changes in response to Milankovitch cycles (Read, 1995). These higher frequency sea level changes also affect the facies stacking pattern of carbonates and the distribution of the reservoir facies because shallow water carbonate systems are sensitive to any variation in sea level.

Long term (2nd order) Mississippian eustatic sea level represents about 40 million years from the Kinderhookian to the Chesterian (Haq and Schutter, 2008). Previous work on the Lower to Middle Mississippian of the Mid-Continent determined that deposition related to global fluctuations in sea level were on the order of 1 to 6 million years (3rd order resolution) (Haq and Schutter, 2008). Haq and Schutter (2008) identified 21 transgressive and regressive (3rd order) cycles over 40 million years, while other workers (Westphal et al., 2004; Elrick and Read, 1991) have recognized higher frequency 4th and 5th order cycles within the Mississippian succession.

SEQUENCE STRATIGRAPHY

Sequence stratigraphy is the branch of stratigraphy that subdivides the rock record using a succession of depositional sequences composed of genetically-related strata as regional and interregional units (Haq et al., 1988). Sequence stratigraphy is a stratigraphic method that uses unconformities (sequence boundaries) and their correlative conformities to package sedimentary successions into spatially and temporally constrained sequences. Sequence stratigraphy integrates time and relative sea level changes to track the migration of facies (Handford and Loucks, 1993). The strength of sequence stratigraphy lies in its

potential to predict facies within a chronostratigraphically constrained framework of unconformity-bound depositional sequences (Handford and Loucks, 1993).

The development of a sequence stratigraphic framework for any given depositional basin provides a temporal and spatial framework for studying depositional change (Kerans and Tinker, 1997). Lithostratigraphy is a sub-discipline of stratigraphy that correlates rock units based on similar lithologic characteristics. Using a strictly lithostratigraphic approach when characterizing a reservoir could result in incorrectly identifying communication between potential reservoirs because a lithostratigraphic correlation between two units does not necessarily indicate the two units are genetically related. Using a chronostratigraphic framework produces a more geologically defined reservoir model by recognizing the appropriate relationship between the lateral and vertical distribution of facies (Figure 9). High-resolution sequence stratigraphy uses depositional spatio-temporal patterns at a smaller scale, such as those generated from Milankovitch band, higher frequency cycles (Kerans and Tinker, 1997).

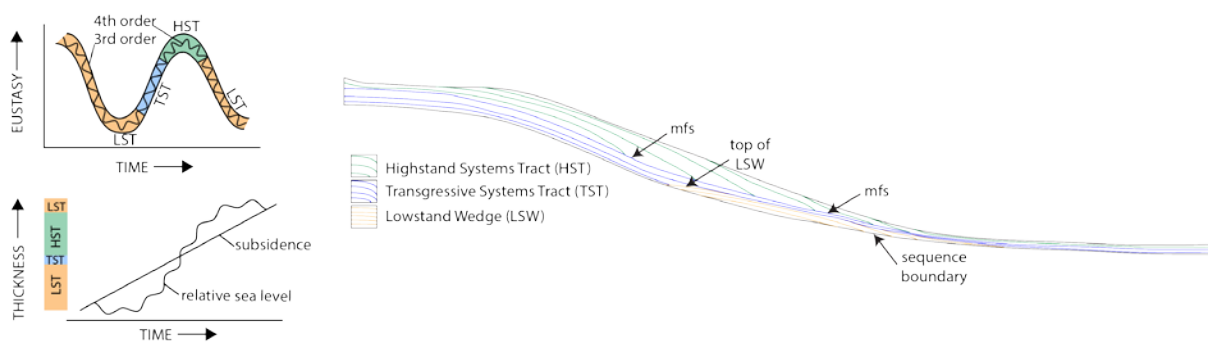


Figure 9: Idealized depositional sequence model for a carbonate ramp within one genetically related package deposited within the same rise and fall of sea level. The thicknesses of each systems tract vary with fluctuations in sea level and rate of subsidence. Higher frequency cycles that are controlled by Milankovitch-band cycles are superimposed on lower order sequences

within these system tracts. Modified from Handford and Loucks (1993) and Kerans and Tinker (1997).

MILANKOVITCH CYCLES

This study focused on identifying high-frequency depositional cycles present within the globally constrained 3rd order sea level changes during the Mississippian in Woods County, Oklahoma and Comanche County, Kansas. This high-frequency cyclicity is interpreted as being driven by Milankovitch cyclicity (changes in orbital variability). Milankovitch cycles are caused by climatic changes that influence the amount of glacial ice on the earth's surface that result from cyclic changes in the shape of the earth's orbit (eccentricity), the earth's tilt (obliquity), and wobble (precession) of the earth's axis (Read, 1995; Figure 10). The earth's relative position to the sun is postulated to control the amount of ice volume present on the earth's surface in a given time due to varying amounts of solar radiation reaching the earth's surface and the variations in temperatures that result. High-frequency sea level changes (4th order/100-400 ky and 5th order/20-40 ky) are superimposed on lower order sequences (3rd order/1-3 Ma) developing a sequence stratigraphic hierarchy in the sedimentary system (Figure 11).

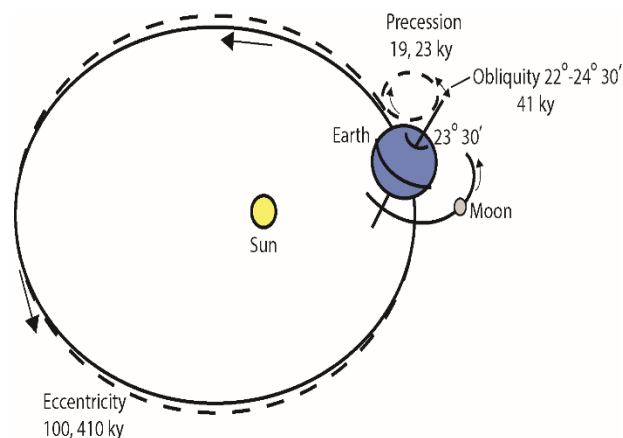


Figure 10: Relationship between Milankovitch orbital patterns of eccentricity, obliquity, and precession. Modified from Read (1995).

Cycle Hierarchy				
Tectono-Eustatic/Eustatic Cycle Order	Sequence Stratigraphic Unit	Duration (n=Ma)	Relative Sea Level Amplitude (m)	Relative Sea Level Rise/Fall Rate (cm/1,000 yr)
First	Supersequence	> 100		< 1
Second	Supersequence	10 - 100	50 - 100	1 - 3
Third	Depositional Sequence, Composite Sequence	1 - 10	50 - 100	1 - 10
Fourth	High-Frequency Sequence	(100 – 400 kyr) 0.1 – 0.4	1 - 150	40 - 500
Fifth	High-Frequency Cycle	(20-40 kyr) 0.02 - 0.04	1 - 150	60 - 700

Figure 11: Cycle hierarchy chart showing the difference between first through fifth order eustatic sea level cycles. This study focuses on the 3rd to 5th order of cyclicity, related to eustatic and regional sea level fluctuations in the Mississippian. Modified from Kerans and Tinker (1997).

REGIONAL STRATIGRAPHY AND GENERALIZED DEPOSITIONAL FABRICS AND ENVIRONMENTAL INTERPRETATIONS

The term “Mississippian Lime” is an informal name used prevalently in the petroleum industry to refer to all Mississippian aged strata that span the Mid-Continent. The “Mississippian Lime” is an unconventional, mixed carbonate/siliciclastic reservoir with multiple reservoir types that underlies an extensive portion of northern Oklahoma and southern Kansas. During the Mississippian, carbonates were deposited across hundreds of miles across the Burlington Shelf in portions of New Mexico, Colorado, Nebraska, Iowa, Illinois, Texas, Kansas, Oklahoma, and Arkansas (Refer to Figure 1) (Gutschick and

Sandberg, 1983; Lane, 1978). The Burlington Shelf transitions into the Illinois Basin to the north and gradually transitions across Missouri, Arkansas, and Oklahoma into the Anadarko Basin and the Ouachita Trough to the south (Gutschick and Sandberg, 1983). In southern Kansas and northern Oklahoma, Mississippian deposits are thought to be mostly shallow-water carbonates (Jewett et al., 1968). Figure 12 represents lithostratigraphic names that commonly appear in the literature for central Kansas and northern Oklahoma, as well as southwest Missouri and northwest Arkansas.

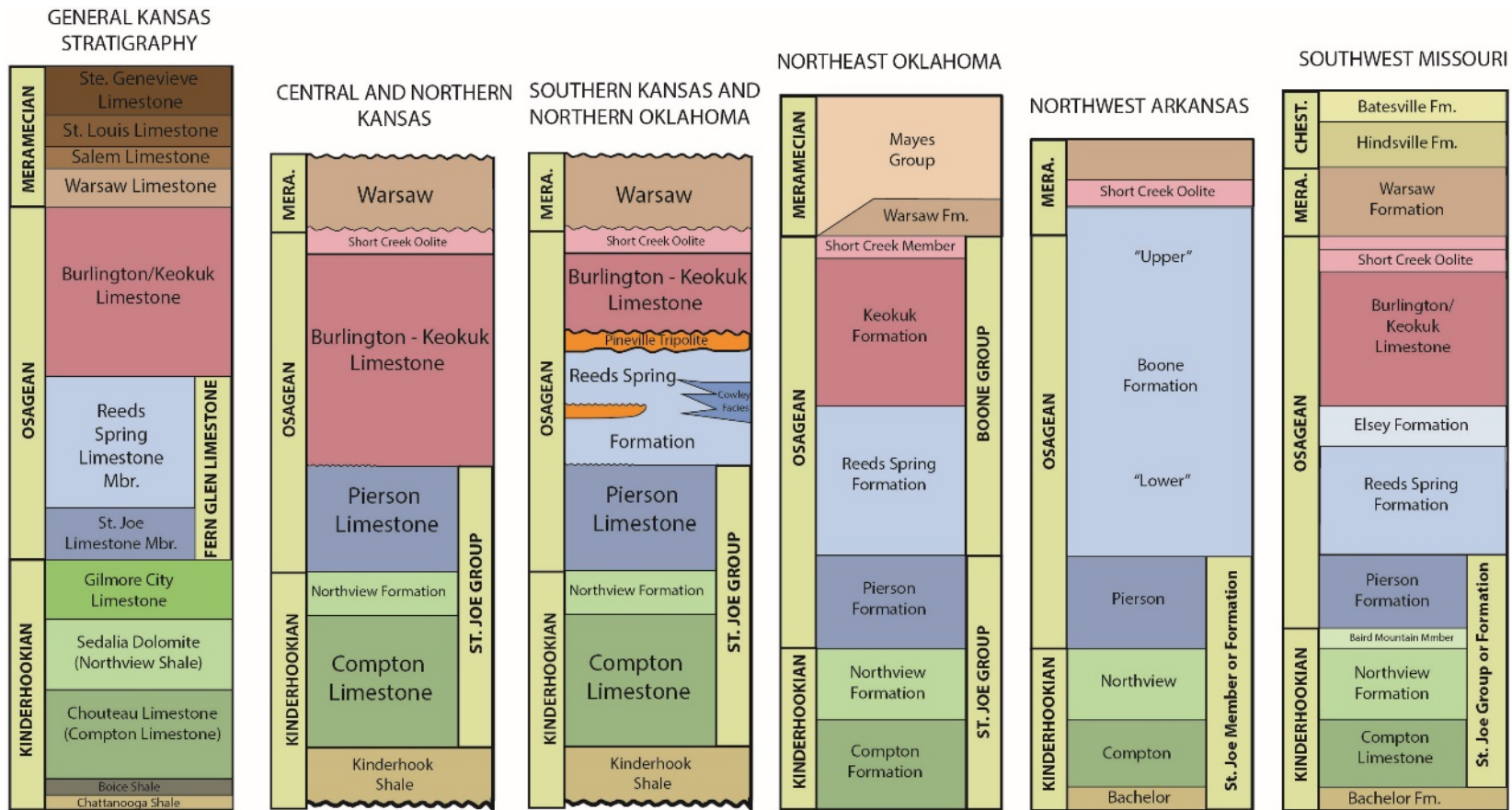


Figure 12: Stratigraphic columns and associated nomenclature for the Mid-Century Mississippian in Kansas, Oklahoma, Arkansas and Missouri. The nomenclature varies considerably across the Mid-Century from the outcrop-based nomenclature in Missouri and Arkansas to the subsurface nomenclature in Oklahoma and Kansas. This study focuses on the stratigraphic names associated with the subsurface in Kansas and northern Oklahoma. Modified from Jewett et al., 1968, Mazzullo, 2011 and Mazzullo et al., 2013.

Kinderhookian-aged strata are generally characterized by dark-gray to green-gray silty shale and green-gray, fine-crystalline limestones, with local siltstones present (Jordan and Rowland, 1959). Kinderhookian-aged strata are interpreted to be deposited on a distally steepened carbonate ramp in a predominantly marine environment, and generally contain less chert than the overlying Osagean-aged strata (Jewett et al., 1968; Wilhite et al., 2011).

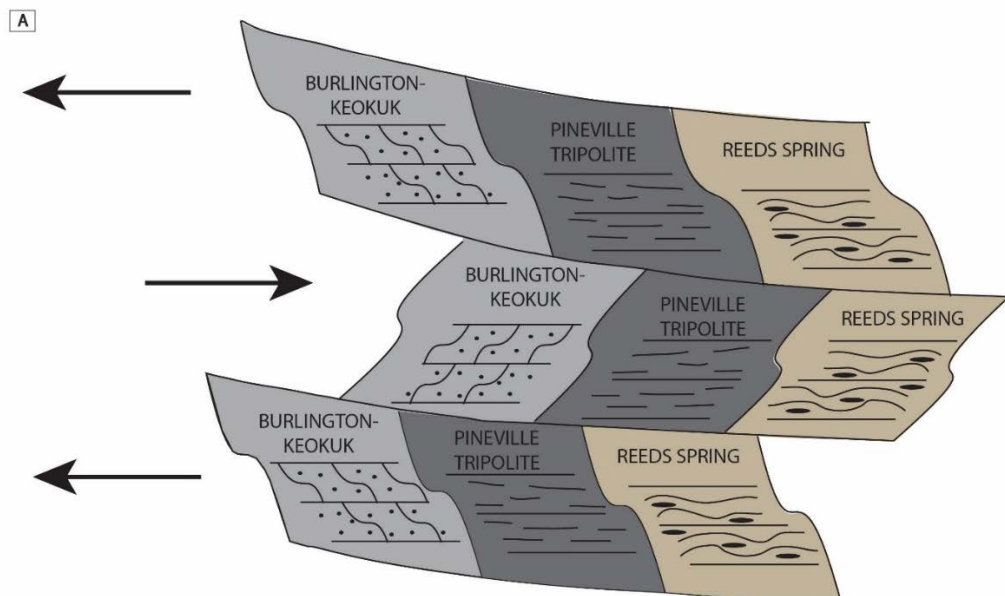
Osagean-aged strata are typically characterized by cherty dolomitic strata in the Mid-Continent comprised of carbonate mudstones to wackestones, sponge spiculitic wackestones to packstones, echinoderm rich wackestones to grainstones, and dolomitic siltstones and shale lithofacies (Franseen, 2006). Osagean-aged strata south of Kansas are interpreted to be deposited on a south-southwest dipping, gently sloping ramp towards the Anadarko Basin, where fluctuations in sea level resulted in the basinward progradation of the strata (Childress and Grammer, 2015; Franseen, 2006; Mazzullo et al., 2011; Wilhite et al., 2011).

In northern and western Oklahoma, Meramecian-aged deposits are characterized by gray-tan, medium to coarse grained fossiliferous grainstones, containing ooids and chert (Jordan and Rowland, 1959). Meramecian-aged deposits are interpreted to be both marine and non-marine (Jewett et al., 1968). In Kansas, Meramecian-aged rocks can be absent and are locally present in the Hugoton embayment (Thompson and Goebel, 1968).

Chesterian-aged strata are thickest in the Ardmore Basin in Oklahoma (up to 2500ft/762m) and are locally absent in northeastern Oklahoma due to erosion or lack of deposition (Curtis and Champlin, 1959). The Chesterian-aged strata are characterized by off-white to gray, fine to medium crystalline fossiliferous limestones containing crinoids and ooids, interbedded gray to brown shales and siltstones and fine to medium-grained

sandstones (Curtis and Champlin, 1959). Subsidence rates increased during the Chester and an influx of siliciclastic sediments spread from the south and southeast in Oklahoma (Curtis and Champlin, 1959).

A prominent issue with the Mid-Century Mississippian carbonates is the tendency to apply a lithologic-based formation name to a unit based solely on its depositional fabric. For example, the petroleum industry characterizes limestones with nodular bedded chert as the Reeds Spring formation, which implies the formation was deposited during the Osagean (Mazzullo et al., 2011). Recent work done by Childress and Grammer (2015), however, highlight the time transgressive problems with applying the lithologic formation name to a rock based just on the lithologic characteristics (Figure 13).



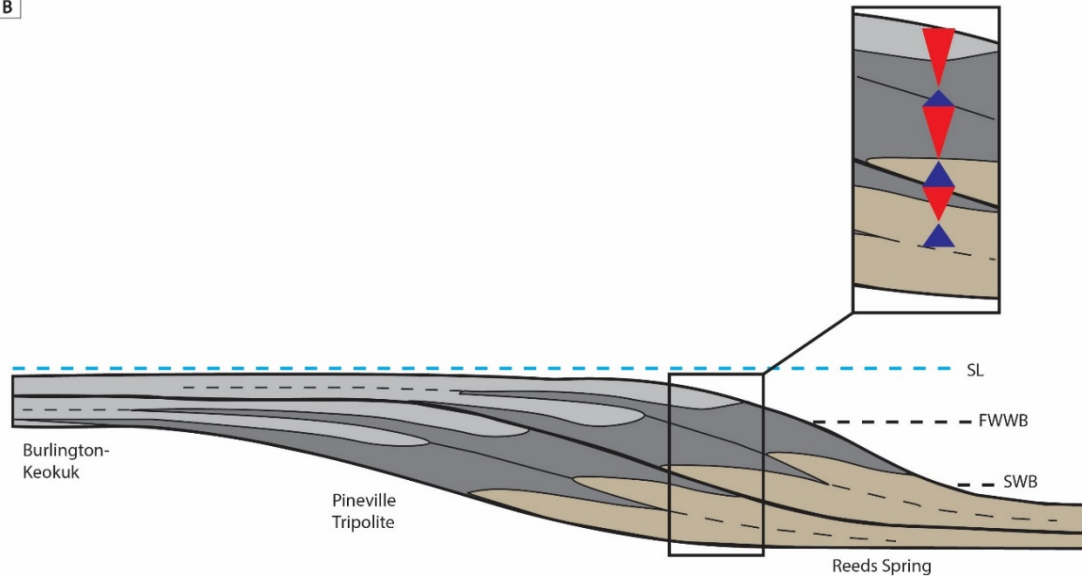
B

Figure 13: **A)** Conceptual diagram displaying a range of Mississippian facies deposited in a transect across the distally steepened ramp from the most proximal position on the ramp (left) to the more distal portion of the ramp (right). The changes in base level (black arrows) display the shift in facies that does not necessarily follow the lithostratigraphically defined “formation” succession. This model helps explain the discrepancy between lithological-based nomenclature and sequence stratigraphy used throughout the Mid-Continent. Modified from Childress and Grammer, 2015. **B)** A side view illustrating an example of stacking patterns formed from a lateral shift in facies on a carbonate ramp related to Milankovitch-scale sea level change, represented by the blue and red triangles, and sequence boundaries represented by thick black lines.

The most commonly targeted petroleum reservoir facies in the Mid-Continent Mississippian-aged strata are thought to be deposited during the Kinderhookian and Osagean stages (Mazzullo et al., 2011). Reservoir types include tripolitic chert, or “chat”, beneath the Pennsylvanian unconformity, dolomitized intervals, mound/build-up and grainstone facies (Montgomery et al., 1998) characterized by low porosity and/or permeability. Mid-Continent Mississippian strata are predominantly carbonates, but the deposits are more accurately described as a mixed system of carbonates and siliciclastics. Due to complex facies distribution, reservoirs in the “Mississippian Lime” are often laterally discontinuous and vertically heterogeneous, leading to a complexly compartmentalized reservoir system.

FACIES ASSOCIATIONS

Four facies associations were identified through analysis for the Oklahoma cores, the Bann 1-14 (Core #1) and the Albus 1-34H (Core #2) in Woods County (241.1ft/73.48m), as well as the Kansas core, the Trophy Farms 32-34-16 1H (Core #3), in Comanche County (199.96ft/60m). These facies associations were distinguished based on texture, composition, sedimentary structures, color and the interpreted environment of deposition. Observations from the core were supplemented with 125 thin sections for Core #1 and #2 and 85 thin sections for Core #3. Grain-rich sediments dominate the northernmost core (Core #3) and gradational changes internally between the sediments made discrete facies distinctions difficult. In order to display this gradational change, facies were delineated by average grain size and relative percentages of observed grain sizes, along with minor changes in skeletal constituents.

Bulk XRD analysis performed by Chesapeake Energy was used to identify mineralogical percentages present in each facies for all three cores. Overall, the XRD analysis for the Kansas facies indicates much higher total carbonate percentages (total carbonate average range 97.5 – 98.2% for all facies) and lower dolomite percentages (average dolomite 1.8% in Kansas Facies 3) compared to the Oklahoma facies (total carbonate average range 52.9 – 78.5%, average dolomite 50.3% in Oklahoma Facies 1). The Oklahoma facies had higher quartz percentages (average range 16.9 – 18.7%) compared to the Kansas facies (average range 0.4 – 0.5%). The quartz observed in Core #1 and #2 was primarily chert and is interpreted as being associated with diagenetic silica replacement (i.e. not detrital quartz). Tables 2A, 2B, 3A and 3B provide detailed summaries of the characteristics of the facies identified in all three cores. Colors were

determined using the GSA rock color designation chart (Goddard et al., 1951). Additional core photos and thin section photomicrographs of each facies for Core #1, Core #2 and Core #3 are located in Appendices C and D.

Oklahoma Facies	Color	Mineralogy (Avg. %)					Dominant Sedimentary Features	Primary Grain Constituents
		Clays	Total Carbonates	Dolomite	Total Non-Clays	Quartz		
Exposure Interval: Skeletal Grainstone to Packstone	Pale Greenish Yellow, Pale Olive, Light Olive Gray, Yellowish Gray, Very Light To Medium Dark Gray, Brownish Gray, Pinkish Gray, White To Blueish White, Grayish Red Purple, Greenish Gray, Very Dark Red, Olive Black	11.9	0.5	0.2	87.6	86.3	Partially Healed and Mineralized Fractures, Massive Bedding	Crinoids (2 - 60%), Bivalves(10 - 15%), Brachiopod (5 -10%) and Bryozoan Fragments (0 -10%), Ostracodes (5%)
4: Skeletal Packstone to Grainstone	Light Olive Gray To Olive Gray, Yellow Gray, Very Light To Medium Dark Gray, Brownish Gray, Pinkish Gray, Bluish White	2.0	78.6	28.9	19.4	18.7	Minor Bioturbation, Open and Mineralized Fractures and Suture Seam Stylolites	Crinoid (10 - 80%), Bivalve (3 - 8%), Bryozoan (10%) and Brachiopod Fragments (5 -10%) and Sponge Spicules (5 -10%)
3: Bioturbated Packstone	Medium Gray To Dark Gray, Light Olive Gray To Olive Gray And Olive Black	3.8	52.9	13.1	43.3	42.9	Moderate to Common Bioturbation, Centimeter-Scale Vertical and Horizontal Burrows	Crinoid (5 - 50%), Bivalve (5%), Brachiopod Fragments (2 - 20%), Microcrystalline Quartz (15 - 60%) and Sponge Spicules (15 - 25%)
2: Burrowed Wackestones to Packstones	Gray To Dark Gray, Light Olive Gray To Olive Gray And Olive Black	5.0	53.7	17.9	41.3	40.7	Millimeter-Scale Horizontal Burrows and Localized Laminated Bedding	Minor Crinoid Fragments (5 - 15%), Thin Shelled Brachiopod Fragments (2 - 10%), Microcrystalline Quartz (10 - 30%) and Sponge Spicules (10 - 30%)
1: Dolomitized Mudstone	Light Olive Gray To Olive Gray, Yellowish Gray, Grayish Red, Very Light Gray To Medium Light Gray, Dark Gray	10.6	72.5	50.3	16.9	16.9	Abundant Silt to Very Fine Sand-Sized Dolomite Crystals, Laminated Bedding	Dolomite (50 - 60%), Microcrystalline Quartz (2 - 5%) and Sponge Spicules (0 - 5%)

Table 2A: Summary of key characteristics of the four depositional facies identified in Core #1 (Bann 1-14) and Core #2 (Albus 1-34H) in Oklahoma. Averages for mineralogy were calculated using core data from Core #1 and #2. Primary grain constituent percentages were estimated from thin sections using visual estimation charts.

Oklahoma Facies	Porosity (Avg. %)	Porosity (Max. %)	Porosity (Min. %)	Permeability (Avg. mD)	Permeability (Max. mD)	Permeability (Min. mD)	No. of Samples	Dominant Pore Type
Exposure Interval: Skeletal Grainstone to Packstone	15.1	22.6	9.2	9.118	100.000	0.022	19	Mold
4: Skeletal Packstone to Grainstone	5.4	14.3	1.1	0.216	3.060	0.0003	20	Vug
3: Bioturbated Packstone	8.1	15.2	1.9	0.292	1.290	0.005	65	Mold
2: Burrowed Wackestones to Packstones	6.3	13.8	2.8	0.009	1.340	0.00001	18	Mold
1: Dolomitized Mudstone	8.2	10.9	4.5	0.011	0.011	0.002	3	Intercrystalline

Table 2B: Continued summary of key characteristics of the four depositional facies identified in Core #1 and #2. Average values for permeability and porosity were calculated using core data from Core #1 and #2. Dominant pore types were estimated from thin sections using visual estimation charts.

Kansas Facies	Color	Mineralogy (Avg. %)					Dominant Sedimentary Features	Primary Grain Constituents
		Clays	Total Carbonates	Dolomite	Total Non-Clays	Quartz		
4: Crinoidal Grainstone To Packstone B	Light Olive Gray, Grayish Green, Yellowish Gray	1.3	98.2	0.5	0.5	0.5	Horizontal Stylolites, Mineralized Vertical Fractures, Skeletal Debris, Graded Bedding, Localized Laminar Bedding	Coarse to Very Coarse Sand-Sized Crinoids (10 - 80%), Brachiopod (2 - 8%), Bivalve (1 - 15%) and Bryozoan Fragments (3 - 25%)
3: Crinoidal Grainstone To Packstone A	Dusky Yellowish Green, Olive Black	1.6	97.9	1.8	0.5	0.5	Horizontal Stylolites, Mineralized Fractures, Skeletal Debris, Massively Bedded	Medium to Coarse Sand-Sized Crinoids (10 - 30%), Bivalves (2 - 15%), Brachiopod (0 - 5%), Foraminifera (0 - 5%) and Bryozoan Fragments (5 - 25%)
2: Bryozoan Grainstone To Packstone	Yellowish Gray, Greenish Gray, Grayish Pink	1.5	98.2	0.0	0.3	0.3	Horizontal Stylolites, Mineralized Fractures, Mottled Massive and Graded Bedding, Localized Centimeter-Sized Horizontal Burrows	Bryozoan (15 - 35%), Bivalve (2 - 20%), Brachiopods (1 - 5%), Foraminifera (0 - 5%) and Crinoid Fragments (10 - 30%)
1: Skeletal Packstone To Wackestone	Olive Black, Light Olive Gray, Yellowish Gray, Pale Yellowish Orange	2.0	97.5	0.0	0.5	0.5	Suture Seam Stylolites, Mottled and Localized Laminar Bedding	Fine to Medium Sand-Sized Crinoids (5 - 10%), Bivalves (0 - 5%) and Bryozoans (0 - 20%)

Table 3A: Summary of key characteristics of the four depositional facies identified in Core #3 (Trophy Farms 32-34-16 1H) in Kansas. Averages for mineralogy were calculated using core data from Core #3. Primary grain constituent percentages were estimated from thin sections using visual estimation charts.

Kansas Facies	Porosity (Avg. %)	Porosity (Max. %)	Porosity (Min. %)	Permeability (Avg. mD)	Permeability (Max. mD)	Permeability (Min. mD)	No. of Samples	Dominant Pore Type(s)
4: Crinoidal Grainstone To Packstone B	2.43	7.30	0.60	0.1946	3.8700	0.0001	28	Intraparticle and Interparticle
3: Crinoidal Grainstone To Packstone A	2.06	9.00	0.70	0.0528	1.0100	0.0001	25	Intraparticle and Interparticle
2: Bryozoan Grainstone To Packstone	2.16	5.20	0.09	0.0128	0.1190	0.0001	30	Interparticle and Moldic
1: Skeletal Packstone To Wackestone	0.70	0.70	0.70	0.0001	0.0001	0.0001	2	Interparticle

Table 3B: Continued summary of key characteristics of the four depositional facies identified in Core #3. Average porosity and permeability values were calculated using core data from Core #3. Dominant pore types were estimated from thin sections using visual estimation charts.

The facies identified in all three cores are presented in a shallowing/shoaling-upward order, beginning with what is interpreted to be the most restricted and relatively distal depositional environment and ending with the most proximal depositional environment, with Core #3 representing an overall more proximal expression of facies.

OKLAHOMA FACIES 1: DOLOMITIZED MUDSTONE

Observations – Oklahoma Facies 1

The dolomitized mudstone facies (Figure 14) is a variety of gray colored facies, composed of silt to clay sized dolomite crystals (50 – 60%) with microcrystalline quartz (2 – 5%) and localized sponge spicules (0 – 5%). Oklahoma Facies 1 contains intercrystalline, vuggy and interparticle porosity (dominant pore type: intercrystalline; average porosity 8.2%) and the second lowest permeability of the Oklahoma facies (average 0.011 mD). XRD analysis indicates this facies has the second highest total carbonate content (average 72.5%), the highest dolomite content (average 50.3%), the highest clay content (average 10.6%) and lowest quartz content (average 16.9%) of the Oklahoma Facies. Oklahoma Facies 1 occurs in both cores and ranges from 0.5ft (0.15m) to 2.8ft (0.9m) thick. Oklahoma Facies 1 exhibits both sharp and gradational contacts with the overlying and underlying Oklahoma facies.

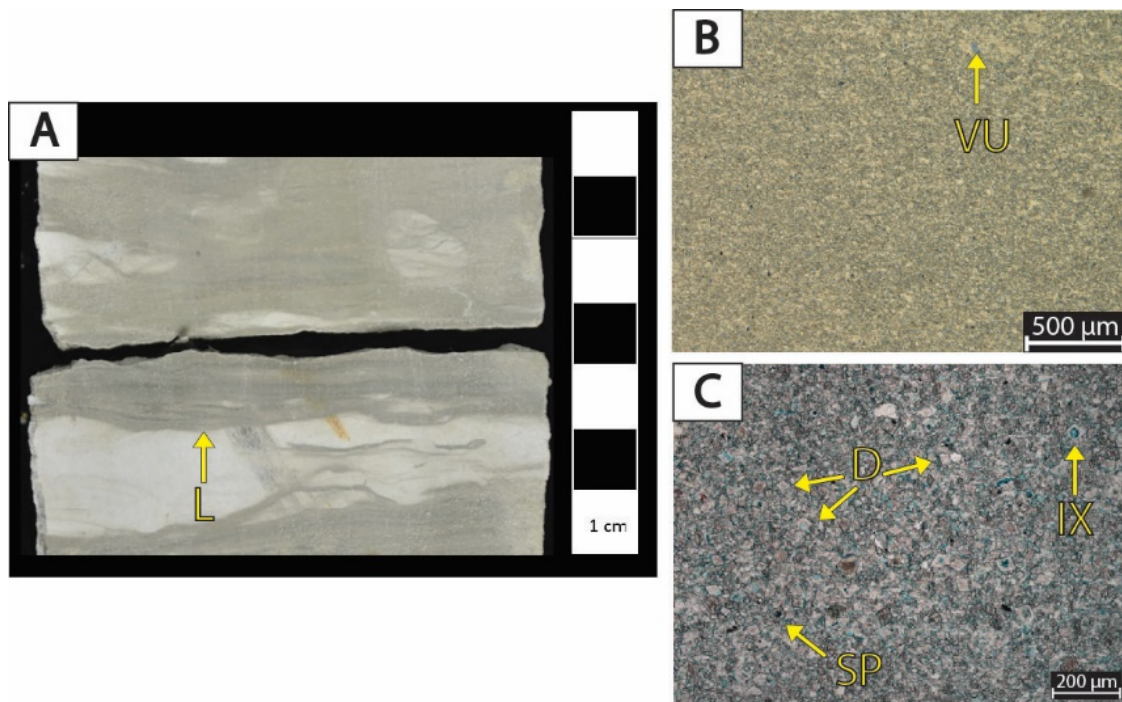


Figure 14: Oklahoma Facies 1: Dolomitized mudstone. **A)** Core photograph from Core #1 (5279.4') in white light. Scale is in centimeters. Oklahoma Facies 1 is light olive gray, yellowish gray and medium dark gray characterized by silt to very fine sized dolomite crystals and laminated bedding (L). **B&C)** Photomicrograph from the Core #1 (5279.4') in plane polarized light. Sample is alizarin red stained and blue epoxy impregnated. Porosity (NCS): 10.9%. Permeability (Klinkenberg): 0.0018 mD. Visual estimation of mineralogical composition: 10% clays, 80% carbonates, and 10% other minerals. Sample contains abundant very fine-grained dolomite (D, 60%) and sponge spicules (SP, 5%). Open and oil-filled vuggy (VU) porosity as well as intracrystalline (IX) porosity observed in dolomite.

Interpretation – Oklahoma Facies 1

The type of dolomite present in Core #1 was characterized by Ewald (in progress, 2016) as micrite selective, unimodal planar-e to planar-s crystals with the highest abundance in Oklahoma Facies 1 (average 50%). Planar textures are common in dolomites that form near surface diagenetic environments, as well as burial environments (Sibley and Gregg, 1987). Ewald (in progress, 2016) interpreted that the dolomite formed early, under near seafloor conditions in equilibrium with Mississippian seawater. Although the exact timing of the dolomite is unknown, the dolomitization in Core #1 likely formed concurrent with or shortly after micritization through evidence of micrite inclusions present within the

dolomite rhombs (Ewald, in progress 2016). XRD patterns showed that the dolomite is slightly calcian 55.5 mol% CaCO₃ (Ewald, in progress 2016), which suggests the dolomite was precipitated in marine seawater and was not further altered during diagenesis. The dolomite in Core #1 occurs as dolomite crystals ‘floating’ in a micrite matrix. The lack of supratidal features, such as mudcracks and/or stromatolites, in core supports the deposition of Oklahoma Facies 1 in a more distal environment. The presence of sponge spicules also infers a relatively low energy environment, as siliceous sponges flourished in quiet water environments during the Paleozoic (Flügel et al., 2010). Based on these observations, Oklahoma Facies 1 is interpreted as a distal mid-ramp environment below storm wave base (SWB) where circulation was limited.

OKLAHOMA FACIES 2: BURROWED WACKESTONE TO PACKSTONE

Observations – Oklahoma Facies 2

Oklahoma Facies 2 (Figure 15) is a gray to olive black facies, composed of fine to medium-grained burrowed wackestone to packstone with microcrystalline quartz (10 – 30%), sponge spicules (10 – 30%), minor crinoid fragments (5 – 15%) and thin-shelled brachiopod fragments (2 – 10%). Localized laminated bedding and a moderate (3 on bioturbation index from Bann et al., 2008) occurrence of millimeter-sized horizontal burrows were observed. Facies 2 contains interparticle, vuggy, moldic and fracture porosity (dominant pore type: mold; average porosity 6.3%) and the lowest permeability of the four Oklahoma facies (average 0.009 mD). Oklahoma Facies 2 occurs in both cores, ranges from 0.5ft (0.15m) to 12ft (3.7m) thick, and has gradational contacts with the overlying and underlying facies (Oklahoma Facies 1, 3 and 4).

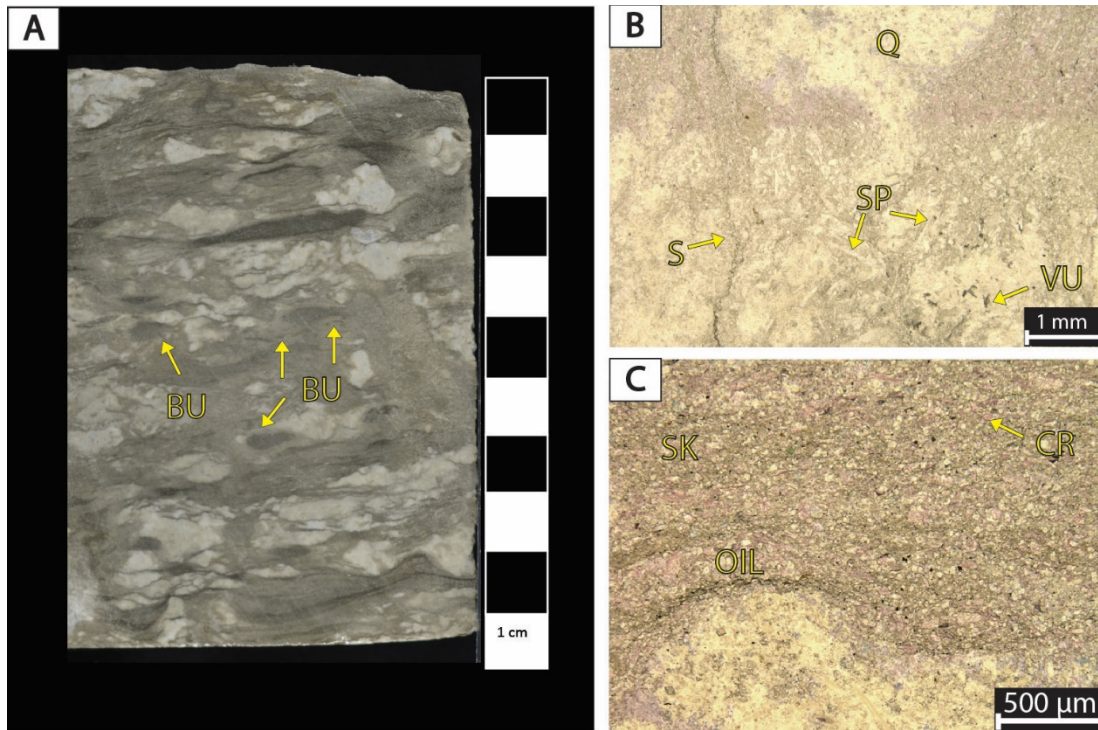


Figure 15: Oklahoma Facies 2: Burrowed wackestone to packstone. **A)** White light core photo from Core #1 (5353.8'). Scale is in centimeters. Facies 2 is gray to olive gray and olive black, characterized by millimeter-sized horizontal burrows (BU). **B&C)** Plane polarized light photomicrograph from Core #1 (5353.8'). Sample is alizarin red stained and blue epoxy impregnated. Porosity (NCS): 6.4%. Permeability (Klinkenberg): 0.0006 mD. XRD: 4.9% clay (4.7% illite/smectite, 0.2% chlorite), 33.2% carbonate (24% calcite, 9.2% dolomite), and 61.9% other minerals (61.5% quartz and trace amounts of pyrite and halite). Sample contains microcrystalline quartz (Q, 30%), stylolites (S), silt-sized quartz grains (30%), crinoid fragments (CR, 15%), sponge spicules (SP, 10%) and undifferentiated skeletal debris (SK). Oil-filled vuggy (VU) porosity observed.

Interpretation – Oklahoma Facies 2

This facies represents the distal outer ramp below fair weather wave base (FWWB) and above SWB and a transitional environment between the underlying dolomitized mudstone facies (Oklahoma Facies 1) and the overlying bioturbated packstone facies (Oklahoma Facies 3). The horizontal millimeter-scale burrows present in this facies have been interpreted as a distal *Cruziana* ichnofacies. *Cruziana* ichnofacies occurs in shallow marine settings below FWWB and above SWB, with moderate energy levels below FWWB varying to lower energy levels in deeper, quieter waters (Ekdale et al., 1984; MacEachern

et al., 2009). Horizontal burrows dominate and vertical burrows occur locally (Ekdale et al., 1984) in this ichnofacies. The minor presence (average 5%) of normal marine fauna (crinoid debris, thin-shelled brachiopods and sponge spicules) favors a more restricted depositional environment interpretation.

OKLAHOMA FACIES 3: BIOTURBATED PACKSTONE

Observations – Oklahoma Facies 3

Oklahoma Facies 3 (Figure 16) is a medium gray to olive black, medium to fine grained, moderately to commonly bioturbated, mottled packstone with centimeter-scale horizontal and vertical burrows, crinoids (5 – 50%), bivalve fragments (0 – 5%), brachiopods (2 – 20%), microcrystalline quartz (15 – 60%) and sponge spicules (15 – 25%). Vuggy, moldic, fracture and interparticle porosity (dominant pore type: mold) are present in Oklahoma Facies 3. This facies has a wide range of porosity values (maximum = 15.2%, minimum = 1.9%, average = 8.1%). Oklahoma Facies 3 has the highest permeability (maximum = 1.29 mD, minimum = 0.005 mD, average = 0.292 mD) of the four depositional Oklahoma facies. XRD analysis revealed that this facies has the lowest total carbonate (average 52.9%) and dolomite content (average 13.1%) and the highest quartz content (average 42.9%) of the depositional facies in Oklahoma. Oklahoma Facies 3 occurs in both cores, ranges from 0.2ft (0.06m) to 10.8ft (3.3m) thick, and has gradational and sharp contacts with overlying and underlying facies (Oklahoma Facies 1, 2 and 4).

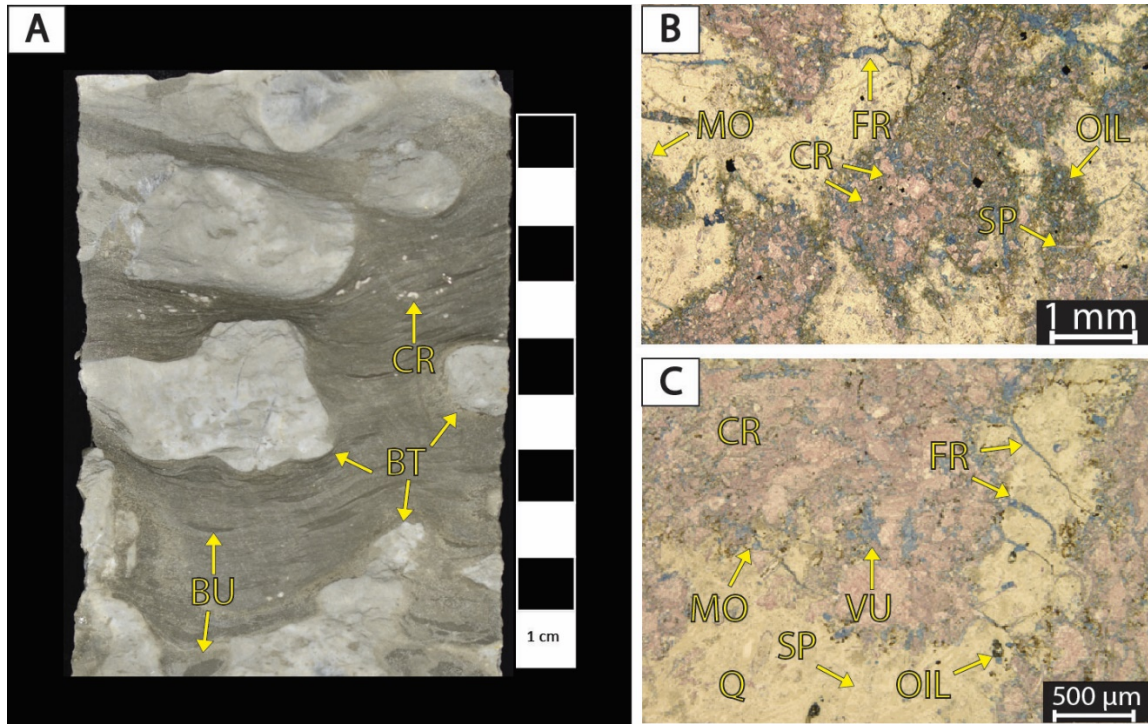


Figure 16: Oklahoma Facies 3: Bioturbated packstone. **A)** Core photo in white light from Core #1 (5342.56'). Scale is in centimeters. Oklahoma Facies 3 is medium gray to olive gray and olive black in appearance, characterized by horizontal centimeter-sized burrows (BU), moderate to common bioturbation (BT) and mottled bedding. Crinoid (CR) debris is common. **B)** Plane polarized light photomicrograph from Core #1 (5342.56') Sample is alizarin red stained and blue epoxy impregnated. Plug Porosity (NCS): 5.3% Permeability (Klinkenberg): 0.0018 mD. XRD: 8.3% clay (8% illite/smectite, 0.3% chlorite), 40.4% carbonate (18.9% calcite, 12.7% dolomite), and 51.3% other minerals (49.7% quartz and trace amounts of potassium feldspar, plagioclase, pyrite, apatite and halite). Sample contains microcrystalline quartz (30%), silt-sized quartz grains (10%), sponge spicules (SP, 15%), crinoid fragments (CR, 20%), brachiopod fragments (15%) and undifferentiated microbioclastic debris. Oil filled fracture porosity observed. Open moldic (MO) and fracture (FR) porosity present. **C)** Plane polarized light photomicrograph from Core #1 (5258.4'). Sample is alizarin red stained and blue epoxy impregnated. Porosity (NCS): 3.8%. Permeability (Klinkenberg): 0.029 mD. XRD: 1.8% clay (illite+mica), 66% carbonates (calcite), and 32.2% other minerals (32% quartz and trace amounts of pyrite). Sample contains crinoid fragments (CR, 40%), sponge spicules (SP, 20%), microcrystalline quartz (Q, 10%), silt-sized quartz grains (3%) and undifferentiated skeletal debris. Fracture (FR), vuggy (VU) and moldic (MO) porosity observed.

Interpretation – Oklahoma Facies 3

Oklahoma Facies 3 represents the mid-ramp environment below FWWB and above SWB. It also represents a transitional environment between the underlying burrowed wackestone to packstone facies (Oklahoma Facies 2) and the overlying skeletal packstone

to grainstone facies (Oklahoma Facies 4). Mid-ramp deposits consist of variable carbonate sediments deposited below FWFB and reflect varying degrees of storm influence. The deposits are dominated by suspension-fall out (mud) and are commonly bioturbated (Burchette and Wright, 1992). The increase of skeletal diversity (up to 50% crinoids, presence of bivalves and more robust brachiopods) in Oklahoma Facies 3 indicates a less restricted environment than Oklahoma Facies 2. *Thalassinoides* is a more proximal expression of the *Cruziana* ichnofacies, characterized by predominantly mottled fabric and centimeter sized burrows (Ekdale et al., 1984; MacEachern et al., 2009). Oklahoma Facies 3 exhibits a blotchy (mottled), heterogeneous fabric that may be due to densely packed *Thalassinoides* burrow systems resulting in a mottled fabric (Ekdale et al., 1984). Bright yellow-orange fluorescence under ultraviolet lighting in several zones of the cores indicates the presence of hydrocarbons in many of these deposits (see Appendix C).

OKLAHOMA FACIES 4: SKELETAL PACKSTONE TO GRAINSTONE

Observations – Oklahoma Facies 4

Oklahoma Facies 4 (Figure 17) is a variable gray to grayish blue, medium to coarse grained skeletal packstone to grainstone with minor bioturbation, open and mineralized fractures, suture seam stylolites, crinoids (10 – 80%), bivalves (3 – 8%), bryozoans (10%), brachiopod fragments (5 – 10%) and sponge spicules (5 – 10%). Traction currents were observed at select intervals (see Appendix C). Vuggy (dominant pore type), moldic, fracture and interparticle porosity are present in Oklahoma Facies 4, creating a wide range of porosity values (minimum = 1.1%, maximum = 14.3%, average = 5.4%) and the third highest permeability (minimum = 0.0001 mD, maximum = 3.06 mD, average = 0.216 mD) of the facies present in Core #1 and #2. XRD analysis indicates this facies has the highest

carbonate content (average 78.5%) and the second highest dolomite content (average 28.9%). Oklahoma Facies 4 occurs in both cores towards the top of the cores (Core #1 above 5291.5', Core #2 above 5163.7') and ranges from 0.2ft (0.7m) to 17.5ft (5.3m) thick. Oklahoma Facies 4 has gradational contacts with underlying Oklahoma Facies 2 and 3 and sharp contacts with underlying Oklahoma Facies 1.

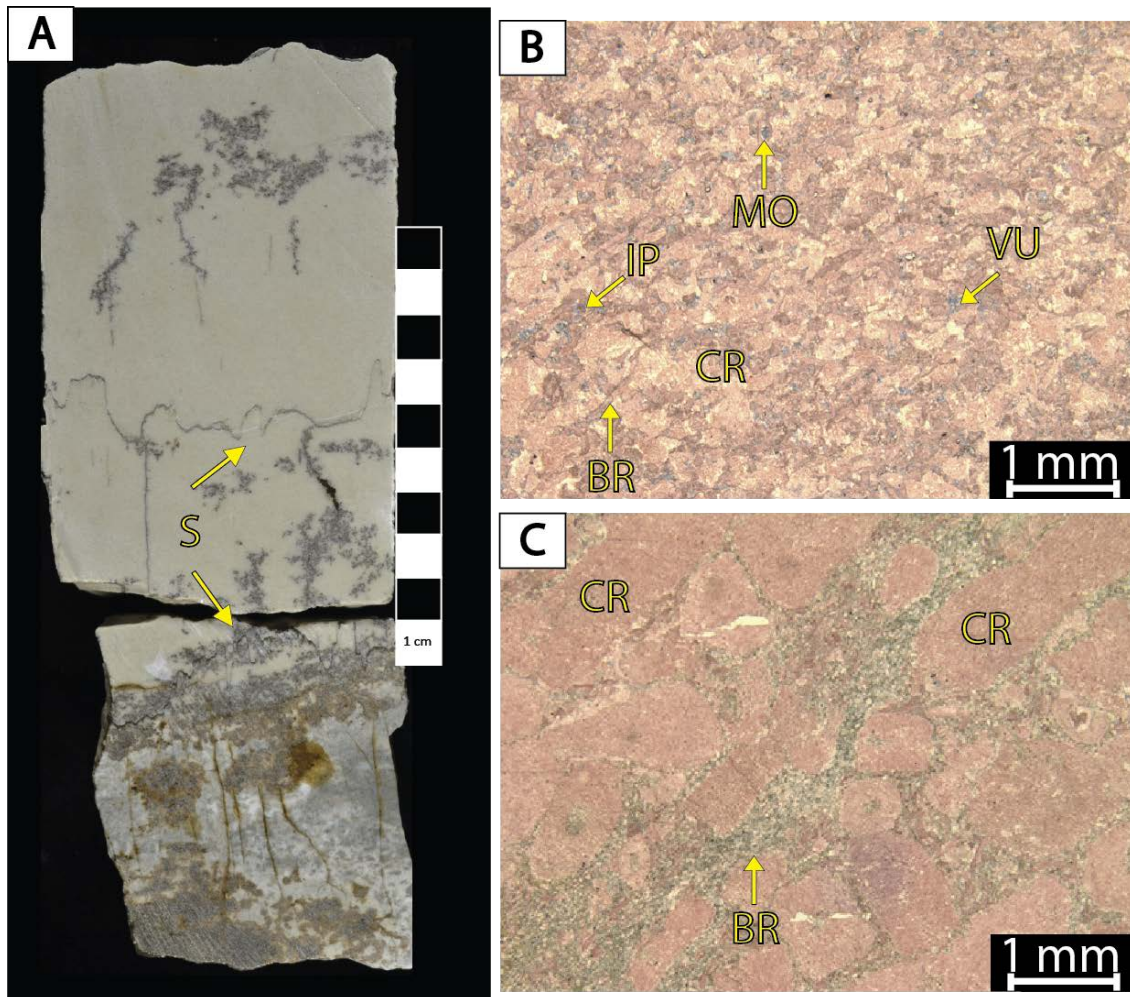


Figure 17: Oklahoma Facies 4: Skeletal grainstone to packstone. **A)** White light photograph of Core #1 (5262.1'). Scale is in centimeters. Oklahoma Facies 4 is characterized by massive bedding, stylolites (S) and a light olive gray to olive gray appearance. Note oil stained vertical fractures. Traction currents were found preserved at select intervals in Core #1 (5246' – 5246.2', 5284'.5 – 5284.8'). **B)** Plane polarized light photomicrograph of Core #1 (5260.66'). Sample is alizarin red stained and blue epoxy impregnated. Porosity (NCS): 2.3%. Permeability (Klinkenberg): <0.0001 mD. Visual estimation of mineralogical content: 1% clay, 97% carbonates, and 2% other minerals. Sample contains crinoid fragments (CR, 80%), sponge spicules (SP, 5%), brachiopod fragments (BR, 5%) and undifferentiated skeletal debris. Open

moldic (MO), vuggy (VU) and interparticle (IP) porosity present. C) Plane polarized light photomicrograph of Core #1 (5277.74'). Sample is alizarin red stained and blue epoxy impregnated. Porosity (NCS): 5.7%. Permeability (Klinkenberg): 0.0020 mD. Visual estimation of mineralogical content: 1% clay, 93% carbonates, and 6% other minerals. Sample contains crinoid fragments (CR, 60%), sponge spicules (10%), brachiopod fragments (BR, 10%), microcrystalline quartz (5%), silt-sized quartz grains (3%) and undifferentiated skeletal debris.

Interpretation – Oklahoma Facies 4

These facies represent deposition within the mid-ramp environment or a more distal portion of the ramp crest environment near or at FWWB. The minor bioturbation present in Oklahoma Facies 4 and grain size (medium to coarse sand-size) indicate a more distal environment of the ramp crest. Some areas in Core #1 (5246' – 5246.2', 5284'.5 – 5284.8'; see Appendix C) have preservation of traction currents, which are common diagnostic features of a higher energy mid-ramp environment. The prevalent diagenetic overprint present in Core #1 and #2 may have obliterated most of these sedimentary features. The presence of normal marine fauna in these facies indicates open marine conditions were present. Yellow-orange fluorescence under ultraviolet lighting indicates hydrocarbons present in select intervals in the Core #1 and #2 (see Appendix C).

KANSAS FACIES 1: SKELETAL PACKSTONE TO WACKESTONE

Observations – Kansas Facies 1

Kansas Facies 1 (Figure 18) is an olive black, light olive gray, yellowish gray, pale yellowish orange, mottled and locally laminated bedded, fine to medium grained skeletal packstone to wackestone with suture seam stylolites, fine to medium sand-sized crinoids (5 - 10%), bivalves (0 -5%) and bryozoans (0 - 20%). The dominant pore type observed in this facies was interparticle. This facies had the lowest porosity (average 0.7%) and the lowest permeability (average <0.0001 mD) of the four Kansas facies. XRD analysis indicates that this facies has the highest clay content (average 2%) and lowest carbonate

percentage (average 97.5%) of the four Kansas Facies. Kansas Facies 1 occurs throughout the bottom 2/3 of the core (5340' – 5346'), varying in thickness (0.25ft/0.07m to 1.5ft/0.5m) with a total thickness of 7.4ft (2.3m), exhibiting both abrupt and gradational contacts with overlying facies (Kansas Facies 2, 3 and 4).

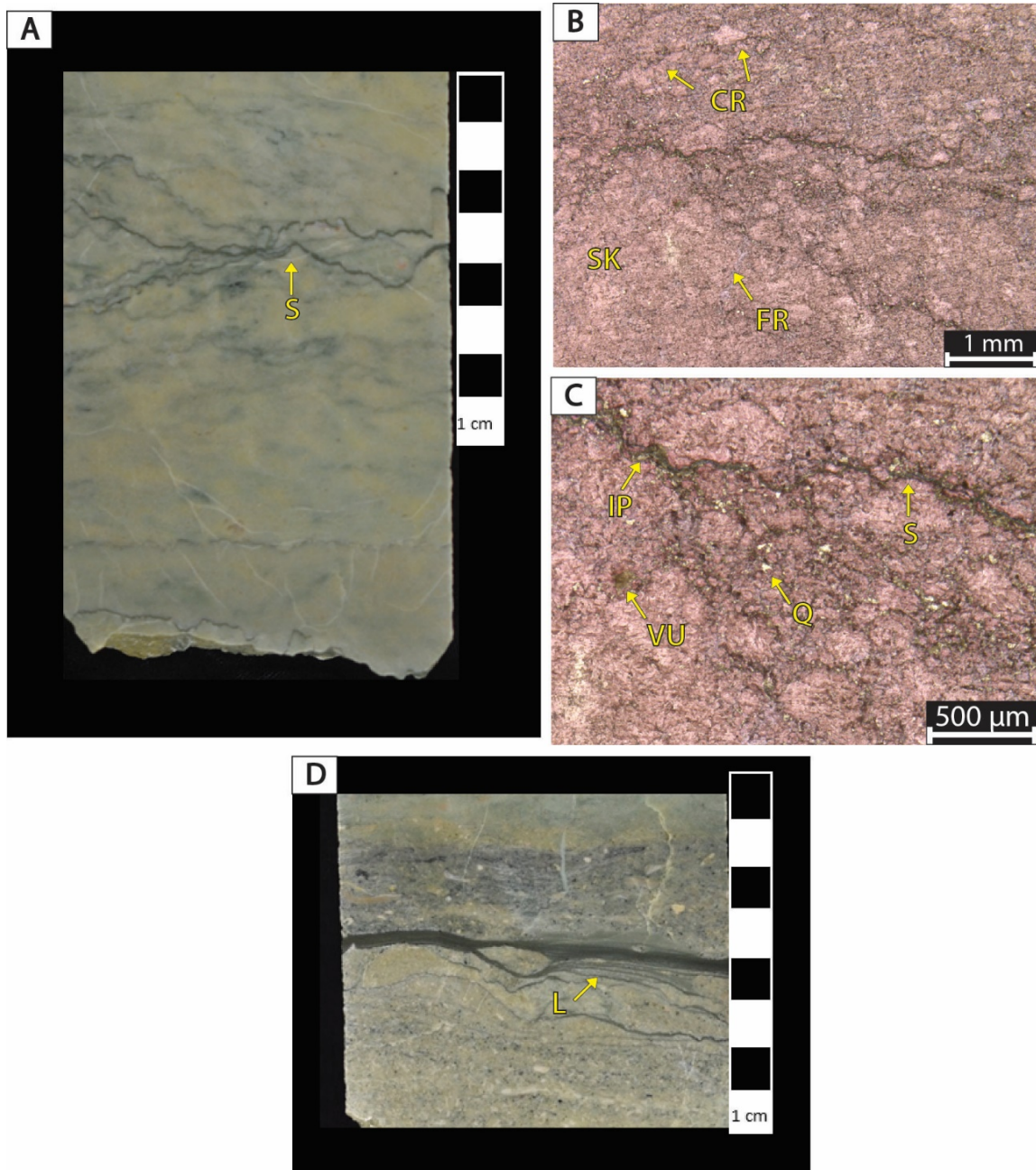


Figure 18: Kansas Facies 1: Skeletal packstone to wackestone. A) White light core photograph of Core #3 (5354.42'). Scale is in centimeters. Facies 1 is characterized by an olive black, light olive

gray, yellowish gray, pale yellowish orange appearance with suture seam stylolites (S). **B&C** Plane polarized light photomicrographs of Core #3 (5354.42'). Sample is alizarin red stained and blue epoxy impregnated. Porosity (NCS): 0.7%. Permeability (Klinkenberg): 0.0001 mD. Visual estimation of mineralogical composition: 2% clays, 97% carbonates, 1% other minerals. Sample contains silt sized quartz (Q, 5%), crinoid fragments (CR, 5%) and undifferentiated skeletal debris (SK). Slight fracture (FR), interparticle (IP) and vuggy (VU) porosity observed. **D**) White light core photograph of Core #3 (5374.5'). Scale is in centimeters. Laminated (L) bedding occurs locally in this facies.

KANSAS FACIES 2: BRYOZOAN GRAINSTONE TO PACKSTONE

Observations – Kansas Facies 2

Kansas Facies 2 (Figure 19) is a yellowish gray, greenish gray, grayish pink mottled to massively bedded, locally graded bedded, medium to very coarse grained bryozoan grainstone to packstone with localized centimeter-sized horizontal burrows, horizontal stylolites, mineralized fractures and medium to very coarse sand-sized bryozoans (15 - 35%), bivalves (2 - 20%), brachiopods (1 - 5%), foraminifera (0 - 5%) and crinoid fragments (10 - 30%). Vuggy, mold, shelter, fracture and inter- and intra- particle porosity were observed in this facies. The dominant pore types are interparticle and moldic pores. Kansas Facies 2 has the second highest porosity (average 2.16%) and second lowest permeability (average 0.013 mD) of the four Kansas facies. Kansas Facies 2 occurs throughout the core below the exposure interval (5330.8' – 5454' interval in Core #3), ranging from 0.5ft (0.15m) to 5.25ft (1.6m) with a total thickness of 41.25ft (12.6m). Kansas Facies 2 exhibits abrupt contacts with underlying Kansas Facies 1 and gradational contacts with Kansas Facies 3 and 4.

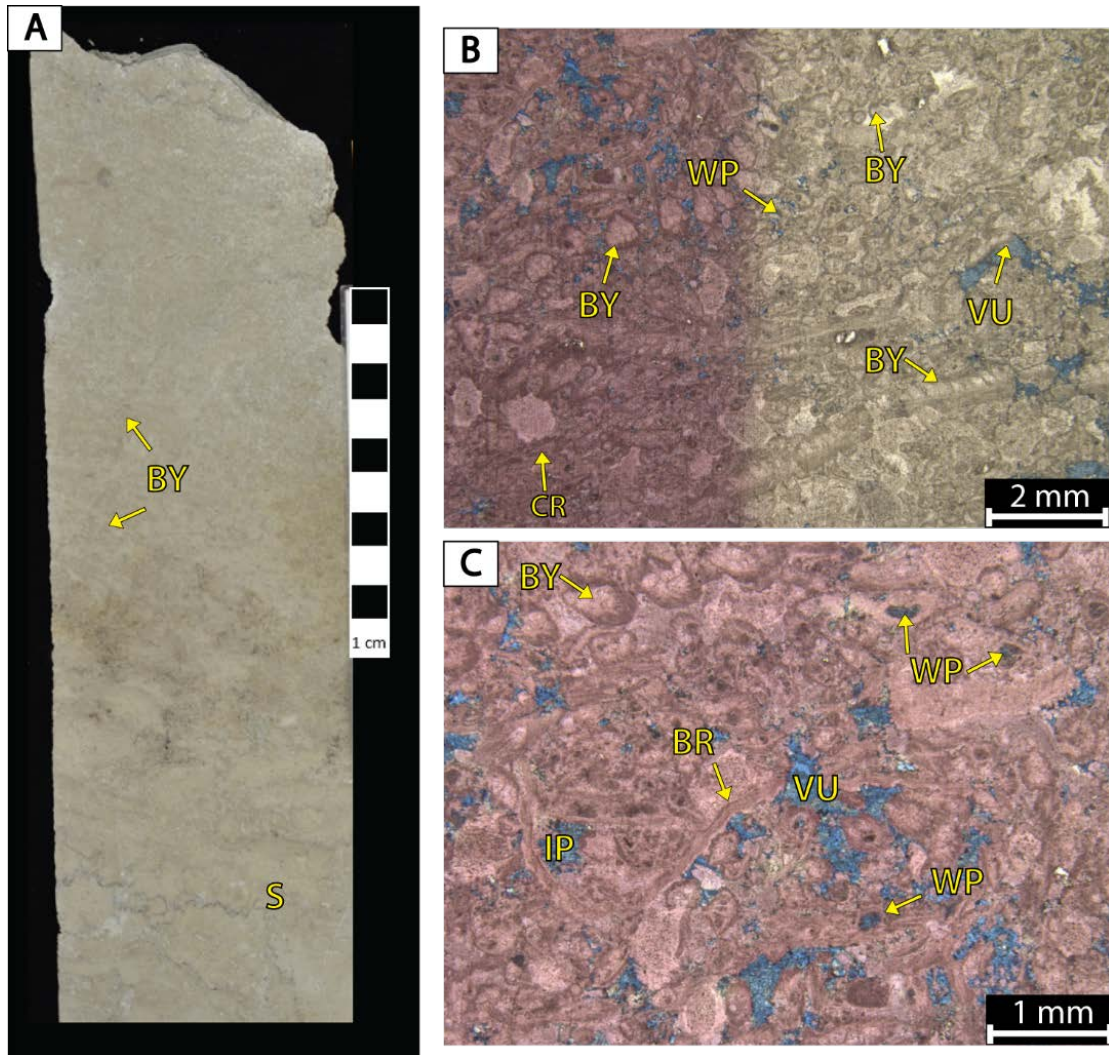


Figure 19: Kansas Facies 2: Bryozoan grainstone to packstone. **A)** White light core photo from Core #3 (5423.36'). Scale is in centimeters. Kansas Facies 2 is yellowish gray, greenish gray, grayish pink in color and is characterized by horizontal stylolites (S), mottled and massive bedding with abundant bryozoans (BY). **B&C)** Plane polarized light photomicrograph from Core #3 (5423.36'). Sample is alizarin red stained (half of slide in **B**) and blue epoxy impregnated. Porosity (NCS): 3.1%. Permeability (Klinkenberg): 0.0063 mD. XRD: 2.7% clay (kaolinite), 96.9% carbonate (calcite), and trace amounts of quartz. Sample contains bryozoans (BY, 20%), brachiopods (BR, 5%), crinoid fragments (CR, 10%) and undifferentiated skeletal debris. Intraparticle (WP), interparticle (IP), mold and vuggy (VU) porosity observed.

Interpretation – Kansas Facies 1 and 2

Kansas Facies 1 and 2 also represent the mid-ramp environment, slightly closer to the inner ramp environment than Oklahoma Facies 3 due to the higher diversity of fauna and coarser grained sediments (fine to very coarse). Kansas Facies 1 and 2 have localized

centimeter horizontal burrows (*Thalassinoides*), mottled fabric and graded bedding, which are also characteristics of the mid-ramp environment below FWFB and above SWB (Burchette and Wright, 1992). The abundance of bryozoans (maximum 35%) in Kansas Facies 2 indicates a relatively more distal environment than the overlying crinoid dominated (Burchette and Wright, 1992) Kansas Facies 3 and 4.

KANSAS FACIES 3: CRINOIDAL GRAINSTONE TO PACKSTONE A

Observations – Kansas Facies 3

The crinoidal grainstone to packstone A (Kansas Facies 3; Figure 20) is a dusky yellowish green, olive black, medium to coarse grained and massively bedded facies with horizontal stylolites, abundant skeletal debris containing fine to coarse sand-sized crinoids (10 - 30%), bivalves (2 -15%), brachiopods (0 - 5%), foraminifera (0 - 5%) and bryozoan fragments (5 - 25%). Inter- and intra- particle were the most common pore type observed in thin section for this facies. Moldic and vuggy porosity were also present in hand sample and thin section for this facies. Average porosity (2.06%) for Kansas Facies 3 is the second lowest of the four Kansas facies and has the second highest permeability (minimum = 0.0001 mD, maximum = 1.01 mD, average = 0.053 mD). XRD analysis indicates the highest dolomite content (average 1.8%) of the total carbonate content (average 97.9%) occurs in this facies. This facies is present throughout Core #3 (5338' – 5456.9'), ranging from 0.25ft (0.08m) to 5ft (1.5m) with a total thickness of 34.75ft (11.5m). Kansas Facies 3 has gradational contacts with Kansas Facies 2 and 4 and abrupt contacts with Kansas Facies 1.

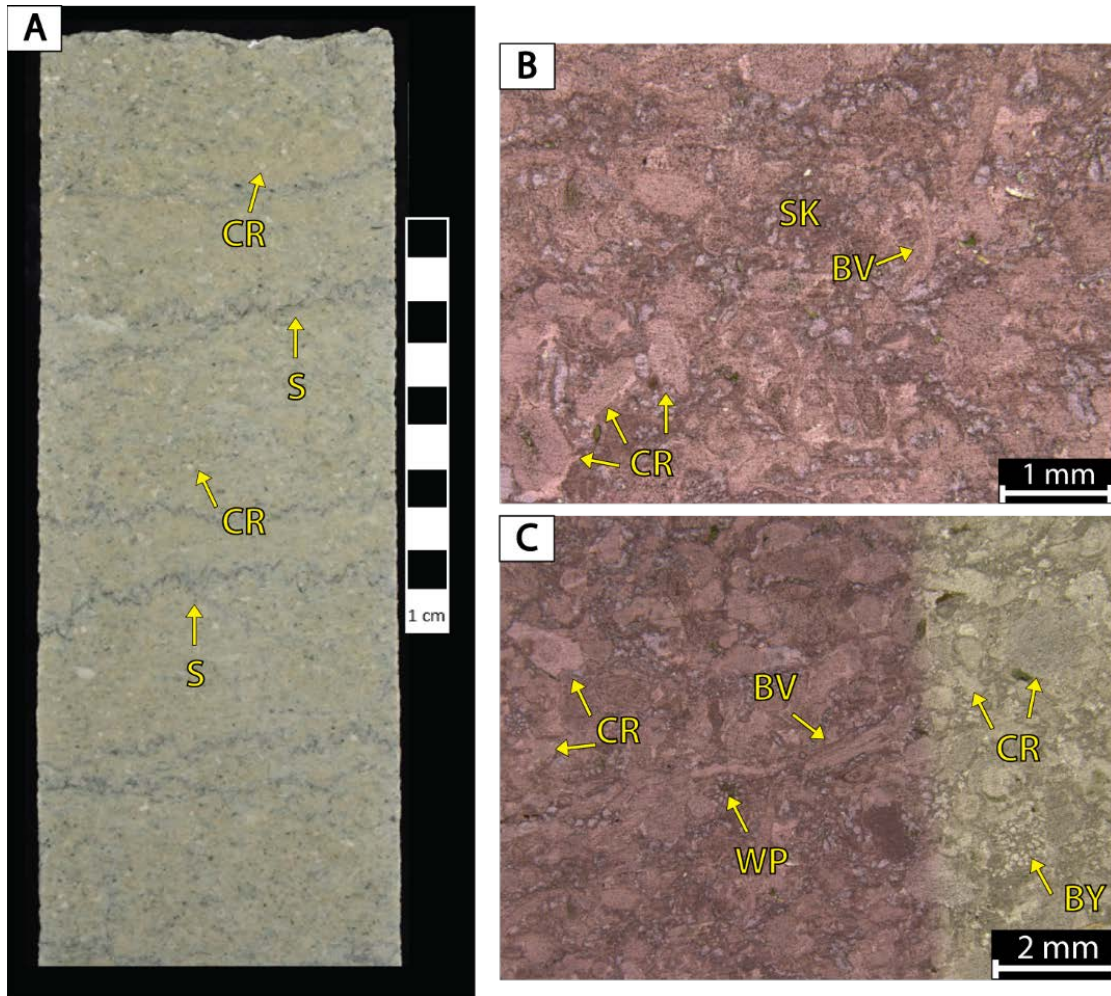


Figure 20: Kansas Facies 3: Crinoidal grainstone to packstone A. **A)** White light core photo from Core #3 (5373.36'). Scale is in centimeters. Kansas Facies 3 is dusky yellowish green and olive black in color. This facies is characterized by horizontal stylolites (S), massive bedding and fine to coarse sand-sized crinoids (CR). **B&C)** Plane polarized light photomicrograph from Core #3 (5373.36'). Sample is alizarin red stained (half of slide in C) and blue epoxy impregnated. Porosity (NCS): 0.9%. Permeability (Klinkenberg): 0.0008 mD. Visual estimation of mineralogical content: 3% clays, 97% carbonates. Sample contains bivalves (BV, 15%), bryozoans (BY, 5%), crinoid fragments (CR, 20%) and undifferentiated skeletal debris (SK). Minor intraparticle (WP) and interparticle porosity observed.

KANSAS FACIES 4: CRINOIDAL GRAINSTONE TO PACKSTONE B

Observations – Kansas Facies 4

The crinoidal grainstone to packstone B (Kansas Facies 4; Figure 21) is a light olive gray, grayish green, yellowish green, graded bedded, locally laminated, coarse to very coarse grained facies with horizontal stylolites, crinoids (10 - 80%), brachiopods (2 - 8%),

bivalves (1 - 15%) and bryozoan fragments (3 - 25%). This facies has the highest porosity (minimum = 0.6%, maximum = 7.3%, average = 2.4%) of the Kansas facies, with predominantly inter- and intra- particle pores in thin section. Kansas Facies 4 also has highest permeability (minimum = 0.0001 mD, maximum = 3.87 mD, average = 0.195 mD) of the four Kansas facies. Kansas Facies 4 occurs in the bottom 2/3 of Core #3 (5349.5' – 5350.2'), ranging 0.5ft (0.15m) to 3ft (0.9m) thick, with a total thickness of 32.95ft (10m). Facies 4 has gradational contacts with Facies 2 and 3 and abrupt contacts with Facies 1.

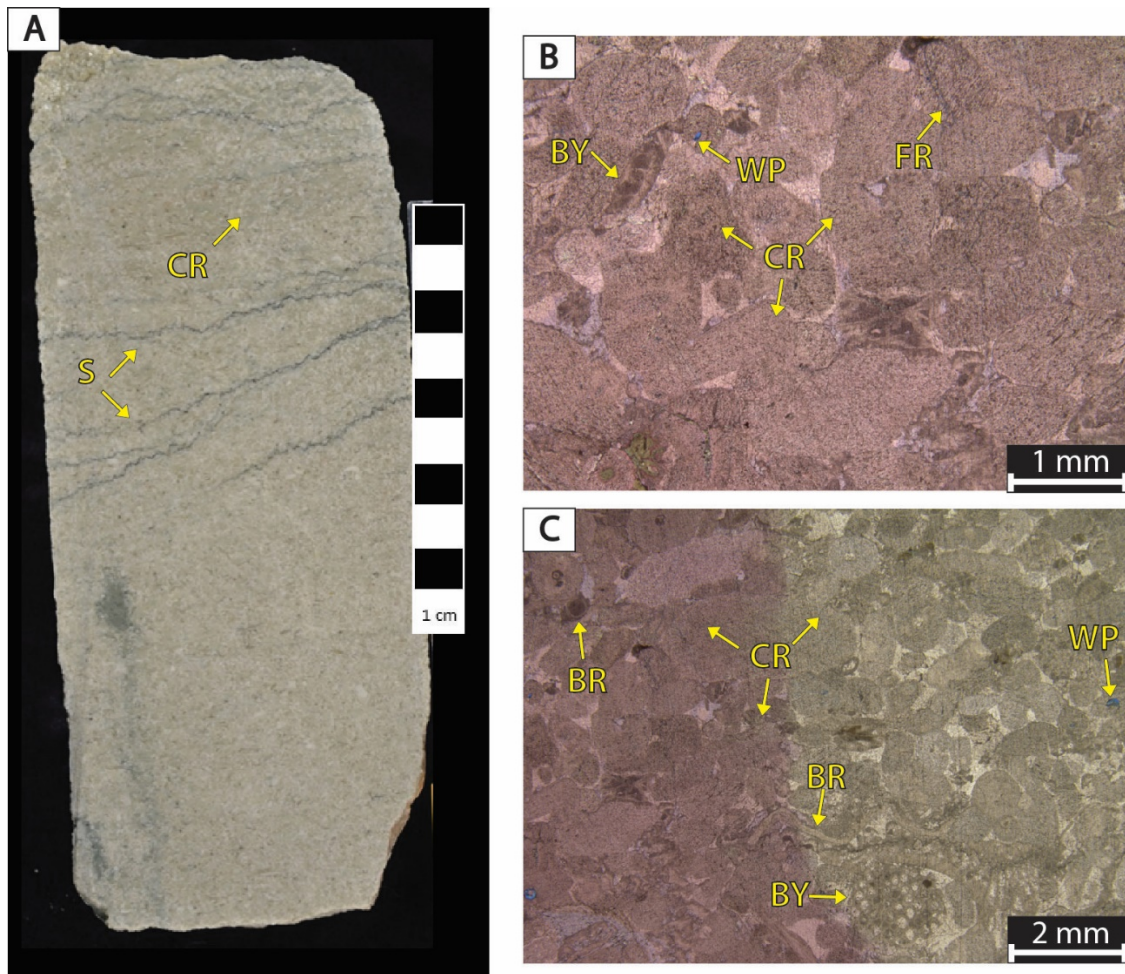


Figure 21: Kansas Facies 4: Crinoidal grainstone to packstone B. **A)** White light core photo from Core #3 (5382.6'). Scale is in centimeters. Kansas Facies 4 is light olive gray, grayish green and yellowish gray in color. This facies is characterized by horizontal stylolites (S), massive bedding and localized laminar bedding and coarse to very coarse sand-sized crinoids (CR). **B&C)** Plane polarized light photomicrograph from Core #3 (5382.6'). Sample is alizarin red stained (half of

slide in C) and blue epoxy impregnated. Porosity (NCS): 1.3%. Permeability (Klinkenberg): 0.0022 mD. Visual estimation of mineralogical content: 2% clays, 98% carbonates. Sample contains bivalves (2%), brachiopods (BR, 3%), bryozoans (BY, 10%), crinoid fragments (CR, 40%) and undifferentiated skeletal debris. Minor intraparticle (WP) and fracture (FR) porosity observed.

Interpretation –Kansas Facies 3 and 4

These facies represent deposition within the mid-ramp environment or a more distal portion of the ramp crest environment near or at FWWB. Kansas Facies 4 contained ~50% more crinoids (coarser grained, up to 80%) than Kansas Facies 3 (up to 30%), indicating that Kansas Facies 4 may have occurred in the inner ramp environment with slightly higher energy conditions than Kansas Facies 3, potentially at FWWB where constant agitating conditions prevailed. The presence of normal marine fauna in these facies indicates open marine conditions were present. Yellow-orange fluorescence under ultraviolet lighting indicates hydrocarbons present in select intervals in Core #3 (see Appendix C).

OKLAHOMA AND KANSAS EXPOSURE INTERVAL

Observations – Exposure Interval

A well-developed exposure interval occurs in Core #1 and #2 towards the top of the cores (Core #1: above 5230', Core #2: above 5152.3') and ranges from 6.5ft (2m) to 13ft (4m) thick, exhibiting sharp contacts with the underlying Oklahoma Facies 4 and 1. The exposure interval in Core #3 occurs at the top (5342.8'-5280') and varies from 1ft (0.3m) to 50ft (15.2m) thick and shares a similar appearance to the exposure interval in Core #1 and #2. Thin section, porosity and permeability data for the exposure interval in Core #3 was not available.

The exposure interval (Figure 22) in Core #1 and #2 is a variable green, gray, black and red that occurs as a massively bedded, coarse grained, poorly sorted skeletal grainstone

to packstone with partially healed and open fractures, crinoids (2 – 60%), bivalves (10 – 15%), brachiopods (5 – 10%), bryozoans fragments (10%) and ostracodes (5%). Vuggy, moldic, fracture and interparticle porosity (dominant pore type: mold; minimum = 9.2%, maximum = 22.65%, average = 15.1%) are present in this interval, with the highest permeability (minimum = 0.022 mD, maximum = 100.0 mD, average= 9.118 mD) for Core #1 and #2. XRD analysis indicates this interval has the highest amount of clays present (average 11.9%) and other mineral constituents (total non-clay minerals average: 87.5%; total quartz average (of the non-clay minerals): 86.3%).

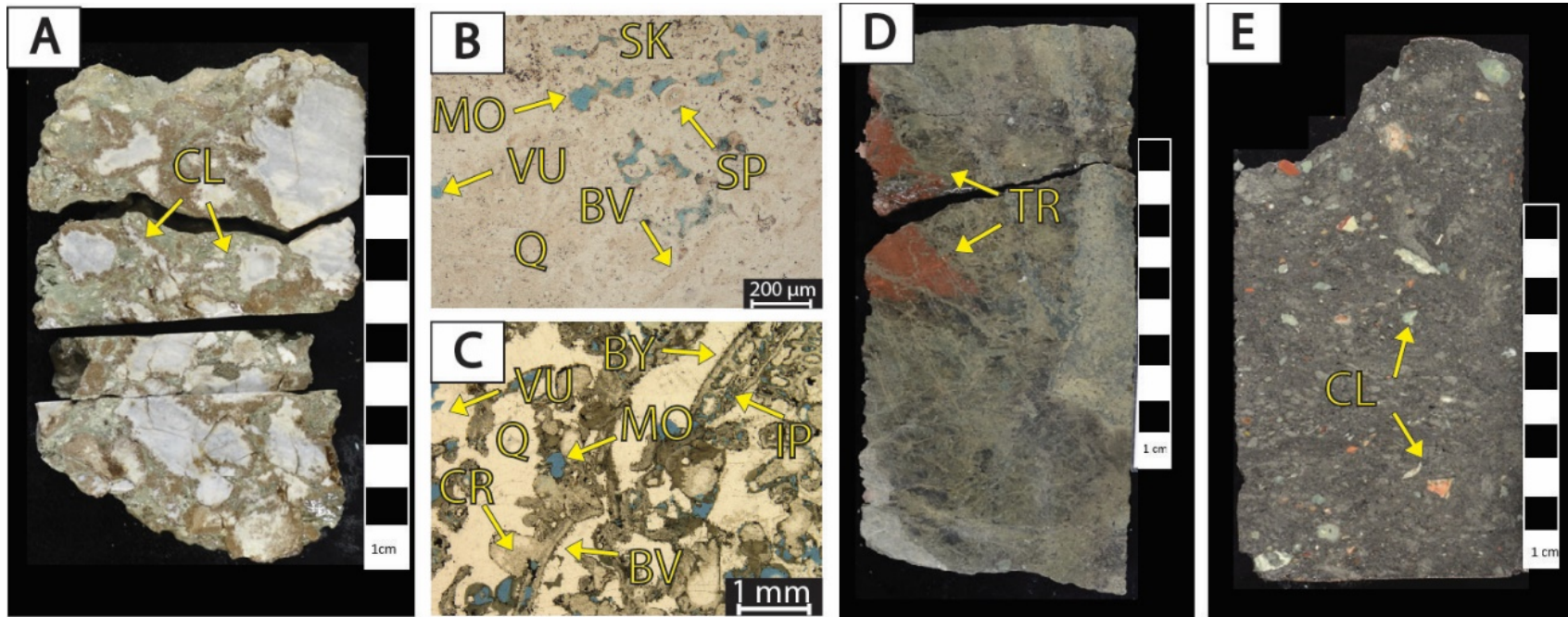


Figure 22: Exposure interval. **A)** White light core photo from Core #2 (5131.9'). Scale is in centimeters. Brecciated clasts (CL) are common. **B)** Plane polarized light photomicrograph from Core #2 (5131.9'). Silicified skeletal packstone. Sample is alizarin red stained and blue epoxy impregnated. Porosity (NCS): 17.05%. Permeability (Klinkenberg): 1.117 mD. XRD: 20.3% clay (13.2% illite/smectite, 4.1% chlorite, 3% kaolinite) and 79.7% other minerals (77.5% quartz, 1.3% potassium feldspar and trace amounts of plagioclase and halite). Sample contains microcrystalline quartz (Q, 60%), silt-sized quartz grains (40%), clay (15%), sponge spicules (SP, 10%), crinoid fragments (CR, 10%), bivalve fragments (BV, 10%) and undifferentiated skeletal debris (SK). Moldic (MO) and vuggy (VU) porosity observed. **C)** Plane polarized light photomicrograph from Core #1 (5227.4'). Silicified skeletal grainstone to packstone. Sample is alizarin red stained and blue epoxy impregnated. Porosity (NCS): 14.2%. Permeability (Klinkenberg): 11.8 mD. XRD: 20.3% clay (4.1% illite+mica, 14.3% chlorite, 1.9% kaolinite), 0.2% carbonate (dolomite), and 79.4% other minerals (79.1% quartz and trace amounts of pyrite). Sample contains microcrystalline quartz (Q, 50%) crinoid fragments (CR, 10%), brachiopod fragments (5%), bivalves (BV, 15%), bryozoans (BY, 10%) and undifferentiated skeletal debris. Moldic (MO), vuggy (VU) and interparticle (IP) porosity observed. **D)** White light core photo from Core #1 (5216.4'). Scale is in centimeters. Terra rosa (TR) is another common feature indicative of exposure. **E)** White light core photo from Core #3 (5325.4') with clasts (CL). Scale is in centimeters.

Interpretation – Exposure Interval

Exposure surfaces are surfaces of sediment or rock that show the effects of being exposed to subaerial conditions at the earth's surface, such as karst features or an interruption in sedimentation (Scholle et al., 1983). Exposure intervals are solely diagenetic features and are not directly related to depositional environments. Most exposure surfaces represent a hiatus in the depositional record and the temporal duration of the exposure intervals was not determined in this study. The abundance of clay, terra rosa and solution pipes in this interval are probably related to subaerial exposure. The high porosity and permeability values in this interval are likely enhanced due to dissolution related to the subaerial exposure.

Summary of Interpretations

Oklahoma Facies 1, the laminated dolomitized mudstone, is interpreted as a distal mid-ramp environment due to the fine grained nature of the sediments, mud content and lack of sedimentary features that would indicate a more proximal environment of deposition for a mudstone such as a tidal flat. XRD patterns in Core #1 showed that the dolomite is slightly calcian 55.5 mol% CaCO₃ and enriched in Ca²⁺ (Ewald, in progress 2016), which suggests the dolomite was precipitated in marine seawater (Dehcheshmehi et al., 2015).

Oklahoma Facies 2 is a wackestone to packstone facies with millimeter-sized horizontal burrows interpreted as being deposited in a low energy and/or restricted environment below FWFB. Oklahoma Facies 3 is a moderate to highly (3 to 6 bioturbation index from Bann et al., 2008) bioturbated packstone characterized by burrows ranging from

localized millimeter-sized horizontal burrows to centimeter-sized vertical burrows. This facies is interpreted to have been deposited in a moderate to low energy depositional environment where more normal marine conditions below FWWB exist.

Oklahoma Facies 4 is a skeletal packstone to grainstone with normal marine fauna and minor bioturbation. The lack of bioturbation and the presence of a higher diversity of normal marine fauna in Oklahoma Facies 4 favors an interpretation of a high to moderate energy depositional environment within FWWB.

Kansas Facies 1, a skeletal packstone to wackestone, and Kansas Facies 2, a bryozoan grainstone to packstone, exhibit graded bedding and localized laminar bedding that is characteristic of a mid-ramp environment with moderate energy between SWB and FWWB. Kansas Facies 3, crinoidal grainstone to packstone A, and Kansas Facies 4, crinoidal grainstone to packstone B, are interpreted as a high to moderate energy depositional environment at FWWB, most likely in constantly agitated conditions and proximal to skeletal shoals.

The presence of these facies types in all three cores indicates deposition on a carbonate ramp, ranging from the distal mid-ramp to outer ramp to the higher energy, more proximal mid-ramp to ramp crest between SWB and FWWB (Figure 23).

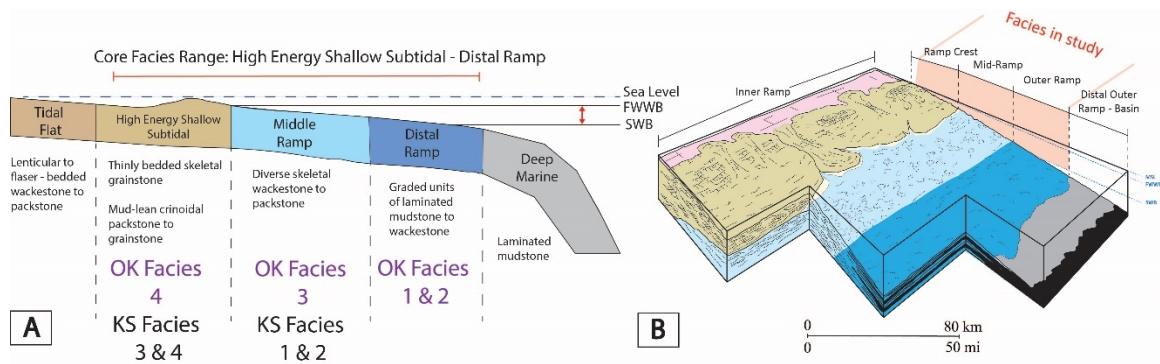


Figure 23: **A)** Cross section diagram of a distally-steepened carbonate ramp. Facies range from mudstones to higher energy skeletal grainstones between FWFB and SWB. Modified from Kaufman and Jameson (2002). **B)** Schematic diagram of a distally steepened carbonate ramp with the main environmental subdivisions and distribution of facies. Modified from Handford (1986).

SEQUENCE STRATIGRAPHIC FRAMEWORK/ INTERPRETATION

Recent sequence stratigraphic based subsurface work to the east of the Nemaha Uplift in Logan and Payne counties (LeBlanc, 2015; see Figure 4 for location) revealed four regionally correlative sequences of probable 3rd order in duration, ranging in thickness from 25ft (7.5m) to 115ft (35m) that correlated to the gamma-ray wireline log curve (Figure 24). The sequences were determined using an idealized shallowing-upward stacking pattern of five facies, similar to the facies identified in this study (Figure 24). The facies in LeBlanc's (2015) study had greater siliciclastic input unrelated to diagenesis compared to the facies in this study. Glauconitic sandstone was present in the Logan and Payne County subsurface cores that was absent in this study. LeBlanc (2015) showed that the sequences thinned in the eastward direction and likely control the distribution of reservoir quality units. Higher frequency cyclicity (possible 4th order) was also identified (thicknesses average about 10ft/3m) but were problematic for regional correlation due to lack of biostratigraphic control, spacing of cores and uncertainty about the controlling mechanisms responsible for the higher frequency deposition (i.e. allocyclic versus autocyclic processes).

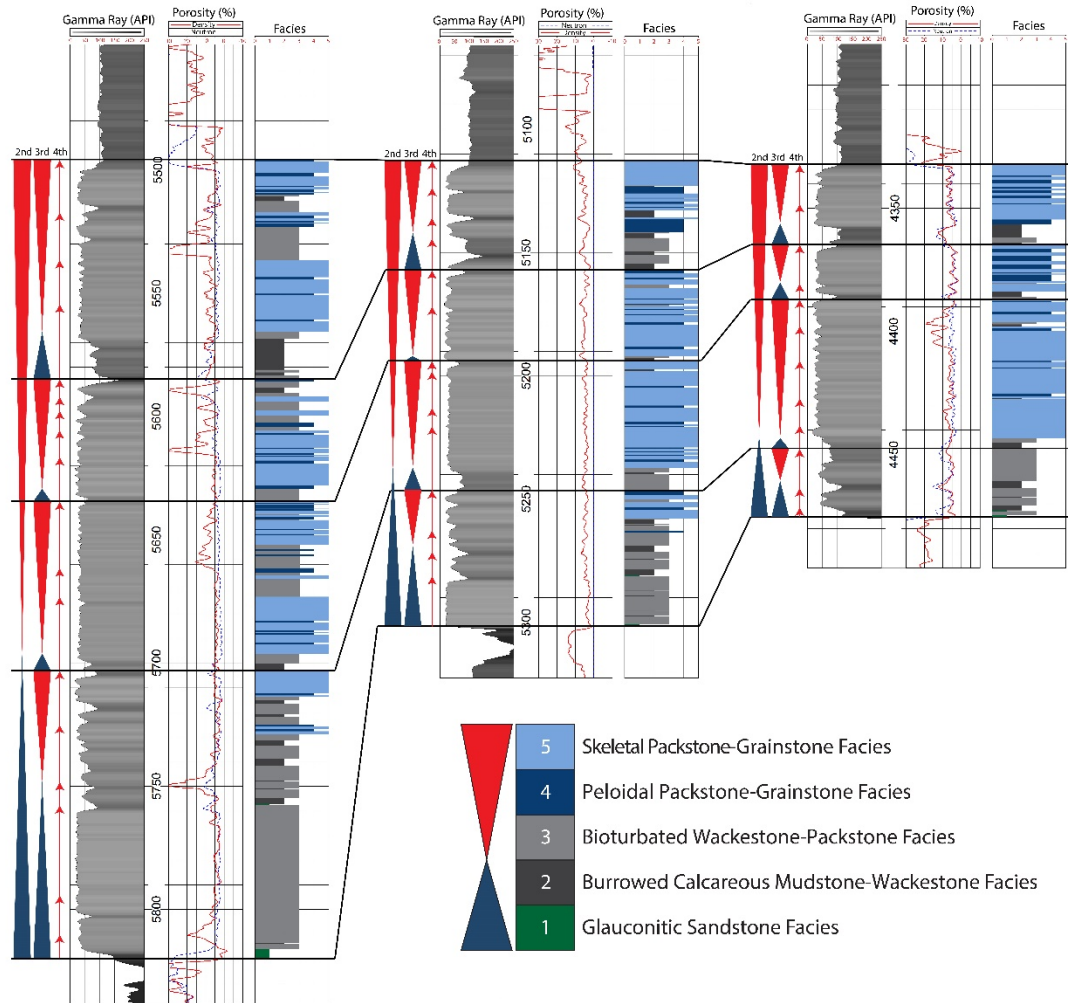


Figure 24: Sequence stratigraphic framework with depositional facies, gamma-ray, neutron and density porosity wireline logs established from LeBlanc (2015) in Logan and Payne counties, Oklahoma. 3rd order sequences correlate to the gamma-ray signature, with the base of the sequences (transgressive phase) corresponding to an increase in total gamma-ray API value. The idealized shallowing upwards succession of the five depositional facies identified for the Mississippian subsurface section in Logan and Payne counties, Oklahoma is shown next to blue and red triangles. The blue triangle represents the transgressive phase of the system and the red triangle represents the regressive phase of the system. The facies from LeBlanc (2015) have greater siliciclastic input compared to the facies in this study. Modified from LeBlanc (2015).

Another recent study utilizing sequence stratigraphy to the southwest of the Nemaha Uplift in Kingfisher County (Flinton, 2016; see Figure 4 for location) also identified four probable 3rd order sequences ranging from 10 to 225 ft. (3-69m) that had a strong correlation to the gamma-ray and resistivity wireline log curves (Figure 25). The sequences

were determined using an idealized shallowing-upward stacking pattern of six facies that also resemble the facies identified in this study (Figure 26). The transgressive facies in Kingfisher County had glauconite present, which differs from the facies identified in this study. The shallowing upward succession of facies (mudstones progressing into skeletal grainstones) are similar to the facies identified in this study. Flinton (2016) indicates that the guard resistivity curve proved to be a more consistent correlation tool for the high-frequency cycles (4th order), but the gamma-ray signature confined the probable 2nd and 3rd order scales of cyclicity. Subsurface cross sections of 3rd order sequences display an overall progradation in the depositional dip direction to the southeast (Figure 27; Flinton, 2016).

NW

SE

Droke Unit #1

< 2.69 mi >
(4.33 km)

Moore Unit #D1

< 1.02 mi >
(1.64 km)

Effie B York Unit #1

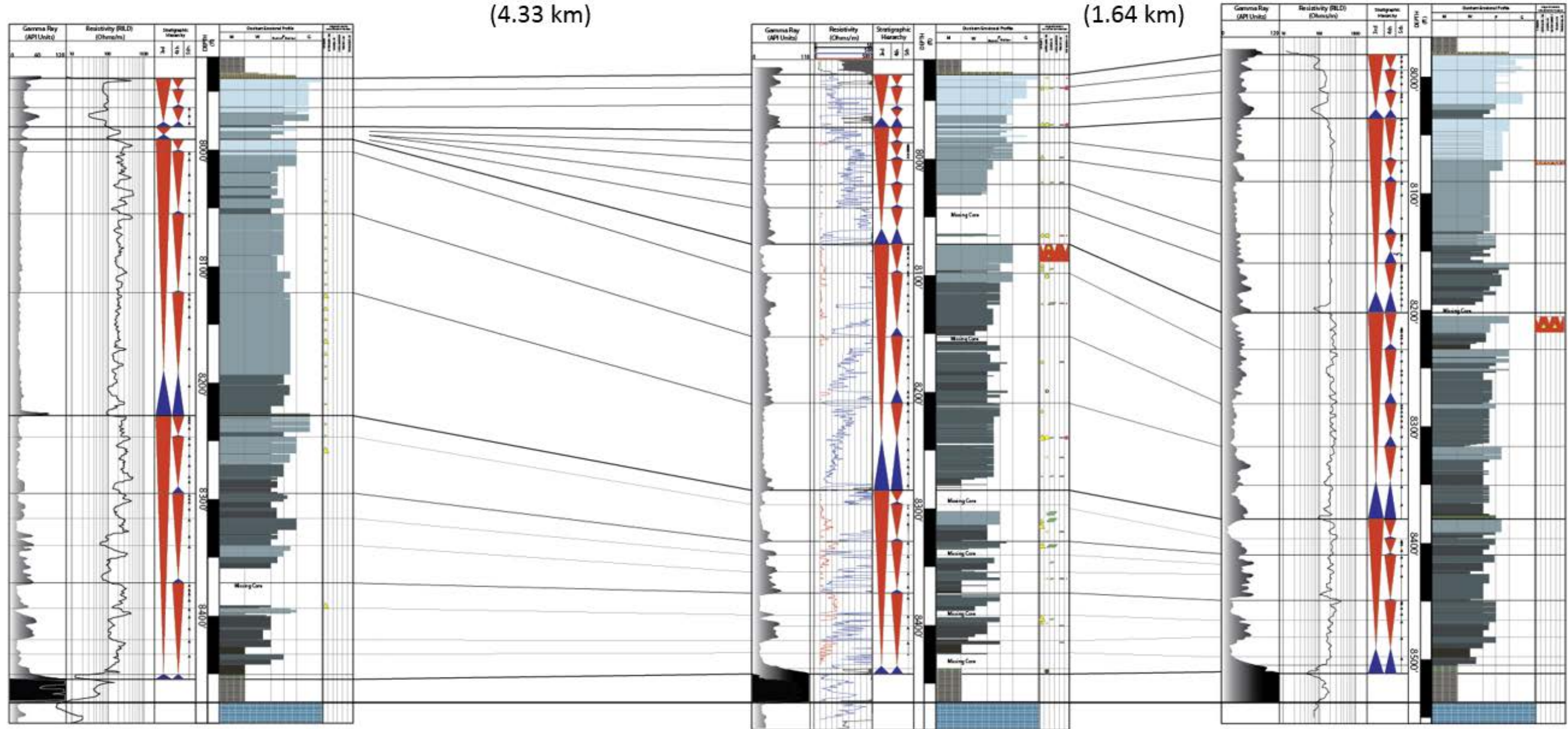


Figure 25: Sequence stratigraphic framework with gamma-ray curve, resistivity curve (guard resistivity curve for the More Unit #D1), sequence stratigraphic hierarchy, Dunham classification and core features of the Mississippian subsurface section in Kingfisher County, Oklahoma (Flinton, 2016). The 3rd order sequence boundaries (bold black lines) correlated to the gamma-ray and guard resistivity increases at the base of each sequence. The 4th order high-frequency cycle boundaries correlated strongly to the guard resistivity curve (thin black lines). From Flinton (2016), used with permission.

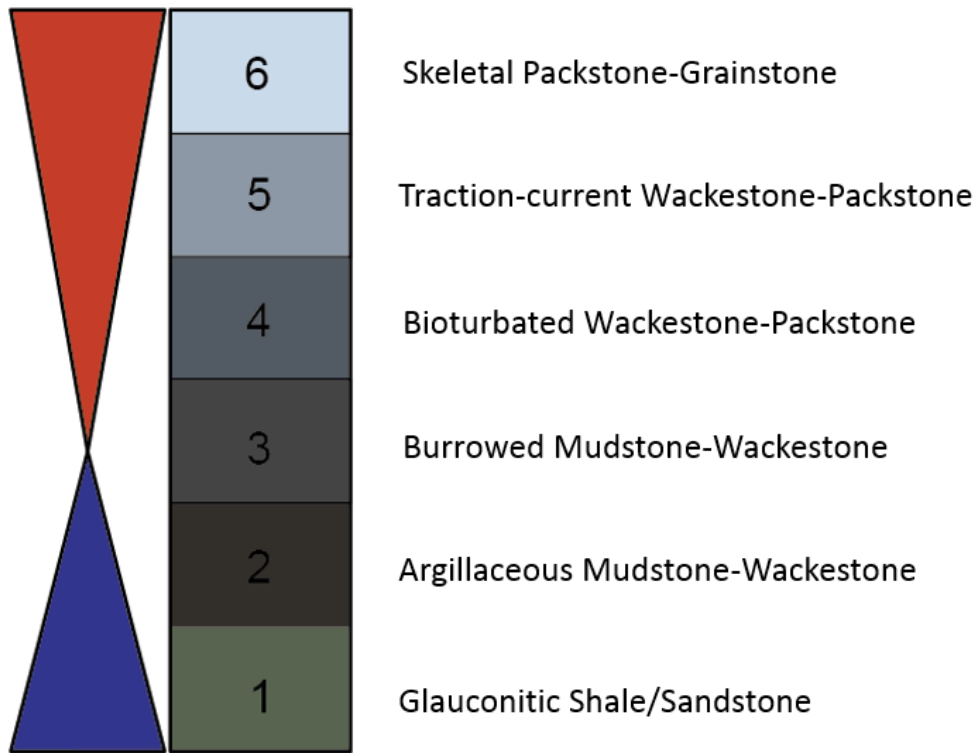


Figure 26: Idealized shallowing upwards succession of the six depositional facies identified for the Mississippian subsurface section in Kingfisher County, Oklahoma. The blue triangle represents the transgressive phase of the system and the red triangle represents the regressive phase of the system. Glauconite is present in the transgressive facies in Flinton (2016), which differs from the facies identified in this study. The shallowing upward succession of facies (mudstones progressing into skeletal grainstones) are similar to the facies identified in this study. From Flinton (2016), used with permission.

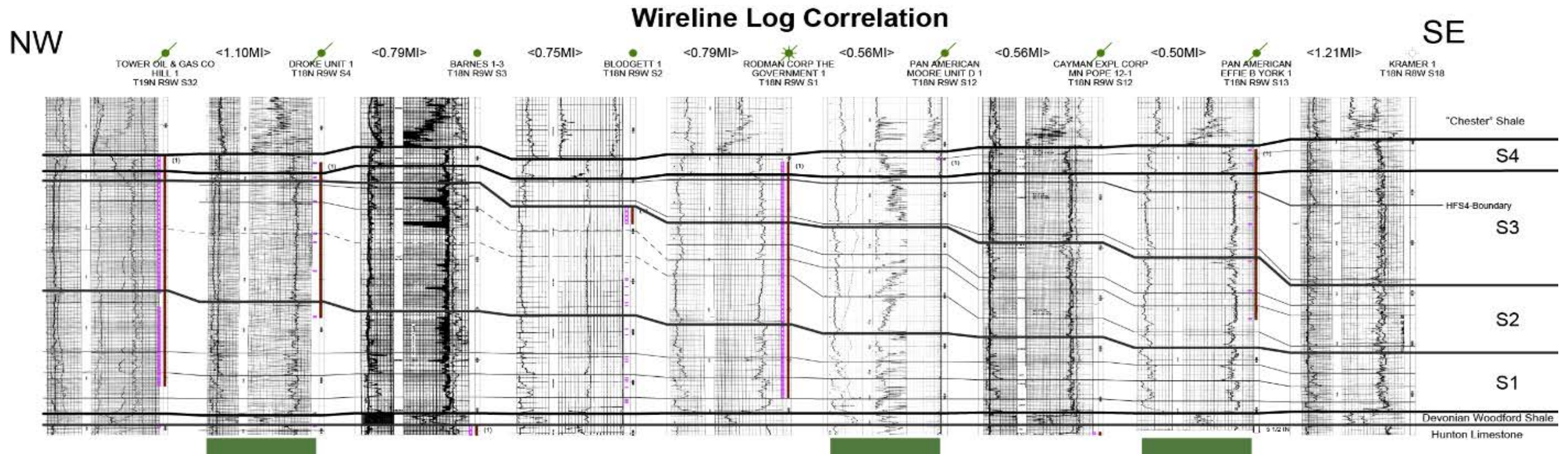


Figure 27: Wireline log correlation of Mississippian subsurface section in Kingfisher County, Oklahoma, perpendicular to depositional strike. Cored wells utilized in the study (Flinton, 2016) are marked by green boxes. Four 3rd order sequences (S1 – S4) were identified (represented by thick black lines), with higher-frequency 4th order cycles shown with thinner black lines. Sequences were correlated in the subsurface using the gamma-ray and resistivity curves. Overall, the 3rd order sequences prograde towards the basin (SE) in a clinoform geometry. S1 and S2 thicken landwards (NW) and S3 and S4 thicken basinward (SE). From Flinton (2016), used with permission.

IDEALIZED FACIES SUCCESSION: OKLAHOMA AND KANSAS

The sequence stratigraphic framework for the Mississippian section in north-central Oklahoma and south central Kansas was constructed using an idealized vertical stacking pattern of facies identified from the Bann 1-14 (Core #1), Albus 1-34H (Core #2) and Trophy Farms 32-34-16 1H (Core #3) subsurface cores as described in the previous section. The idealized stacking patterns of the facies represent an overall shallowing- or shoaling-upwards package within a transgressive and regressive phase of a single fluctuation in relative sea level (Figure 28). The idealized vertical stacking patterns were utilized to identify cycles and sequences present in the cores and delineate a hierarchy of these cycles and sequences. Once these cycles and sequences were vertically constrained for Core #1 and #2, their boundaries were correlated laterally. Core #3 did not correlate directly to Core #1 and #2 due to the proximal expression of facies present (implying a more proximal depositional environment on the distally steepened ramp) and the distance from Core #2 (17mi/27.6km). Flooding surfaces in all three cores were characterized by an abrupt change from shallow water to deeper water deposits, as identified by the vertical facies succession. The abrupt facies change was interpreted as a deepening of the depositional environment related to sea level rise.

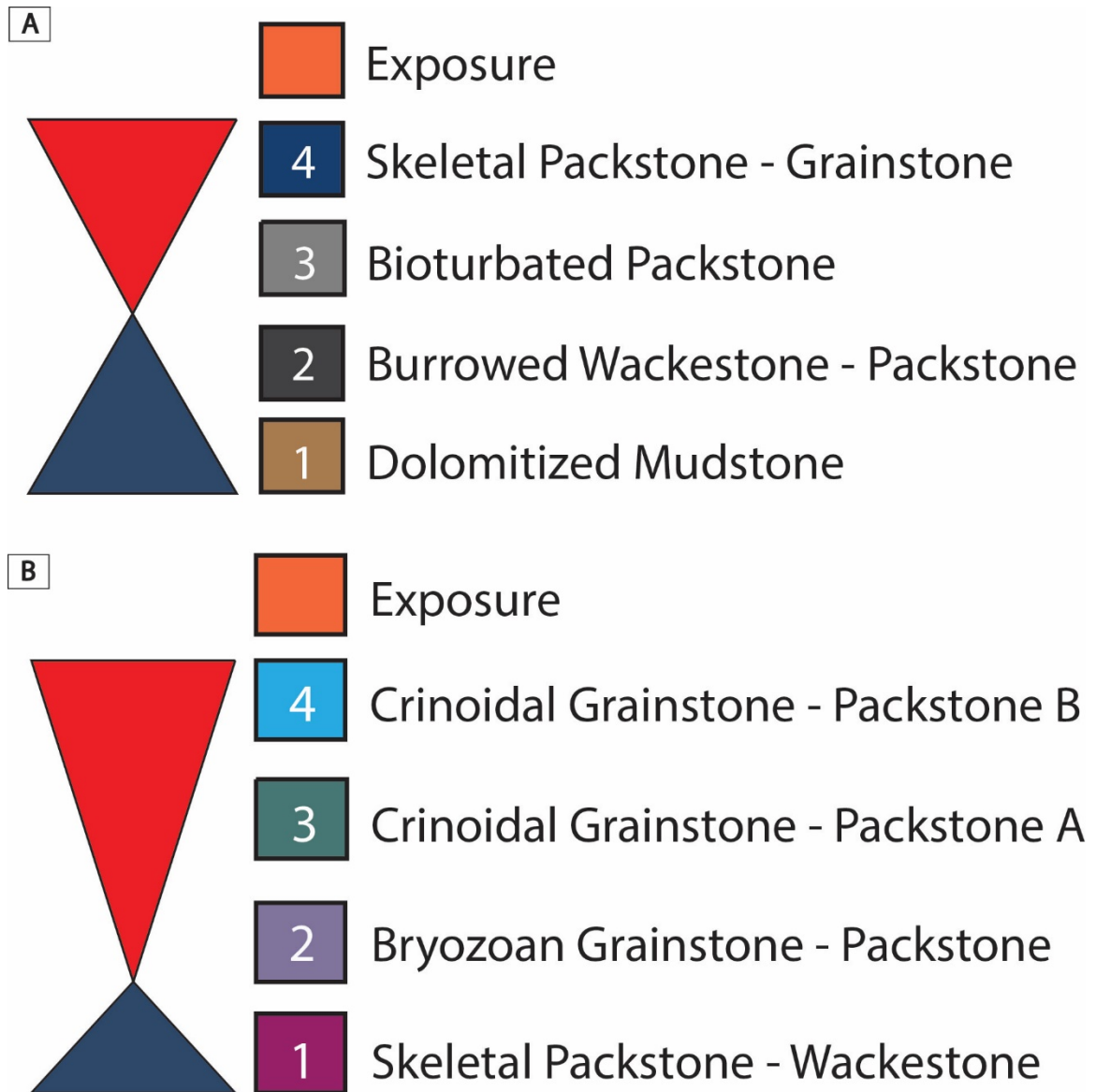


Figure 28: Idealized shoaling-upward facies succession established for the Mississippian section for Core #1 and Core #2 (A) and Core #3 (B). The blue triangle represents the transgressive phase of the system and the red triangle represents the regressive phase of the system. Deviations to the idealized stacking pattern could be due to autogenic processes.

SEQUENCE STRATIGRAPHIC HIERARCHY

The three cores analyzed in this study display a three-fold sequence stratigraphic hierarchy similar to that defined in other recent studies (LeBlanc, 2015 and Flinton, 2016).

It is important to note that the temporal resolution of the cores utilized in this study is unknown and the characterization of 3rd, 4th and 5th order cyclicity in this study is meant to

convey the observation of the three-fold hierarchy, without any specific time interval associated with each sequence and cycle. Conodont biostratigraphy has a maximum temporal resolution of approximately one million years (Boardman et al., 2013), which would aid in constraining the 3rd order sequences but cannot provide definition for the higher order 4th and 5th sequences and cycles.

“THIRD” ORDER SEQUENCES

Four probable 3rd order sequences (S1 – S4, Figure 20A&B) were identified in all three cores. In the Oklahoma cores, Bann 1-14 (Core #1) and Albus 1-34H (Core #2), 3rd order sequences ranged from 11.2ft (3.4m) to 41.8ft (12.8m) in thickness, with overall thicker sequences to the southeast (basinward), towards Core #1 (Figure 29A). In the Kansas core, Trophy Farms 32-34-16 1H (Core #3), 3rd order sequences ranged from 30ft (9.1m) to 73ft (22.3m) in thickness, with S4 being the thickest (Figure 29B). Overall, the 3rd order sequences are thicker in the Kansas core (compared to the Oklahoma cores), which is a more proximal position relative to the basin. Refer to Appendix A for details. For all three cores, the sequences are bounded by transgressive facies (Oklahoma Facies 1 and 2, Kansas Facies 1) at the base and progress into regressive facies (Oklahoma Facies 3 and 4, Kansas Facies 2, 3 and 4) at the top. S4 in all three cores is bounded at the top by an extensive subaerial exposure horizon possibly related to the Pennsylvanian/Mississippian unconformity.

“FOURTH” ORDER HIGH- FREQUENCY SEQUENCES

Within the four probable 3rd order sequences, three to five 4th order high-frequency sequences (HFS) were identified for Core #1 and #2. Two to eight HFS within the four probable 3rd order sequences were identified for Core #3 (Figures 29 A&B). There were

only two discernable HFS in S4 in Core #3 (due to exposure overprint) which may explain the HFS number variation within one core. The HFS thicknesses ranged from 3ft (0.9m) to 20ft (6.1m) in all three cores. Refer to Appendix A for details. The identification of the HFS is important because they are among the smaller scale (meter scale) genetic units that make up the fundamental reservoir units (Eberli and Grammer, 2010) and likely control the distribution of the petroleum reservoir units.

HIGHER-FREQUENCY CYCLES

Higher-frequency cycles characterized by very thin packages, generally less than 1ft (0.3m) thick, were also identified in these cores. These cyclic packages are consisted of facies repetition consistent with portions of the overall facies stacking pattern. These cycles are interpreted as autocyclic tempestites because the cores were deposited in a depositional environment that was heavily influenced by storms, where FWWB fluctuations may have caused abrupt variations in the facies stacking pattern, resulting in the deposition of thin packages unrelated to sea level change. Since storms occur locally and have variable preservation in the sedimentary record, correlation of these units in these cores are probably not related to the distribution of reservoir flow units. These highest frequency cycles are not shown because of this regionally discontinuous and autocyclic nature.

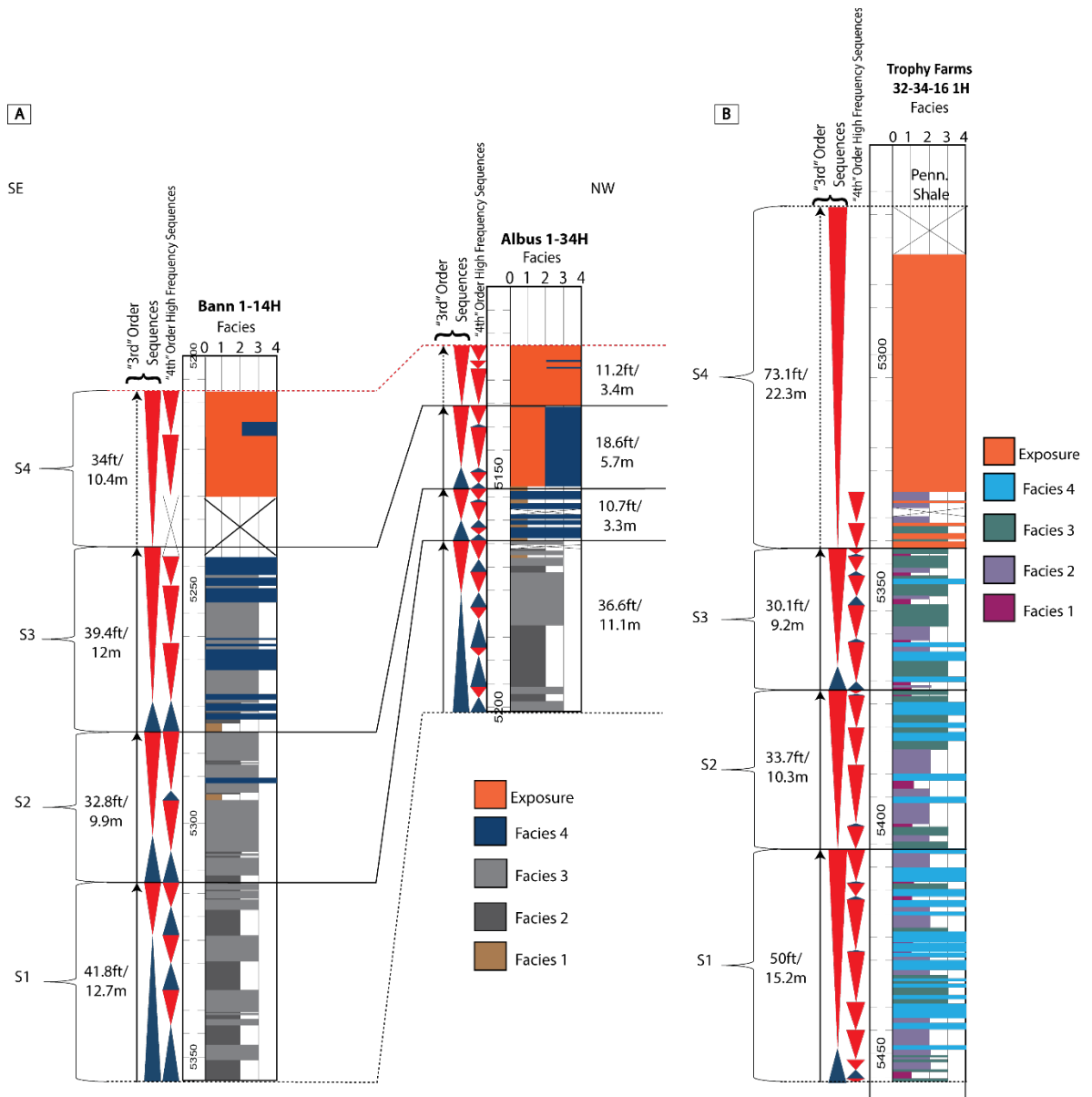


Figure 29: **A**) Southeast to northwest cross section of Core #1 and #2 with 3rd and 4th order sequences and depositional facies identified in core. The entire cored sections represent an overall shallowing-upward succession, probably of 2nd order duration. This cross section demonstrates the thickness variabilities of the sequences observed, with thicker 3rd order sequences (S1 – S4) and 4th order HFS to the southeast (basinward). S4 is represented by a dashed line to convey the probable confidence in the identified sequences, since this interval is dominated by exposure. Black (X's) represent missing intervals in the core. Each 3rd order sequence contains three to five 4th order high-frequency sequences (HFS) that were not regionally correlative. Higher frequency cyclicity related to storm deposition is not shown due to the regionally discontinuous and autocyclic nature of these cycles. **B**) Sequence stratigraphic hierarchy of Core #3 with 3rd and 4th order sequences and depositional facies identified in core. The entire cored section represented an overall shallowing-upward succession, possibly 2nd order in duration. This figure demonstrates the thickness variabilities of the 3rd order sequences observed, labeled S1 – S4, with thickest 3rd order (S4) towards the top of the core. Overall, the 3rd order sequences in a more proximal

position are thicker than those observed in the Oklahoma cores (A). Each 3rd order sequence contains two to eight 4th order HFS. Black (X's) represent missing intervals in the core. The majority of S4 is an exposure interval (represented by a dashed line) and 4th order HFS for the entire sequence could not be readily identified in the core. Higher frequency cyclicity is not shown due to the regionally discontinuous and autocyclic nature of these cycles.

WIRELIN LOG CORRELATION

In order to correlate and map sequences across the study area, multiple data sets were integrated regionally. The established facies and sequences from the cores were tied to wireline logs to identify correlative trends in order to aid in the subsurface mapping of the sequences. The 3rd order sequence boundaries were “ground truthed” to the cores and were chosen based on the presence of transgressive facies overlying a succession of regressive facies present in the cores.

GAMMA – RAY

Borehole measured gamma-ray logs were analyzed to facilitate the subsurface correlation of the identified sequences. For all three cores, 3rd order sequence boundaries correlated to an increase in the gamma-ray signature (greater than 18 API units). The greater API values corresponded with the transgressive phase of the 3rd order sequences and the signature decreased as the sequence progressed into the regressive phase (Figure 30A&B). There was a variable correlation to the 4th order HFS. The thin (less than 1ft/0.3m) 5th order HFC were below the resolution of the tool for an accurate reading and did not correlate.

Not all increases in gamma-ray corresponded with a 3rd order sequence boundary, as seen in S1 for Core #1 and Core #2 (Figure 30A). These subtle increases in the gamma-ray in S1 reflected the relatively transgressive facies and correlated strongly with the 4th

order HFS boundaries. S1 in Core #1 and #2 had the best correlation at the HFS scale and the HFS in the other sequences were not correlative.

DENSITY AND NEUTRON POROSITY

Density and neutron porosity logs were analyzed in this study to identify any porosity trends for reservoir considerations. The density logs were acquired using a limestone matrix value of 2.71g/cc. The Mid-Continent Mississippian is considered a mixed carbonate siliciclastic system and the density porosity values may be an overestimate of the true porosity for Core #1 and #2 in the areas where quartz accounts for over 40% of the facies (refer to Table 2A for values; Asquith and Krygowski, 2004).

Overall, the density porosity plots in S1, S2 and S3 range from 0 – 10% in Core #1 and #2 and 0 – 5% in Core #3. Density porosity for S4 in all three cores plots higher, ranging from 15 – 30% in the Oklahoma cores (Core #1 and #2) and 20 – 30% in the Kansas core (Core #3). The neutron porosity in S1, S2 and S3 generally plots between 5 – 25% in Core #1 and #2 and 0 – 5% in Core #3. Neutron porosity values for S4 in all three cores also plot higher, ranging 25 – 30% in Core #1 and #2 and 15 – 30% in Core #3. The high porosity values in S4 are most likely erroneous due to the rubbled and irregular nature of the exposure horizon that would provide poor contact for the pads of the tool in the borehole to gather accurate readings.

Generally, the porosity values tend to increase at the top of the 3rd order sequence boundaries in the regressive phase for all three cores. There was not the same consistent correlation trend for the 3rd order sequence boundaries observed using the density and neutron porosity logs as seen with the gamma-ray signature (Figure 30A&B).

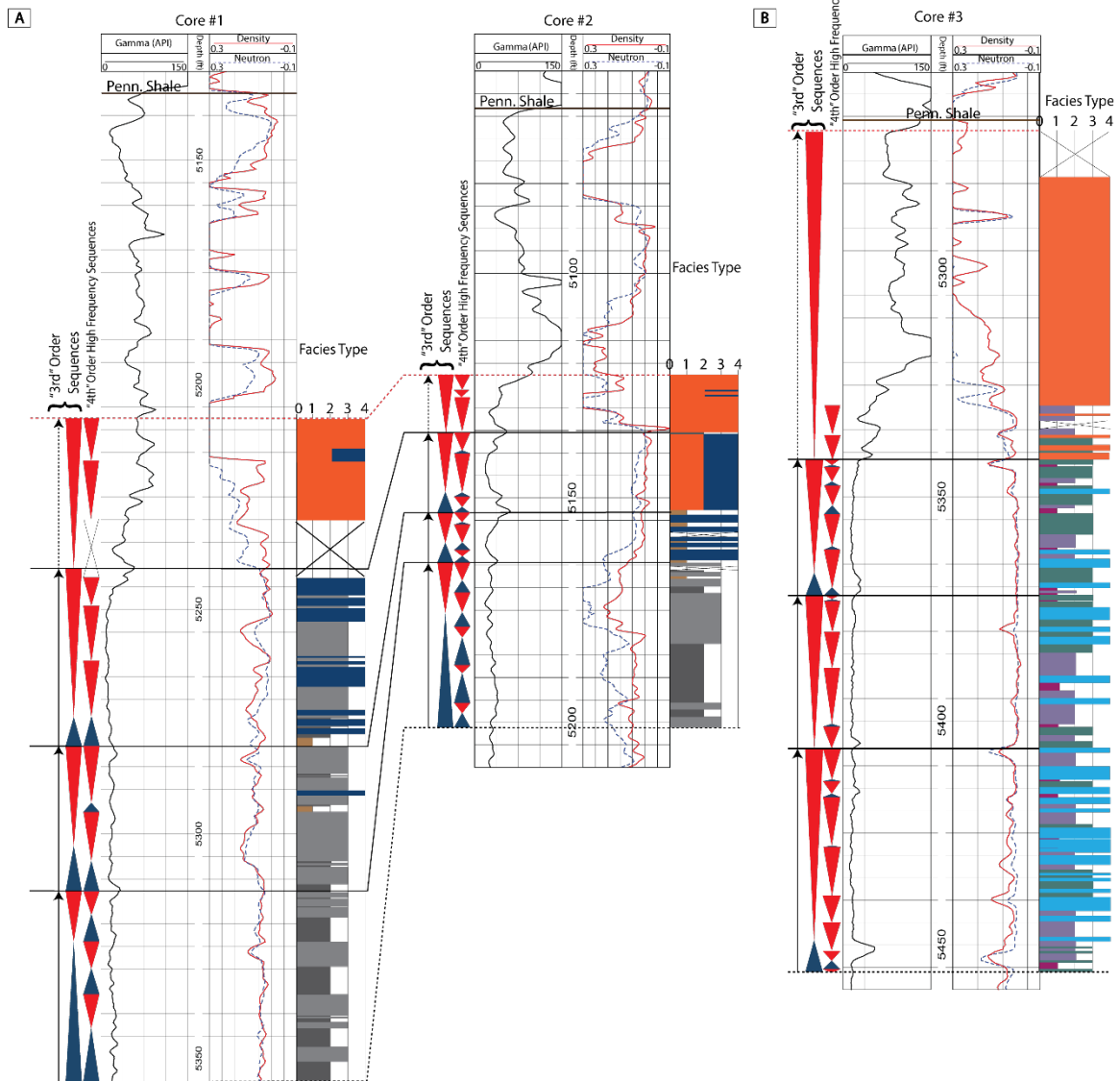


Figure 30: **A)** Southeast to northwest cross section of Core #1 and #2 with 3rd and 4th order sequences identified in core correlated to the gamma-ray and density (red solid line) and neutron (blue dashed line) porosity curves, along with depositional facies. Refer to Figure 20A for depositional facies and sequence label key. The 3rd order sequence boundaries correlate with an increase (>18 API) in the gamma-ray signature which represent the transgressive phase of the sequence. 4th order HFS have the strongest correlation to increases in the gamma-ray signature in the transgressive phases of S1. Generally, the density and neutron porosity increases towards the top of the regressive phase of the 3rd order sequences, with higher values in S4 (density ranging 5 – 10% in S1 – S3, 15 – >30% in S4, neutron ranging 5 – 20% in S1 – S3, 20 – >30% in S4). **B)** Sequence stratigraphic hierarchy of Core #3 with 3rd and 4th order sequences identified in core correlated to the gamma-ray and density (red solid line) and neutron (blue dashed line) porosity curves, along with depositional facies. Refer to Figure 20B for depositional facies and sequence

label key. The 3rd order sequence boundaries correlate with an increase (>18 API) in the gamma-ray signature, which represent the transgressive phase of the sequence. The 4th order HFS did not correlate consistently to increases in the gamma-ray signatures. Generally, the density and neutron porosity increases towards the top of the regressive phase of the 3rd order sequences, with higher values in S4 (density ranging 5 – 15% in S1 – S3, 10 – > 30% in S4, neutron ranging 5 – 15% in S1 – S3, 8 – >30% in S4).

RESISTIVITY

The resistivity curves for all three cores were analyzed primarily to evaluate their effectiveness as an additional correlation tool for the 3rd and 4th order sequence boundaries based on the successful results from Flinton (2016). Generally, the resistivity within the 3rd order sequences was relatively higher (100 – 1000 ohm-m) in the grainstones and packstones compared to the wackestones and mudstones (10 – 50 ohm-m) for all three cores. Other than these general increases, the increases in the resistivity curve did not show any consistent correlation to the 4th order HFS boundaries. There was not the consistent increase in resistivity among the 3rd order sequences (S1 – S4), unlike the results from Flinton (2016). This could also be due to Flinton (2016) utilizing a guard resistivity curve, which has a vertical resolution of 3-6in (8-16cm) that can detect flooding surfaces/sequence boundaries that can be this thin. For the Oklahoma cores, Core #1 showed a strong correlation in resistivity increases for S1 and S3 and weakened in S2 and S4. Core #2 showed a strong correlation for S2 and S3 that was not present in S1 and S4. For the Kansas core, Core #3, there was also a strong correlation for S1 and S3, however the correlation weakened in S2 and S4 (Figure 31A&B).

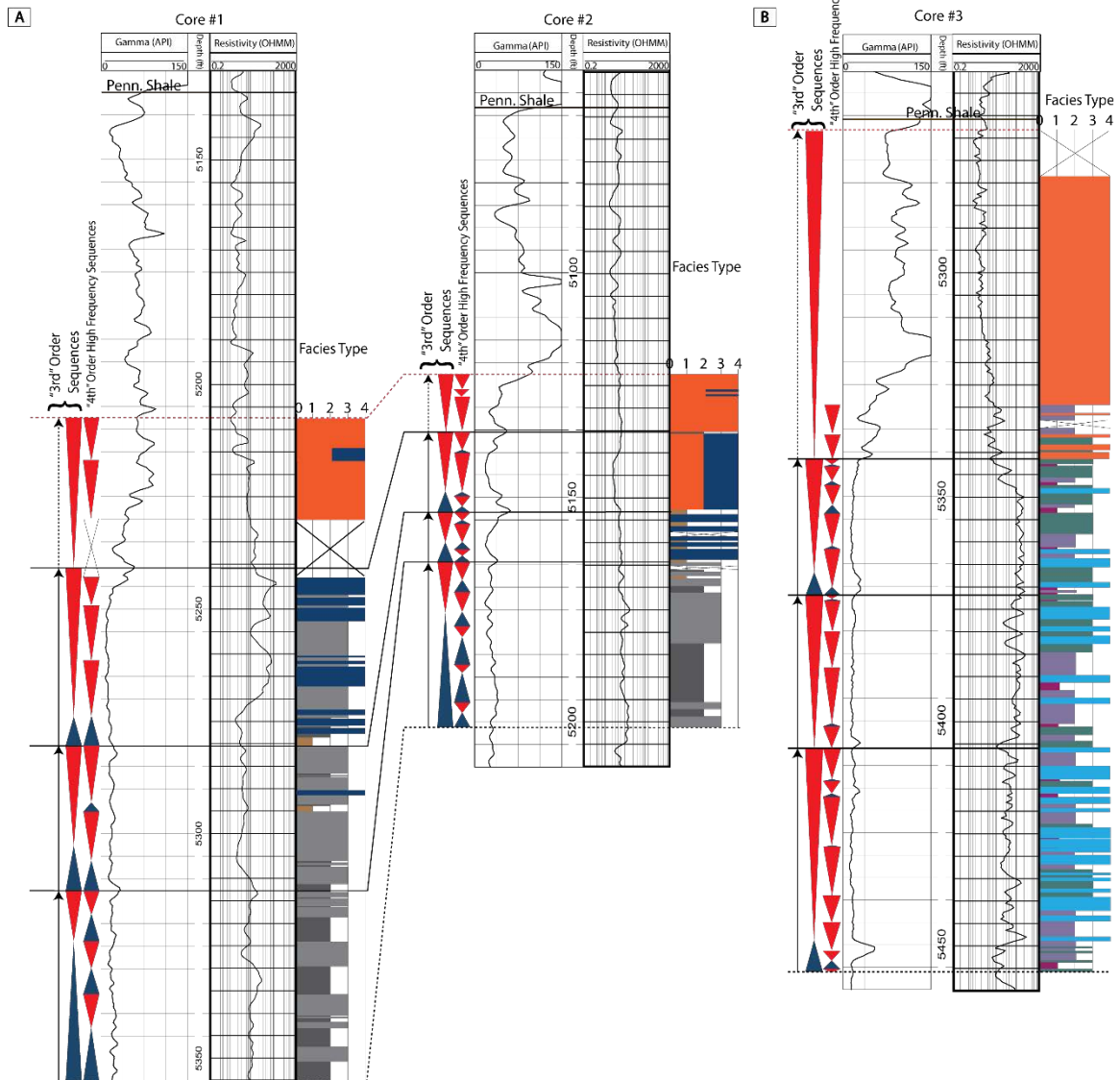


Figure 31: **A)** Southeast to northwest cross section of Core #1 and #2 with 3rd and 4th order sequences identified in core, correlated to the gamma-ray and deep resistivity curve and depositional facies. Refer to Figure 20A for depositional facies and sequence label key. The 3rd order sequences correlate with an increase in resistivity in S1 and S3 for Core #1 and S2 and S3 for Core #2. A majority of the increases in resistivity correspond with the grainstone and packstone facies but did not consistently correlate to the 4th order HFS boundaries. An increase in deep resistivity curve response was not consistent among the 3rd order sequence boundaries (weak correlation with S2 and S4 for Core #1, S1 and S4 Core #2). **B)** Sequence stratigraphic hierarchy for Core #3, 3rd and 4th order sequences identified in core correlated to the gamma-ray and deep resistivity curve and depositional facies. Refer to Figure 20B for depositional facies and sequence label key. The 3rd order sequence boundaries correlate with an increase in resistivity in S1 and S3. A majority of the increases in resistivity also correspond with the grainstone and packstone facies but did not consistently correlate with the 4th order HFS boundaries. There was a weak correlation of an increase in the resistivity curve in S2 and S4 3rd order sequence boundaries.

CHAPTER III

DISCUSSION

RESULTS/SEQUENCE STRATIGRAPHIC ARCHITECTURE AND REGIONAL CORRELATION

Three subsurface cross sections (Figure 32) in Comanche, Barber (Kansas), Woods and Harper (Oklahoma) counties were constructed using the gamma-ray and resistivity wireline log curves tied to the sequence stratigraphic framework established from Cores #1, #2 and #3. As explained previously, the neutron and density porosity logs were not as effective for correlation between sequences compared to the gamma-ray curve.

The sequence stratigraphic framework from each core was superimposed on the corresponding wireline logs for each core, highlighting the correlation between the 3rd order sequence boundaries and an increase in the gamma-ray signature (represented by solid green lines in the subsurface cross sections). Applying the “ground truthed” correlation to the increases in gamma-ray API units from the sequence stratigraphic framework, sequences were picked in shoaling- or shallowing-upwards packages throughout the Mississippian section (from the top of the Devonian Woodford to the base of the Pennsylvanian/ Mississippian unconformity) on the wireline log for each core.

After identifying sequences on the wireline logs with the core and increases in the gamma-ray signature, additional sequences were marked on the wireline logs within the study area. Once the gamma-ray increases were marked on the dip-oriented cross sections, down dip depositional (southwest direction) sequences were correlated. For strike-oriented cross sections, the sequences were correlated along regional depositional strike (northwest to southeast).

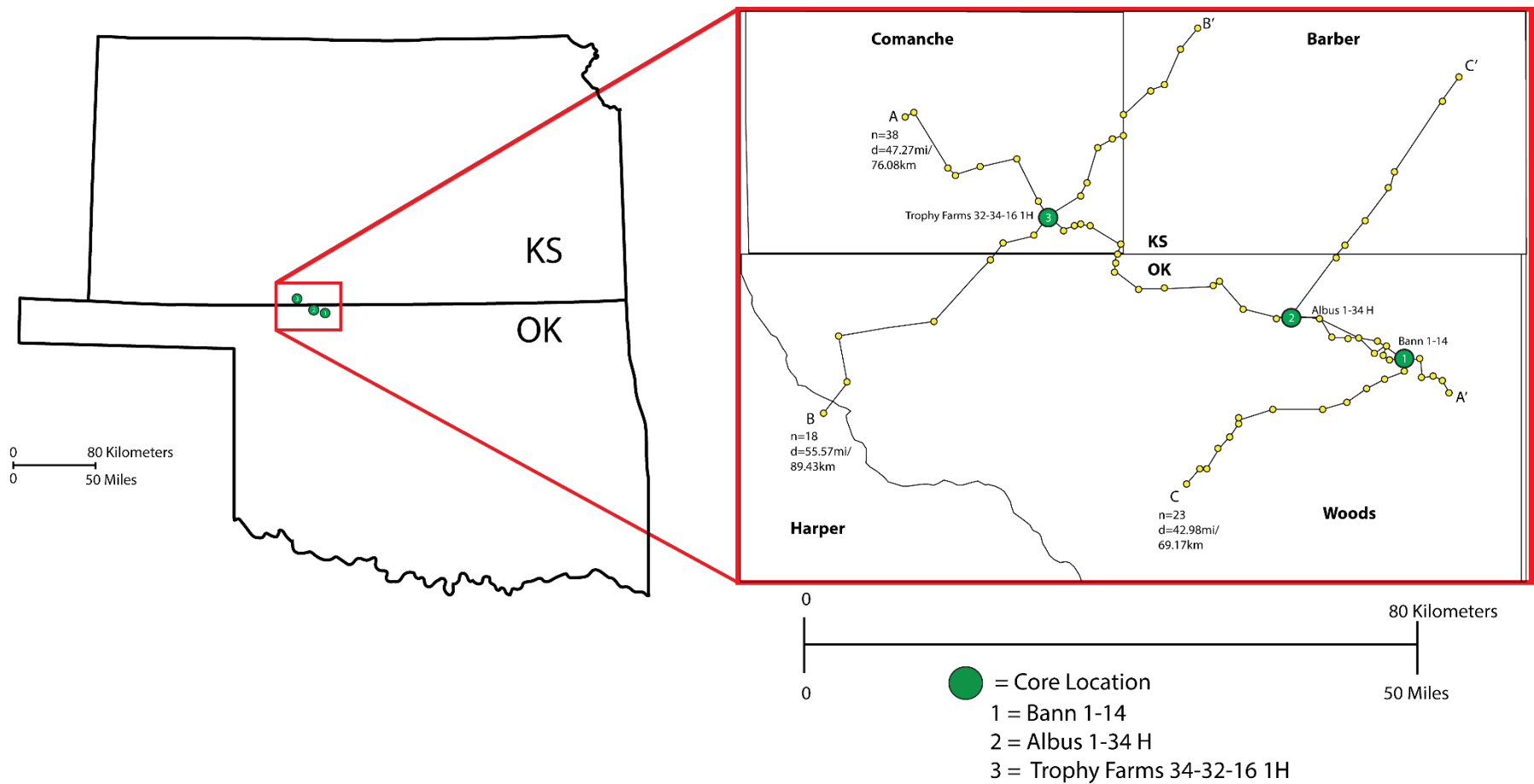


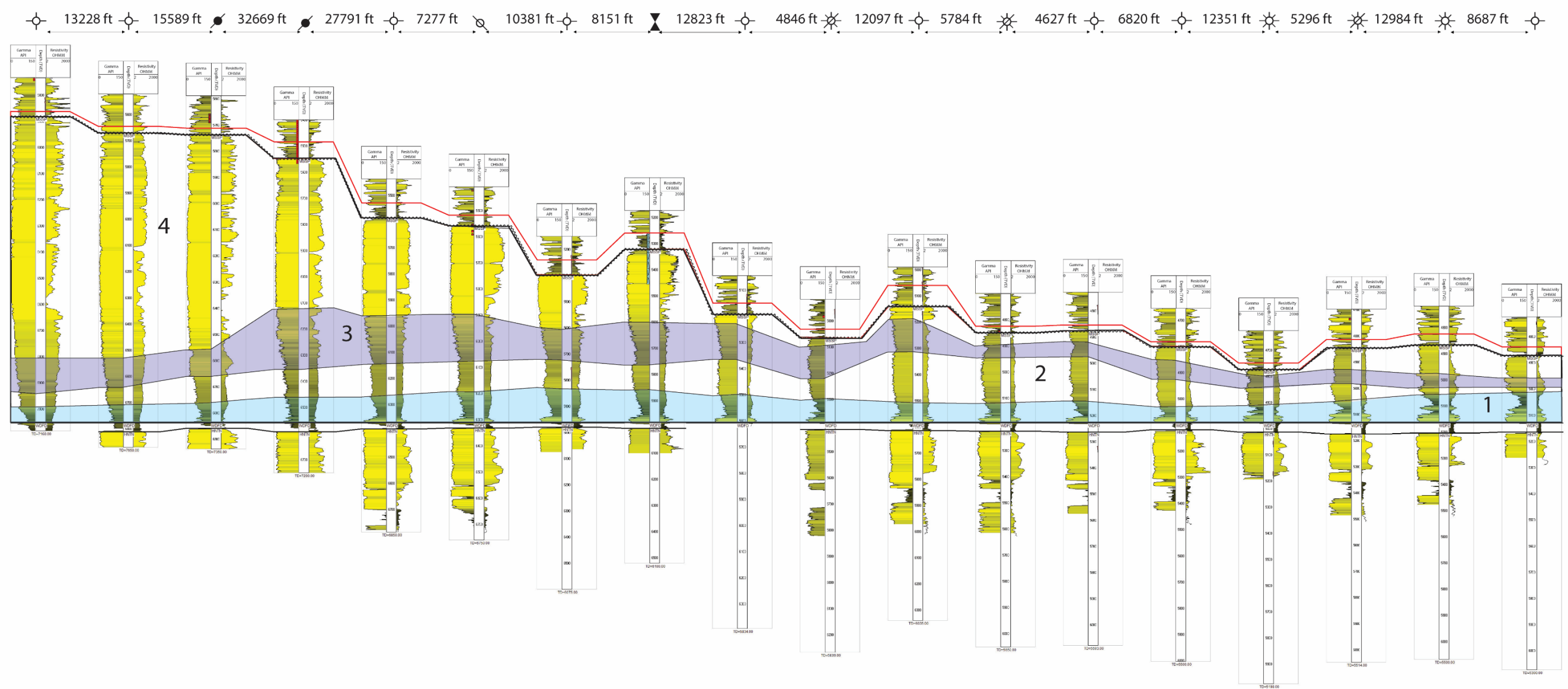
Figure 32: Location map of subsurface cross section lines (A to A', B to B', C to C') covering 146mi/235km within Oklahoma and Kansas, with core locations represented by green circles. A total of 79 wells with wireline logs were utilized to create the subsurface cross sections.

A sequence stratigraphic approach versus a lithostratigraphic approach (which is often diachronous in respect to facies) provides the ability to predict the vertical and lateral distribution of facies within a chronostratigraphically constrained sequence. Figure 33A&B is an example of how a lithostratigraphic correlation compared to a chronostratigraphic correlation can be misleading. Without a regard for time surfaces, a lithostratigraphic correlation (Figure 33A) of reservoir intervals interprets the units as laterally and vertically continuous and/or in communication. When time surfaces are considered (Figure 33B), these 'continuous' units have internal compartmentalization and potentially impermeable sequence boundaries that disrupt the continuity of the sequences.

SUBSURFACE CROSS SECTIONS

The three subsurface cross sections presented below utilize both equidistant as well as actual distance scaled sections. This comparison highlights the potential issues associated with looking at the geometries using the equidistant cross sections exclusively. For example, the apparent dip in the equidistant cross section might be vertically exaggerated up to 186 times. Considering structural dip values on a low declivity ramp typically range from one to three degrees, this is a crucial consideration when mapping these systems.

A



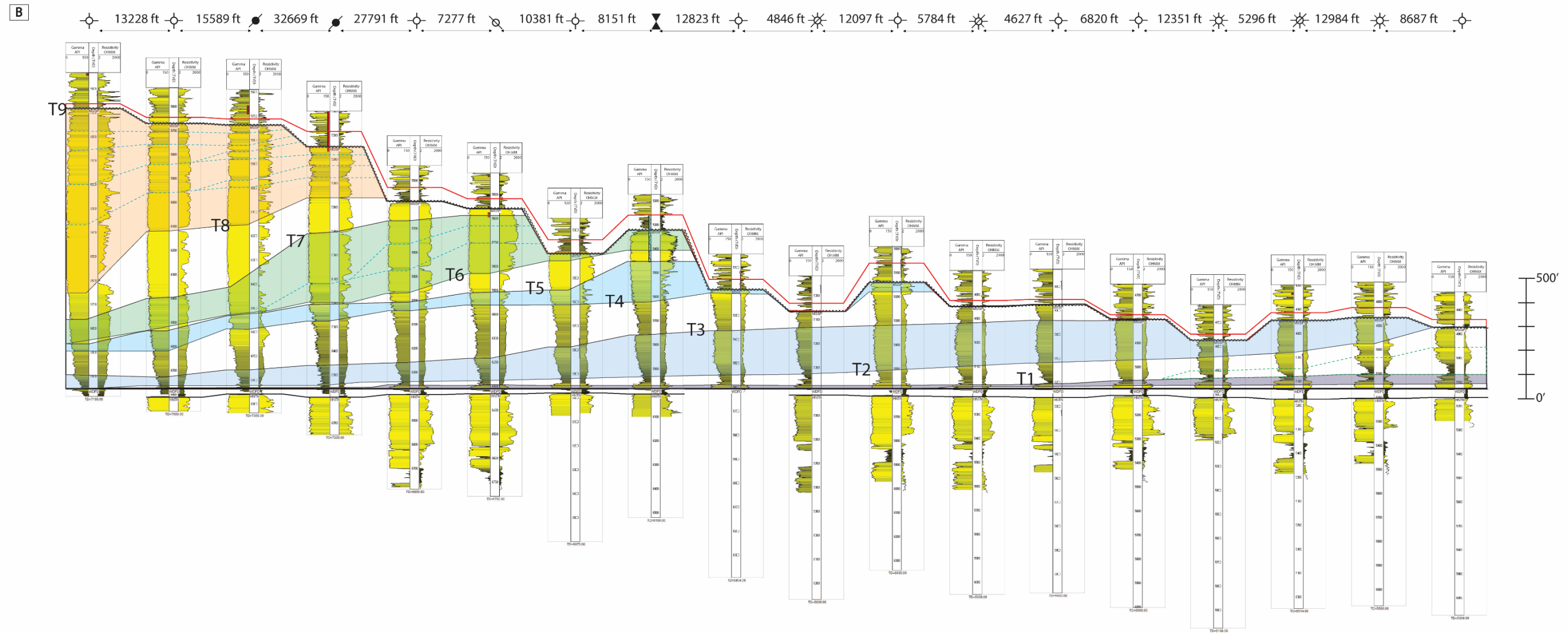


Figure 33: Lithostratigraphic interpretation (A) (sequences numbered 1 – 4) compared to a chronostratigraphic interpretation (B) (time surfaces labeled T1 – T9). Gamma-ray logs are on the left track (0 – 150 API) and resistivity logs (0.2 – 2000 ohm-m) are on the right track. The lithostratigraphic interpretation correlates similar gamma-ray signatures into continuous packages without a regard for the system geometry or chronostratigraphic surfaces. This correlation can be misleading because it can show potential reservoir units in communication or continuous (i.e. sequence 3 in (A)) when in actuality they maybe compartmentalized or baffled by an impermeable sequence boundary, as seen in (B) T4 – T7. Average V.E. = 186x.

Subsurface cross section A to A' (Figure 34A - D) represents a depositional strike-oriented (N-NW to S-SE) cross section, spanning 47.27mi (76.08km) with 38 wells. In this interpretation, there are 13 mapped sequences with four total potential sequences (possibly systems tracts or sequence boundaries) in sequence 5, sequence 3 and sequence 9. Carbonates deposit in a strike elongate pattern and the strike-oriented cross sections show more 'laterally' continuous sequences. In general, the sequences towards the southeast are thinner (less than 75ft/22.8m, near Core #1 (Bann 1-14) and #2 (Albus 1-34H)) and less aggradational than the sequences to the northwest (greater than 100ft/30.4m, near Core #3 (Trophy Farms 32-34-16 1H)) (Figure 34 A-D). Core #3 in the study area is interpreted as being in a relatively more proximal depositional environment compared to Core #1 and #2. This northwest section may represent the mid-ramp depositional environment where sequences are best preserved due to base level fluctuations not effectively drowning or exposing this depositional environment. Another possibility to explain these thicker sequences is there was locally more accommodation space. This local increase of accommodation space could be (morphology wise) a shoal complex that developed parallel to the shoreline, where aggradation occurred along the shoals and infilled in between the shoals. Additionally, tectonic events associated with the Nemaha and Central Kansas Uplifts (refer to Figure 4) could have created local accommodation space. Sedimentation rates could also account for thicker sequences to the northwest, which is the most likely scenario. Sedimentation rates in the more proximal area could have been greater than the relatively distal positions due to better water conditions being more favorable to carbonate productivity.

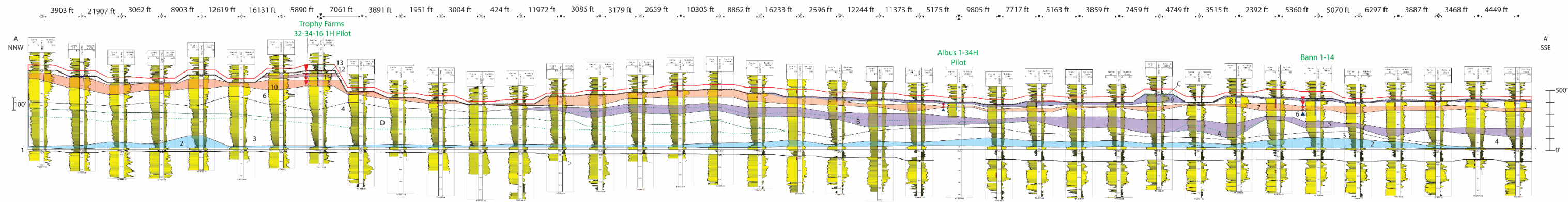


Figure 34A: Equidistant scaled subsurface cross section A to A' flattened on the Devonian Woodford. A to A' is a strike-oriented (N-NW to S-SE) cross section, spanning 47.27mi (76.08km) with 38 wells. Gamma-ray logs are on the left track (0 – 150 API) and resistivity logs (0.2 – 2000 ohm-m) are on the right track. The sequence stratigraphic framework for each core (Core #1 = Bann 1-14, Core #2 = Albus 1-34H, Core #3 = Trophy Farms 32-34-16 1H) is represented by the 3rd order sequence boundaries shown in solid green lines and the transgressive and regressive triangles. The Woodford (Devonian) and Mississippian thickness is represented by a solid black outline, with the interpreted Mississippian/Pennsylvanian unconformity thickness represented by a red outline. 13 sequences (labeled 1 -13, represented by solid black lines) are mapped in this interpretation, with four total potential sequences (labeled A-D, possibly systems tracts or sequence boundaries) represented by green dashed lines in sequence 5 (A&B), sequence 3 (D) and sequence 9 (C). The geometry of the sequences are elongate in the strike direction. In general, the sequences thin towards the southeast (less than 75ft/22.8m, near Core #1 and #2) and less aggradational than the sequences to the northwest (thicknesses greater than 100ft/30.4m, near Core #3) which could be due to local accommodation space, deposition in the mid-ramp environment or sedimentation rates. See text for discussion. Average V.E. 134x.

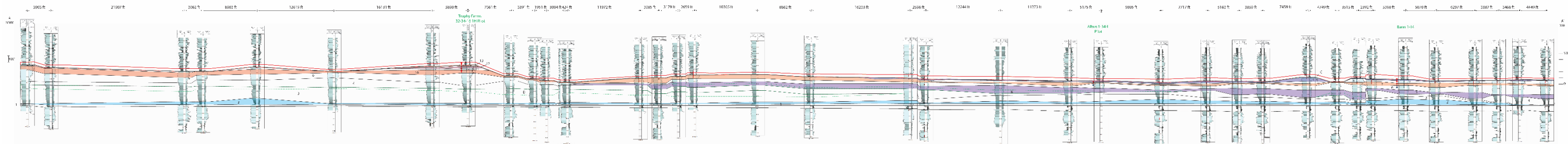


Figure 34B: Actual distance scaled subsurface cross section A to A'. Gamma-ray logs are on the left track (0 – 150 API) and resistivity logs (0.2 – 2000 ohm-m) are on the right track. Refer to Figure 34A for explanation. This version displays the more realistic distribution of the sequences. See text for discussion.

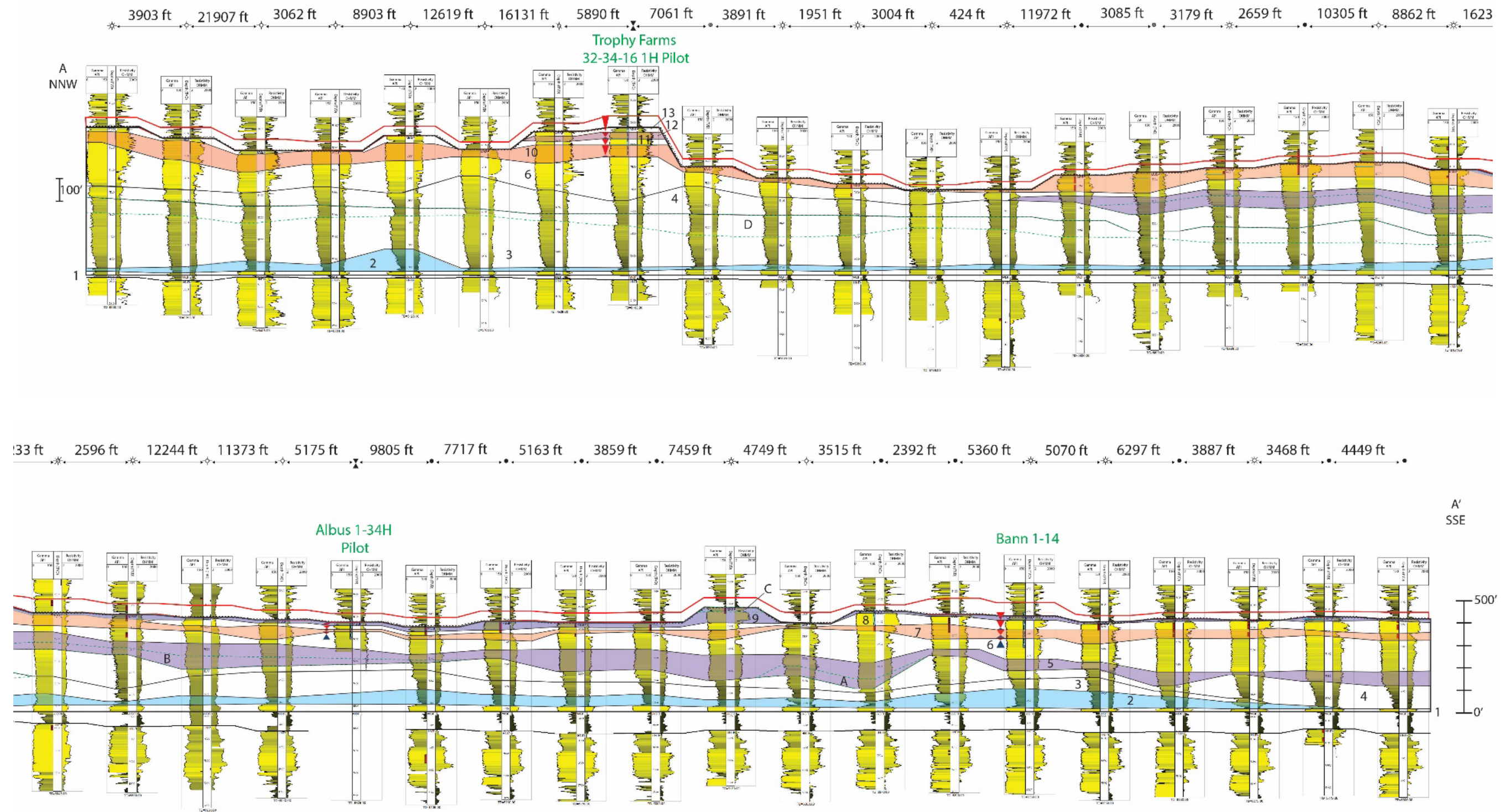


Figure 34C: Cropped version of equidistant scaled subsurface cross section A to A'. Refer to Figure 34A for explanation.

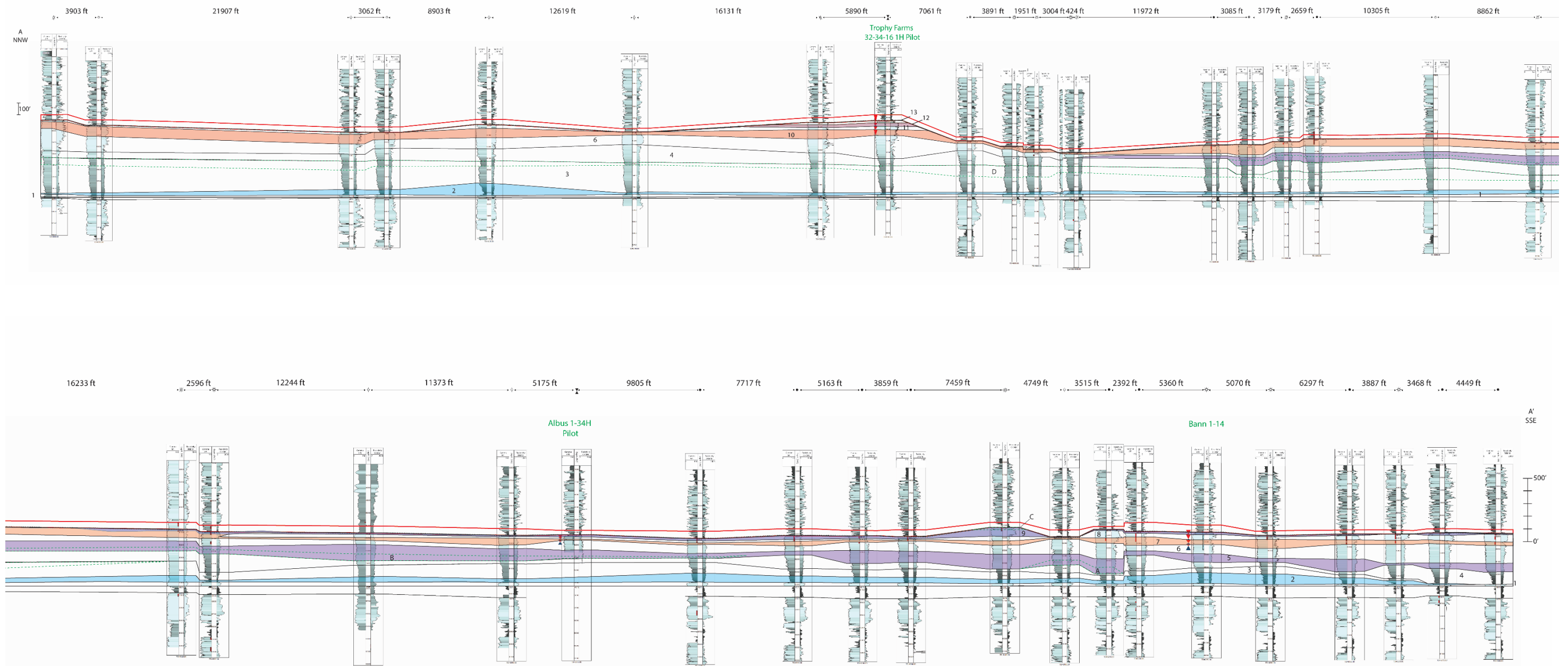


Figure 34D: Cropped actual distance scaled A to A' subsurface cross section. Refer to Figure 34A&B for explanation.

Subsurface cross section B to B' represents a dip-oriented (S-SW to N-NE) cross section, spanning 55.57 mi (89.43km) with 18 wells. Two alternative interpretations are presented for sequence stratigraphic correlations. B to B' was chosen for multiple correlations because Core #3 (Trophy Farms 32-34-16 1H) has the thickest cored Mississippian section (199.96ft of 710ft) of the three cores utilized in this study, and the dip direction orientation provides a better approximation for the geometry of the system.

Interpretation 1 (Figure 35A&B) displays five sequences with eight potential sequences within the fifth sequence. The potential sequences could either be systems tracts boundaries within a sequence (lowstand, transgressive and highstand system tracts) or sequence boundaries that would divide the sequence into other sequences. The distinction between which type of boundary they could be is uncertain since this dataset lacks chronostratigraphic constrains. The thickness of the sequences ranges from ~300ft (91.4m) to 50ft (15.2m). The sequences are progradational clinofolds dipping towards the basin, similar to the geometries described by Flinton (2016). Sequences 4, A and B (Figure 35A&B) are representations of how the sequence stratigraphic framework from Core #3 could be correlated to surrounding wells using the tie to the gamma-ray log. The interpreted base of the Pennsylvanian/Mississippian unconformity 1.5mi (2.4km) west of Core #3 is ~50ft (15.2m) deeper than Core #3, making the correlation of the sequences to the southwest equivocal and therefore represented by dashed lines. Sequences 1 and 4 maybe too laterally continuous for a dip-oriented cross section to be an accurate sequence stratigraphic correlation in this representation.

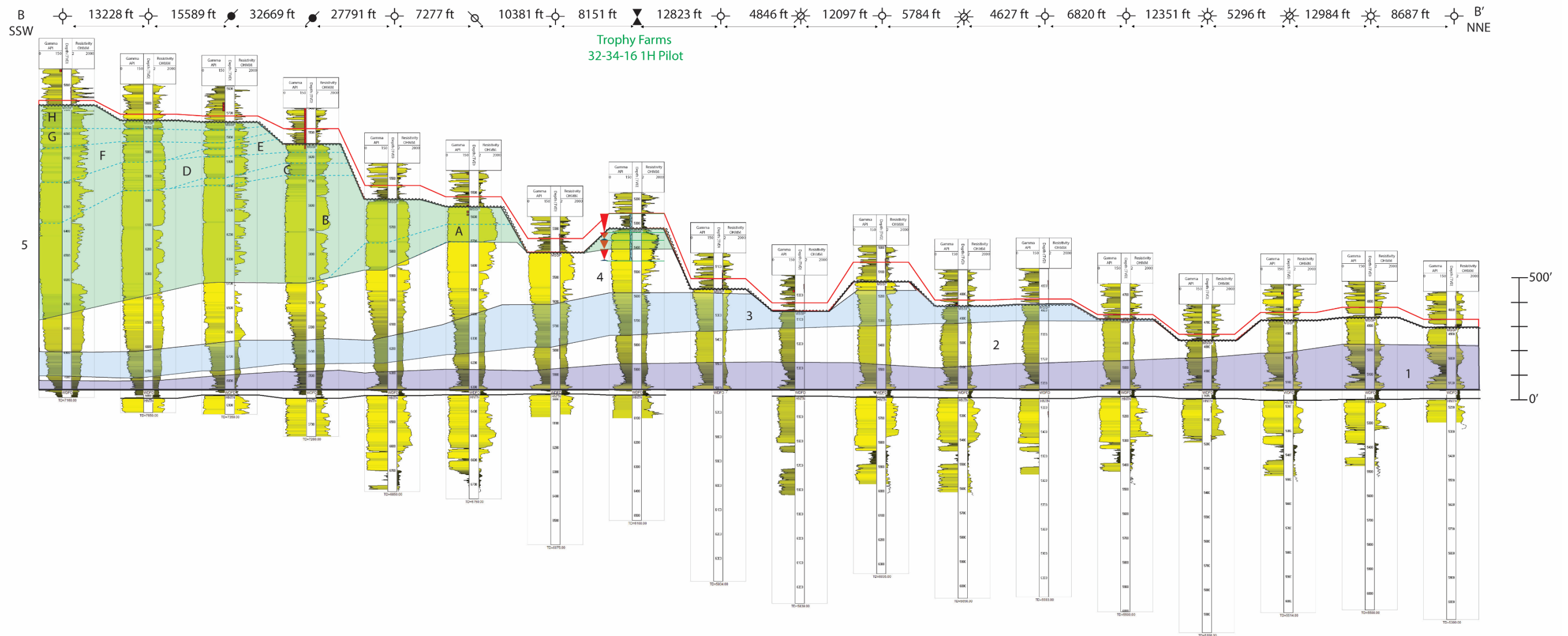


Figure 35A: Interpretation 1 of dip-oriented (S-SW to N-NE) subsurface cross section B to B' flattened on the Devonian Woodford, spanning 55.57 mi (89.43km) with 18 wells (equidistant spacing). Gamma-ray logs are on the left track (0 – 150 API) and resistivity logs (0.2 – 2000 ohm-m) are on the right track. The Woodford (Devonian) and Mississippian thickness is represented by a solid black outline, with the interpreted thickness of the Mississippian/Pennsylvanian unconformity represented by a red outline. The sequence stratigraphic framework for Core #3 is represented by the 3rd order sequence boundaries highlighted by solid green lines and the transgressive and regressive triangles. Five sequences were mapped (labeled 1-5, represented by solid lines) with eight potential sequences (possibly systems tracts or sequence boundaries) within the fifth sequence (5), represented by dashed lines (labeled A-H). Sequences 4, A and B (labeled S1 – S3 in Figure 29B) could be related to the 3rd order sequences identified in Core #3, however the unconformity cutting into Sequence 4 and 5 makes these correlations probable, therefore represented by dashed lines. The overall geometry of the sequences is a progradation towards the basin (SW). Sequences 1 and 4 maybe too laterally continuous for a sequence stratigraphic interpretation in this representation. Average V.E. = 186x.

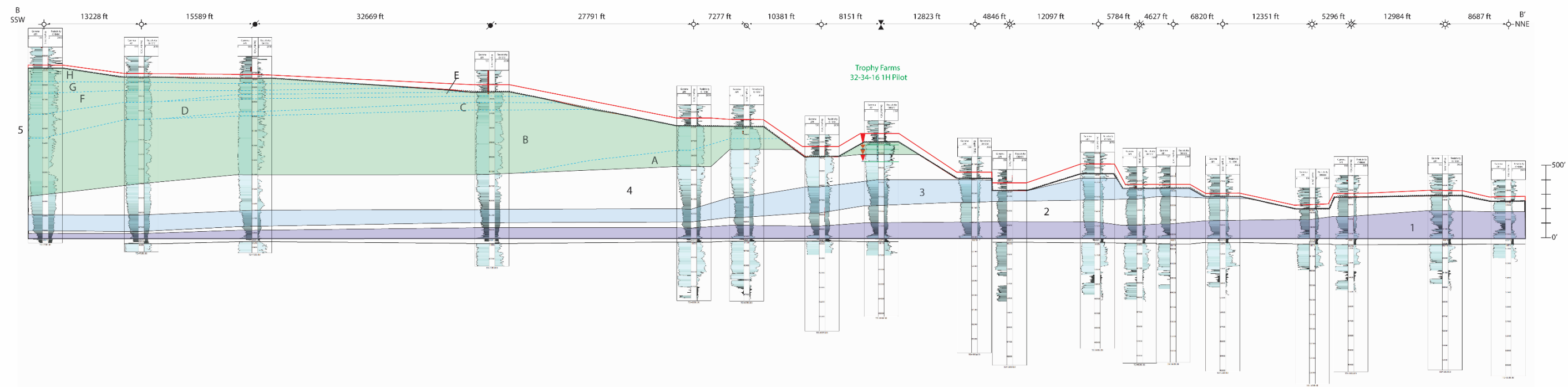


Figure 35B: Actual distance scaling of Interpretation 1 dip-oriented (S-SW to N-NE) subsurface cross section B to B', spanning 55.57 mi (89.43km) with 18 wells. Gamma-ray logs are on the left track (0 – 150 API) and resistivity logs (0.2 – 2000 ohm-m) are on the right track. Refer to Figure 35A for explanation. In this interpretation, prograding clinofoms are clearly defined and less vertically exaggerated.

Interpretation 2 (Figure 36A&B) displays 10 sequences compared to the five sequences in Interpretation 1. These 10 sequences (probable 3rd order) are represented by solid lines and 10 additional internal sequences (labeled A – J, possibly systems tracts or sequence boundaries) within sequences 3 (A), 8 (B&C) and 10 (D – J) are represented by dashed lines. Overall, the mapped sequences are thinner (25ft/7.6m to ~200ft/61m) in Interpretation 2 compared to Interpretation 1. Even though the sequences are thinner, the prograding clinoform geometry of these sequences towards the basin is still visible. Sequence 1, 2 and A in Interpretation 2 were combined into sequence 1 in Interpretation 1. Correlating these sequences in smaller, less continuous packages displays the potential for further vertical and lateral reservoir compartmentalization within a sequence. Interpretation 2 sequences 3, 4 and 5 were sequences 2 and 3 in Interpretation 1. Sequences 7, B, and C show another variation of using the sequence stratigraphic framework to correlate sequences away from the “ground truthed” log, with the dashed lines representing a probable correlation for the reasons mentioned previously in Interpretation 1.

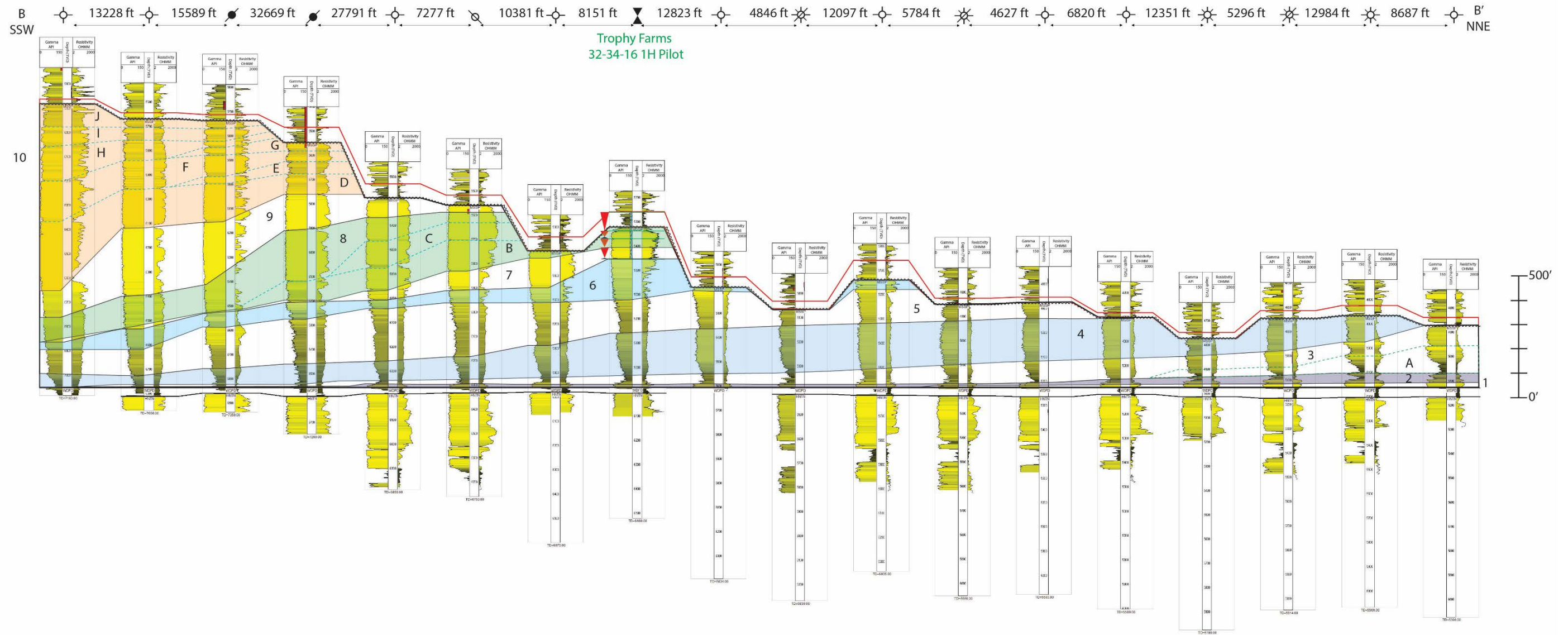


Figure 36A: Equidistant scaled version of Interpretation 2, the dip-oriented (S-SW to N-NE) subsurface cross section B to B'. Gamma-ray logs are on the left track (0 – 150 API) and resistivity logs (0.2 – 2000 ohm-m) are on the right track. The Woodford (Devonian) and Mississippian thickness is a solid black outline, with the interpreted Mississippian/Pennsylvanian unconformity thickness represented by a red outline. The sequence stratigraphic framework for Core #3 is represented by the 3rd order sequence boundaries highlighted by solid green lines and the transgressive and regressive triangles. 10 sequences were identified in this interpretation compared to the five sequences from Interpretation 1, offering an interpretation with further compartmentalization within the sequences. The 10 sequences are represented by solid lines (labeled 1-10) and 10 additional internal sequences (possibly systems tracts or sequence boundaries) represented by dashed lines (labeled A – J) within sequence 3 (A), 8 (B&C) and 10 (D – J). Overall, the sequences are thinner (25ft/7.6m to ~200ft/61m) in this interpretation compared to Interpretation 1. Sequences 7, B and C (labeled S1 – S3 in Figure 29B) could be related to the sequence stratigraphic framework established for Core #3. Average V.E. = 186x.

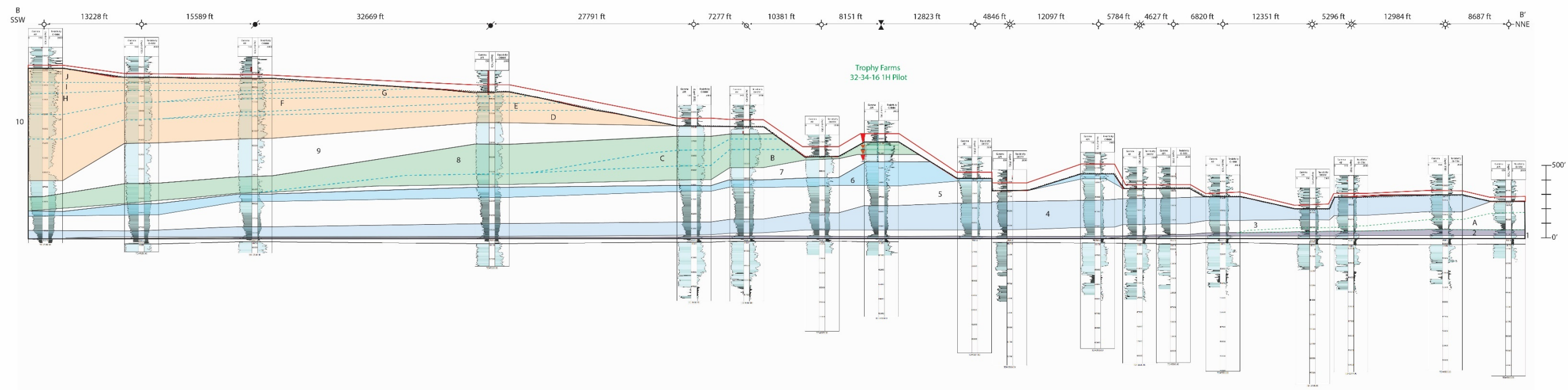


Figure 36B: Actual distance scaled version of Interpretation 2 dip-oriented (S-SW to N-NE) subsurface cross section B to B'. Gamma-ray logs are on the left track (0 – 150 API) and resistivity logs (0.2 – 2000 ohm-m) are on the right track. Refer to Figure 36A for explanation.

Subsurface cross section C to C' (Figure 37A-C) represents a dip-strike-dip oriented (S-SW to N-NE) cross section, covering 42.98mi (69.17km) with 23 wells. A total of 19 sequences were mapped in this interpretation, varying 50ft (15.2m) to 13ft (4m) thick, with seven potential internal sequences (possibly systems tracts or sequence boundaries) varying 50ft (15.2m) to 25ft (7.6m) thick. Since carbonate facies tracts are elongate in a strike direction, the dip orientation provides an approximation for the limits of the facies tracts within the depositional system, which provides valuable insight for reservoir distribution. Cross section C to C' exhibits these characteristics, with more elongate sequences in a strike direction and prograding clinoforms basinward in the dip direction (SW). The first three sequences (labeled 8, 9 and 10) for Core #1 and #2 correlate, although an unconformity cuts through the top sequence (11), making the correlation less probable.

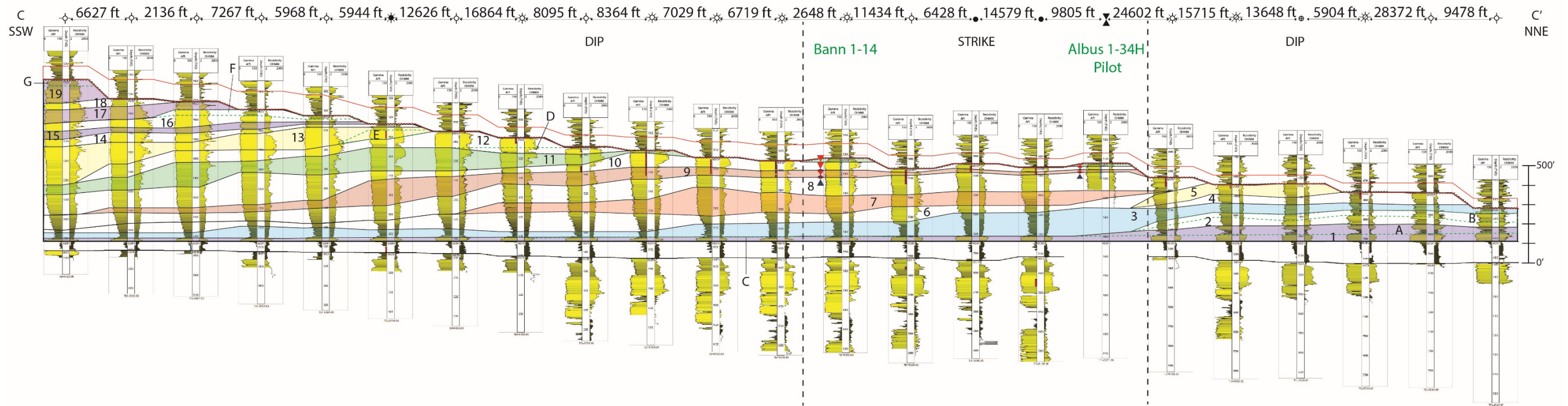


Figure 37A: Equidistant scaled subsurface cross section C to C' with gamma-ray (left track, 0-150 API) and resistivity (right track, 0.2 – 2000 ohm-m) in a dip-strike-dip orientation including Core #1 (Bann 1-14) and #2 (Albus 1-34H). The Woodford (Devonian) and Mississippian thickness is represented by a solid black outline, with the interpreted Mississippian/Pennsylvanian unconformity thickness represented by a red outline. The sequence stratigraphic framework for Core #1 and #2 is represented by the 3rd order sequence boundaries highlighted by solid lines and the transgressive and regressive triangles. 19 sequences (labeled 1-19) were mapped in this interpretation. Seven additional internal sequences are represented by dashed lines (labeled A-G). Dip-oriented sections (labeled DIP) exhibit a prograding clinoform geometry dipping basinwards (SW). The strike-oriented section (labeled STRIKE) sequences are more elongate. The strike-oriented section also shows correlation of sequences 8, 9 and 10 between Core #1 and #2 sequence stratigraphic framework (S1 – S3 in Figure 29A). The interpreted Mississippian/Pennsylvanian unconformity cuts through the top sequence (11; S4 in Figure 29A) making this correlation less probable. Average V.E. = 152x.

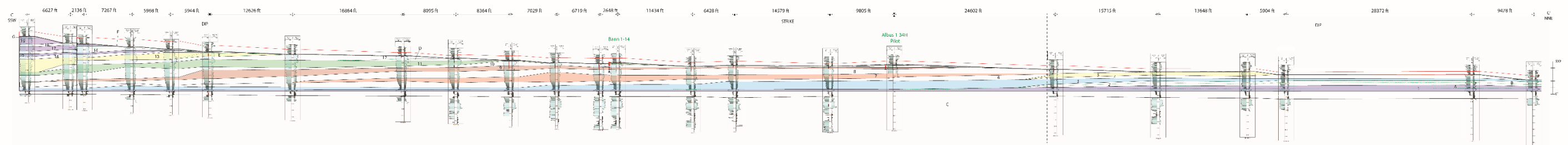


Figure 37B: Actual distance scaled version of subsurface cross section C to C'. Gamma-ray logs are on the left track (0 – 150 API) and resistivity logs (0.2 – 2000 ohm-m) are on the right track. Refer to Figure 37A for explanation.

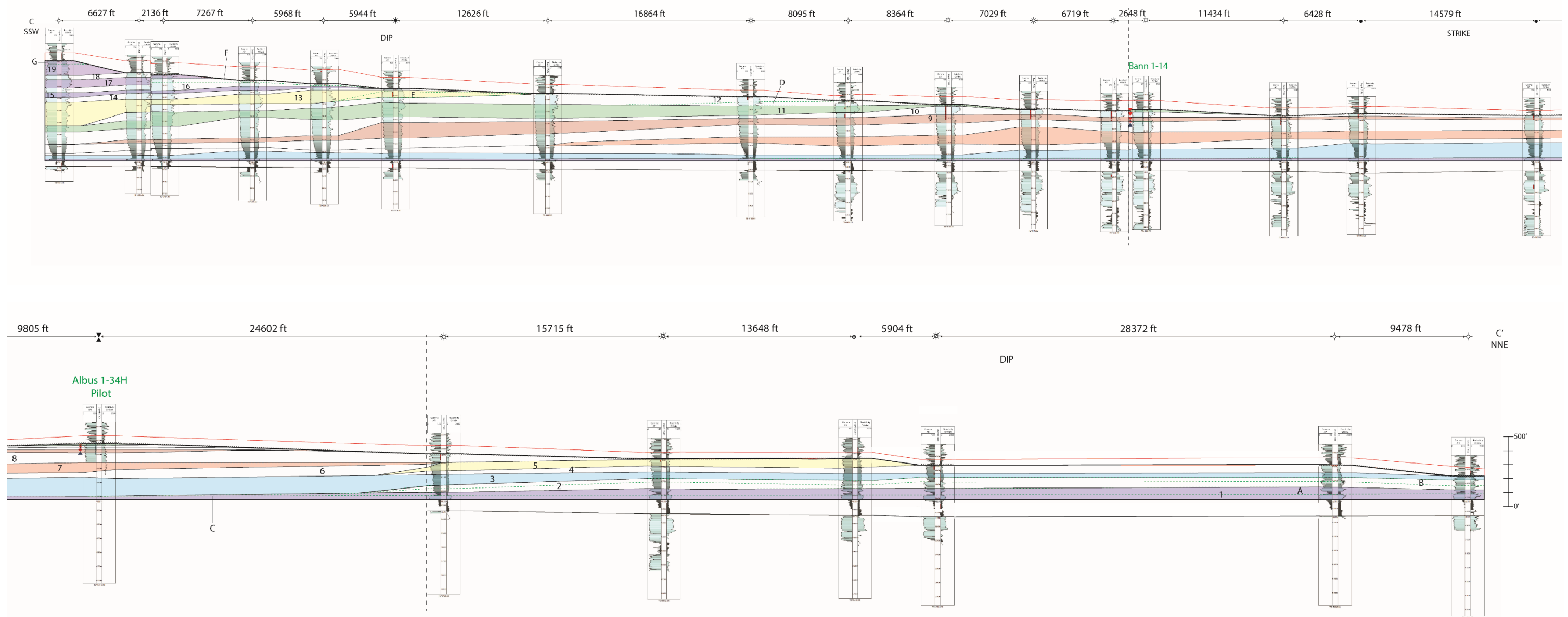


Figure 37C: Cropped version of subsurface cross section C to C' (actual distance scale). Refer to Figure 37A&B for explanation.

RESERVOIR CONSIDERATIONS

With the completion of subsurface sequence mapping, potential petroleum reservoir quality controls were evaluated with porosity and permeability cross-plots comparing facies, dominant pore type, sequences, and the transgressive versus regressive phases of the sequences related to these features. If a trend of porosity and permeability enhancement is correlative to specific depositional facies, sequences, and/or the regressive and transgressive phases of the sequences, extrapolation of vertical and lateral heterogeneity in facies distribution and reservoir quality away from the study area will be more accurate.

FACIES

The range of porosity and permeability values for the different depositional facies identified in this study are shown in Figure 38 (refer to Tables 2B and 3B for values). Overall, there are only general facies relationships tied to porosity and permeability enhancement for the three cores, suggesting other factors other than primary facies type (such as diagenesis, structural influence or exposure) were responsible for controlling the reservoir quality within the facies.

The exposure horizon (most likely related to the Pennsylvanian/Mississippian unconformity) for Core #1 and #2 has the highest porosity and permeability values (refer to Table 2B for values), however, it is not an ideal reservoir interval because most of the hydrocarbons have been leaked off by the lack of an effective overlying seal above the exposure interval (Figure 38A). Exposure interval values were excluded to focus on the porosity and permeability relationships that exist amongst the depositional facies (Figure 38B). In general, for Core #1 and #2, Oklahoma Facies 3 (bioturbated packstone) has the

best porosity and permeability (refer to Table 2B for values) and is the most volumetrically significant facies (41.6%). Oklahoma Facies 4 (skeletal packstone to grainstone) has the next best porosity and permeability (refer to Table 2B for values) and the second highest volumetric significance (21%). Oklahoma Facies 2 (burrowed wackestone to packstone) and 1 (dolomitized mudstone) have the lowest permeability values (0.009 mD and 0.011 mD) potentially creating internal baffles within the sequences.

In general, for Core #3, Kansas Facies 4 (crinoidal grainstone to packstone B) has the best porosity and permeability values (refer to Table 3B for values) of the depositional facies identified in Kansas (Figure 38C). It is the third most volumetrically significant facies (28%). Kansas Facies 3 (crinoidal grainstone to packstone A) has the second highest porosity and permeability (refer to Table 3B for values) and is the second most volumetrically significant facies (29%). It is important to reiterate that Kansas Facies 4 and 3 only differed by relative abundance of crinoids and grain size and the changes between these depositional facies were gradual. Kansas Facies 1 (skeletal packstone to wackestone) has the lowest average porosity and permeability (0.7%, 0.0001 mD), potentially creating an impermeable barrier between the coarser grained facies. Kansas Facies 2 (bryozoan grainstone to packstone) has the second lowest permeability (0.0128 mD) that could also inhibit hydrocarbon migration through the sequences.

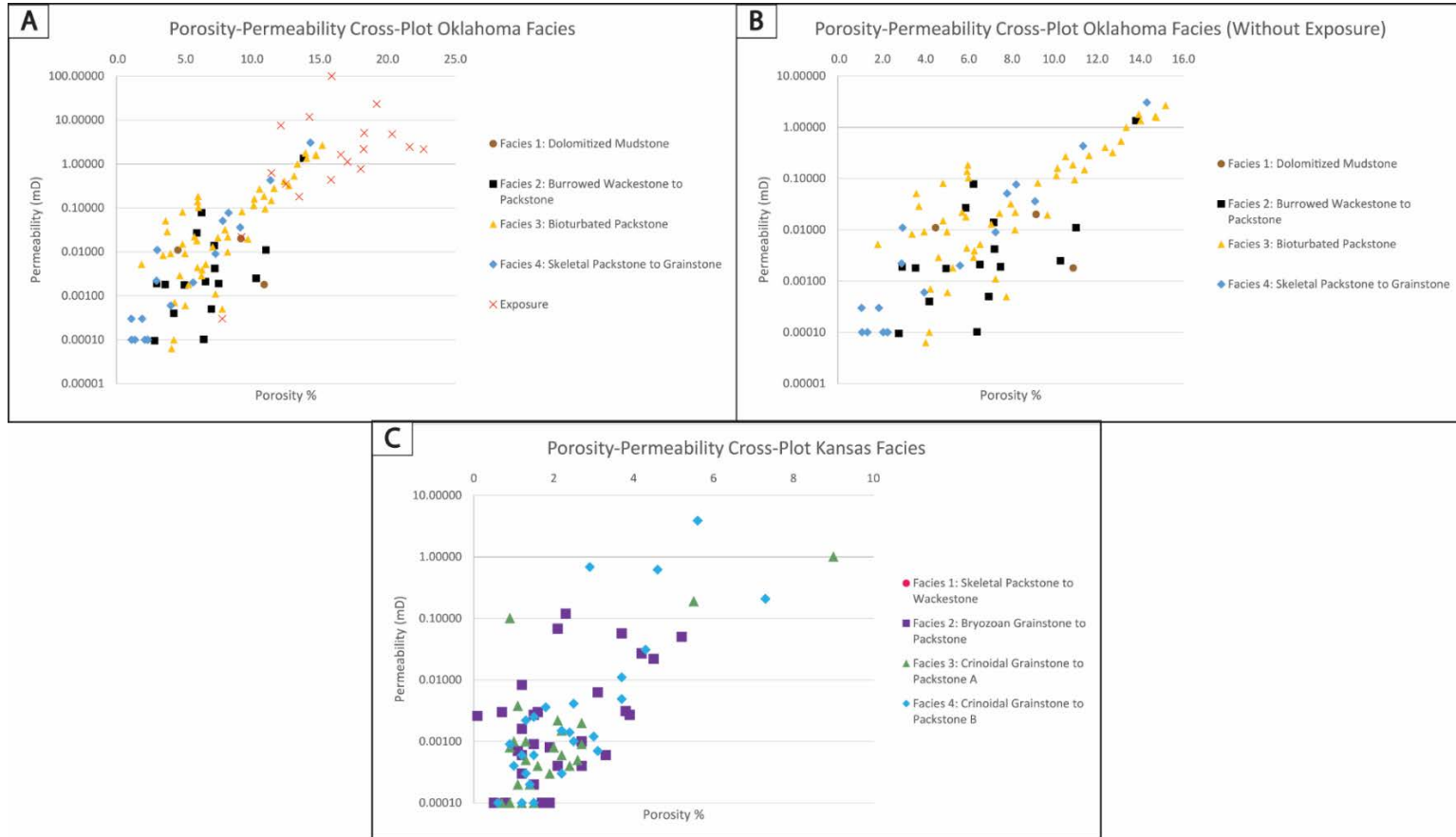


Figure 38: Porosity and permeability cross-plots for Oklahoma depositional facies (Core #1 and #2, **(A)** and **(B)**) and Kansas depositional facies (Core #3, **(C)**). Porosity is plotted along the x-axis in percentage with values ranging 0 – 25% in graph **(A)**, 0 – 16% in graph **(B)** and 0 – 10% in graph **(C)**. Permeability is plotted along the y-axis expressed in mD in a logarithmic scale with values ranging 0.00001 – 100 mD in graph **(A)**, 0.00001 – 10 mD in graph **(B)** and 0.0001 – 10 mD in graph **(C)**. Graph **(B)** for Core #1 and #2 show values without exposure display how the exposure values **(A)** skew the data (porosity values over 20% and permeability values up to 100 mD), as well as focusing on the depositional facies as reservoir target intervals. Oklahoma Facies 3 has the best reservoir potential of the depositional facies for Core #1 and #2 **(B)**. Kansas Facies 4 has the best reservoir potential of the depositional facies for Core #3 **(C)**.

DOMINANT PORE TYPE

There are no specific trends comparing dominant pore type to porosity and permeability values (Figure 39), although a general trend of lower porosity and permeability values (<12% phi, <0.1 mD) where localized intercrystalline pores occur with vugs in Core #1 and #2 (Figure 39A). For Core #3, the highest porosity and permeability values (>4% phi, >0.01 mD) are associated with inter- and intra- particle porosity (Figure 39B).

A comparison of the cross-plots to the depositional facies in each core was done to evaluate any trends between dominant pore types within each facies (Figure 39). Fracture and vug are non-fabric selective pore types whereas mold and inter- and intra-particle pores are fabric selective (Choquette and Pray, 1970). This can give clues as to the conditions and timing of porosity generation. Moldic porosity in grain-supported rocks may lead to more effective and interconnected pores compared to moldic porosity in mud-supported rocks due to finer grained material, such as *in-situ* clay minerals, occluding pore throats. Oklahoma Facies 1 and 2 are more mud rich compared to Oklahoma Facies 3 and 4, which may explain the porosity and permeability distribution being higher for the moldic porosity in Oklahoma Facies 3 compared to the moldic porosity in Oklahoma Facies 2 (Figure 39C).

In Core #3, the prolific moldic porosity development in the grain-supported facies is absent and generally has lower permeability values compared to Core #1 and #2 (refer to Tables 2B and 3B for values). Fabric selective inter- and intra- particle porosity are the most common pore types observed in the Kansas facies. This could partially explain the lower permeability values seen in Core #3 compared to Core #1 and #2 (Figure 39D).

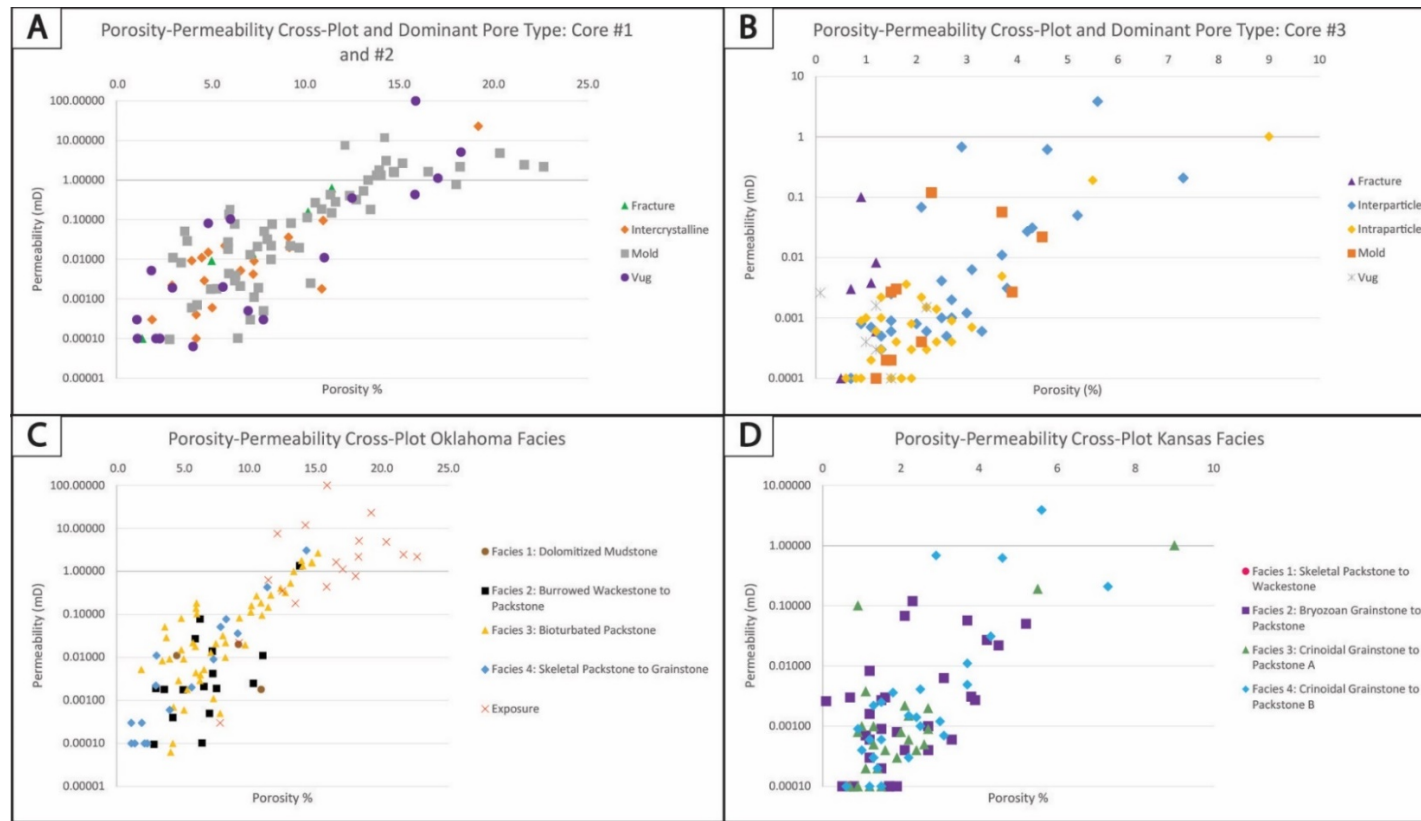


Figure 39: Porosity – permeability cross-plots compared to dominant pore types for Core #1 and #2 (**A**) and Core #3 (**B**) along with depositional facies for Core #1 and #2 (**C**) and Core #3 (**D**) ((**C**) and (**D**) are from Figure 38A&C; duplicate display is for visual correlation purposes). Porosity is plotted along the x-axis in percentage with values ranging 0 – 25% in graphs (**A**) and (**C**) and 0 – 10% in graphs (**B**) and (**D**). Permeability is plotted along the y-axis expressed in mD in a logarithmic scale with values ranging 0.00001 – 100 mD in graphs (**A**) and (**C**) and 0.001 – 10 mD in graphs (**B**) and (**D**). Fabric selective moldic porosity associated with the grain-supported facies in Core #1 and #2 (Oklahoma Facies 3 and 4; plots **A** and **C**) generally have higher porosity and permeability values (>8% phi, >0.1 mD) compared to the moldic porosity in the mud-supported facies (Oklahoma Facies 1 and 2; <8% phi, <0.01 mD). Inter- and intra-particle porosity is associated with the highest porosity and permeability values (>4% phi, >0.1 mD) in Core #3 (**B** and **D**). Overall, the permeability is lower in Core #3 compared to Core #1 and #2, which may be in part due to this fabric selective porosity development. See text for discussion.

SEQUENCES

Sequence 4 (S4) has the highest porosity and permeability development for Core #1 and #2 but these values are most likely related to dissolution related to subaerial exposure (Figure 40A). From a hydrocarbon reservoir standpoint however, the lack of a top seal has led to hydrocarbon leak off, diminishing the reservoir potential of the sequence. Sequence 2 (S2) for Core #1 offers the best reservoir potential (10.1% average porosity and 0.57 mD average permeability) and has an abundance of oil staining (~80%; refer to Appendix C) in hand sample. Sequence 1 (S1) and 2 (S2) in Core #2 have the best reservoir potential from whole core inspection (~70-80% oil staining with bright gold fluorescence; refer to Appendix C). S1 and S2 for Core #2 also show the greatest separation of neutron and density wireline logs and high resistivity values (80 – 1000 ohm-m; see Figure 30A&B). S1 in Core #1 has little to no separation between the neutron and density wireline logs, potentially depressing the average porosity and permeability values for S1. The cross-plot (Figure 40A) shows S2 and S3 have the next highest porosity and permeability development (compared to S4) for Core #1 and #2, although the majority of S3 in Core #2 is exposed. In summary, S2 offers the best reservoir potential since it has the highest average porosity and permeability (10.15% phi, 0.572 mD) with hydrocarbon shows in Core #1 and #2.

Sequence 1 (S1) for Core #3 has the highest porosity and permeability development (average 2.95% phi, 0.157 mD) and offers the best reservoir potential of the four identified 3rd order sequences (Figure 40B). Sequence 2 (S2) has lower porosity values (average 1.1%) than Sequences 3 (S3) and 4 (S4) (average 1.5% and 1.7%, respectively), but has higher permeability values (average S2 0.014 mD compared to

<0.0007 mD averages in S3 and S4), making it a better secondary reservoir interval. S3 and S4 are comprised predominantly of Kansas Facies 1 and 2, which have lower porosity and permeability values compared to Kansas Facies 3 and 4 (refer to Table 3B for values). S4 has the poorest reservoir quality but this may be due to paucity of data in this interval. Tables 4 and 5 summarize the sequence porosity and permeability values and rank for the cores.

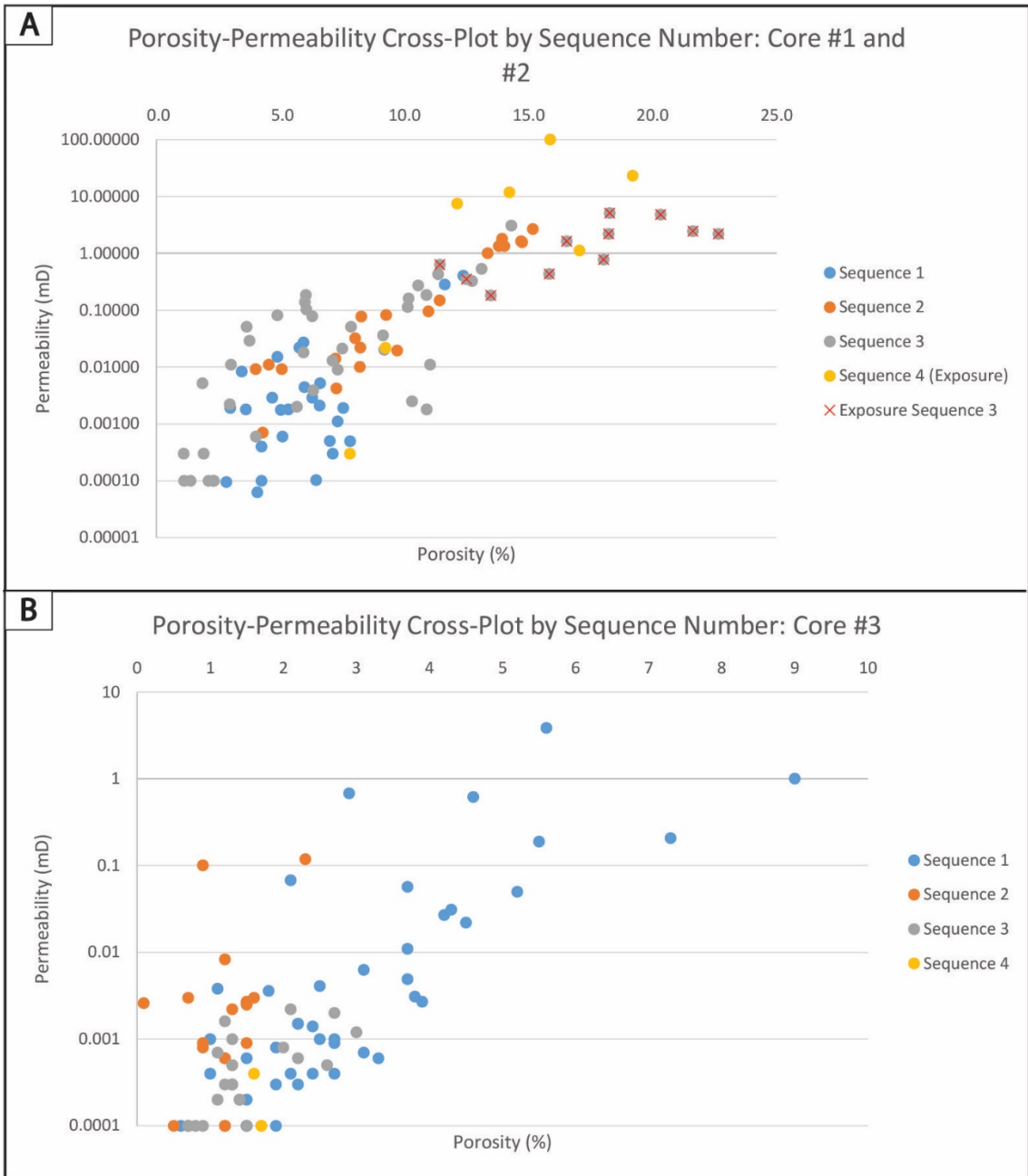


Figure 40: Porosity- permeability cross-plot compared to 3rd order sequences in Core #1 and #2 (A) and Core #3 (B). Porosity is plotted along the x-axis in percentage with values ranging 0 – 25% in graph (A) and 0 – 10% in graph (B). Permeability is plotted along the y-axis expressed in mD in a logarithmic scale with values ranging 0.00001 – 100 mD in graph (A) and 0.001 – 10 mD in graph (B). Even though S4 has the highest porosity and permeability values for Core #1 and #2 (A), it is a poor reservoir interval due to an upper seal breach. Exposure is also present in the high porosity and permeability values S3 of Core #2 (A). S2 offers the best reservoir potential for Core #1 and #2 (A). S1 in Core #3 (B) has the best porosity and permeability development of the four 3rd order sequences.

Oklahoma 3rd Order Sequence Numbers: Core #1 & Core #2	Average Porosity (%)	Average Permeability (mD)	Reservoir Potential Rank
Sequence 1	5.9	0.1	3
Sequence 2	10.1	0.572	1
Sequence 3	8.8	0.543	2
Sequence 4*	12.6	20.49	4

Table 4: Summary of sequence porosity and permeability values for Core #1 and Core #2 and reservoir rank (1 = highest, 4 = lowest). The asterisk indicates a sequence dominated by exposure (most likely related to the Pennsylvanian/Mississippian unconformity) and where hydrocarbons leaked off, diminishing the reservoir quality of this sequence. Sequence 2 (S2) offers the best reservoir potential for Core #1 and Core #2.

Kansas 3rd Order Sequence Numbers: Core #3	Average Porosity (%)	Average Permeability (mD)	Reservoir Potential Rank
Sequence 1	2.95	0.157	1
Sequence 2	1.1	0.014	2
Sequence 3	1.5	0.0006	3
Sequence 4	1.7	0.0002	4

Table 5: Summary of sequence porosity and permeability values and reservoir rank (1 = highest, 4 = lowest). Sequence 1 (S1) offers the best reservoir potential for Core #3.

TRANSGRESSIVE VERSUS REGRESSIVE PHASE

There is no obvious trend between the combined regressive and transgressive phases for the three cores in respect to porosity and permeability development (Figure 41A&B). The average of the combined regressive and transgressive phases compared to the porosity and permeability did, however, reveal general trends regarding porosity and permeability development (Figure 41C&D).

For Core #1 and #2, the combined average of the regressive phases has better porosity (8.7%) and significantly higher permeability (2.3 mD) values compared to the overall average values of the transgressive phases (8.4% phi and 0.51 mD) (Figure 41C). The regressive phase of each sequence offers the best reservoir potential for Core #1 and #2.

For Core #3, there is better porosity development associated with the combined average of the transgressive phases (average phi = 2.4 %) compared to the combined

average of the regressive phases (average phi = 2.1 %). The regressive phases have a wider range of porosity values (minimum phi = 0.09%, maximum phi = 9%, median phi = 1.5%) than the transgressive phases (minimum phi = 1.1%, maximum phi = 4.5%, median phi = 2%) in Core #3 (Figure 41B). Although the overall average porosity values are higher in the transgressive phase, the combined average permeability associated with the regressive phases (average = 0.1 mD, median = 0.0009 mD) is higher compared to the transgressive phases (average = 0.01 mD, median = 0.0007 mD) (Figure 41D).

Permeability in a low porosity and/or permeability reservoir like the “Mississippian Lime” is an important factor in producing economic hydrocarbons. For this reason, the regressive phases within each sequence have a better reservoir potential compared to the transgressive phases in Core #3.

Although it's not always the case, the regressive phase of base level change in carbonates can lead to better reservoir development because the water conditions maybe more conducive to diagenetic and physical processes that can enhance primary porosity and permeability.

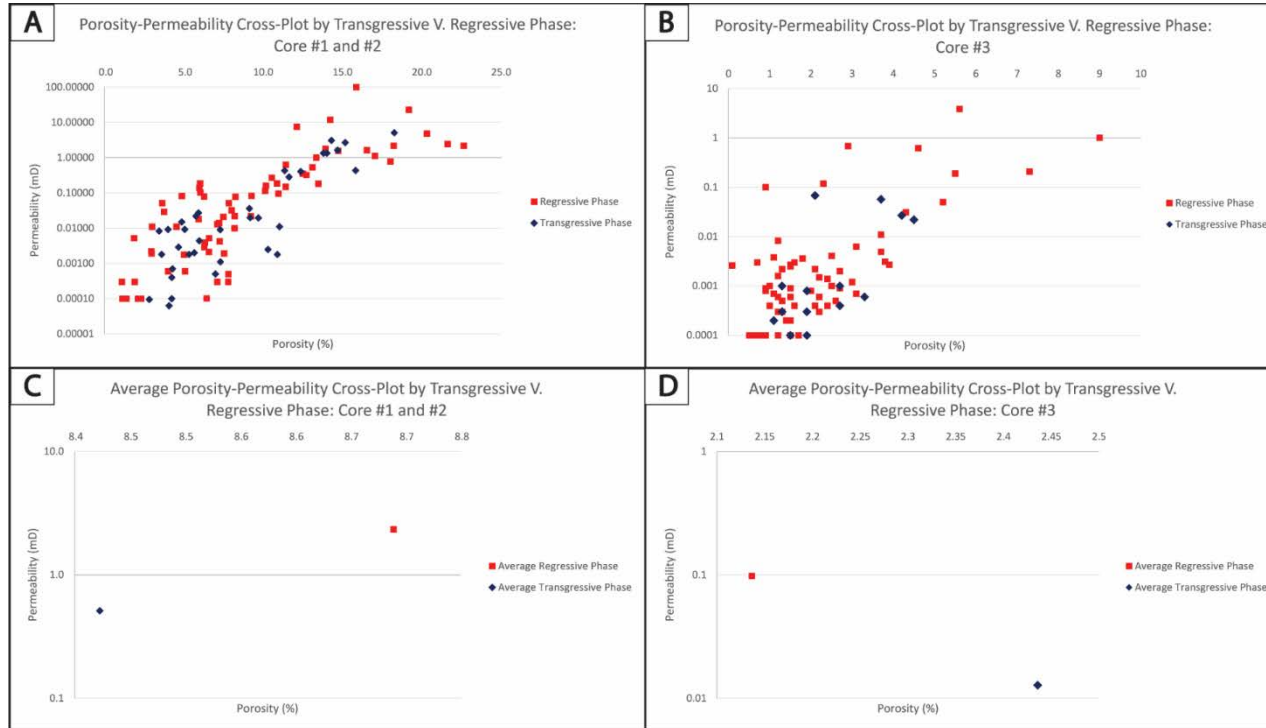


Figure 41: Porosity - permeability cross-plots comparing the total and average regressive and transgressive phases of each sequence for Oklahoma (Core #1 and #2, (A&C)) and Kansas (Core #3, (B&D)). Porosity is plotted on the x-axis in percentage ranging from 0 – 25% for graph (A), 0 – 10% for graph (B), 8.4 – 8.8% for graph (C) and 2.1 – 2.5% for graph (D). Permeability is plotted along the y-axis in a logarithmic scale ranging from 0.00001 – 100 mD for graph (A), 0.001 – 10 mD for graph (B), 0.1 – 10 mD for graph (C) and 0.01 – 1 mD for graph (D). There is no obvious trend between the combined regressive and transgressive phases for each core (A&B). The average porosity and permeability values for the regressive and transgressive phases for Core #1 and #2 (C) reveals the regressive phases have better porosity (8.7%) and significantly higher permeability (2.3 mD) development compared to the transgressive phases (8.4% phi and 0.51 mD). The average porosity and permeability values for the regressive and transgressive phases for Core #3 (D) shows that there is better porosity development associated with the transgressive phases (average = 2.4%) compared to the regressive phases (average = 2.1%). There is higher permeability associated with the regressive phases (average = 0.1 mD, median = 0.0009 mD) compared to the transgressive phases (average = 0.01 mD, median = 0.0007 mD) in Core #3, maximizing the reservoir potential within the regressive phases of the sequences.

TRANSGRESSIVE VERSUS REGRESSIVE PHASE BY SEQUENCE

Since there is a general correlation of enhanced porosity and permeability within the combined average regressive phases in all three cores, the transgressive and regressive phases of each 3rd order sequence were analyzed to identify any trends between the regressive phase and the identified reservoir sequences (Figures 42 – 45). Along with these analyses, dominant pore type (Figures 42C and 43C) and reservoir facies (Figures 44C and 45C) within the reservoir sequences were examined for further correlations.

All four 3rd order sequences were plotted by transgressive and regressive phases against porosity and permeability for Core #1 and Core# 2 in Figure 42A to delineate any correlations of porosity and permeability values in the regressive phases of each sequence. S3 and S4 have the highest porosity and permeability values associated with regressive phases of the sequences (S3 maximums = 22.6% phi, 4.7 mD; S4 maximums = 15.9% phi, 100 mD) however, S1 and S2 have higher porosity and permeability values associated with both the transgressive and regressive phases (>8% phi, >0.1 mD). S2 is plotted separately (Figure 42B) from the four identified sequences because this sequence offers the best reservoir potential for Core #1 and #2 (refer to Figure 40). Dominant pore types (Figure 42C) within S2 were cross-plotted for identification of any correlations between dominant pore types and the regressive or transgressive phase of S2. There does not seem to be any consistent trend associated with the regressive or transgressive phase of S2 and dominant pore types. Generally, the higher porosity and permeability values (>10% phi, >0.01 mD) are associated with moldic porosity development within the grain supported facies (refer to Figure 39) of the regressive phase of S2 (Figure 42B&C).

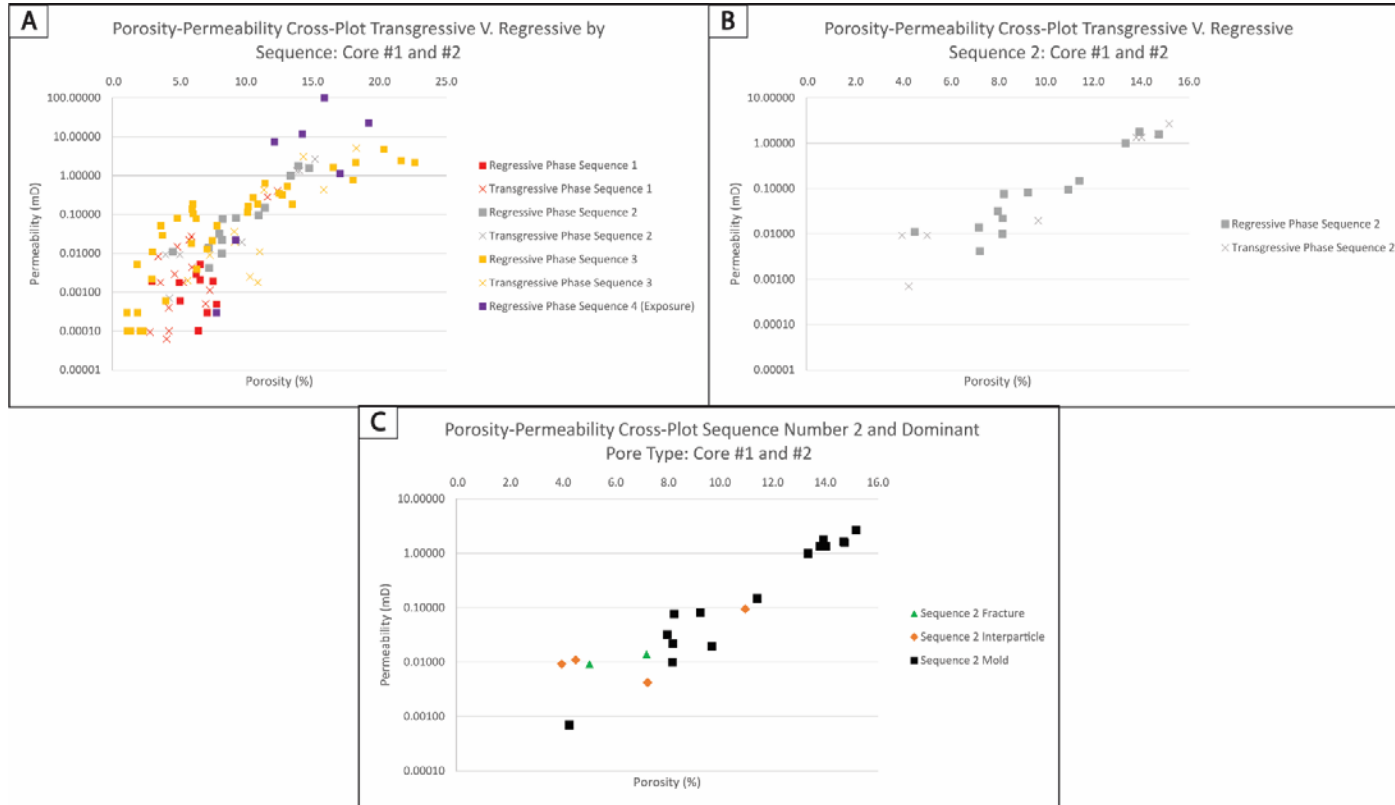


Figure 42: Porosity – permeability cross-plots compared to the regressive and transgressive phases of each sequence (A), Sequence 2 (S2) transgressive and regressive phases (B) and dominant pore types within S2 (C) for Core #1 and Core #2. Porosity is plotted along the x-axis with values in percentage ranging from 0 – 25 % in graph (A) and 0 – 16% in graphs (B) and (C). Permeability is plotted along the y-axis in a logarithmic scale ranging from 0.00001 – 100 mD for graph (A), 0.00001 – 10 mD in graph (B) and 0.0001 – 10 mD in graph (C). S2 is plotted separately (B) from the four identified sequences (A) because this sequence offers the best reservoir potential for Core #1 and #2 (refer to Figure 40). Dominant pore types (C) within S2 are cross-plotted for any correlations between dominant pore types and the regressive or transgressive phase of S2. There does not seem to be any consistent trend associated with the regressive or transgressive phase of S2 and dominant pore types. Generally, the higher porosity-permeability values (>10%, >0.01 mD) are associated with moldic porosity within the regressive phase of S2 (B&C).

Core #3 underwent the same analysis and the four identified 3rd order sequences were cross-plotted by transgressive and regressive phases against porosity and permeability (Figure 43A) to discern any correlations of porosity and permeability development in the regressive phases of each sequence. There is a correlation between the regressive phase and the highest porosity and permeability values for each sequence (Figure 43A; S1 maximums: >5% phi, >0.1 mD; S2 maximums: >1% phi, >0.01 mD; S3 maximums: >2% phi, >0.001 mD; S4 maximums: >1% phi, > 0.0001 mD). S1 is plotted separately from the four identified sequences (Figure 43B) because this sequence offers the best reservoir potential for Core #3 (refer to Figure 40). Dominant pore types (Figure 43C) within S1 were cross-plotted to identify potential correlations between dominant pore type and the regressive or transgressive phase of S1 associated with porosity and permeability development. There does not seem to be any consistent trend associated with the regressive or transgressive phase of S1 and dominant pore types, since there is overlap of pore type in each phase. Generally, inter- and intra- particle porosity is associated with the higher porosity-permeability values (>5%, >0.1 mD) within the grain supported facies (refer to Figure 39) in the regressive phase of S1 (Figure 43 B&C).

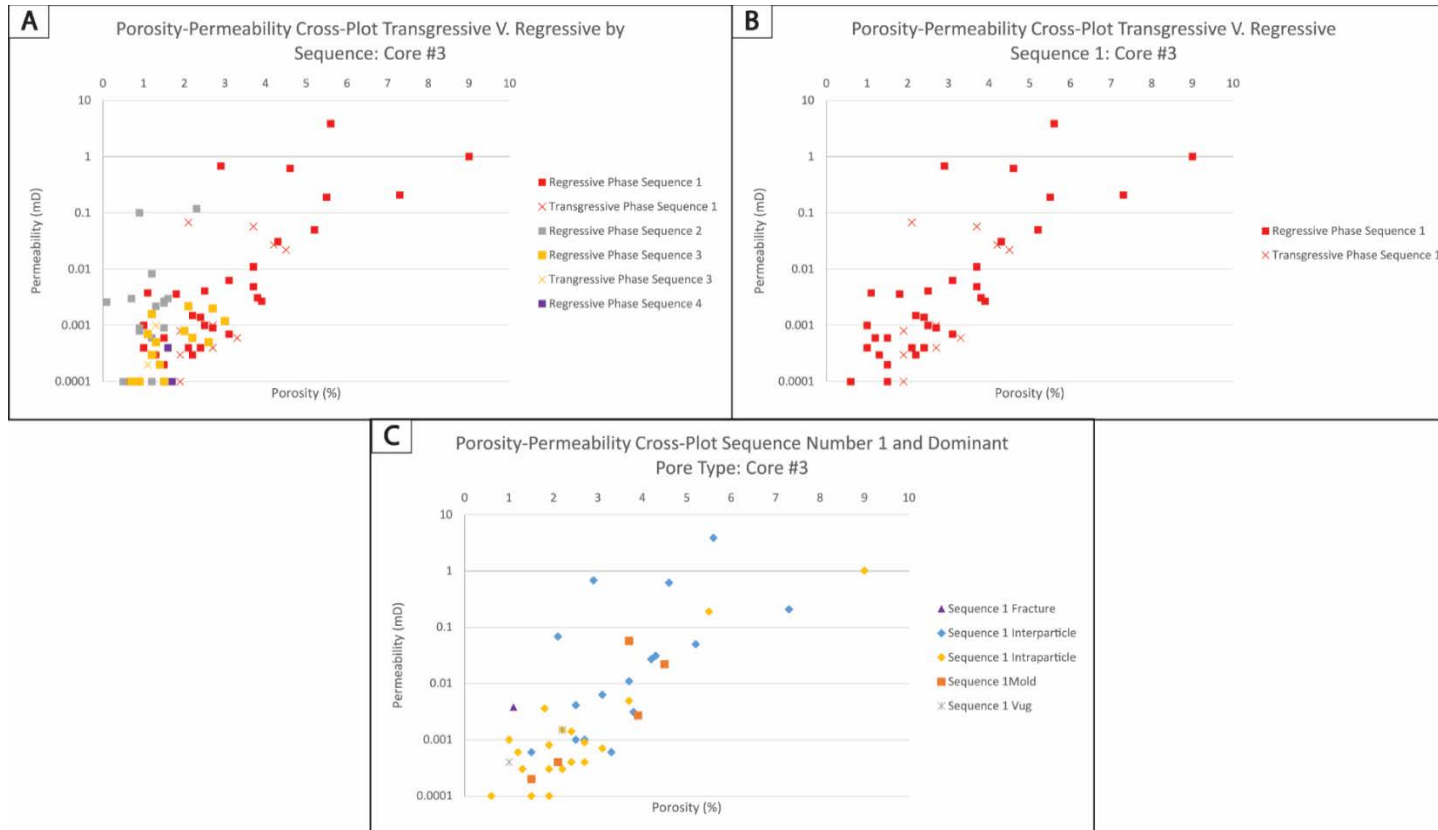


Figure 43: Porosity – permeability cross-plots compared to the regressive and transgressive phases of each sequence (A), Sequence 1 (S1) transgressive and regressive phases (B) and dominant pore types within S1 (C) for Core #3. Porosity is plotted along the x-axis with values in percentage ranging from 0 – 10 % for graphs (A), (B) and (C). Permeability is plotted along the y-axis in a logarithmic scale ranging from 0.0001 – 10 mD for (A), (B) and (C) graphs. S1 is plotted separately (B) from the four identified sequences (A) because this sequence offers the best reservoir potential for Core #3 (refer to Figure 40). Dominant pore types (C) within S1 are cross-plotted for potential correlations between dominant pore type and the regressive or transgressive phase of S1 associated with porosity-permeability development. There does not seem to be any consistent trend associated with the regressive or transgressive phase of S1 and dominant pore types. Generally, inter- and intra- particle porosity is associated with the higher porosity-permeability values (>5% phi, >0.1 mD) in the regressive phase of S1 (B&C).

The transgressive and regressive phases of the sequences in the three cores were compared to the identified reservoir facies to distinguish any porosity and permeability relationships with either phase (Figures 44 and 45). The depositional facies with the highest reservoir potential for the three cores (Core #1 and #2: Oklahoma Facies 3, Figure 44C; Core #3: Kansas Facies 4, Figure 45C) were plotted compared to the transgressive and regressive phases of the identified reservoir sequence (Core #1 and #2: S2; Core #3: S1) to identify these potential trends.

For Core #1 and #2, the reservoir facies in S2 are associated with both the transgressive and regressive phases of the sequence, with a majority (69%) of the highest porosity and permeability values ($>10\%$ phi, >0.1 mD) associated with the regressive phase of the sequence (Figure 44C). These values also correspond with moldic porosity development (refer to Figure 42C).

For Core #3, all of the reservoir facies within S1 are associated with the regressive phase of the sequence (Figure 45B&C). These facies are also associated with the highest porosity and permeability values ($>2\%$ phi, >0.1 mD) (Figure 45C) and inter- and intra- particle porosity development (refer to Figure 43C).

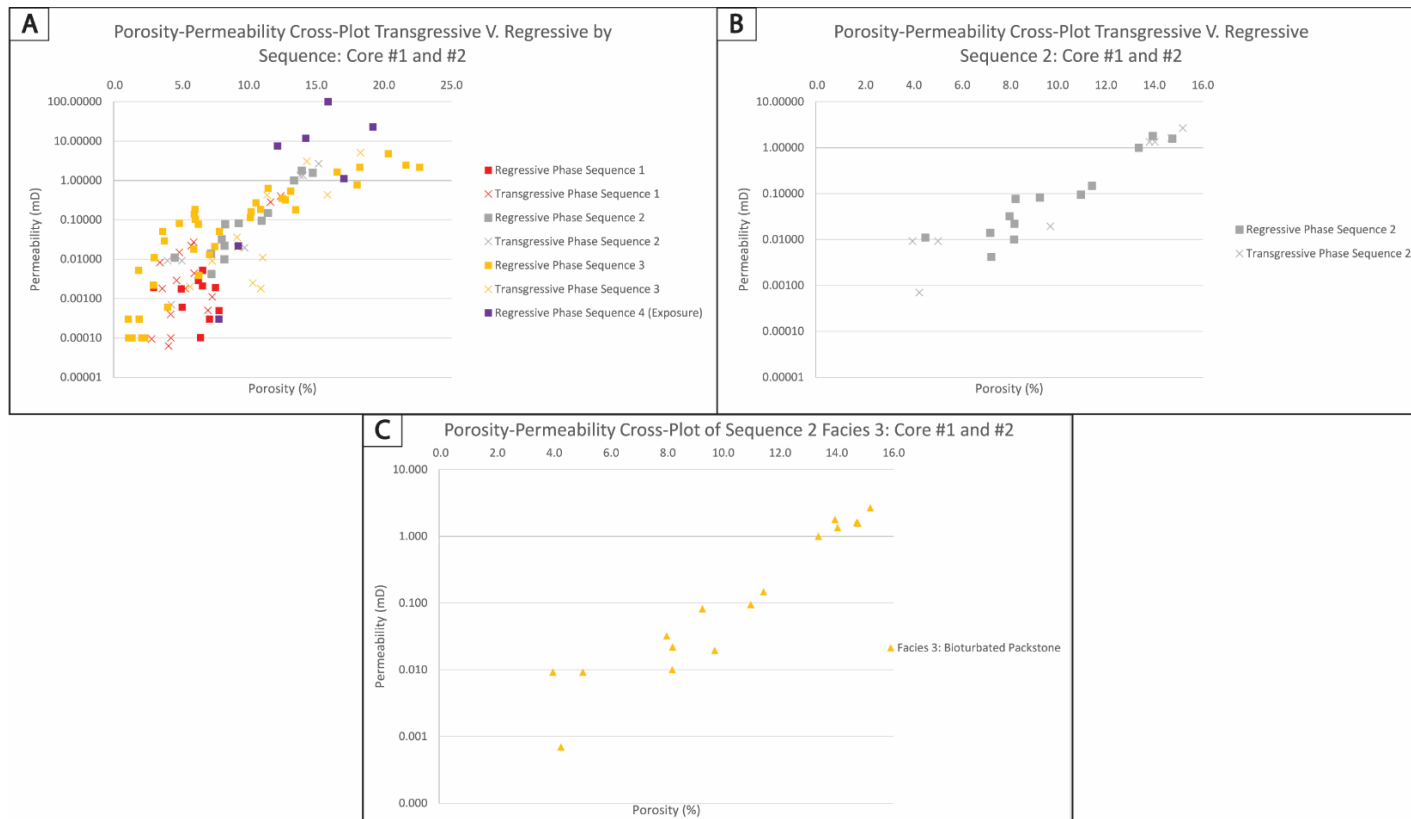


Figure 44: Porosity – permeability cross-plots compared to the regressive and transgressive phases of each sequence (A), Sequence 2 (S2) transgressive and regressive phases (B) and Oklahoma Facies 3 within S2 (C) for Core #1 and Core #2 (graphs (A) and (B) are duplicated from Figure 42A&B for visual correlation purposes). Porosity is plotted along the x-axis with values in percentage ranging from 0 – 25 % in graph (A) and 0 – 16% in graphs (B) and (C). Permeability is plotted along the y-axis in a logarithmic scale ranging from 0.00001 – 100 mD for graph (A), 0.00001 – 10 mD in graph (B) and 0.001 – 1 mD in graph (C). Refer to Figure 42 for (A) and (B) explanation. The depositional facies with the highest reservoir potential (Oklahoma Facies 3, (C)) is cross-plotted comparing the transgressive and regressive phases to identify any trend between porosity and permeability development. The reservoir facies in S2 are associated with both the transgressive and regressive phases of the sequence, with a majority (69%) of the highest porosity and permeability values (>10% phi, >0.1 mD) associated with the regressive phase of the sequence.

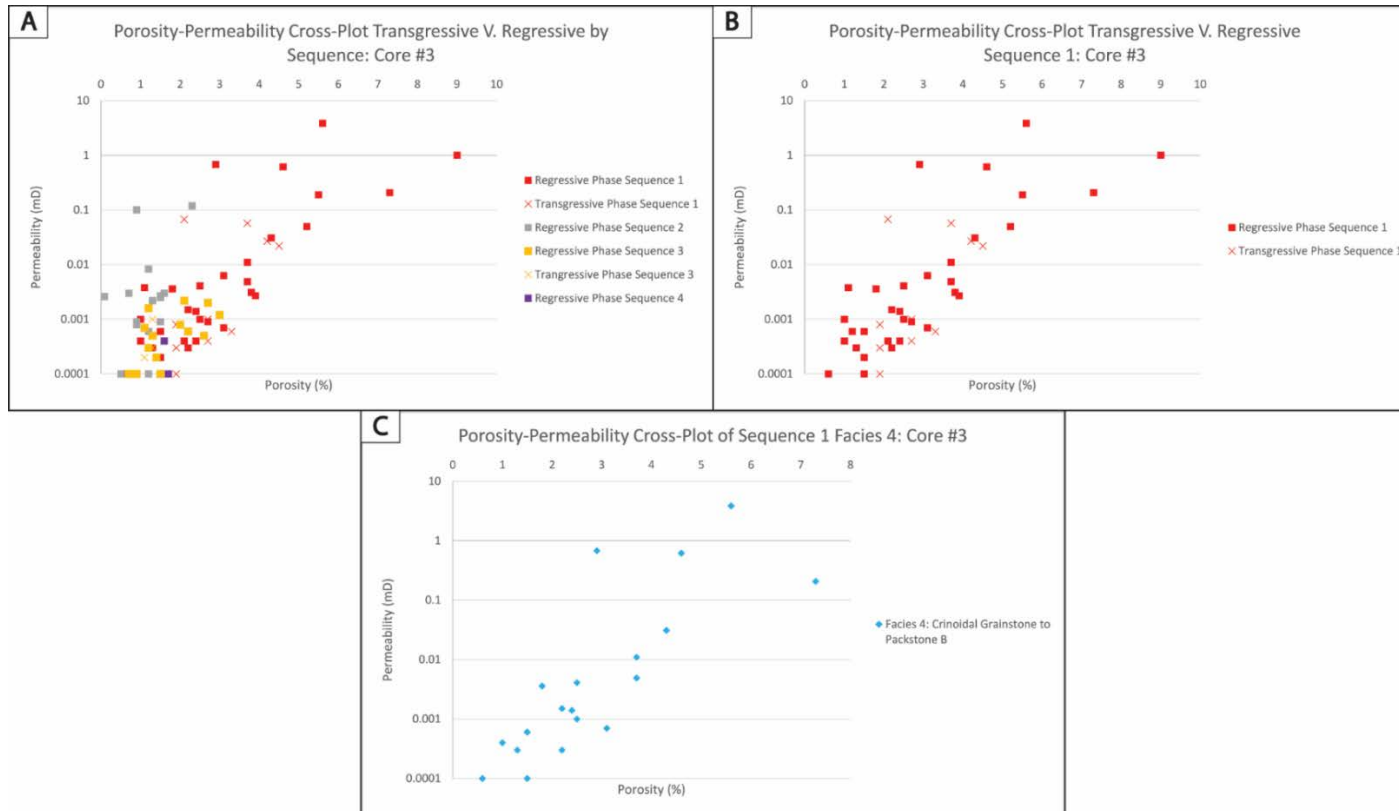


Figure 45: Porosity – permeability cross-plots compared to the regressive and transgressive phases of each sequence (A), Sequence 1 (S1) transgressive and regressive phases (B) and Kansas Facies 4 within S1 (C) for Core #3 (graphs (A) and (B) are duplicated from Figure 43A&B for visual correlation purposes). Porosity is plotted along the x-axis with values in percentage ranging from 0 – 10 % in graphs (A) and (B) and 0 – 8% in graph (C). Permeability is plotted along the y-axis in a logarithmic scale ranging from 0.0001 – 10 mD for (A), (B) and (C) graphs. Refer to Figure 43 for (A) and (B) explanation. The depositional facies with the highest reservoir potential (Kansas Facies 4, (C)) is cross-plotted comparing the transgressive and regressive phases to identify any trend between porosity and permeability development. All of the identified reservoir facies are associated with the regressive phase of S1 and the highest porosity and permeability values (>2% phi, >0.1 mD).

In summary, the regressive phase of S2 targeting Oklahoma Facies 3 for Core #1 and #2 offers the best reservoir potential in the Oklahoma cores. S3 in Core #1 and #2 offers the best secondary target potential, with Oklahoma Facies 4 being the best secondary target facies (Table 6).

The regressive phase of S1 targeting Kansas Facies 4 in Core #3 offers the best reservoir potential in the Kansas core. S2 in Core #3 is the best secondary target, with Kansas Facies 3 being the best secondary target facies (Table 7). Overall, Core #1 and Core #2 offer better reservoir potential compared to Core #3.

Oklahoma 3rd Order Sequence Numbers: Core #1 & Core #2	Average Porosity (%)	Average Permeability (mD)	Reservoir Potential Rank (Regressive Phase)	Target Facies
Sequence 1	5.9	0.1	3	Primary: Facies 3
Sequence 2	10.1	0.572	1	
Sequence 3	8.8	0.543	2	Secondary: Facies 4
Sequence 4*	12.6	20.49	4	

Table 6: Summary of Core #1 and #2 reservoir characteristics (combined with data from Table 5A). The regressive phase of each sequence is ranked 1 – 4 (1 = highest, 4 = lowest). The asterisk indicates a sequence dominated by unconformity exposure (possibly related to the Pennsylvanian/Mississippian unconformity) and where hydrocarbons leaked off, diminishing the reservoir quality of this sequence.

Kansas 3rd Order Sequence Numbers: Core #3	Average Porosity (%)	Average Permeability (mD)	Reservoir Potential Rank (Regressive Phase)	Target Facies
Sequence 1	2.95	0.157	1	Primary: Facies 4
Sequence 2	1.1	0.014	2	
Sequence 3	1.5	0.0006	3	Secondary: Facies 3
Sequence 4	1.7	0.0002	4	

Table 7: Summary of Core #3 reservoir characteristics (combined with data from Table 5B). The regressive phase of each sequence is ranked 1 – 4 (1 = highest, 4 = lowest). The overall reservoir quality in Core #3 (maximum porosity/permeability: 2.95% phi, 0.157 mD) is lower compared to Core #1 and #2 (minimum porosity/permeability: 5.9%, 0.1 mD).

PREDICTION CAPABILITIES

As mentioned earlier, the strength of creating the subsurface cross sections with a sequence stratigraphic approach is the enhanced prediction of the lateral and vertical distribution of facies. Utilizing the porosity and permeability cross-plots, individual core reservoir facies and sequences identification was completed. Figure 46 displays the potential application (using strike-oriented Core #1 from cross section A to A'; refer to Figure 34) of predicting where the primary and secondary reservoir facies could potentially lie within a sequence. The next step would be to tie the facies to a wireline log signature to correlate the facies away from the cored well. This prediction would maximize hydrocarbon drilling target locations and production extraction efficiency.

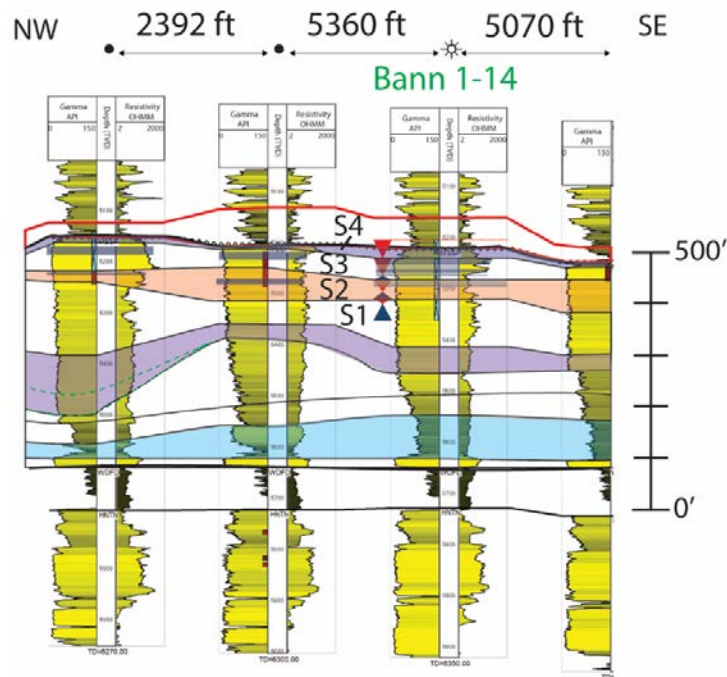


Figure 46: Application of facies identification and correlating identified reservoirs away from the cored well. Oklahoma Facies 3 and 4 (primary and secondary reservoir facies) are highlighted in blue and gray rectangles in the regressive phases of S2 and 3 (primary and secondary reservoir intervals). The rectangles highlight the gamma-ray signature associated with facies and where potential reservoir intervals could be in the strike direction. Average V.E. = 42x.

CONTROLS ON RESERVOIR DEVELOPMENT

Well log analysis for this study reveals about 354ft (107.8m) missing Mississippian section for Core #1 (total Mississippian thickness 494ft/150.6m), at least 61ft (18.6m) for Core #2 (total Mississippian thickness at least 138ft/42m) and about 520ft (158.5m) for Core #3 (total Mississippian thickness 710ft/216.4m). The Mississippian section in a more proximal area can be up to four times thicker than sections in a more distal position (144ft/43.9m – 324ft/98.7m from LeBlanc, 2015).

As mentioned previously, potential factors that could account for this thickness variability include depositional environment, structural influence and sedimentation rates. Since these cores are located in a ramp environment, the most proximal position may be in the mid-ramp environment where preservation potential was highest because sea level fluctuations did not effectively drown or expose the carbonate factory. For structural considerations, it is possible tectonic events related to the Nemaha and the Central Kansas Uplifts locally created the needed accommodation space for the carbonate factory to 'keep up' with sea level change. If the factory 'kept up' with variations in sea level, there could be 'missed beats' in previous studies (Flinton, 2016; LeBlanc, 2015) in a more distal position. Rapid sedimentation rates (meters to tens of meters per thousand years) can cause carbonates to build up considerable thickness as the basin subsides and can even surpass subsidence rates and prograde basinward (Halley, 1983). Carbonate production is intimately tied to the seawater chemistry and environment (Schlager, 1992). The Mississippian was a period of aragonite precipitating seas and a transition between icehouse and greenhouse conditions, offering a unique combination of diagenetic susceptibility and large amplitude sea level changes that greatly affected the study area.

CHAPTER IV

SUMMARY AND CONCLUSIONS

This study used an integrated approach to characterize the Mississippian-aged sediments to the west of the Nemaha Uplift using cores located in Woods County, Oklahoma and Comanche County, Kansas. Detailed core and thin section analysis, a better understanding of the depositional environment, establishing a sequence stratigraphic framework, subsurface cross sections and reservoir considerations provide an enhanced understanding of the “Mississippian Lime” reservoirs. The key conclusions from this study are:

1. Four depositional facies for Oklahoma and Kansas (eight total) were established in this study utilizing core and thin section analysis. The facies present are consistent with regional descriptions and deposition on a distally-steepened ramp, between FWWB and SWB.
2. There are identifiable idealized vertical stacking patterns of facies (shallowing upwards packages) that aided in subsurface correlation. Facies in the transgressive phase of sea level change are fine-grained mudstones to wackestones and progress into coarser grained packstones and grainstones in the regressive phase.
3. The idealized stacking pattern revealed a three-fold sequence stratigraphic hierarchy consisting of probable 3rd order sequences, 4th order high-frequency sequences and higher frequency cycles related to storm deposition, with an overall 2nd order scale regressive pattern represented in the entire cored interval. The 3rd order sequences appear to be the primary control on correlative the sequence

distribution within the study area, with 4th order high-frequency sequences accounting for the internal heterogeneity. Higher frequency cyclicity observed in vertical facies variability are most likely autocyclic tempestites and are not correlative in the study area.

4. The 3rd order sequence boundaries are readily defined in the gamma-ray wireline log signature. This gamma-ray signature provides the primary correlation unit to facilitate subsurface mapping in the study area.
5. Subsurface cross sections revealed that the 3rd order sequences have variable thicknesses in a strike-oriented direction (roughly east-west), with overall thicker yet more discontinuous sequences to the northwest. The dip-oriented (roughly north-south) subsurface cross sections displayed the 3rd order sequences prograding as clinoforms basinward, which is consistent with regional studies, with generally thicker sequences basinward. Overall, the relatively proximal (northwest) cross sections have thicker sequences than the relatively distal (southeast) cross section sequences.
6. Reservoir quality shows a correlation between the sequence stratigraphic framework and depositional facies. The highest reservoir quality is related to the regressive phases of the 3rd order sequences. Oklahoma Facies 3 (8.1% avg. porosity, 0.292 mD avg. permeability) and Kansas Facies 4 (2.43% avg. porosity, 0.192 mD avg. permeability) offer the best reservoir potential for Core #1/Core #2 and Core#3, respectively, with Oklahoma Facies 1 and 2 and Kansas Facies 1 acting as permeability barriers. Sequence 2 (Core #1 and #2) and Sequence 1

(Core #3) possess the greatest reservoir potential. Overall, Core #1 and Core #2 offer better reservoir quality sequences compared to Core #3.

REFERENCES

- Adkison, W.L., 1972, Stratigraphy and Structure of Middle and Upper Ordovician Rocks in the Sedgwick Basin and Adjacent Areas, South-Central Kansas, State Geological Survey of Kansas, Geological Survey Professional Paper 702, p. 1-32.
- Ahr, W.M., 1973, the carbonate ramp: an alternative to the shelf model: Transactions Gulf Coast Association of Geological Societies, v. 23, p. 221-225.
- Anderson, N.L. and Hedke, D.E., 1995, Geophysical atlas of selected oil and gas fields in Kansas, Kansas Geological Survey, Bulletin 237, p. 1- 164.
- Asquith, G. and Krygowski, D., 2004, Second edition Basic well log analysis, AAPG Methods in Exploration Series No. 16, American Association of Petroleum Geologists, Tulsa, Oklahoma, p. 1-244.
- Bann, K.L., Tye, S.C., MacEachern, J.A., Fielding, C.R., and Jones, B.G., 2008, Ichnological Signatures and Sedimentology of Mixed Wave- and Storm-dominated Deltaic Deposits: Examples from the Early Permian, Southern Sydney Basin of Southeastern Australia, in Hampson, G., Steel, R., Burgess, P., and Dalrymple, R. (eds.), Recent Advances in Models of Siliciclastic Shallow-Marine Stratigraphy, SEPM Special Publication 90, p. 293-332.
- Blakey, Ron, 2014, Paleogeography and Geologic Evolution of North America, <http://www2.nau.edu/rcb7/nam.html>. Accessed November 2014.
- Boardman, D. R., Thompson, T.L., Godwin, C., Mazzullo, S.J., Wilhite, B.W., Morris, B. T., 2013, High-Resolution Conodont Zonation for Kinderhookian (Middle Tournaisian) and Osagean (Upper Tournaisian Lower Viséan) Strata of the Western Edge of the Ozark Plateau, North America, Shale Shaker, September/October, p. 98 – 151.
- Burchette, T. P., and Wright, V. P., 1992, Carbonate ramp depositional systems, Sedimentary Geology, V. 79, p. 3-57.
- Catuneanu, O., Abreu, V., Bhattacharya, J. P., Blum, M. D., Dalrymple, R. W., Eriksson, P. G., Fielding, Christopher R., Fisher, W. L.; Galloway, W. E., Gibling, M. R.; Giles, K. A., Holbrook, J. M., Jordan, R., Kendall, C. G. St.C., Macurda, B., Martinsen, O. J., Miall, A. D., Neal, J. E., Nummedal, D., Pomar, L., Posamentier, H. W., Pratt, B. R., Sarg, J. F., Shanley, K. W., Steel, R. J., Strasser, A., Tucker, M. E., and Winker, C., 2009, Towards the Standardization of Sequence Stratigraphy, Papers in the Earth and Atmospheric Sciences, Paper 238 <http://digitalcommons.unl.edu/geosciencefacpub/238>, p.1-35.

- Chaplin, J.R., 2010, Stratigraphic analysis of the Permian Chase group in northern Oklahoma – outcrop analogs of reservoir rocks in the Hugoton Embayment of northwestern Oklahoma and southwestern Kansas, Oklahoma Geological Survey, Guidebook 36, p. 1-124.
- Childress, M., 2015, High resolution sequence stratigraphic architecture of a Mid-Continent Mississippian outcrop in southwest Missouri: Oklahoma State University, 273p.
- Childress, M. and Grammer, G.M., 2015, High Resolution Sequence Stratigraphic Architecture Of A Mid-Continent Mississippian Outcrop In Southwest Missouri , Shale Shaker, July/August, p. 206 - 234.
- Choquette, Philip W., and Pray, Lloyd C., 1970, Geologic Nomenclature and Classification of Porosity in Sedimentary Carbonates, AAPG Bulletin, v. 54, no. 2, p. 207-250.
- Curtis, Doris M. and Champlin, Stephen C., 1959, Depositional Environments of Mississippian Limestones of Oklahoma, Tulsa Geological Society Digest, v. 27, no. 1, p. 90-103.
- Dehcheshmehi, S. M., Gregg, J. M., Shelton, K. L., and Appold, M.S., 2015, Influence of Diagenetic Fluids on Mississippian Carbonate Rock Properties in the Southern Midcontinent, AAPG Search and Discovery Article #51165. 25 p.
- Dunham, R.J., 1962, Classification of Carbonate Rocks According to Depositional Texture, AAPG Special Volumes, Memoir 1: Classification of Carbonate Rocks, v. 1, p. 108-121.
- Eberli, G.P. and Grammer, G.M., 2010, Carbonate sequence stratigraphy from Eberli, G.P., Grammer, G.M. and P.M. Harris, 2010, Distribution and Geometry of Potential Carbonate Reservoir Facies – Great Bahama Bank, AAPG Field Course Notes, p. 1-15.
- Ekdale, A.A., Bromley, R.G., and Pemberton, S.G., 1984, Ichnology – Trace Fossils in Sedimentology and Stratigraphy, SEPM Short Course No. 15, 317 p.
- Elrick, M. and Read, J.F., 1991, Cyclic ramp-to-basin carbonate deposits, Lower Mississippian, Wyoming and Montana: A combined field and computer modeling study: Journal of Sedimentary Petrology, v. 61, p. 1194-1224.
- Evans, C.S., and Newell, K., 2013, The Mississippian Limestone play in Kansas: oil and gas in a complex geological setting, Kansas Geological Survey, Public Information Circular 33, March, p. 1-6.

Ewald, T.A., 2015, Integrated diagenesis and high-resolution sequence stratigraphy of the Mississippian Lime, north-central Oklahoma: Oklahoma State University, unpublished thesis, 75p.

Flinton, K, 2016, The effects of high-frequency cyclicity on reservoir characteristics of the “Mississippian Limestone”, Anadarko basin, Kingfisher County, Oklahoma: Oklahoma State University, 175p.

Flügel, Erik, 2010, *Microfacies of Carbonate Rocks: Analysis, Interpretation, and Application*, 2nd Ed., Springer-Verlag, Berlin, Heidelberg, New York, 1007 p.

Franseen, E.K., 2006, Mississippian (Osagean) Shallow-Water, Mid-Latitude Siliceous Sponge Spicule and Heterozoan Carbonate Facies: An Example from Kansas with Implications for Regional Controls and Distribution of Potential Reservoir Facies, *Current Research in Earth Sciences, Bulletin 252*, pg. 1-23.

Gay, Parker S. Jr., 2003, The Nemaha Trend – A System of Compressional Thrust-Fold, Strike-Slip Structural Features in Kansas and Oklahoma, Part 1, *Shale Shaker*, July-August, p. 9-49.

Grammer, G. M., P. M. Harris, G. P. Eberli, 2004, Integration of Outcrop and Modern Analogs in Reservoir Modeling: Overview with Examples from the Bahamas, in G. M. Grammer, P. M. Harris, and G. P. Eberli, eds., *Integration of Outcrop and Modern Analogs in Reservoir Modeling: American Association of Petroleum Geologists Memoir 80*, p. 1-22.

Goddard, E. N., Trask, P. D., De Ford, R. K., Rove, O. N., Singewald, J. T., and Overbeck, R. M., 1951, *Rock Color Chart*, Geological Society of America, Boulder, Colorado.

Gutschick, Raymond, and Sandberg, Charles A., 1983, Mississippian Continental Margins Of the Conterminous United States, *SEPM Special Publication No. 33*, p. 79-96.

Handford, C.R., 1986, Facies and bedding sequences in shelf-storm-deposited carbonates Fayetteville shale and Pitkin Limestone (Mississippian), Arkansas: *Journal of sedimentary petrology*, v. 56, p. 123-137.

Handford, C.R. and Loucks, R.G., 1993. Carbonate depositional sequences and systems tracts- responses of carbonate platforms to relative sea-level changes, in Loucks, R.G. and Sarg, J.F., eds., *Carbonate sequence stratigraphy- recent developments and applications: American Association of Petroleum Geologists Memoir 57*, p. 3-41.

Harris, S.A., 1987, Hydrocarbon Accumulation in “Meramec-Osage” (Mississippian) Rocks, Sooner Trend, Northwest-Central Oklahoma, Tulsa Geological Society, Special Publication No. 3: Petroleum Geology of the Mid-Continent.

Halley, R.B., 1983. An outline of carbonate sedimentation and diagenesis, the Rocky Mountain Section SEPM, p. 1 -133.

Haq, B.U., Hardenbol, J., and Vail, P.R., 1988, Mesozoic and Cenozoic chronostratigraphy and cycles of sea-level change, SEPM Special Publication No.42, p. 71 – 108.

Haq, B. U., and Schutter, S. R., 2008, A chronology of Paleozoic sea-level changes, Science, v. 322, October 2008, p. 64-68.

Jewett, J.M., Bayne, C.K, Gobel, E.D., O’Connor, H.G., Swineford, A., and Zeller, D.E., 1968, Stratigraphic succession in Kansas, *in* Kansas Geological Survey, Zeller, D.E. eds., Bulletin 189, <http://www.kgs.ku.edu/Publications/Bulletins/189/index.html>.

Jordan, L. and Rowland, T.L., 1959, Mississippian Rocks in Northern Oklahoma, Tulsa Geological Society Digest, v. 27, p. 124-136.

Kaufman, J. and Jameson, J., 2002, Sequence Stratigraphy, Facies, and Reservoir Quality of Lower Devonian Carbonates in Roman Trebsa Field, Timan-Pechora Basin, C.I.S., SEPM Special Publication No. 74, p. 43-68.

Kerans, C. and Tinker, S.W., 1997, Sequence stratigraphy and characterization of carbonate reservoirs: SEPM, short course notes no. 40, p. 1-130.

Lane, H. R., 1978, the Burlington Shelf (Mississippian, North-Central United States): *Geologica et Palaeontologica*, v. 12, p. 165-175.

Lane, H. R., and DeKyser, T. L., 1980, Paleogeography of the Late Early Mississippian (Tournasian 3) in the Central and Southwestern United States, Paleozoic Paleogeography of West-Central United States: Rocky Mountain Paleogeography Symposium 1, p. 149-162.

LeBlanc, S., 2015, High resolution sequence stratigraphy and reservoir characterization of the “Mississippian Limestone” in north-central Oklahoma: Oklahoma State University, 418p.

Lehrmann, D.J., and Goldhammer, R.K., 1999, Secular variation in parasequence and facies stacking patterns of platform carbonates: a guide to application of stacking patterns analysis in strata of diverse ages and settings: SEPM Special Publication No.63, p.188-225.

MacEachern, J. A., Bann, K. L., Gingras, M. K., and Pemberton, S. G., 2009, Applied Ichnology, SEPM Short Course Notes 52: Revised Edition, Society for Sedimentary Geology (SEPM), Tulsa, OK, 145 p.

Mazzullo, S.J., 2011, Mississippian Oil Reservoirs in the Southern Midcontinent: New Exploration Concepts for a Mature Reservoir Objective, AAPG Search and Discovery, Article no. 10373, November, p. 1-34.

Mazzullo, S.J., Boardman, Darwin R., Wilhite, Brian W., Godwin, Cory, and Morris, Beau T., 2013, Revisions of Outcrop Lithostratigraphic Nomenclature in the Lower to Middle Mississippian Subsystem (Kinderhookian to Basal Meramecian Series) Along the Shelf-Edge in Southwest Missouri, Northwest Arkansas, and Northeast Oklahoma, Shale Shaker, v. 63, no. 6, p. 414-454.

Mazzullo, S.J., Wilhite, B.W., and Boardman, D.R., 2011, Lithostratigraphic Architecture of the Mississippian Reeds Spring Formation (Middle Osagean) in Southwest Missouri, Northwest Arkansas, and Northeast Oklahoma: Outcrop Analog of Subsurface Petroleum Reservoirs, Shale Shaker, March/April, p. 254-269.

Mazzullo, S.J. Wilhite, B.W., Woolsey, I.W., 2009, Petroleum reservoirs within a spiculite dominated depositional sequence: Cowley Formation (Mississippian: Lower Carboniferous), south-central Kansas: AAPG Bulletin, v. 93, p. 1649-1689.

Montgomery, S. L., Mullarkey, J.C., Longman, M.W., Colleary, W.M., and Rogers, J.P., 1998, Mississippian "Chat" Reservoirs, South Kansas: Low-Resistivity Pay in Complex Chert Reservoir, E&P Notes, AAPG Bulletin, v. 82, no. 2, p. 187 – 205.

Northcutt, R. A., and Campbell, J. A., 1996, Geologic Provinces of Oklahoma, Transactions of the 1995 AAPG Mid-Continent Section Meeting, 1996, p. 128-134.

Plint, A.G., et al., 1992, Control of sea level change, in R.G. Walker and N.P. James, eds., Facies Models, Response to Sea Level Change, Chapter 2, p. 15-25.

Price, B., 2014, High resolution sequence stratigraphic architecture and reservoir characterization of the Mississippian Burlington/Keokuk formation, northwestern Arkansas: Oklahoma State University, 143p.

Price, B., and Grammer, G.M., 2015, Sequence Stratigraphic Control on Distribution and Porosity Evolution in Cherts in the Mississippian of the Mid-Continent, AAPG Search and Discovery Article #51123, 32 p.

Read, J.F., 1995, Overview of Carbonate Platform Sequences, Cycle Stratigraphy and Reservoirs in Greenhouse and Icehouse Worlds, In: Read, J. F., Kearns, C., Weber, L. J., Sarg, J. F., and Wright, F. M., (eds.) Milankovitch Sea Level Changes, Cycles, and

Reservoirs on Carbonate Platforms in Greenhouse and Ice-House Worlds: SEPM Short Course 35, p. 1-102.

Roundtree, R., Wright, J., and Miskimins, J., 2010, Unconventional Resource Recovery Improvement Using Conventional Reservoir Engineering Strategies, AAPG Search and Discovery Article #80088, 15 p.

Schlager, W., 1992. Sedimentology and sequence stratigraphy of reefs and carbonate platforms: a short course, AAPG Course Notes n.34, p.1-71.

Scholle, P. A., Bebout, D.G., and Clyde, H.M, 1983. Carbonate Depositional Environments: American Association of Petroleum Geologists, Memoir 33, p. 1-708.

Scholle, P.A., and Ulmer-Scholle, D.S., 2003, A Color Guide to the Petrography of Carbonate Rocks: Grains, Textures, Porosity, Diagenesis, AAPG Memoir 77, Tulsa, The American Association of Petroleum Geologists, 474 p.

Sibley, D. F. and Gregg, J. M. 1987. Classification of Dolomite Rock Textures, Journal of Sedimentary. Petrology, no.57, p. 967-975.

Thompson, T.L. and Goebel, E.D., 1968, Conodonts and Stratigraphy of the Meramecian Stage (Upper Mississippian) in Kansas, Kansas Geological Survey, Bulletin 192, <http://www.kgs.ku.edu/Publications/Bulletins/192/index.html>

Tucker, M.E., and V.P. Wright, 1990, Carbonate Sedimentology: Blackwell Scientific Publications, 482 p.

Westphal, H., Eberli, G.P., Smith, L.B., Grammer, G.M., Kislak, J., 2004, Reservoir characterization of the Mississippian Madison Formation, Wind River basin, Wyoming: AAPG Bulletin, v. 88, p. 405-432.

Wilhite, Brian W., Mazzullo, S.J., Morris, Beau T., and Boardman, Darwin II, 2011, Syndepositional Tectonism and its Effects on Mississippian (Kinderhookian to Osagean) Lithostratigraphic Architecture: Part 1 – Based on Exposures in the Midcontinent USA, AAPG Search and Discovery Article #30207, 43 p.

APPENDICES

APPENDIX A
WRITTEN CORE DESCRIPTIONS AND SEQUENCE STRATIGRAPHIC
FRAMEWORK

Core descriptions presented below. Colors correspond to the rock color chart (Table 8) from Goddard et al., 1951. Descriptions of the degree of bioturbation refer to the bioturbation index from Bann et al., 2008 (Table 9). Fracture density is designated by foot per number, as shown in Table 10. Locations of thin sections follow “TS” in written descriptions.

Rock-Color Chart			
Color Name	Numerical Designation	Color Name	Numerical Designation
Bluish White	5 B 9/1	Medium Light Gray	N6
Brownish Gray	5 YR 4/1	Medium Gray	N5
Dark Gray	N3	Olive Black	5 Y 2/1
Dark Yellowish Green	10 GY 3/2	Olive Gray	5 Y 4/1
Grayish Green	10 G 4/2	Pale Olive	10 Y 6/2
Grayish Pink	5 R 8/2	Pale Greenish Yellow	10 Y 8/2
Grayish Red	5 R 5/2	Pale Orangeish Yellow	10 YR 8/6
Grayish Red Purple	5 RP 4/2	Pinkish Gray	5 YR 8/1
Greenish Gray	5 G 6/1	Very Dark Red	5 R 2/6
Yellowish Gray	5 Y 8/1	Very Light Gray	N8
Light Olive Gray	5 Y 6/1	White	N9
Medium Dark Gray	N4	Yellowish Gray	5 Y 8/1

Table 8: Modified from the Rock-Color Chart prepared by the Rock-Color Chart Committee and distributed by The Geological Society of America. Reprinted in 1970, after Goddard et al., 1951.

Bioturbation Index			
#	Characteristics	Mud-Dominated Facies	Grain-Dominated Facies
0	Bioturbation absent		
1	Sparse bioturbation, bedding distinct, few discrete traces		
2	Uncommon bioturbation, bedding distinct, low trace density		
3	Moderate bioturbation, bedding boundaries sharp, traces discrete, overlap rare		
4	Common bioturbation, bedding boundaries indistinct, high trace density with overlap common		
5	Abundant bioturbation, bedding completely disturbed (just visible)		
6	Complete bioturbation, total biogenic homogenization of sediment		

Table 9: Bioturbation index used in Illustrator core descriptions. From Bann et al., 2008.

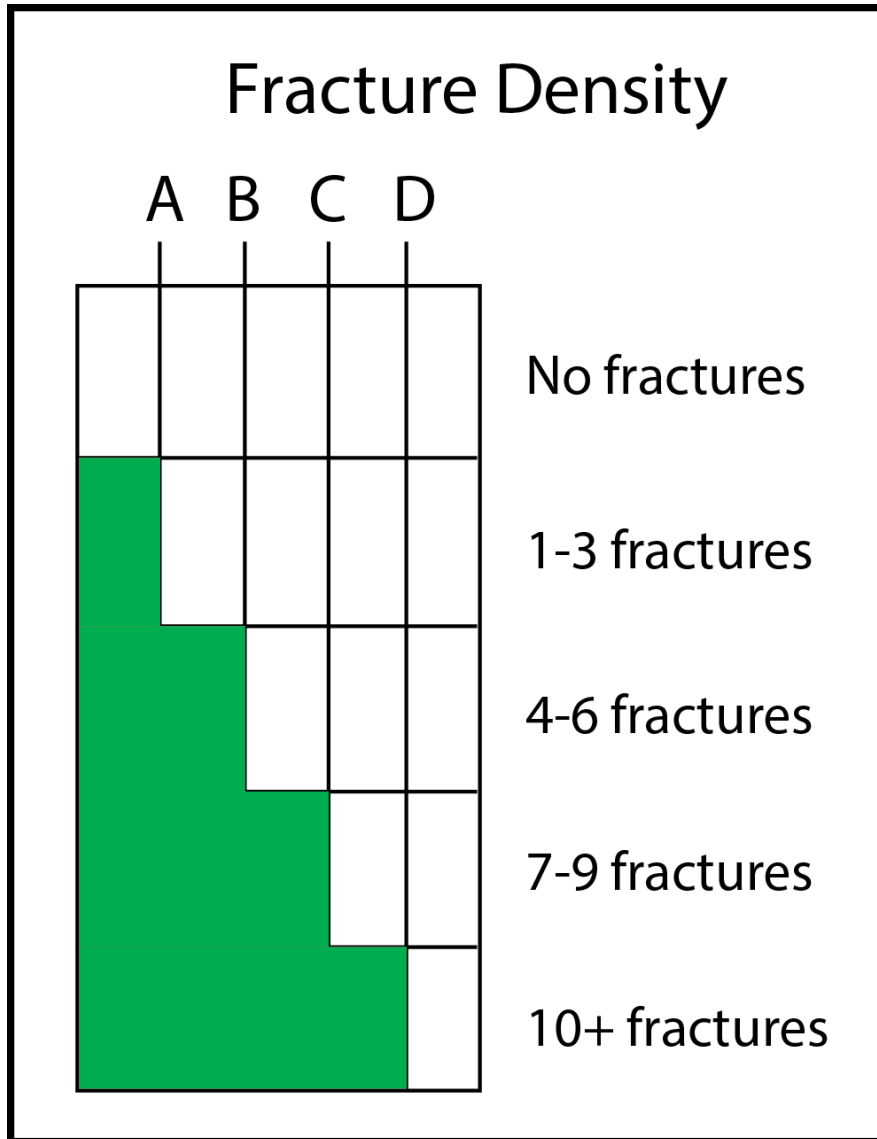


Table 10: Fracture numbers per foot as listed on core description.

WRITTEN CORE DESCRIPTIONS

Core #1: Bann #1-14 - Chesapeake Energy

Woods County, OK

Cored Interval: 5205.0' – 5355.0'

Examined Interval: 5207.0' – 5355.0'

Base of Penn. /Miss. Unconformity: 5207.0' (from core)

Formation: “Mississippian Limestone”

5355.0' – 5347.7' = Facies #2 and Facies #3. Burrowed wackestones to packstones with intermittent bioturbated packstones. Mottled medium gray to dark gray, with olive gray and light bluish gray chert. Bioturbation common with abundant bioturbation at 5355' – 5353' and 5351'—5350', horizontal burrows ranging from 1 to 3 mm in size with differential compaction. Scattered, light bluish gray chert nodules throughout the interval (~1 inch in diameter). One vertical burrow present at 5348.6' (0.02' long). Fine to medium grained cherty, dolomitic, burrowed wackestone to packstone. Interval of bioturbated packstones at 5351.7' - 5347.7'. Sand sized pyrite crystal present at 5354.9'. Coarse sand sized crinoid fragments present at 5349.9' and 5348.6'. Partially filled (calcite) vertical fractures (~0.15') present at 5351.1' and (0.3' long) at 5348.5', calcite filled ptigmatic fracture at 5350.5' (0.035' long). No visible porosity. Oil staining and fluorescence under ultraviolet light observed in moderately bioturbated zones where chert is absent (5355.1' – 5352.5', 5352.1' – 5351.2', 5351.1' - 5350.5', 5350.0', 5349.9' – 5349.2', 5348.5' – 5347.7'). Base of Core.

TS 5353.8', TS 5349.36', TS 5347.9'

5347.7' – 5340.7' = Facies #2 and Facies #3. Bioturbated packstones with intermittent burrowed wackestones to packstones. Mottled medium gray to dark gray, light olive gray to olive gray. Moderate to common bioturbation. Horizontal burrows ranging from 1 - 3 mm in size at 5347.3' – 5347.2' and 5346.3', from 1 to 5 mm in size at 5342.3' – 5341.8' and 1 – 5 cm at 5342.9' - 5342.5', 5341.8' – 5340.7' and range 5 – 10 mm throughout the interval. Fine to medium grained cherty, dolomitic, burrowed wackestone to mud rich packstone. Scattered, light bluish gray chert nodules throughout the interval (~1 inch in diameter) with differential compaction. Intervals of burrowed wackestones at 5347.7' – 5343.7', 5342.3' – 5341.8' and 5341.0' – 5340.7'. Coarse sand-sized crinoid fragments present at 5346.8', 5344.5', 5342.6' and 5340.8'. Sand sized pyrite crystals present at 5342.8'. Partially healed (calcite) vertical and sub-vertical fractures (6, ~0.3' long) present at 5342.3' – 5341.8'. No visible porosity. Oil staining and fluorescence under ultraviolet light observed in moderately bioturbated zones where chert is absent (5347.7' – 5344.0', 5345.0' - 5342.5', 5341.9 – 5340.7).

TS 5346.4', TS 5344.8', TS 5342.56', TS 5341.6', TS 5340.7'

5340.7' – 5335.95' = Facies #3. Bioturbated packstones. Mottled medium gray to dark gray, light olive gray to olive gray and olive black. Moderate to common bioturbation throughout interval. Horizontal burrows ranging 1 – 5 cm at 5340.7' – 5340.0'. Horizontal burrows ranging from 1 to 3 mm in size at 5335.9' – 5335.7', 5334.6' – 5334.3' and 10 – 50 mm at 5340.0' – 5335.9'. Vertical burrow (0.1' long) present at 5339.4'. Fine to medium grained cherty, dolomitic, bioturbated mud rich packstone to wackestone. Coarse sand sized crinoid fragments present at 5340.6', 5340.3', 5339.9', 5338.6', 5338.2', 5337.9' and 5336.4'. Cement filled fracture at 5340.2' (~0.1' long). Partially healed (calcite) vertical (~0.3' long) present at 5335.8' – 5335.5' and cement filled fractures at 5338.7', 5338.2', 5337.7'. No visible porosity. Oil staining and fluorescence under ultraviolet light observed in moderately bioturbated zones where chert is absent (5340.7 – 5340.0).

TS 5340.7', TS 5337.9', TS 5337.8', TS 5337.2', TS 5336.3'

5335.95' – 5329.4' = Facies #2. Burrowed wackestones to mud rich packstones. Mottled medium gray to dark gray, light olive gray to olive gray and olive black. Moderate to common bioturbation. Horizontal burrows ranging from 1 to 3 mm in size throughout interval with 10 – 50 mm horizontal burrows at 5335.95' – 5335.9'. Fine to medium grained cherty, dolomitic, burrowed mud rich packstone to wackestone. Sand-sized pyrite crystals present at 5331.7' and 5330.2'. Healed (calcite) vertical and sub vertical (2, ~0.02' long) fractures present at 5333.8'. Partially healed (calcite) vertical (~0.3' long) present at 5335.8' – 5335.5' and cement filled fractures at 5334.2' (0.02' - 0.05' long). Coarse sand sized crinoid fragments present at 5334.8', 5334.2', 5333.9' and 5330.5'. Traction currents observed in the chert interval at 5334.8'. Olive black lamination features (~0.05' thick) present at 5332.8' and 5330.5'. No visible porosity. Oil staining and fluorescence under ultraviolet light observed in moderately bioturbated zones where chert is absent (5340.0' – 5334.0', 5335.0' - 5334.1', 5333.0' – 5331.2').

TS 5337.9', TS 5337.8', TS 5337.2', TS 5336.3', TS 5333.3', TS 5331.2'

5329.4' – 5324.1' = Facies #3. Bioturbated mud rich to grain rich packstones. Mottled medium gray to dark gray, grayish red, light olive gray, olive black, yellowish gray. Moderate to abundant bioturbation. Horizontal burrows ranging from 1 to 5 mm in sized scattered throughout the interval. Vertical burrow (0.25' long) present at 5327.2', 5326.8', and 5325.35'. Fine to medium grained cherty, dolomitic, burrowed mud rich to grain rich packstones. Grayish red color (possible iron) surrounding bioturbation at 5327.1' – 5324.5', 5324.2' - 5324.1'. Open vertical fractures at 5328.4' (6+) and 5327.0' (1) (~0.4' long). Olive black lamination features (~0.05' thick) present at 5328.5', and 5327.8'. Coarse to medium sand-sized crinoid fragments present at 5330.5', 5328.5, 5327.4', and 5325.2'. Sand sized pyrite crystals present at 5328.4'. No visible porosity. Oil staining and fluorescence under ultraviolet light observed in moderately bioturbated zones where chert is absent (5329.2' – 5327.1'). Bright fluorescence under ultraviolet light observed at 5326.2 – 5324.0'.

TS 5328.0', TS 5326.26', TS 5325.2', TS 5324.8'

5324.1' – 5319.7' = Facies #2. Burrowed wackestones to packstones. Mottled light gray to dark gray, light olive gray, grayish red. Moderate to abundant bioturbation. Horizontal burrows ranging from 1 to 10 mm scattered throughout the interval. Vertical burrow (~0.1') present at 5322.4'. Fine to medium grained cherty, dolomitic, burrowed mud rich packstones to wackestones. Partially healed (calcite) sub vertical (0.02' long) fracture present at 5323.6'. Healed (calcite) vertical (0.7' long) present at 5322.3' and 5321.5' (0.1' long). Grayish red color (possible iron or oil stain) surrounding bioturbation at 5322.7', 5322.2', and 5321.4'. Olive black laminations (~0.2' thick) present at 5323.0 - 5322.8'. Coarse sand-sized crinoids present at 5322.8', 5320.3' and 5319.7'. No visible porosity. Oil staining and fluorescence under ultraviolet light observed in moderately bioturbated zones where chert is absent (5323.2' – 5322.8', 5322.3' – 5319.8', 5319.7').

TS 5321.1', TS 5320.4', TS 5319.7'

5319.7' – 5306.3' = Facies #2 and Facies #3. Bioturbated mud rich packstones with intermittent burrowed wackestones to packstones. Mottled medium to medium dark gray, olive gray to light olive gray, grayish red, yellowish gray, olive black. Moderate to abundant bioturbation. Horizontal burrows ranging 1 – 4 mm in size at 5318.75', 5316.9' - 5316.3', 5314.8' – 5314.6' and range 1 – 4 cm throughout the interval. Vertical burrows (~0.2' – 0.5') present at 5318.7', 5316.3', and 5306.3'. Fine to medium grained cherty, dolomitic, bioturbated mud rich packstones to wackestones. Intervals of burrowed wackestones to packstones at 5319.7' – 5318.6', 5316.95' - 5316.25', 5314.8' - 5314.5', 5313.2' - 5311.2', 5307.1' - 5307.0', 5306.8' - 5306.3'. Healed (calcite) vertical and sub vertical fractures (~0.2' – 0.5' long) present at 5313.1' (2), 5312.8', 5312.5', 5312.2' (3), and 5311.8'. Grayish red color (possible iron or oil stain) surrounding bioturbation at 5318.2', 5317.25', 5316.2', 5315.5', 5314.2', 5313.8', 5313.2', 5310.7', 5310.1', 5309.2', 5308.7', 5307.1' – 5307.6'. Olive black laminations (~0.05' thick) present at 5318.1', 5317.55', 5315.1', 5313.8', 5313.6', 5313.5', 5311.3', 5311.15', 5309.9', 5309.3', 5309.05'. Coarse to medium sand sized crinoids present at 5318.1', 5317.5', 5316.8', 5315.15', 5314.4', 5313.7', 5312.7' – 5311.8', 5311.2', 5311.0' – 5309.7', 5309.3', 5308.8'. No visible porosity. Oil staining and fluorescence under ultraviolet light observed in moderately bioturbated zones where chert is absent (5319.7' – 5319.1', 5318.5' – 5316.95', 5316.2' – 5314.8', 5314.3' – 5313.2', 5311.8' – 5309.2'). Bright oil staining present at 5309.1' - 5308.1', 5307.9' – 5307.1', 5307.0' – 5306.85'.

TS 5318.2', TS 5315.36', TS 5315.26', TS 5313.66', TS 5310.86', TS 5309.5', TS 5309.5', TS 5308.6', TS 5307.7'

3rd order Sequence 1 boundary at 5313.2'.

5306.3' – 5295.1' = Facies 3#. Bioturbated grain rich packstones. Mottled olive gray to light olive gray, yellowish gray, medium dark gray, grayish brown to brownish gray. Moderate to

abundant bioturbation. Horizontal burrows range from 5 – 20 mm present throughout the interval and from less than 1 – 4 mm in size at 5298.3' – 5298.0'. Vertical burrows (~0.1' long) present at 5302.8' and 5299.8'. Vertical burrow (0.15' long) present at 5297.7'. Medium to fine grained cherty, dolomitic, bioturbated grain rich to mud rich packstones. Grayish brown to brownish gray color surrounds burrows throughout the interval. Scattered, light bluish gray chert nodules throughout the interval (~1 inch in diameter). 5303.0' – 5299.2' interval exhibits a highly fractured rubble zone. Partially healed vertical fractures (0.2' long) present at 5303.2' (2). Partially healed vertical fractures (~0.25' long) present at 5298.1' (2), 5296.1' (2), and 5295.3'. Coarse sand sized crinoids visible in hand sample at 5304.5'. Medium sand-sized crinoids visible (~3 cm in diameter) at 5296.1' with thin shelled bivalves (~ 2 mm). No visible porosity. Olive black laminations present at 5295.1' – 5295.0'. Oil staining and fluorescence under ultraviolet light observed in moderately bioturbated zones where chert is absent (5306.3'-5303.3', 5297.8' - 5295.1). Bright fluorescence present at 5301.1' - 5300.4', 5299.3' – 5298.3'.

TS 5306.16', TS 5305.3', TS 5304.86', TS 5303.6', TS 5299.3', TS 5298.7', TS 5296.1'

5295.1' – 5293.9' = Facies #1. Dolomitized bioturbated mudstone. Mottled light olive gray to olive gray, yellowish gray, grayish red, very light gray to medium light gray, dark gray. Horizontal burrows range from 1 – 5 mm in size scattered throughout the interval. Very fine grained cherty, dolomitized mudstone. Medium sand-sized crinoids visible (~1 cm diameter) at 5294.7'. Grayish red color surrounds chert at 5294.8' -5295.0'. No visible porosity. Oil staining and fluorescence under ultraviolet light observed throughout the interval.

TS 5294.5'

5293.9' – 5290.8' = Facies #3 and Facies #2. Bioturbated grain rich to mud rich packstones with intermittent burrowed wackestones. Mottled light olive gray to olive gray, yellow gray, light to medium dark gray, and grayish brown. Moderate to abundant bioturbation. Horizontal burrows range from 1 - 3 cm in size at 5292.5' – 5295.2' and 10 – 20 mm throughout the interval. Medium to fine grained cherty, dolomitic, bioturbated grain rich to mud rich packstones and burrowed wackestones. Burrowed wackestone interval at 5293.9' – 5293.5' with mud rich, very fine grained interval at 5293.48' – 5293.5' and 5291.2' – 5290.8'. Coarse sand-sized crinoid fragments (~0.5 mm) visible at 5292.3'. Partially healed vertical fractures (5, 0.6' long) at 5293.5'. Horizontal stylolite at 5293.4'. Brownish gray color surrounds bioturbation features throughout the interval. No visible porosity. Oil staining and fluorescence under ultraviolet light observed throughout the interval.

TS 5293.39', TS 5292.6', TS 5291.6', TS 5290.9'

5290.8' – 5280.4' = Facies #3 and Facies #2. Bioturbated packstones and burrowed packstones to wackestones. Mottled light olive gray to olive gray, yellow gray, light to medium dark gray, and grayish brown. Moderate to abundant bioturbation. Horizontal burrow size ranges 0.5 mm to 3 mm. Vertical burrows (~0.1' long) present at 5290.4', 5289.8' and 5288.2'. Medium

to fine grained cherty, dolomitic, bioturbated grain rich to mud rich packstones. Grayish brown to brownish gray color surrounds bioturbation throughout the interval. Intervals of burrowed wackestones at 5290.8' – 5290.4', 5287.2' – 5287.0' and 5286.7' – 5286.5'. Crinoids visible (~1 mm) at 5290.1' -5290.6', 5288.68' – 5288.7', 2586.9', 5286.6', 5285.5' – 5285.6', 5285.2' - 5285.25', 5284.6', 5284.1' – 5284.4', 5281.1', and 5280.8'. Open and partially healed vertical fractures (~0.5' long) present at 5289.95', 5288.2', 5285.95', 5284.5', 5283.8', 5281.1', 5280.5'. No visible porosity. Oil staining and fluorescence under ultraviolet light observed throughout the interval.

TS 5289.8', TS 5288.26', TS 5288.9', TS 5286.72', TS 5287.2', TS 5285.64', TS 5284.8', TS 5283.2', TS 5282.2', TS 5281.4'

3rd order Sequence 2 boundary at 5280.4' (dark olive gray/olive black organic rich seam (mud) 0.01' thick).

5280.4' – 5278.8' = Facies #1. Dolomitized bioturbated mudstone. Mottled light olive gray to olive gray, yellowish gray, grayish red, very light gray to medium light gray, dark gray. Moderate bioturbation throughout the interval. Horizontal burrow ranges from 1 mm to 5 mm in size scattered throughout the interval. Very fine grained cherty, dolomitized mudstone. Olive black laminations present at 5280.4' – 5280.05' (~.01' thick). Partially healed vertical fractures (0.05' long) present at 5279.8' – 5279.9', and 5278.8'. Fossils not visible in hand sample. No visible porosity. Oil staining and fluorescence under ultraviolet light observed throughout the interval.

TS 5279.94', TS 5279.4'

5278.8' – 5273.8' = Facies #4, Facies #3 and Facies #2. Bioturbated skeletal grainstones to packstones with intermittent burrowed wackestones. Mottled light olive gray to olive gray, yellow gray, very light to medium dark gray, brownish gray. Moderate bioturbation. Horizontal burrows range from 1 mm to 30 mm in size throughout the interval. Medium to fine grained cherty, dolomitic, bioturbated and skeletal grain rich to mud rich packstones and wackestones. Burrowed wackestone intervals at 5278.8' – 5277.9', 5276.8' – 5276.3' and 5274.6' – 5274.4'. Bioturbated packstone interval present at 5276.3' – 5276.1', 5275.6' – 5275.4' and 5274.4' – 5274.0'. Grayish brown to brownish gray color surrounds bioturbation throughout the interval between 5276.2' – 5274.4'. Sand sized crinoids visible (~1 mm) at 5277.6' - 5277.8'. Horizontal stylolites at 5274.8' and 5274.65'. Open vertical fracture at 5276.4' (0.6' long). Open vertical fractures (0.1' long) at 5277.0', 5275.5', and 5274.5'. Fracture and vuggy porosity visible at 5274.6'. Oil staining and fluorescence under ultraviolet light observed throughout the interval.

TS 5278.66', TS 5277.74', TS 5276.1', TS 5277.3', TS 5275.66', TS 5275.94', TS 5274.4'

5273.8' – 5267.5' = Facies #3 and Facies #4. Bioturbated packstones with intermittent skeletal grainstones. Mottled light olive gray to olive gray, yellow gray, very light to medium

dark gray, brownish gray. Moderate bioturbation. Horizontal burrows range from 5 mm to 30 mm in size throughout the interval. Vertical burrow present at 5268.85' (0.05' long). Medium grained cherty, dolomitic, bioturbated and skeletal grain rich to mud rich packstones. Skeletal grainstone interval 5273.4' – 5272.3'. Grayish brown to brownish gray color surrounds bioturbation throughout the interval. Medium sand sized crinoids visible (~1 mm) at 5273.8' - 5273.9', 5272.1' – 5271.2', 5271.9' – 5270.86'. Horizontal stylolites at 5268.5' and 5268.3' and 5268.2'. Sand-sized pyrite crystal visible at 5268.5'. Open vertical fracture at 5273.0' (0.2' long). Open vertical fractures (2/ft., 0.1' long) throughout interval between 5272.1' – 5268.5'. Oil staining and fluorescence under ultraviolet light observed at 5274.4' - 5272.2', 5271.5' - 5271.1', 5270.8' – 5269.0' and 5268.2' – 5267.5'.

TS 5273.56', TS 5273.86, TS 5271.16', TS 5270.2', TS 5269.8'

5267.5' – 5263.0' = Facies #4. Skeletal grainstones to packstones. Mottled light olive gray to olive gray, yellow gray, very light to medium dark gray, brownish gray, pinkish gray, blueish white. Moderate bioturbation. Burrows range from 1 mm to 3 cm in size throughout the interval. Medium grained cherty, slightly bioturbated skeletal grain rich to mud rich packstones. Grayish brown to brownish gray color surrounds bioturbation throughout the interval. Horizontal stylolites at 5266.96', 5266.5, 5266.4', 5265.6', 5265.3', 5264.8', 5264.3', 5264.4', 5264.2'. Fossil fragments not visible in hand sample. Oil staining and fluorescence under ultraviolet light observed at 5267.5' – 5265.55', 5264.75' – 5263.85', 5263.6' – 5263.0'.

TS 5267.5', TS 5265.16', TS 5264.14', TS 5263.2'

5263.0' – 5252.5' = Facies #3 and Facies #4. Bioturbated skeletal grain rich packstones. Mottled light olive gray to olive gray, yellow gray, very light to medium dark gray, brownish gray. Moderate bioturbation. Horizontal burrows range from 1 mm to 50 mm in size throughout the interval. Vertical burrows at 5253.9' (0.2' long) and 5253.3' (0.25' long). Medium grained cherty, slightly bioturbated skeletal grain rich to mud rich packstones. Intervals of skeletal packstones to grainstone at 5262.1' – 5261.8' and 5260.7' – 5260.2'. Grayish brown to brownish gray color surrounds bioturbation throughout the interval. Light olive green gray laminations (0.02' thick) present at 5161.95', 5161.9' and 5260.2'. Medium sand-sized crinoids visible at 5260.55'. Horizontal stylolites at 5262.3', 5262.2', 5260.8', 5260.7', 5260.5', 5258.8', 5258.5', 5258.4', 5258.1', 5256.95', 5256.5', 5256.1', 5255.5', 5255.4', 5255.2', 5254.9', 5254.4', 5254.2', 5252.9', 5252.8', 5252.7' and 5252.25'. Healed vertical fractures (0.45' long) at 5259.55' (6), 52529.0 (4). Healed vertical fractures (0.07' long) at 5254.5' (5), 5254.1' (4), and 5253.8' (3). Oil staining and fluorescence under ultraviolet light observed at 5263.0' – 5262.55', 5261.8' – 5261.0', 5260.5' – 5260.4' and 5260.1' – 5252.5'.

TS 5262.86', TS 5261.5', TS 5262.1', TS 5260.66', TS 5259.2', TS 5258.66', TS 5258.4', TS 5257.2', TS 5257.8', TS 5256.44', TS 5256.56' TS 5255.5', TS 5255.9', TS 5253.3', TS 5254.7'

5252.5' – 5243.0' = Facies #4, Facies #3 and Exposure. Skeletal grainstones with intermittent bioturbated packstones. Mottled light olive gray to olive gray, yellow gray, very light to medium dark gray, brownish gray, pinkish gray, blueish white. Moderate bioturbation. Burrows ranges from 1 mm to 3 cm in size throughout the interval. Medium grained cherty, slightly bioturbated skeletal grain rich to mud rich packstones. Bioturbated packstone interval at 5249.6' – 5249.2' and 5247.2' – 5246.9'. Grayish brown to brownish gray color surrounds bioturbation throughout the interval. Light olive green clay present at 5244.1' – 5243.9' (Exposure related). Fossil fragments not visible in hand sample. Horizontal stylolites at 5251.1', 5251.7', 5250.75', 5250.55', 5250.4', 5250.2', 5248.9', 5248.3', 5245.9', 5243.5'. Open vertical fracture at 5251.1' (0.2' long). Healed vertical fractures (0.1' - 0.2' long, 5-7/ft.) throughout interval between 5250.1' – 5245.95', 5245.1' – 5244.1' and 5243.8' – 5243.0'. Oil staining and fluorescence under ultraviolet light observed at 5151.45' – 5250.8', 5250.0' – 5244.1', 5243.82' – 5243.0'.

TS 5250.6', TS 5249.5', TS 5248.8', TS 5247.2', TS 5246.9', TS 5246.5', TS 5245.4', TS 5244.8', TS 5244.0', TS 5243.2'

5243.0' – 5230.0' = No recovery. 3rd order sequence 3 boundary from GR log at 5241.0'.

5230.0' – 5207.0' = Exposure Interval and Facies 4. Silicified skeletal grainstones to packstones. Brecciated pale yellowish green, pale olive, light olive gray, yellowish gray, very light to medium dark gray, brownish gray, pinkish gray, white to blueish white, grayish red purple, greenish gray, very dark red, olive black. No visible bioturbation. Very coarse to fine grained silicified, brecciated, skeletal grain rich to mud rich packstones with skeletal mud rich packstones at 5217.0' – 5214.0'. Collapse breccia at 5221.5' – 5222.0'. Breccia clasts throughout interval are sub angular, ranging 1 – 5 cm in size. Solution pipe 5226.1' – 5225.0'. Light olive green clay at 5226.2', 5219.9'. Pyrite nodules (0.5mm) at 5212.3' – 5212.8'. Bryozoan fragments at 5226.9' (1 cm) and mold (~2 cm) visible at 5222.8'. Partially healed vertical fractures (0.1' – 0.4' long) at 5229.2' (2), 5228.8' – 5228.5' (12), and 5226.6' – 5226.3' (4). Rubbled interval 5211.9' – 5207.0'. Vuggy and mold porosity (less than 1mm – 1.5cm in size) visible in hand sample at 5229.4' – 5229.3', 5229.0' – 5228.5', 5227.7' – 5227.1', 5226.9', 5225.9' – 5225.2', 5224.8', 5224.0' - 5222.5', 5220.0' – 5219.0', 5218.8' – 5216.1'. Dark oil staining in plain white light at 5229.7' – 5229.3', 5225.1', 5219.0', and 5218.6'. Oil staining and fluorescence under ultraviolet light observed 5230' – 5228.2', 5227.84' – 5222.6', 5221.56' – 5220.45', 5219.9' – 5218.2', 5218.0 – 5217.8', 5213.0' – 5211.9', 5208.4' – 5208.0'. Contact with Mississippian/Pennsylvanian unconformity base at 5207.0'.

TS 5227.4', TS 5226.8', TS 5225.8', TS 5221.7', TS 5219.8', TS 5219.3', TS 5218.5'

3rd order Sequence 4 boundary at 5207'.

Core #2: Albus 1-34H - Chesapeake Energy

Woods County, OK

Cored Interval: 5110.0' – 5201.1'

Examined Interval: 5123.98' – 5201.1'

Base of Penn. /Miss. Unconformity: 5123.98' (from core)

Formation: “Mississippian Limestone”

5201.1' – 5195.2' = Facies #3 and Facies 2. Bioturbated packstones with intermittent burrowed wackestones. Mottled medium gray to dark gray, with olive gray and light bluish gray chert. Moderate bioturbation with horizontal burrows ranging from 1 to 5 mm in size with differential compaction throughout the interval. Scattered, light bluish gray chert nodules at 5197.5' and 5196.0' – 5195.2'. (~2 cm in diameter). One vertical burrow present at 5197.5' and 5196.8' (0.1' long). Fine to medium grained cherty, dolomitic, burrowed wackestone to packstone. Burrowed wackestones at 5198.7' – 5197.1', 5195.8' – 5195.2'. Sand-sized pyrite crystal present at 5200.9'. Medium sand-sized crinoid fragments present at 5200.6', 5200.4', 5197.3' – 5197.0'. Thin shelled bivalve shell fragments (5mm to 1 cm) at 5198.6', 5197.8' – 5195.2'. Healed (calcite) vertical fractures (~0.02') present at 5200.8' (3) and 5197.4 (2). No visible porosity. Oil staining and fluorescence under ultraviolet light observed from 5200.5' – 5198.2' and bright fluorescence observed from 5198.0' – 5195.2'. Base of Core.

TS 5197.2'

5195.2' – 5182.35' = Facies #2. Burrowed wackestones to packstones. Mottled medium gray to dark gray, light olive gray to olive gray, yellowish gray, blueish white. Moderate to common bioturbation. Horizontal burrows ranging from 1 - 3 mm in size at throughout interval, from 5 mm to 3 cm in size at 5194.2' – 5190.5', 5189.7' – 5187.2', and 5186.2' – 5182.7'. Vertical burrows (0.1' long) at 5194.8', 5193.6', 5190.2', 5185.8', 5185.8', 5183.4', 5182.6'. Fine to medium grained cherty, dolomitic, burrowed wackestone to mud rich packstone. Olive black laminations surrounding burrows at 5193.5 – 5193.1', 5191.9' – 5191.7' and 5189.8' – 5189.6'. Scattered, light bluish gray chert nodules throughout the interval (~1 inch in diameter) with differential compaction. Medium sand-sized crinoid fragments present at 5195.2', 5194.8', 5193.5', 5192.9', 5190.68', 5187.6', 5183.02' and 5182.6'. Bivalve shells (2 mm – 8 mm) present at 5194.5', 5193.0' and 5189.3'. Sand sized-pyrite crystals present at 5183.02' and 5182.4'. Partially healed (calcite) vertical (2, ~0.3' – 0.2' long) present at 5195.2 – 5194.8', 5192.7' – 5192.5'. Calcite nodules (2 cm in diameter) at 5191.8' and 5189.8'. No visible porosity. Oil staining and fluorescence under ultraviolet light observed from 5195.2' – 5188.0', 5185.0' – 5182.35' and bright fluorescence from 5187.8' – 5185.2'.

TS 5194.8', TS 5189.2'

5182.35' – 5167.9' = Facies #3 and Facies #2. Bioturbated packstones with intermittent burrowed wackestones and mudstones. Mottled light gray to dark gray, light olive gray to olive gray, yellowish gray, reddish gray and olive black. Moderate to common bioturbation throughout interval. Horizontal burrows ranging 2 mm – 3 cm at 5182.35' – 5169.8'. Horizontal burrows ranging from 1 to 3 mm in size at 5169.2' – 5169.0'. Vertical burrows present at 5180.3' (0.1' long), 5177.65' (0.2' long), 5175.7' (0.1' long), and 5168.3' (0.2' long). Dark blueish gray chert infilling burrows at 5180.1', 5179.8' – 5179.35', 5178.2 – 5177.9', 5175.8', 5174.2', 5172.55' – 5172.0', 5171.7' - 5171.3', 5168.9' – 5168.7', 5168.5' – 5168.4' (reddish gray surrounding burrows), and 5168.2' – 5168.0'. Fine to medium grained cherty, dolomitic, bioturbated mud rich packstone to wackestone. Olive black laminations around burrows at 5181.9' - 5181.7'. Dark olive gray laminations present at 5167.95 – 5167.9'. Medium sand-sized crinoids present at 5179.35', 5178.4', 5177.8' – 5177.7', 5176.1', 5175.6', 5172.4' – 5172.1', 5170.6', 5169.5' – 5169.1' and 5168.9' – 5168.8'. Ostracodes (1cm) at 5181.8', 5181.45' and 5181.4'. Thin shelled bivalves (5mm) at 5181.7', 5178.2' and 5174.8'. Cement filled vertical fracture at 5182.3' (~0.3' long). Pyrite crystal present at 5179.5'. Potential traction currents at 5175.9'. Vuggy/moldic porosity visible at 5173.35'. Rubbled interval at 5170.0' – 5169.0'. Oil staining and fluorescence under ultraviolet light observed at 5178.2' – 5176.5', 5173.0' – 5172.5', 5169.0' – 5167.9' and bright fluorescence at 5181.0' – 5178.6', 5176.2' – 5172.5'.

TS 5181.1', TS 5173.4'

5167.9' – 5164.5' = Facies #1, Facies #2 and Facies #3. Bioturbated mud rich packstones with intermittent burrowed mud rich packstones and dolomitized mudstone. Mottled yellowish gray, greenish gray, light greenish gray, medium gray, grayish red, light olive gray to olive gray and olive black. Fine to medium grained cherty, dolomitic, bioturbated mud rich to packstones with intermittent fine grained dolomitic mudstones. Laminated bedding features at 5167.8' and 5167.7'. Dark blueish gray chert infilling burrows at 5164.9'. Grayish red color (oil or iron) surrounding bioturbation at 5167.2' – 5166.9', 5166.6' – 5166.2', 5165.0' – 5164.4'. Healed vertical fractures at 5167.8' (0.2' long), 5166.05' (0.05' long), 5164.5' (4, 0.05' long). Missing interval 5166.0' – 5165.18'. No visible porosity. Oil staining and bright fluorescence under ultraviolet light observed in moderately bioturbated zones where chert is absent (5167.9' – 5166.0', 5165.1' – 5164.5').

3rd order Sequence 1 boundary at 5164.5'.

TS 5166.4'

5164.5' – 5153.8' = Facies #4 and Facies #1. Skeletal packstones to grainstones with intermittent mudstones and bioturbation. Mottled yellowish gray, greenish gray, light greenish gray, medium gray, grayish red, pale greenish yellow, light olive gray. Moderate bioturbation. Horizontal burrows ranging from 1 to 3 cm in sized in select intervals (5162.7' – 5162.5', 5161.9 – 5161.8'). Vertical burrow (0.02' long) present at 5163.5'. Medium to coarse

grained, cherty skeletal mud rich to grain rich packstones and grainstones with intermittent fined grained mudstones. Dark blueish gray chert infilling burrows at 5164.5', 5162.4', and 5161.2'. Grayish red color (possible iron or oil) surrounding bioturbation at 5163.9', 5163.6' – 5163.2', 5162.95' – 5162.8', 5162.4' – 5162.2', 5161.9' – 5160.9', 5160.6' – 5159.8'. Healed vertical fractures at 5163.5 (3, 0.15' long), 5162.9' – 5162.7' (3), 5160.36' – 5160.0 (10+, 0.02' long, calcite healed). Greenish gray lamination features (~0.1' thick) present at 5160.4' and 5159.7', 5154.1' – 5153.8'. Medium sand-sized shell fragments present at 5160.8'. Sand sized pyrite crystals present at 5161.2'. No visible porosity. Oil staining and fluorescence under ultraviolet light observed in moderately bioturbated zones where chert is absent (5164.55' – 5160', 5159.8' – 5158.9', 5157.2' – 5153.8'). Oil staining and bright fluorescence under ultraviolet light observed at 5164.5' – 5163.2'.

3rd order Sequence 2 boundary at 5153.8' (green argillaceous interval).

TS 5163.1', TS 5159.5'

5153.8' – 5135.2' = Exposure, Facies #1, Facies #4 and Facies #2. Exposure interval with intermittent skeletal grainstones, mudstones and burrowed wackestones. Mottled, brecciated light gray to dark gray, light olive gray, grayish red, pale greenish yellow, brownish gray. Horizontal burrows ranging from 1 to 2 cm visible at 5136.5' – 5135.2'. Medium grained cherty, subaerially exposed skeletal grainstones with burrowed packstones and mudstones. Overall brecciated appearance with sub angular clasts ranging 0.5cm – 4cm. Solution pipe at 5151.3 – 5152.0'. Greenish yellow clay fill at 5141.2' – 5140.1'. Open fractures (0.01' – 0.02' long, 10+) present within sub angular clasts throughout the interval. Grayish red color (possible iron or oil stain) surrounding clasts at 5149.2' – 5141.0', 5135.5' – 5135.2'. Coarse sand-sized crinoids present at 5147.9', 5147.5', 5144.75' and 5137.5'. Brachiopod fragments visible at 5137.1'. Vuggy porosity (up to 1mm) visible at 5149.4', 5148.0' – 5147.0', 5145.9', 5145.7', 5141.4' – 5140.0', 5137.9' – 5137.0'. Oil staining and fluorescence under ultraviolet light observed in throughout interval (5153.8' – 5143.5', 5142' – 5141', 5140.5' – 5135.2).

3rd order Sequence 3 boundary 5135.2'.

TS 5152.9', TS 5149.8', TS 5148.7' TS 5147.7', TS 5147.4', TS 5145.7', TS 5144.4', TS 5143.8', TS 5143.5', TS 5141.6', TS 5138.3', TS 5138.3', TS 5136.6', TS 5136.2'

5135.2' – 5123.98' = Exposure interval and Facies #4. Silicified skeletal grainstones.

Brecciated pale yellowish green, pale olive, light olive gray, yellowish gray, very light to medium dark gray, brownish gray, pinkish gray, white to blueish white, grayish red purple, greenish gray, very dark red. No visible bioturbation. Very coarse to fine grained silicified, brecciated, skeletal grainstones with coarse grained skeletal grainstones at 5127.2' and 5125.8'. Interval rubbled. Collapse breccia at 5127.5' – 5127.0'. Breccia clasts throughout interval are sub angular, ranging 1 – 5 cm in size. Light olive green clay at 5130.8', 5127.5' – 5127.2'. Coarse sand-sized crinoids at 5133.7', 5133.1', 5131.1', 5127.2', 5126.1', 5125.8' and 5124.5'.

Horizontal stylolite at 5129.9'. Vuggy and moldic porosity (less than 1mm – 15mm in size) visible in hand sample at 5133' – 5131', 5129'. Dark oil staining in plain white light at 5133.5', 5130.5' and 5129.5' – 5129.0'. Oil staining and fluorescence under ultraviolet light observed 5135.2' – 5130.0', 5129.8' – 5128.5', 5127.95' – 5127.6', 5127.2' – 5126.8', 5125.1' – 5124.2'. Contact with Mississippian/Pennsylvanian unconformity base at 5123.98'.

3rd order Sequence 4 boundary at 5123.98'.

TS 5133.9', TS 5131.9'

Core #3: Trophy Farms 32-34-16 1H - Chesapeake Energy

Comanche Co., Kansas

Cored Interval: 5260' – 5459.96'

Examined Interval: 5269.8' – 5459.6'

Top “Mississippian Limestone”: 5269.8” (from core)

Formations: “Mississippian Limestone” and Pennsylvanian

5456.96' – 5407.0' = Facies #1, Facies #2, Facies #3 and Facies #4. Skeletal grainstones to packstones with intermittent wackestones. Grayish pink, dusky yellowish green, grayish green, olive black. Horizontal burrows ranging from 2 mm to 1 cm in size at 5424.7' - 5424.5' and 5422.95' - 5422.8'. Very coarse to medium sand-sized skeletal grainstones and packstones with mud rich packstones to wackestones with abundant stylolites. Intervals of wackestones (Facies #1) at 5456.45' – 5455', 5427.5' – 5427.4', 5418.35' – 5417.35' and 5414.3' – 5413.0'. Coarse and medium sand-sized crinoid fragments present throughout interval at 5449.2', 5456.96' – 5452.2', 5451.6', 5450.8', 5450.0' and 5449.0' – 5407.0'. Bivalves and bryozoans (1cm – 2cm) scattered throughout 5451' – 5407.0'. Banded bedding feature at 5436.45' – 5438.25', 5436.2' – 5432.8'. Partially filled (calcite) vertical fractures (~0.2' – 0.5' long) present at 5441.1', 5439', 5437.8', 5436.8', 5431.3', 5424.7', 5420.25' (clay fill), 5417.2', and 5410.8'. Open vertical fractures at 5439.65' - .1', 5436.0' – 5435.5' and calcite filled ptigmatic fracture at 5432.95' – 5432.7'. Horizontal stylolites present throughout the interval. Organic rich seam at 5252.2', 5418.3' - .1', 5407.0'. Visible moldic and vuggy porosity (2mm – 1 cm) at 5456' – 5454', 5452.8', 5454.2', 5451.2', 5449.6', 5448.8', 5448.2', 5447.8', 5447.4', 5447.1', 5446.9', 5446.8', 5446.5', 5446.4', 5446.2', 5445.5', 5445.2', 5443.3', 5443.2', 5442.8' - .6', 5442.3' - 5442.0', 5440.2', 5439.9', 5439.85', 5439.05', 5435.05', 5436.8', 5436.5' - 5436.0', 5436.0' – 5434', 5433.3' - 5433.0', 5430.7' – 5429.0', 5423.8' - 5423.6', 5423.0' - 5422.0', 5421.3' – 5421.3', 5421.0' – 5420.0', 5418.5' – 5418.2', 5414.3' – 5414.3' and 5408.9. Rubbled intervals

at 5432.7' – 5432.3', 5428.95' – 5428.6' and 5427.2' – 5426.6. Oil staining and fluorescence under ultraviolet light observed throughout interval. Base of Core.

3rd order Sequence 1 boundary 5407.0.

TS 5474.74', TS 5454.2', TS 5453.74', TS 5452.3', TS 5451.04', TS 5449.6', TS 5448.28', TS 5447.66', TS 5446.88', TS 5446.16', TS 5445.74', TS 5445.06', TS 5444.14', TS 5442.86', TS 5442.3', TS 5440.88', TS 5439.82', TS 5438.5', TS 5436.32', TS 5435.36, TS 5435.18', TS 5434.34', TS 5433.7', TS 5433.04', TS 5430.64', TS 5430.12', TS 5429.62', TS 5429.12', TS 5427.32', TS 5425.84', TS 5424.68', TS 5423.36', TS 5422.6', TS 5421.52', TS 5420.44', TS 5419.2', TS 5416.84', TS 5415.14', TS 5413.12', TS 5411.46', TS 5408.52', TS 5407.84'

5407.0' – 5373.6' = Facies #3, Facies #2, Facies #4 and Facies #1. Skeletal grain rich packstones to grainstones with intermittent wackestones. Grayish pink, dusky yellowish green, grayish green, olive black. Stylolitic coarse to medium grained skeletal packstone to grainstones with fracturing and intermittent wackestones. Intervals of wackestones at 5402.15' – 5401.9', 5394.1' – 5392.5' and 5374.5' – 5374.0'. Organic seams present at 5407.0', 5402.2', 5389.2', 5381.1', 5374.45', and 5373.6' – 5373.3'. Mottled grayish green interval at 5386.9' – 5386.0'. Coarse to medium sand sized crinoid fragments present throughout the interval. Bryozoans and bivalve fragments (3 mm – 3 cm) visible sporadically throughout the interval. Partially healed (calcite) and healed vertical (~0.3 – 0.5' long) present at 5407.7', 5400.9' (6), 5398.95' (6), 5398.0' (10+), 5392.8' (6), 5392.0' – 5388.3', 5387.9' – 5385', 5382.9', 5379.1', 5378.2' and 5375.7' – 5374.2'. Rubbled intervals at 5397.35' – 5395.9'. Moldic and vuggy porosity visible at 5403.0' – 5402.0', 5399.0' – 5398.0', 5393.0' – 5392', 5387.2', 5376.2'. Oil staining and fluorescence under ultraviolet light observed throughout interval except at 5374.0' – 5373.6'.

3rd order Sequence 2 boundary at 5373.6'.

TS 5405.58', TS 5404.5', TS 5403.7' TS 5400.78', TS 5398.26', TS 5395.7', TS 5393.86', TS 5392.22', TS 5390.68', TS 5389.66', TS 5386.76', TS 5384.6', TS 5382.6', TS 5380.9', TS 5379.5', TS 5378.14', TS 5376.36', TS 5375.04', TS 5373.36'

5373.6' – 5342.9' = Facies #3, Facies #2, Facies #4 and Facies #1. Skeletal grain rich packstones to grainstones with intermittent wackestones. Grayish pink, dusky yellowish green, grayish green, reddish gray, olive black. Fine to very coarse grained stylolitic grain rich packstone to grainstones with localized wackestones. Intervals of wackestone to mud rich packstones at 5373.6' – 5372.2', 5371.7' – 5371.55', 5362.9' – 5362.5', 5354.75' – 5353.6', 5348.7' - 5348.0' and 5344.4' – 5343.9'. Coarse to medium sand sized crinoid fragments present throughout the interval along with sporadic bivalves and bryozoans (2 mm – 3cm). Rubbled interval at 5366.0' – 5365'. Organic rich seam at 5344.35, 5344.2' and 5342.9'. Partially healed and healed (calcite) vertical (~0.1' – 0.4' long) fractures present at 5371.3' – 5342.9'. Calcite cement filled fracture (0.2' long) at 5363.15', 5360.8', and 5353.2'. Visible moldic and vuggy

porosity at 5366.7' - 5366.5', 5362.98' - 5362.7', 5360.7', 5358.5' - 5358.0', 5354.9', 5352.2' - 5352.0', 5343.0' - 5342.0'. Fluorescence under ultraviolet light observed throughout interval except at 5372.5' - 5372.0', 5371.75' - 5371.6', 5354.75' - 5353.9', 5348.7' - 5348.5'.

3rd order Sequence 3 boundary 5342.9'.

TS 5370.82', TS 5369.4', TS 5368.28', TS 5367.14', TS 5364.62', TS 5363.42', TS 5361.24', TS 5358.98', TS 5357.36', TS 5356.36', TS 5355.6', TS 5354.42', TS 5353.18', TS 5352.4', TS 5351.08', TS 5350.14', TS 5349.08', TS 5347.5', TS 5345.06', TS 5343.12'

5342.9' - 5269.8' = Exposure, Facies #3 and Facies #2. Subaerial exposure with intermittent skeletal grain rich packstones to grainstones. Olive black, yellow green, grayish red, yellow gray, olive gray. No recovery at 5335.0' - 5334.34', 5280.0' - 5270.0'. Intervals of skeletal packstones to grainstones at 5341.25' - 5340.9', 5339.54' - 5338.0', 5337.6' - 5336.2', 5334.34' - 5333.1', 5332.7' - 5329.9', 5314.0 - 5313.45'. Very coarse to fine grained brecciated, exposure horizon with skeletal grain packstones to grainstones. Coarse sand-sized crinoid fragments present at intervals of skeletal packstones to grainstones and 5328.0' - 5327.5'. Bryozoan fragments visible at 5321.6'. Breccia clasts throughout interval are subangular, range 1 - 5 cm in size. Terra rosa at 5341.7' - 5341.3', 5340.5' - 5340.0', 5339.9', 5338.1' - 5337.6', 5322.7' - 5322.4', 5321.2' - 5321.0', 5320.6' - 5319.8'. Rubbled interval 5333.0' - 5332.8', 5330.9' - 5329.0'. Oil staining and fluorescence under ultraviolet light observed at 5341.25' - 5340.9', 5339.54' - 5338.0', 5337.6' - 5336.2', 5334.34' - 5333.1', 5332.7' - 5329.9', 5314.0 - 5313.45'. Pennsylvanian/ Mississippian Unconformity base at 5330.9'. Pennsylvanian Shale base at 5269.8'.

3rd order Sequence 4 boundary at 5269.8'.

TS 5336.62', TS 5331.68'

SEQUENCE STRATIGRAPHIC FRAMEWORK SUMMARY

Third Order Sequences

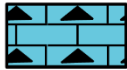



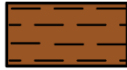

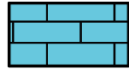
S4 in Core #1 and #2 was mostly comprised of an exposure interval, except at 5217.0' – 5214.8' in Core #1 where Oklahoma Facies 4 was identifiable in core and 5315.2' – 5315.1', 5126.8' – 5126.4' and 5126.0' – 5126.8' in Core #2, where Oklahoma Facies 2 and Oklahoma Facies 4 (respectively) were discernable in core. S4 in Core #3 was also dominated by an exposure interval, except at 5341.06' and 5339.8' – 5337', where Kansas Facies 3 was identifiable in core within the exposure interval, as well as 5337.5' – 5333.0' and 5332.8' – 5330.8', where Kansas Facies 2 was discernable in core. S2 and S4 in Core #1 and #2 show the most drastic thickness change. This could be due to the cores being oblique to strike/dip, potential structural influence from the Central Kansas Uplift and local antecedent topography affecting the accommodation space available.

Fourth Order High-Frequency Sequences

















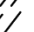


In Core #1 and #2, the HFS in 3rd order S1 and S2 consisted mainly of Oklahoma Facies 2 and 3. The HFS in 3rd order S3 consisted primarily of Oklahoma Facies 3 and 4, with Oklahoma Facies 1 occurring at the base of the first HFS within S3. S4 in Core #1 and Core #2 exhibited areas (5217.0' – 5214.8' in Core #1, 5315.2' – 5315.1', 5126.8' – 5126.4', 5126.0' – 5126.8' in Core #2) where Oklahoma Facies 2 and 4 were discernable from the exposure features and three HFS boundaries were picked at these locations. In Core #3, the HFS in 3rd order S1, S2 and S3 consisted of all four Kansas facies, with the majority of S1 containing Kansas Facies 4. The majority of the 3rd order S4 in Core #3 was an exposure interval and only two HFS were readily identifiable in core that consisted of Kansas Facies 3 and 2 (5341.06', 5339.8' – 5337', 5337.5' – 5333.0' and 5332.8' – 5330.8').

APPENDIX B
GRAPPHICAL CORE DESCRIPTIONS

LITHOLOGIC SYMBOLS

	Cherty Limestone		Calcareous Shale		Dolomite		Clay
	Shale		Sandstone		Limestone		

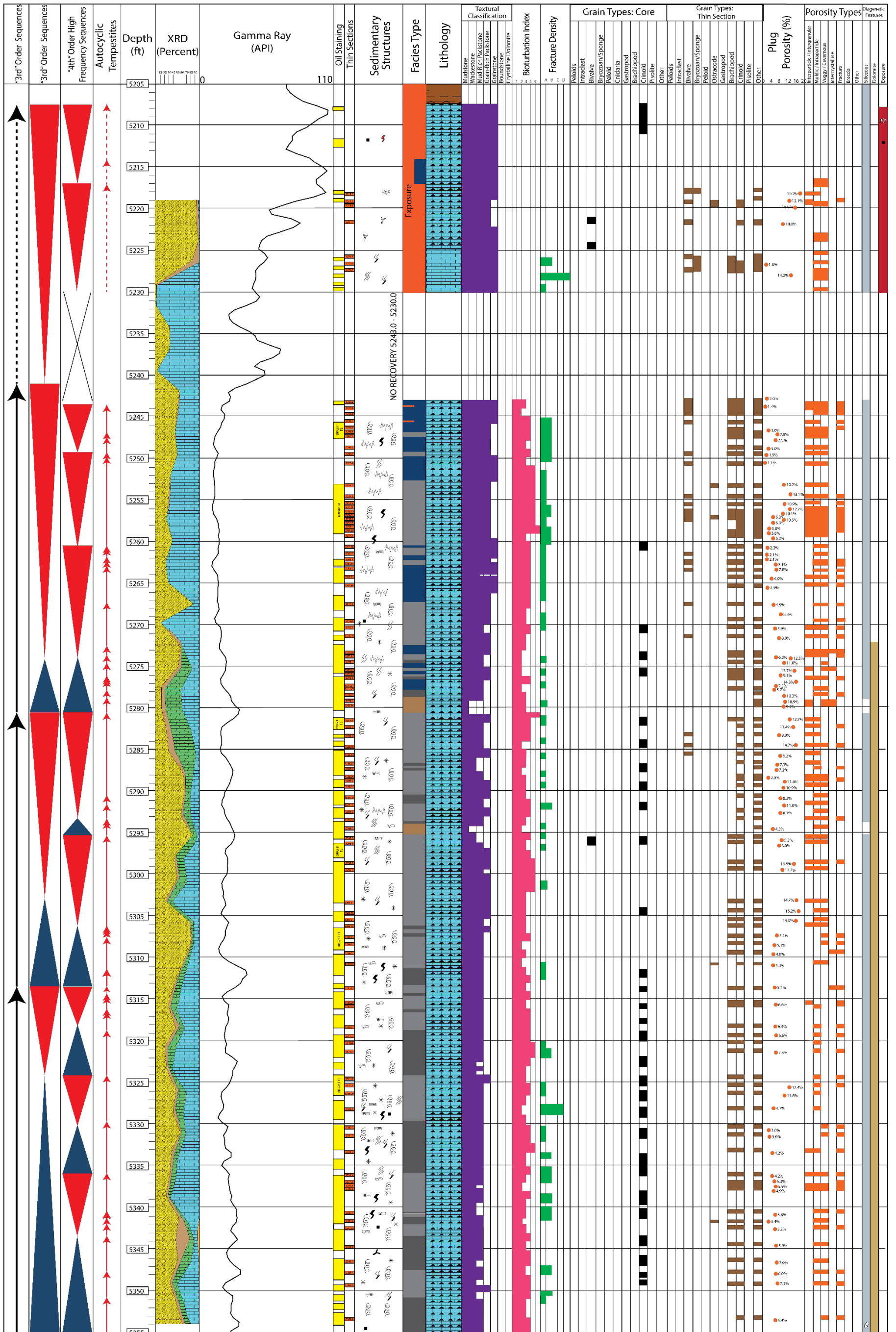
GRAIN TYPES, SEDIMENTARY STRUCTURES AND DIAGENETIC FEATURES

<ul style="list-style-type: none">  Brachiopod  Bryozoon  Crinoid  Sponge Spicules  Undifferentiated Fossils  Pyritic 	<ul style="list-style-type: none">  Burrowed  Stylolitic  Stylolite Swarms  Organic-Rich Seam  Erosional Surface  Exposure Surface  Brecciated Zone 	<ul style="list-style-type: none">  Brecciated  Open Fracture  Fracture Swarm  Partially Filled Fracture  Cement Filled Fracture  Silicious Nodule
---	---	--

Bann #1-14, Woods County, Oklahoma

Formation: Mississippian Limestone Depth Interval: 5205'-5355'

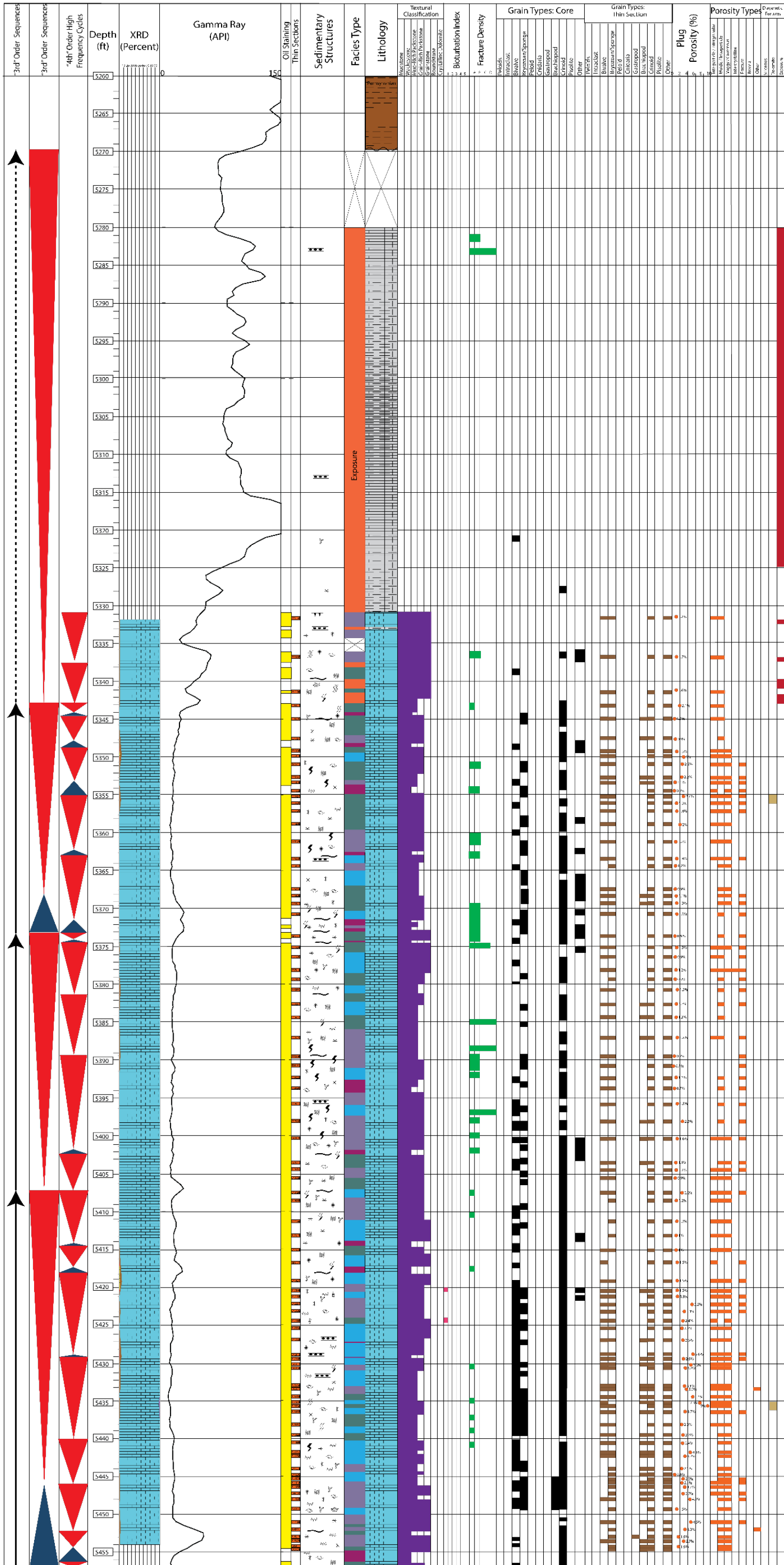
Core #1



Trophy Farms 32-34-16 1H Comanche County, Kansas

Formation: Mississippian Limestone Depth Interval: 5260'-5459.96'

Core #3

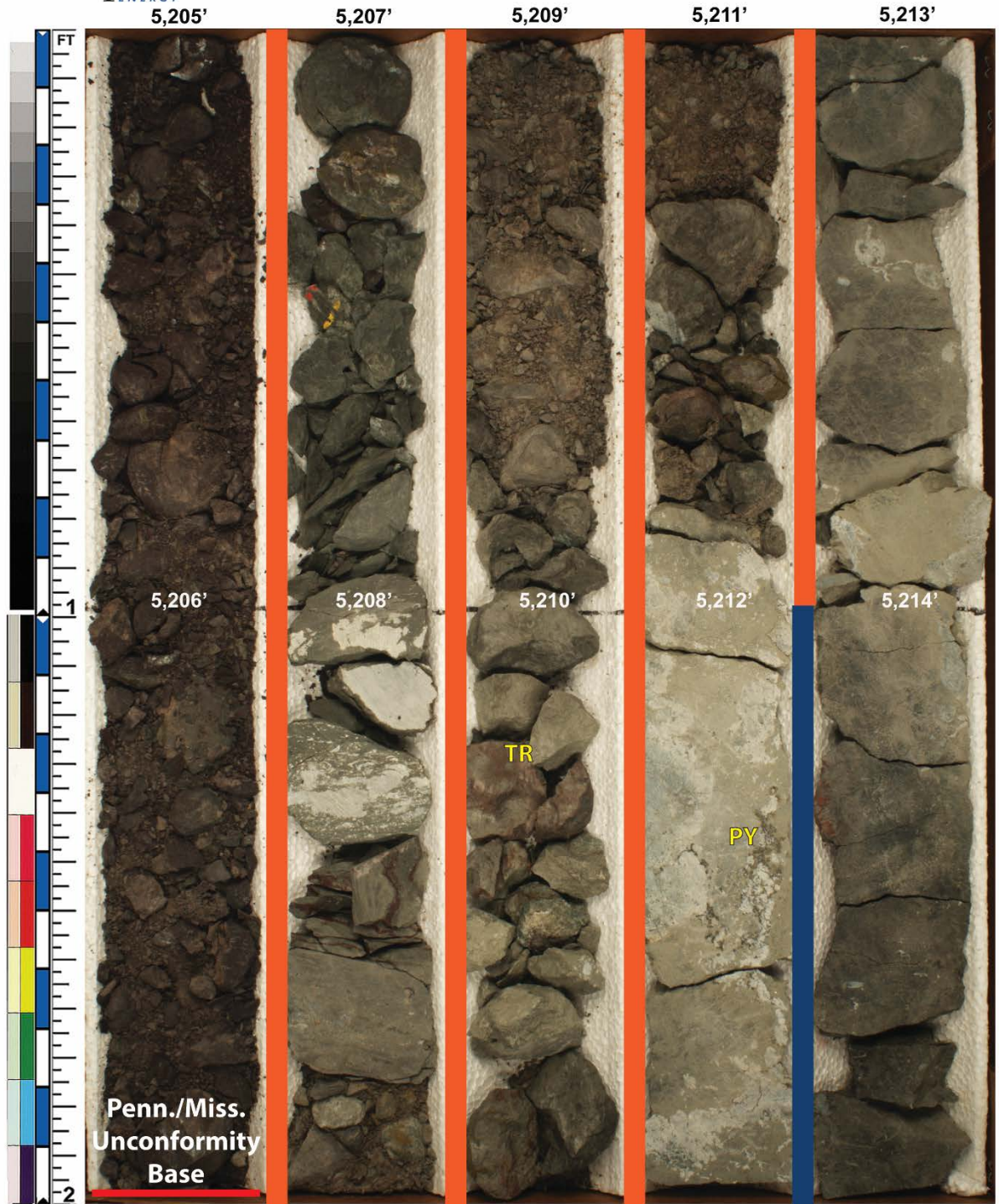


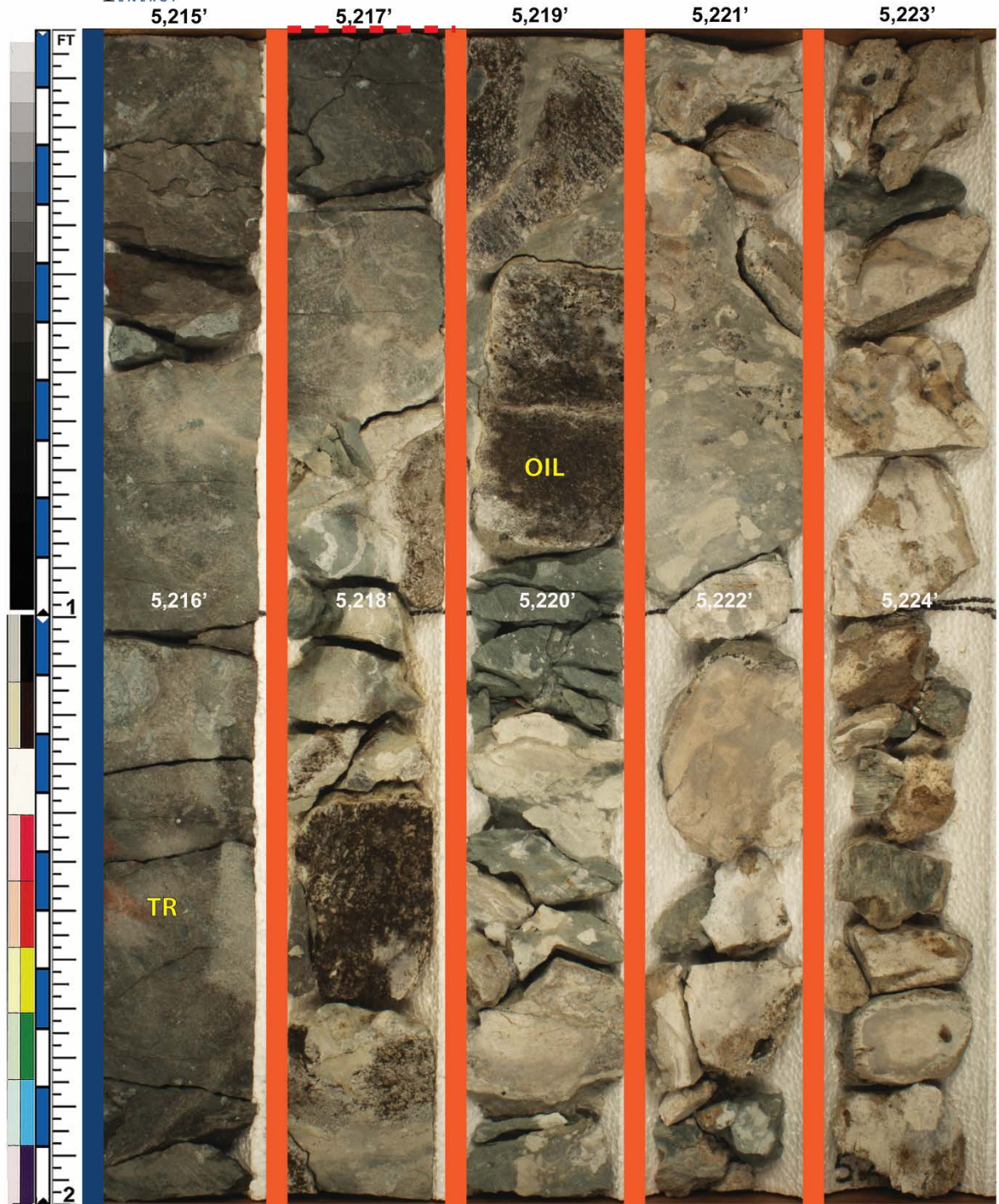
APPENDIX C
WHOLE CORE PHOTOGRAPHS

Core photographs are shown in white light and ultraviolet light and labeled with the abbreviations in the chart below. All cores are photographed in boxes with the shallowest depth at the top left and deepest depth at the bottom right. Each core box represents 10 feet of core and are divided into 2 foot sections. The scale to the far left is in tenths of feet. To the left of each foot intervals, facies types are shown in a colored box. The color corresponds to the color associated with the stacking pattern colors. The base of the Pennsylvanian is represented by a solid yellow line in Core #3. 3rd order sequence boundaries and the base of the Pennsylvanian/Mississippian unconformity are represented by a solid red lines in Core #1 and #2. 4th order high-frequency sequence boundaries and the Pennsylvanian/Mississippian unconformity base for Core #3 are represented by a dashed red line.

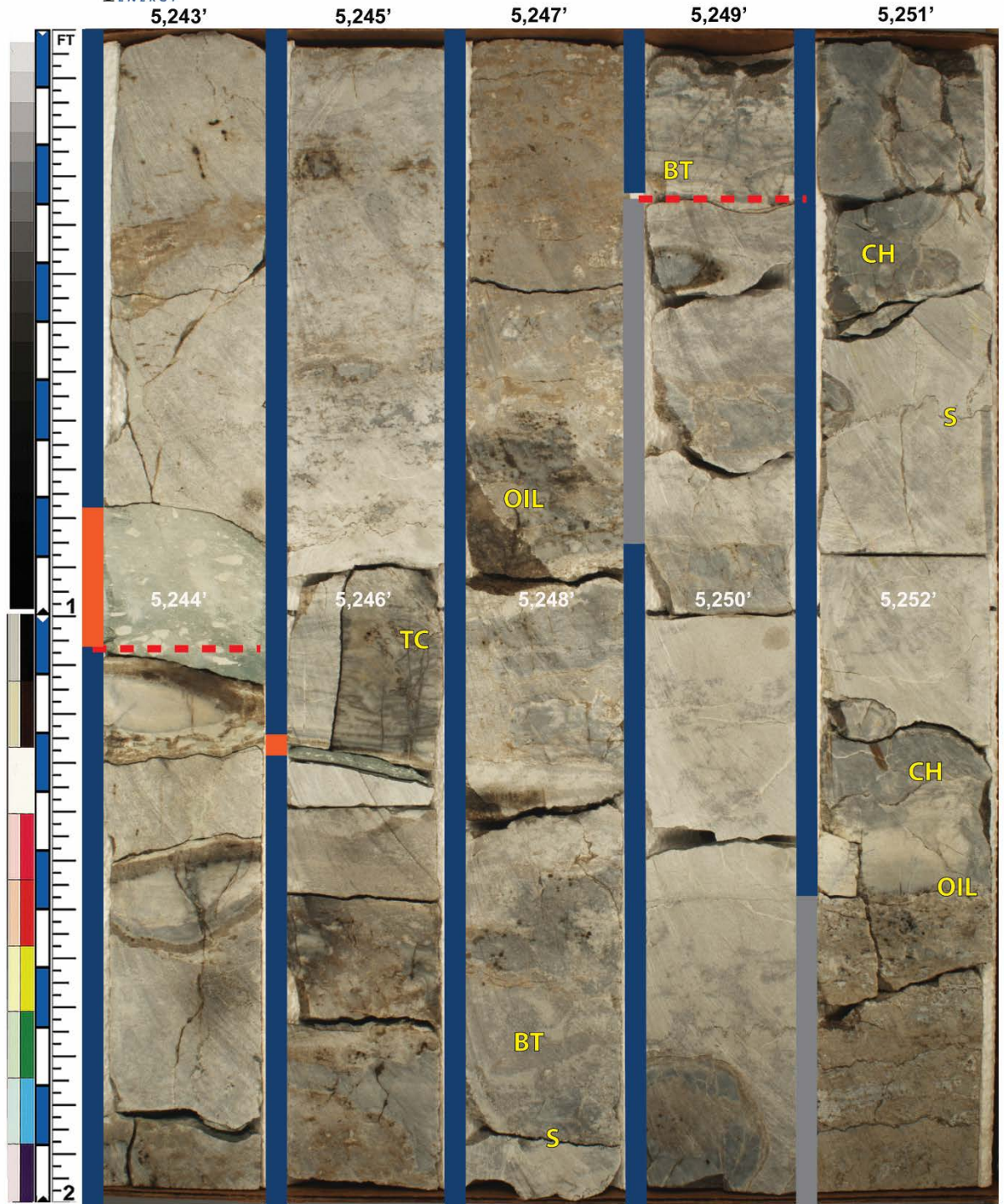
Core and Thin Section Image Labels					
Feature Key				Porosity Key	
BR	brachiopod	OIL	oil/dead oil	FR	fracture
BU	burrow	PY	pyrite	IP	interparticle
BY	bryozoan	Q	quartz	IX	intercrystalline
CH	chert	S	stylolite	MO	moldic
CR	crinoid	SK	undifferentiated skeletal fragments	VU	vug
D	dolomite	SP	spicule	WP	intraparticle
FL	fluorescence	TC	traction current	WX	intracrystalline
FR	fracture	TR	terra rosa		
GST	gastropod	CL	clast		
L	lamination	BT	bioturbation		
M	mud/mudstone				
O	ostracode				

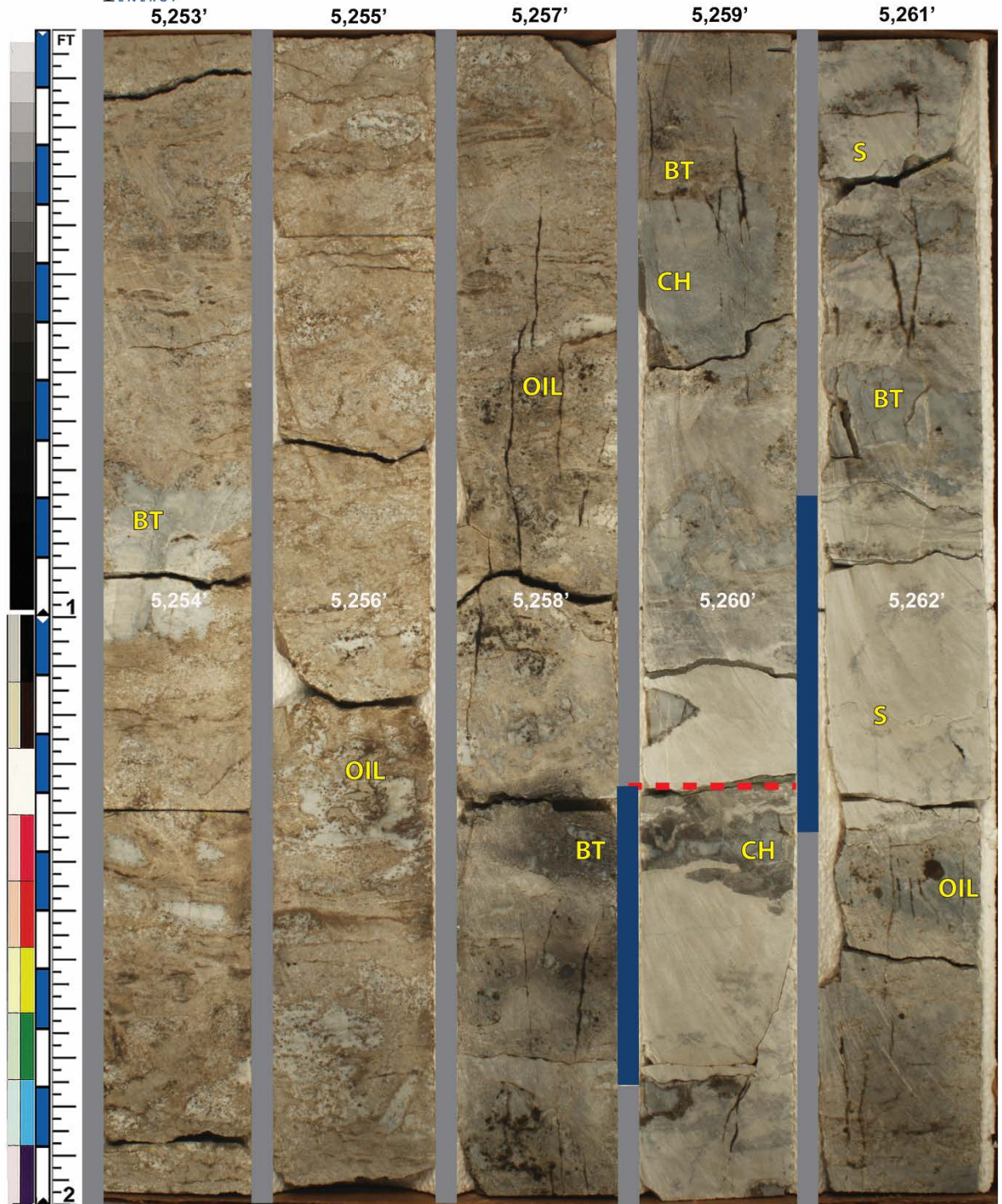
CORE #1: WHITE LIGHT (BANN 1-14)

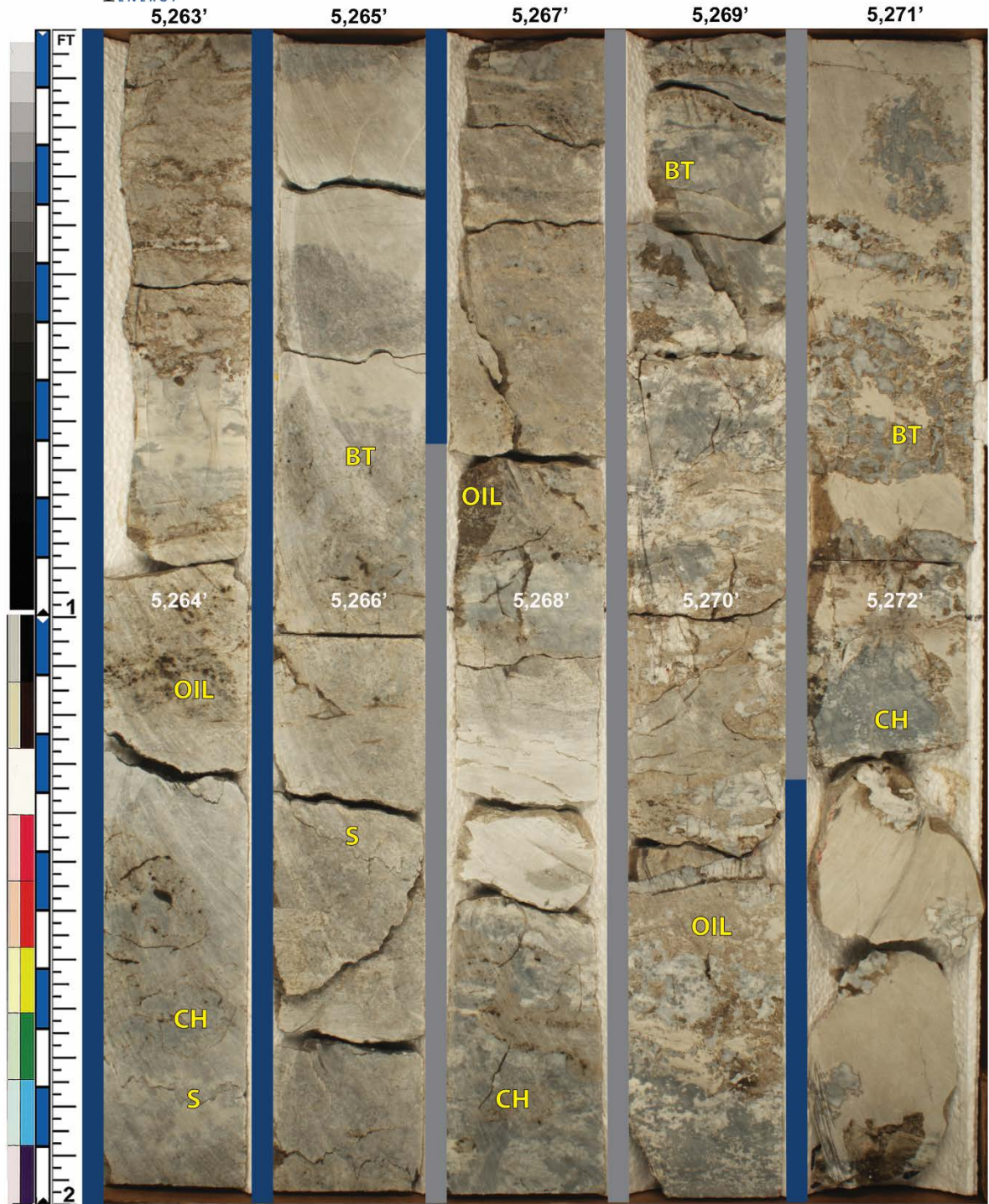


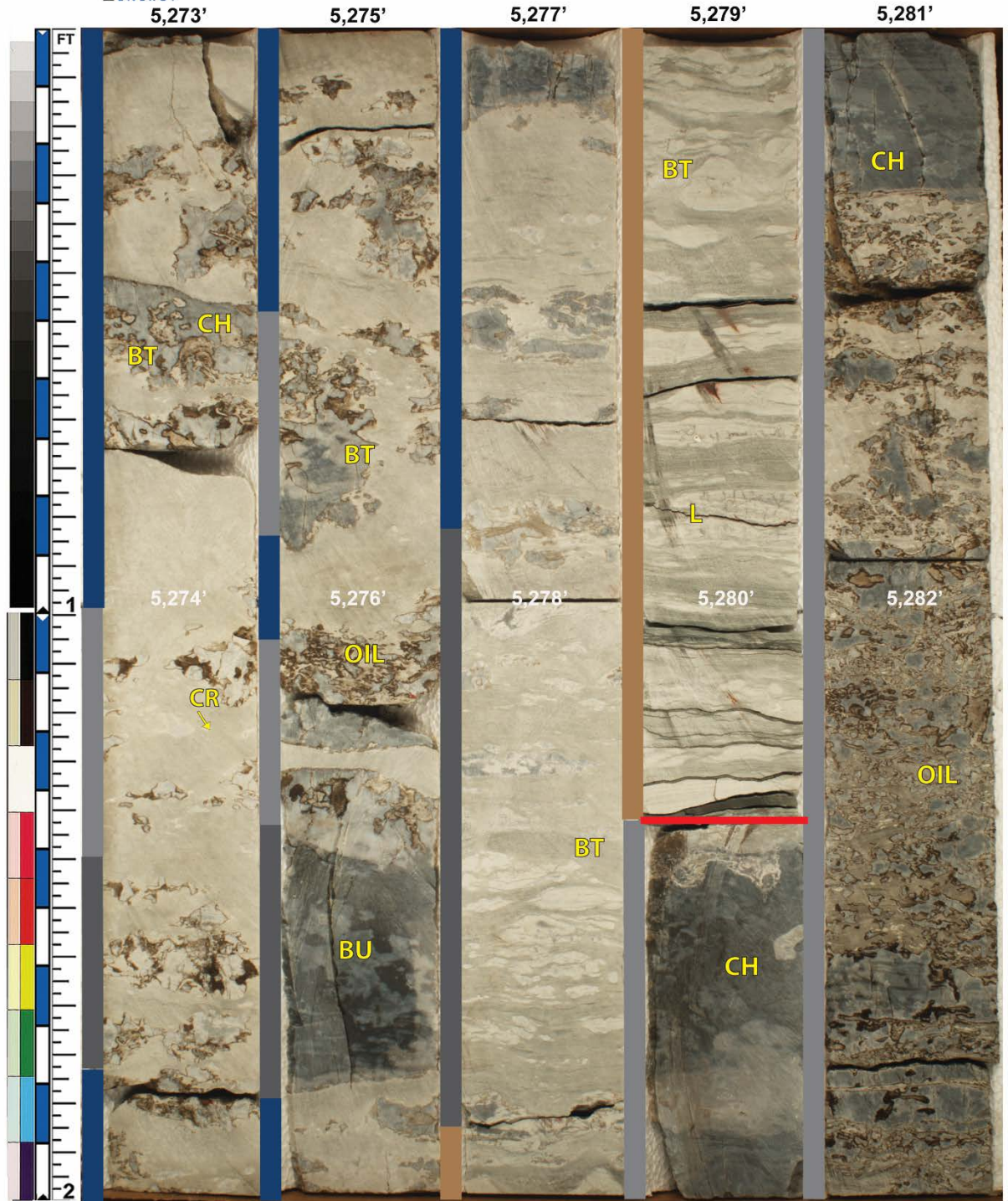


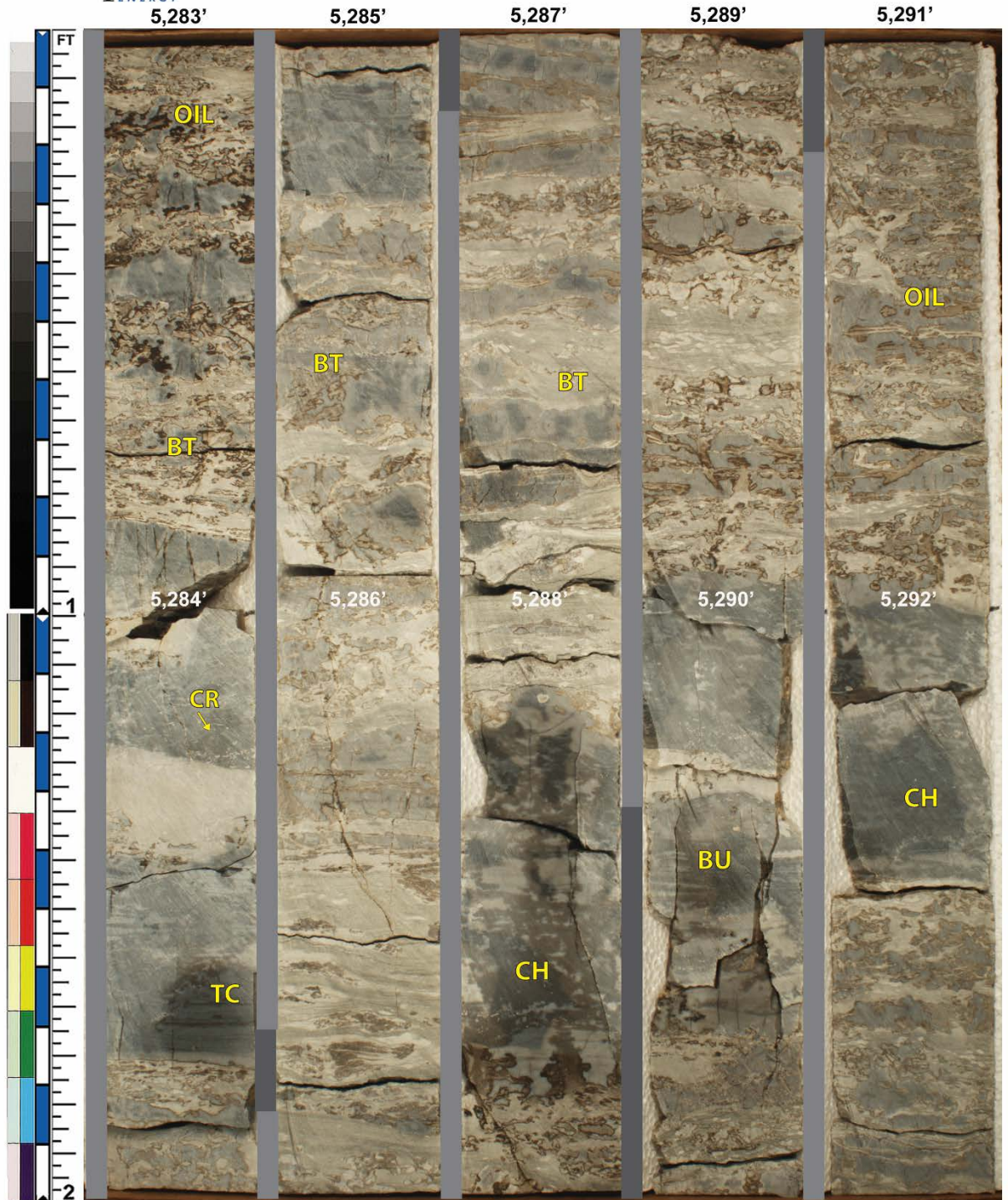


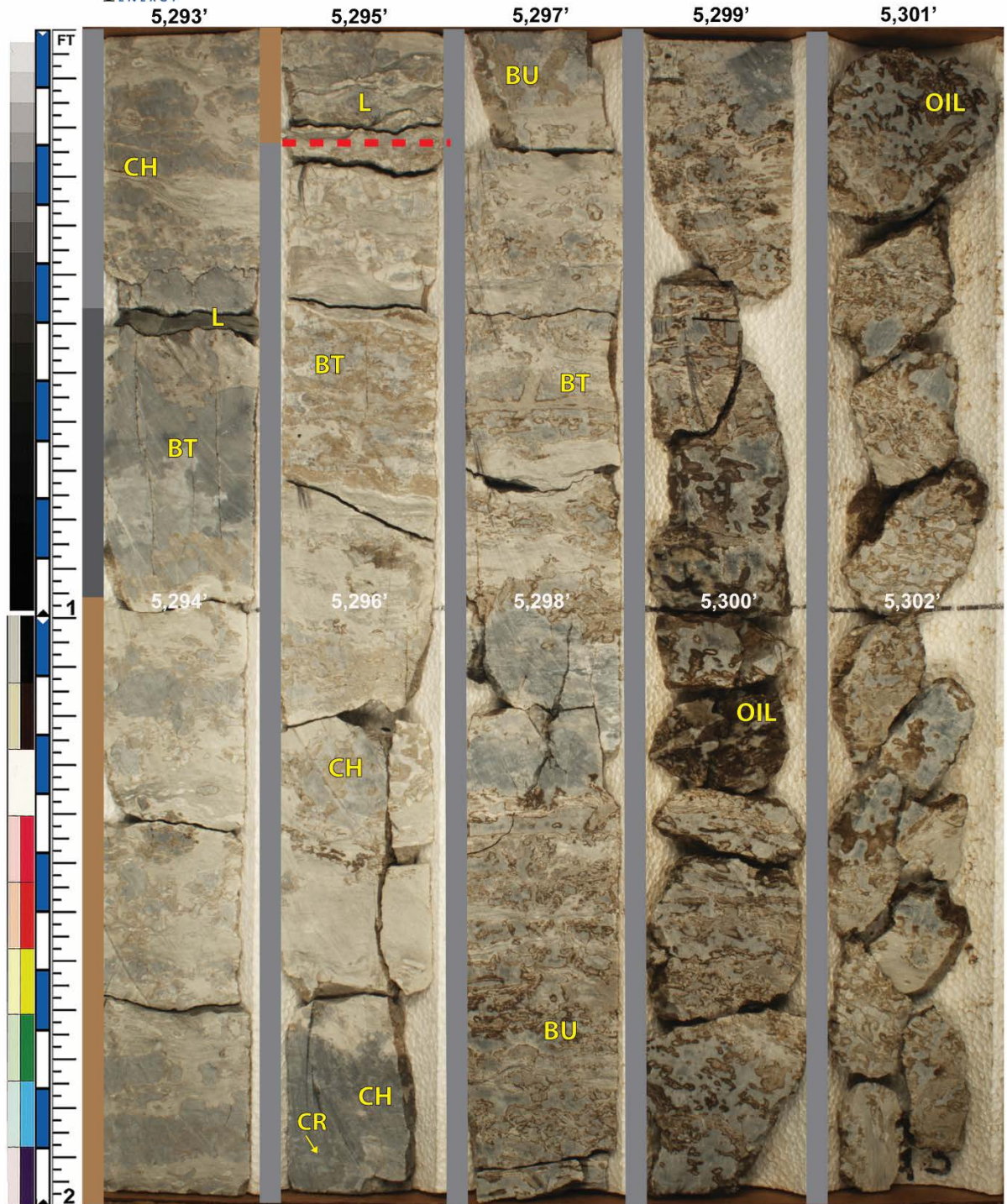


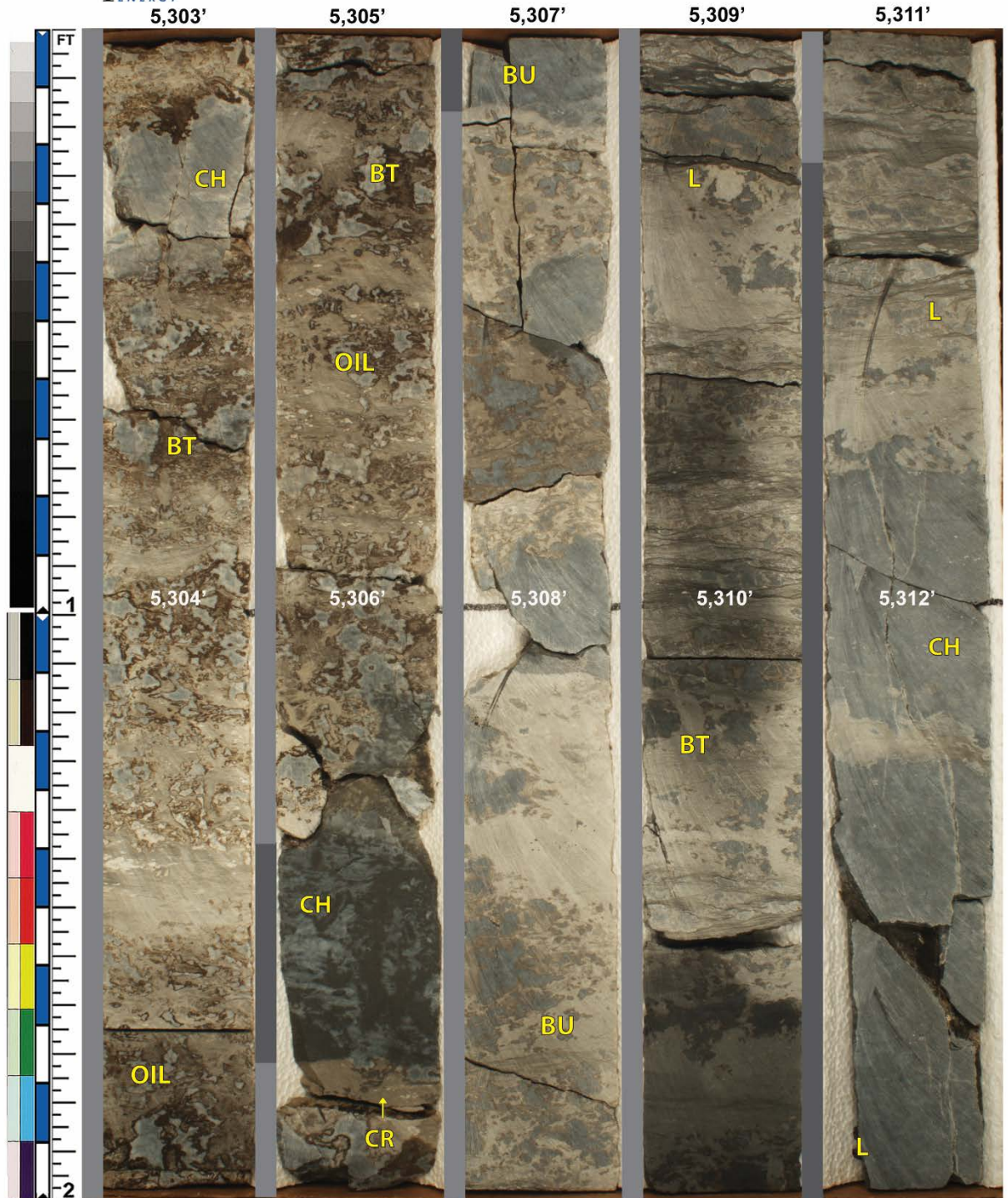


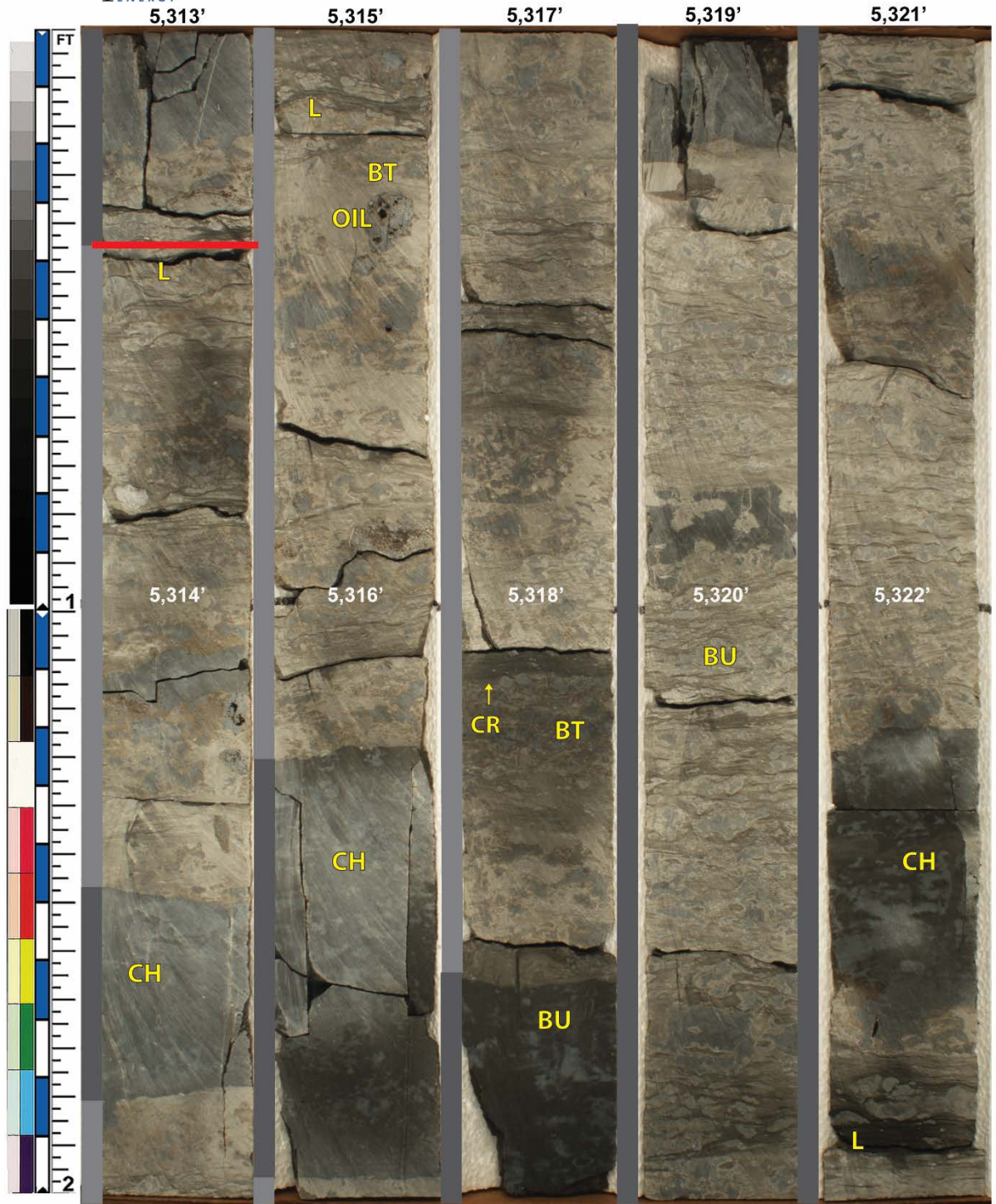


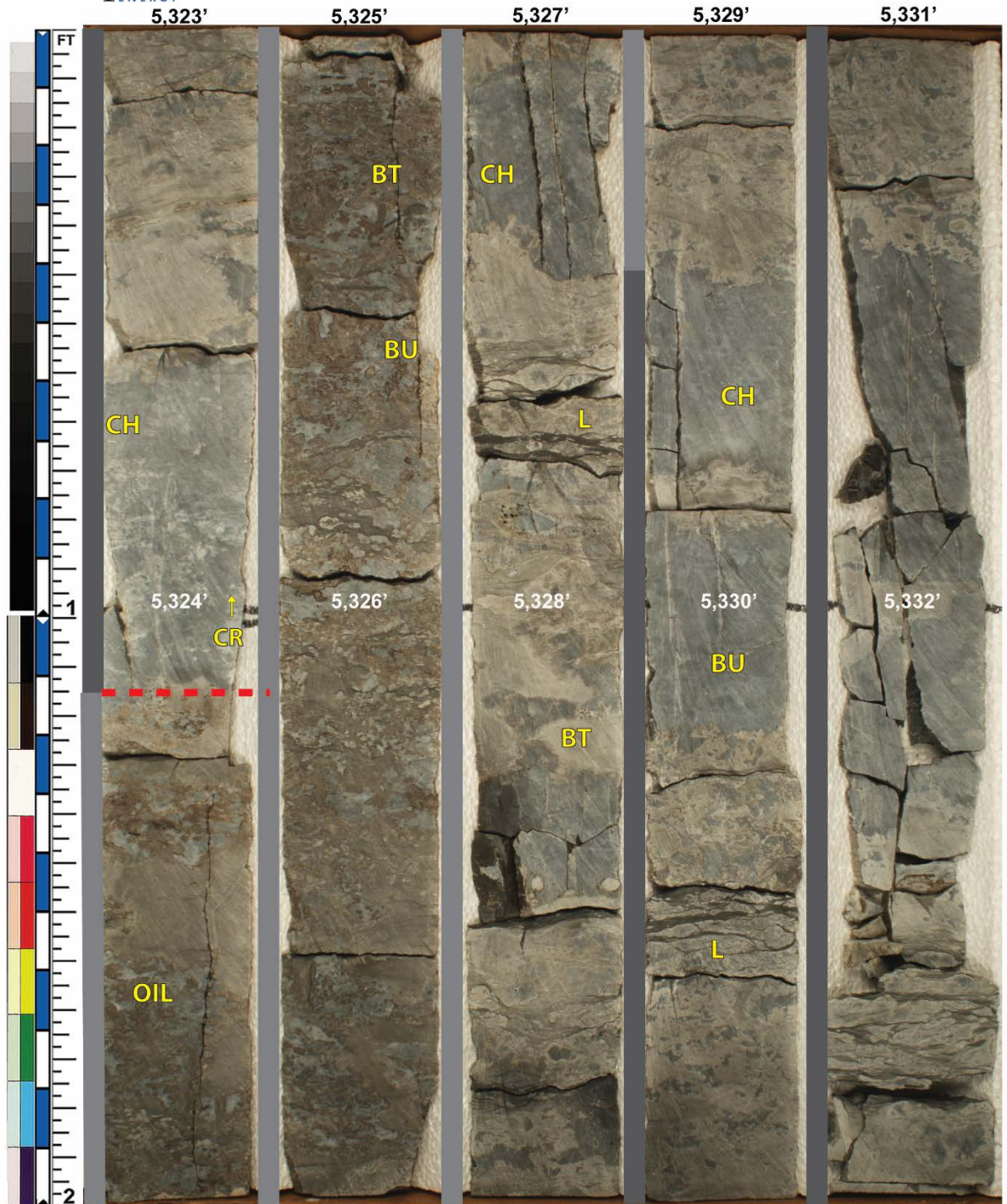


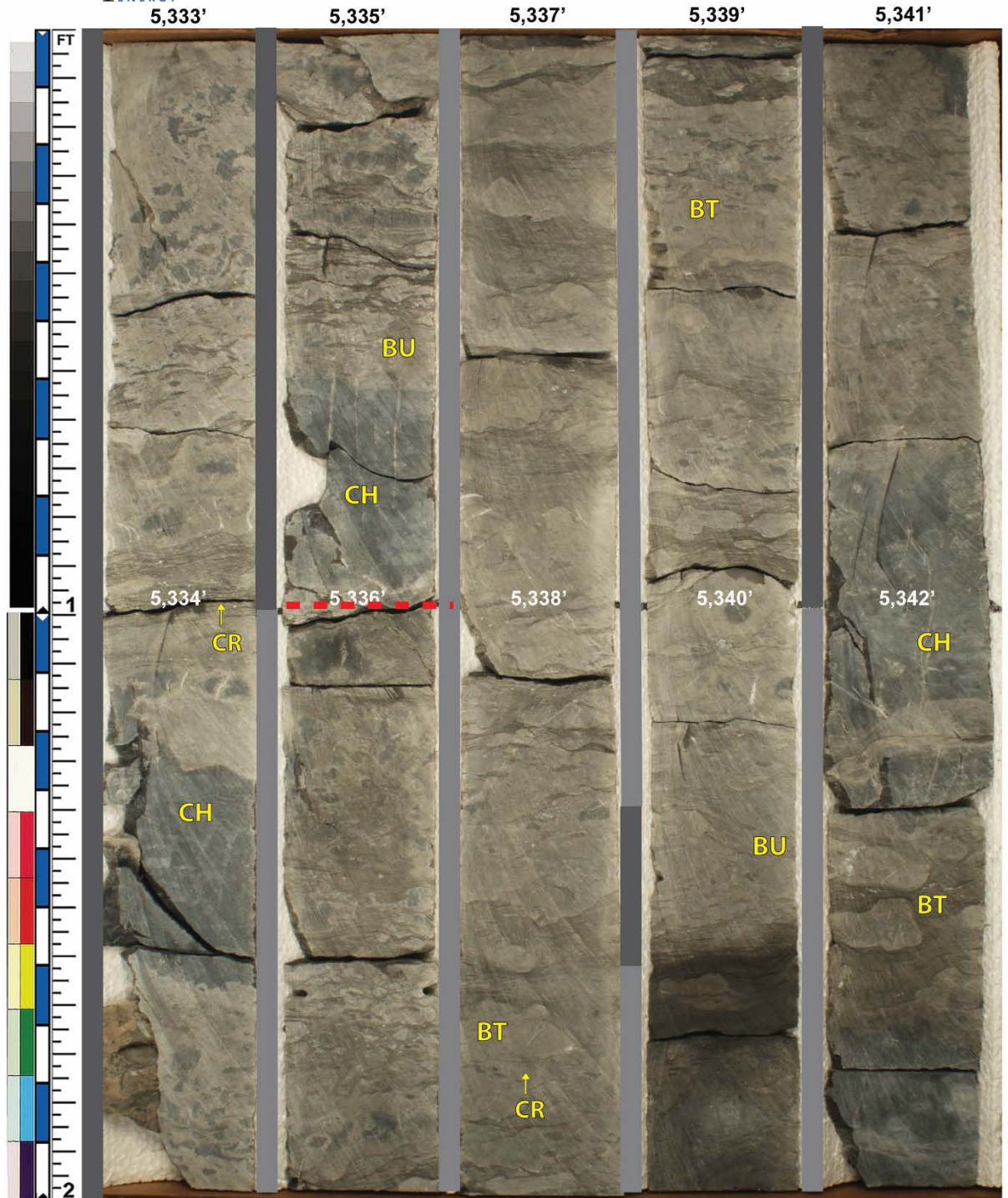


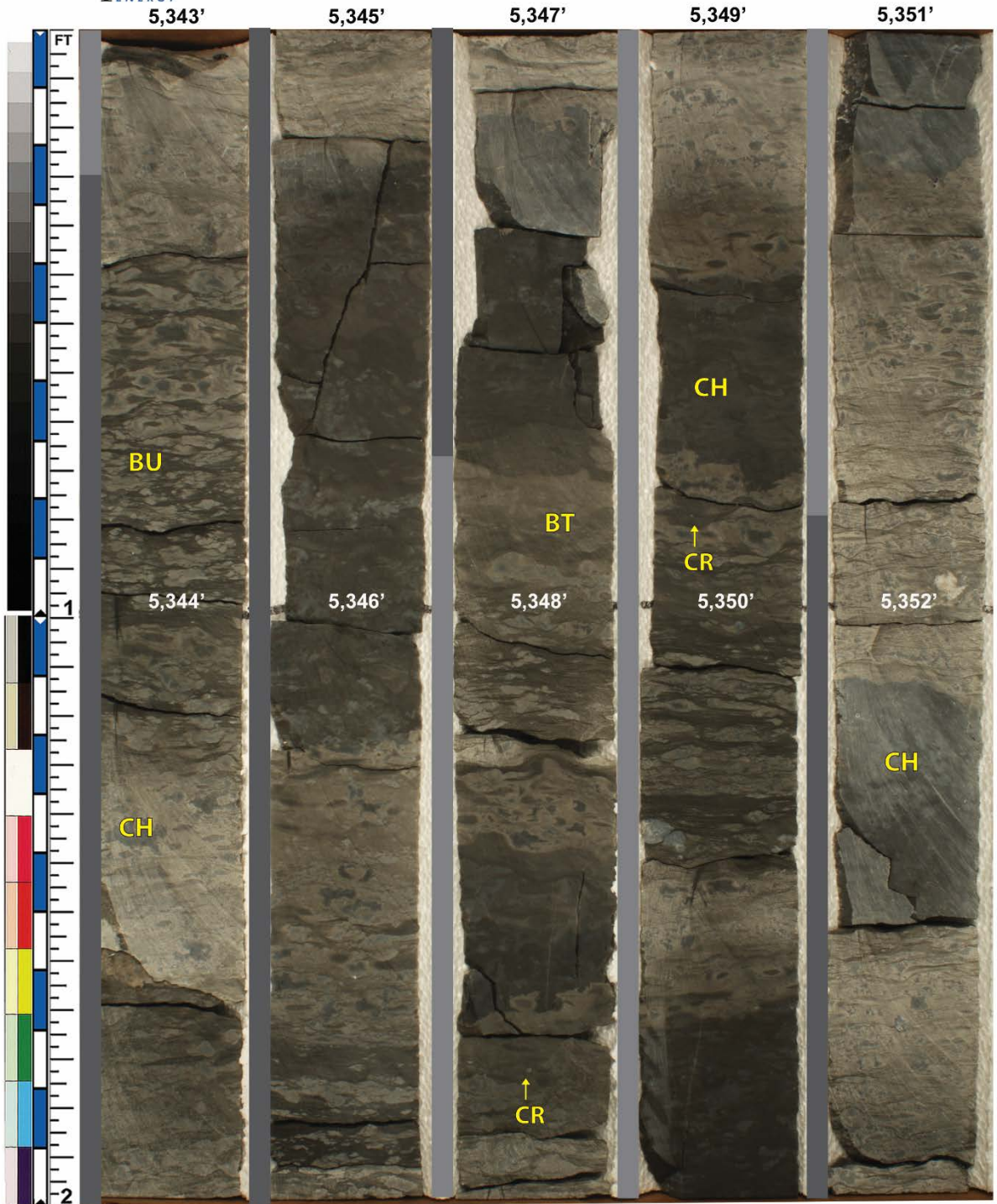


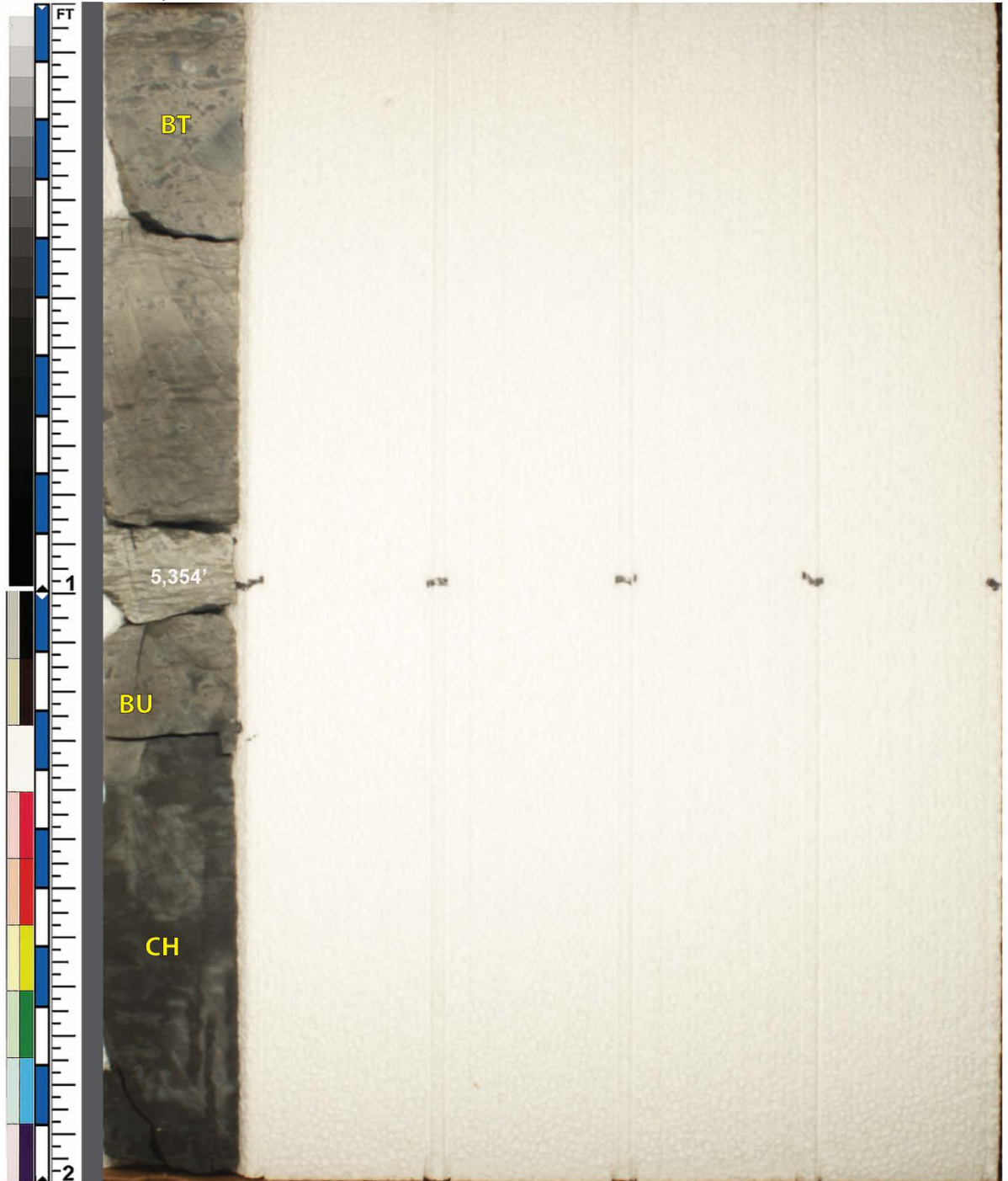










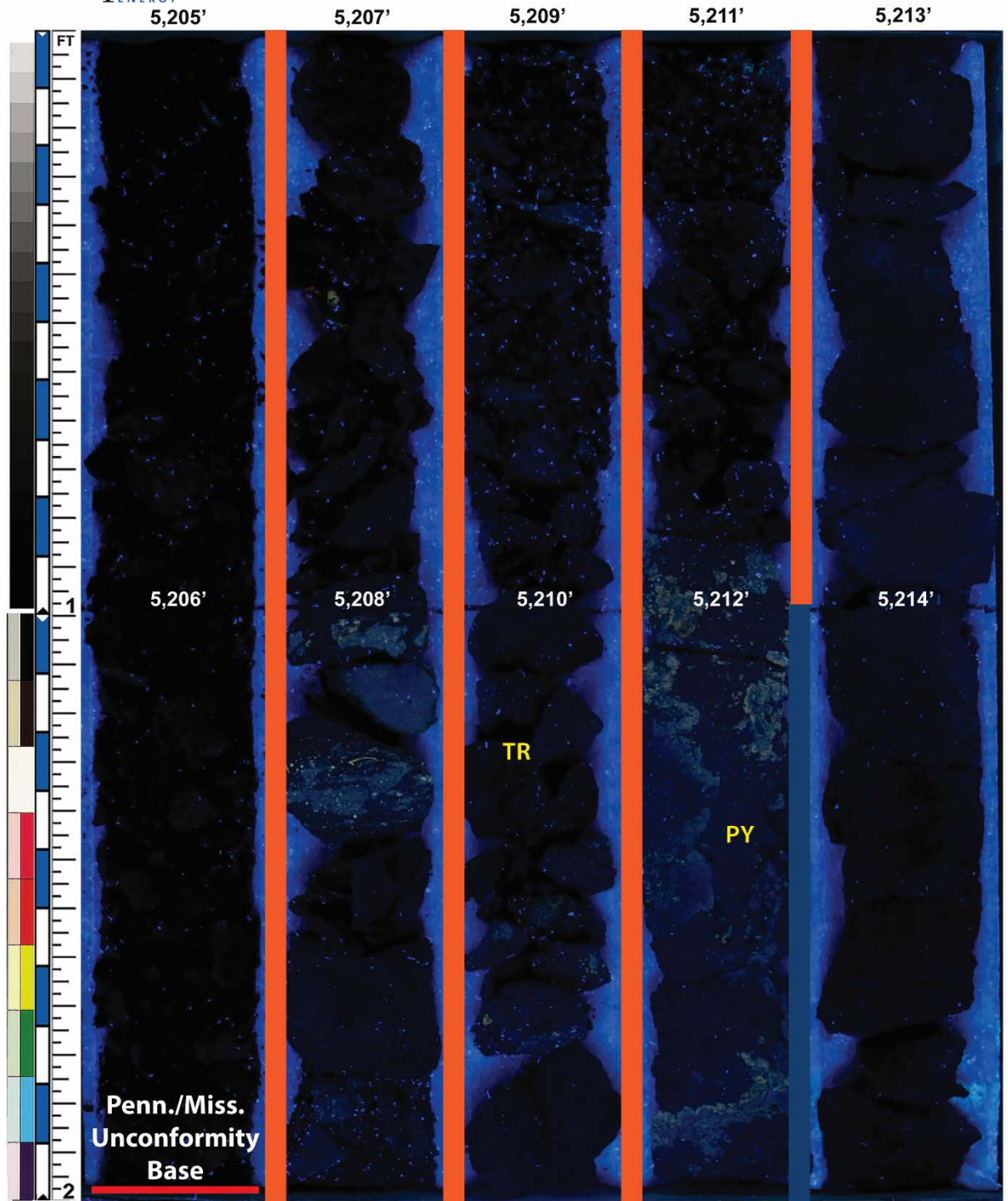


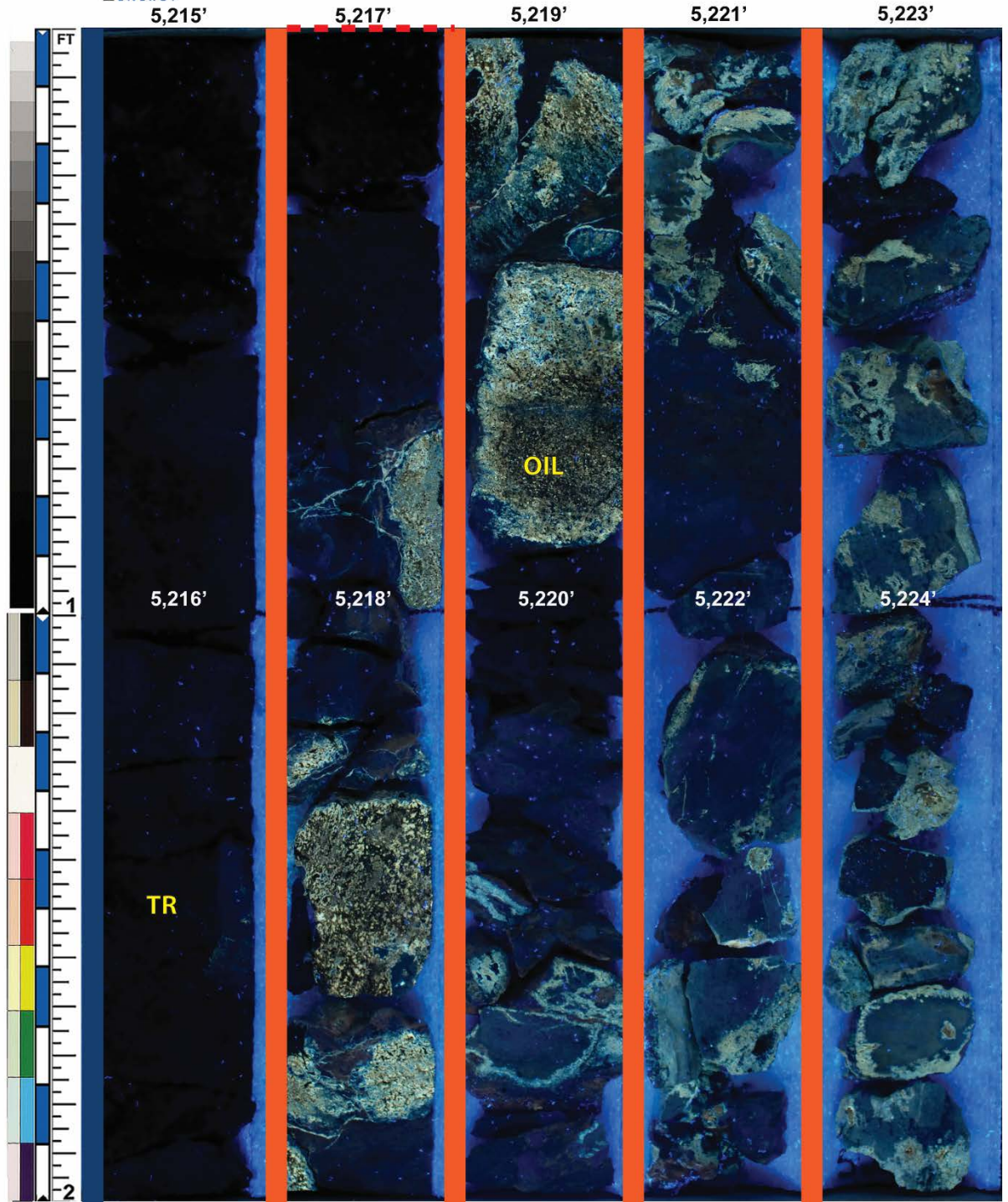
CORE #1: UV LIGHT (BANN 1-14)

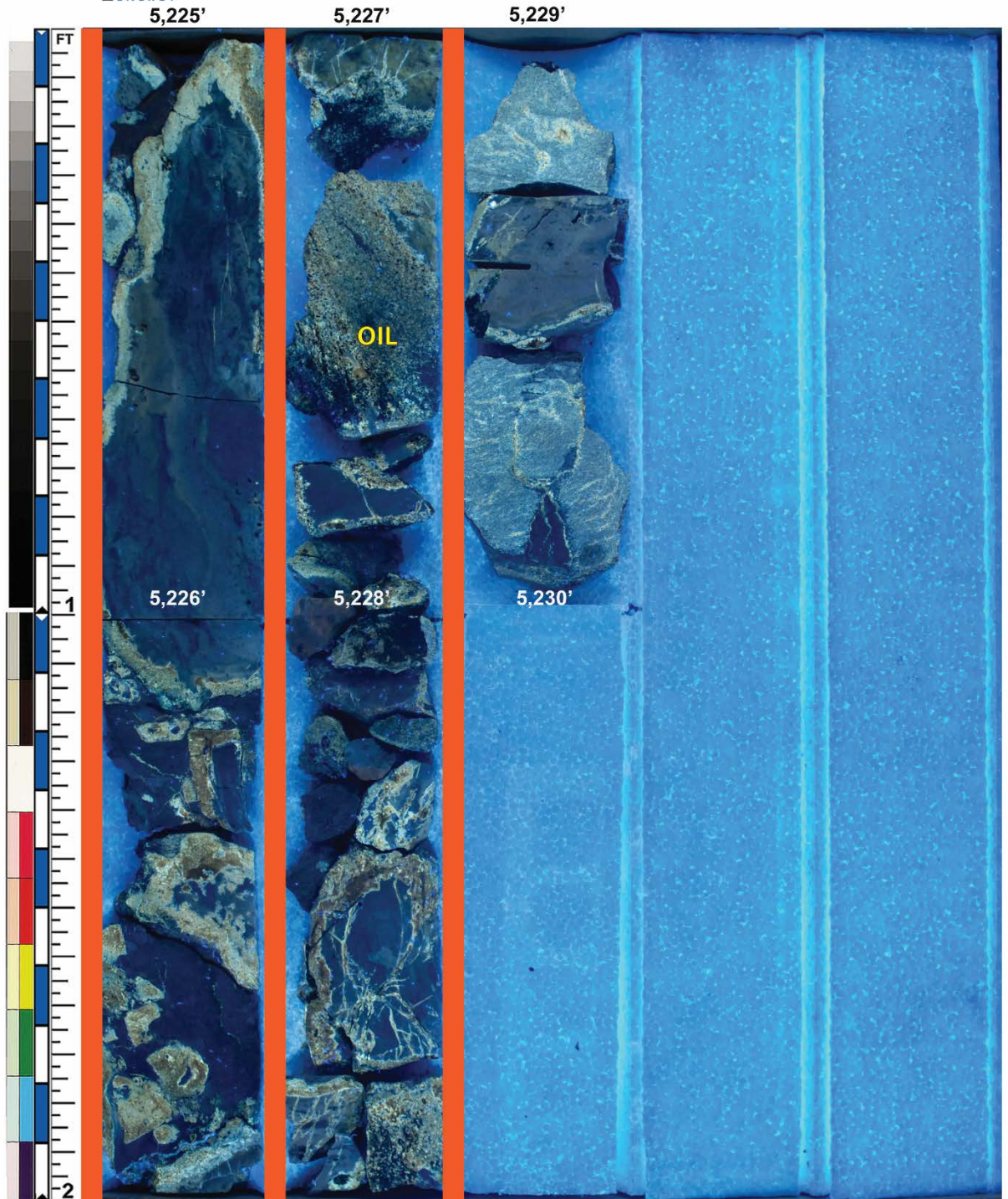


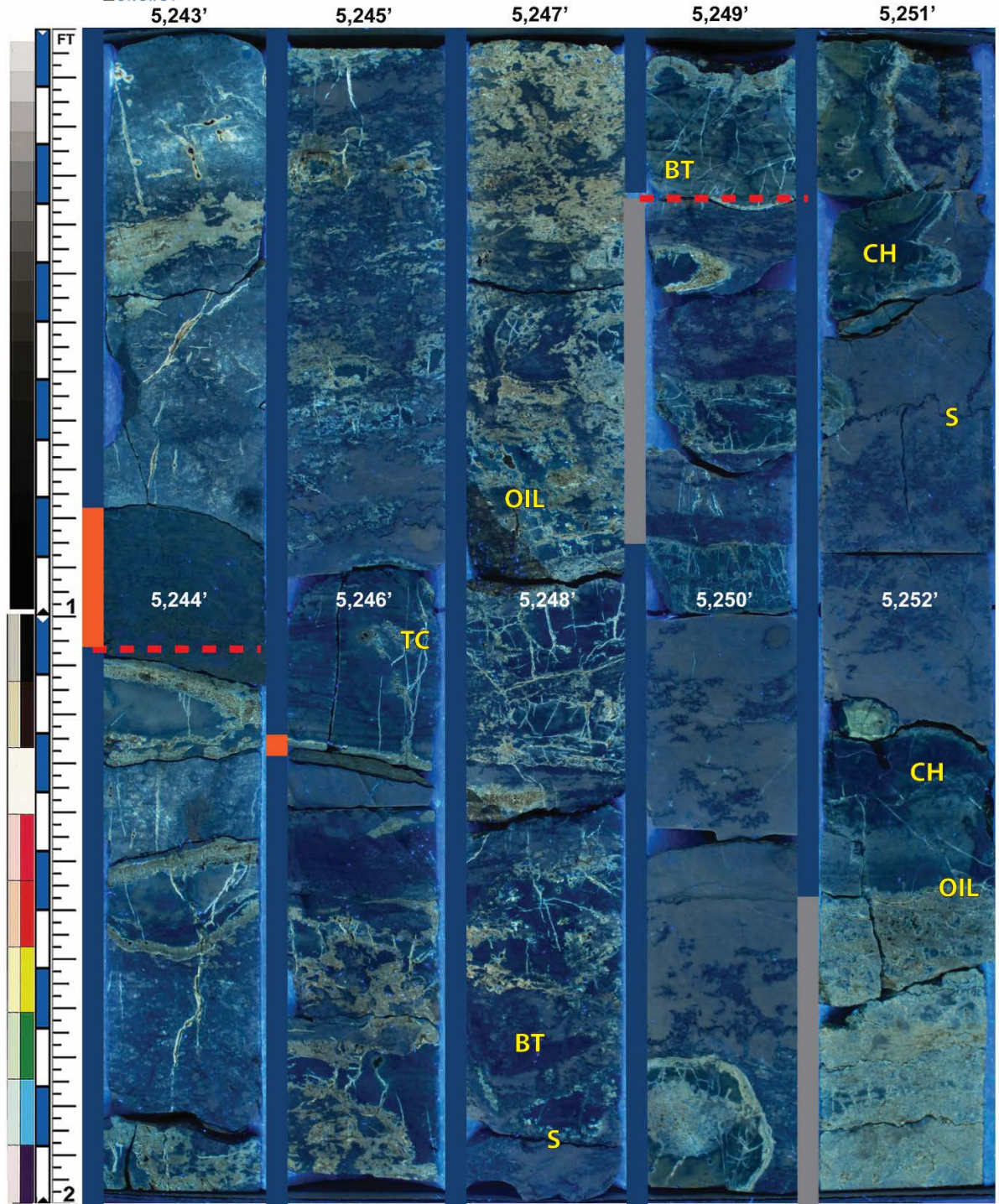
Well: Bann 1-14
Location: Woods Co., OK
Formation: Miss Lime

Job: 07-0904
Core: 1 Box 1 of 2
Depth: 5,205 - 5,215





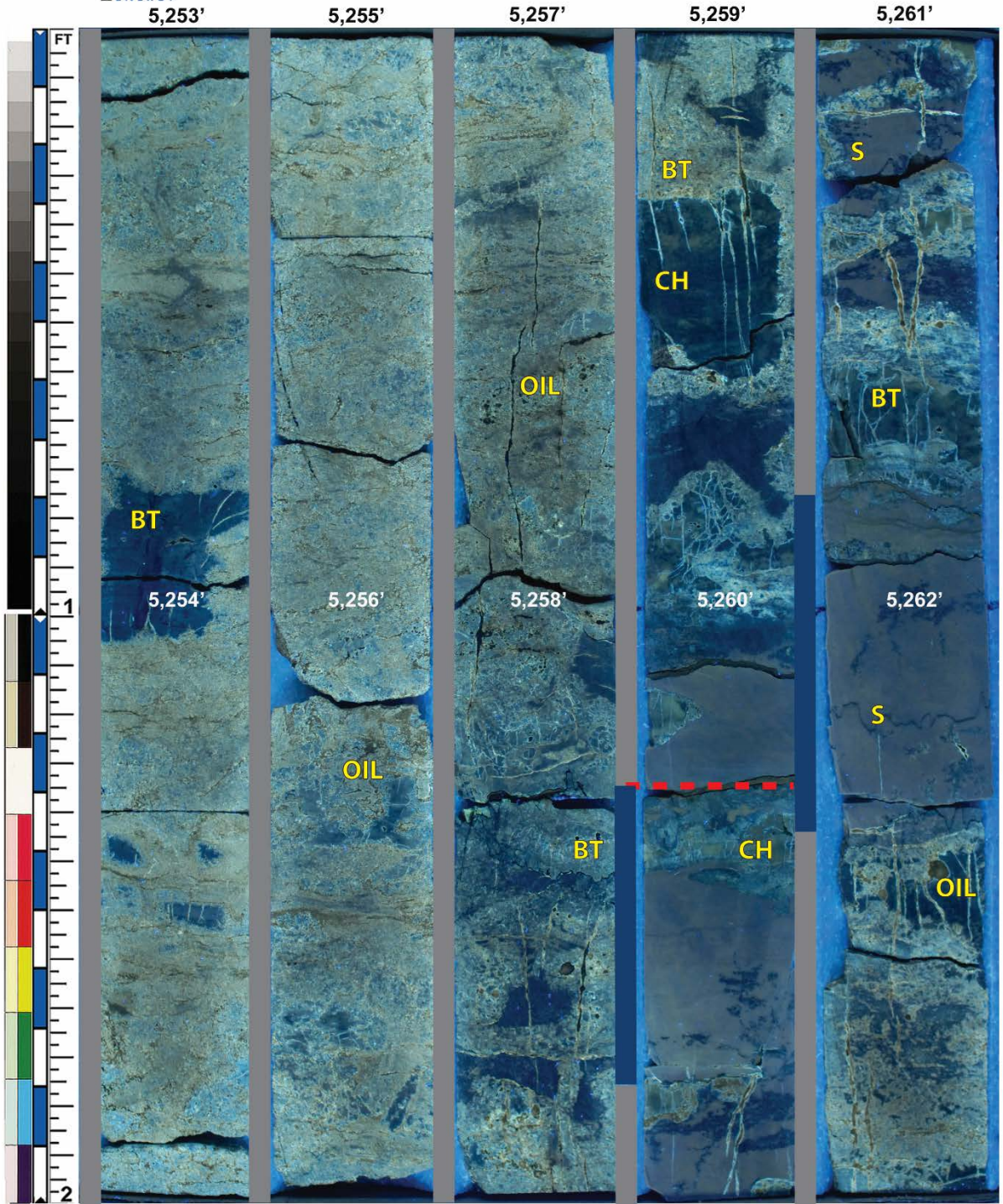


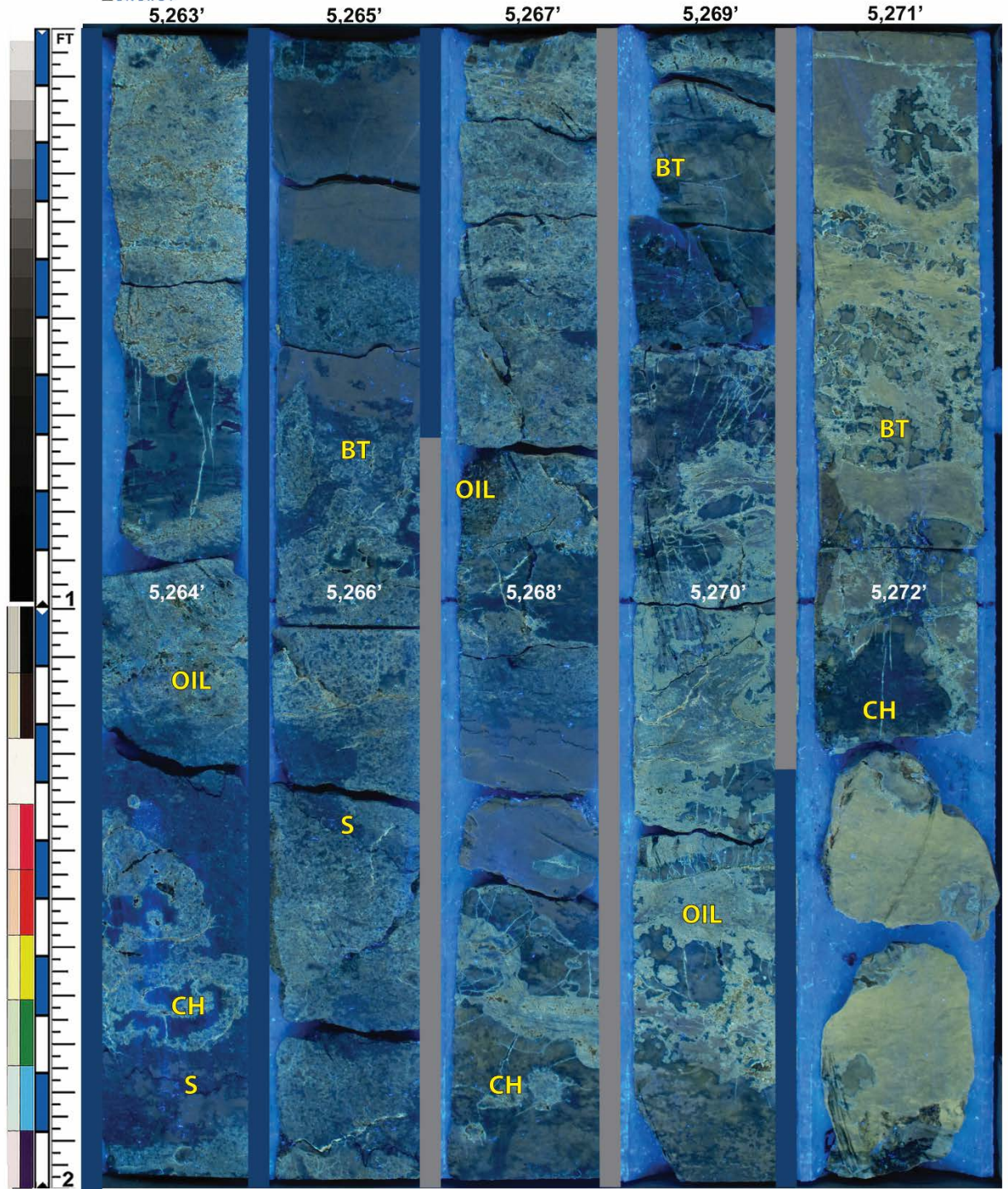


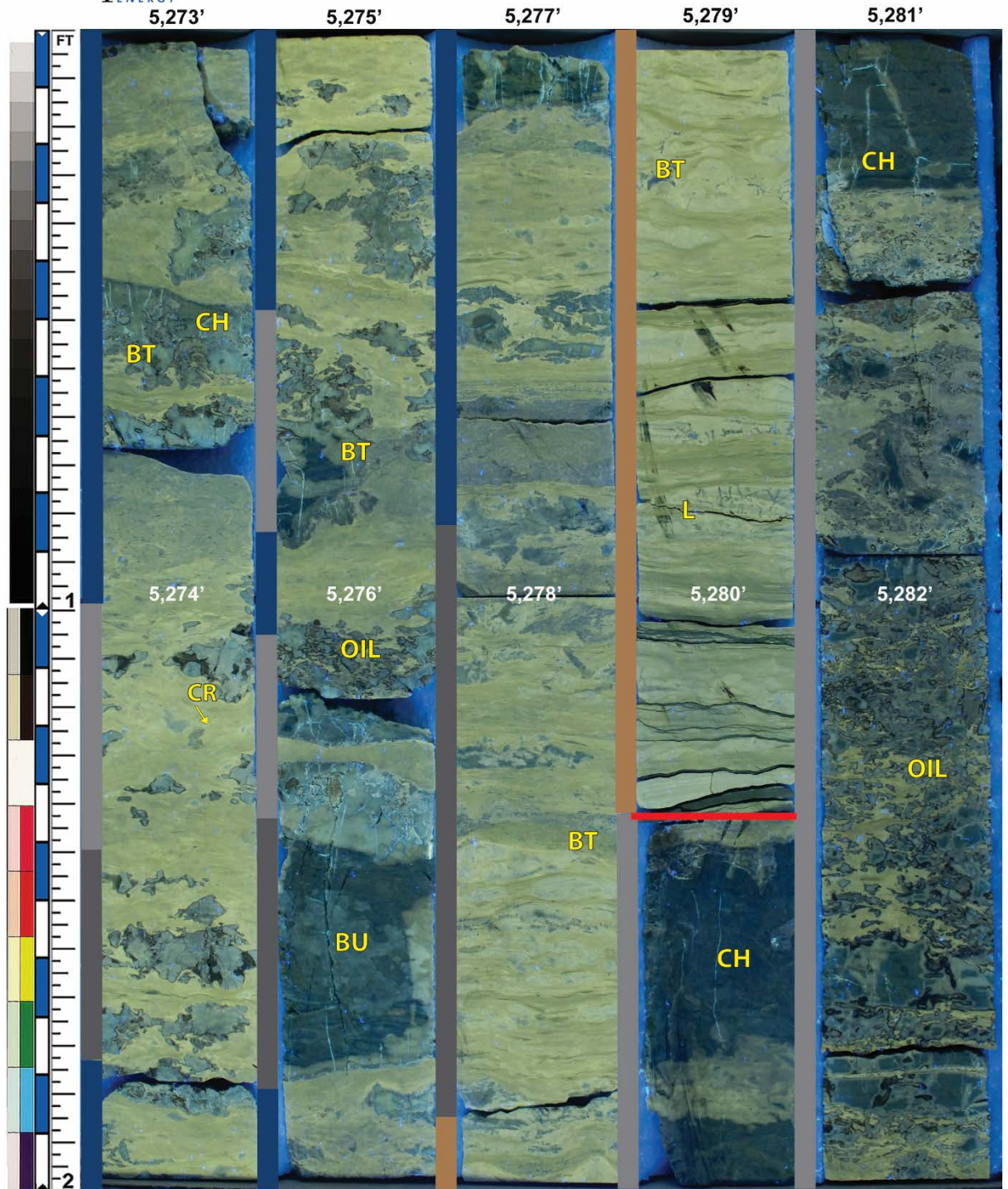


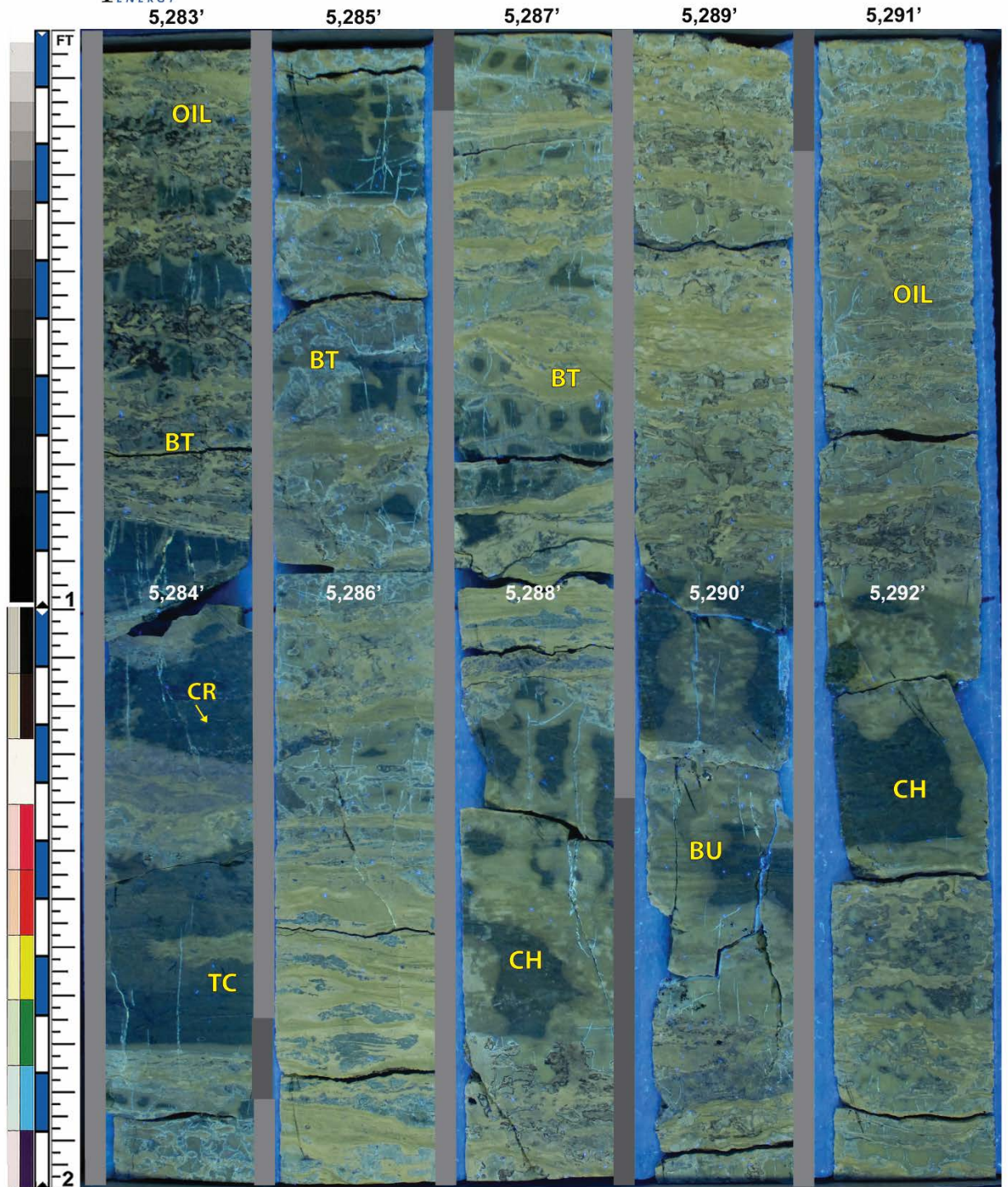
Well: Bann 1-14
Location: Woods Co., OK
Formation: Miss Lime

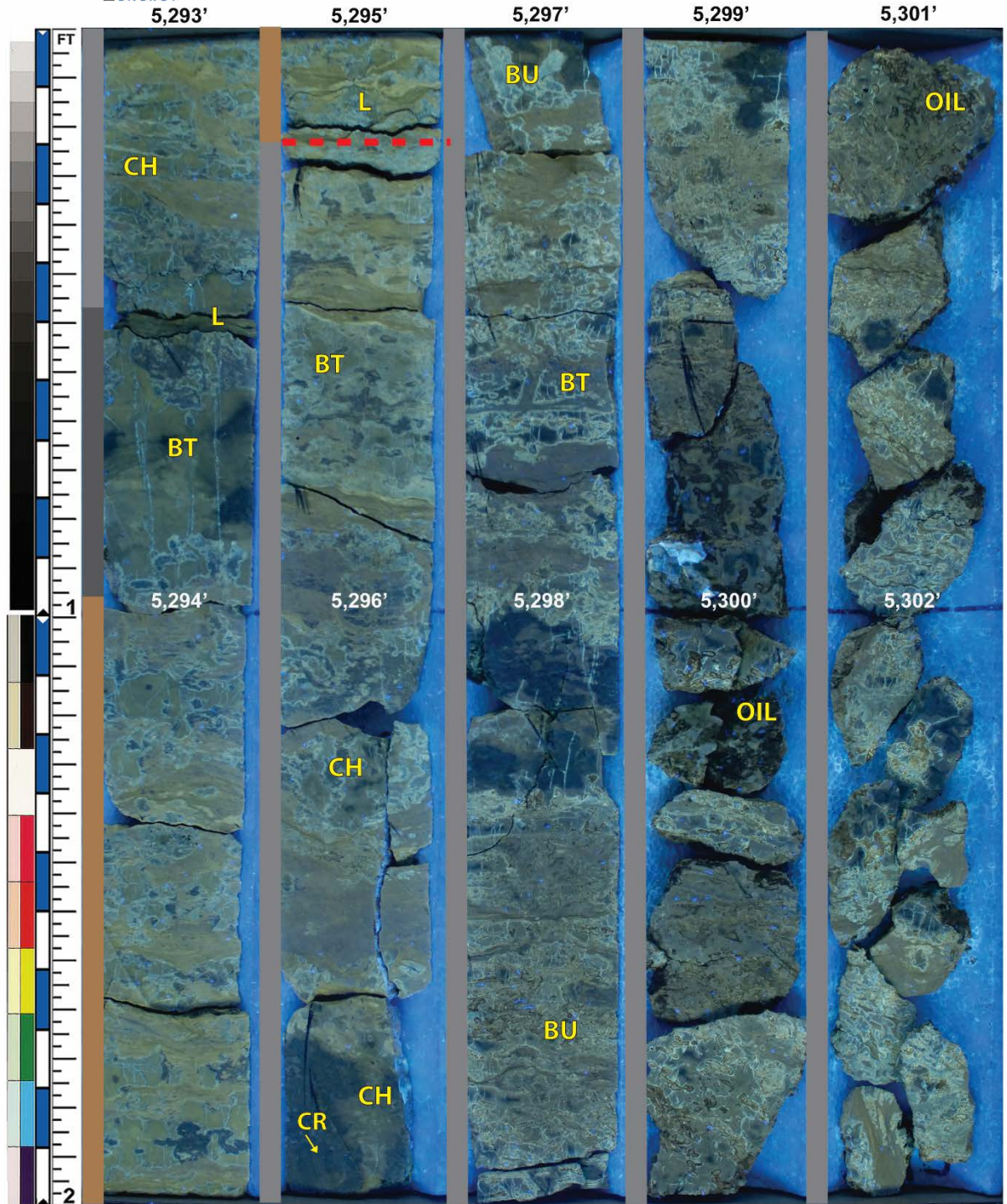
Job: 07-0904
Core: 3 Box 2 of 6
Depth: 5,253 - 5,263

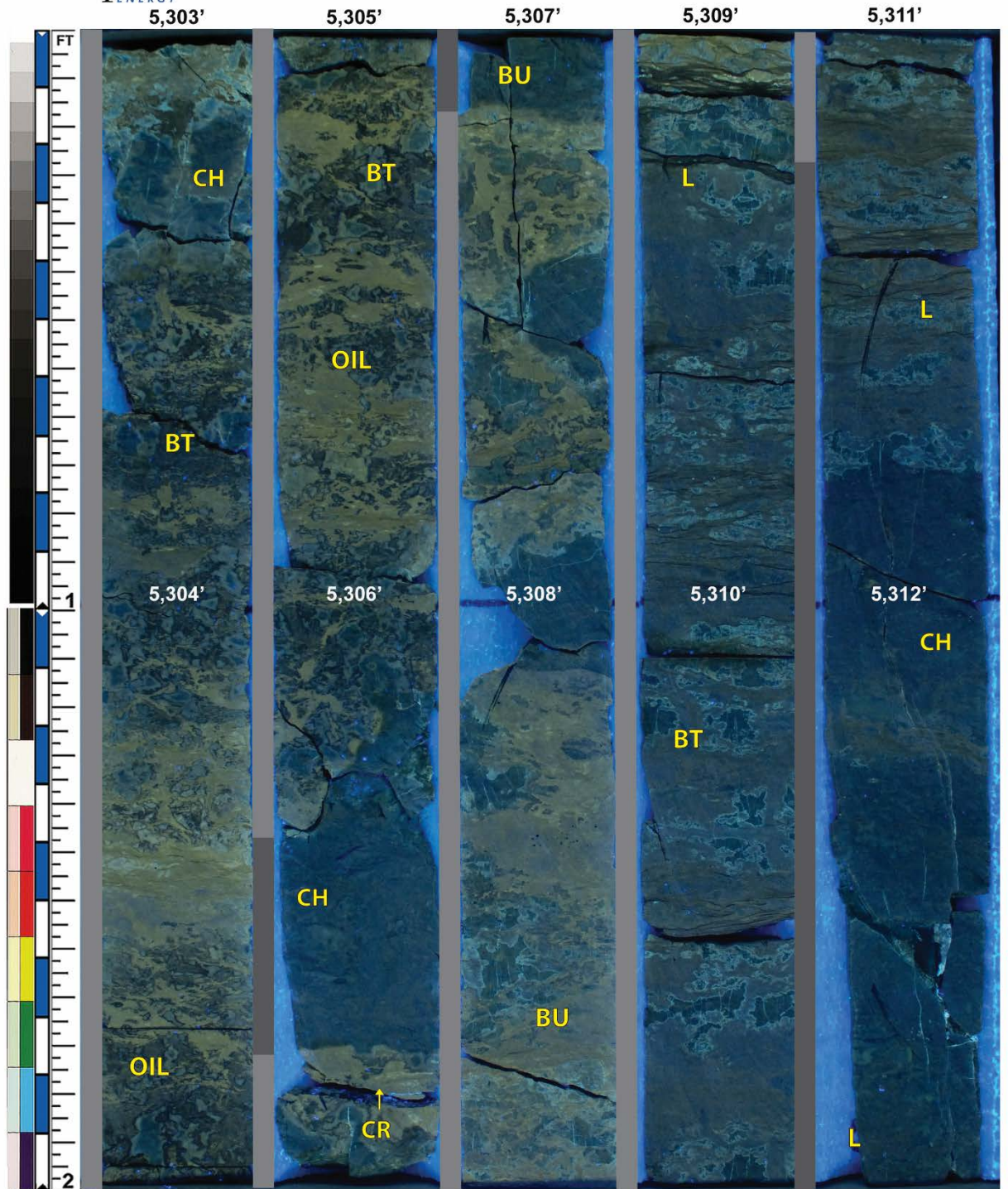








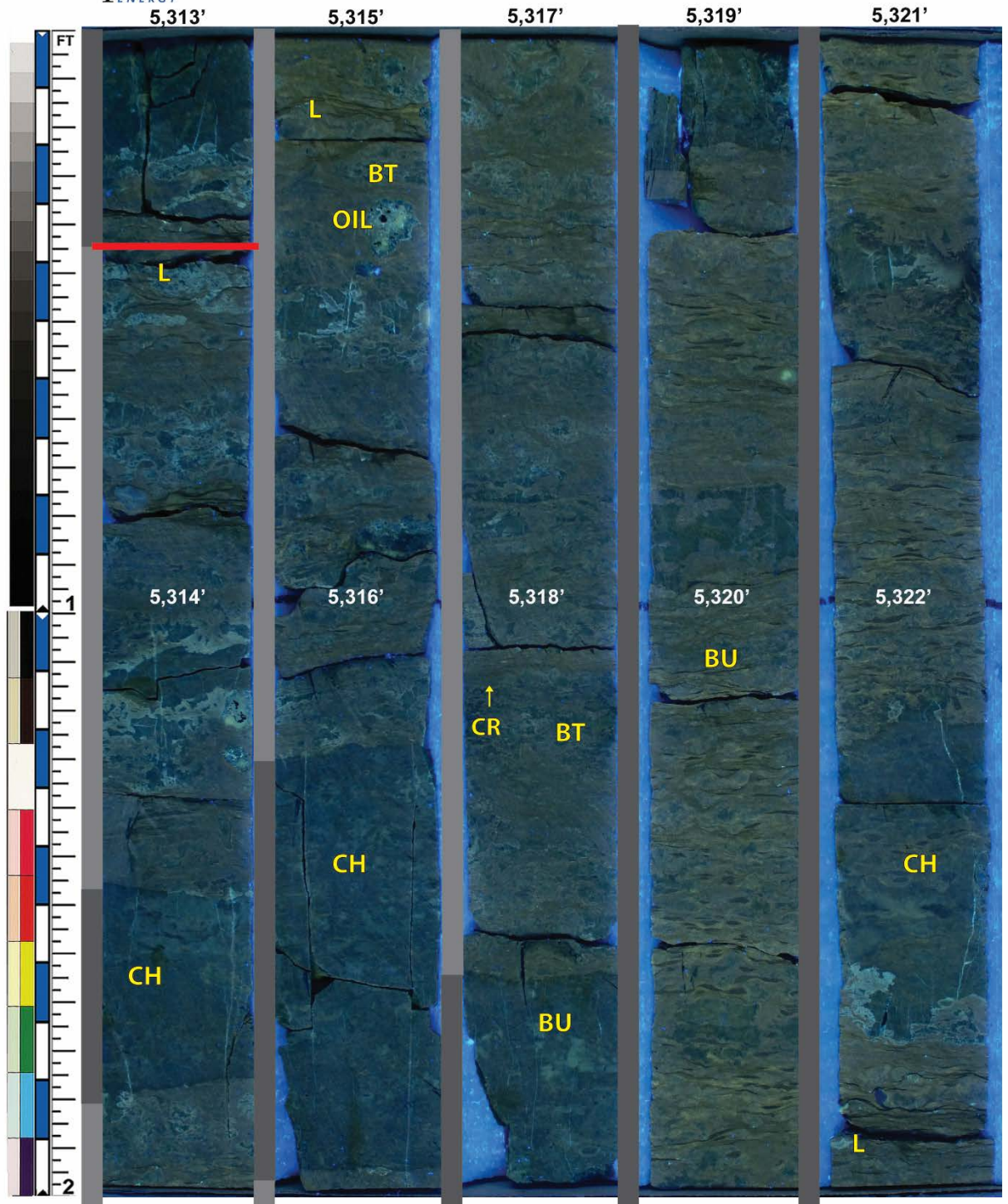






Well: Bann 1-14
Location: Woods Co., OK
Formation: Miss Lime

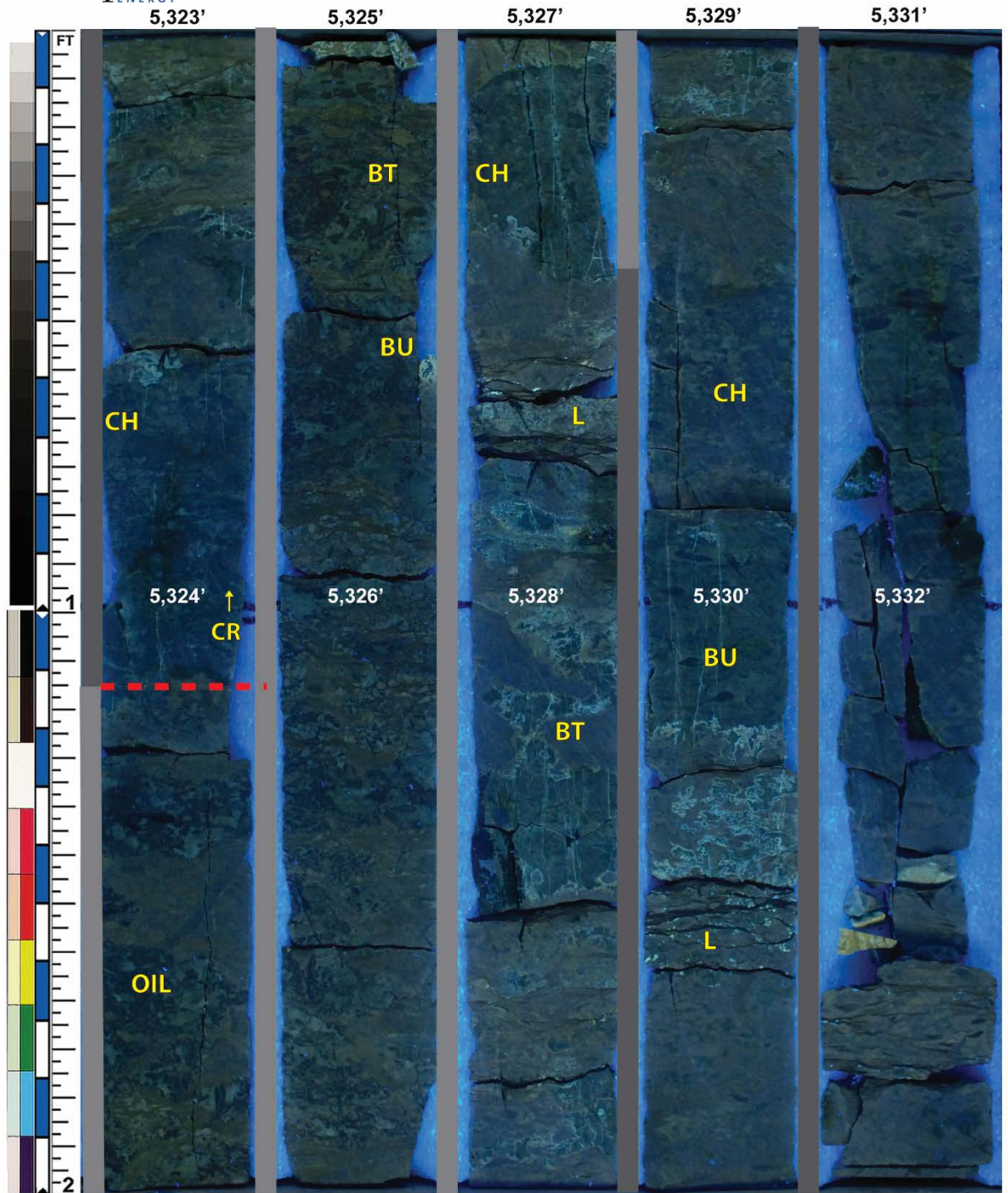
Job: 07-0904
Core: 4 Box 2 of 6
Depth: 5,313 - 5,323

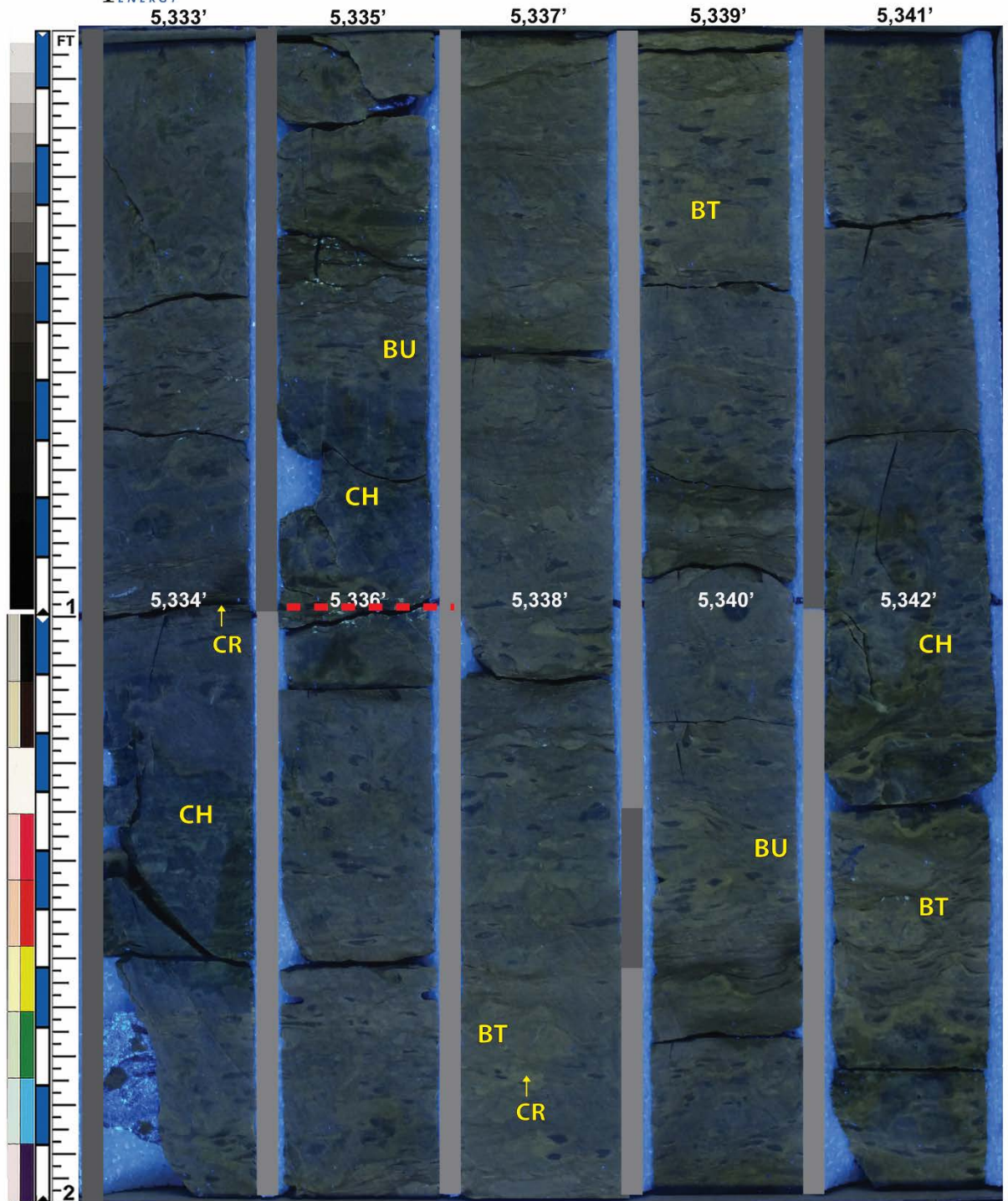


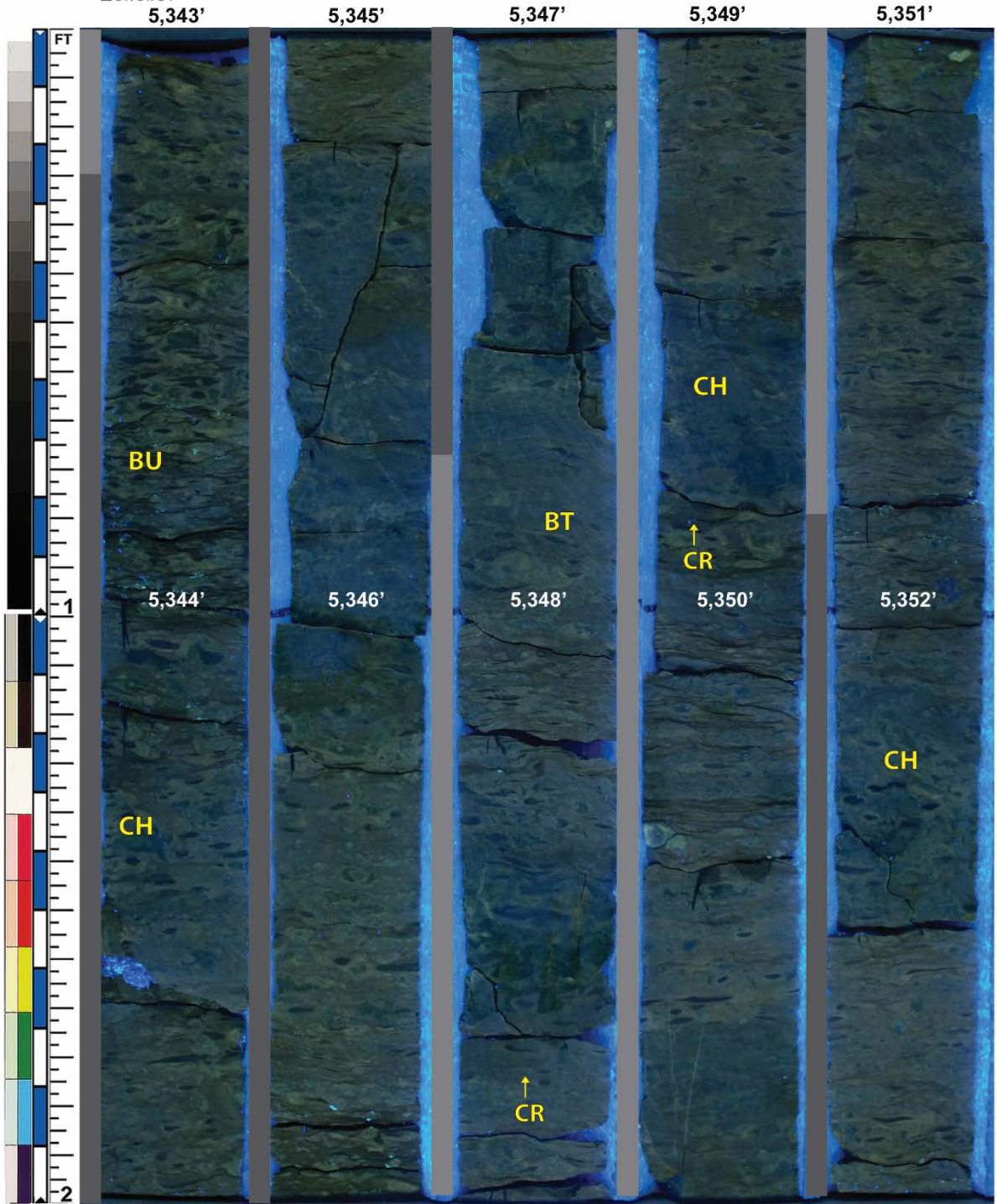


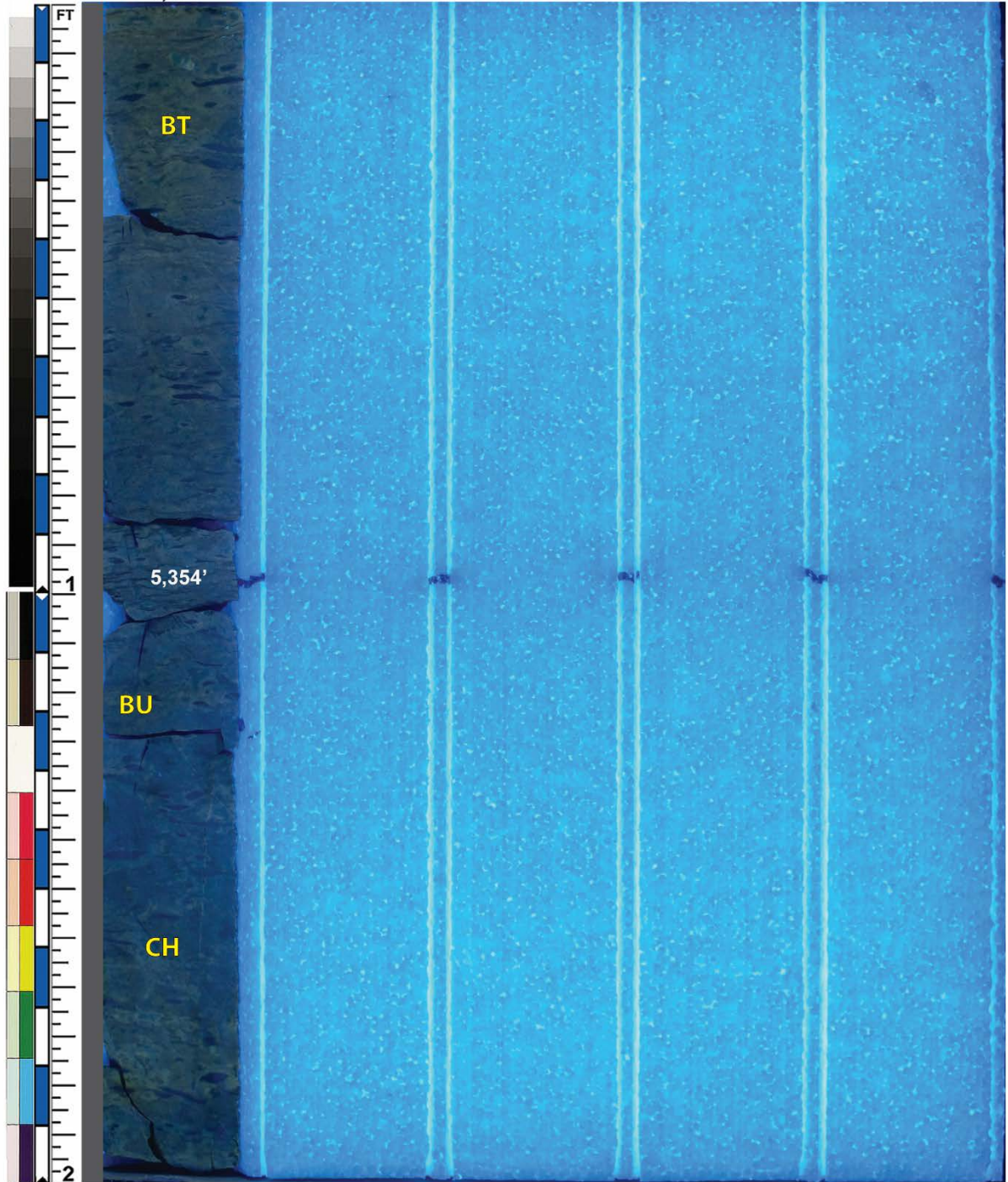
Well: Bann 1-14
Location: Woods Co., OK
Formation: Miss Lime

Job: 07-0904
Core: 4 Box 3 of 6
Depth: 5,323 - 5,333

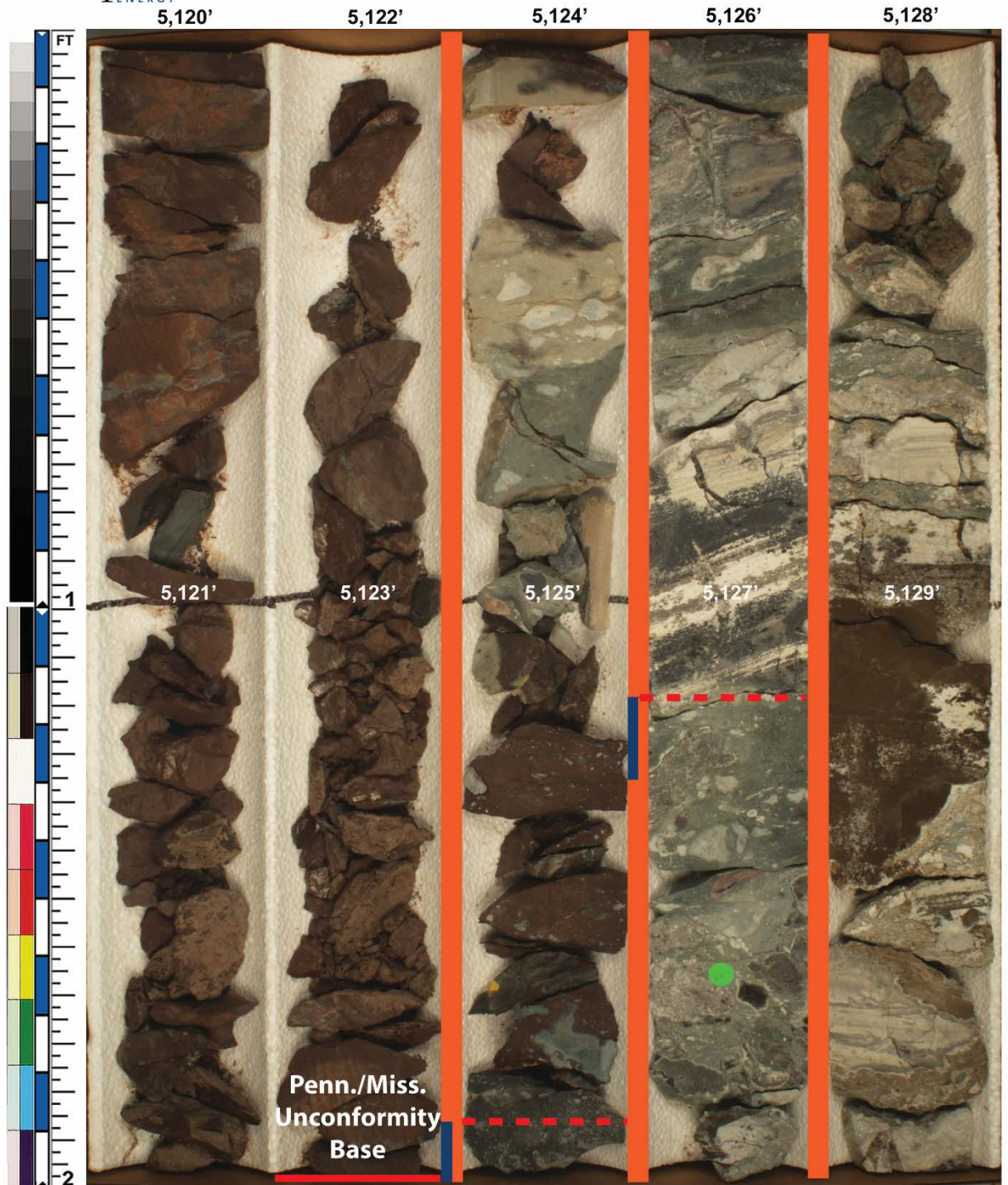


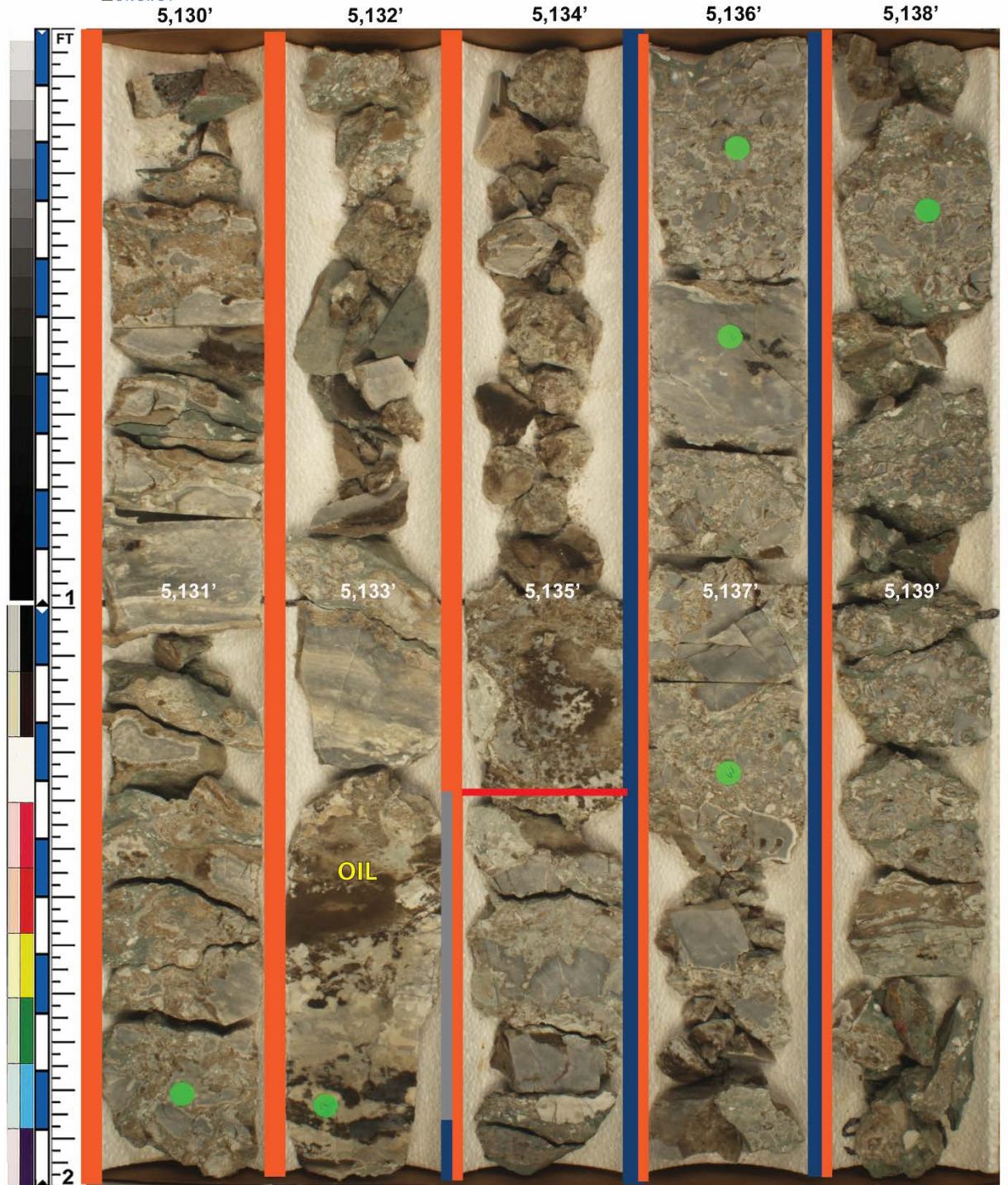


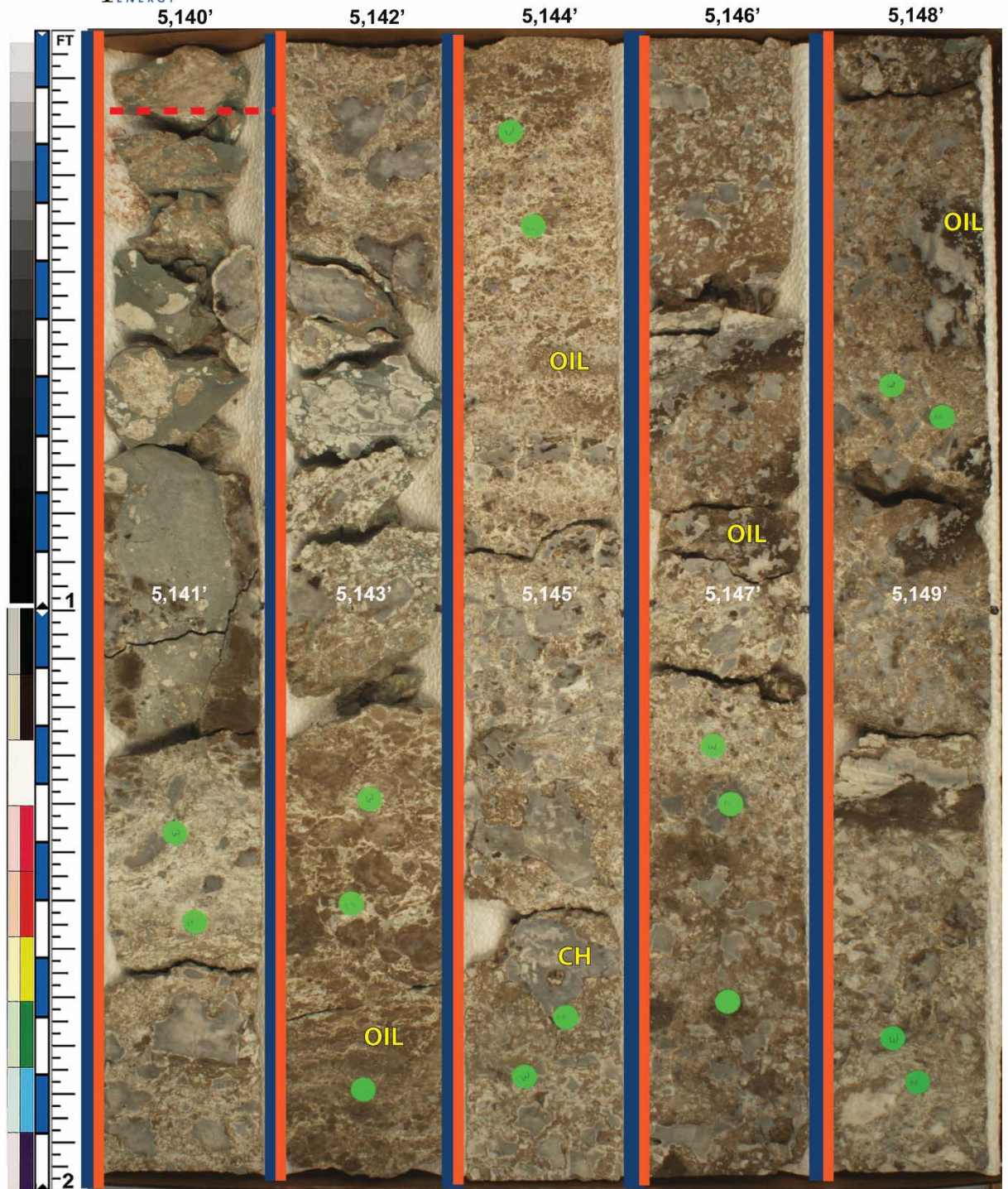


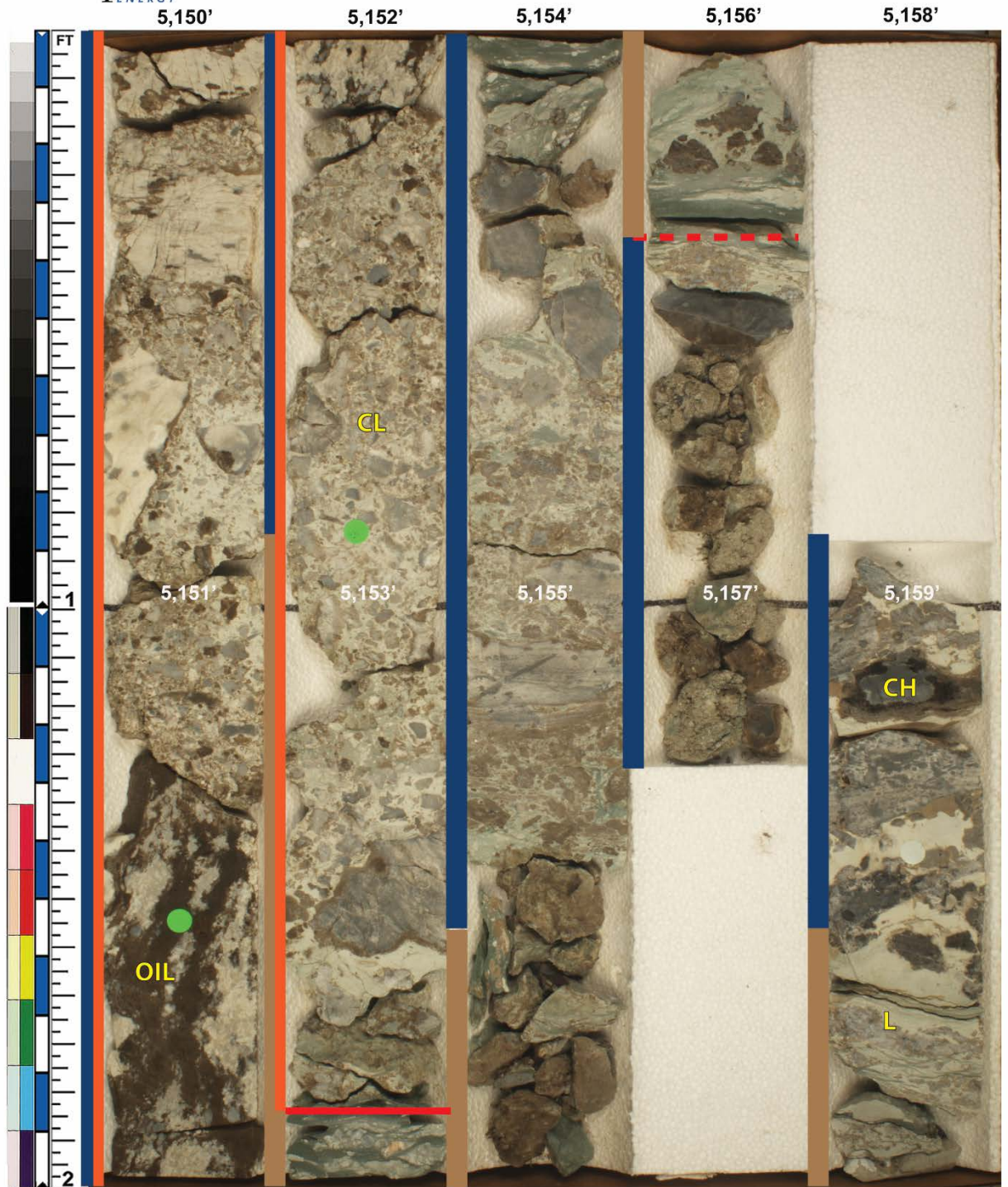


CORE #2: WHITE LIGHT (ALBUS 1-34H)





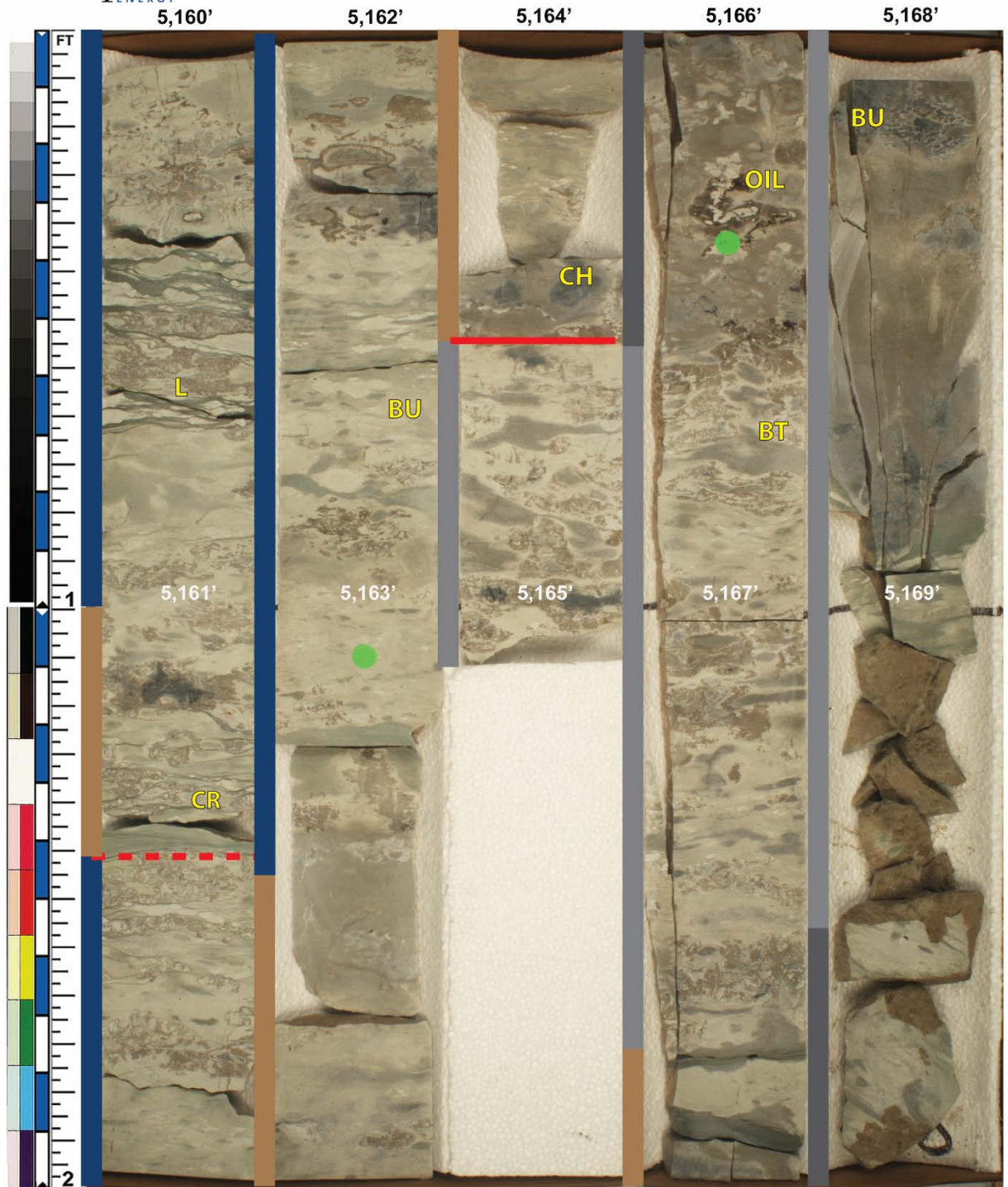


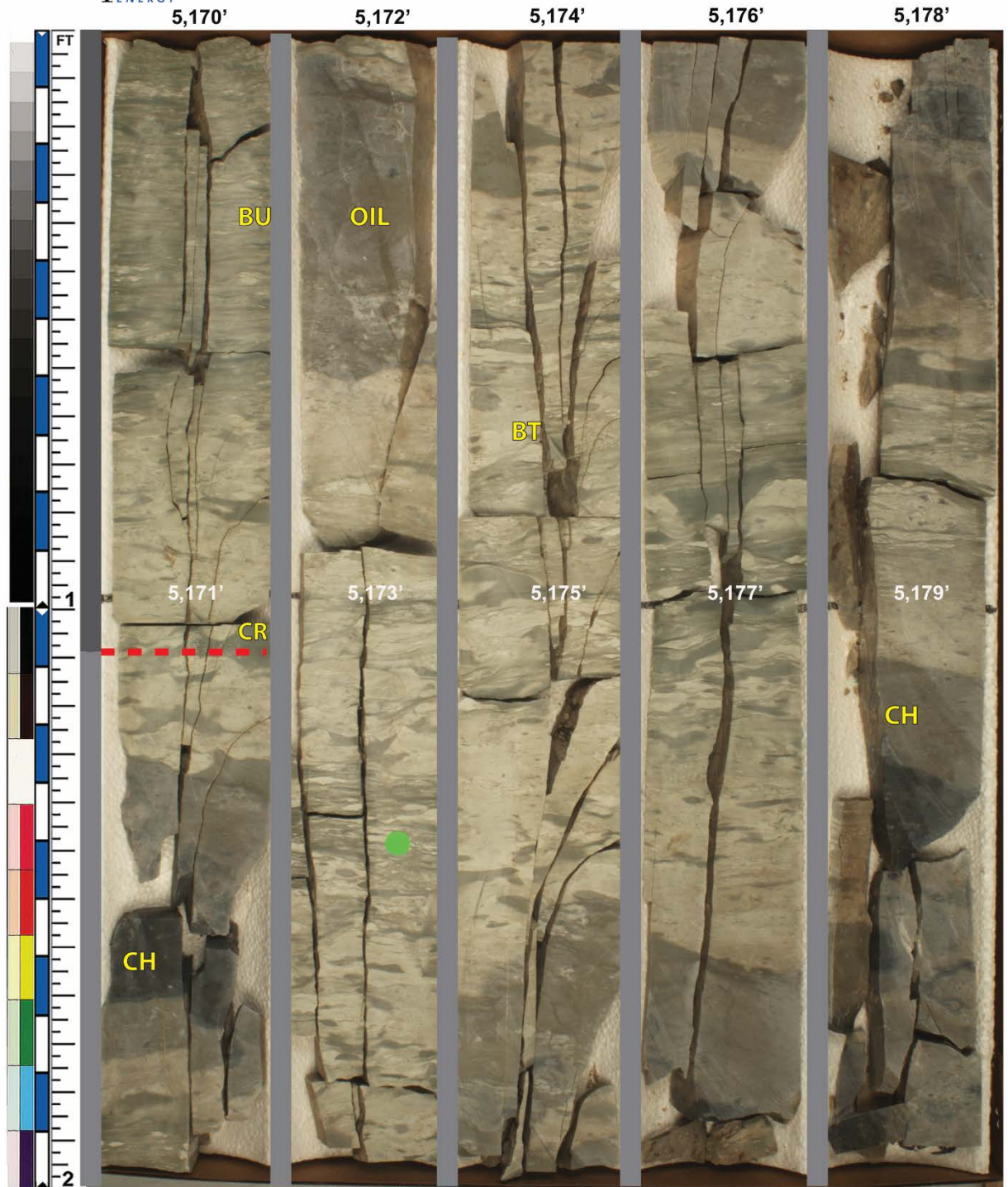


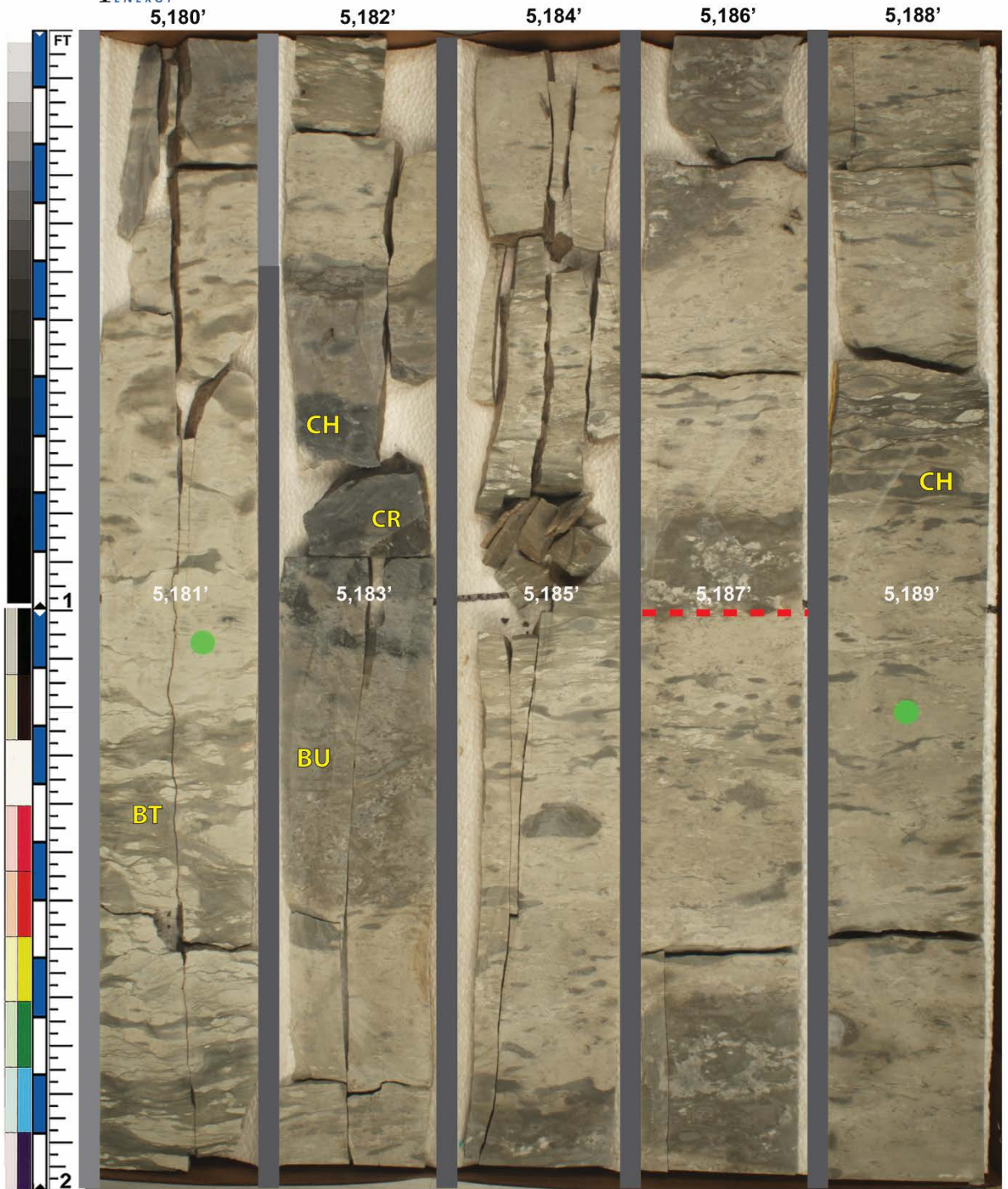


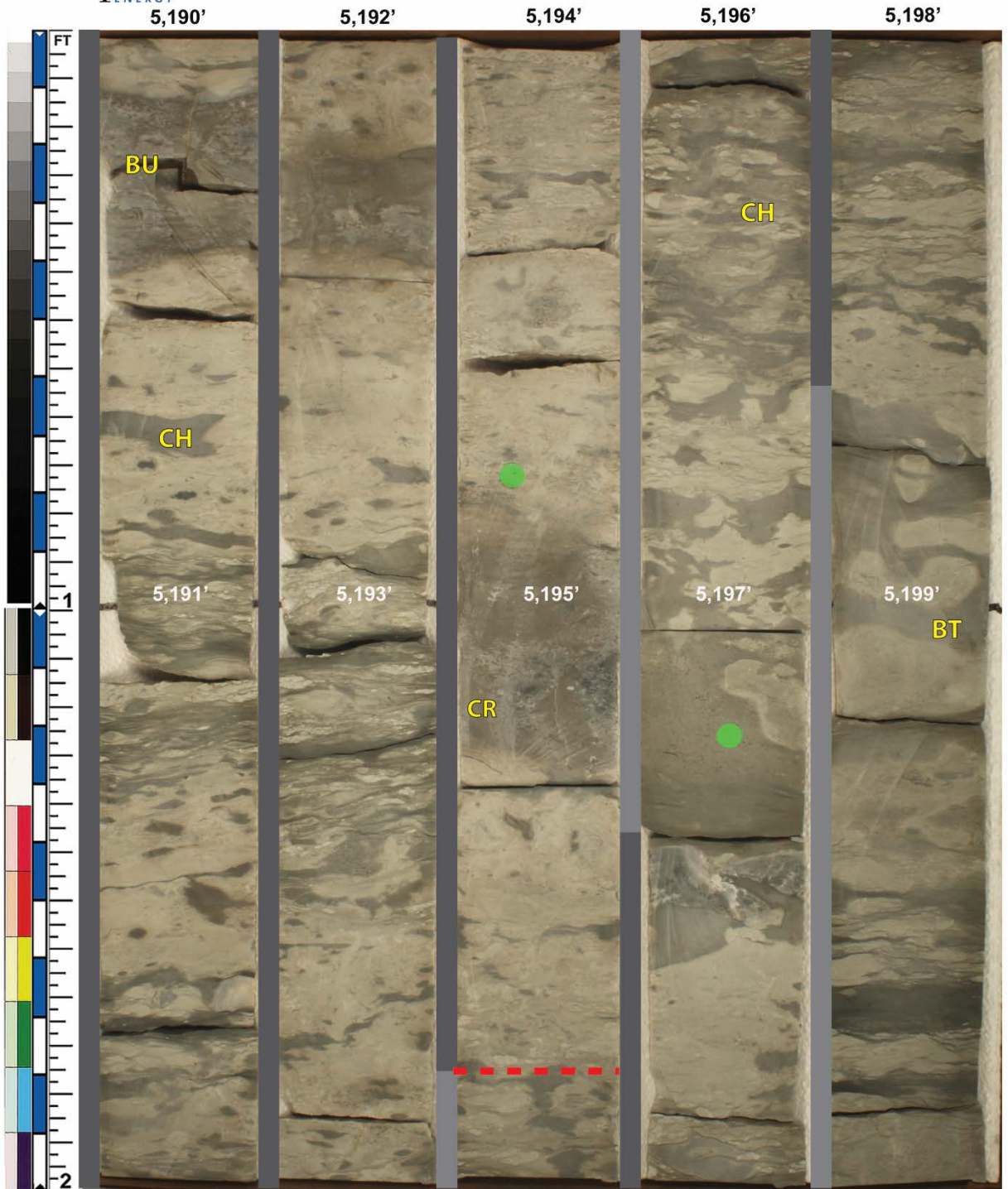
Well: Albus 1-34 H
Location: Woods Co., OK
Formation: Osage

Job: 09-0818
Core 3: box 2 of 2 Depth: 5,160 - 5,165.18
Core 4: box 1 of 5 Depth: 5,166 - 5,170



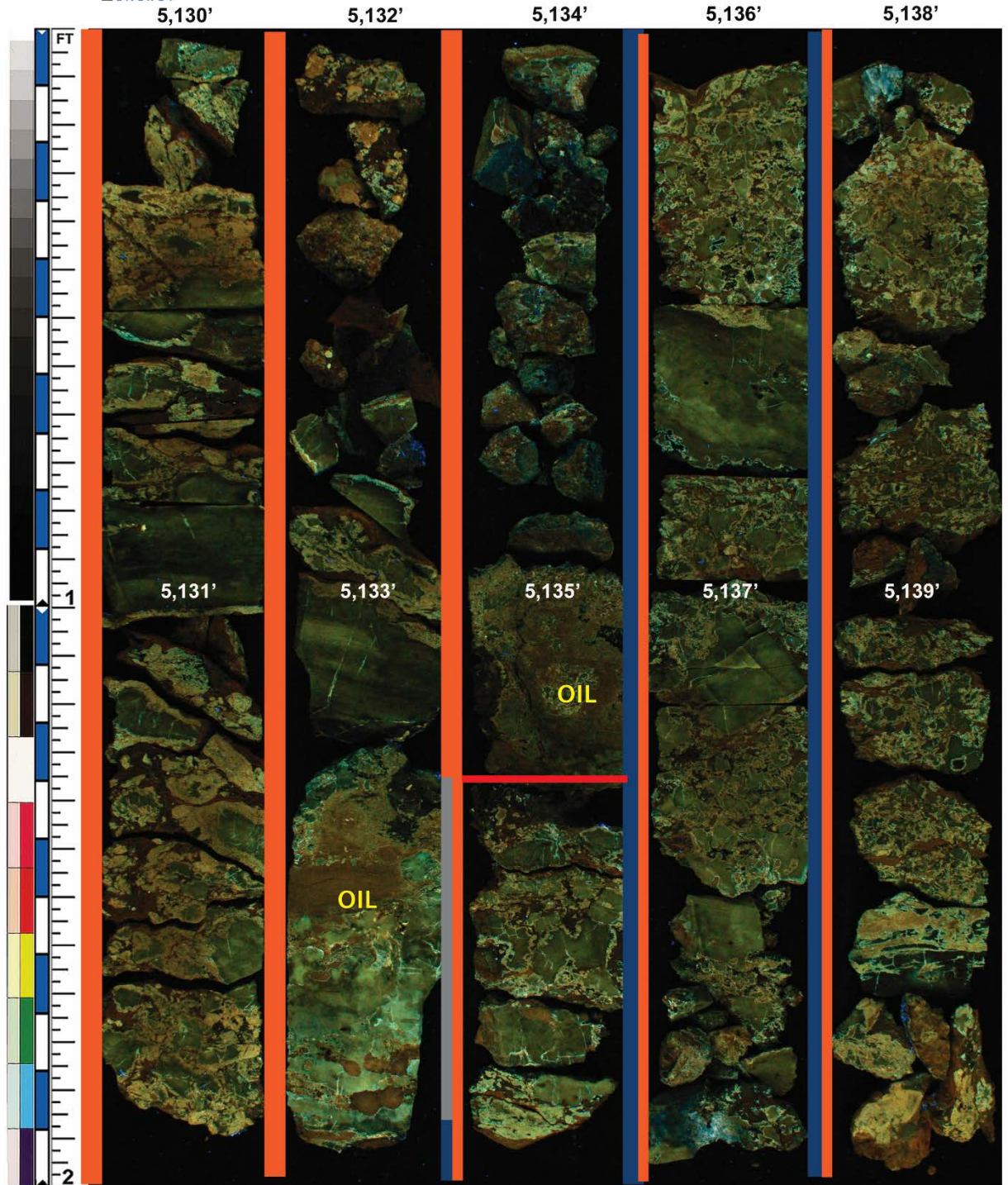


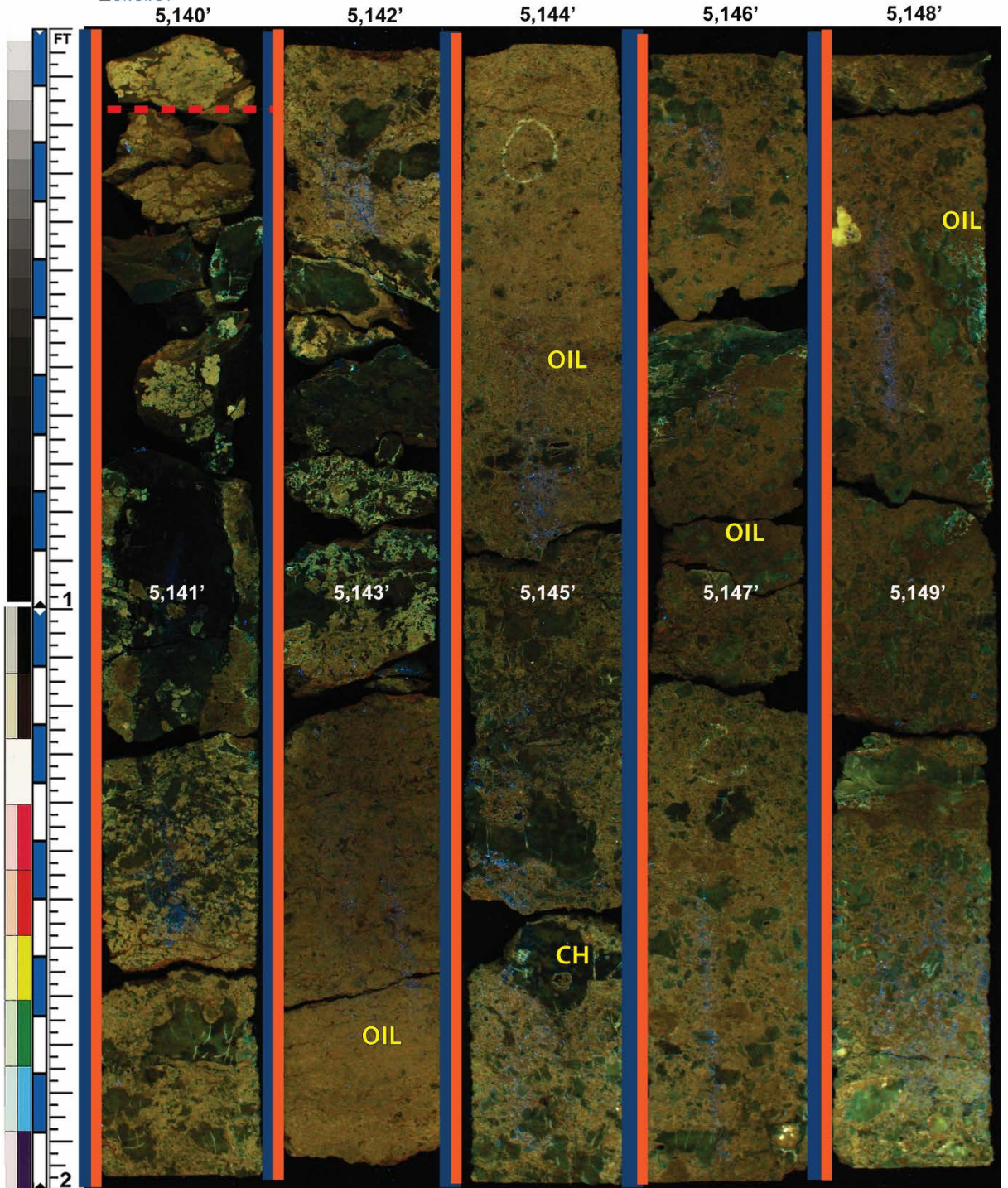


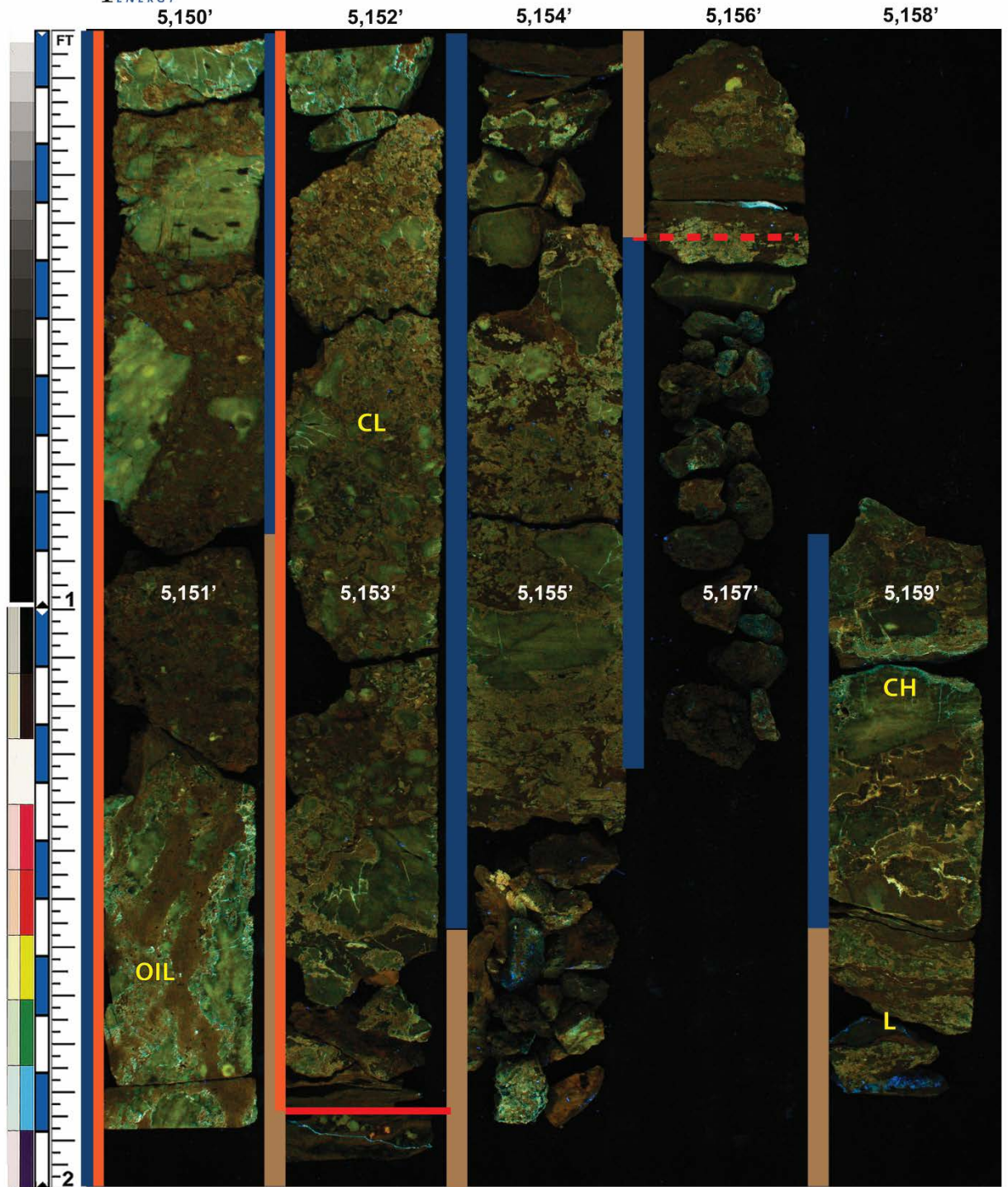




CORE #2: UV LIGHT (ALBUS 1-34H)



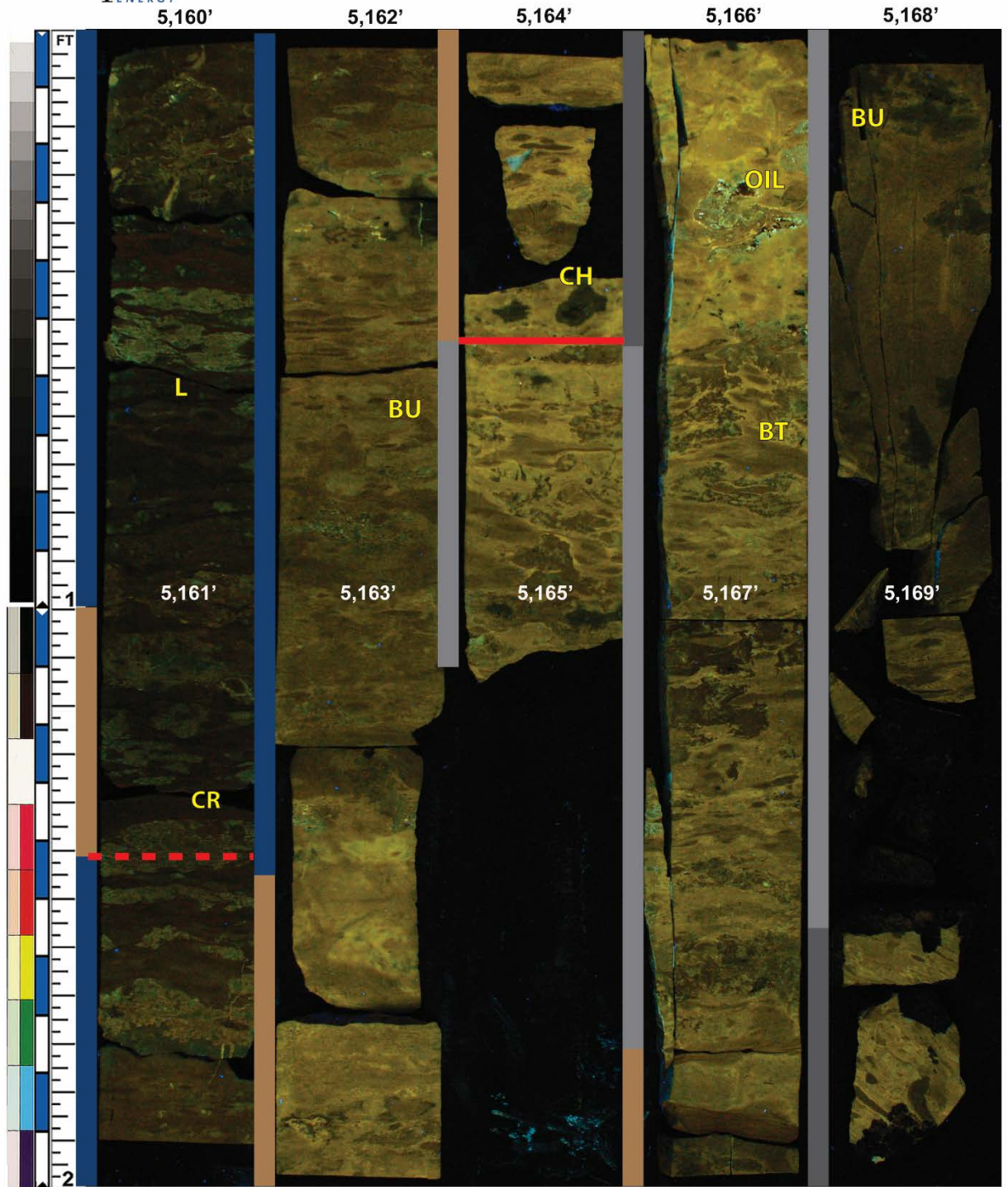


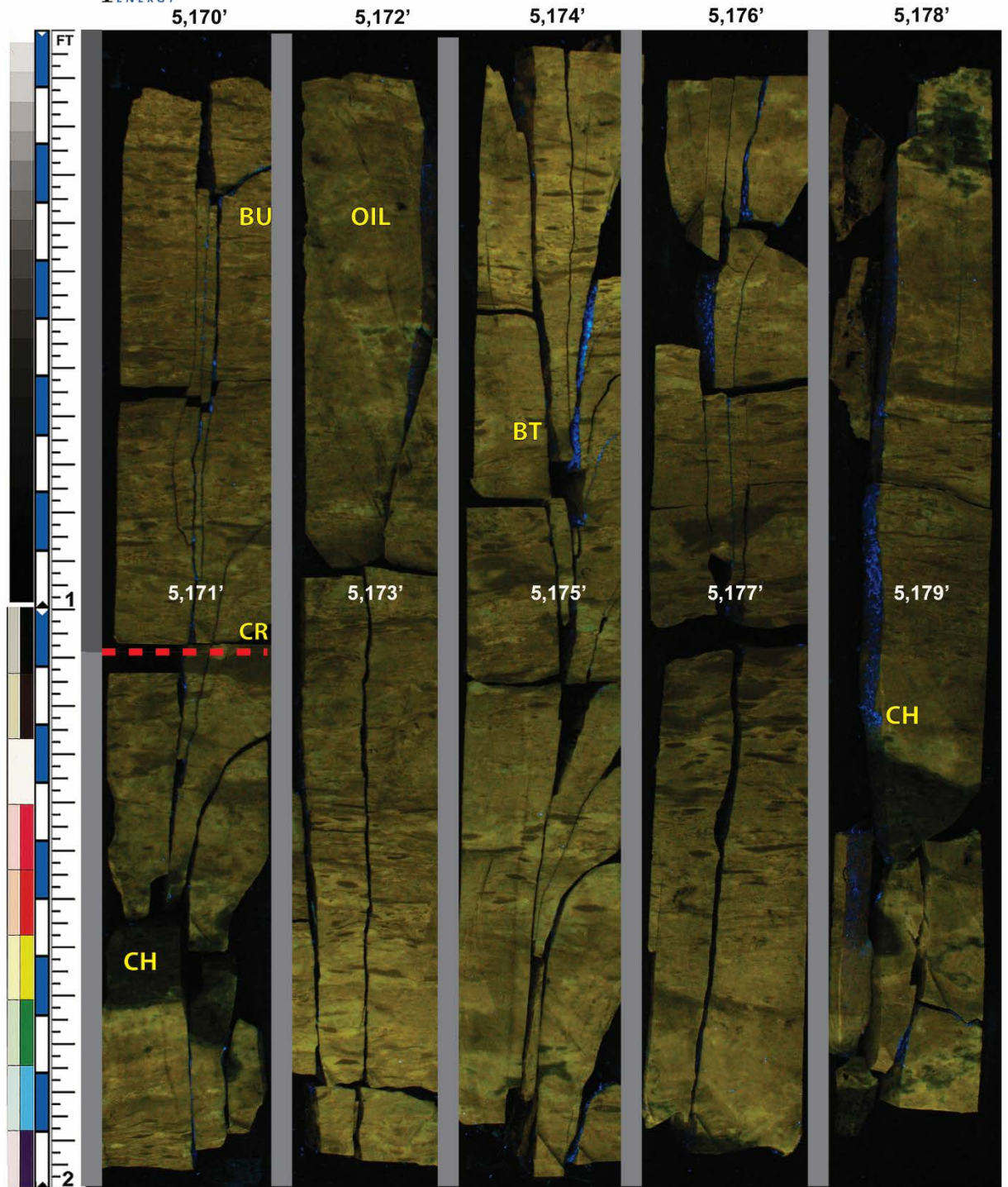




Well: Albus 1-34 H
Location: Woods Co., OK
Formation: Osage

Job: 09-0818
Core 3: box 2 of 2 Depth: 5,160 - 5,165.18
Core 4: box 1 of 5 Depth: 5,166 - 5,170

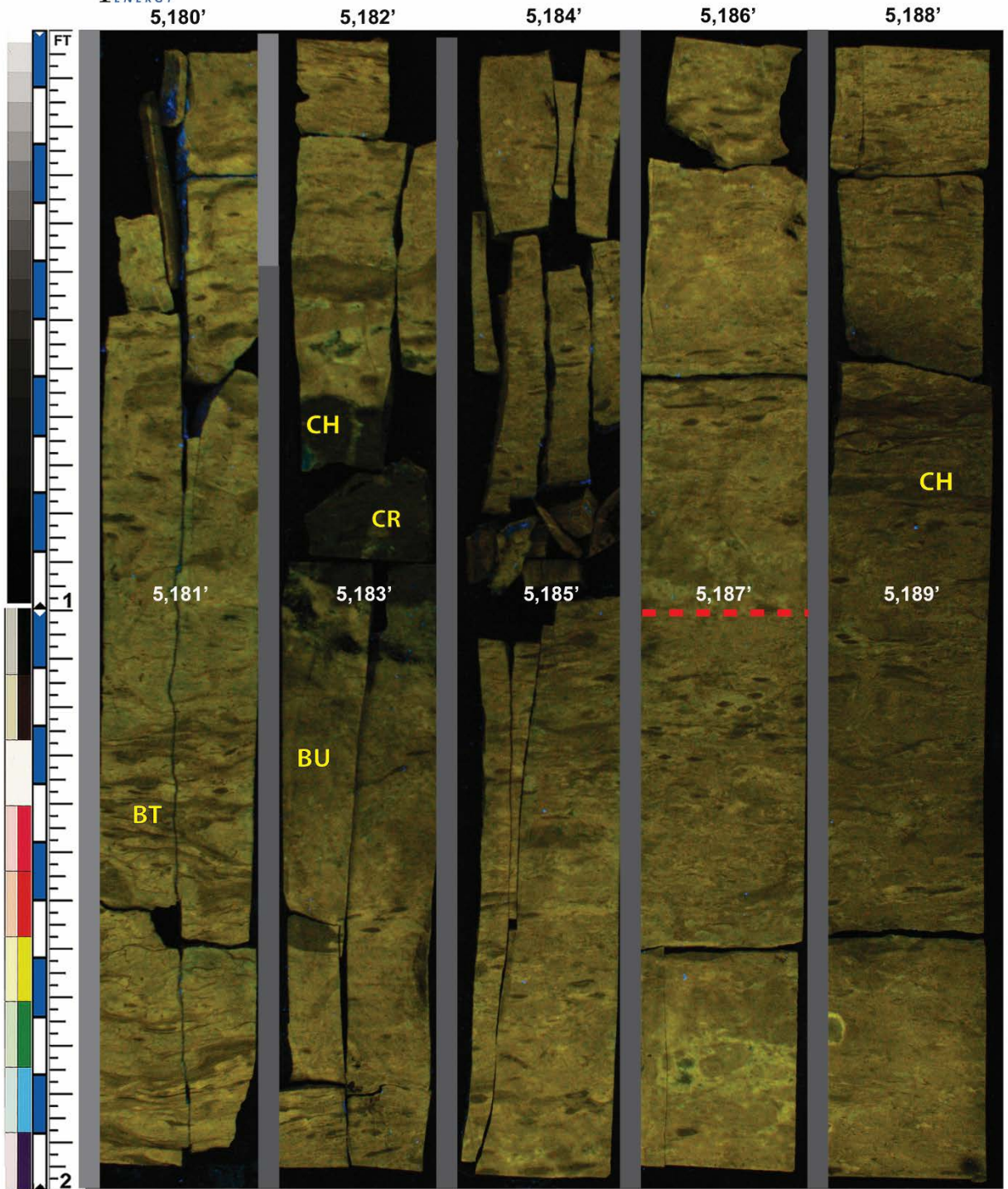






Well: Albus 1-34 H
Location: Woods Co., OK
Formation: Osage

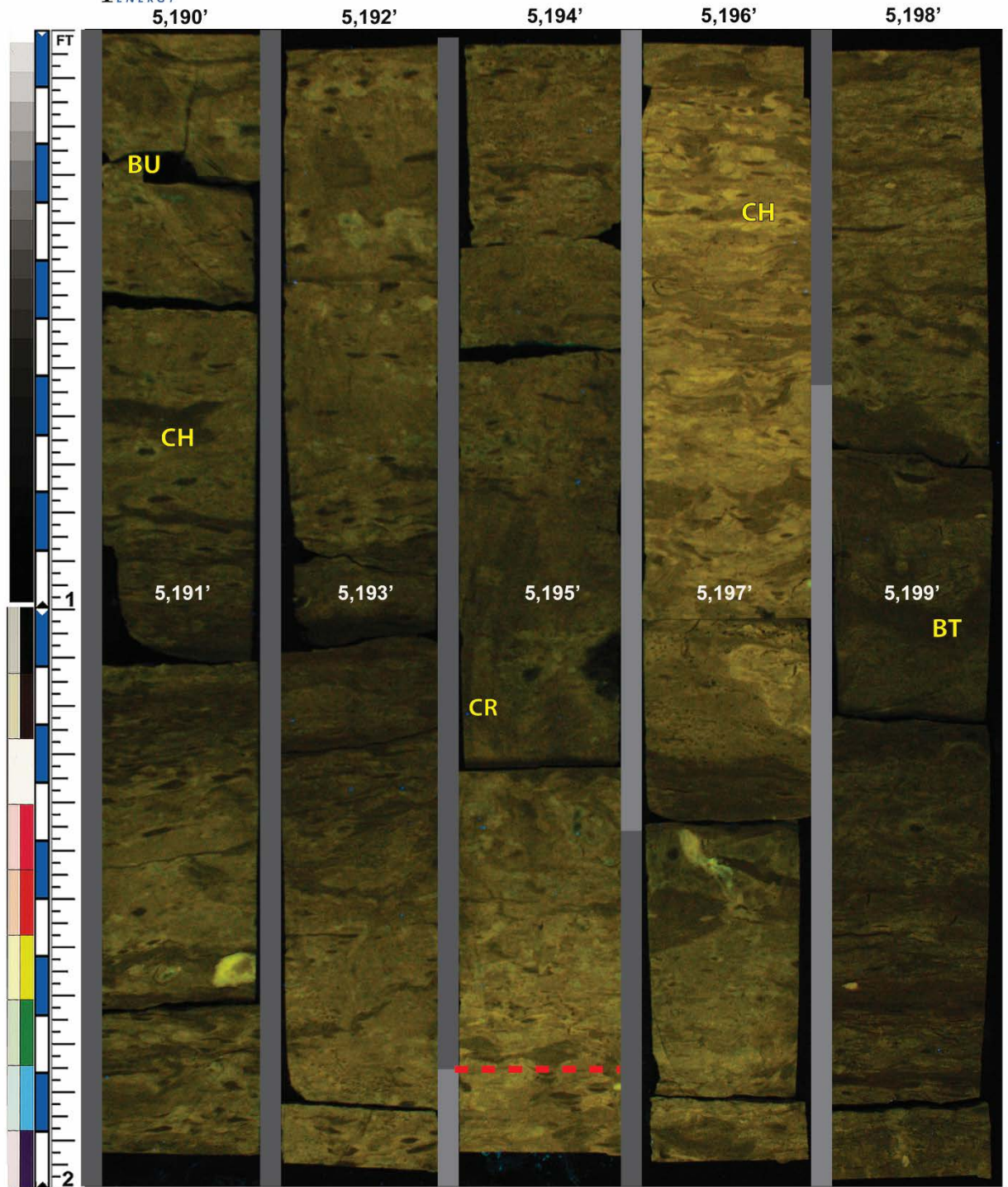
Job: 09-0818
Core 4: box 3 of 5
Depth: 5,180 - 5,190





Well: Albus 1-34 H
Location: Woods Co., OK
Formation: Osage

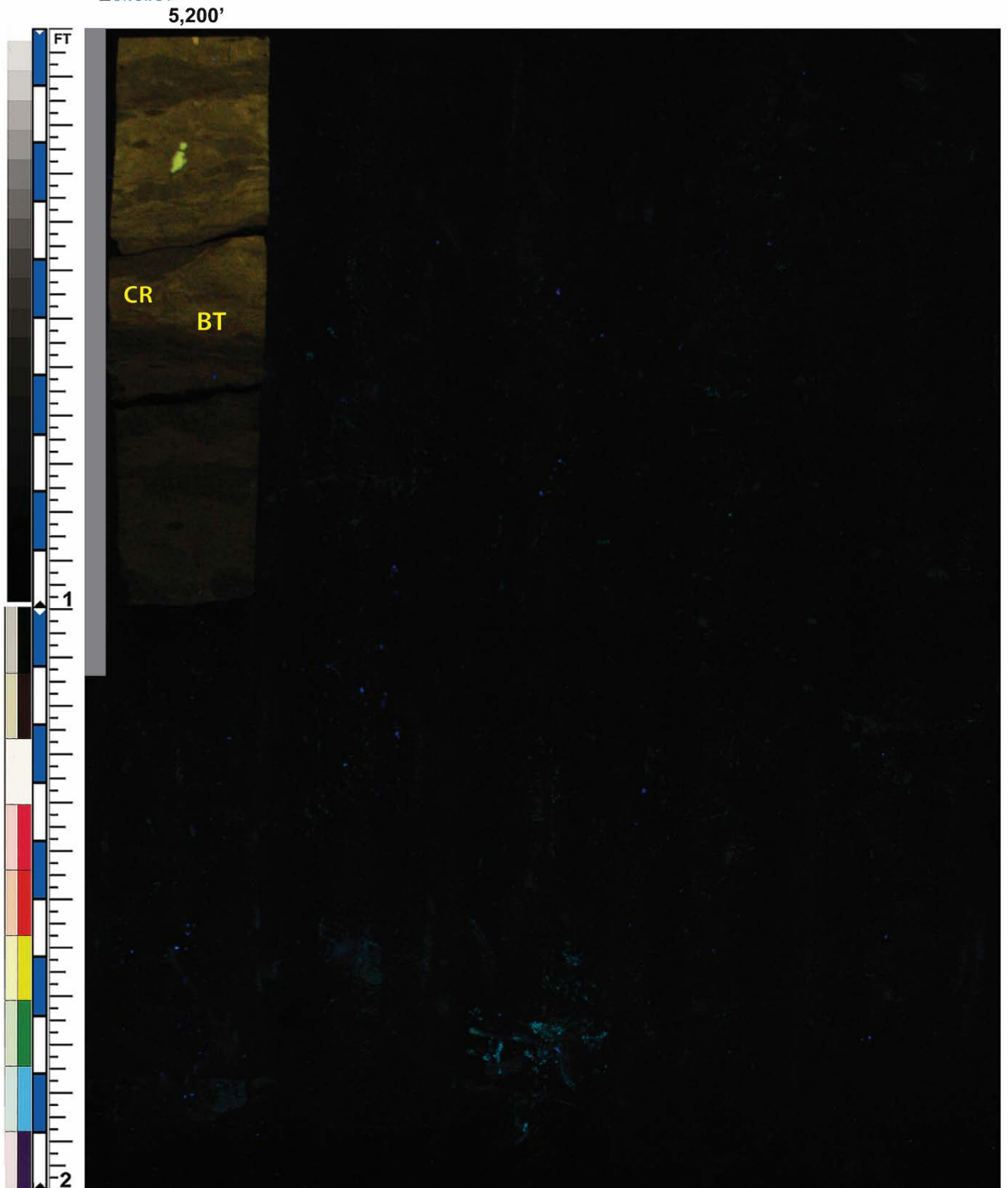
Job: 09-0818
Core 4: box 4 of 5
Depth: 5,190 - 5,200





Well: Albus 1-34 H
Location: Woods Co., OK
Formation: Osage

Job: 09-0818
Core 4: box 5 of 5
Depth: 5,200 - 5,201.1

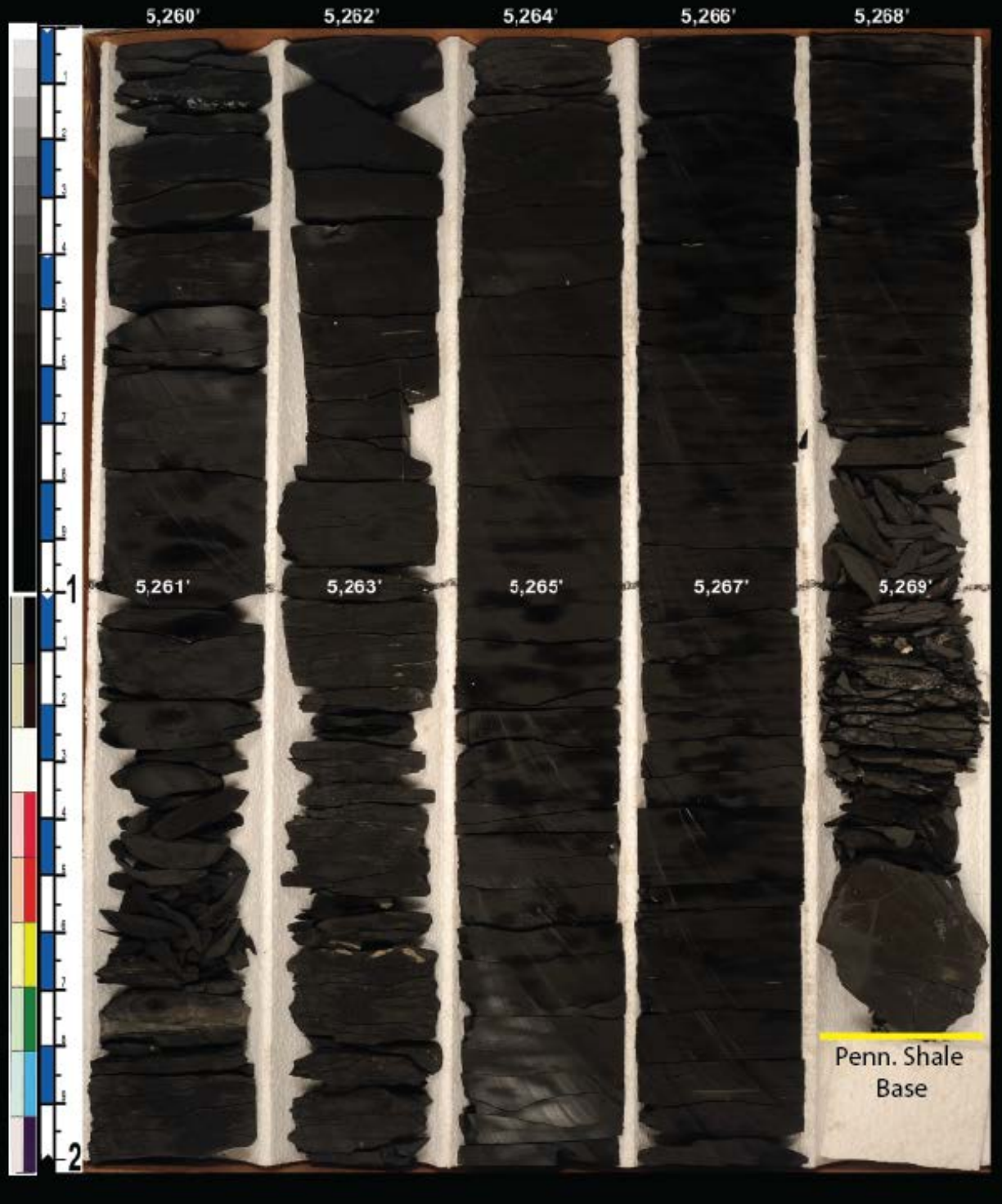


CORE #3: WHITE LIGHT (TROPHY FARMS 32-34-16H)



Well: Trophy Farms 32-34-16 1H
Location: Comanche Co., KS
Formation: Cherokee

Job: #11-1002
Core 1: box 1 of 1
Depth: 5,260' - 5,269.8'





Well: Trophy Farms 32-34-16 1H
Location: Comanche Co., KS
Formation: Cherokee

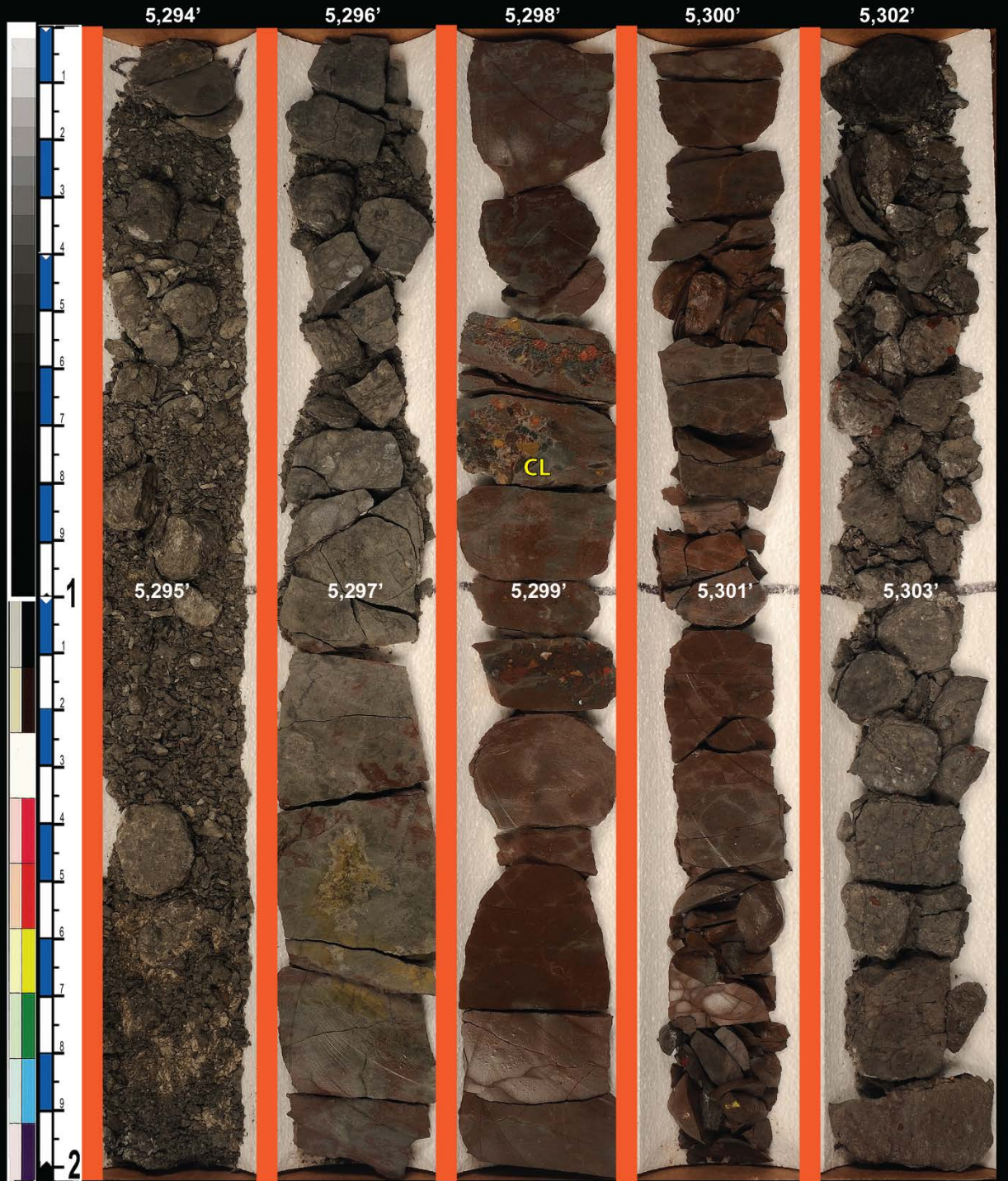
Job: #11-1002
Core 2: box 1 of 1
Depth: 5,280' - 5,290'





Well: Trophy Farms 32-34-16 1H
Location: Comanche Co., KS
Formation: Cherokee

Job: #11-1002
Core 3: box 1 of 2
Depth: 5,294' - 5,304'

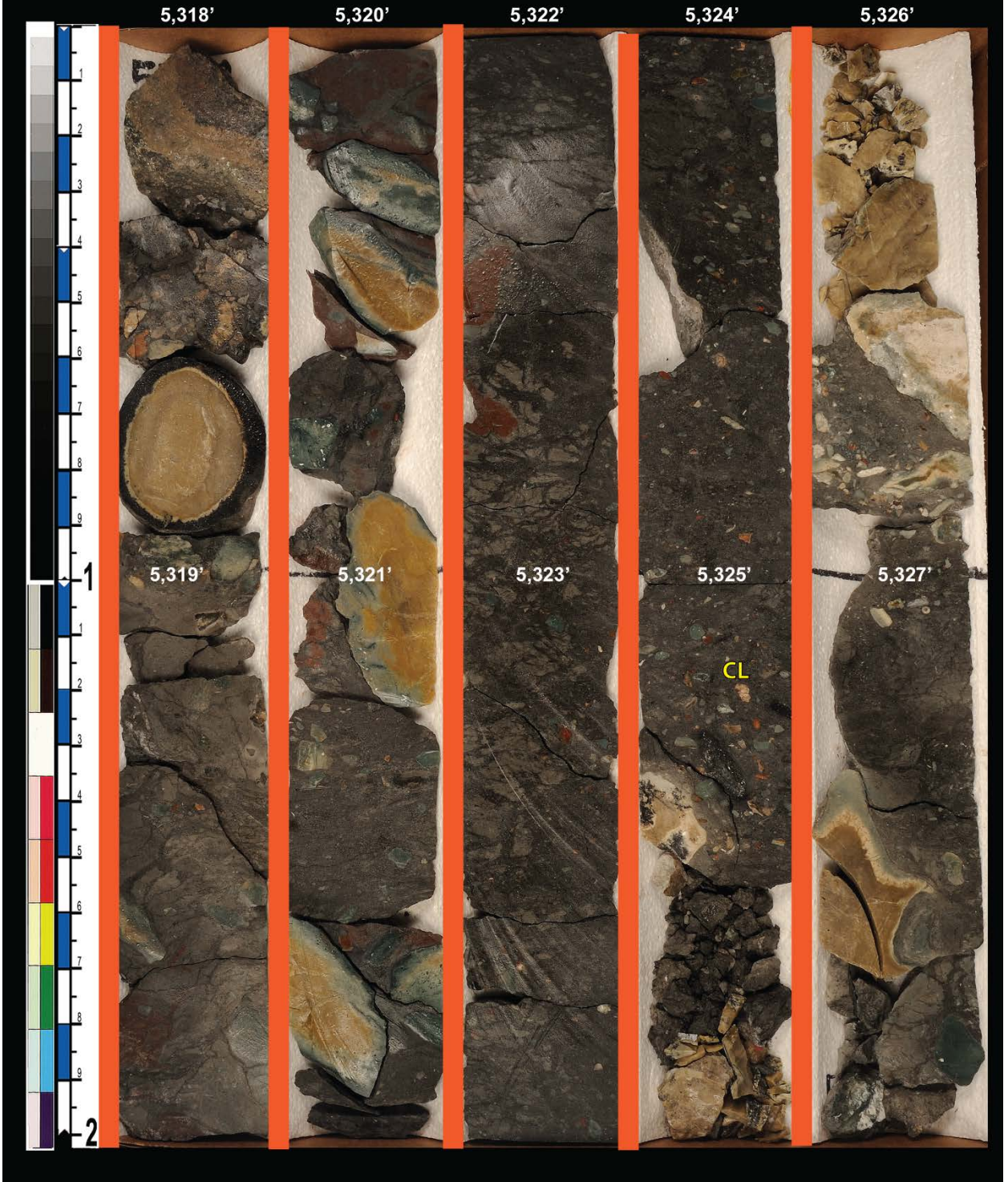




Well: Trophy Farms 32-34-16 1H
Location: Comanche Co., KS
Formation: Cherokee

Job: #11-1002
Core 3: box 2 of 2
Depth: 5,304' - 5,313.55'







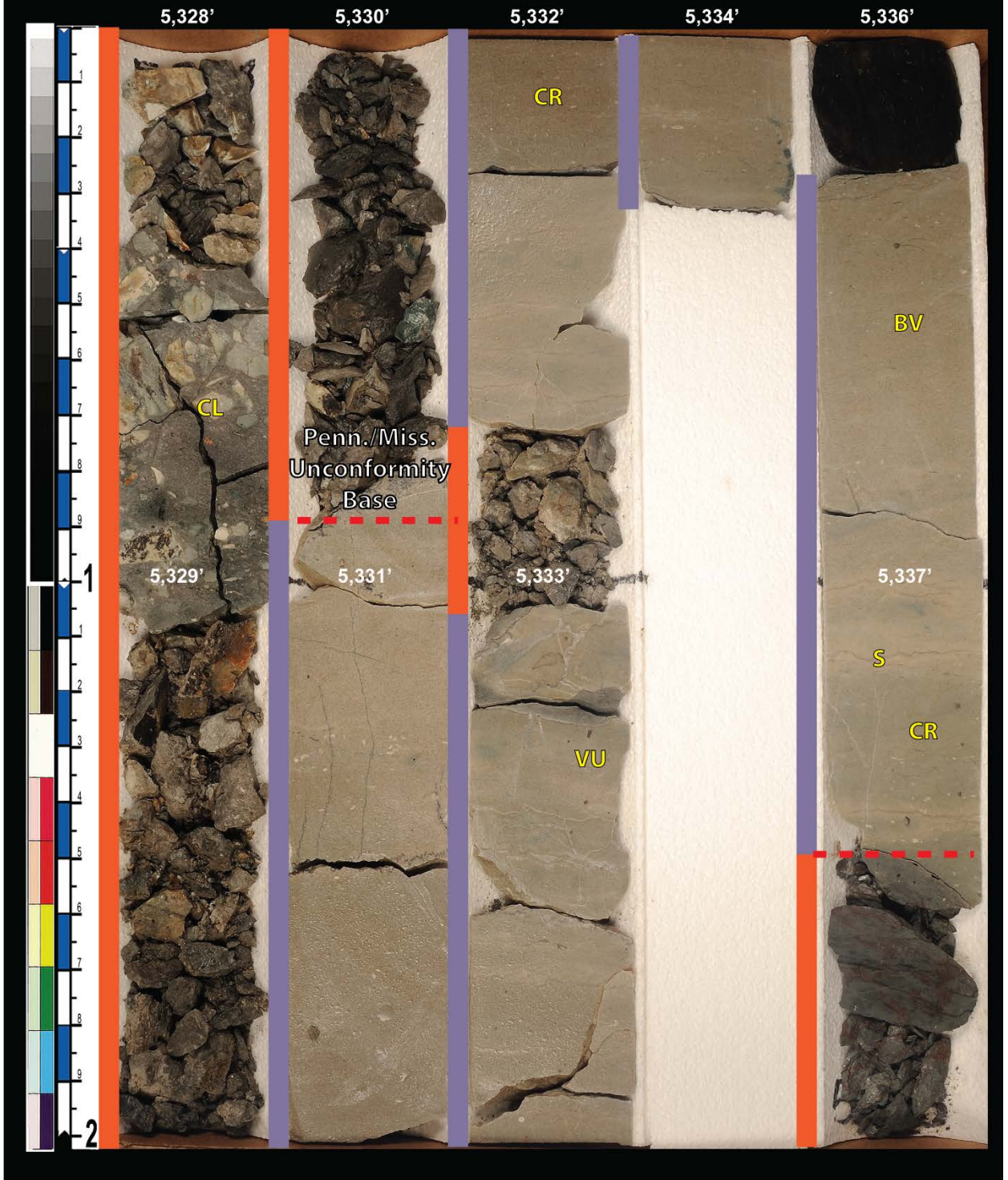
Well: Trophy Farms 32-34-16 1H

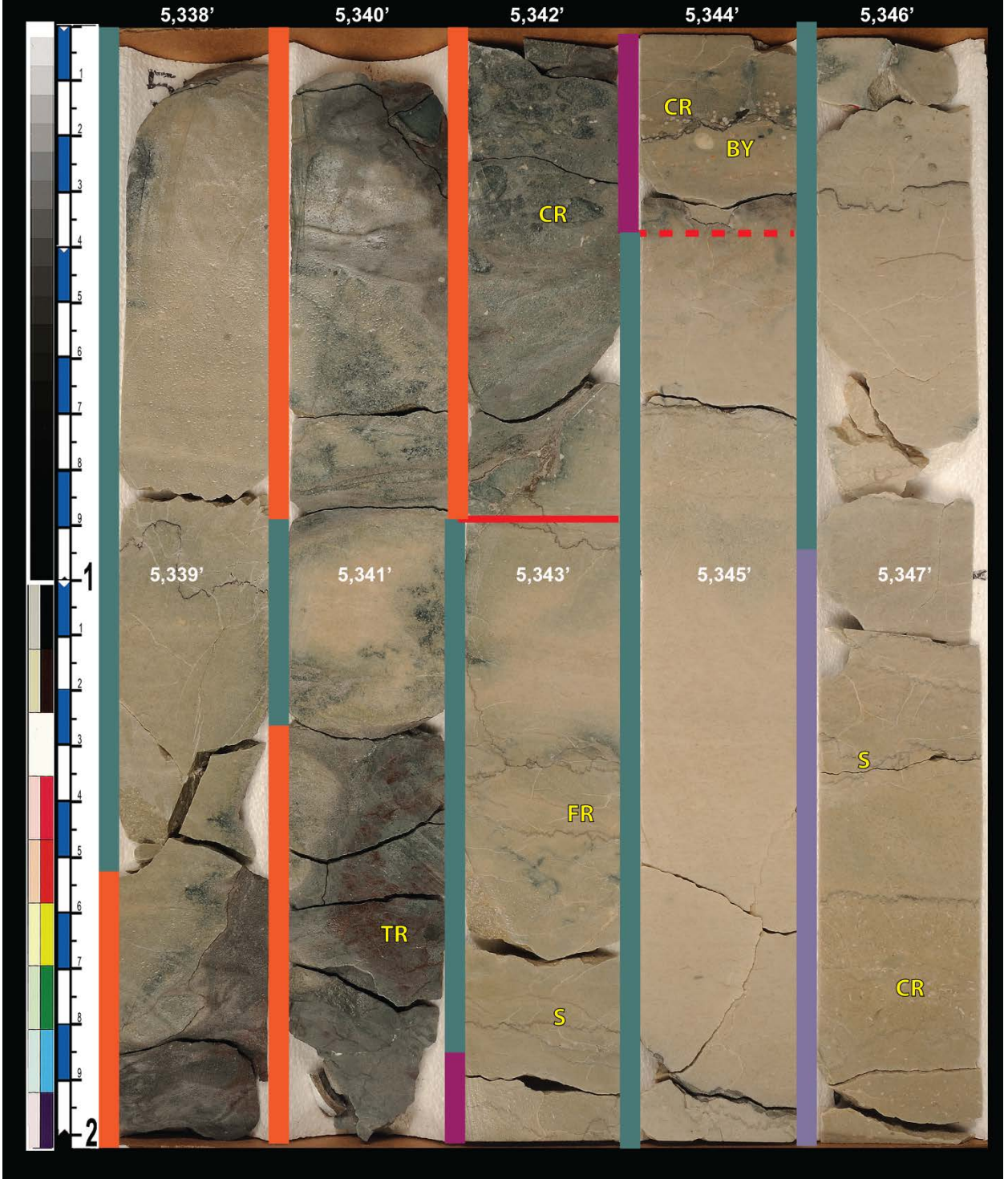
Job: #11-1002

Location: Comanche Co., KS

Core 4: box 2 of 2 Depth: 5,328' - 5,334.34'

Formation: Cherokee, Mississippi Lime Core 5: box 1 of 7 Depth: 5,336' - 5,338'

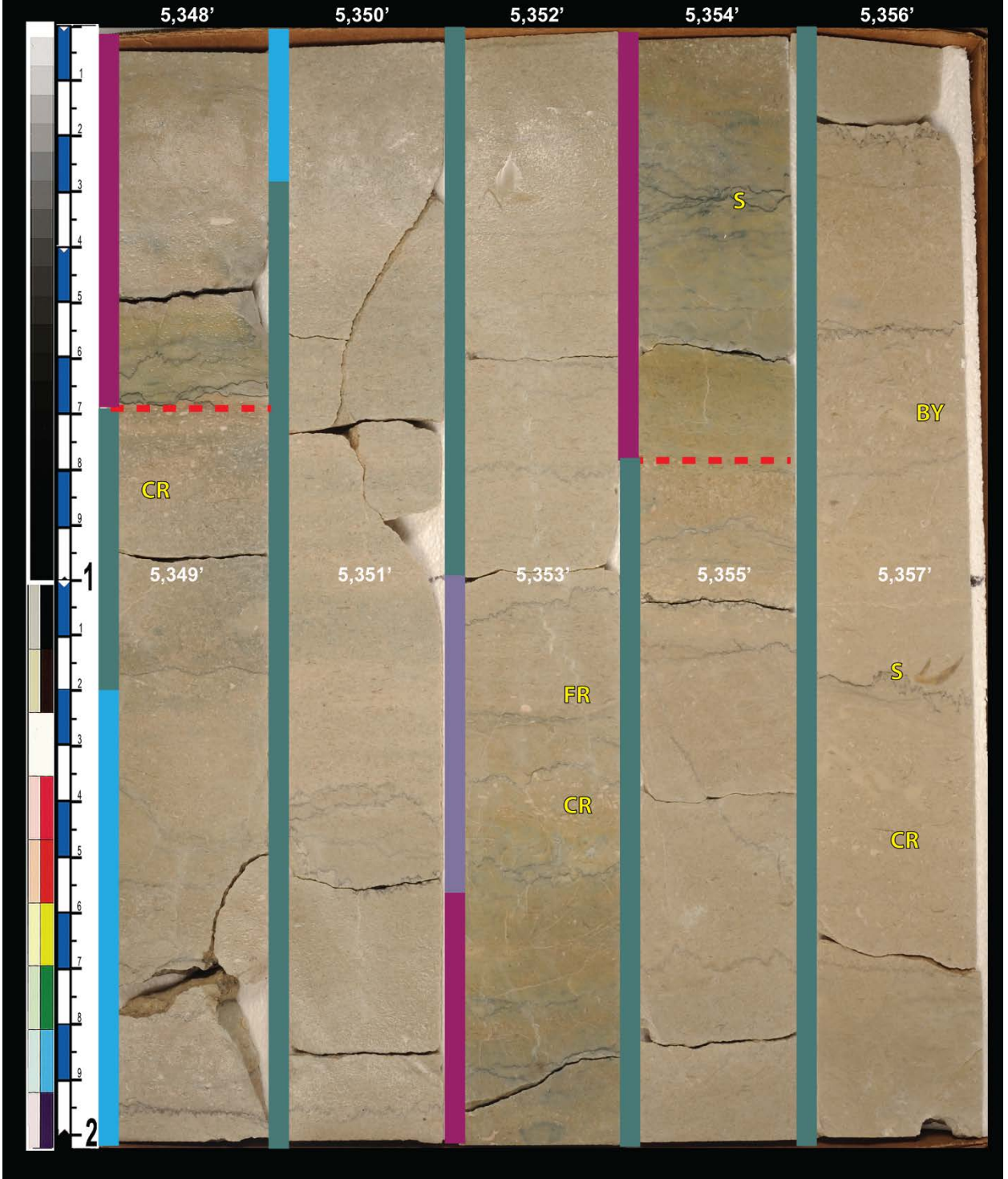


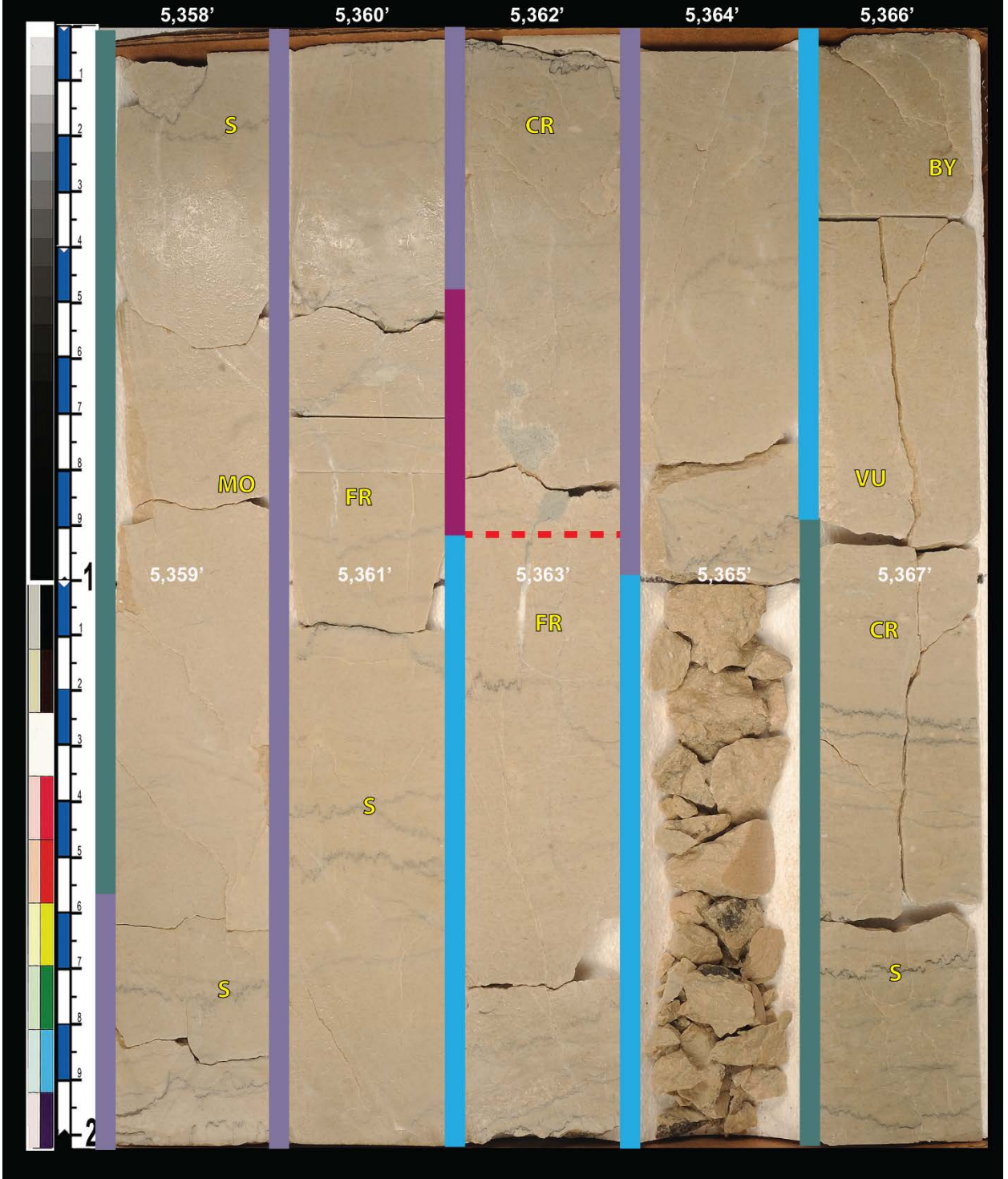


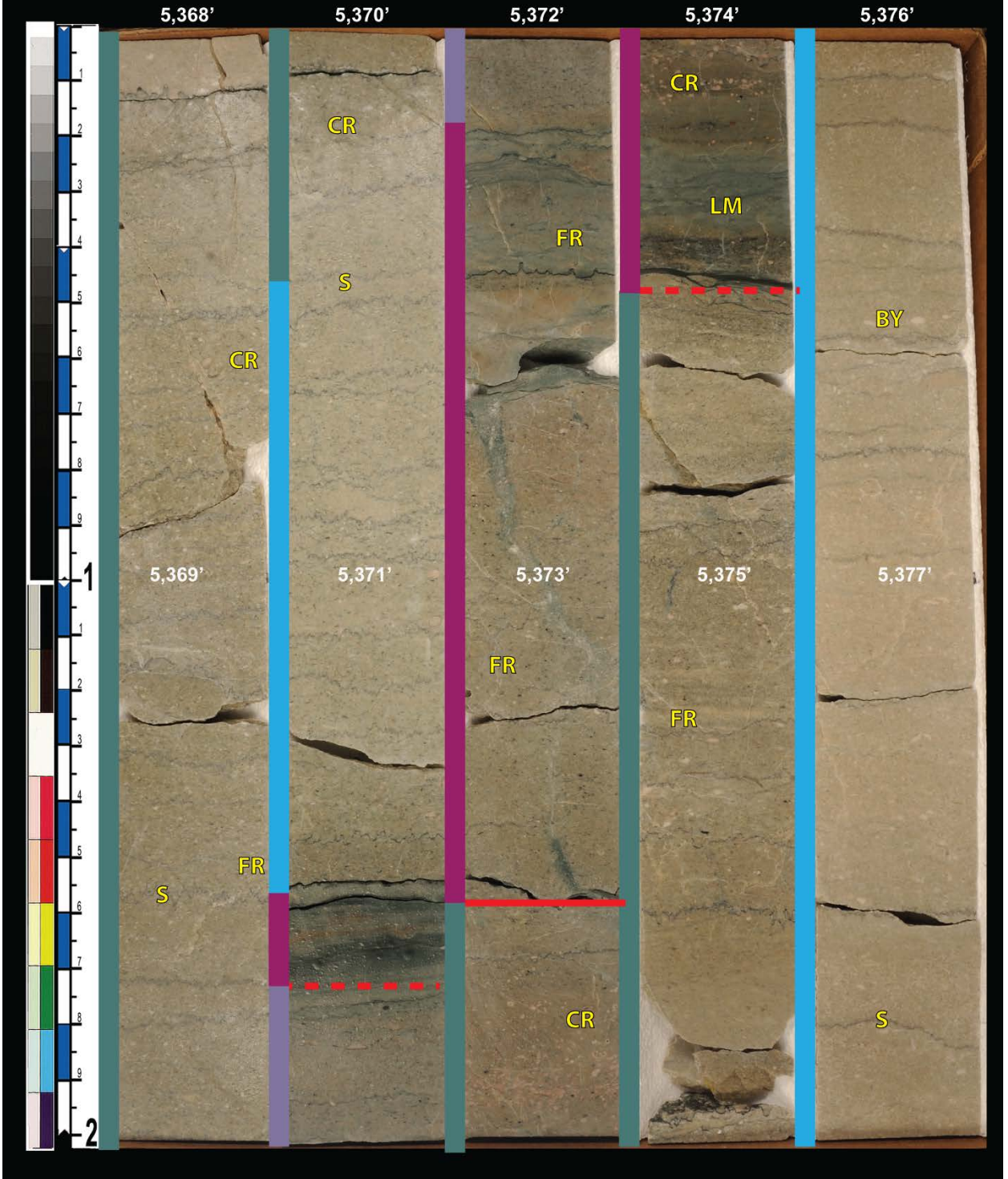


Well: Trophy Farms 32-34-16 1H
Location: Comanche Co., KS
Formation: Mississippi Lime

Job: #11-1002
Core 5: box 3 of 7
Depth: 5,348' - 5,358'



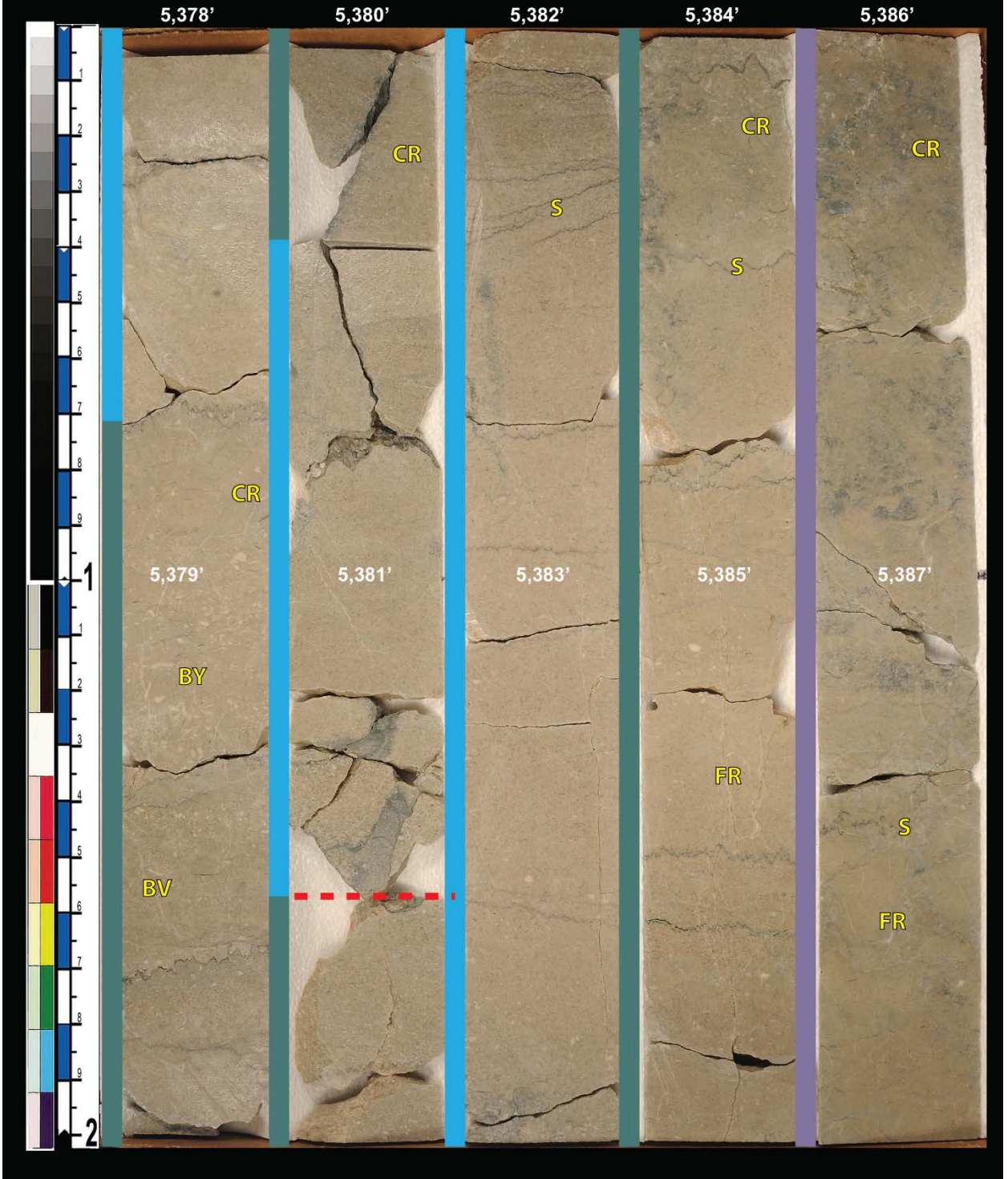






Well: Trophy Farms 32-34-16 1H
Location: Comanche Co., KS
Formation: Mississippi Lime

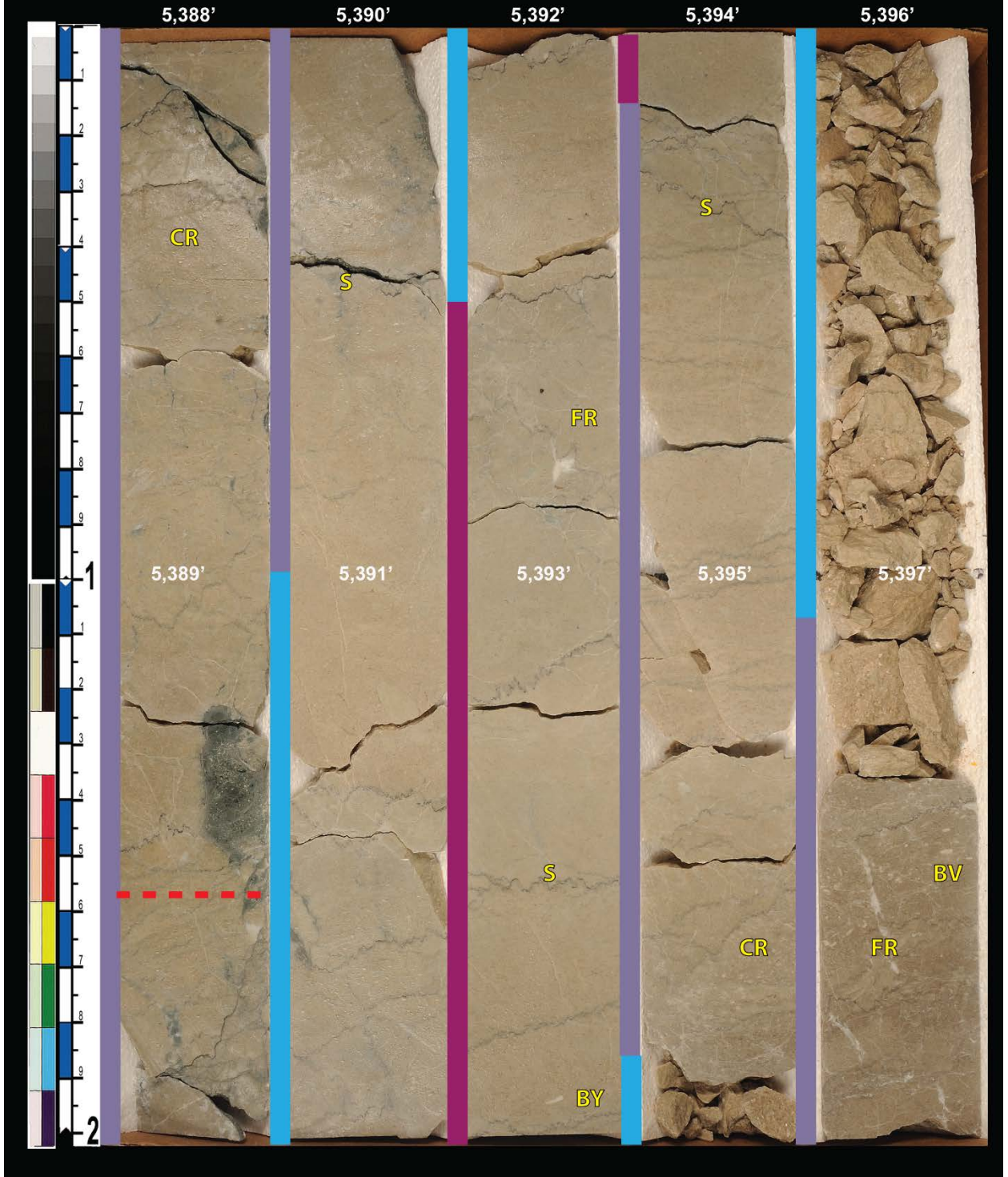
Job: #11-1002
Core 5: box 6 of 7
Depth: 5,378' - 5,388'





Well: Trophy Farms 32-34-16 1H
Location: Comanche Co., KS
Formation: Mississippi Lime

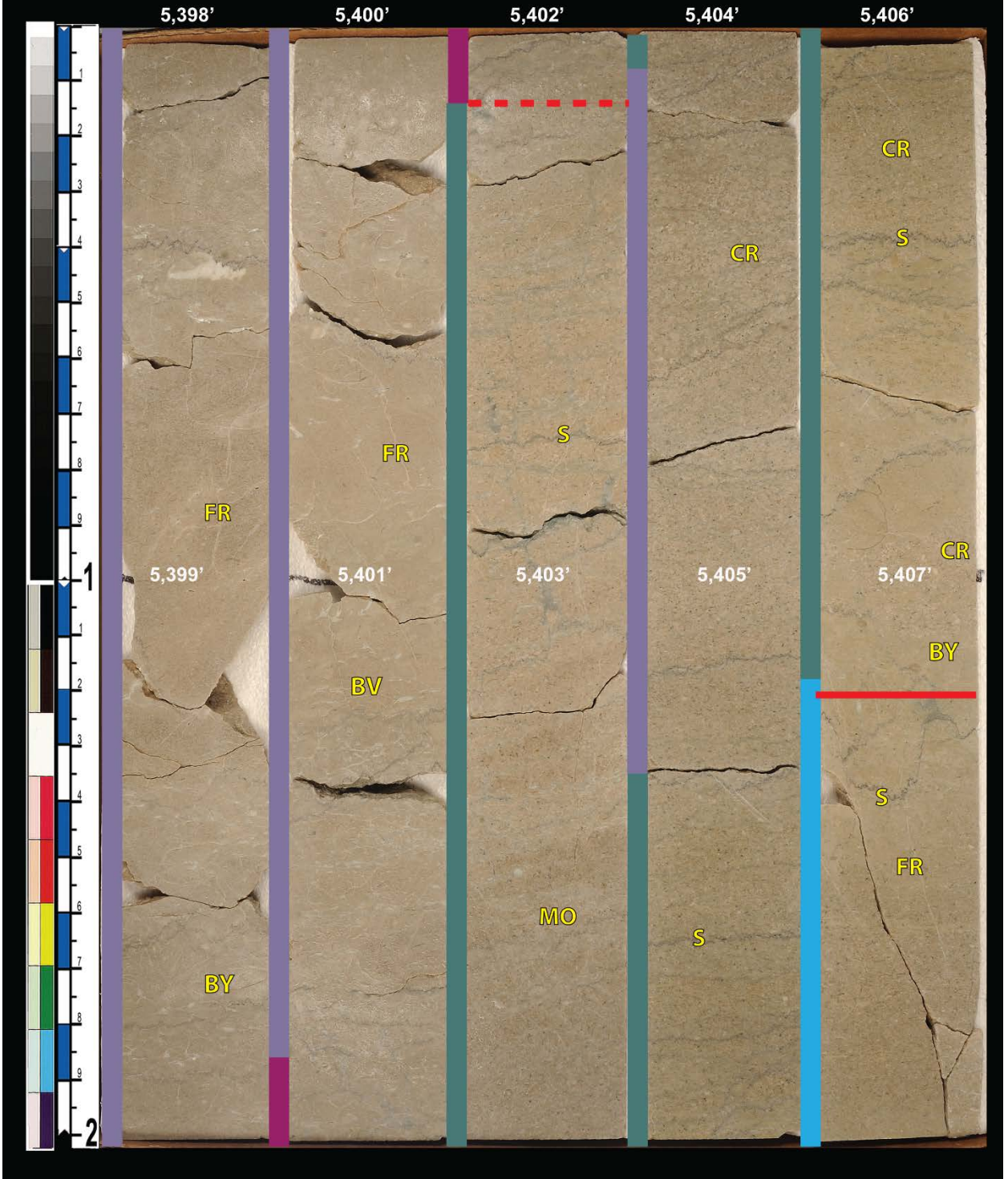
Job: #11-1002
Core 5: box 7 of 7 Depth: 5,388' - 5,397.36'
Core 6: box 1 of 7 Depth: 5,397.36' - 5,398'

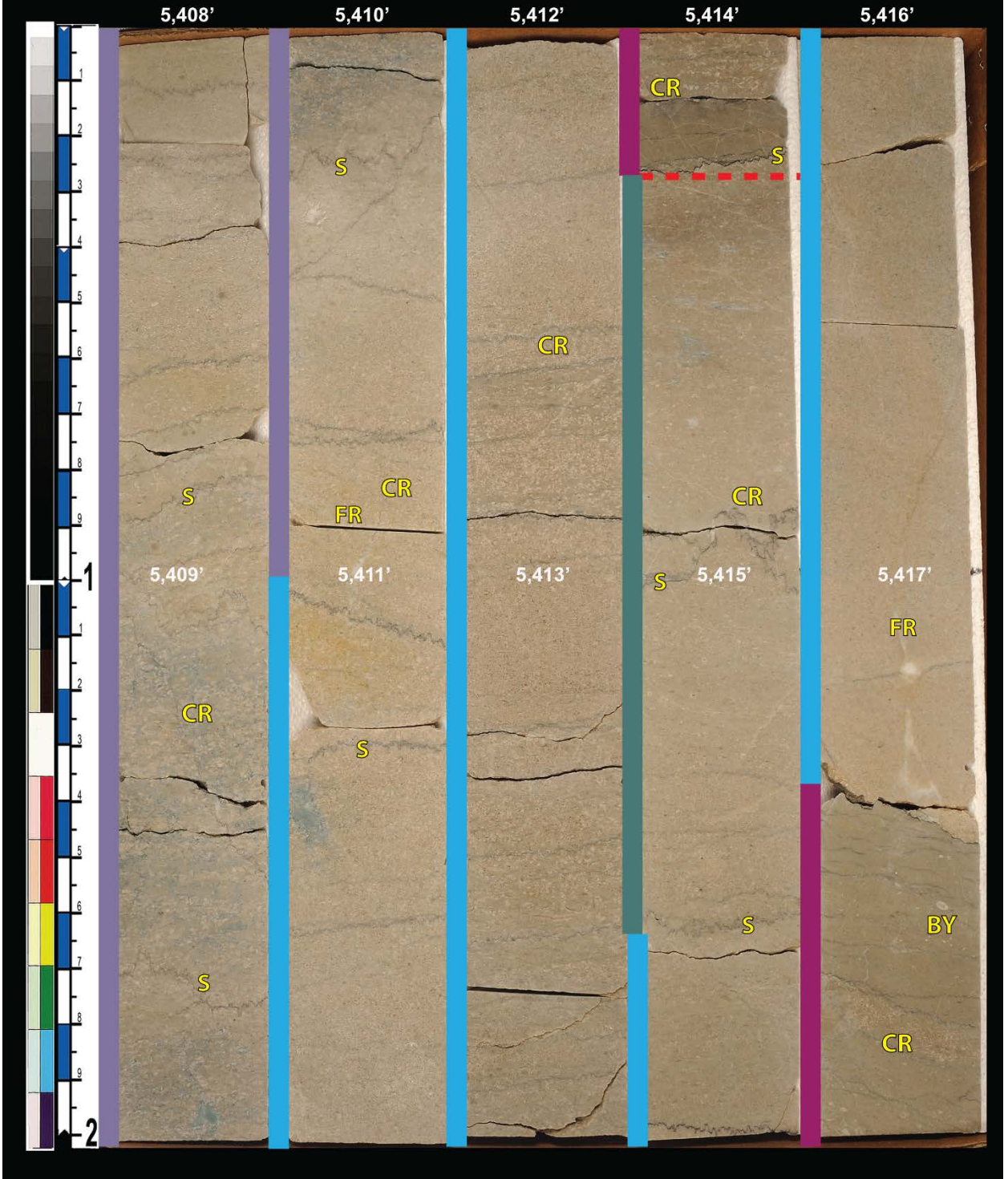




Well: Trophy Farms 32-34-16 1H
Location: Comanche Co., KS
Formation: Mississippi Lime

Job: #11-1002
Core 6: box 2 of 7
Depth: 5,398' - 5,408'

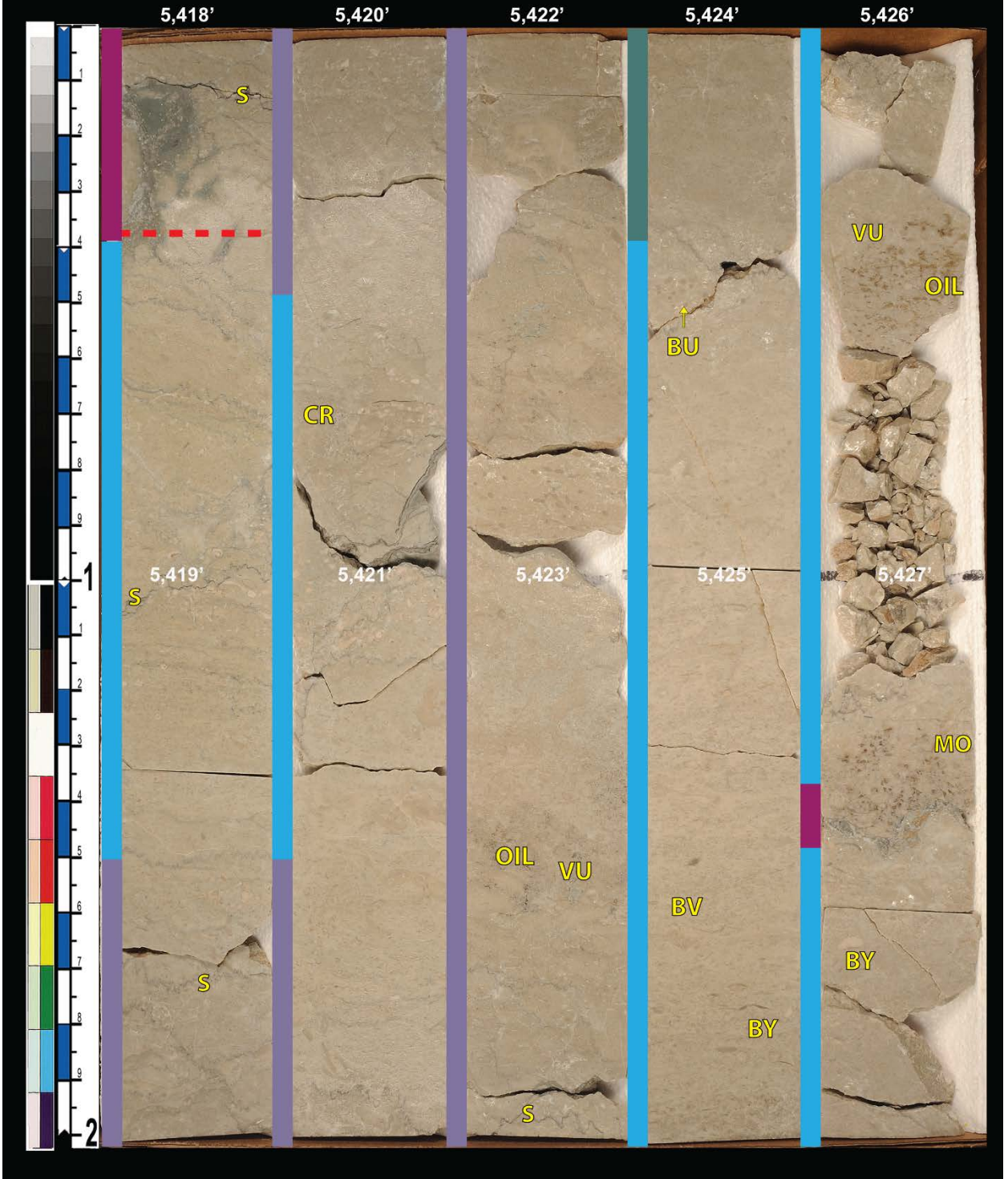






Well: Trophy Farms 32-34-16 1H
Location: Comanche Co., KS
Formation: Mississippi Lime

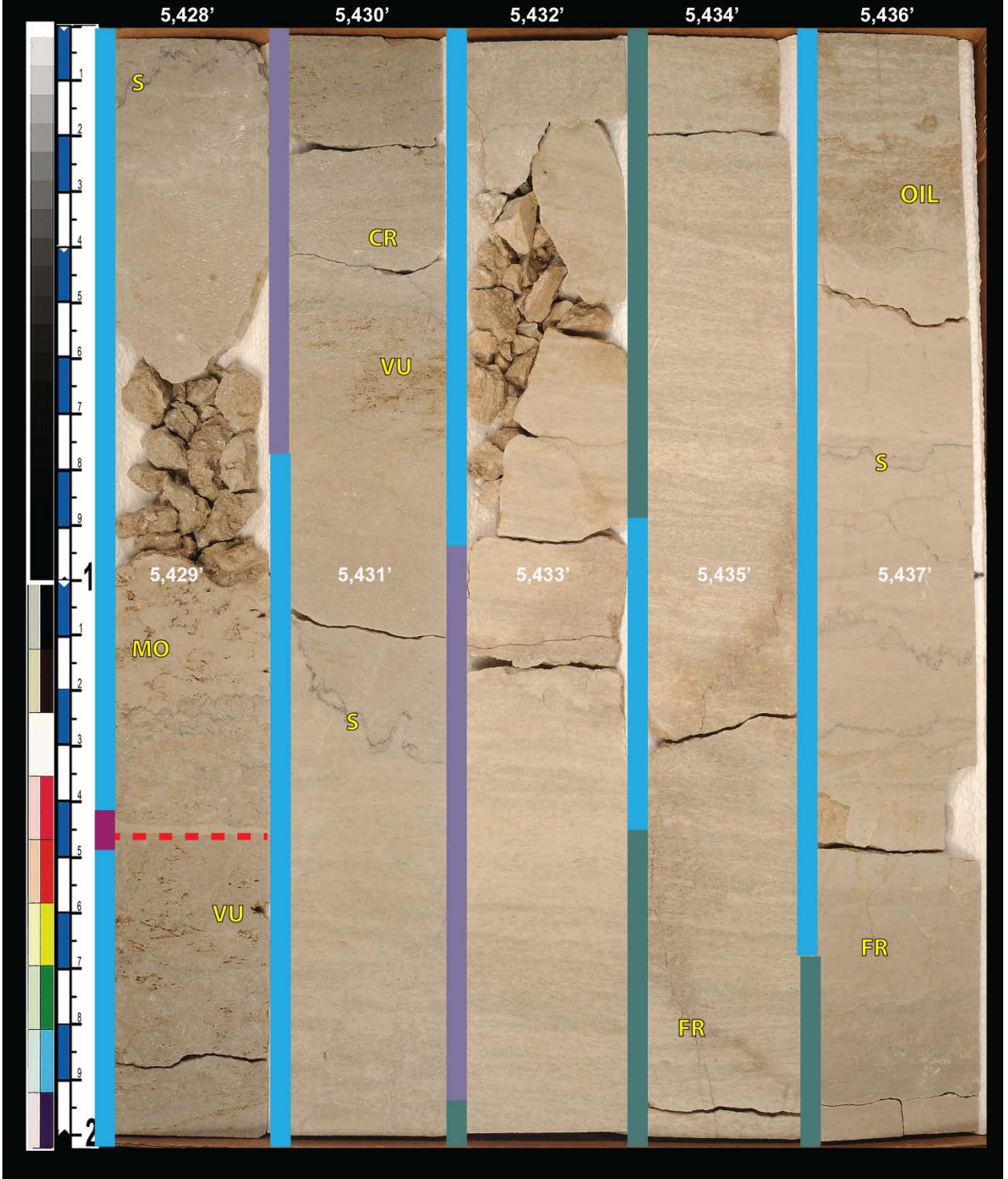
Job: #11-1002
Core 6: box 4 of 7
Depth: 5,418' - 5,428'





Well: Trophy Farms 32-34-16 1H
Location: Comanche Co., KS
Formation: Mississippi Lime

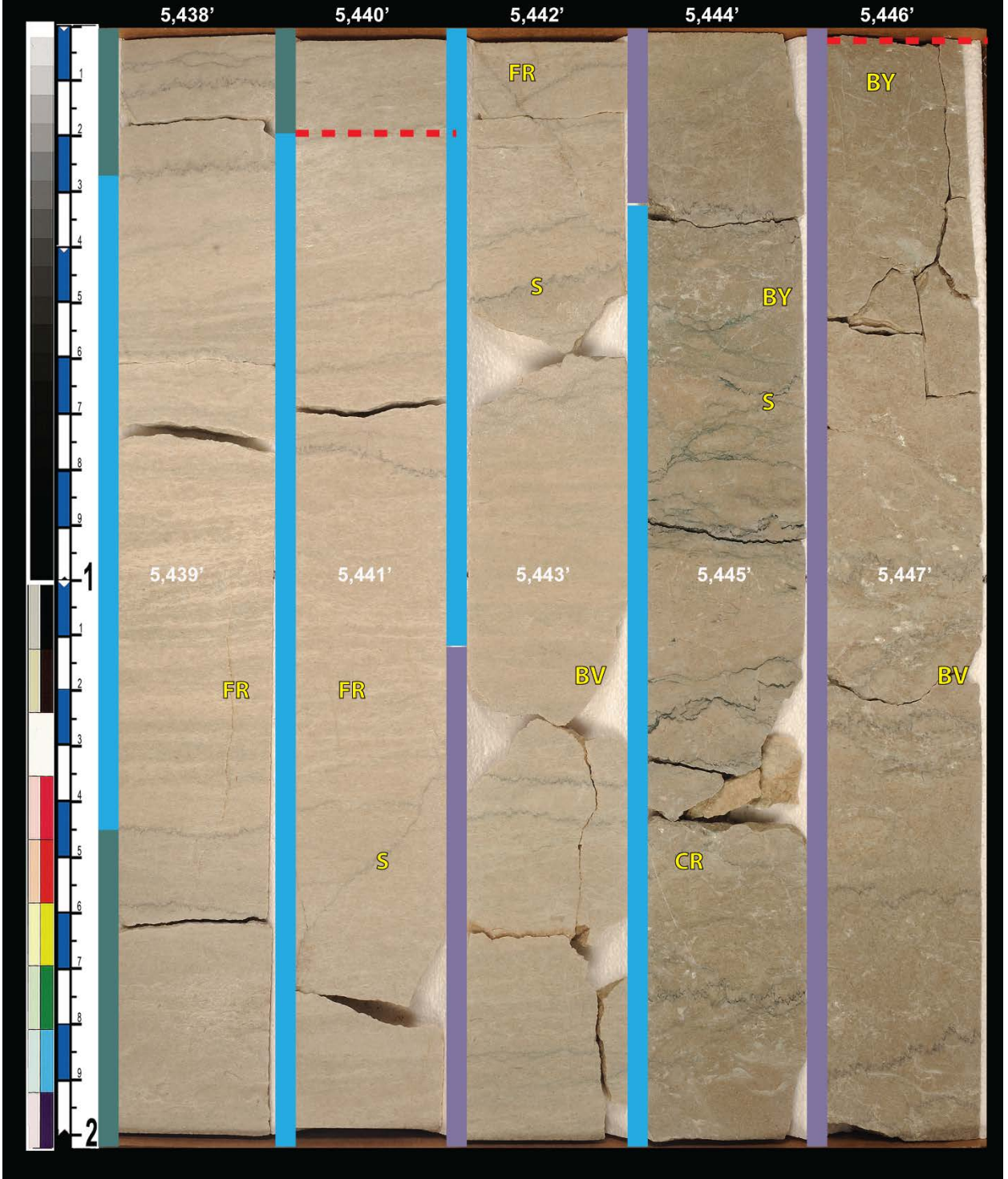
Job: #11-1002
Core 6: box 5 of 7
Depth: 5,428' - 5,438'





Well: Trophy Farms 32-34-16 1H
Location: Comanche Co., KS
Formation: Mississippi Lime

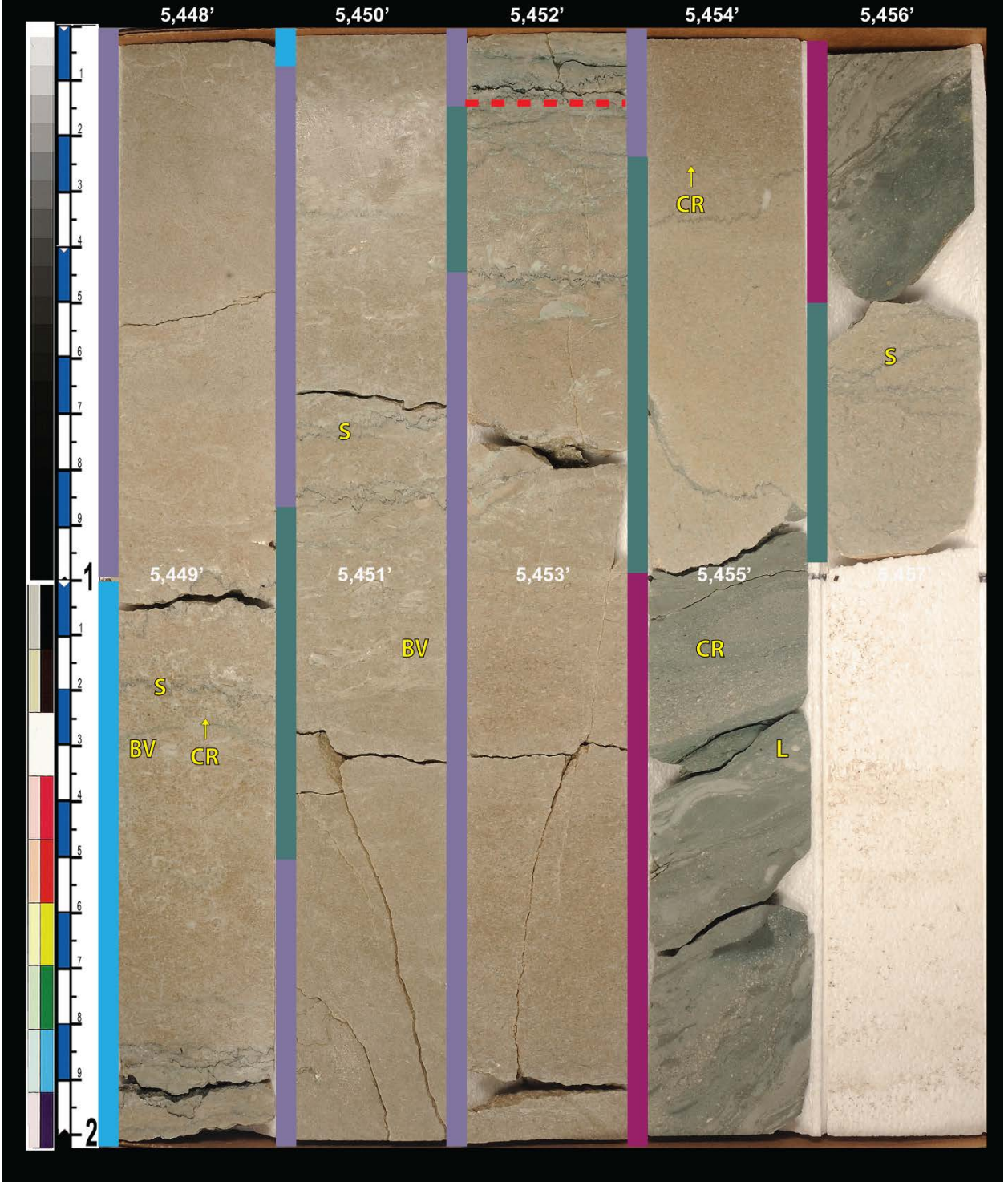
Job: #11-1002
Core 6: box 6 of 7
Depth: 5,438' - 5,448'





Well: Trophy Farms 32-34-16 1H
Location: Comanche Co., KS
Formation: Mississippi Lime

Job: #11-1002
Core 6: box 7 of 7
Depth: 5,448' - 5,456.96'

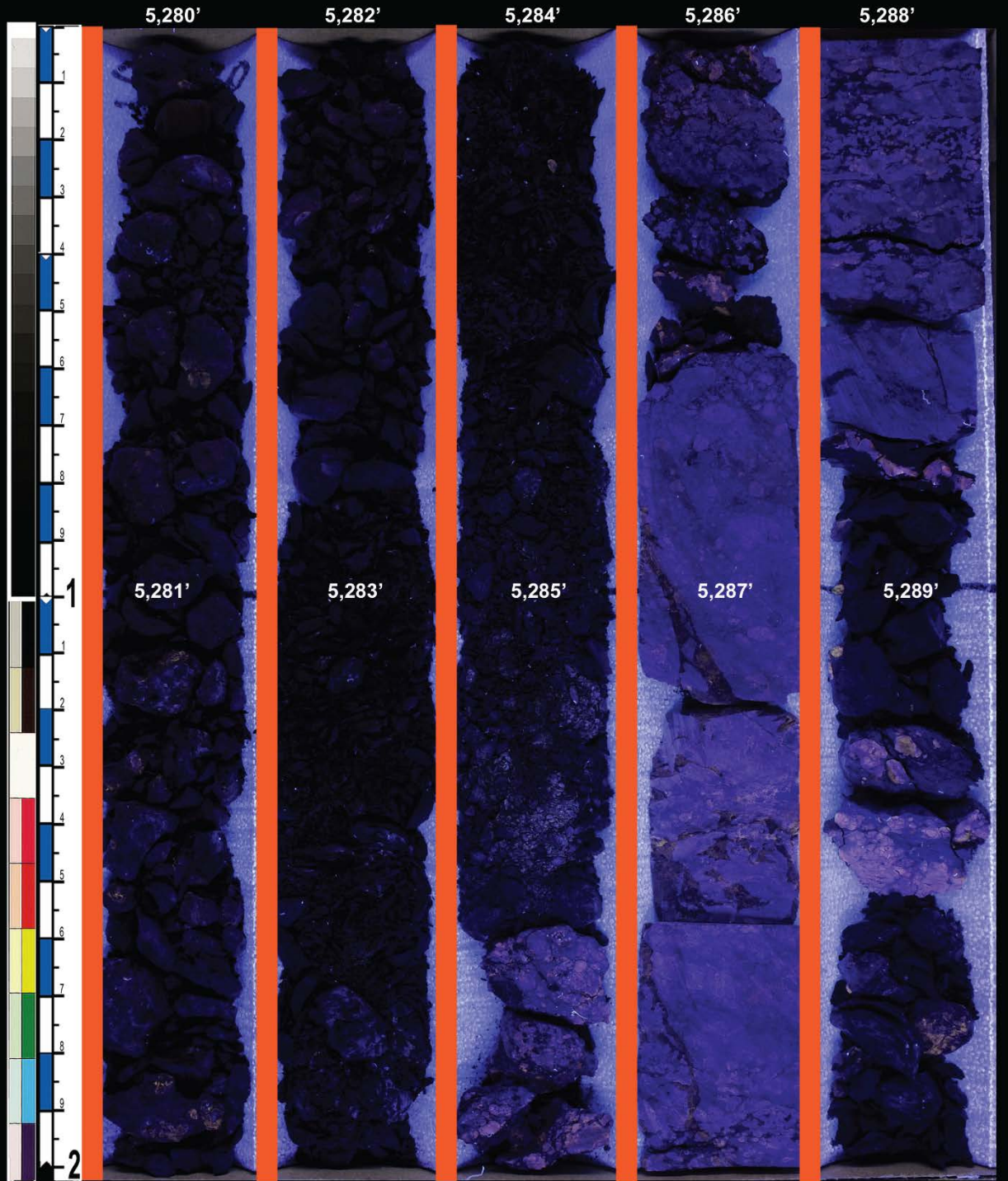


CORE #3: UV LIGHT (TROPHY FARMS 32-34-16H)



Well: Trophy Farms 32-34-16 1H
Location: Comanche Co., KS
Formation: Cherokee

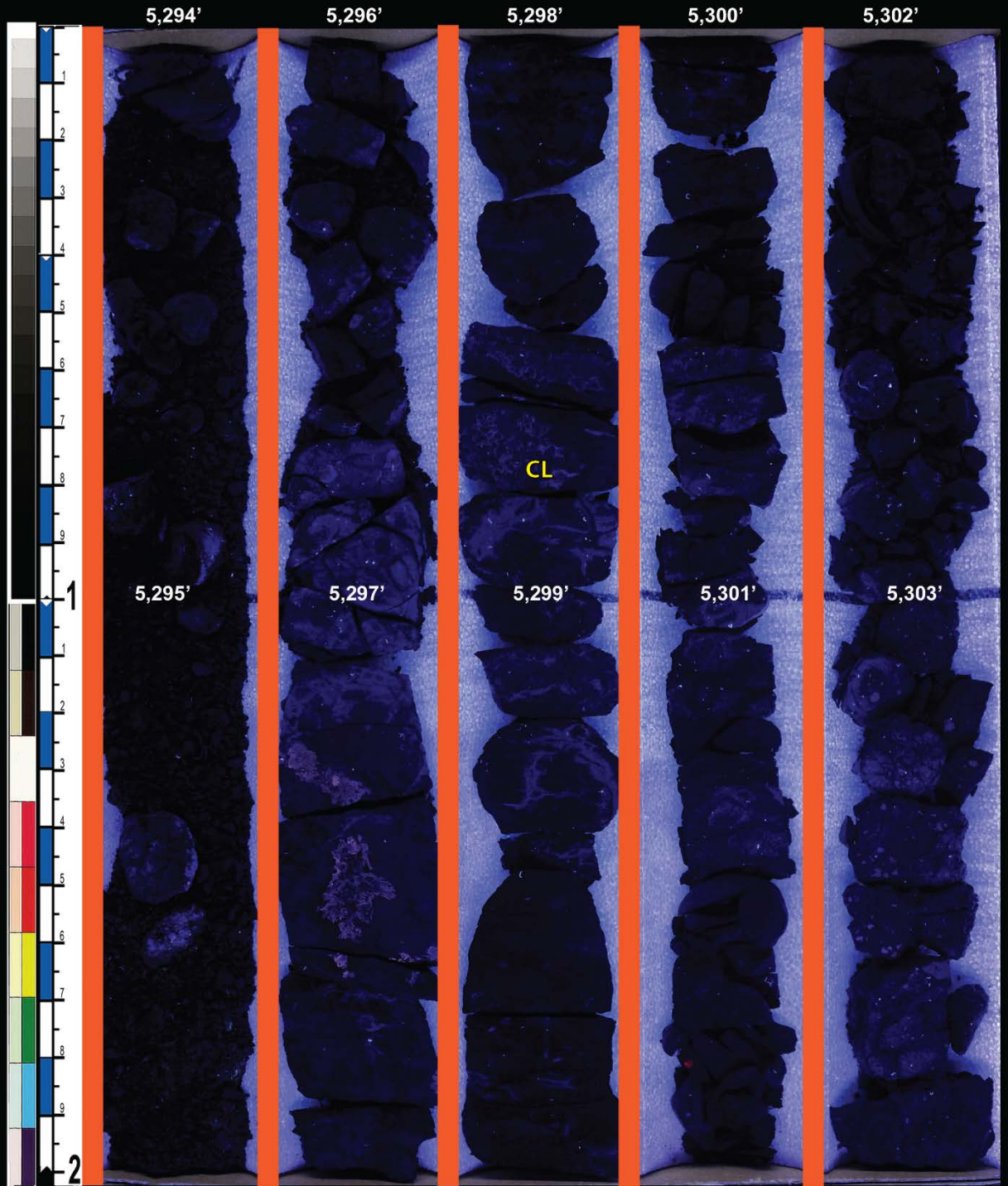
Job: #11-1002
Core 2: box 1 of 1
Depth: 5,280' - 5,290'





Well: Trophy Farms 32-34-16 1H
Location: Comanche Co., KS
Formation: Cherokee

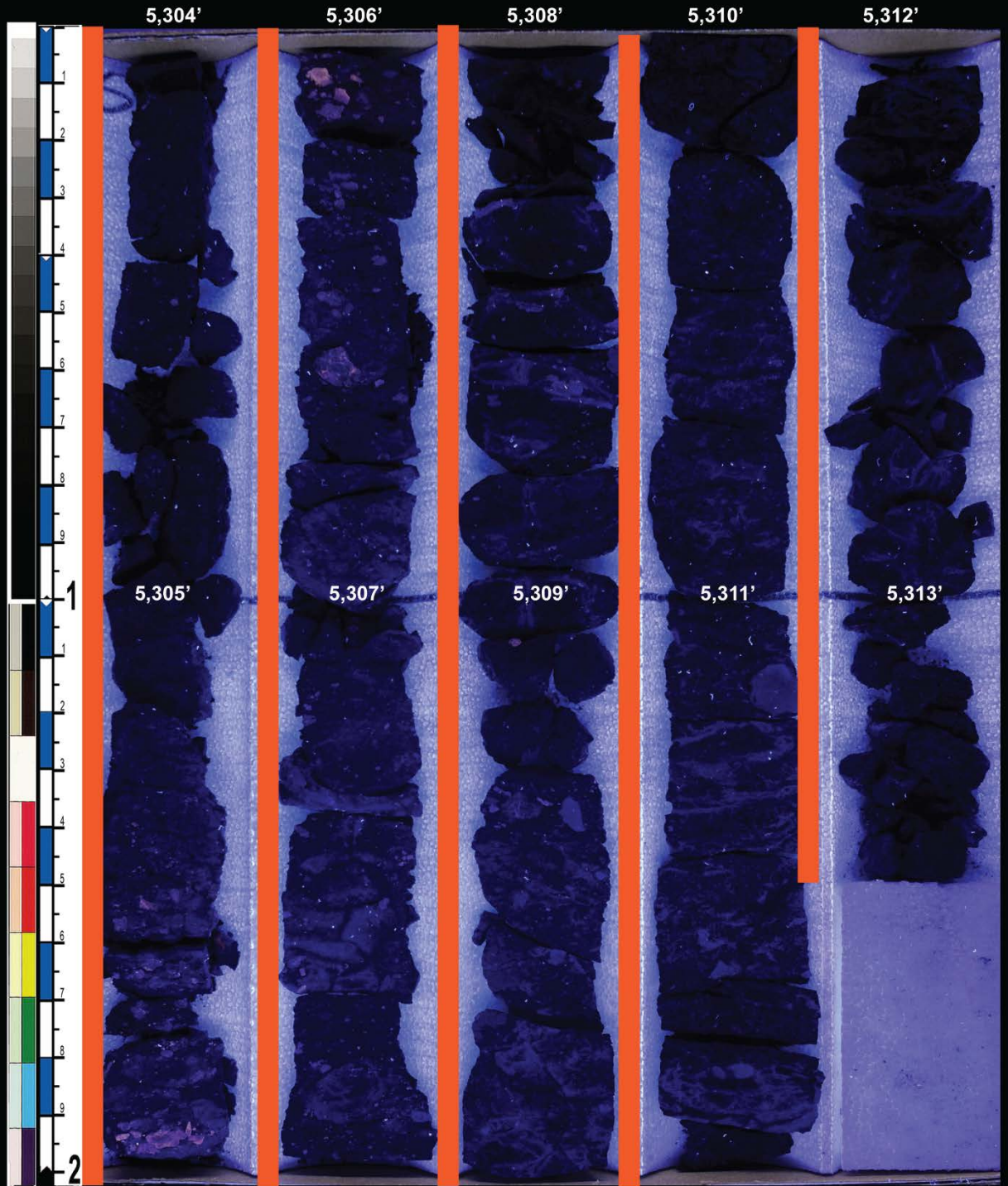
Job: #11-1002
Core 3: box 1 of 2
Depth: 5,294' - 5,304'





Well: Trophy Farms 32-34-16 1H
Location: Comanche Co., KS
Formation: Cherokee

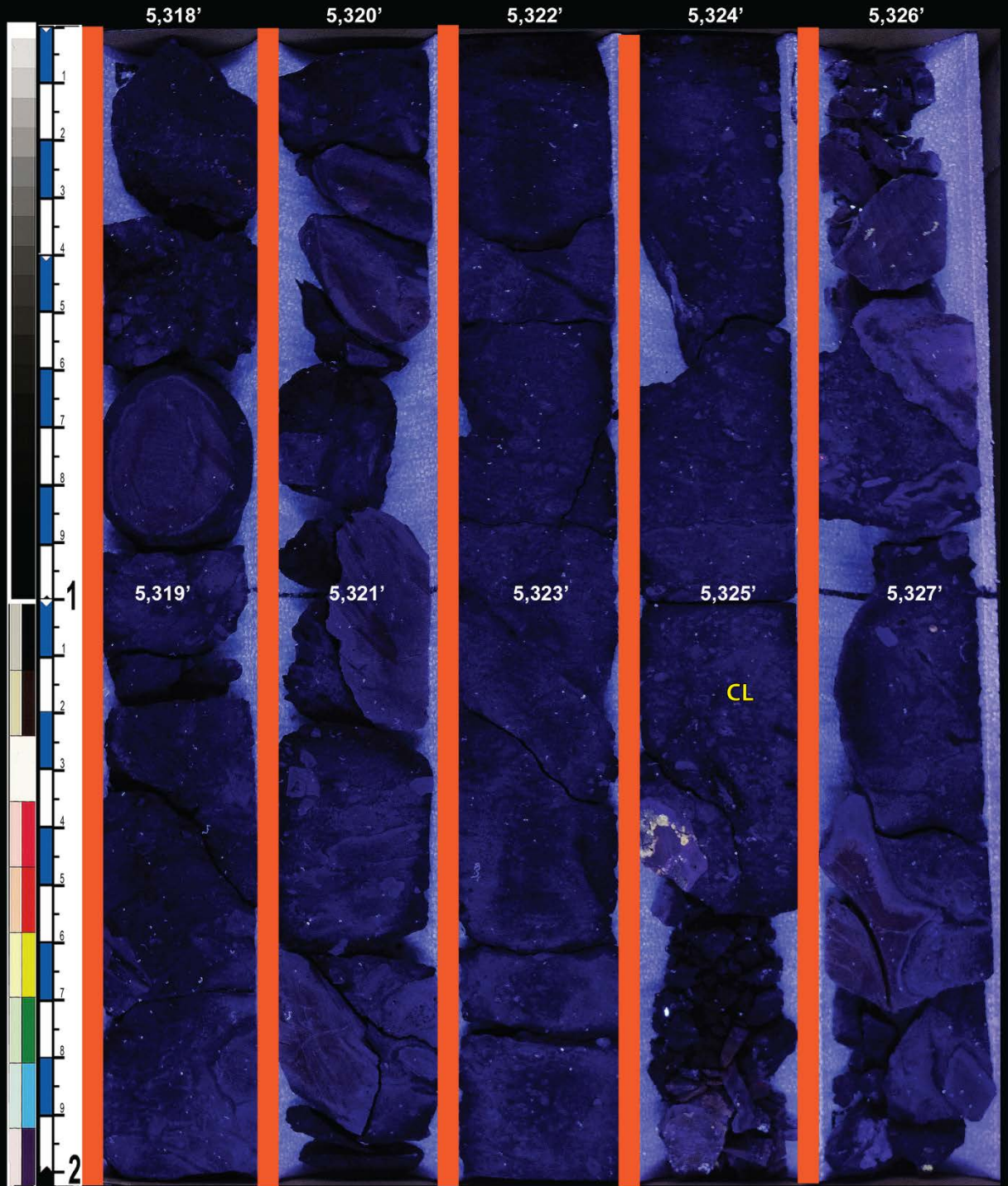
Job: #11-1002
Core 3: box 2 of 2
Depth: 5,304' - 5,313.55'





Well: Trophy Farms 32-34-16 1H
Location: Comanche Co., KS
Formation: Cherokee

Job: #11-1002
Core 4: box 1 of 2
Depth: 5,318' - 5,328'





Well: Trophy Farms 32-34-16 1H

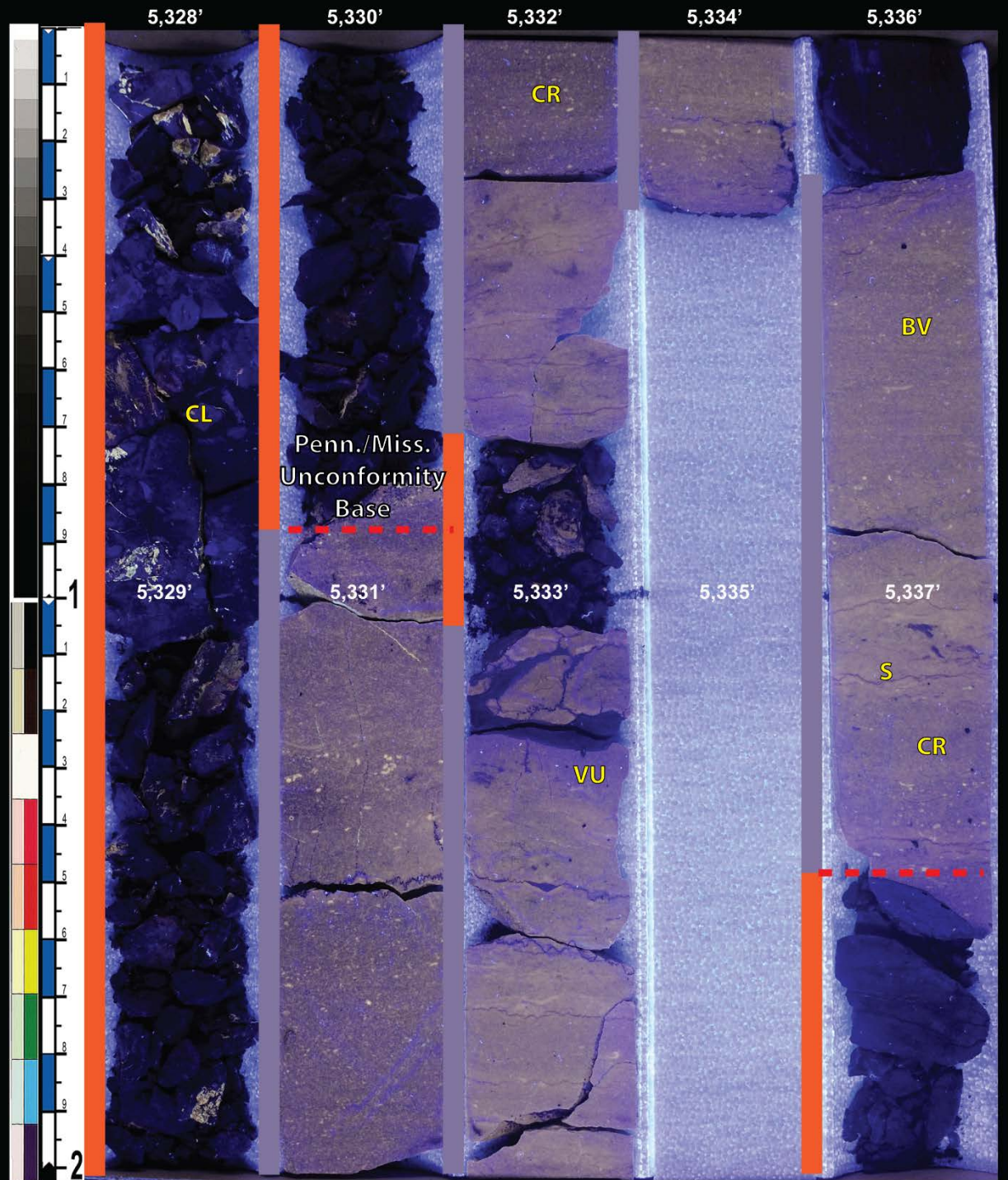
Job: #11-1002

Location: Comanche Co., KS

Core 4: box 2 of 2 Depth: 5,328' - 5,334.34'

Formation: Cherokee, Mississippi Lime

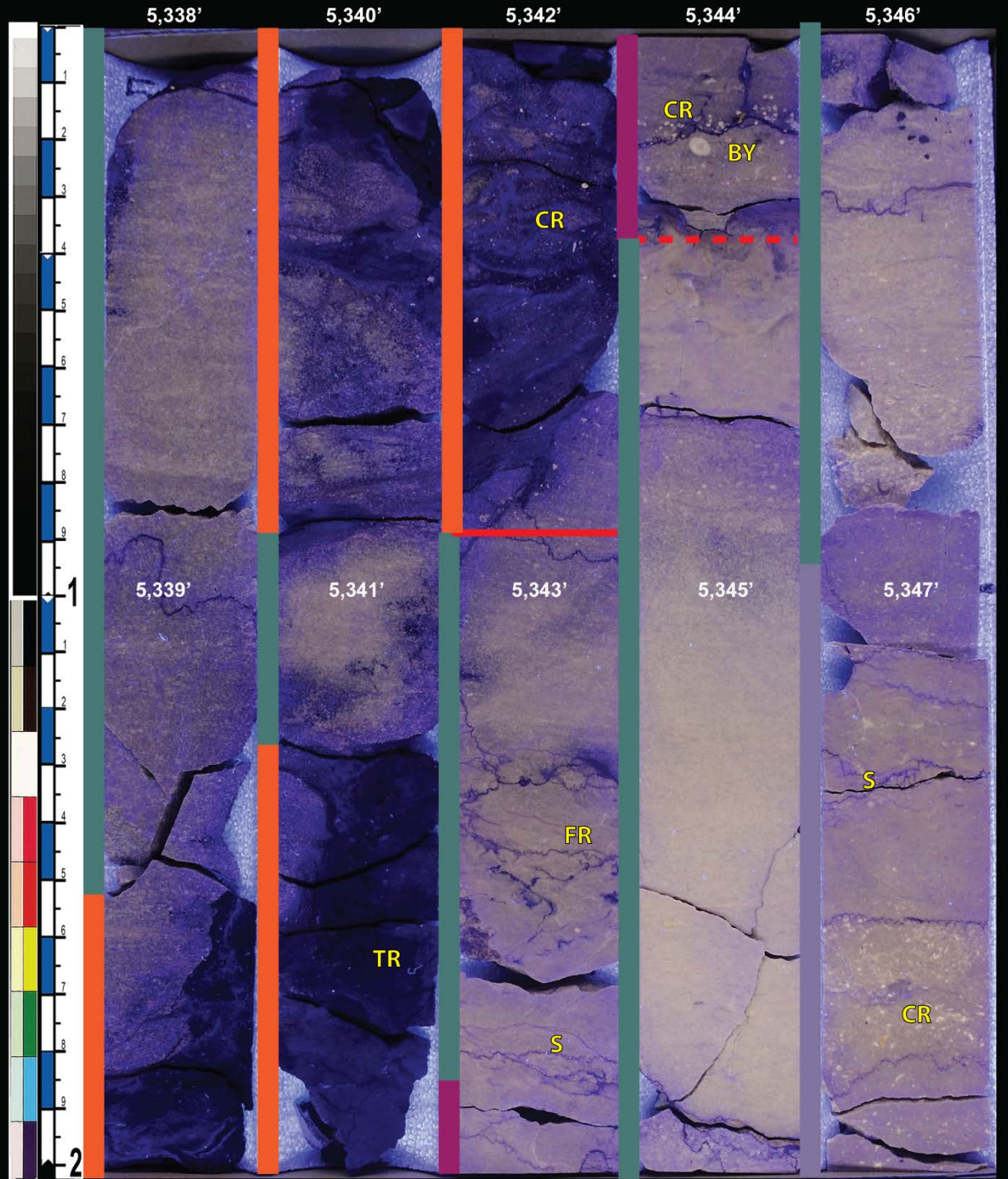
Core 5: box 1 of 7 Depth: 5,336' - 5,338'





Well: Trophy Farms 32-34-16 1H
Location: Comanche Co., KS
Formation: Mississippi Lime

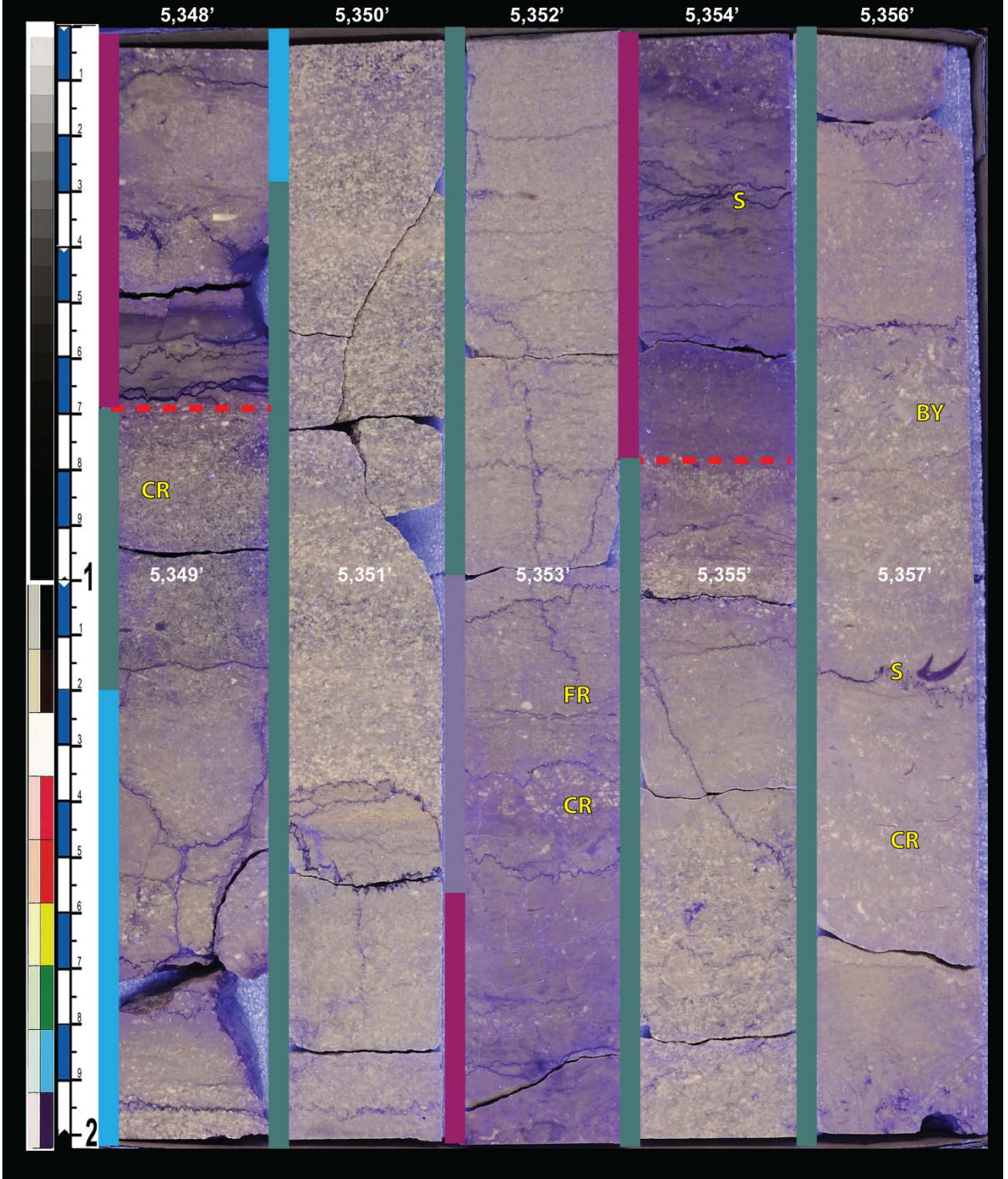
Job: #11-1002
Core 5: box 2 of 7
Depth: 5,338' - 5,348'

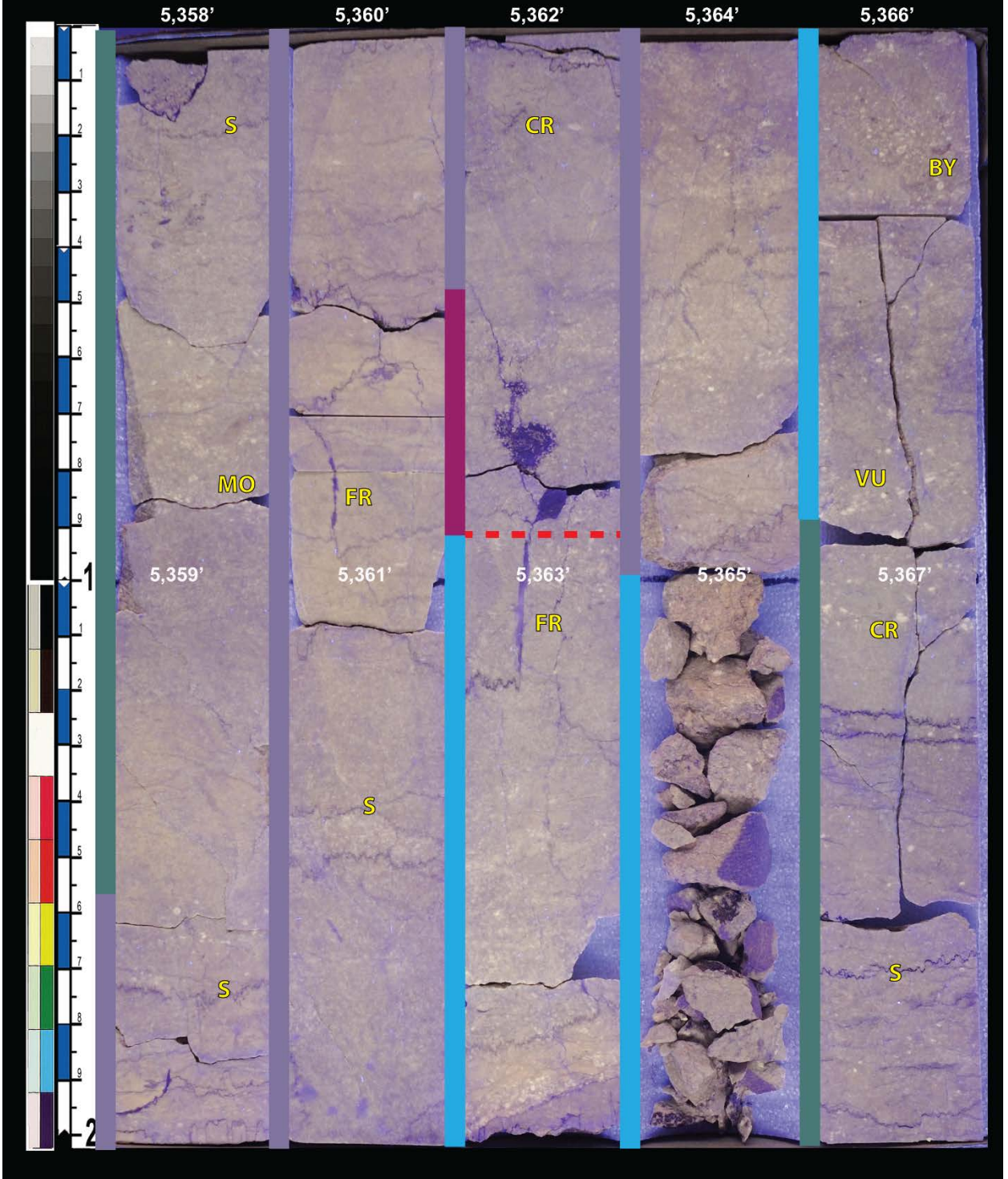


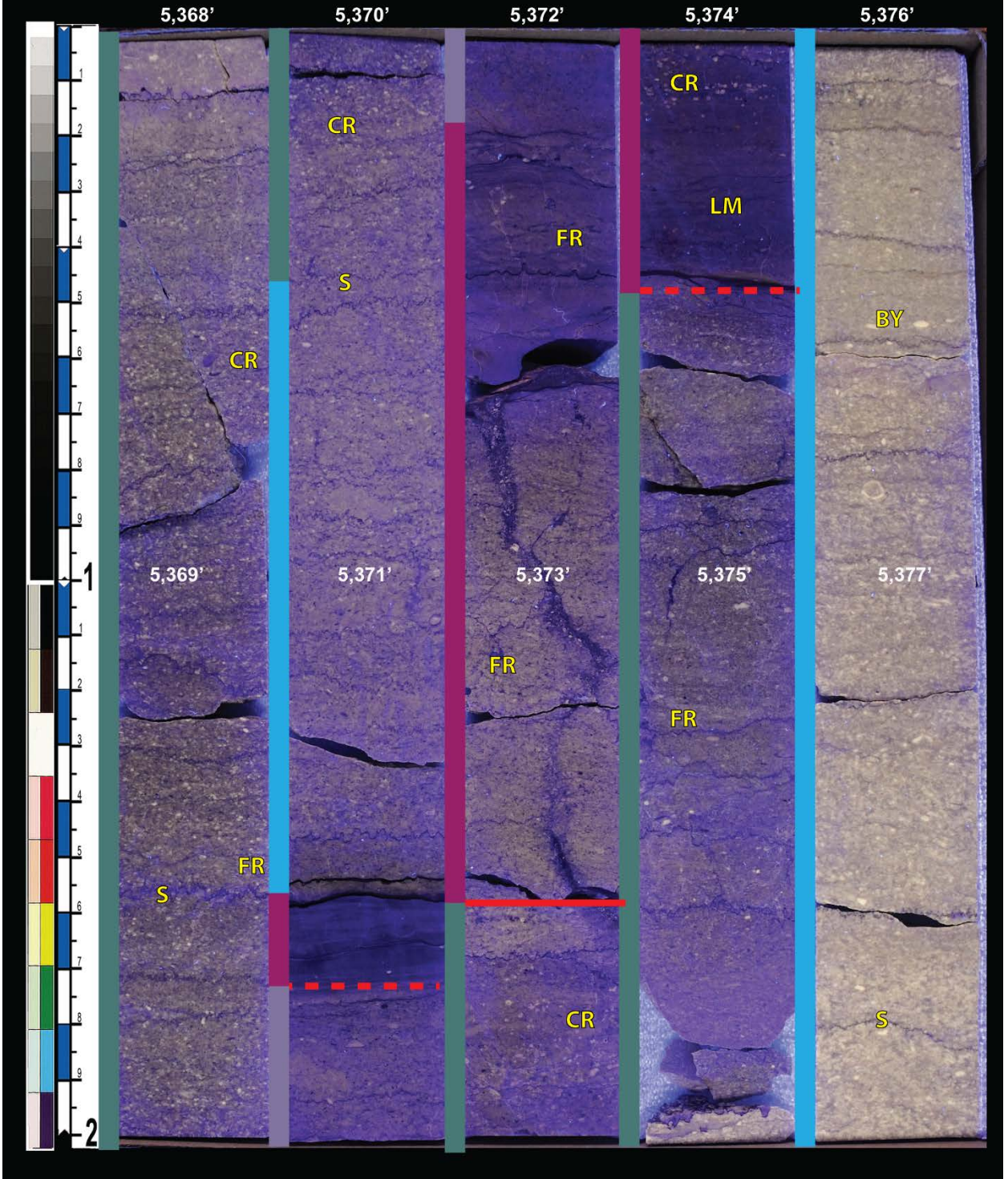


Well: Trophy Farms 32-34-16 1H
Location: Comanche Co., KS
Formation: Mississippi Lime

Job: #11-1002
Core 5: box 3 of 7
Depth: 5,348' - 5,358'



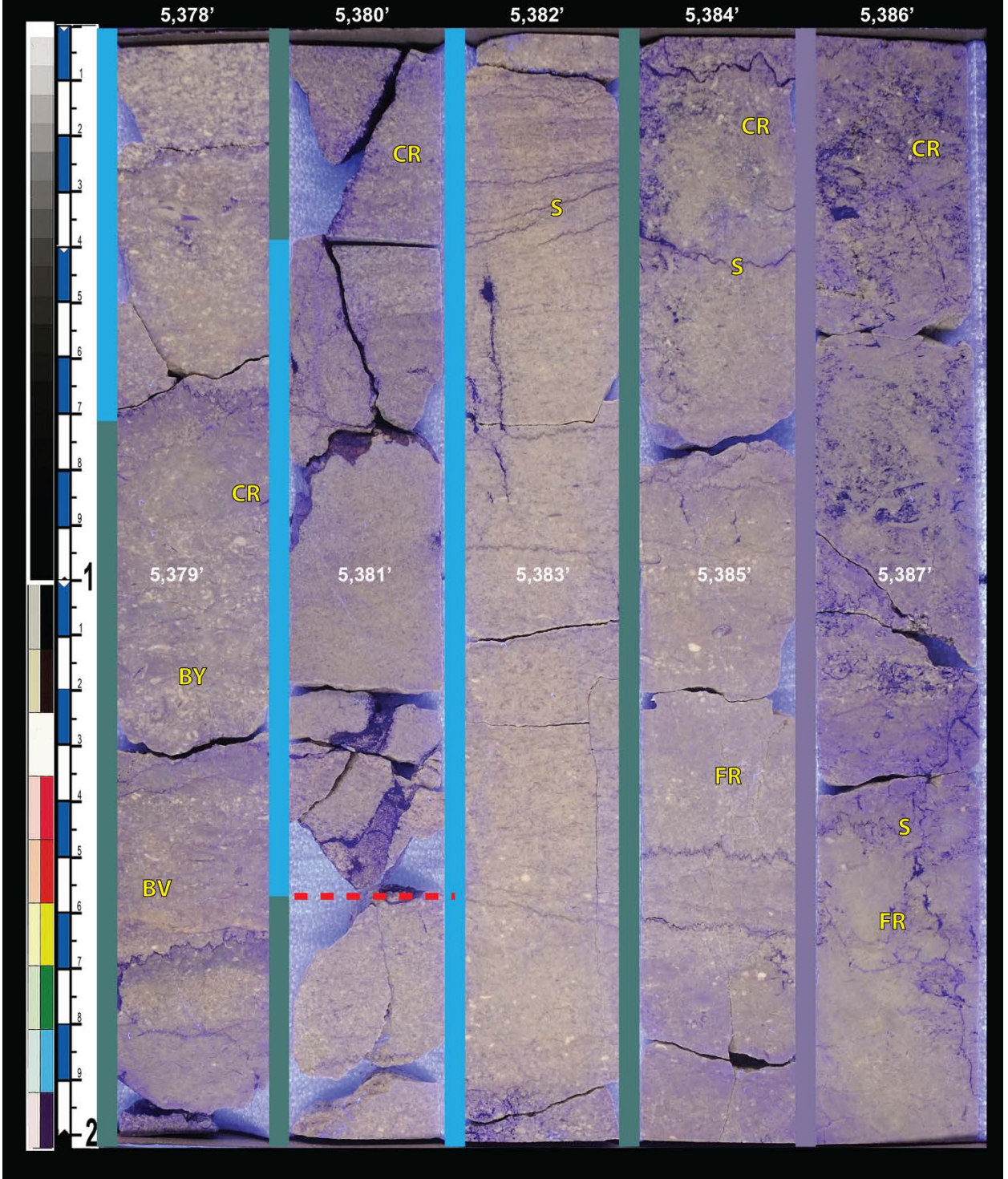






Well: Trophy Farms 32-34-16 1H
Location: Comanche Co., KS
Formation: Mississippi Lime

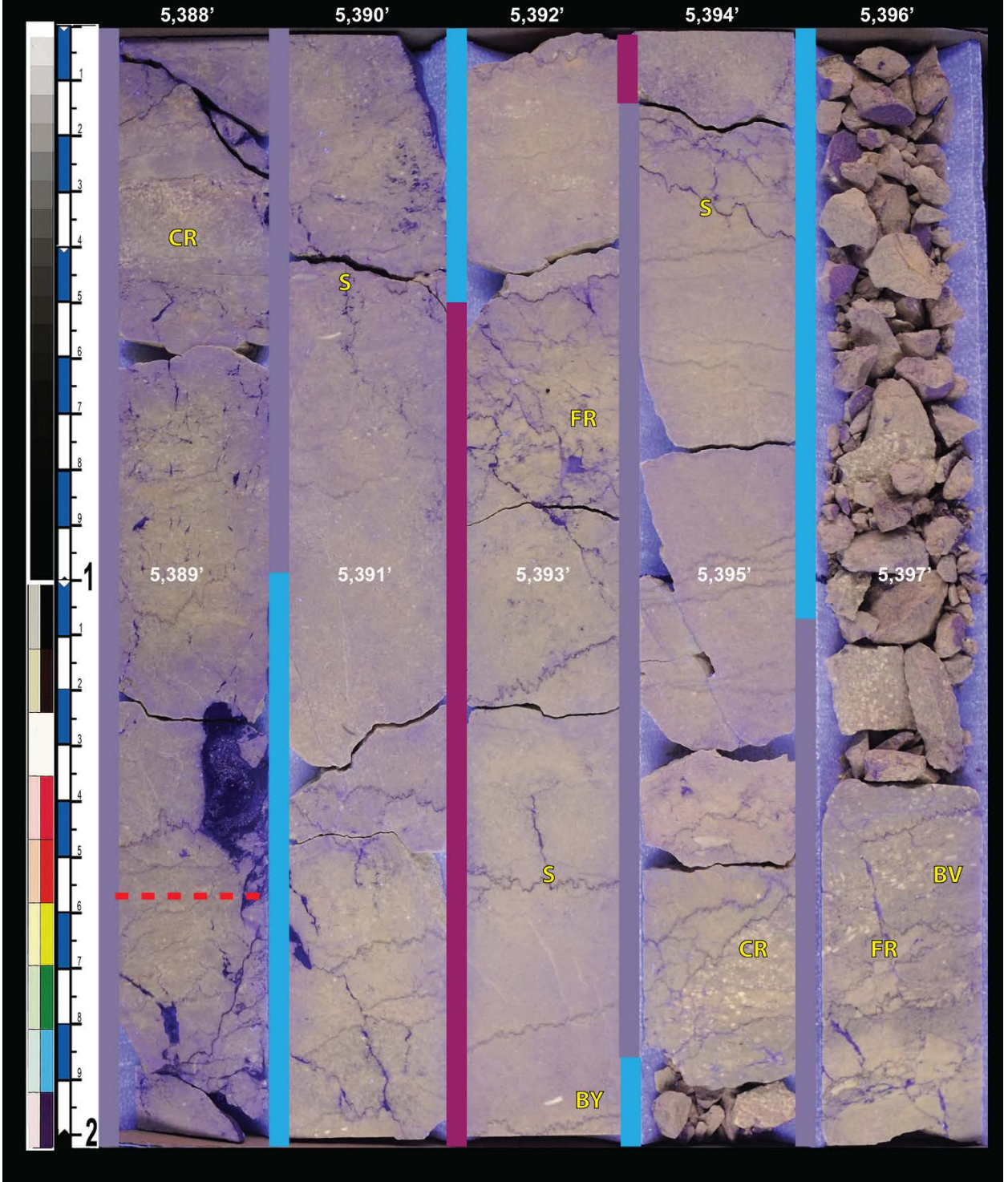
Job: #11-1002
Core 5: box 6 of 7
Depth: 5,378' - 5,388'

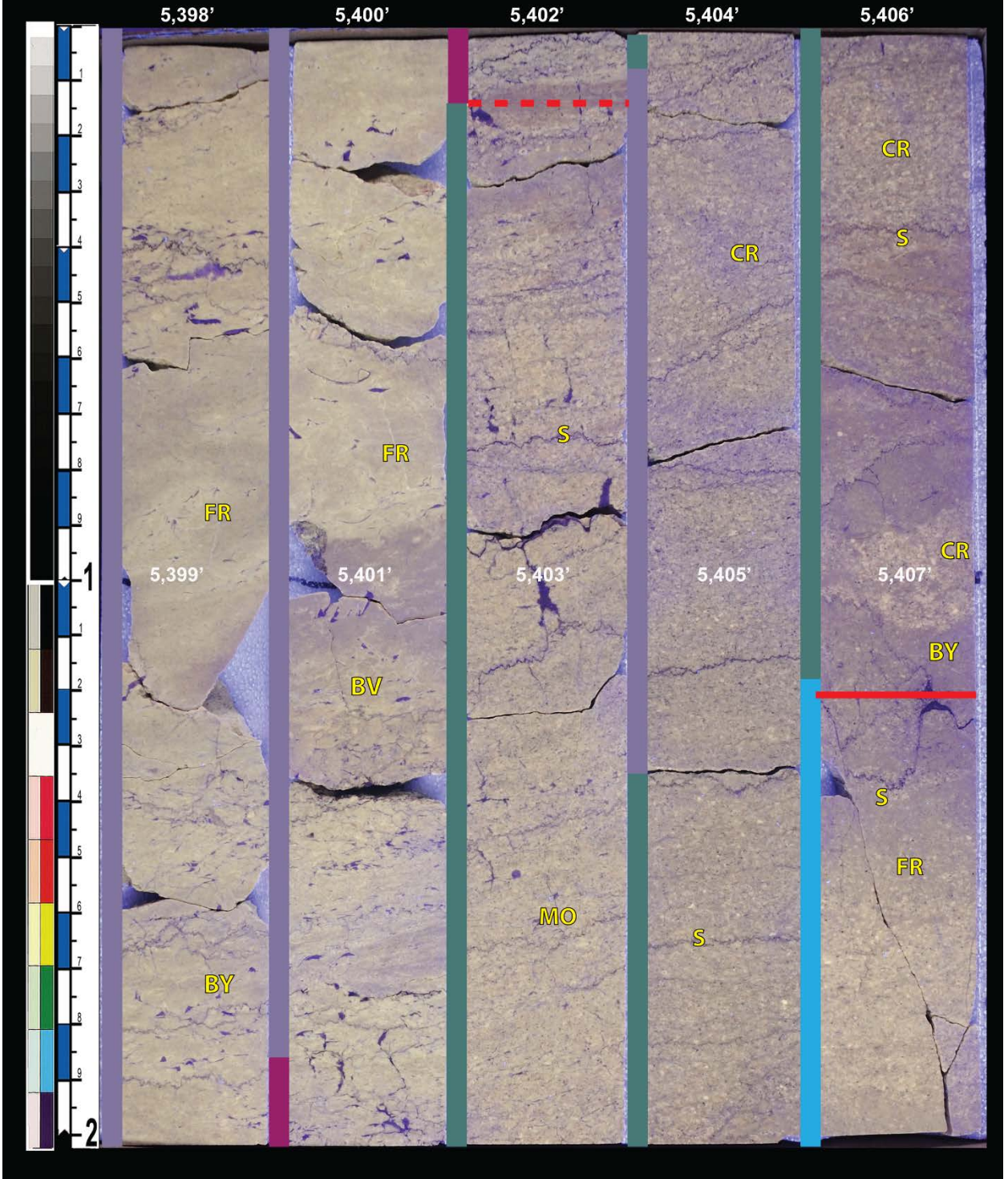


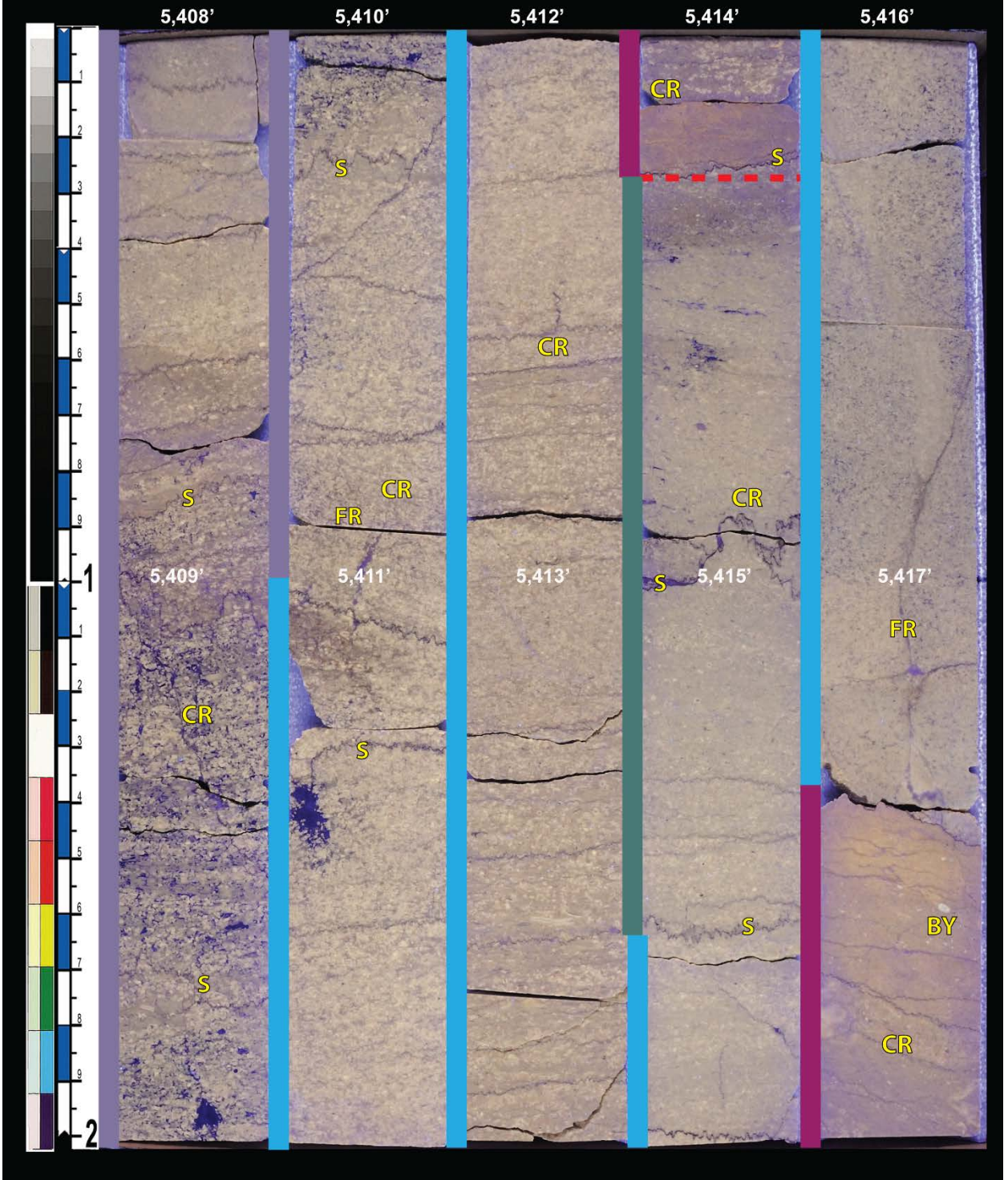


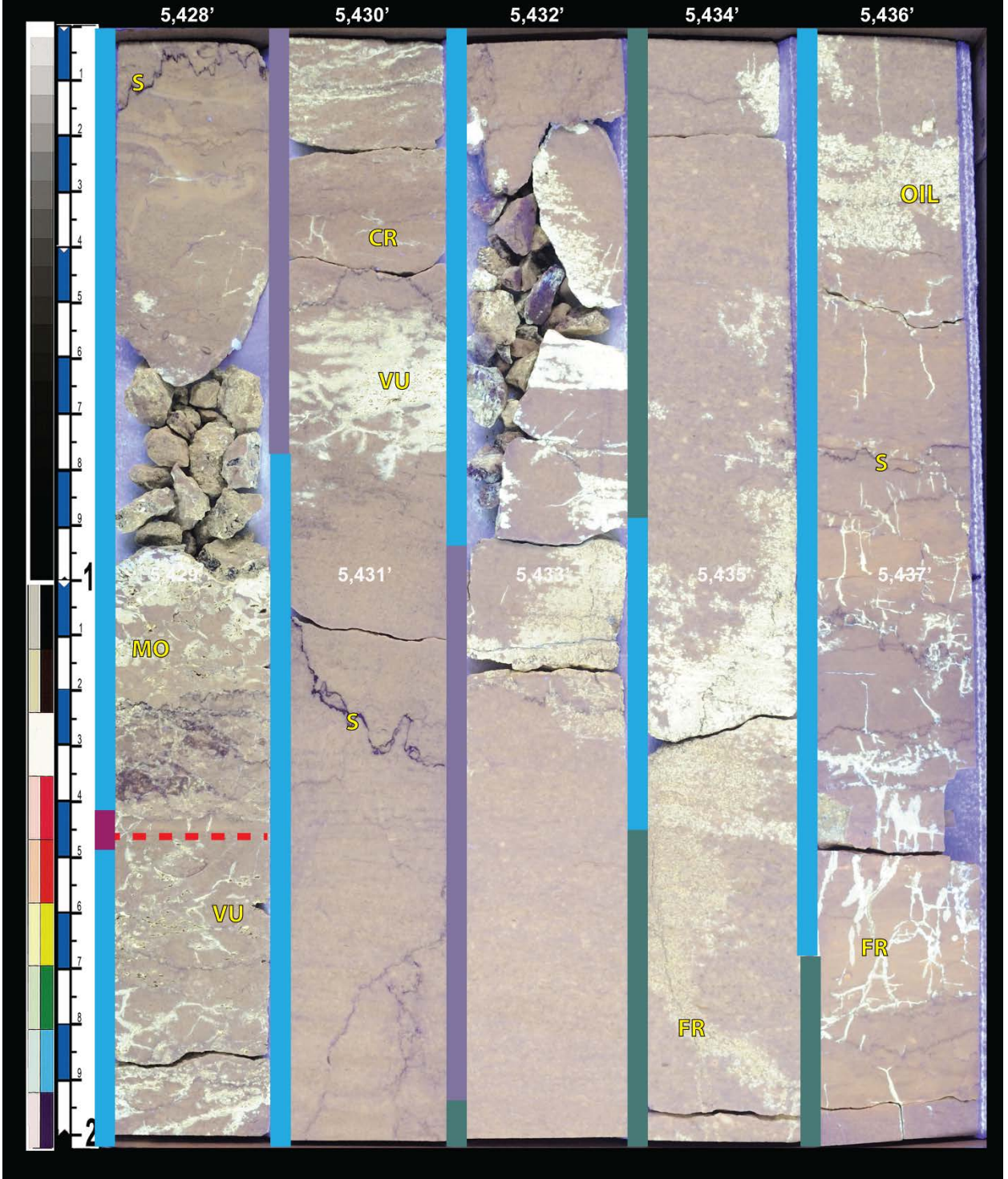
Well: Trophy Farms 32-34-16 1H
Location: Comanche Co., KS
Formation: Mississippi Lime

Job: #11-1002
Core 5: box 7 of 7 Depth: 5,388' - 5,397.36'
Core 6: box 1 of 7 Depth: 5,397.36' - 5,398'





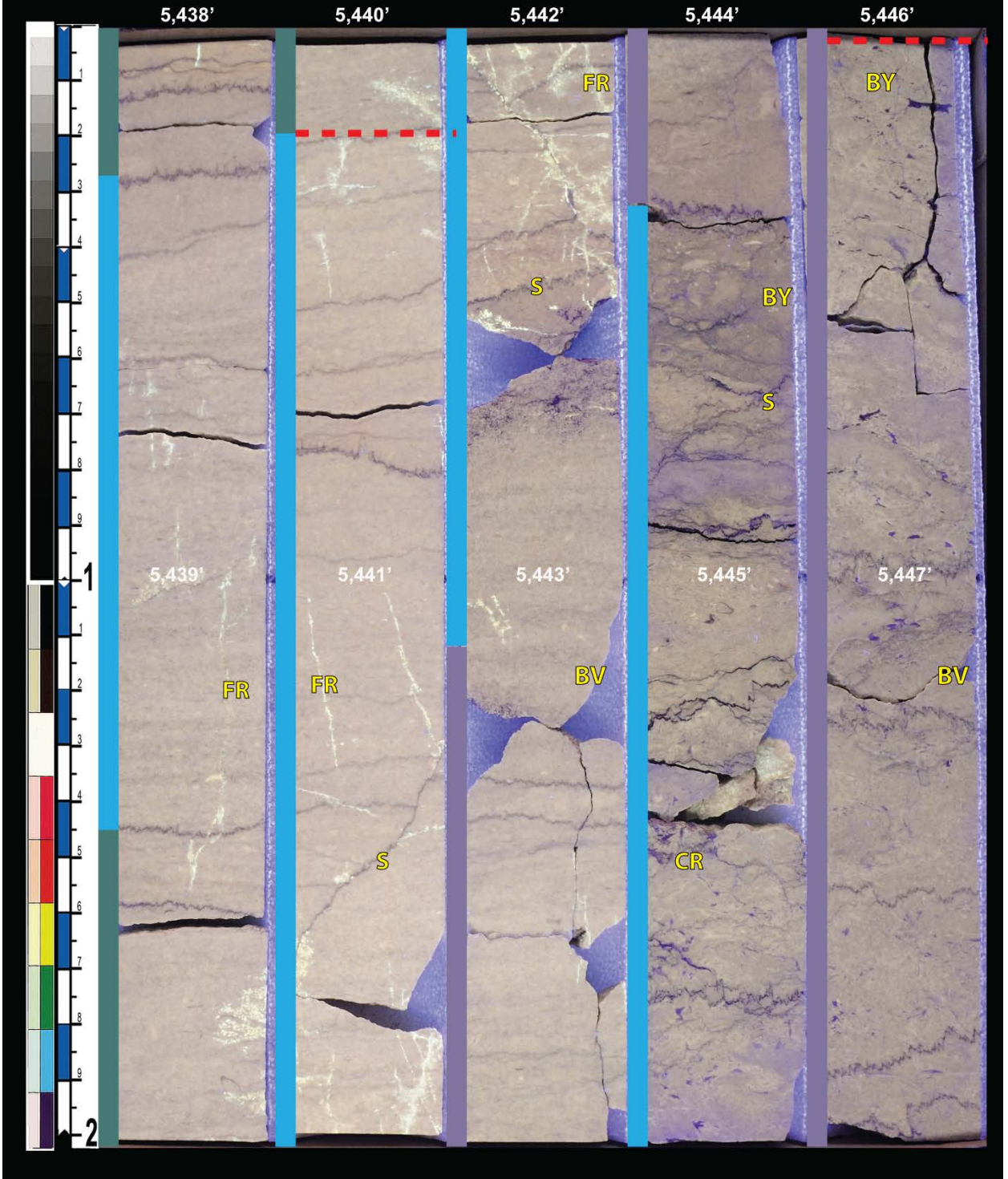






Well: Trophy Farms 32-34-16 1H
Location: Comanche Co., KS
Formation: Mississippi Lime

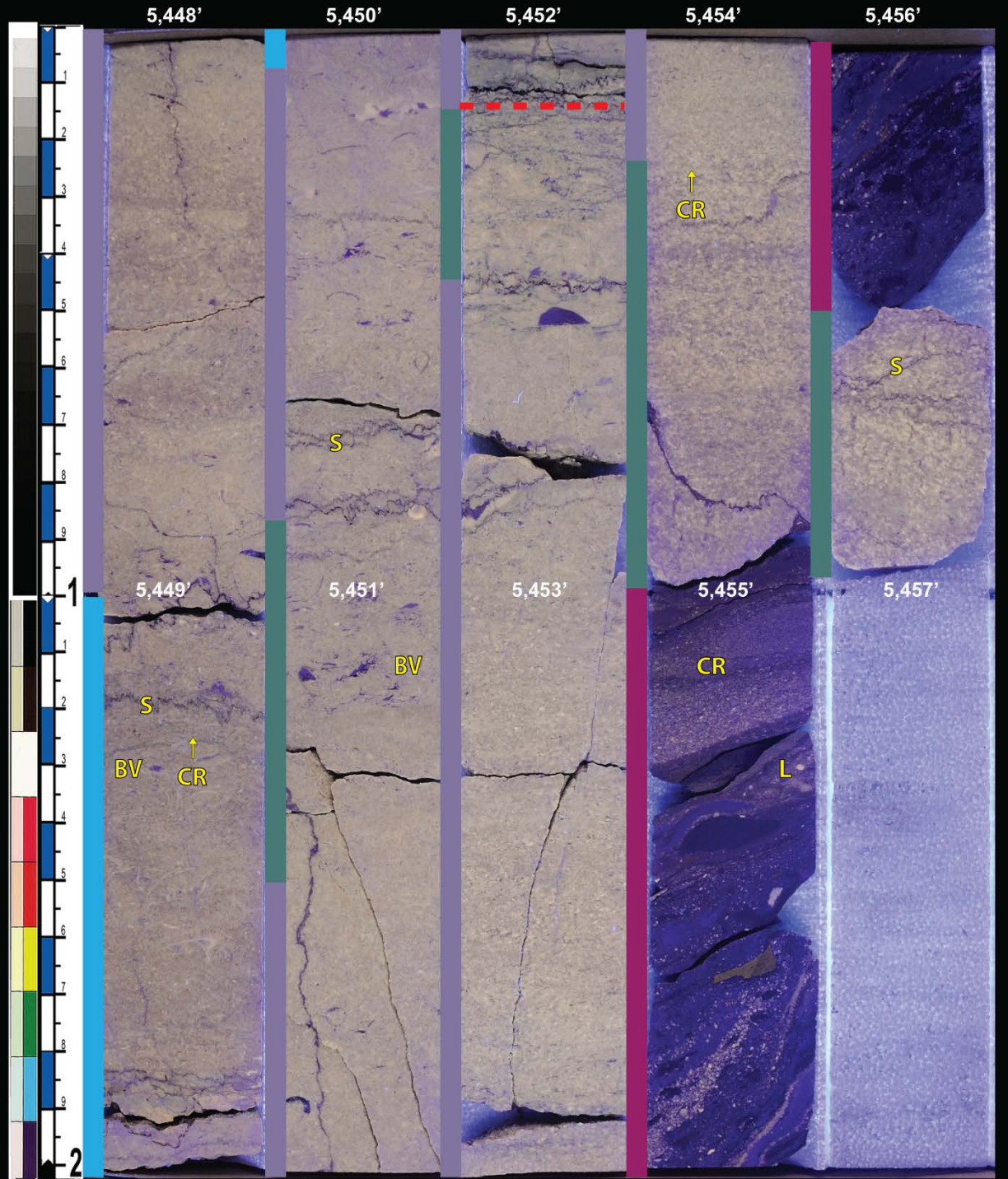
Job: #11-1002
Core 6: box 6 of 7
Depth: 5,438' - 5,448'





Well: Trophy Farms 32-34-16 1H
Location: Comanche Co., KS
Formation: Mississippi Lime

Job: #11-1002
Core 6: box 7 of 7
Depth: 5,448' - 5,456.96'



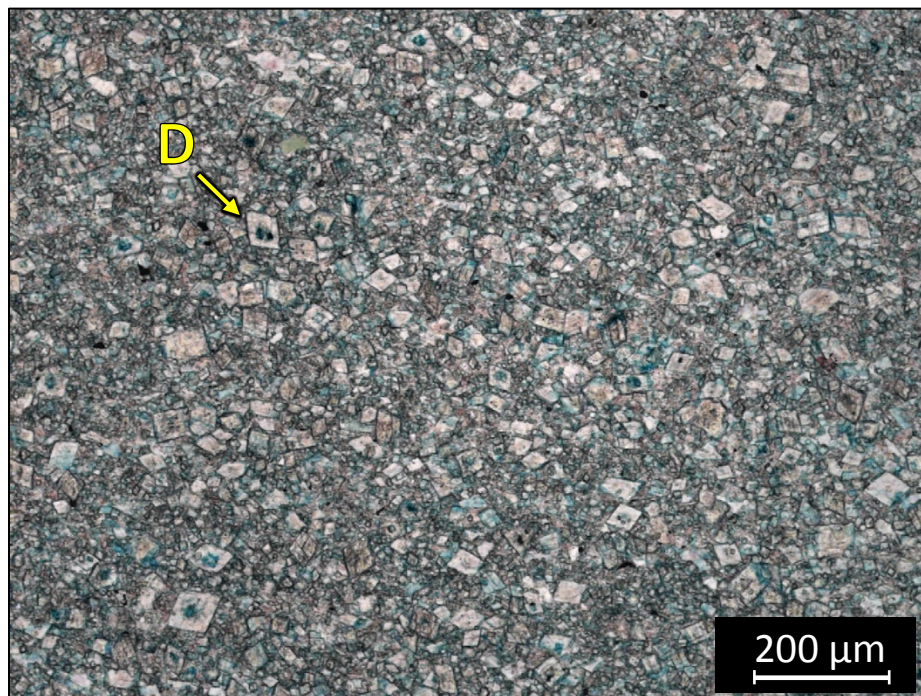
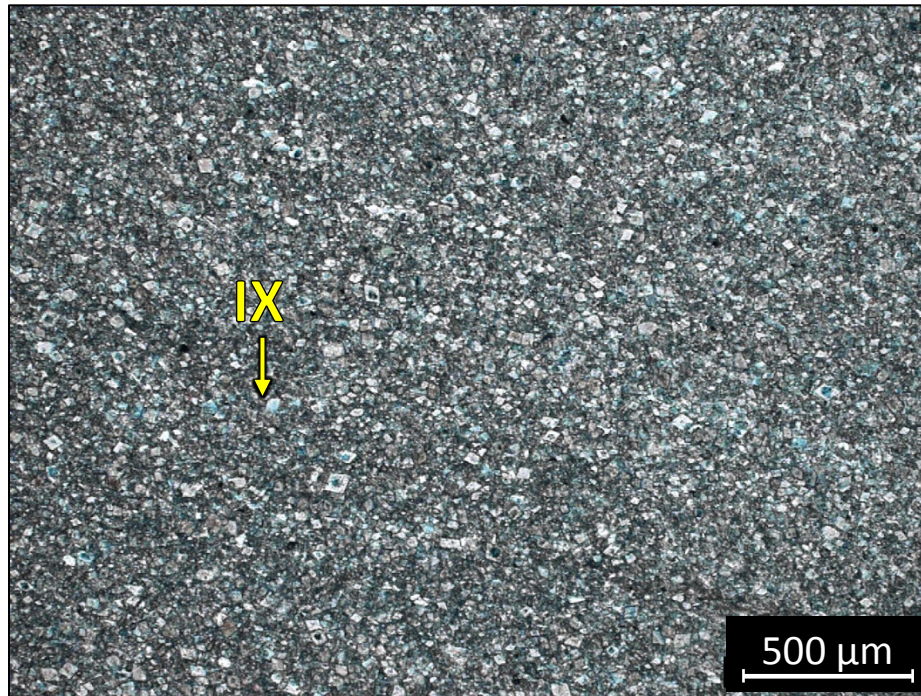
APPENDIX D
THIN SECTION PHOTOMICROGRAPHS

Thin section photomicrographs display the grain size, pore types, fossil content and textural classification that cannot be accurately described in hand sample due to the fine-grained nature and microscopic variabilities within these units. Samples are organized by representative Oklahoma and Kansas facies in a shallowing-upward order, well number and depth from deepest to shallowest. Samples are shown in plane polarized light (unless otherwise noted) and labeled according to the chart below.

Core and Thin Section Image Labels					
Feature Key				Porosity Key	
BR	brachiopod	OIL	oil/dead oil	FR	fracture
BU	burrow	PY	pyrite	IP	interparticle
BY	bryozoan	Q	quartz	IX	intercrystalline
CH	chert	S	stylolite	MO	moldic
CR	crinoid	SK	undifferentiated skeletal fragments	VU	vug
D	dolomite	SP	spicule	WP	intraparticle
FL	fluorescence	TC	traction current	WX	intracrystalline
FR	fracture	TR	terra rosa		
GST	gastropod	CL	clast		
L	lamination	BT	bioturbation		
M	mud/mudstone				
O	ostracode				

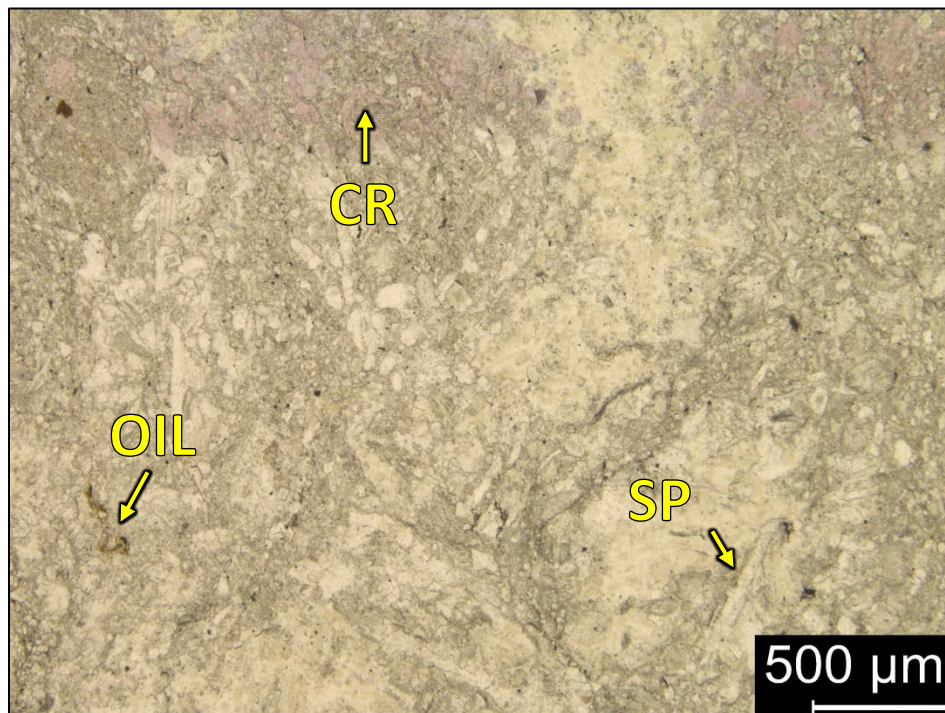
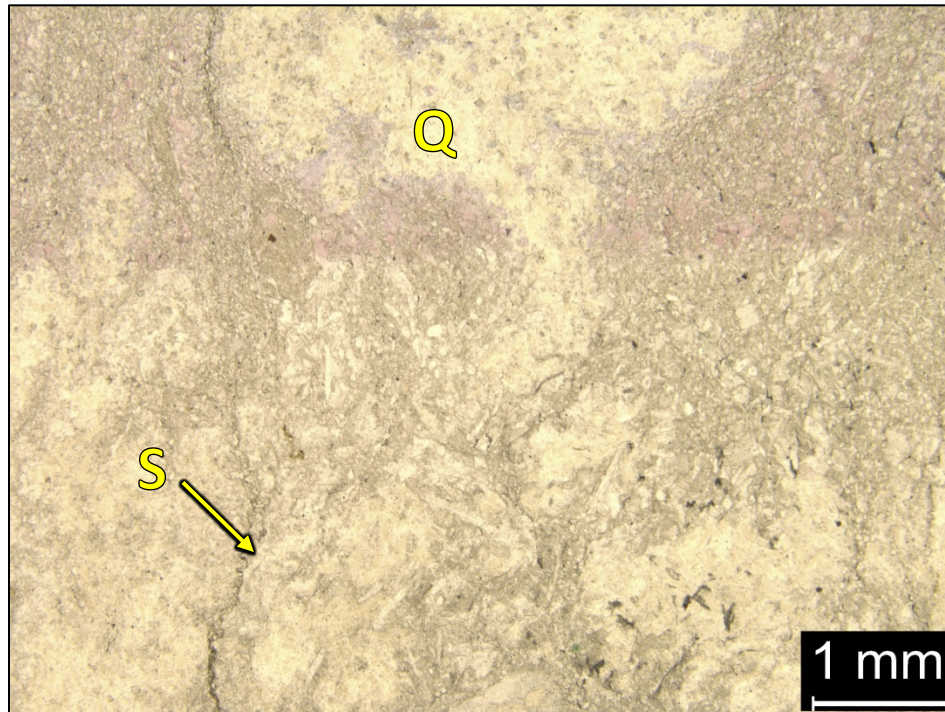
OKLAHOMA FACIES

Facies 1



1 BN - 5279.94': Dolomitized mudstone. Sample is alizarin red stained and blue epoxy impregnated. Porosity (NCS): 9.2%. Permeability (Klinkenberg): 0.020 mD. XRD: 14.9% clay (14% illite+mica, 0.9% chlorite), 57.4% carbonate (7.1% calcite, 50.3% dolomite), and 27.7% other minerals (27.6% quartz and trace amounts of halite). Sample contains sponge spicules (2%), microcrystalline quartz (2%), dolomite (60%) and undifferentiated skeletal debris. Slight intercrystalline and interparticle porosity present.

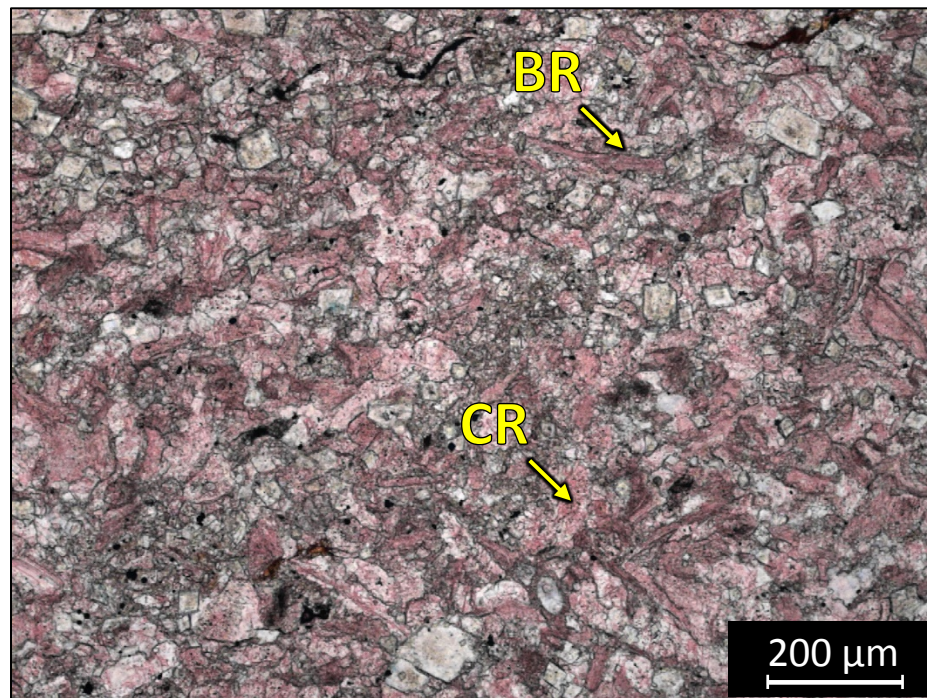
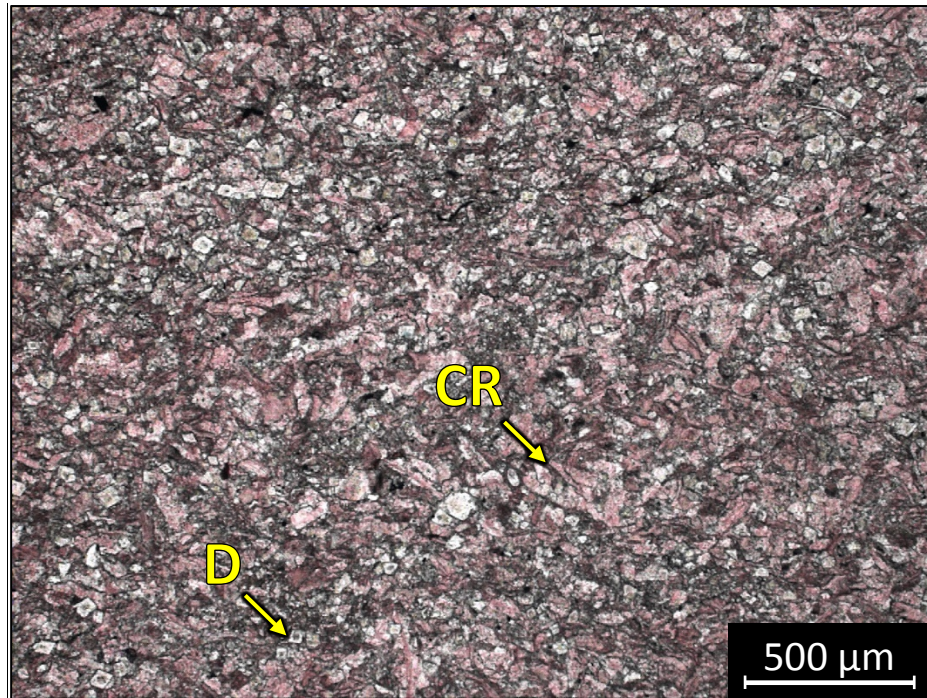
Facies 2



1 BN – 5353.8: Burrowed wackestone to packstone. Sample is alizarin red stained and blue epoxy impregnated. Porosity (NCS): 6.4%. Permeability (Klinkenberg): 0.0006 mD. XRD: 4.9% clay (4.7% illite/smectite, 0.2% chlorite), 33.2% carbonate (24% calcite, 9.2% dolomite), and 61.9% other minerals (61.5% quartz and trace amounts of pyrite and halite). Sample contains microcrystalline quartz (30%), silt-sized quartz grains (30%),

sponge spicules (10%), crinoid fragments (15 %) and undifferentiated skeletal debris.
Vuggy porosity observed.

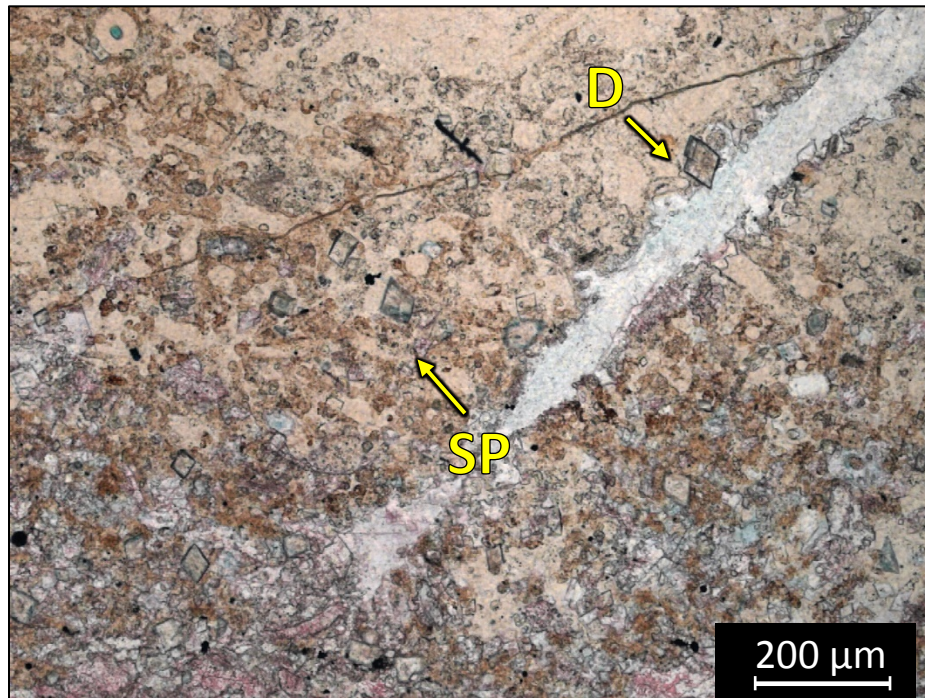
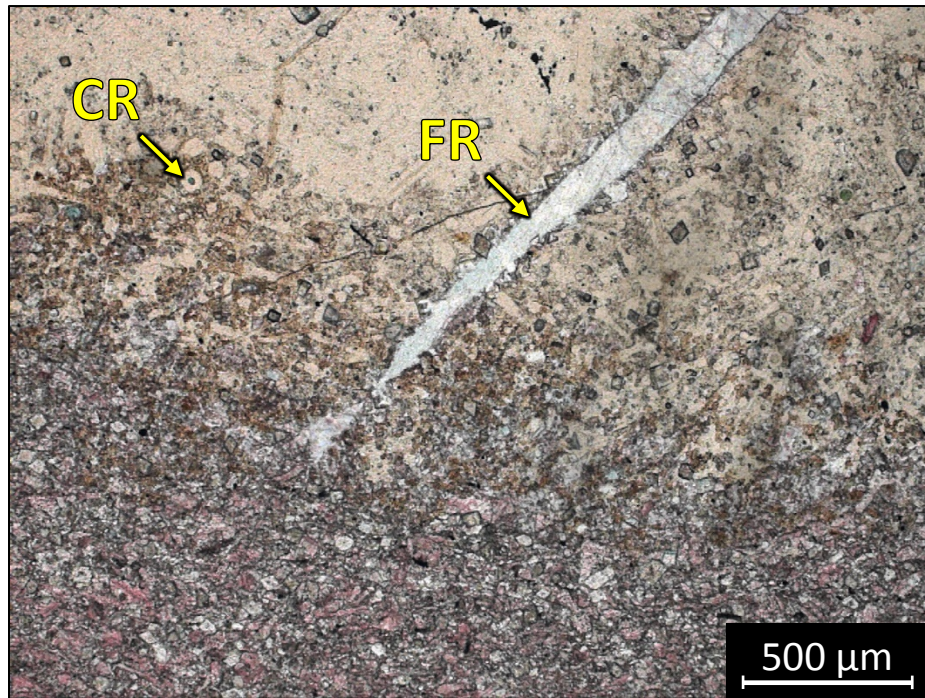
Facies 2



1 BN – 5331.2': Burrowed wackestone to packstone. Sample is alizarin red stained and blue epoxy impregnated. Plug Porosity (NCS): 3.6%. Permeability (Klinkenberg): 0.0018 mD. XRD: 4.2% clay (4% illite+mica, 0.2% chlorite), 64.3% carbonate (54.2% calcite, 10.1% dolomite), and 31.5% other minerals (31.1% quartz and trace amounts of pyrite). Sample contains microcrystalline quartz (10%), sponge spicules (20%), crinoid fragments

(10%), brachiopod fragments (15%), and undifferentiated microbioclastic debris. No visible porosity.

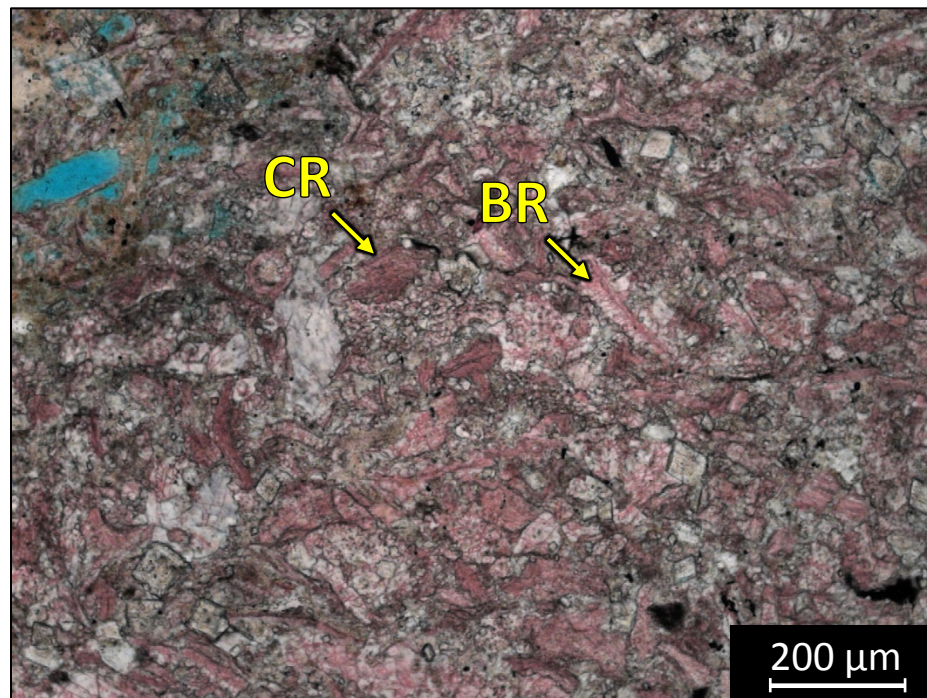
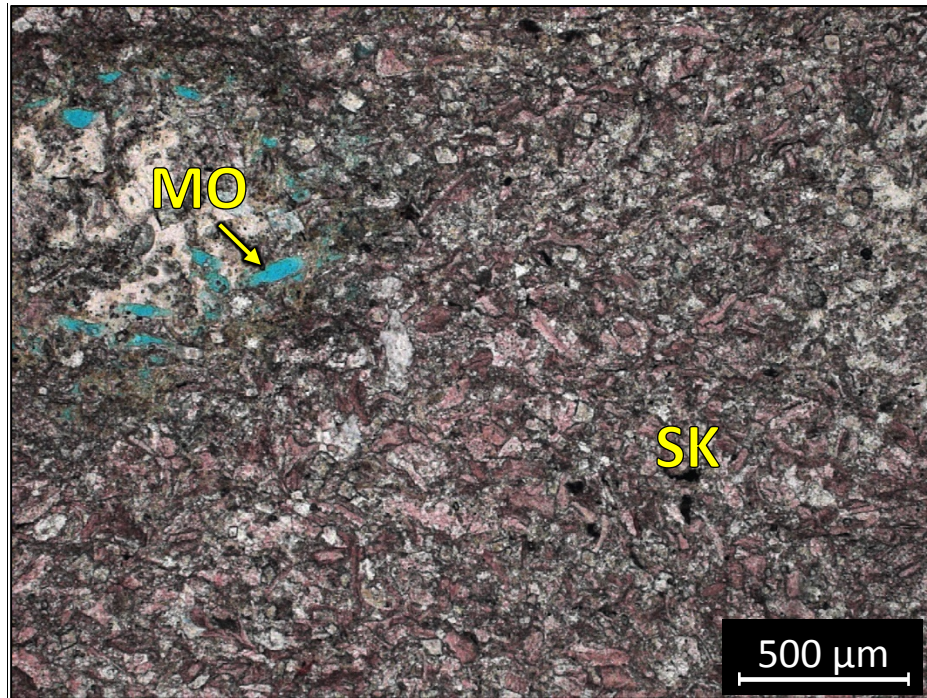
Facies 2



1 BN – 5330.4': Burrowed wackestone to packstone. Sample is alizarin red stained and blue epoxy impregnated. Plug Porosity (NCS): 3.0%. Permeability (Klinkenberg): 0.0019 mD. Visual estimation: 1% clays, 75% carbonates and 24% other minerals. Sample contains microcrystalline quartz (30%), silt-sized quartz grains (5%), sponge spicules

(20%), crinoid fragments (15%), brachiopod fragments (2%), dolomite (15%) and undifferentiated microbioclastic debris. Minor vuggy and fracture porosity present.

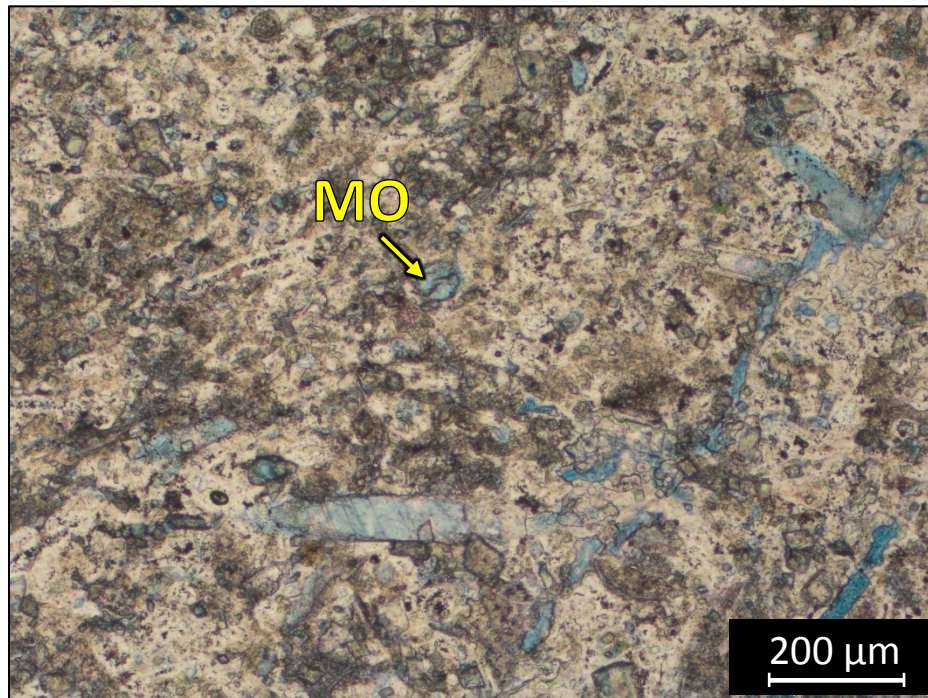
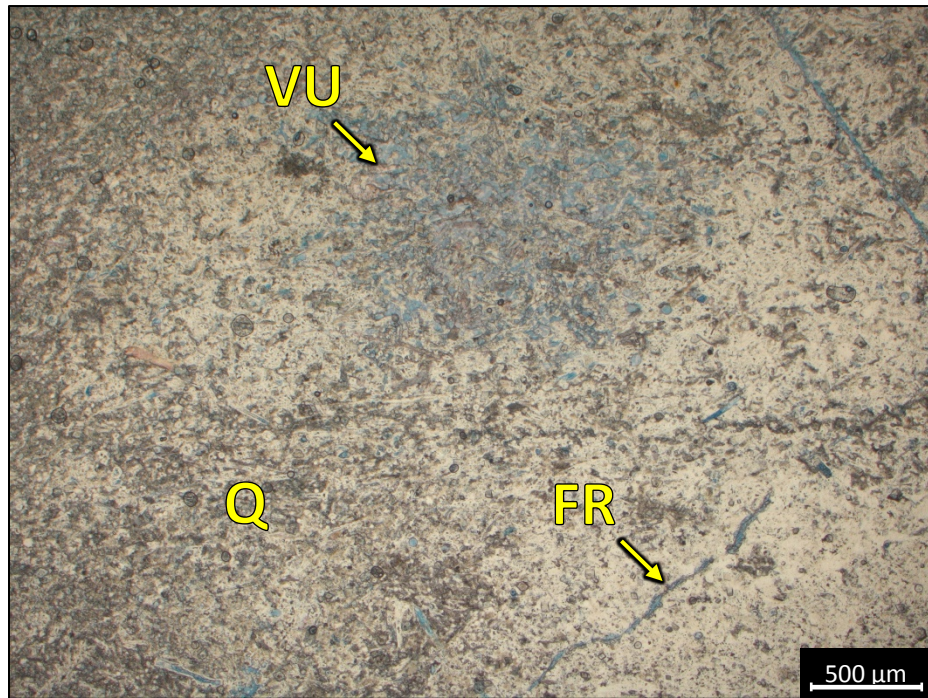
Facies 2



1 BN – 5321.1': Burrowed wackestone to packstone. Sample is alizarin red stained and blue epoxy impregnated. Plug Porosity (NCS): 7.5%. Permeability (Klinkenberg): 0.0019 mD. XRD: 3.9% clay (3.8% illite+mica, 0.1% chlorite), 55.8% carbonate (35.7% calcite, 20.1% dolomite), and 40.3% other minerals (39.4% quartz and trace amounts of pyrite, apatite and halite). Sample contains microcrystalline quartz (5%), sponge spicules (10%),

crinoid fragments (25%), brachiopod fragments (5%), dolomite (7%) and undifferentiated microbioclastic debris. Minor moldic porosity present.

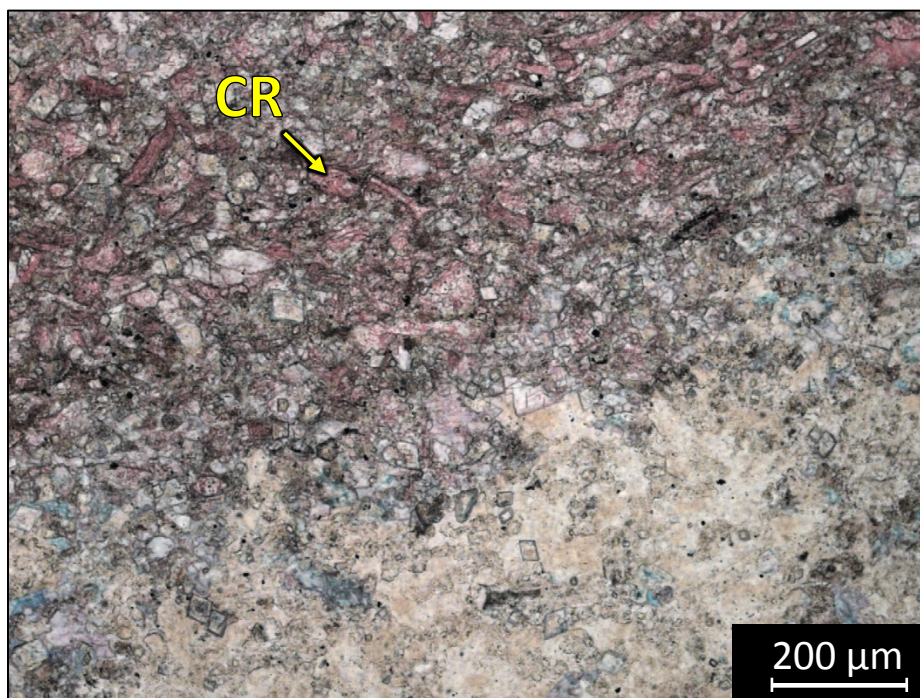
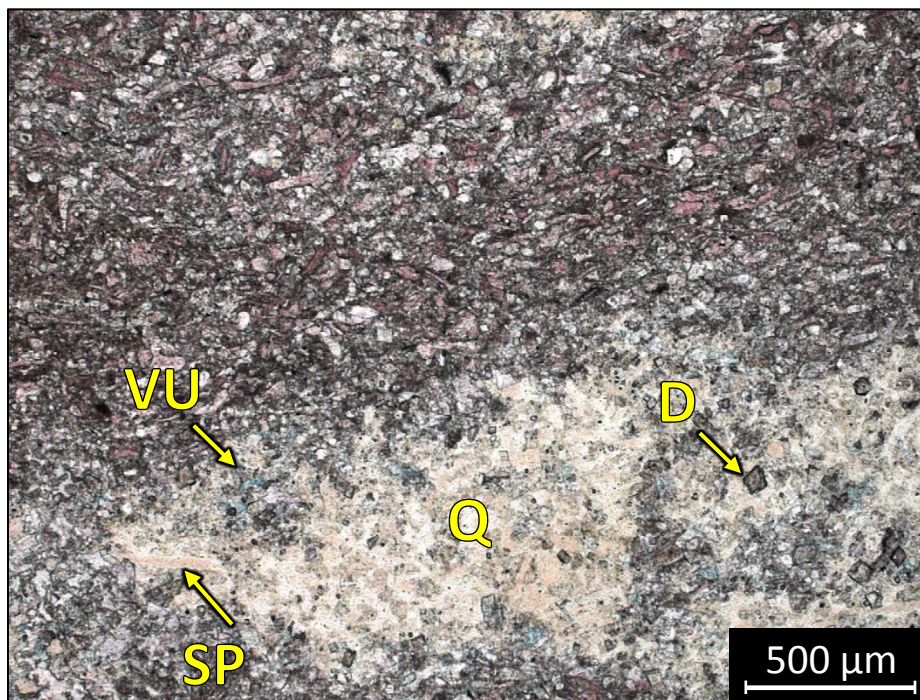
Facies 2



2 ALB – 5166.38': Burrowed wackestone. Sample is alizarin red stained and blue epoxy impregnated. Porosity (NCS): 5.01%. Permeability (Klinkenberg): 0.001763 mD. XRD: 7.5% clay (6.9% illite/smectite, 0.6% kaolinite), 39.6% carbonate (24.3% calcite, 15.3% dolomite), and 52.9% other minerals (49.5% quartz, 2% potassium feldspar, and trace amounts of plagioclase and apatite). Sample contains microcrystalline quartz (15%),

brachiopod fragments (5%), brachiopod spines (10%), sponge spicules (2%), crinoid fragments (5%) and undifferentiated skeletal debris. Fractures, vuggy and moldic porosity observed.

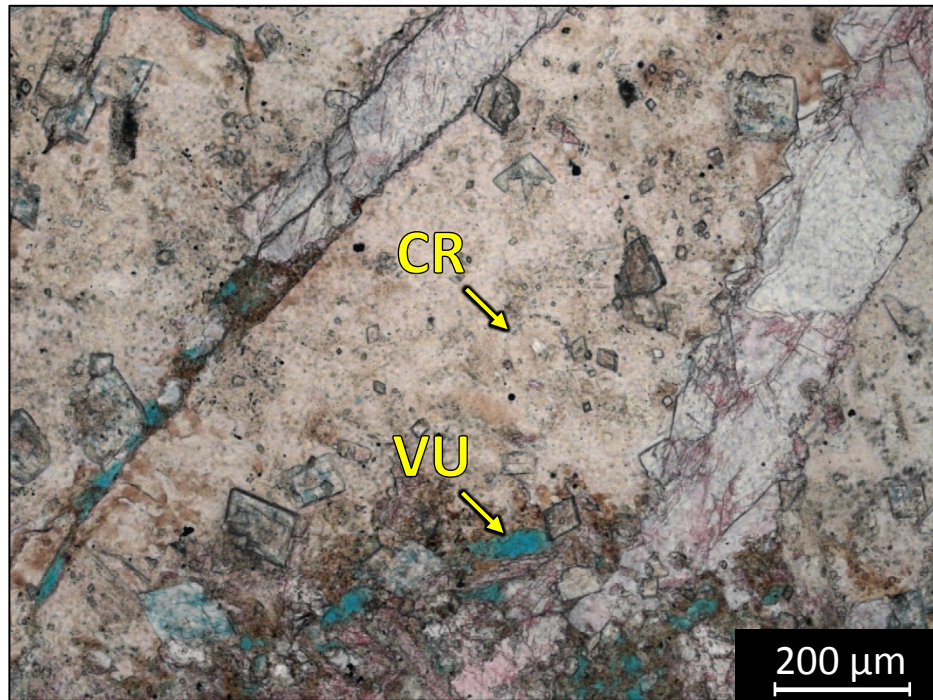
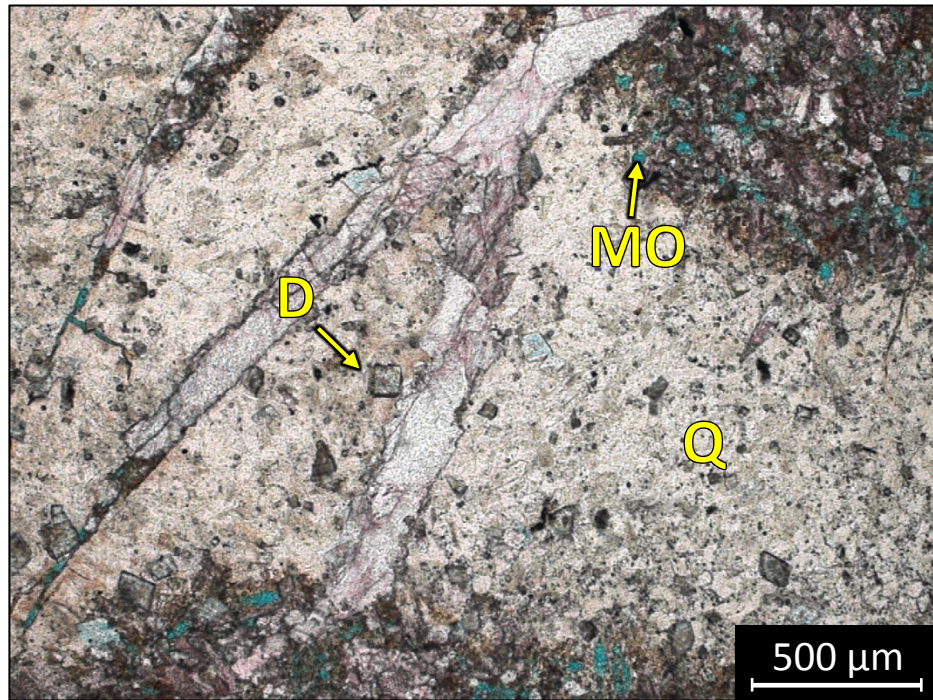
Facies 3



1 BN – 5336.3: Bioturbated packstone. Sample is alizarin red stained and blue epoxy impregnated. Plug Porosity (NCS): 4.2%. Permeability: <0.0001 mD. XRD: 3.5% clay (3.4% illite+mica, 0.1% chlorite), 73.2% carbonate (66% calcite, 7.2% dolomite), and 23.3% other minerals (23.1% quartz and trace amounts of pyrite). Sample contains microcrystalline quartz (15%), silt-sized quartz grains (3%), sponge spicules (10%), crinoid fragments (35%), brachiopod fragments (15%), and undifferentiated

microbioclastic debris. Minor moldic, vuggy, interparticle and intercrystalline porosity present.

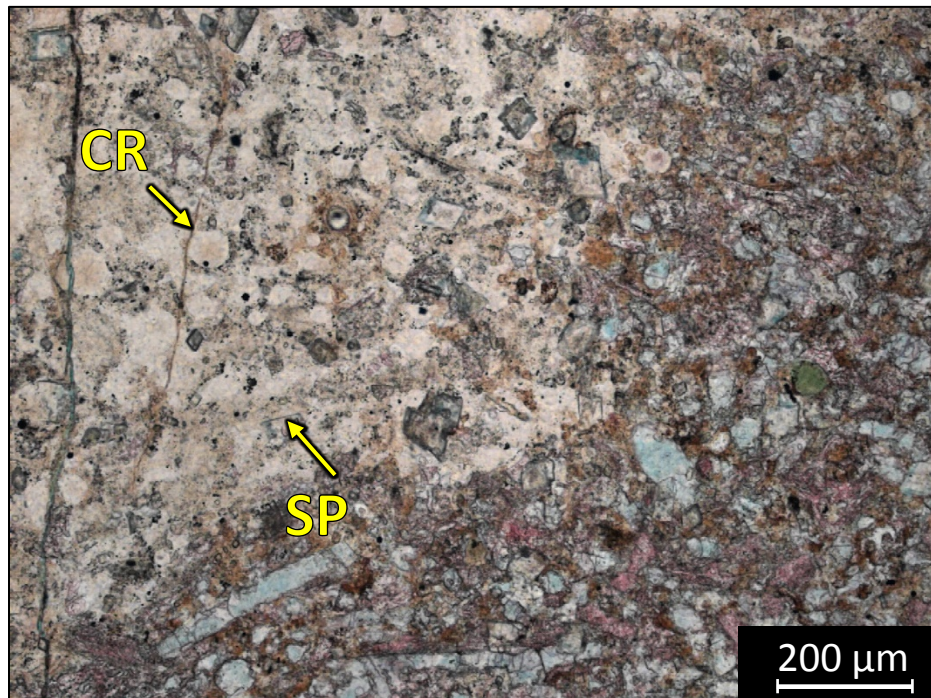
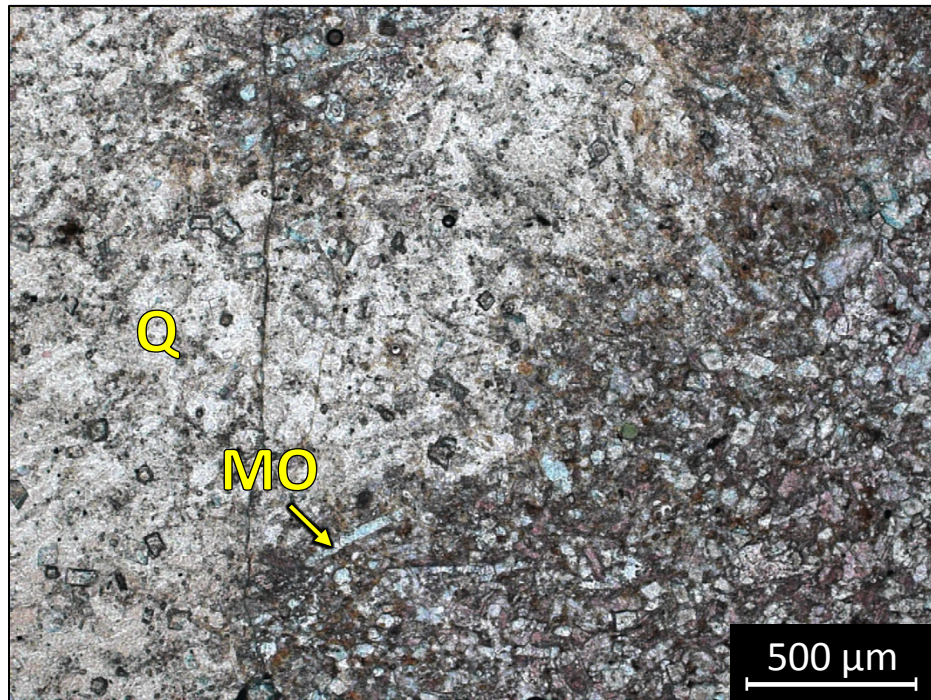
Facies 3



1 BN – 5325.20: Bioturbated packstone to wackestone. Sample is alizarin red stained and blue epoxy impregnated. Plug Porosity (NCS): 12.4%. Permeability (Klinkenberg): 0.404 mD. XRD: 2.2% clay (2.1% illite+mica, 0.1% chlorite), 41% carbonate (30.4% calcite, 10.4% dolomite), and 56.8% other minerals (56.2% quartz and trace amounts of pyrite and halite). Sample contains microcrystalline quartz (50%), sponge spicules (15%),

crinoid fragments (7%), brachiopod fragments (5%), dolomite (10%) and undifferentiated microbioclastic debris. Slight moldic and vuggy porosity present.

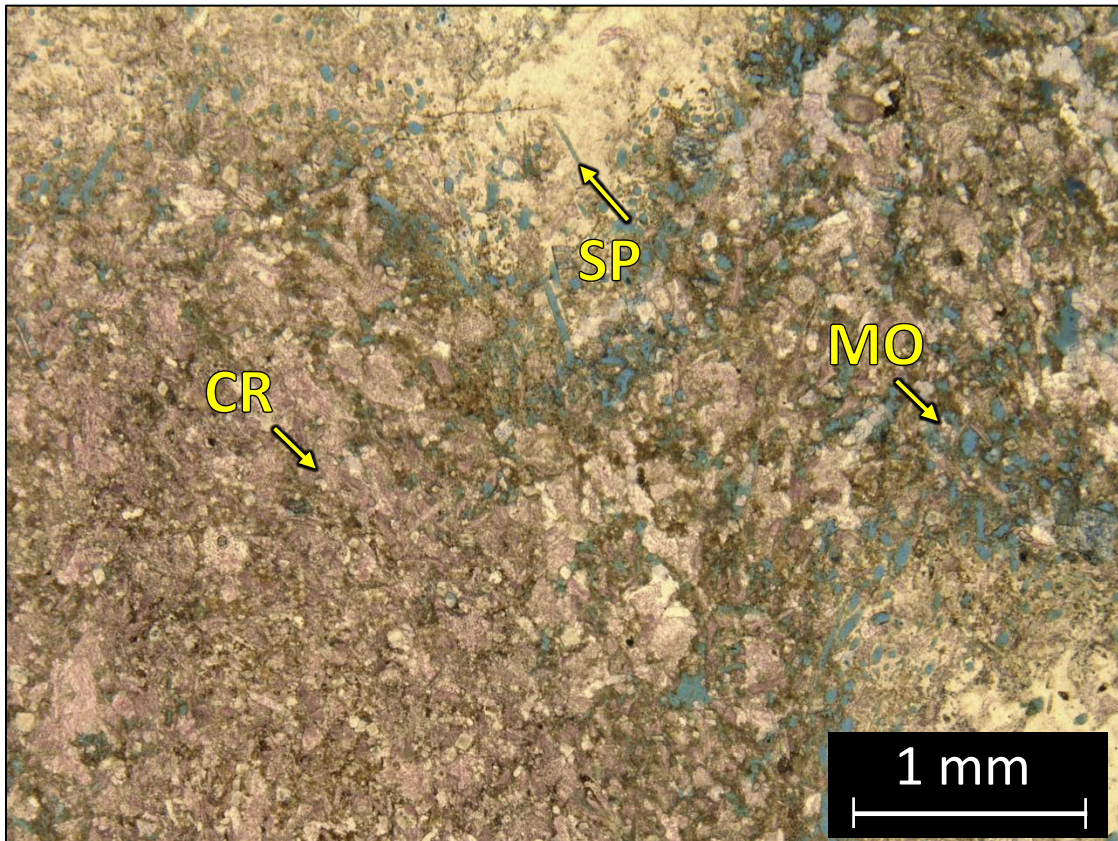
Facies 3



1 BN – 5318.20: Bioturbated packstone to wackestone. Sample is alizarin red stained and blue epoxy impregnated. Plug Porosity (NCS): 6.3%. Permeability (Klinkenberg): 0.0029 mD. Visual estimation: 2% clays, 65% carbonates and 33% other minerals. Sample contains microcrystalline quartz (20%), sponge spicules (5%), crinoid fragments (10%),

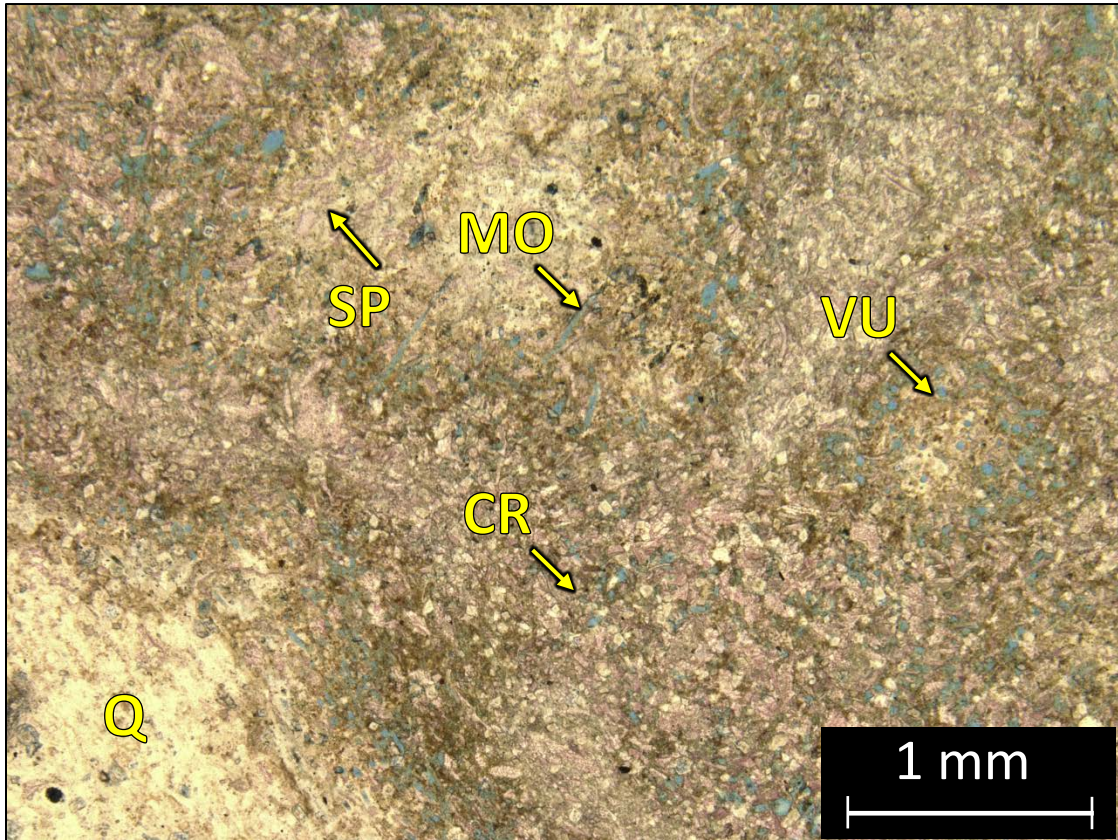
brachiopod fragments (10%), dolomite (20%) and undifferentiated microbioclastic debris. Slight fracture and moldic porosity present.

Facies 3



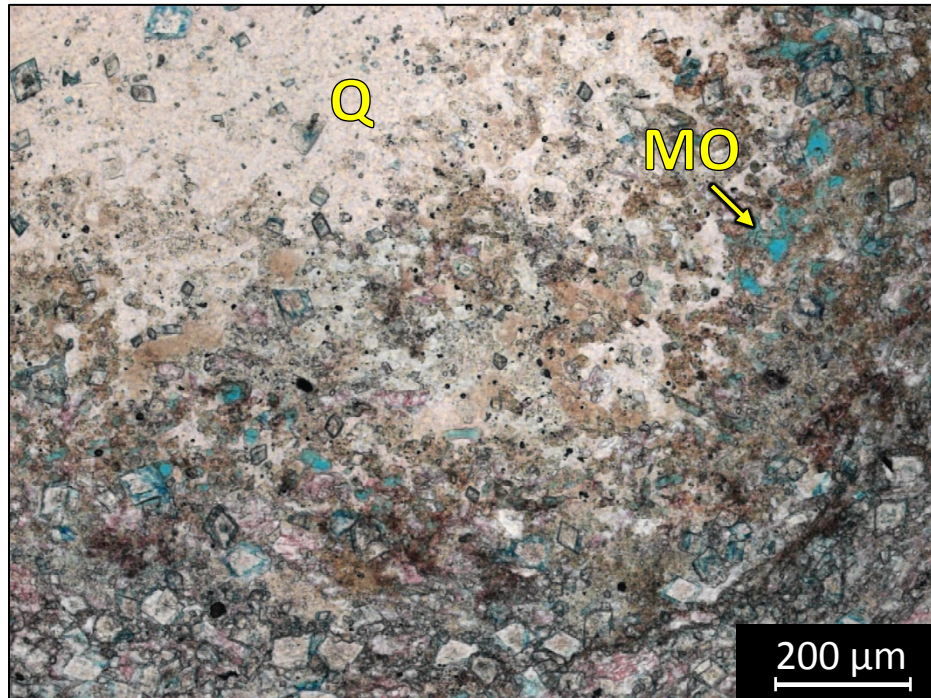
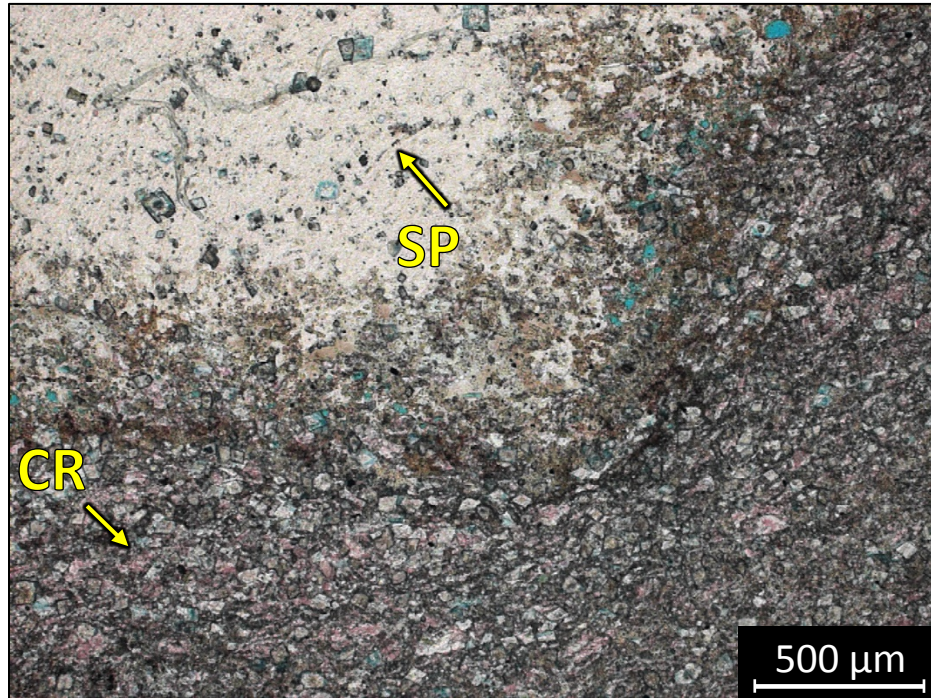
1 BN – 5306.16: Bioturbated packstone to wackestone. Sample is alizarin red stained and blue epoxy impregnated. Porosity (NCS): data not available. Permeability (Klinkenberg): 1.29 mD. Visual estimation: 3% clay, 85% carbonates, and 12% other minerals. Sample contains crinoid fragments (40%), sponge spicules (5%), brachiopod fragments (10%), microcrystalline quartz (15%), dolomite (5%) and undifferentiated skeletal debris. Abundant moldic, interparticle and vuggy porosity present.

Facies 3



1 BN – 5303.6: Bioturbated packstone. Sample is alizarin red stained and blue epoxy impregnated. Porosity (NCS): 14.7%. Permeability (Klinkenberg): 1.63 mD. XRD: 1.8% clay (1.7% illite+mica, 0.1% chlorite), 36.6% carbonate (26.7% calcite, 9.9% dolomite), and 61.6% other minerals (61.1% quartz and trace amounts of halite). Sample contains crinoid fragments (30%), sponge spicules (5%), brachiopod fragments (15%), microcrystalline quartz (10%), dolomite (3%) and undifferentiated skeletal debris. Abundant moldic, interparticle and vuggy porosity present.

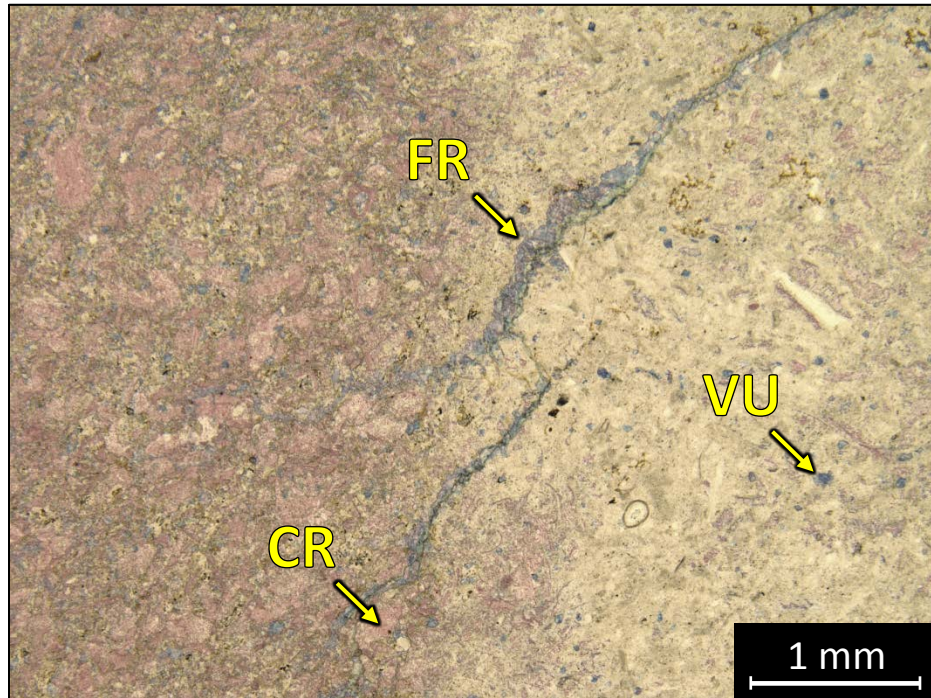
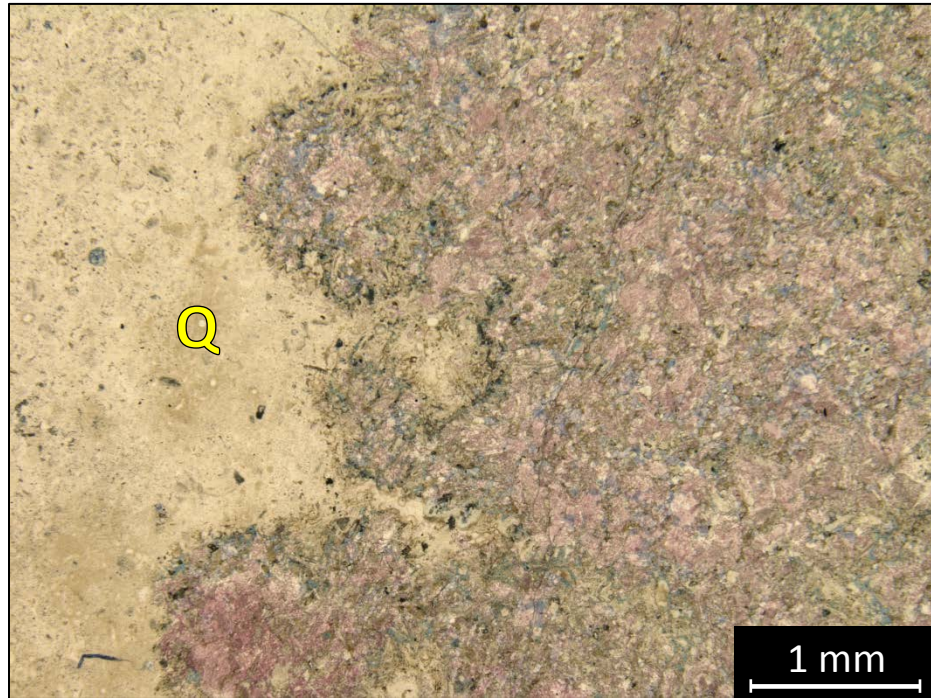
Facies 3



1 BN – 5289.80: Bioturbated packstone to wackestone. Sample is alizarin red stained and blue epoxy impregnated. Porosity (NCS): 10.9%. Permeability (Klinkenberg): data not available. XRD: 4% clay (3.8% illite+mica, 0.2% chlorite), 54.4% carbonate (35.6% calcite, 18.8% dolomite), and 41.6% other minerals (41.3% quartz and trace amounts of halite). Sample contains crinoid fragments (15%), sponge spicules (5%), microcrystalline

quartz (20%), dolomite (15%) and undifferentiated skeletal debris. Moldic, vuggy and interparticle porosity present.

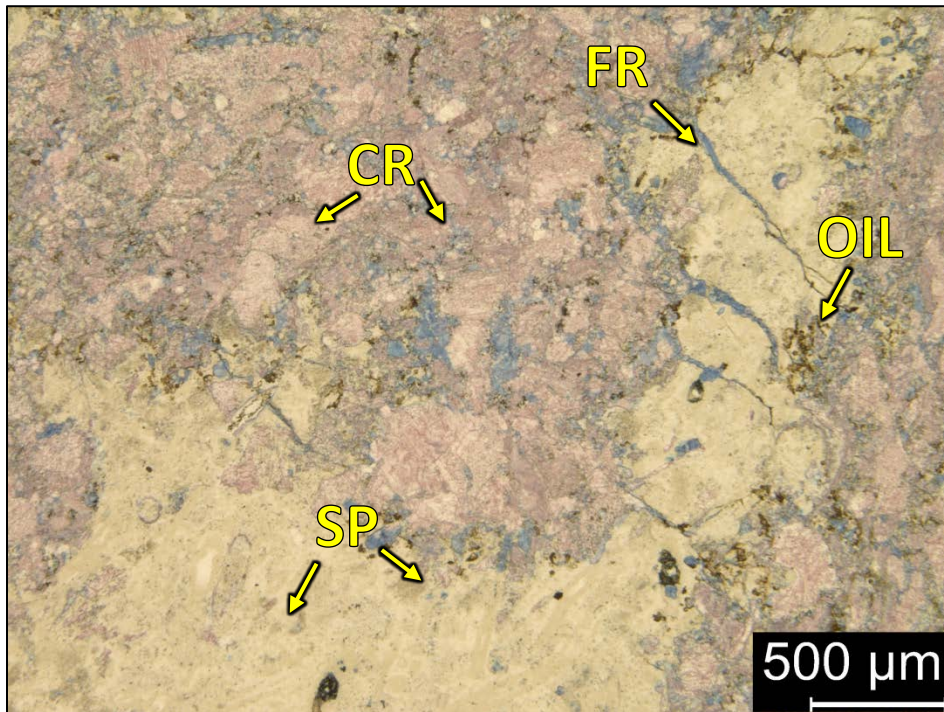
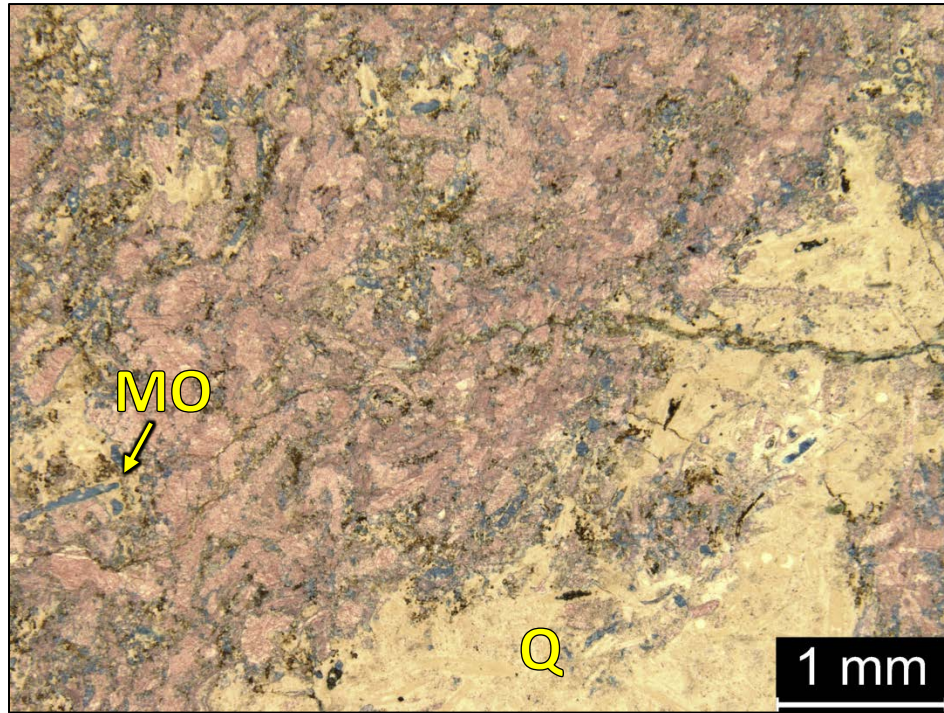
Facies 3



1 BN – 5269.8: Skeletal bioturbated packstone. Sample is alizarin red stained and blue epoxy impregnated. Porosity (NCS): 8.3%. Permeability (Klinkenberg): data not available. XRD: 0.6% clay (8% illite/smectite, 0.3% chlorite), 12.3% carbonate (11% calcite, 1.3% dolomite), and 87.1% other minerals (86.7% quartz and trace amounts of pyrite and halite). Sample contains crinoid fragments (20%), sponge spicules (15%),

brachiopod fragments (5%), microcrystalline quartz (50%) and undifferentiated skeletal debris. Moldic, fracture and vuggy porosity observed.

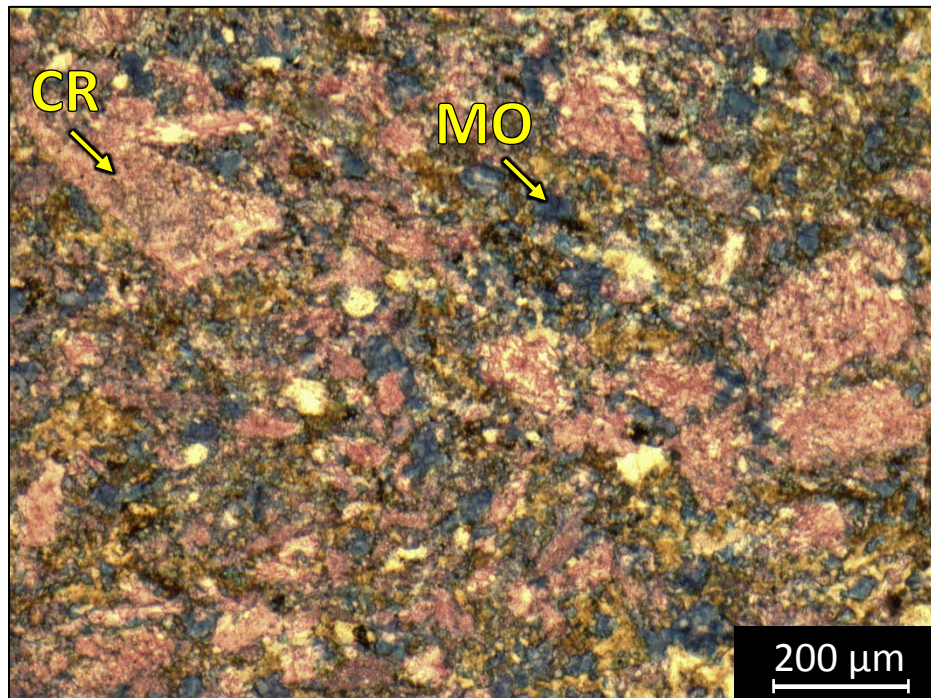
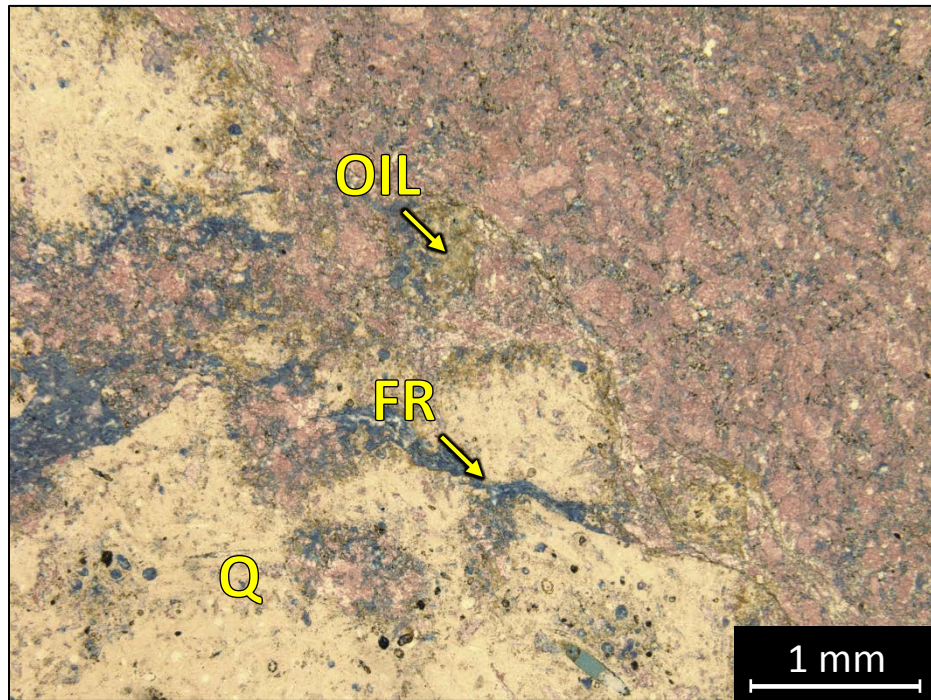
Facies 3



1 BN – 5258.4': Bioturbated packstone. Sample is alizarin red stained and blue epoxy impregnated. Porosity (NCS): 3.8%. Permeability (Klinkenberg): 0.029 mD. XRD: 1.8% clay (illite and mica), 66% carbonates (calcite), and 32.2% other minerals (32% quartz)

and trace amounts of pyrite). Sample contains crinoid fragments (40%), sponge spicules (20%), microcrystalline quartz (10%), silt-sized quartz grains (3%) and undifferentiated skeletal debris. Oil-filled fracture and vuggy porosity observed, as well as open moldic and fracture porosity.

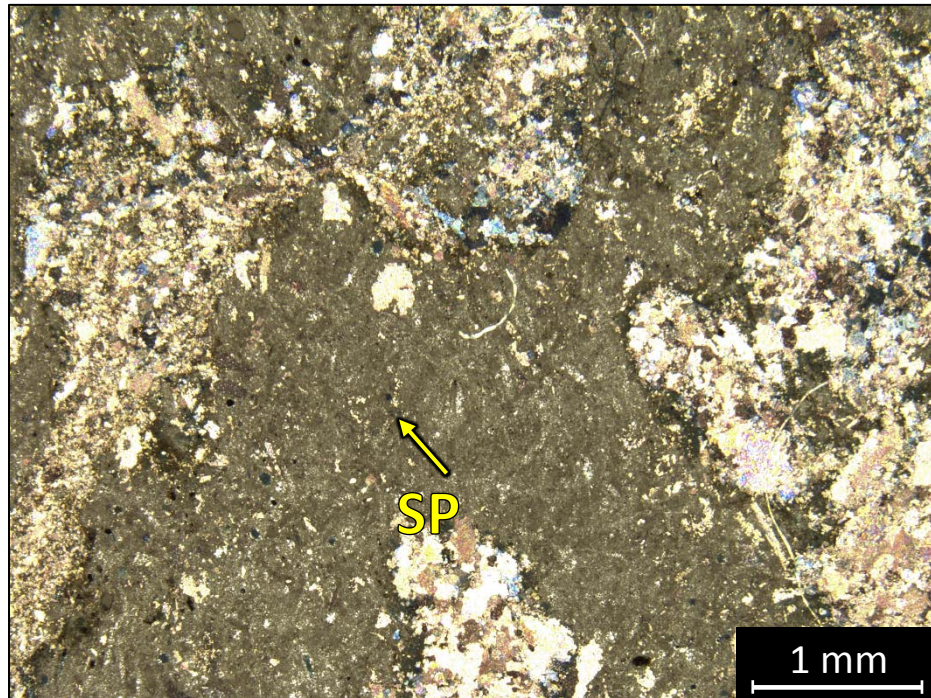
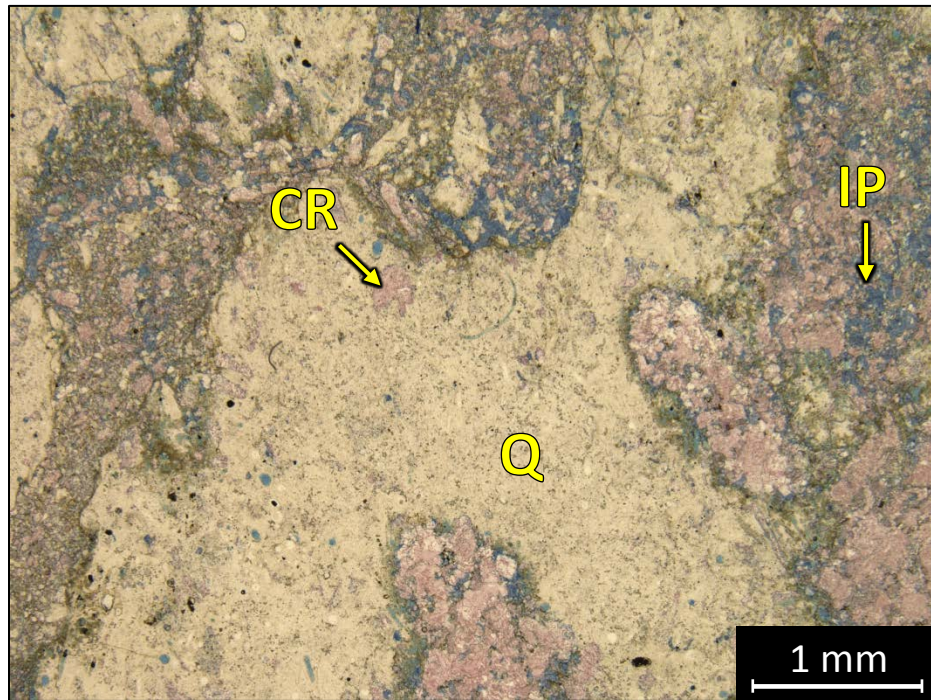
Facies 3



1 BN – 5257.8: Bioturbated packstone. Sample is alizarin red stained and blue epoxy impregnated. Porosity (NCS): 6%. Permeability (Klinkenberg): 0.1030 mD. Visual estimation: 2% clay, 70% carbonates, and 28% other minerals. Sample contains crinoid fragments (30%), sponge spicules (15%), brachiopod fragments (5%) and

undifferentiated skeletal debris. Oil filled fracture and vuggy porosity observed, as well as open moldic, interparticle and fracture porosity.

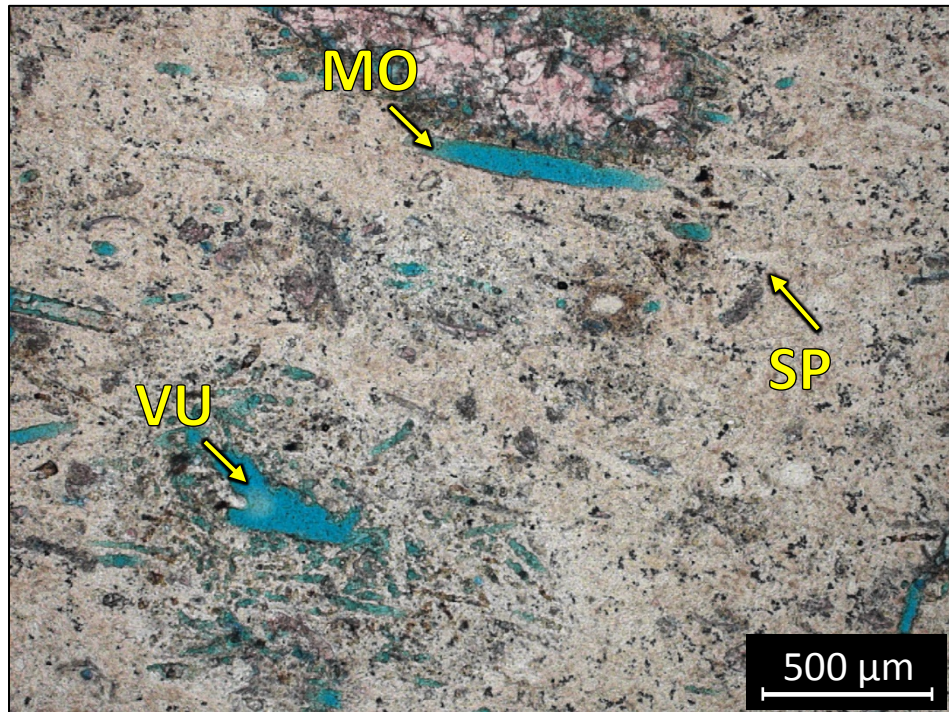
Facies 3



1 BN – 5256.4: Bioturbated packstone. Sample is alizarin red stained and blue epoxy impregnated (PPL and XPL). Porosity (NCS): 10.1%. Permeability (Klinkenberg): 0.1140 mD. Visual estimation: 3% clay, 55% carbonates, and 42% other minerals. Sample contains crinoid fragments (20%), sponge spicules (25%), brachiopod fragments (5%) and

undifferentiated skeletal debris. Moldic, interparticle, vuggy and fracture porosity also observed.

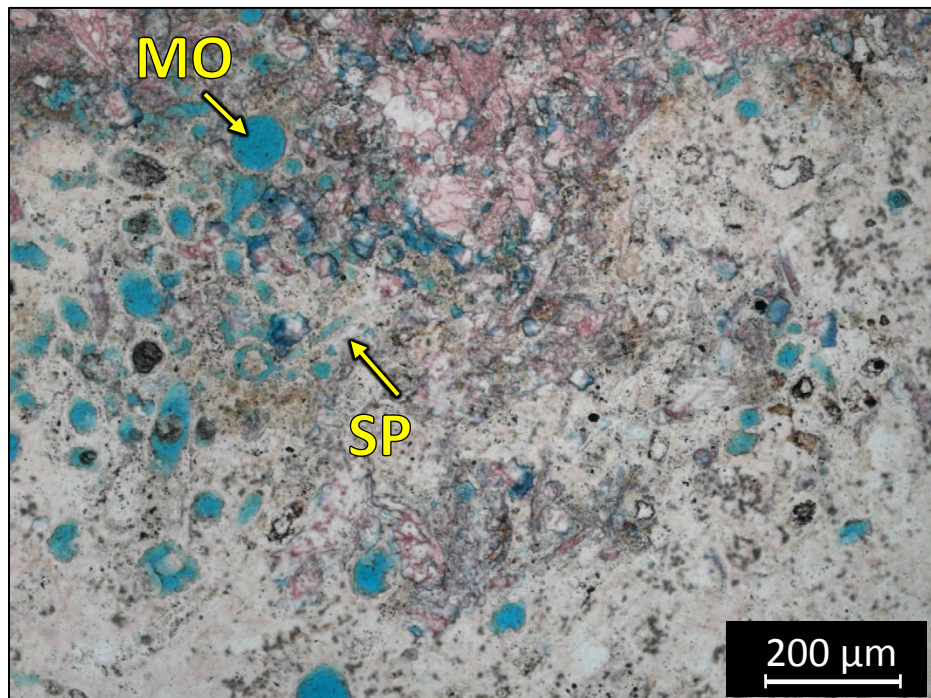
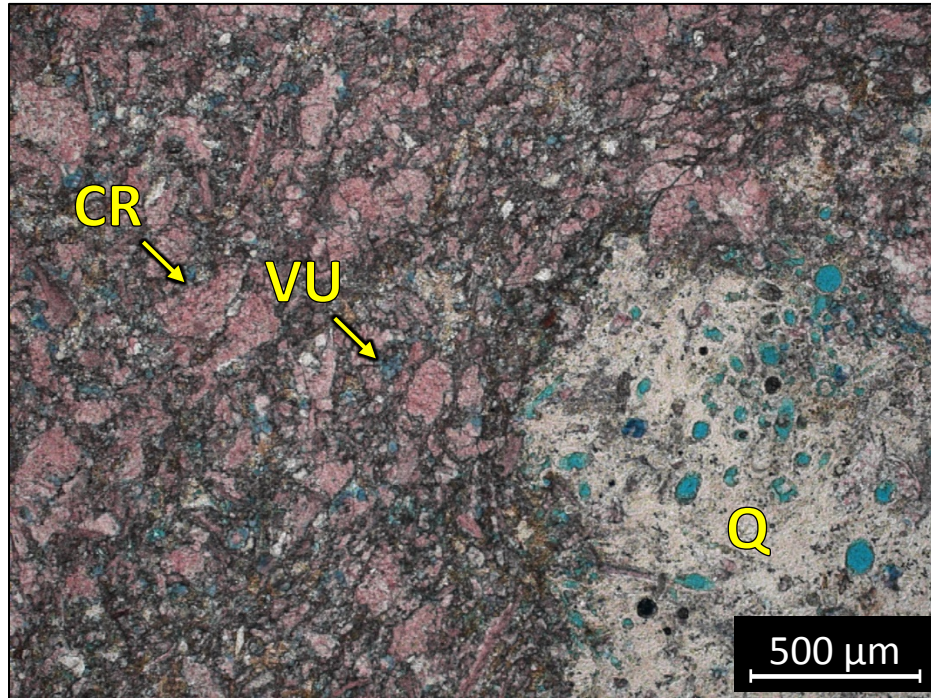
Facies 3



1 BN – 5255.90': Bioturbated wackestone to packstone. Sample is alizarin red stained and blue epoxy impregnated. Porosity (NCS): 12.7%. Permeability (Klinkenberg): 0.323 mD. XRD: 0.5% clay (illite+mica), 56.1% carbonate (calcite), and 43.4% other minerals (43.2% quartz and trace amounts of pyrite and halite). Sample contains crinoid fragments

(15%), sponge spicules (10%), brachiopod fragments (5%), microcrystalline quartz (25%), and undifferentiated skeletal debris. Moldic and vuggy porosity observed.

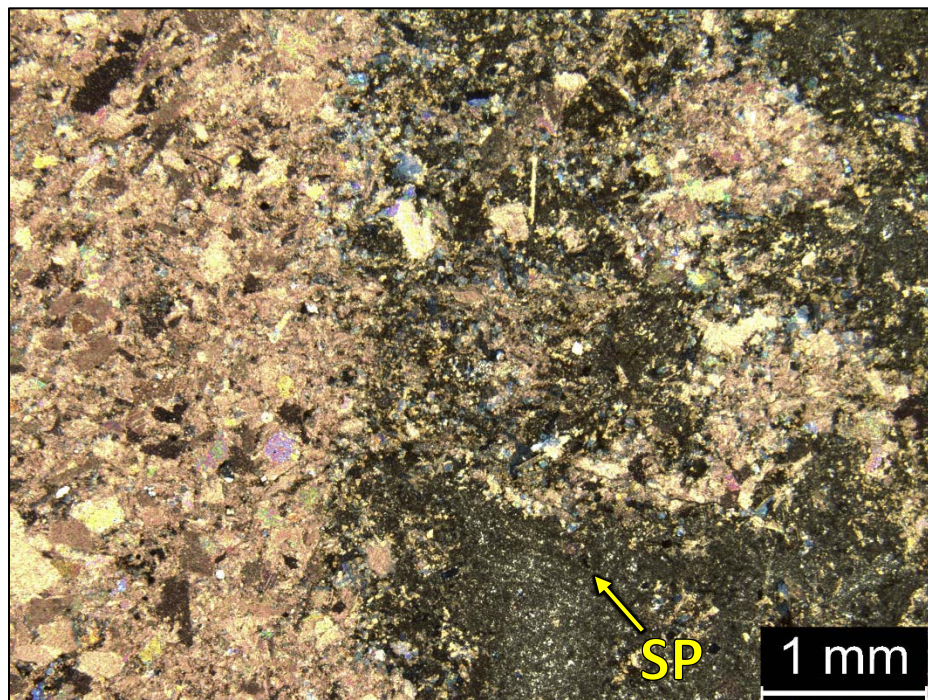
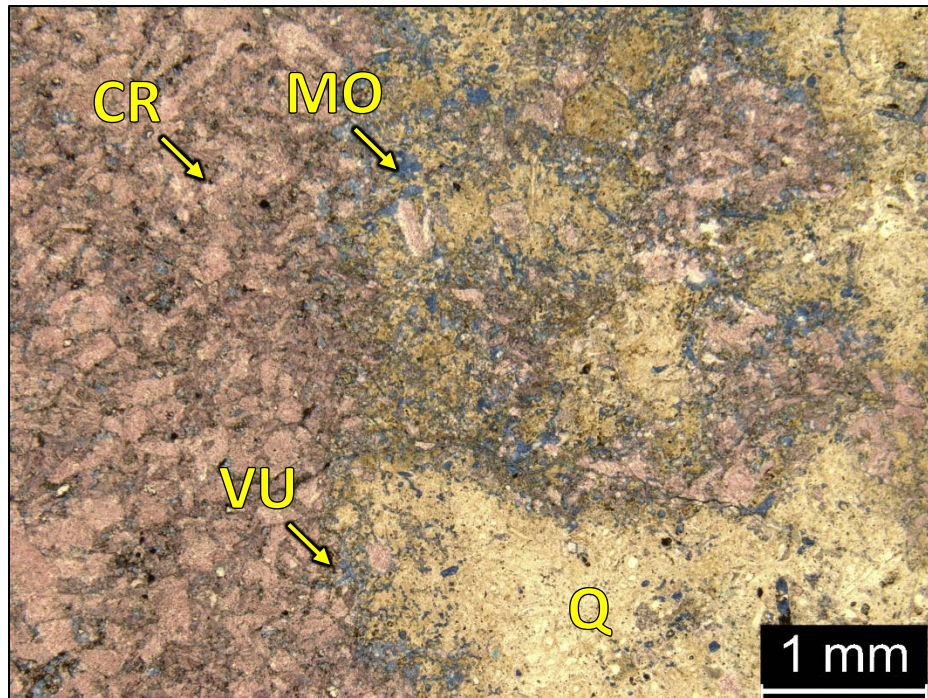
Facies 3



1 BN – 5255.50: Bioturbated skeletal packstone. Sample is alizarin red stained and blue epoxy impregnated. Porosity (NCS): 10.9%. Permeability (Klinkenberg): 0.1850 mD. Visual estimation: 2% clay, 60% carbonates, and 38% other minerals. Sample contains

crinoid fragments (25%), sponge spicules (15%), brachiopod fragments (5%), microcrystalline quartz (20%), ostracodes (3%) and undifferentiated skeletal debris. Moldic and vuggy porosity observed.

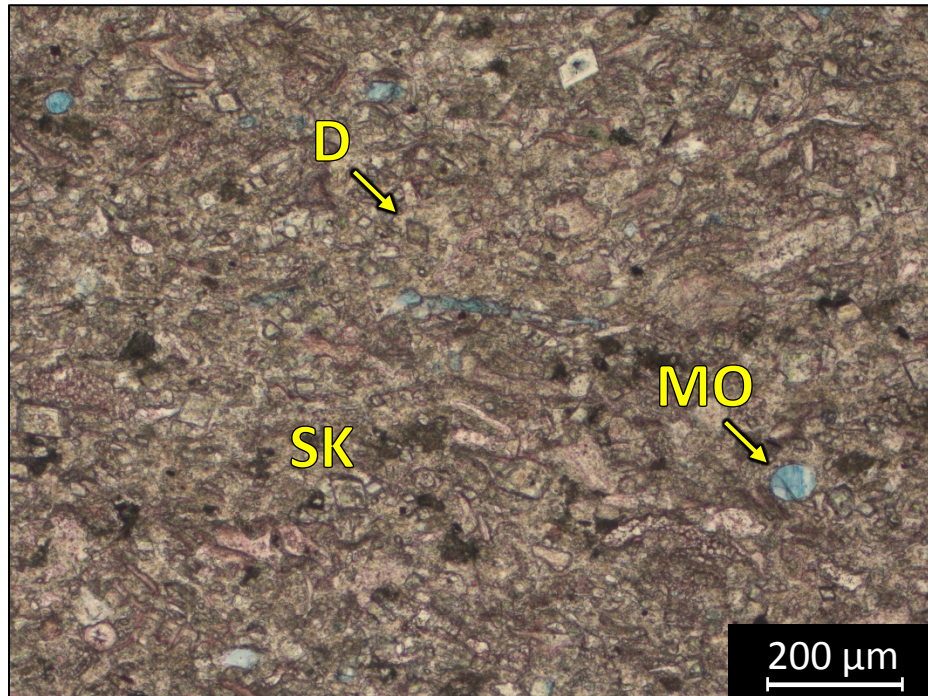
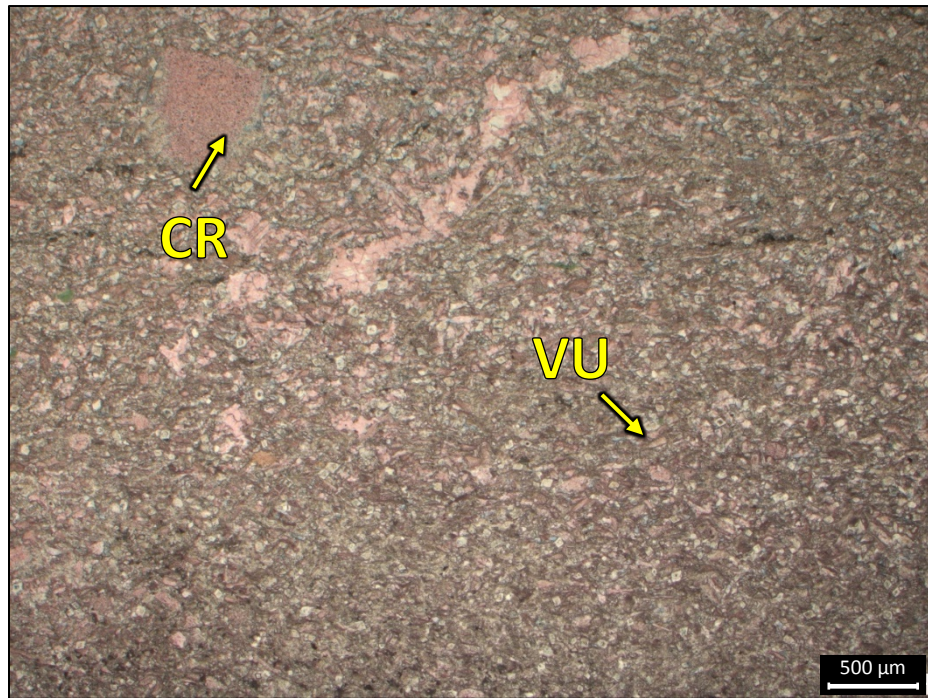
Facies 3



1 BN – 5247.2': Packstone to wackestone. Sample is alizarin red stained and blue epoxy impregnated (PPL and XPL). Porosity (NCS): 7.5%. Permeability (Klinkenberg): 0.02100 mD. XRD: 0.5% clay (illite+mica), 67.5% carbonate (calcite), and 32% other minerals (31.4% quartz and trace amounts of pyrite and apatite). Sample contains crinoid fragments (25%), brachiopod fragments (10%), microcrystalline quartz (15%), sponge

spicules (5%) and undifferentiated skeletal debris. Abundant moldic, interparticle and vuggy porosity observed.

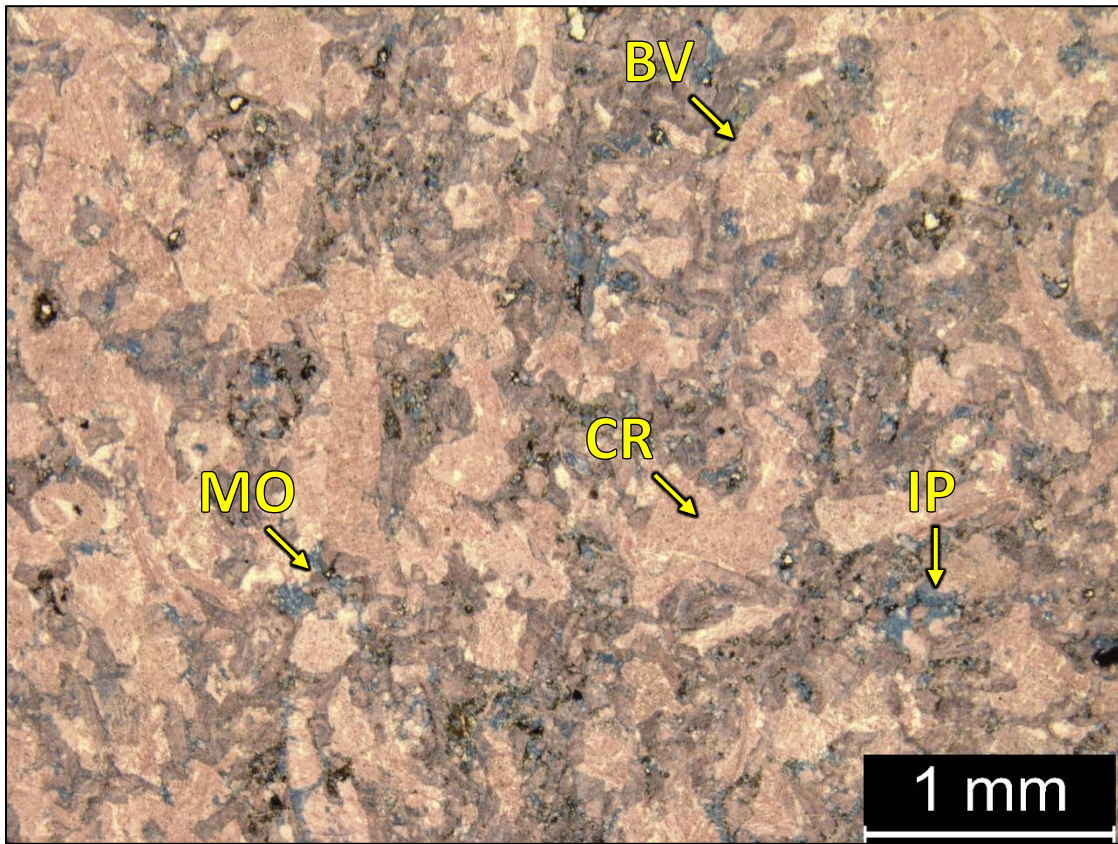
Facies 3



2 ALB – 5181.1': Bioturbated wackestone to packstone. Sample is alizarin red stained and blue epoxy impregnated. Porosity (NCS): 7.31%. Permeability (Klinkenberg): 0.001104 mD. XRD: 14.4% clay (13.6% illite/smectite, 0.5% chlorite, 0.3% kaolinite), 39.8% carbonate (20.1% calcite, 19.7% dolomite), and 45.8% other minerals (44.3% quartz and trace amounts of potassium feldspar, plagioclase and halite). Sample contains

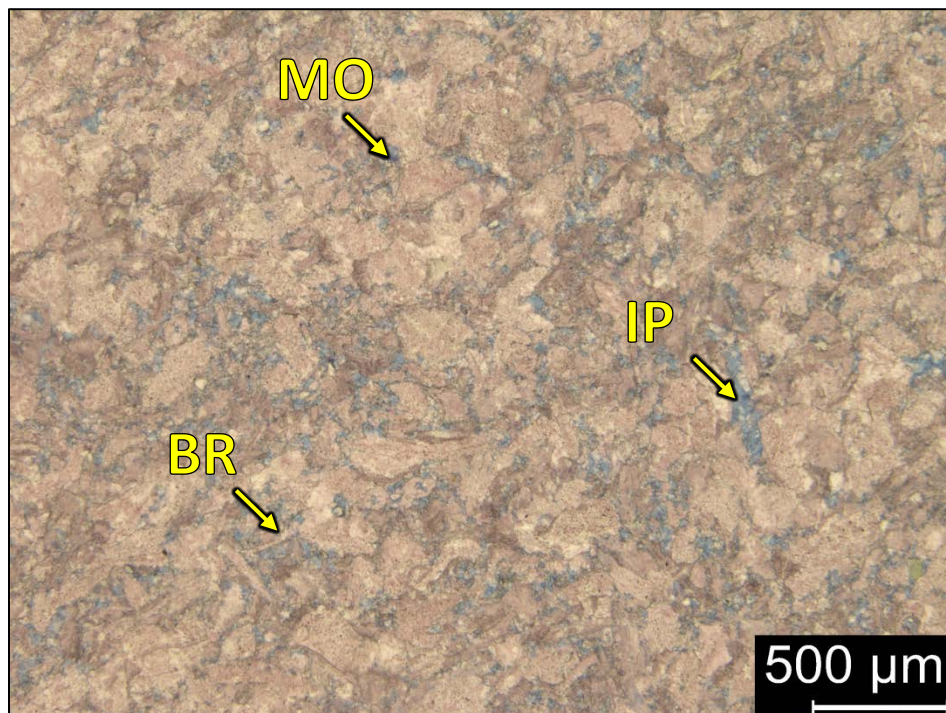
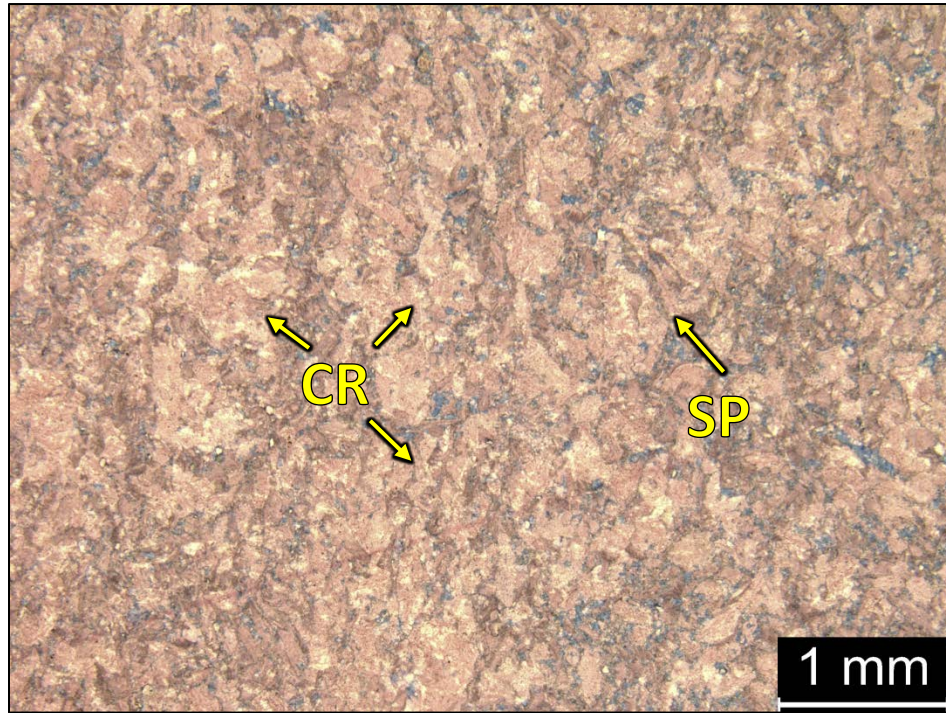
microcrystalline quartz (5%), sponge spicules (7%), crinoid fragments (10%) and undifferentiated skeletal debris. Moldic and vuggy porosity observed.

Facies 4



1 BN – 5243.2’: Skeletal grainstone to packstone. Sample is alizarin red stained and blue epoxy impregnated. Porosity (NCS): 2%. Permeability (Klinkenberg): data not available. XRD: 0.1% clay (chlorite), 97.9% carbonate (calcite), and 2% other minerals (1.9% quartz and trace amounts of pyrite). Sample contains crinoid fragments (80%), brachiopod fragments (5%), bivalves (15%) and undifferentiated skeletal debris. Moldic, vuggy and interparticle porosity observed.

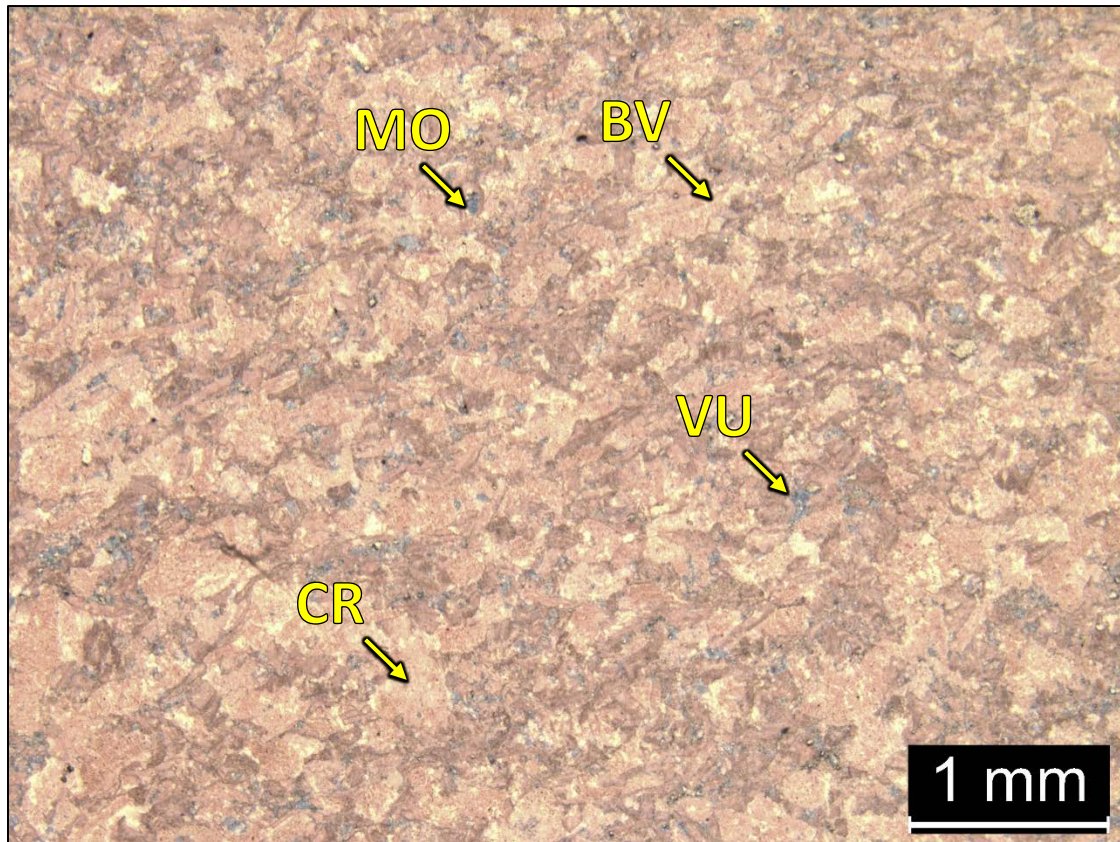
Facies 4



1 BN – 5260.66': Skeletal grainstone. Sample is alizarin red stained and blue epoxy impregnated. Porosity (NCS): 2.3%. Permeability (Klinkenberg): <0.0001 mD. Visual estimation: 1% clay, 97% carbonates, and 2% other minerals. Sample contains crinoid

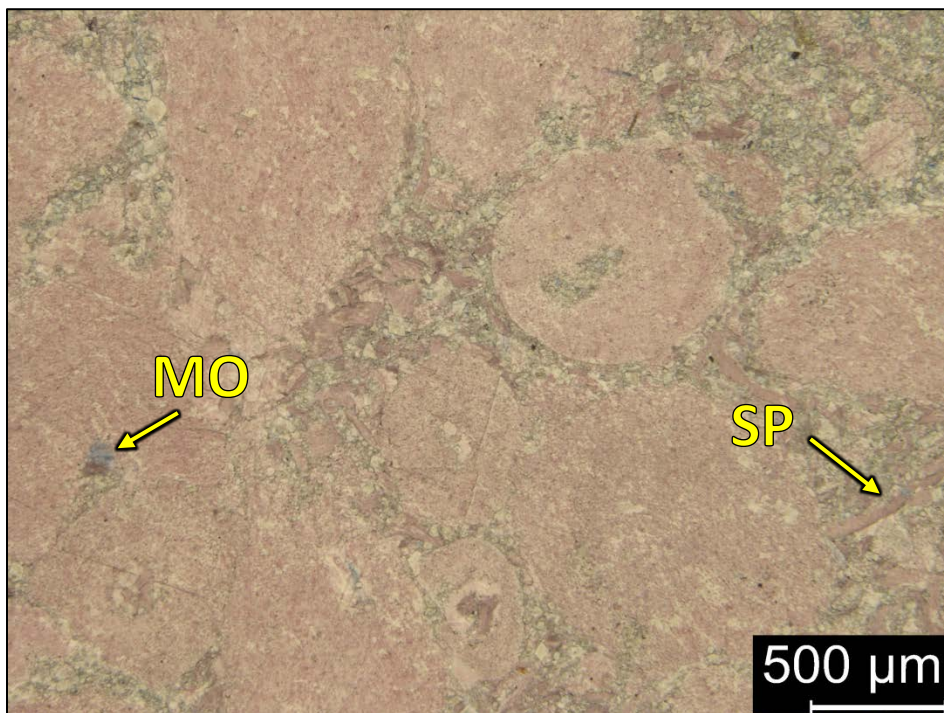
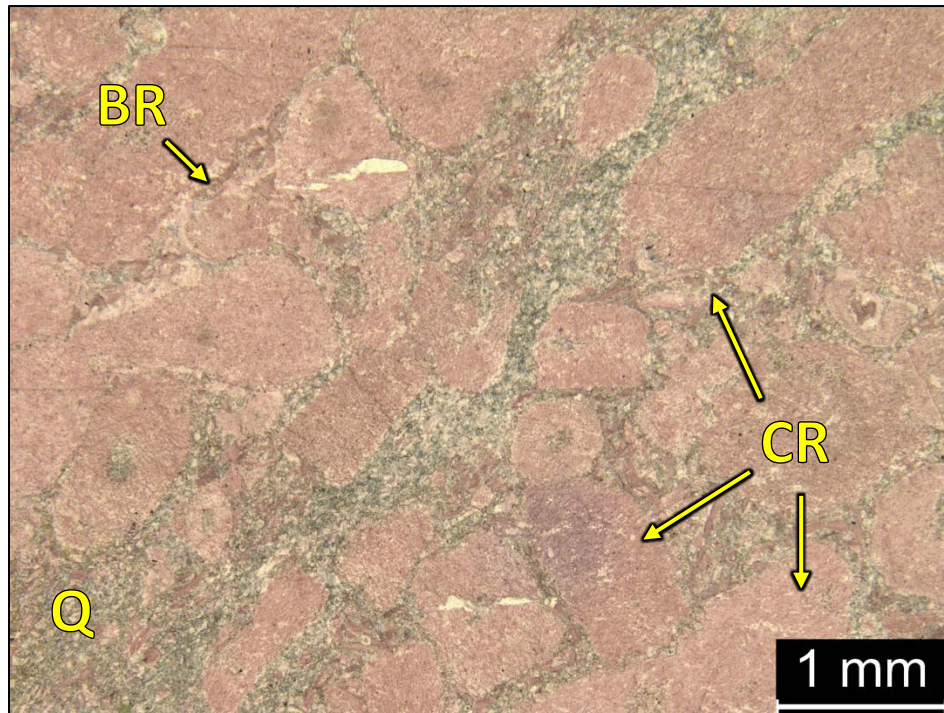
fragments (80%), sponge spicules (5%), brachiopod fragments (5%) and undifferentiated skeletal debris. Open moldic, vuggy, and interparticle porosity present.

Facies 4



1 BN – 5262.1': Skeletal packstone. Sample is alizarin red stained and blue epoxy impregnated. Porosity (NCS): 2.1%. Permeability (Klinkenberg): 0.0001 mD. Visual estimation: 2% clay, 96% carbonates, and 2% other minerals. Sample contains crinoid fragments (60%), brachiopod fragments (5%), bivalves (8%), microcrystalline quartz (2%) and undifferentiated skeletal debris. Slight moldic, interparticle and vuggy porosity observed.

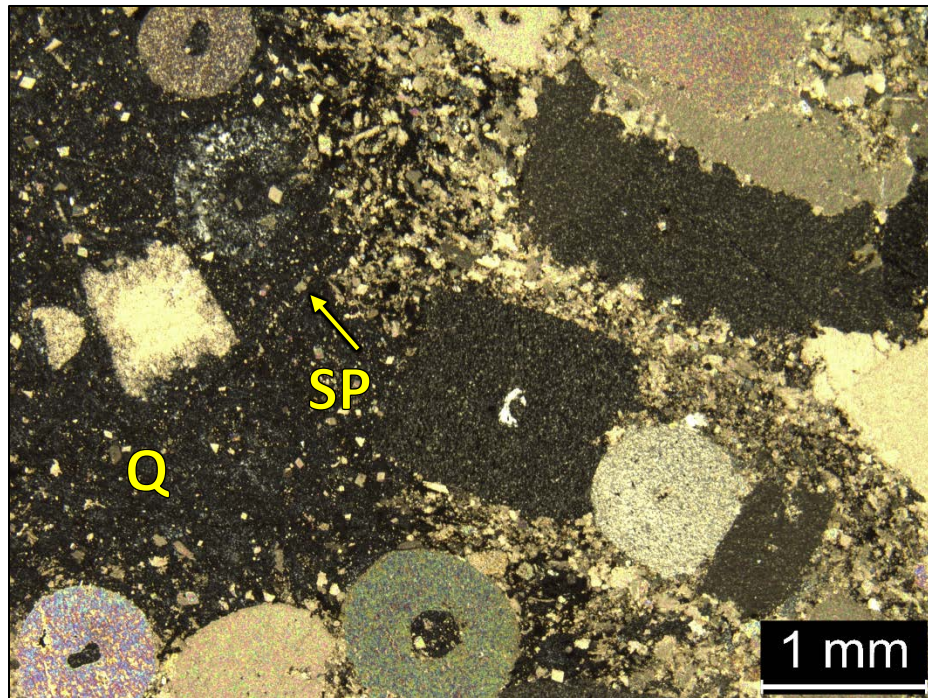
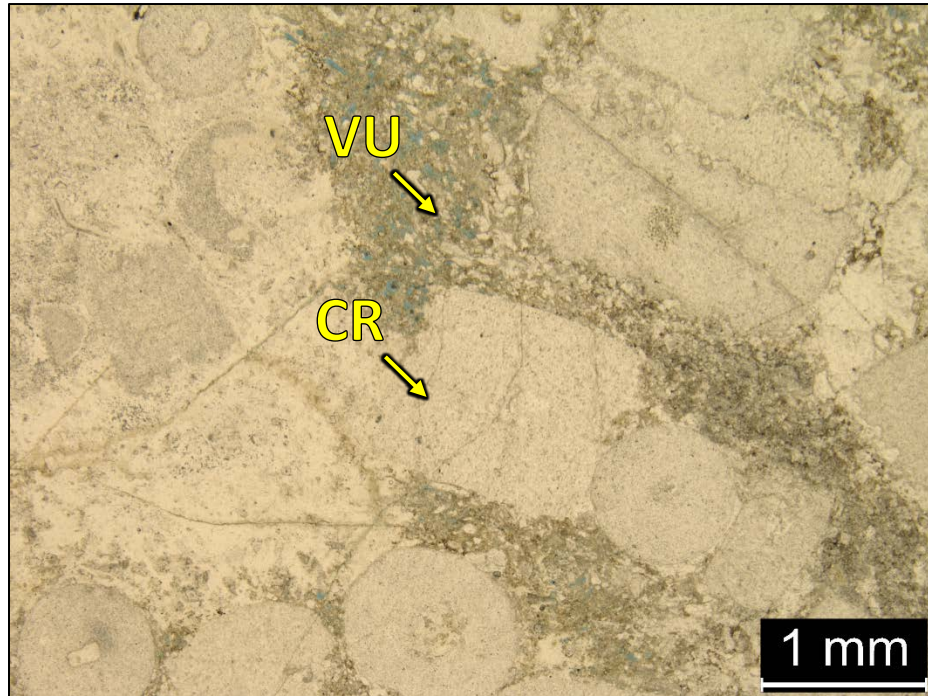
Facies 4



1 BN – 5277.74': Skeletal grain rich packstone. Sample is alizarin red stained and blue epoxy impregnated. Porosity (NCS): 5.7%. Permeability (Klinkenberg): 0.0020 mD. Visual estimation: 1% clay, 93% carbonates, and 6% other minerals. Sample contains crinoid fragments (60%), sponge spicules (10%), brachiopod fragments (10%),

microcrystalline quartz (5%), silt-sized quartz grains (3%) and undifferentiated skeletal debris. Open moldic and vuggy porosity present.

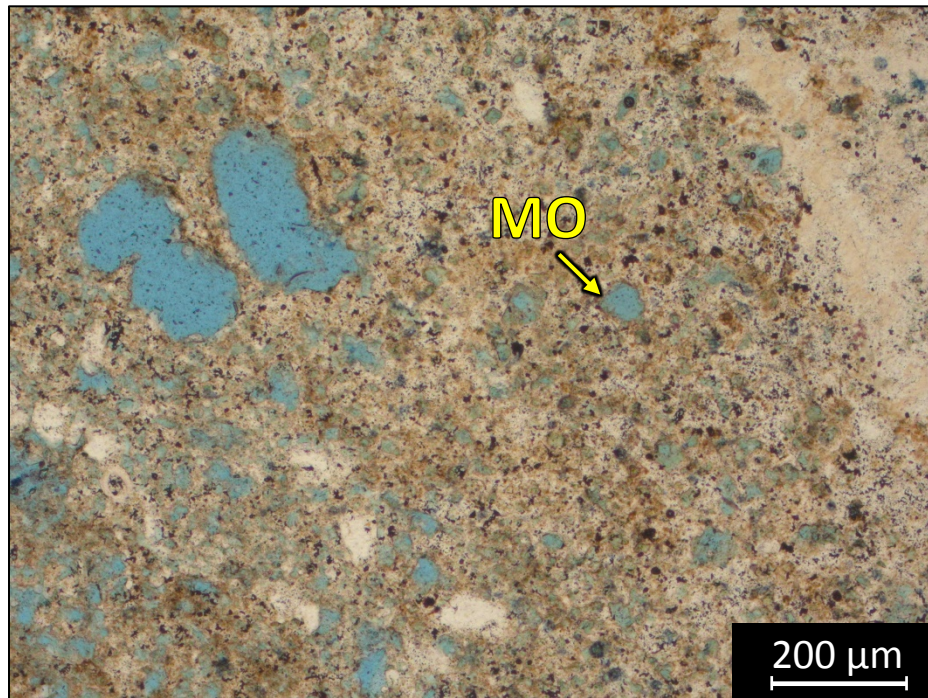
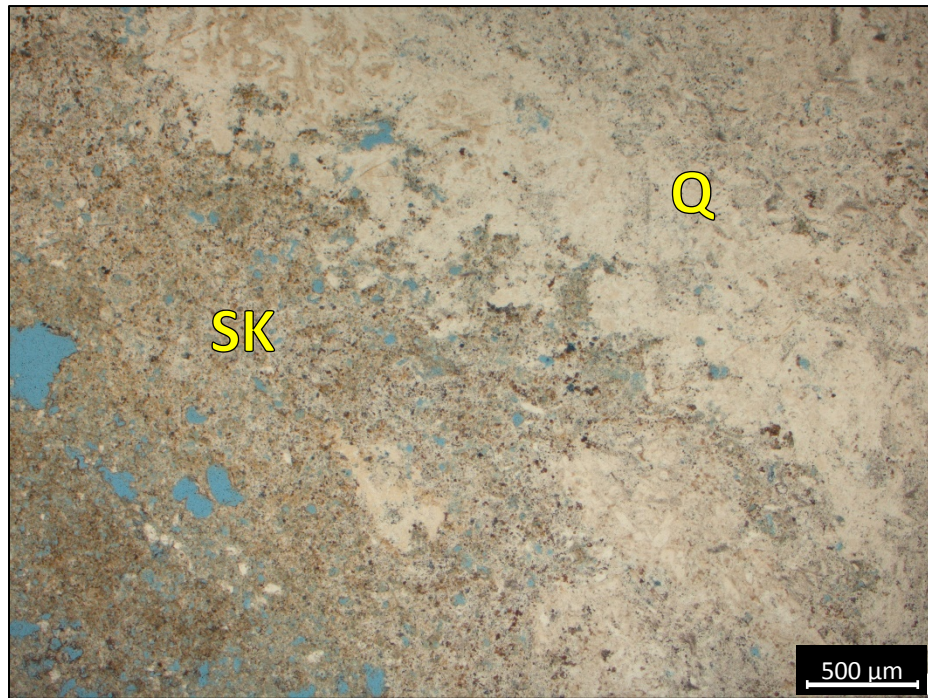
Facies 4



1 BN – 5290.9': Skeletal packstone to grainstone. Sample is alizarin red stained and blue epoxy impregnated (PPL and XPL). Porosity (NCS): 8.3%. Permeability (Klinkenberg): 0.077 mD. Visual estimation: 2% clay, 15% carbonates, and 78% other minerals. Sample

contains crinoid fragments (45%), sponge spicules (5%), microcrystalline quartz (30%), dolomite (5%) and undifferentiated skeletal debris. Moldic and vuggy porosity present.

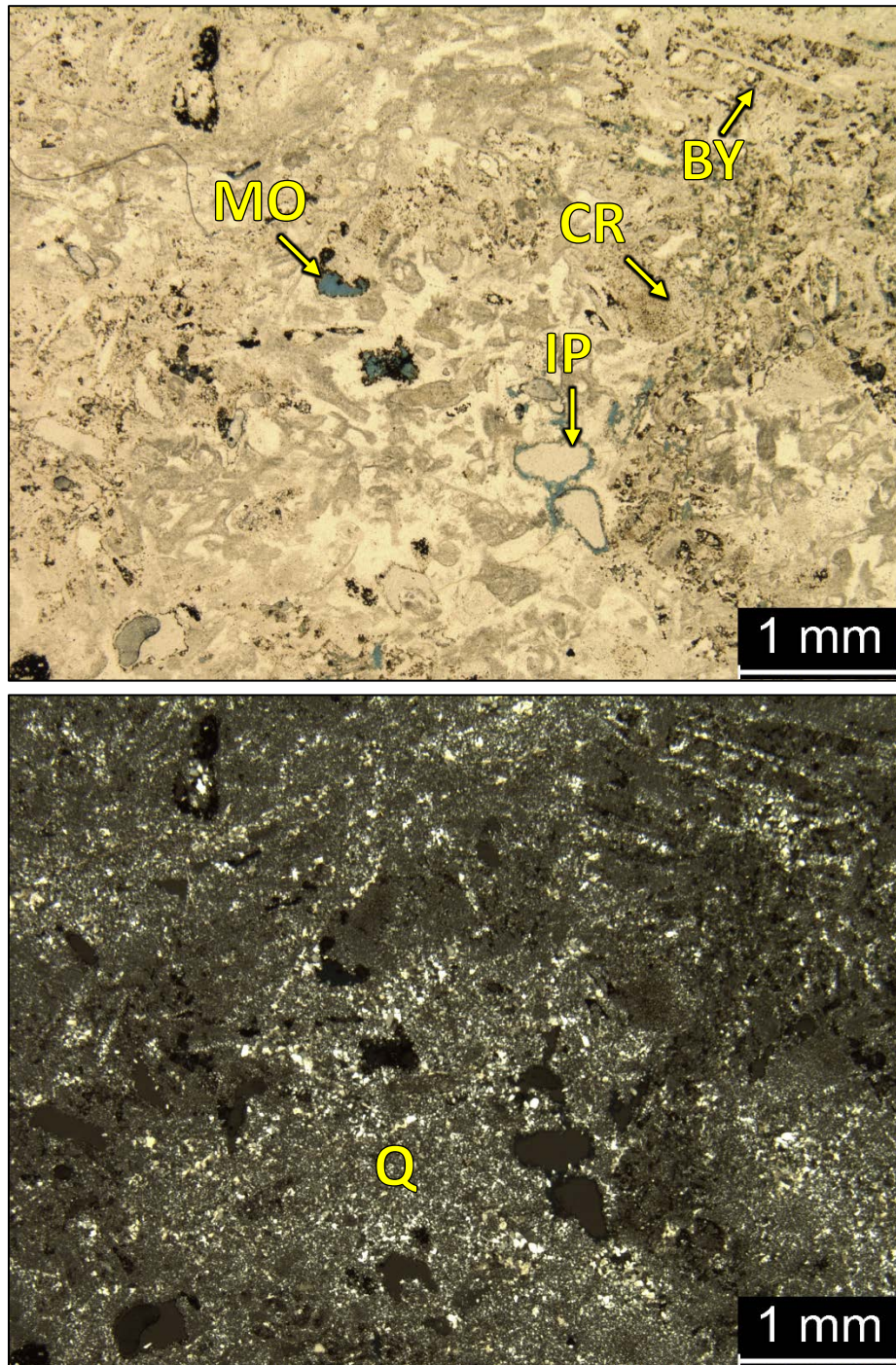
Facies 4



2 ALB – 5152.86': Silicified skeletal packstone. Sample is alizarin red stained and blue epoxy impregnated. Porosity (NCS): 11.36%. Permeability (Klinkenberg): 0.429188 mD. XRD: 2.1% clay (illite/smectite) and 97.9% other minerals (96.7% quartz and trace amounts of potassium feldspar, plagioclase and halite). Sample contains microcrystalline quartz (40%), silt-sized quartz grains (43%), sponge spicules (2%), brachiopod shells

(1%), crinoid fragments (2%) and undifferentiated skeletal debris. Oil filled and open moldic and vuggy porosity observed.

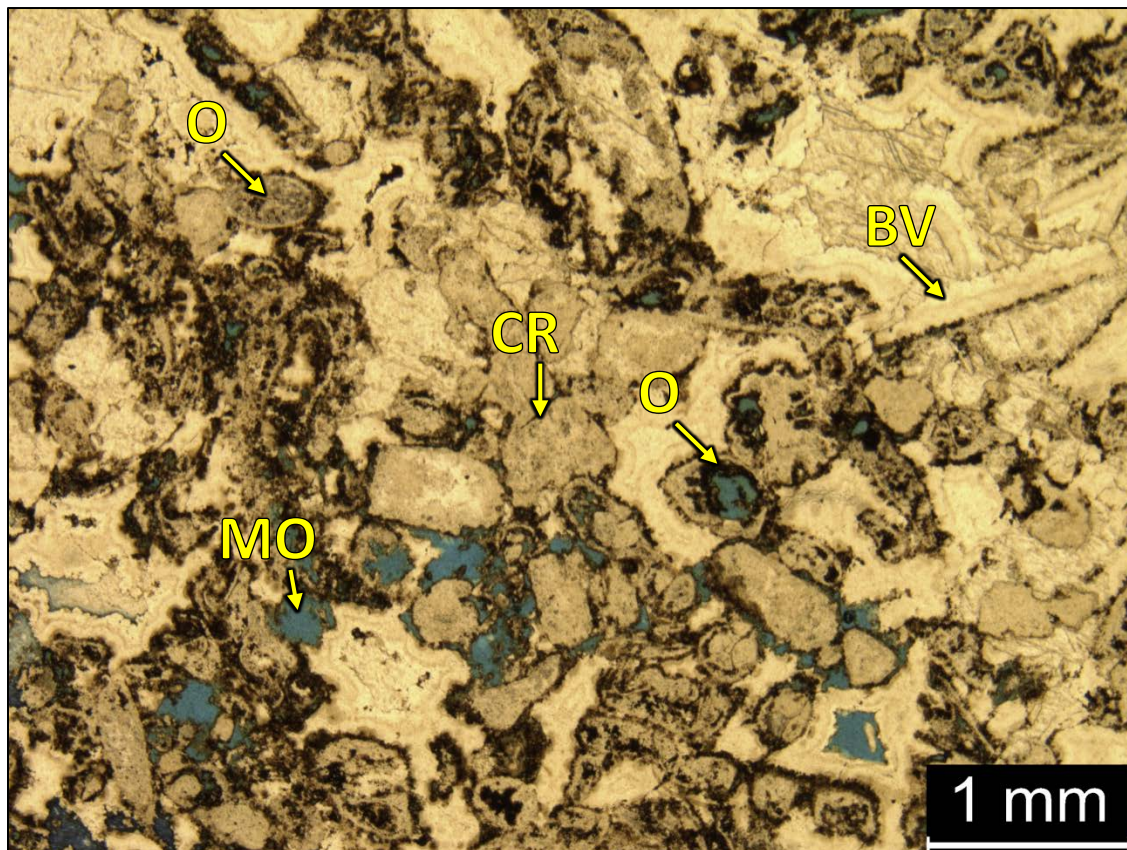
Exposure



1 BN – 5218.5': Silicified skeletal grainstone. Sample is alizarin red stained and blue epoxy impregnated (PPL and XPL). Plug Porosity (NCS): 19.2% Permeability (Klinkenberg): 23 mD. XRD: 4.3% clay (4.0% kaolinite, 0.1% illite/smectite, 0.2% chlorite), 3.7% carbonate (calcite), and 92% other minerals (91.9% quartz and trace

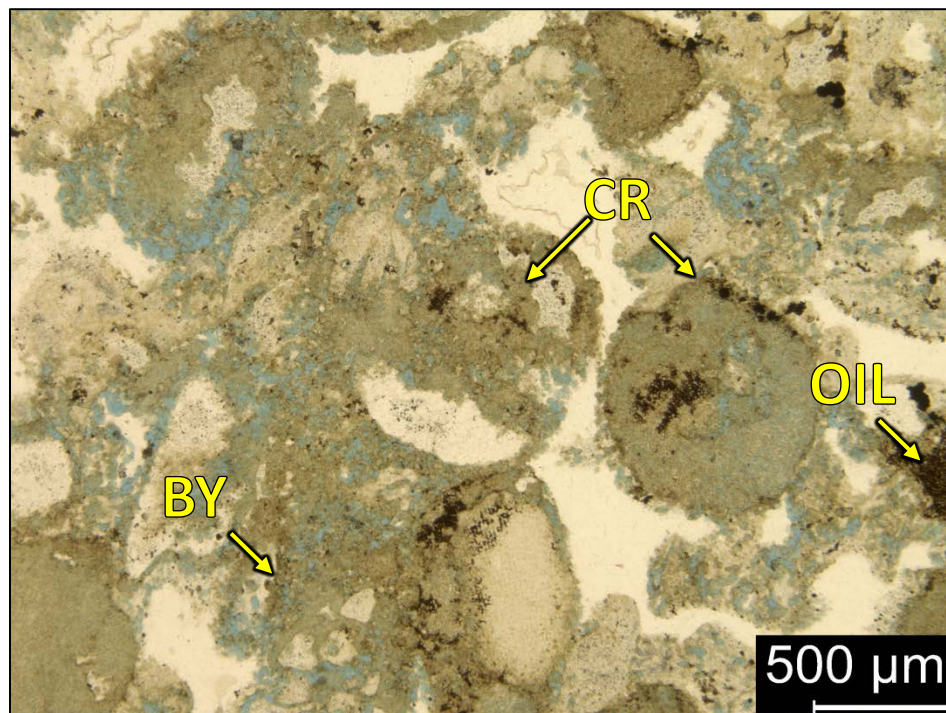
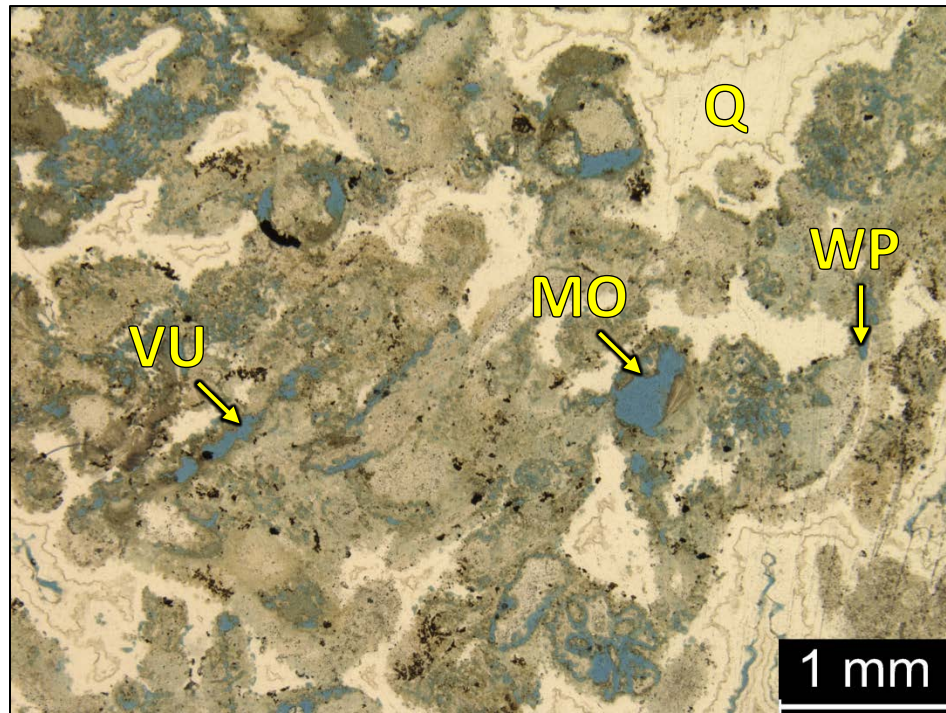
amounts of pyrite). Sample contains crinoid fragments (5%), silt-sized quartz grains (5%), bivalve fragments (5%), bryozoan fragments (10%), microcrystalline quartz (20%), brachiopod fragments (5%) and undifferentiated skeletal debris. Vuggy and interparticle porosity present.

Exposure



1 BN - 5219.8': Silicified skeletal grainstone to packstone. Sample is alizarin red stained and blue epoxy impregnated. Porosity (NCS): 15.9%. Permeability (Klinkenberg): 100 mD. XRD: 6.1% clay (5.5% kaolinite, 0.4% illite+mica, 0.3% chlorite), 1.5% carbonate (1.4% calcite, 0.1% dolomite), and 92.4% other minerals (92.2% quartz and trace amounts of pyrite). Sample contains crinoid fragments (2%), silt-sized quartz grains (5%), bivalve fragments (10%), ostracodes (5%) and undifferentiated skeletal debris. Abundant vuggy, intergranular porosity and some moldic porosity present.

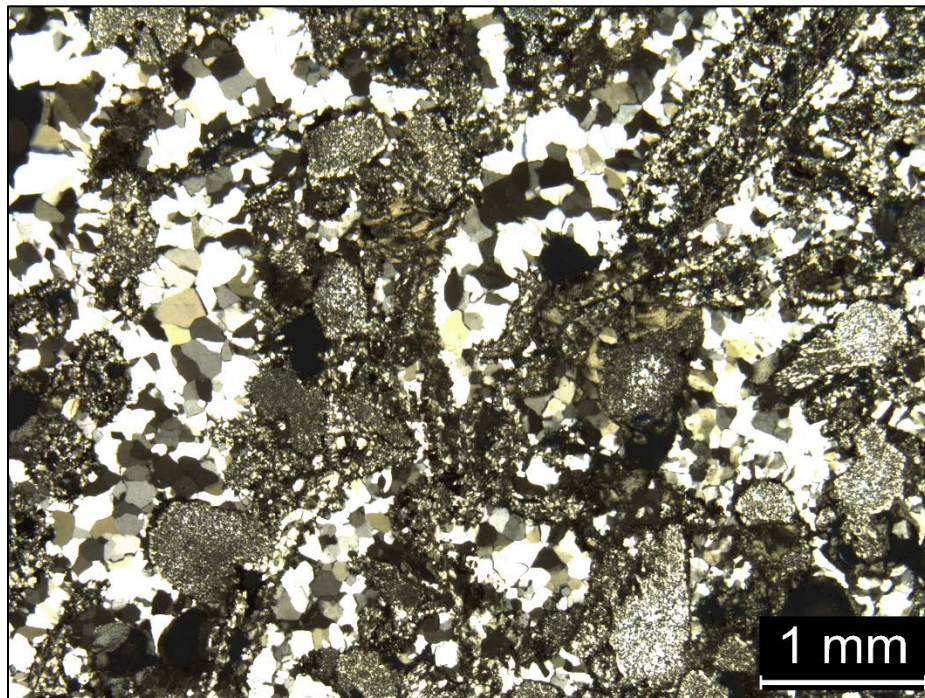
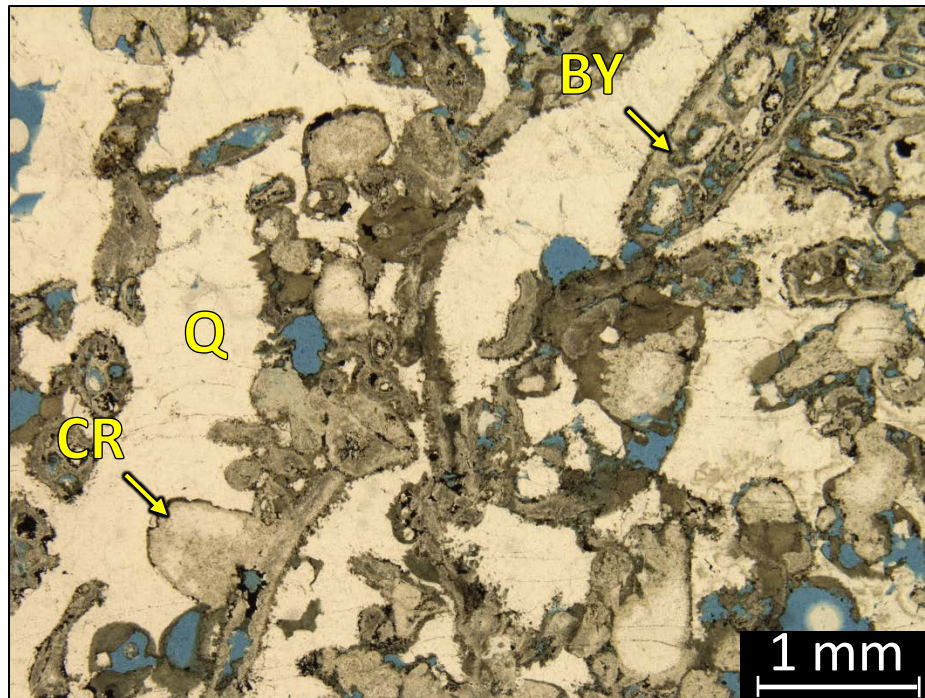
Exposure



1 BN – 5226.8': Skeletal grainstone. Sample is alizarin red stained and blue epoxy impregnated. Porosity (NCS): 1.8%. Visual estimation: 10% clay, 1% carbonates, and 89% other minerals. Sample contains crinoid fragments (60%), bryozoan debris (15%),

sponge spicules (5%), brachiopod fragments (5%) and undifferentiated skeletal debris.
Open and oil filled moldic, vuggy, and interparticle porosity present.

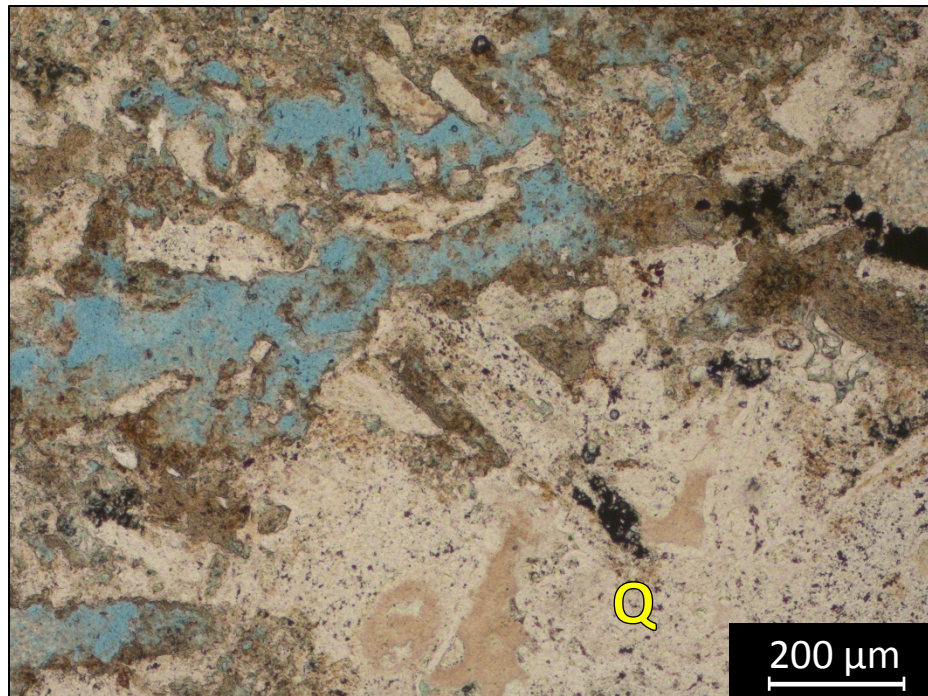
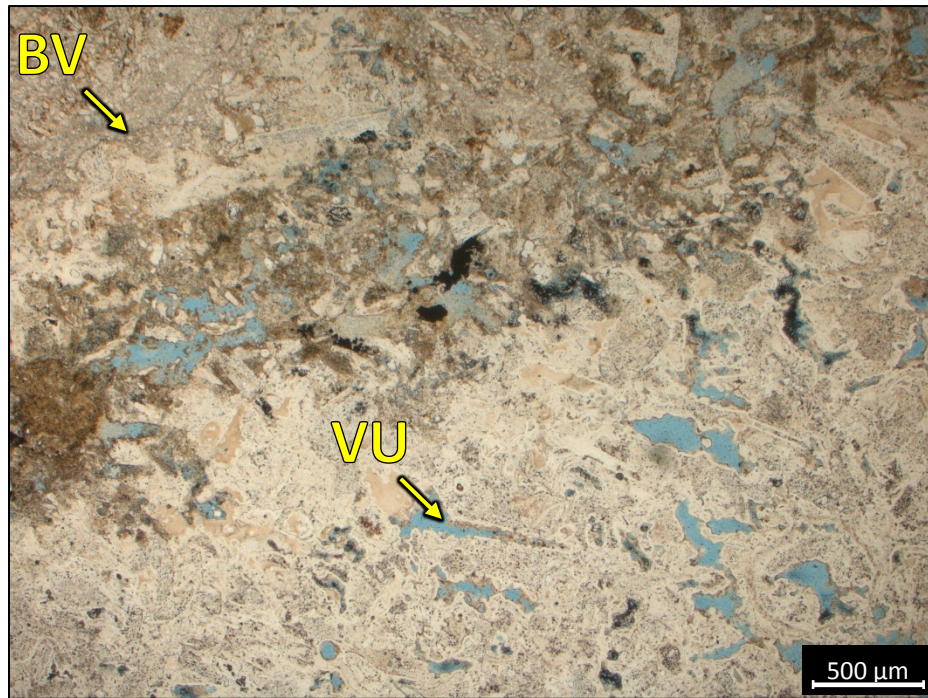
Exposure



1 BN – 5227.4': Silicified skeletal grainstone to packstone. Sample is alizarin red stained and blue epoxy impregnated (PPL and XPL). Porosity (NCS): 14.2%. Permeability (Klinkenberg): 11.8 mD. XRD: 20.3% clay (4.1% illite+mica, 14.3% chlorite, 1.9% kaolinite), 0.2% carbonate (dolomite), and 79.4% other minerals (79.1% quartz and trace amounts of pyrite). Sample contains crinoid fragments (10%), brachiopod fragments

(5%), bivalves (15%), bryozoans (10%) and undifferentiated skeletal debris. Moldic, vuggy and interparticle porosity observed.

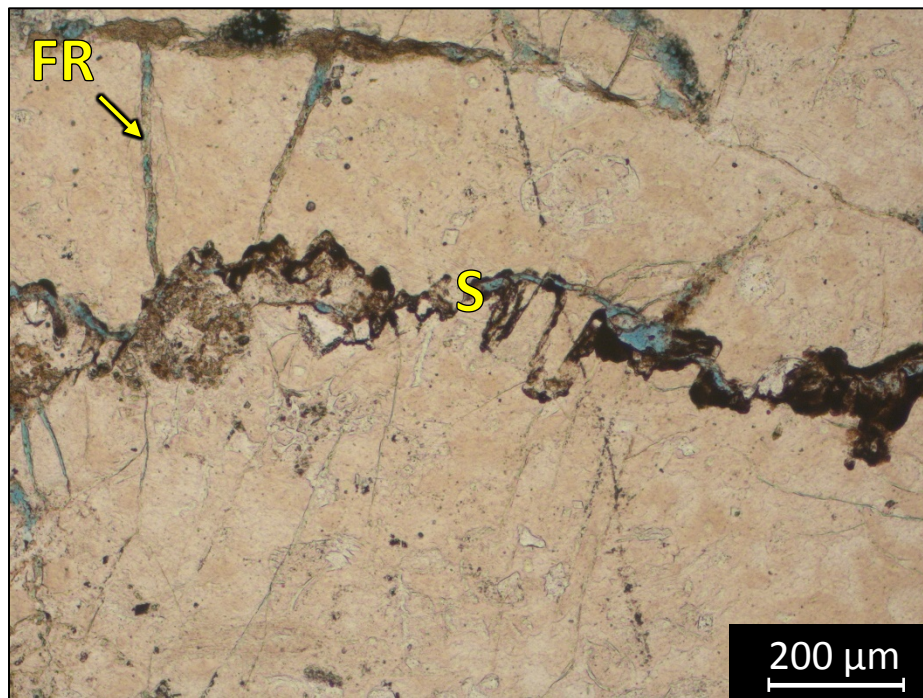
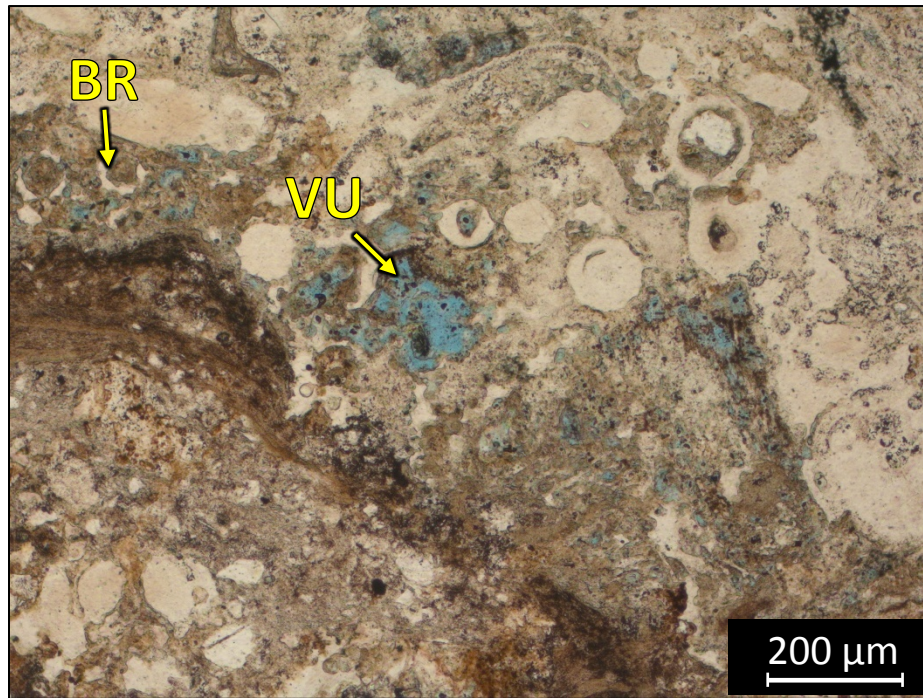
Exposure



2 ALB – 5131.88': Silicified skeletal packstone. Sample is alizarin red stained and blue epoxy impregnated. Porosity (NCS): 17.05%. Permeability (Klinkenberg): 1.117 mD. XRD: 20.3% clay (13.2% illite/smectite, 4.1% chlorite, 3% kaolinite) and 79.7% other minerals (77.5% quartz, 1.3% potassium feldspar and trace amounts of plagioclase and

halite). Sample contains microcrystalline quartz (60%), silt-sized quartz grains (40%), clay (15%), sponge spicules (10%), crinoid fragments (10%), bivalve fragments (10%) and undifferentiated skeletal debris. Filled and open interparticle porosity present, as well as moldic and vuggy porosity observed.

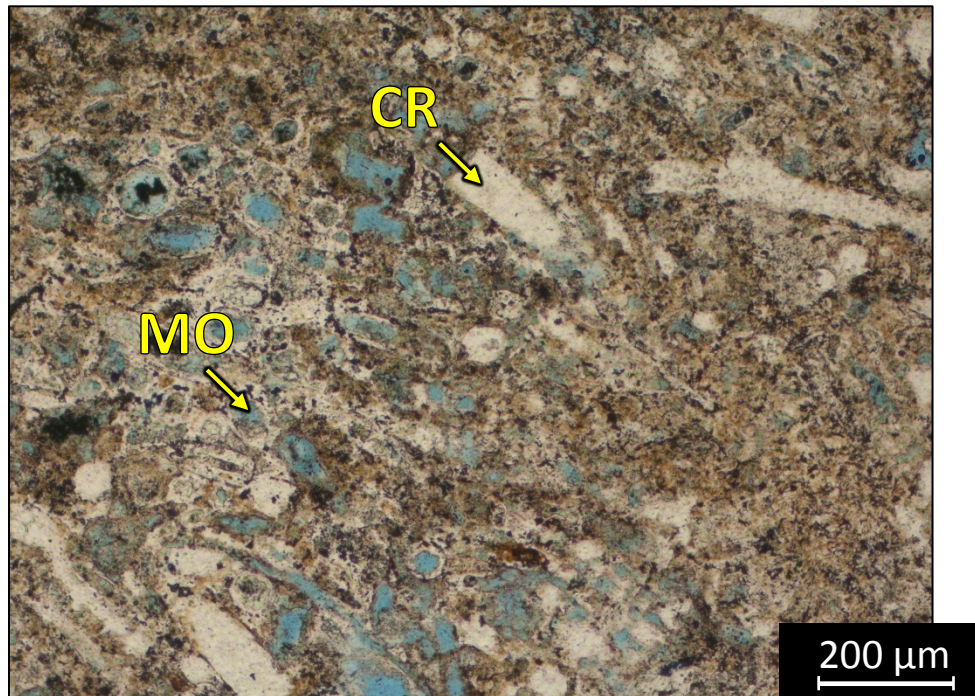
Exposure



2 ALB – 5136.2': Silicified skeletal mud rich packstone. Sample is alizarin red stained and blue epoxy impregnated. Porosity (NCS): 11.43%. Permeability (Klinkenberg): 0.628032 mD. XRD: 19.9% clay (10% illite/smectite, 2.1% chlorite, 7.8% kaolinite), 0.1% carbonate (calcite), and 80.1% other minerals (78.3% quartz, 1.1% plagioclase and trace amounts of potassium feldspar and halite). Sample contains microcrystalline quartz

(40%), silt-sized quartz grains (5%), clay (15%) sponge spicules (15%), crinoid fragments (10%), ostracodes (2%), brachiopod spines (2%), bivalve fragments (2%) and undifferentiated skeletal debris. Oil and clay filled fracture porosity present, as well as moldic and vuggy porosity observed. Solution seam present.

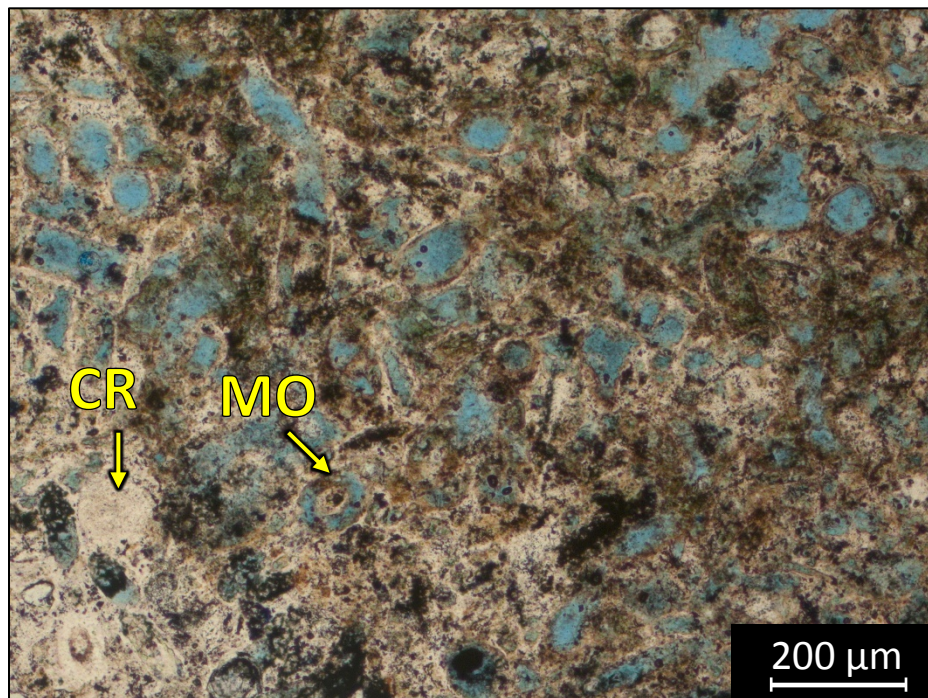
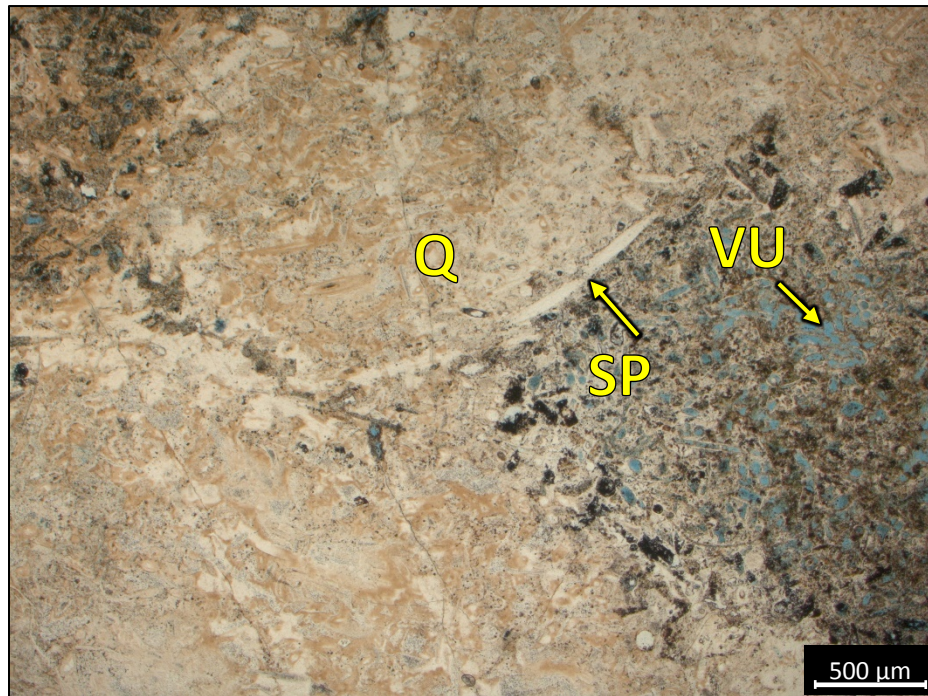
Exposure



2 ALB – 5143.84': Silicified mud rich skeletal packstone. Sample is alizarin red stained and blue epoxy impregnated. Porosity (NCS): 22.65%. Permeability (Klinkenberg): 2.182 mD. XRD: 10.5% clay (7.1% illite/smectite, 3.1% chlorite, 0.3% kaolinite) and 89.5% other minerals (88.8% quartz and trace amounts of potassium feldspar, plagioclase and halite). Sample contains microcrystalline quartz (30%), silt-sized quartz grains (10%),

sponge spicules (10%), brachiopod spines (30%), crinoid fragments (10%) and undifferentiated skeletal debris. Slight clay filled and open fracture porosity and abundant moldic and vuggy porosity observed.

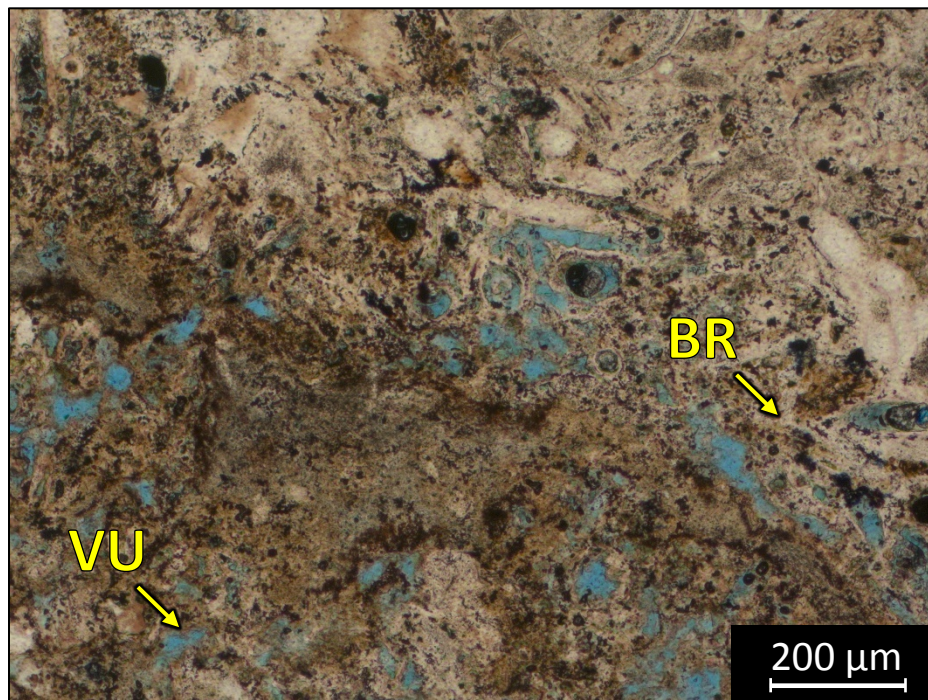
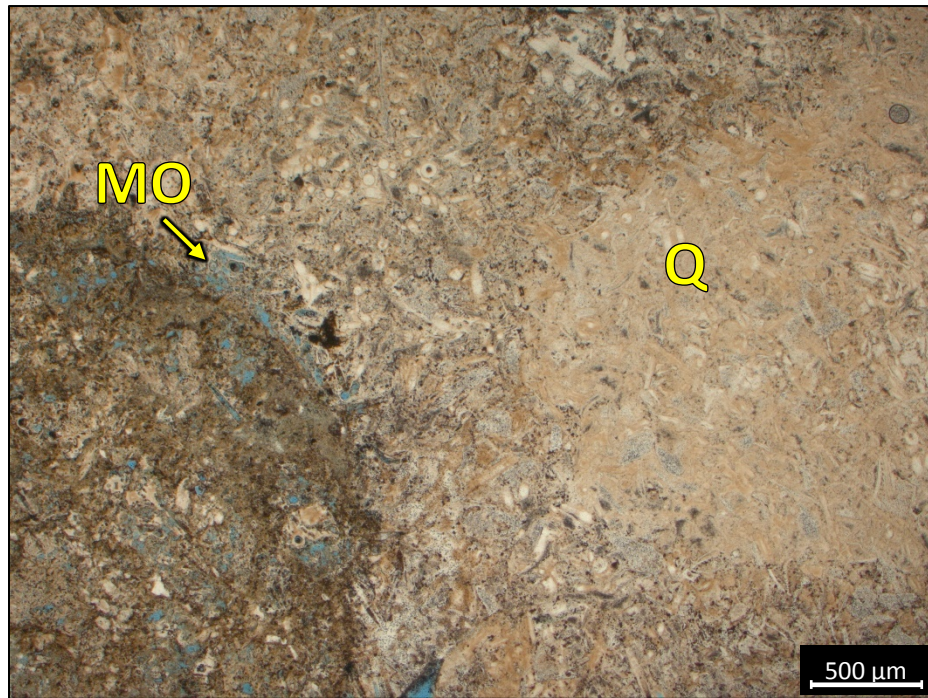
Exposure



2 ALB – 5145.72': Skeletal grain rich packstone. Sample is alizarin red stained and blue epoxy impregnated. Porosity (NCS): 16.54%. Permeability (Klinkenberg): 1.623 mD. XRD: 9.1% clay (7.8% illite/smectite, 1.1% chlorite, 0.2% kaolinite), 0.5% carbonate (0.2% calcite, 0.3% dolomite), and 90.4% other minerals (87.8% quartz, 1.1% potassium feldspar, 0.8% plagioclase and trace amounts of halite). Sample contains microcrystalline

quartz (30%), silt-sized quartz grains (5%), sponge spicules (10%), brachiopod spines (7%), crinoid fragments (2%) and undifferentiated skeletal debris. Abundant moldic and vuggy porosity observed.

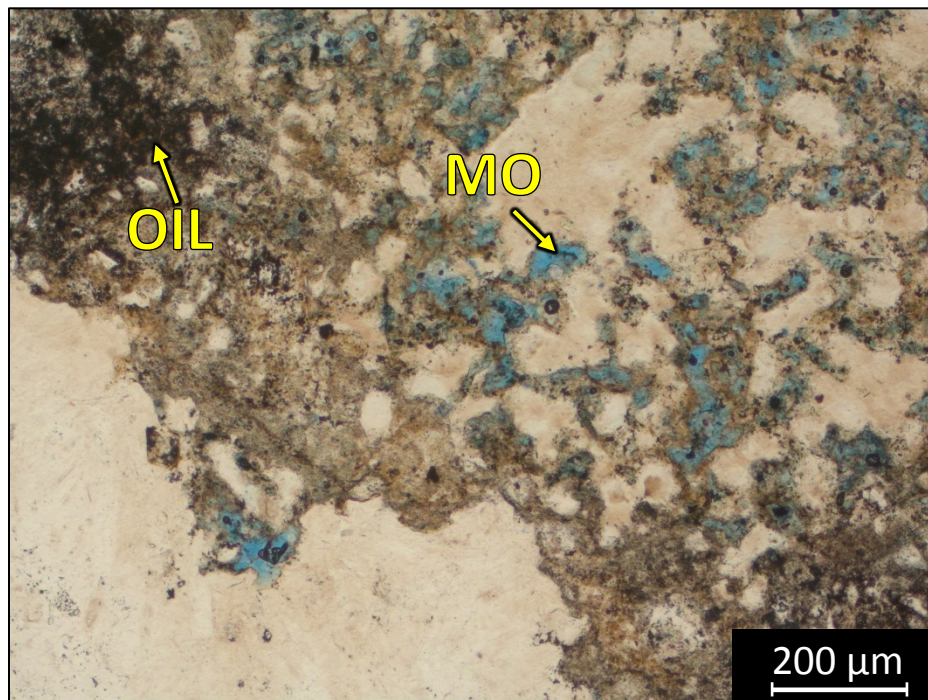
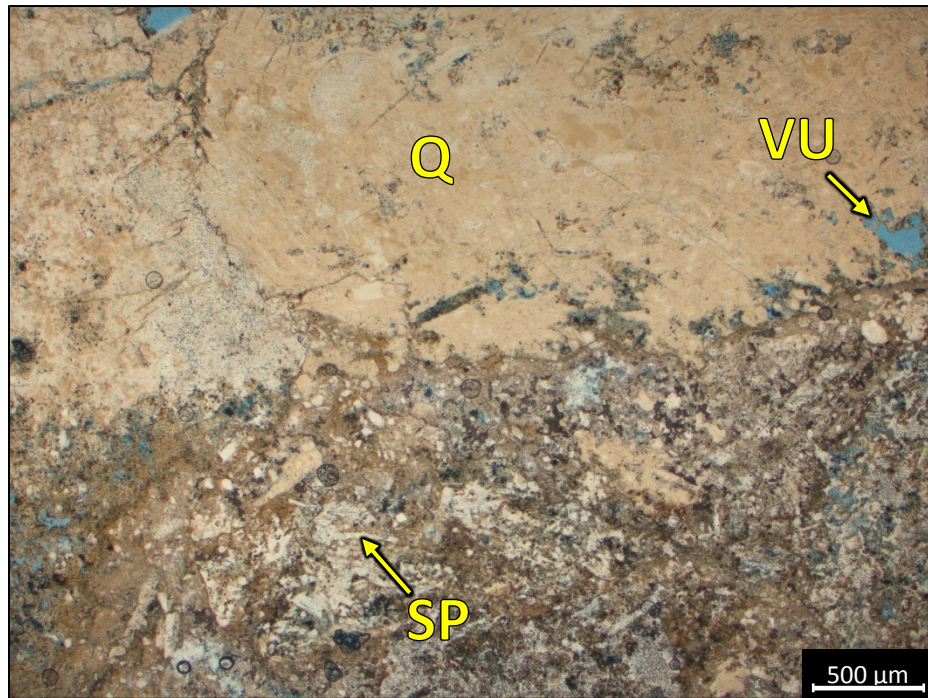
Exposure



2 ALB – 5147.36': Silicified skeletal packstone. Sample is alizarin red stained and blue epoxy impregnated. Porosity (NCS): 18.02%. Permeability (Klinkenberg): 0.774317 mD. XRD: 8.8% clay (7% illite/smectite, 0.6% chlorite, 1.2% kaolinite) and 91.2% other minerals (88.4% quartz, 1.3% potassium feldspar, 1.2% plagioclase and trace amounts of halite). Sample contains microcrystalline quartz (30%), silt-sized quartz grains (10%),

sponge spicules (20%), brachiopod spines (5%), crinoid fragments (2%) and undifferentiated skeletal debris. Abundant moldic and vuggy porosity observed.

Exposure

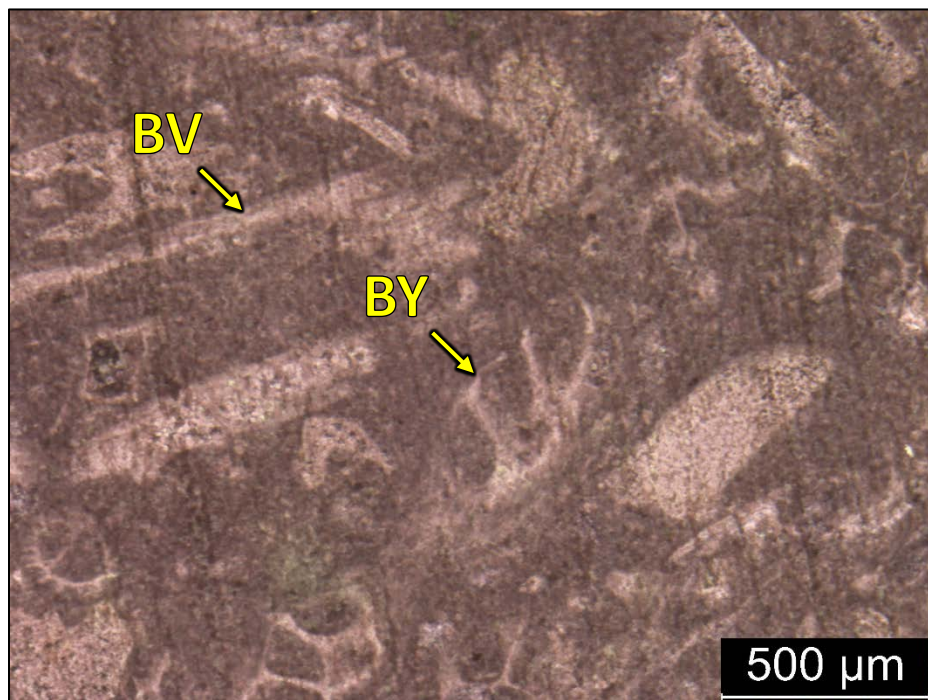
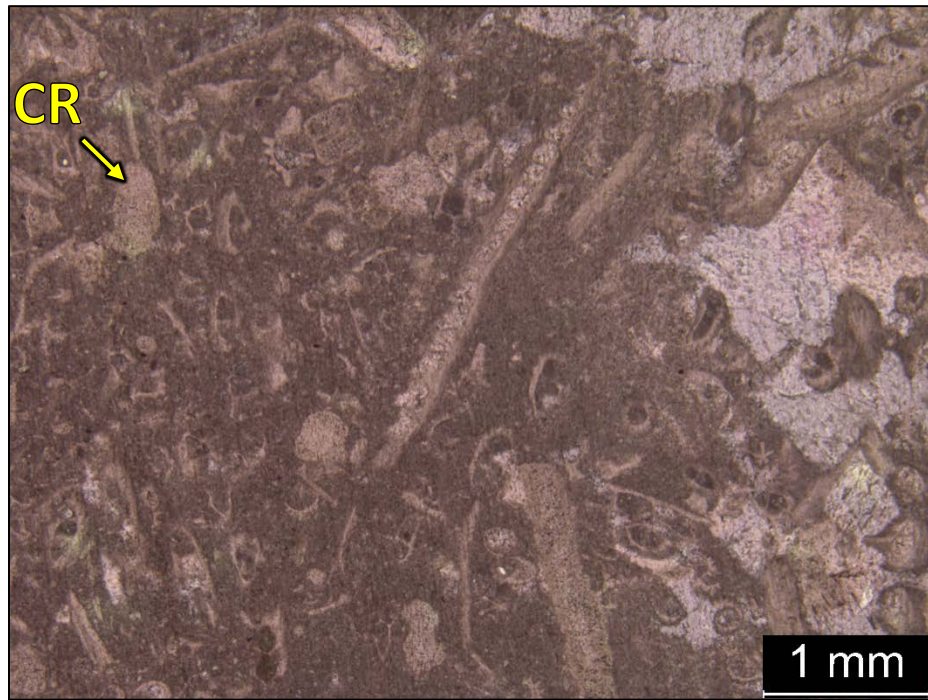


2 ALB – 5149.84': Silicified grain rich packstone. Sample is alizarin red stained and blue epoxy impregnated. Porosity (NCS): 15.83%. Permeability (Klinkenberg): 0.433548 mD. XRD: 10.2% clay (8.9% illite/smectite, 1% chlorite, 0.3% kaolinite) and 89.8% other minerals (87.1% quartz, 1% potassium feldspar, 1.2% plagioclase and trace amounts of halite). Sample contains microcrystalline quartz (30%), silt-sized quartz grains (50%),

megaquartz (40%), sponge spicules (2%), crinoid fragments (3%) brachiopod spines (2%) and undifferentiated skeletal debris. Clay filled and open moldic and vuggy porosity observed.

KANSAS FACIES

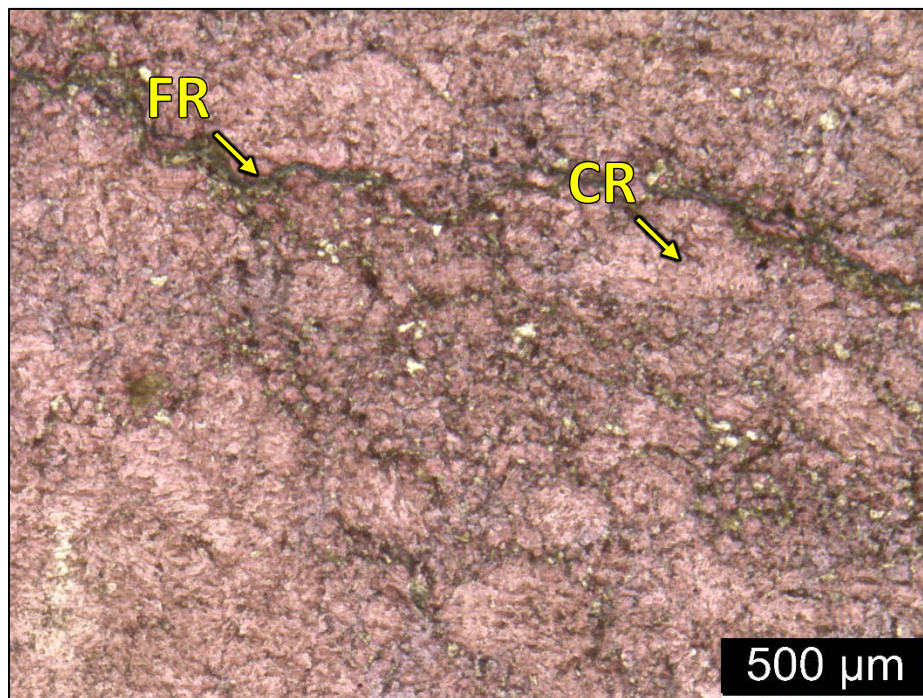
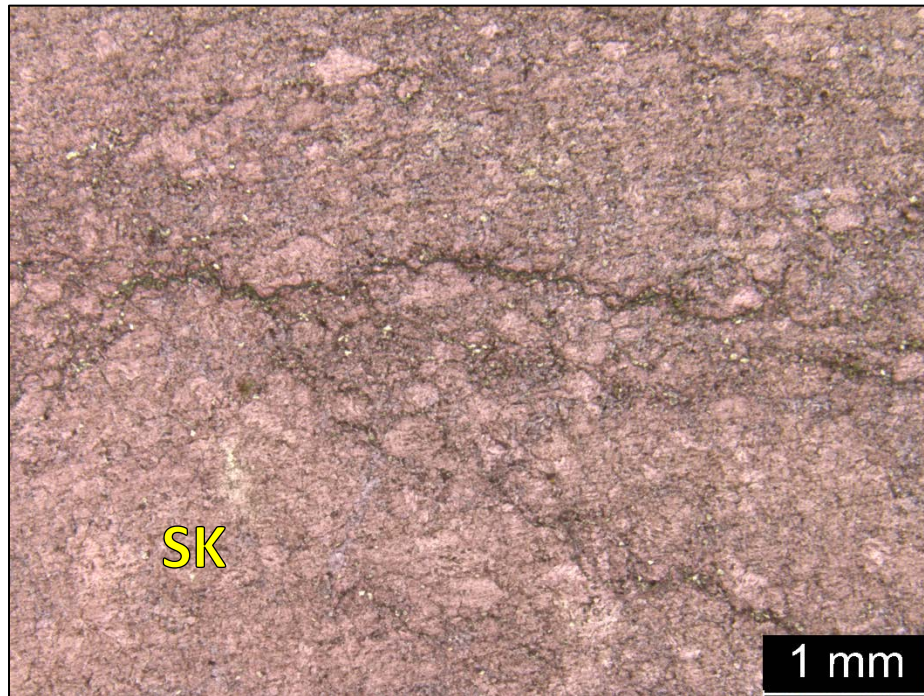
Facies 1



3 TF – 5393.86’: Skeletal grain rich packstone to wackstone. Sample is alizarin red stained and blue epoxy impregnated. Porosity (NCS): 0.7%. Permeability (Klinkenberg): 0.0001 mD. Visual estimation: 2% clays, 98% carbonates. Sample contains bivalves

(5%), bryozoans (20%), crinoid fragments (10%) and undifferentiated skeletal debris. No porosity observed.

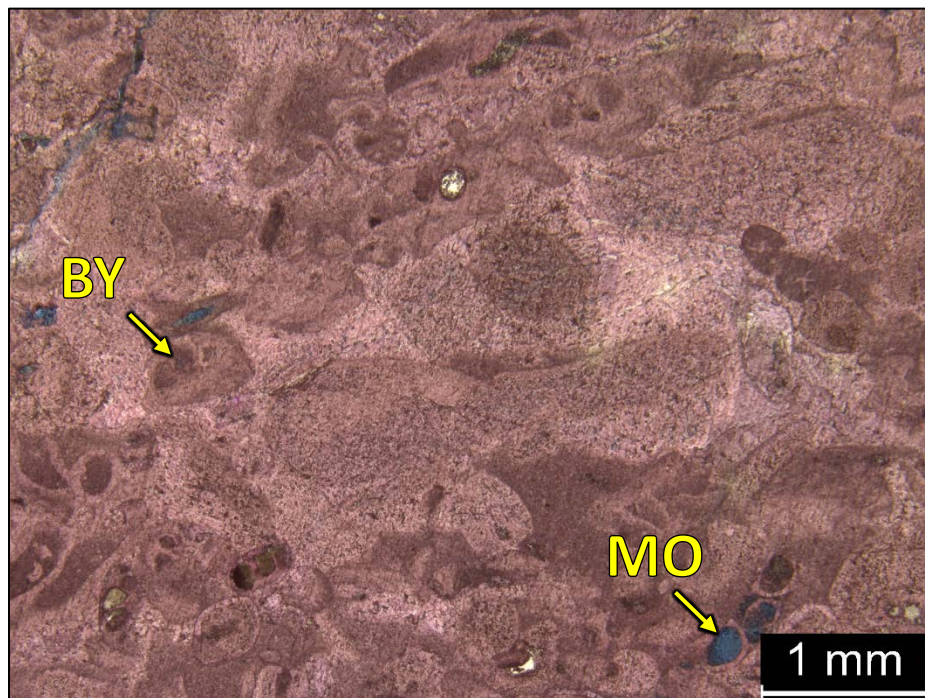
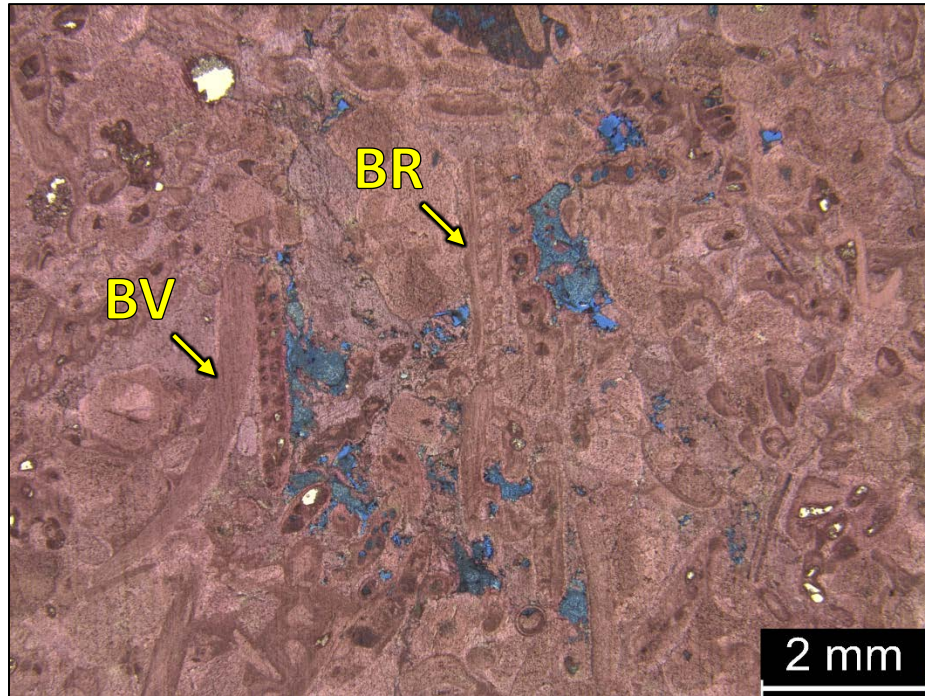
Facies 1



3 TF – 5354.42': Packstone to wackestone. Sample is alizarin red stained and blue epoxy impregnated. Porosity (NCS): 0.7%. Permeability (Klinkenberg): 0.0001 mD. Visual estimation: 2% clays, 97% carbonates, 1% other minerals. Sample contains

microcrystalline quartz (5%), crinoid fragments (5%) and undifferentiated skeletal debris. Slight fracture, interparticle and vuggy porosity observed.

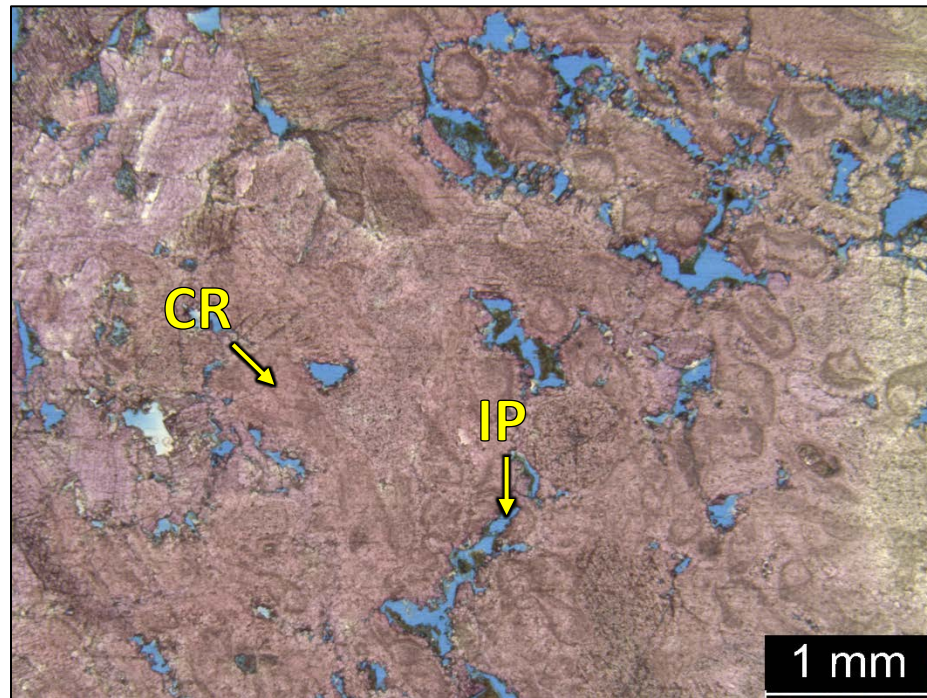
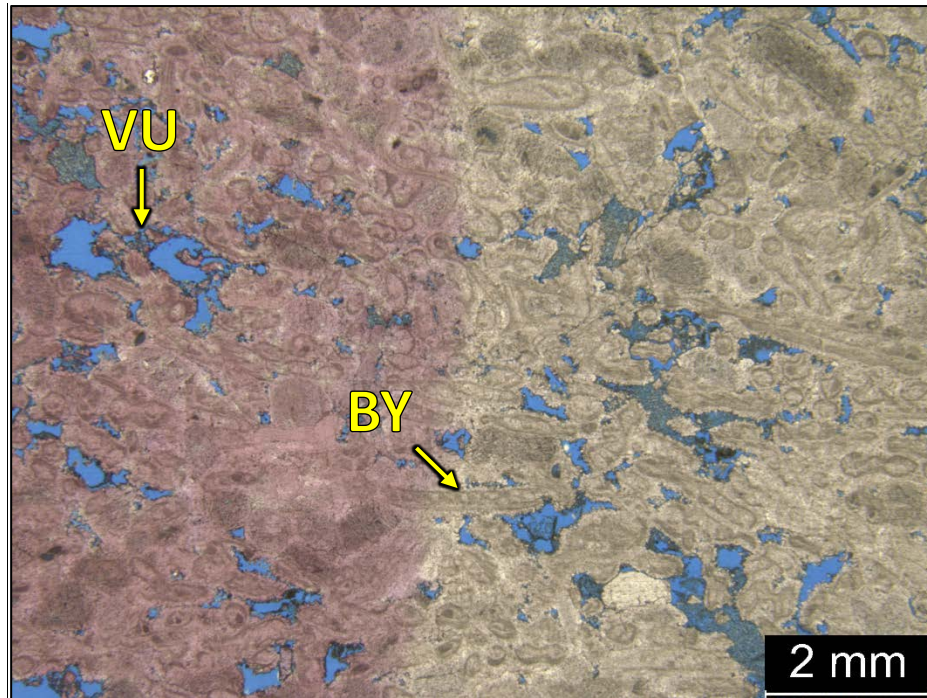
Facies 2



3 TF – 5447.66’: Skeletal grainstone. Sample is alizarin red stained and blue epoxy impregnated. Porosity (NCS): 2.7%. Permeability (Klinkenberg): 0.001 mD. XRD: 1.5%

clay (1.1% illite/mica, 0.5% kaolinite), 97.8% carbonate (calcite), and trace amounts of other minerals (quartz and apatite). Sample contains brachiopods (5%), bivalves (5%), bryozoans (20%), crinoid fragments (15%) and undifferentiated skeletal debris. Slight moldic, vuggy, interparticle, intraparticle and fracture porosity observed.

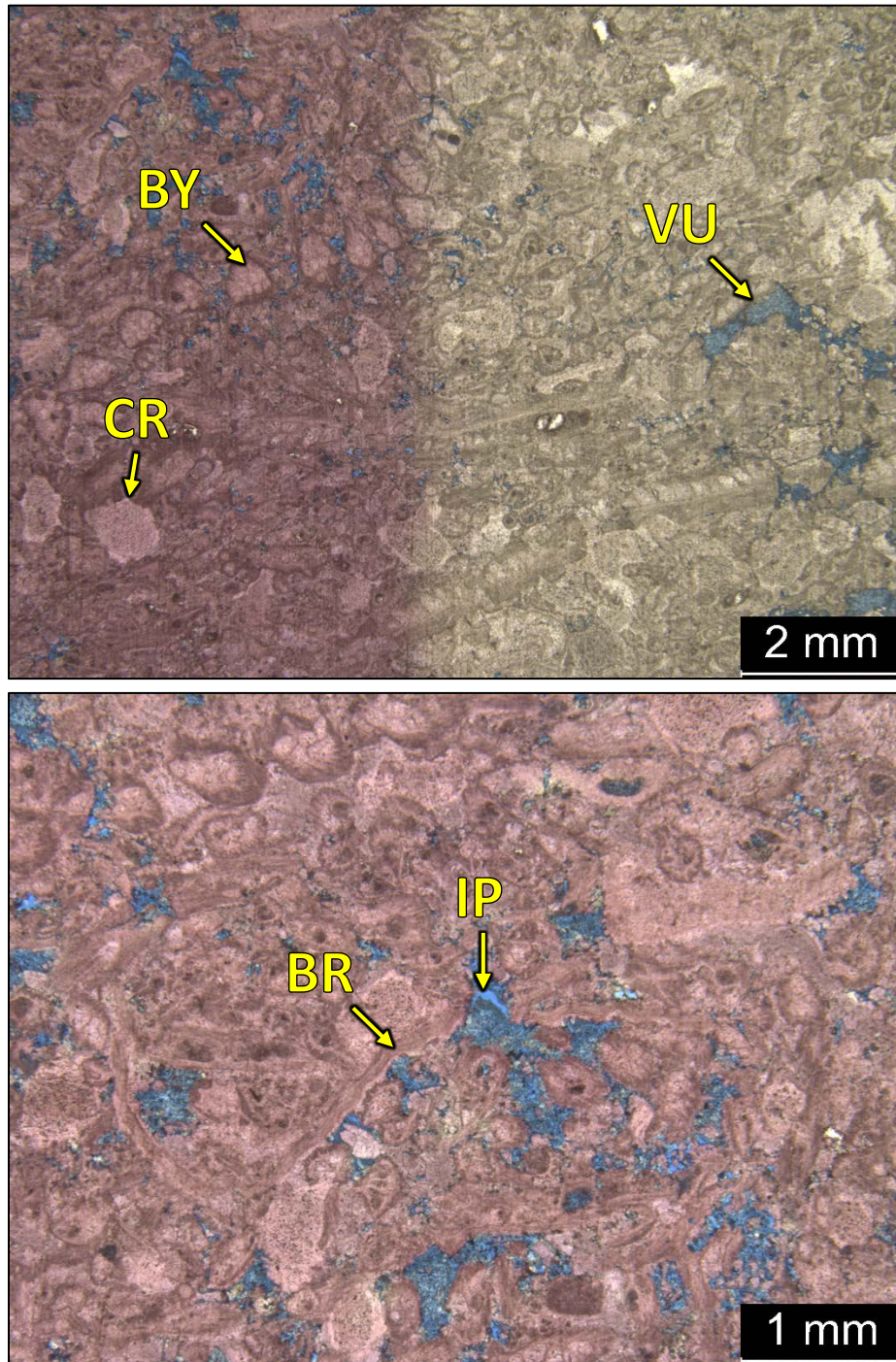
Facies 2



3 TF – 5430.64': Skeletal grain rich packstone to grainstone. Sample is alizarin red stained (half slide) and blue epoxy impregnated. Porosity (NCS): 3.8%. Permeability (Klinkenberg): 0.0031 mD. Visual estimation: 2% clays, 98% carbonates. Sample contains bivalves (3%), bryozoans (20%), crinoid fragments (10%) and undifferentiated

skeletal debris. Abundant moldic, intraparticle, interparticle and partially oil filled vuggy porosity observed.

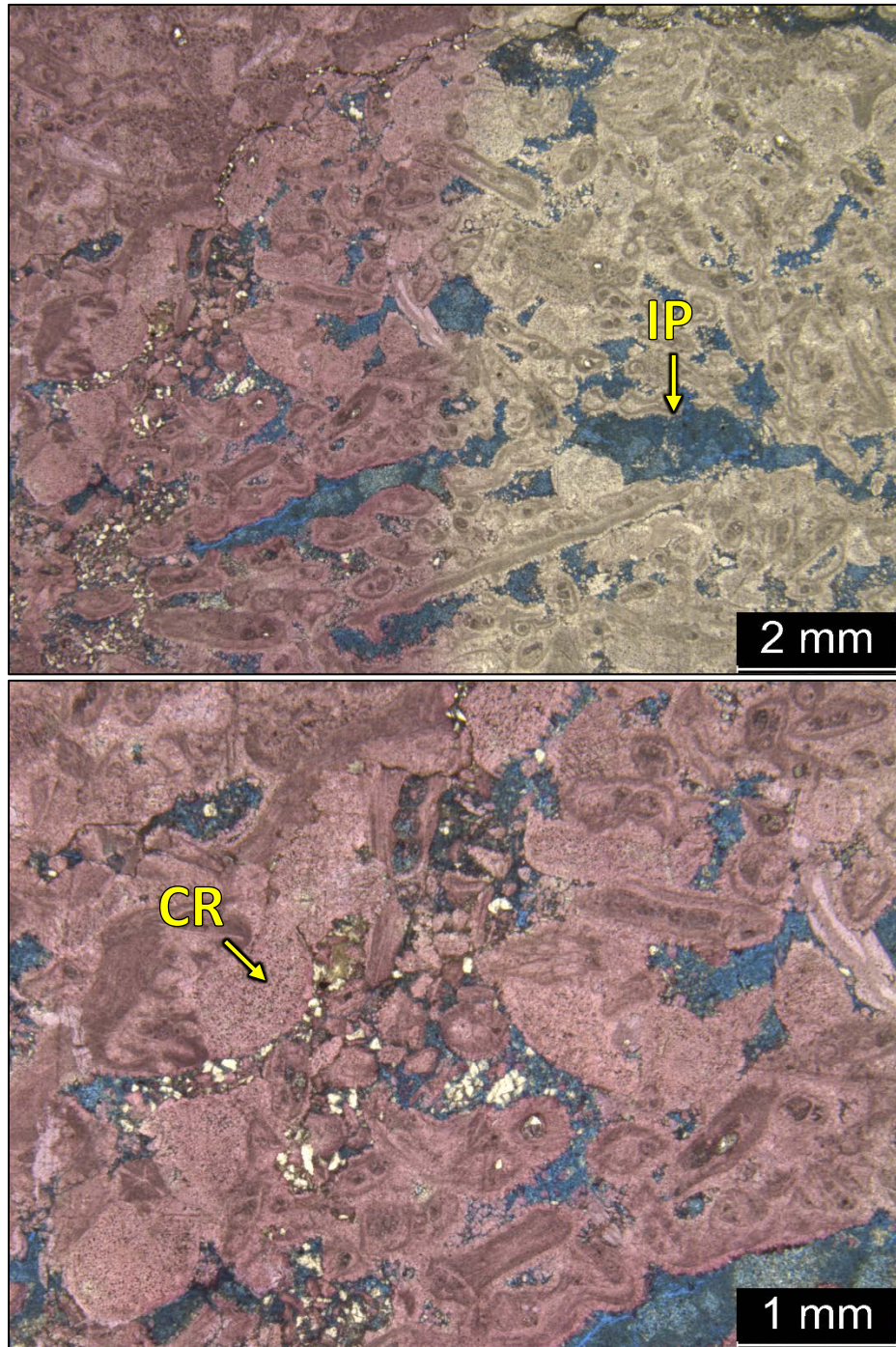
Facies 2



3 TF – 5423.36’: Skeletal (bryozoan) grain rich packstone to grainstone. Sample is alizarin red stained (half slide) and blue epoxy impregnated. Porosity (NCS): 3.1%. Permeability (Klinkenberg): 0.0063 mD. XRD: 2.7% clay (kaolinite), 96.9% carbonate

(calcite), and trace amounts of quartz. Sample contains bryozoans (20%), bivalves (5%), brachiopods (2%), crinoid fragments (10%) and undifferentiated skeletal debris. Intraparticle, interparticle, moldic and vuggy porosity observed.

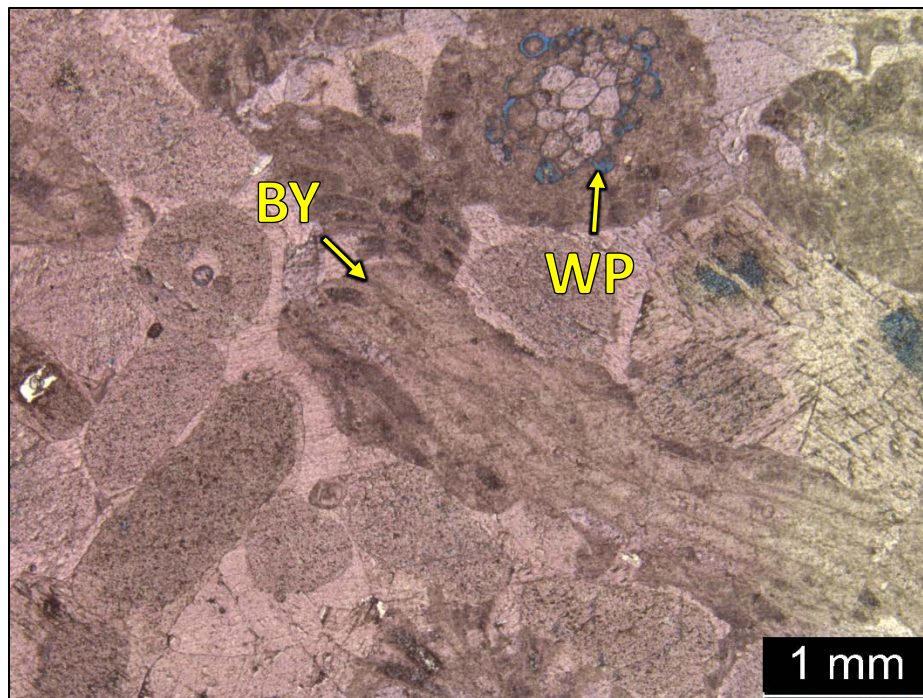
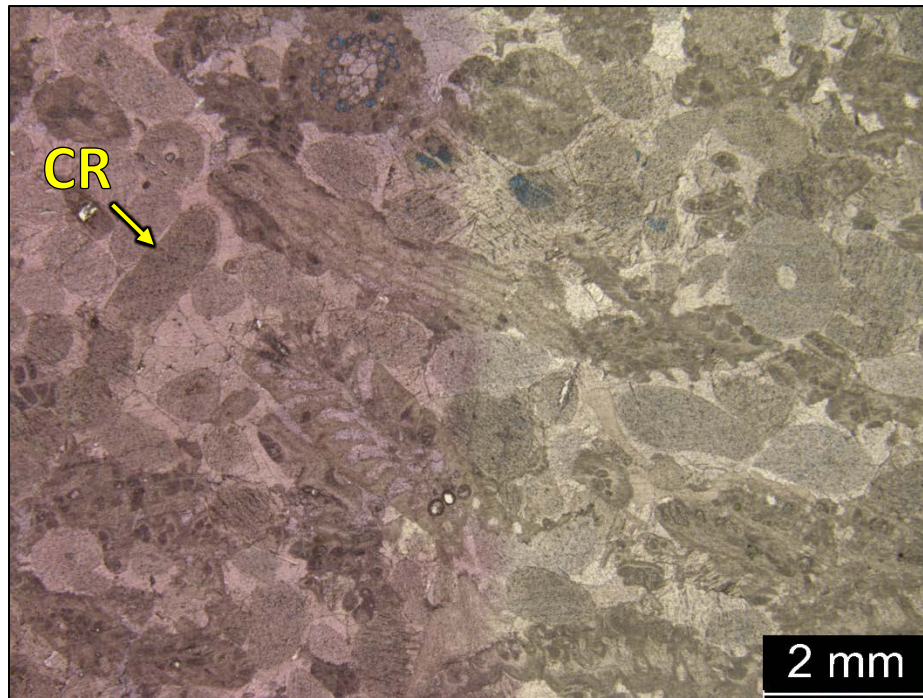
Facies 2



3 TF – 5422.6’: Skeletal grain rich packstone to grainstone. Sample is alizarin red stained (half slide) and blue epoxy impregnated. Porosity (NCS): 5.2%. Permeability (Klinkenberg): 0.05 mD. Visual estimation: 2% clays, 97% carbonates, 1% other minerals. Sample contains bryozoans (25%), silt-sized quartz grains (1%), bivalves (3%),

brachiopods (2%) crinoid fragments (10%) and undifferentiated skeletal debris.
Intraparticle, interparticle, moldic and vuggy porosity observed.

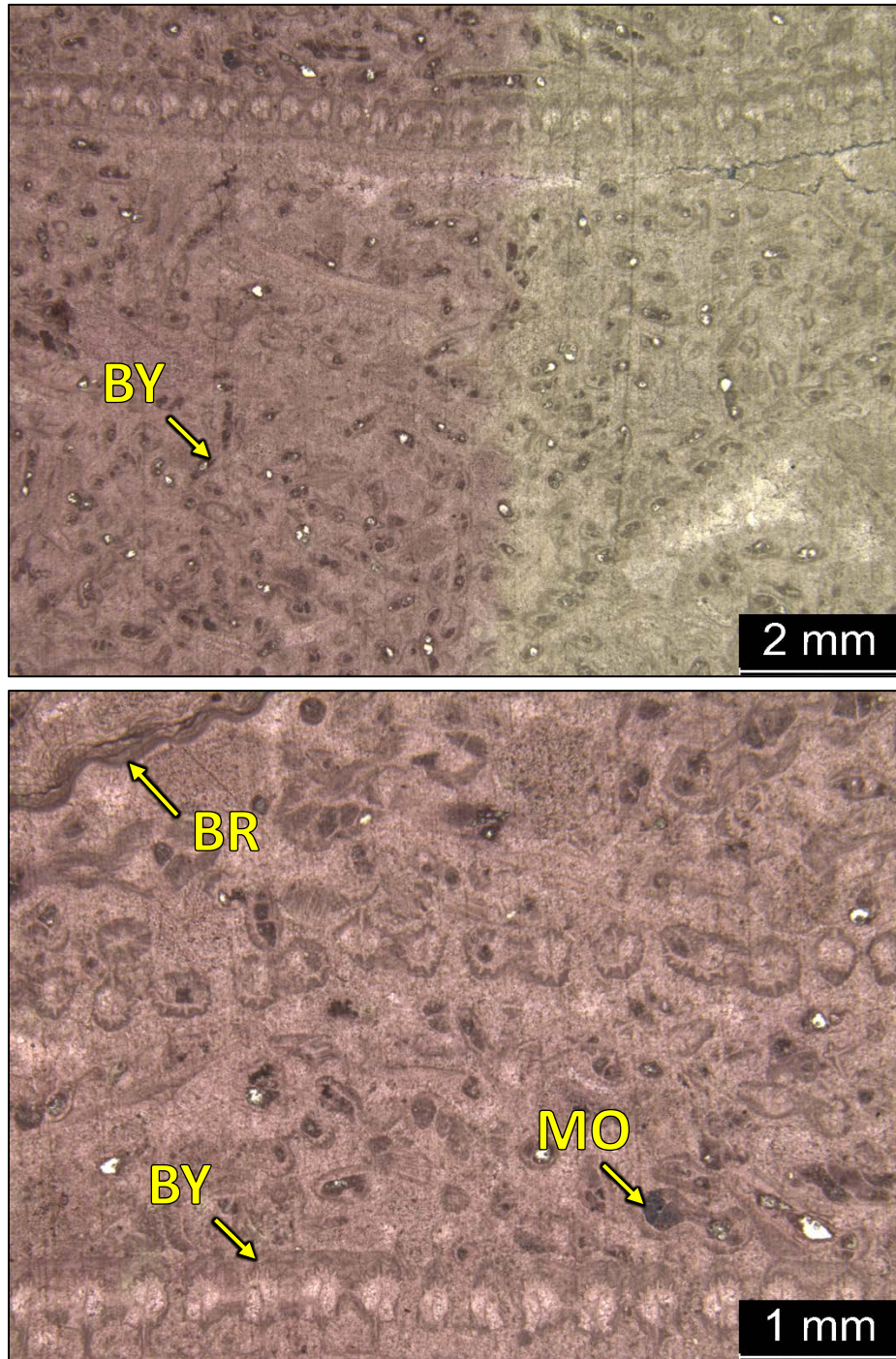
Facies 2



3 TF – 5408.52': Skeletal (bryozoan) grainstone to grain rich packstone. Sample is alizarin red stained and blue epoxy impregnated. Porosity (NCS): 1.2%. Permeability (Klinkenberg): 0.0006 mD. Visual estimation: 1% clays, 99% carbonates. Sample

contains bryozoans (25%), crinoid fragments (15%) and undifferentiated skeletal debris. Interparticle, intraparticle and vuggy porosity observed.

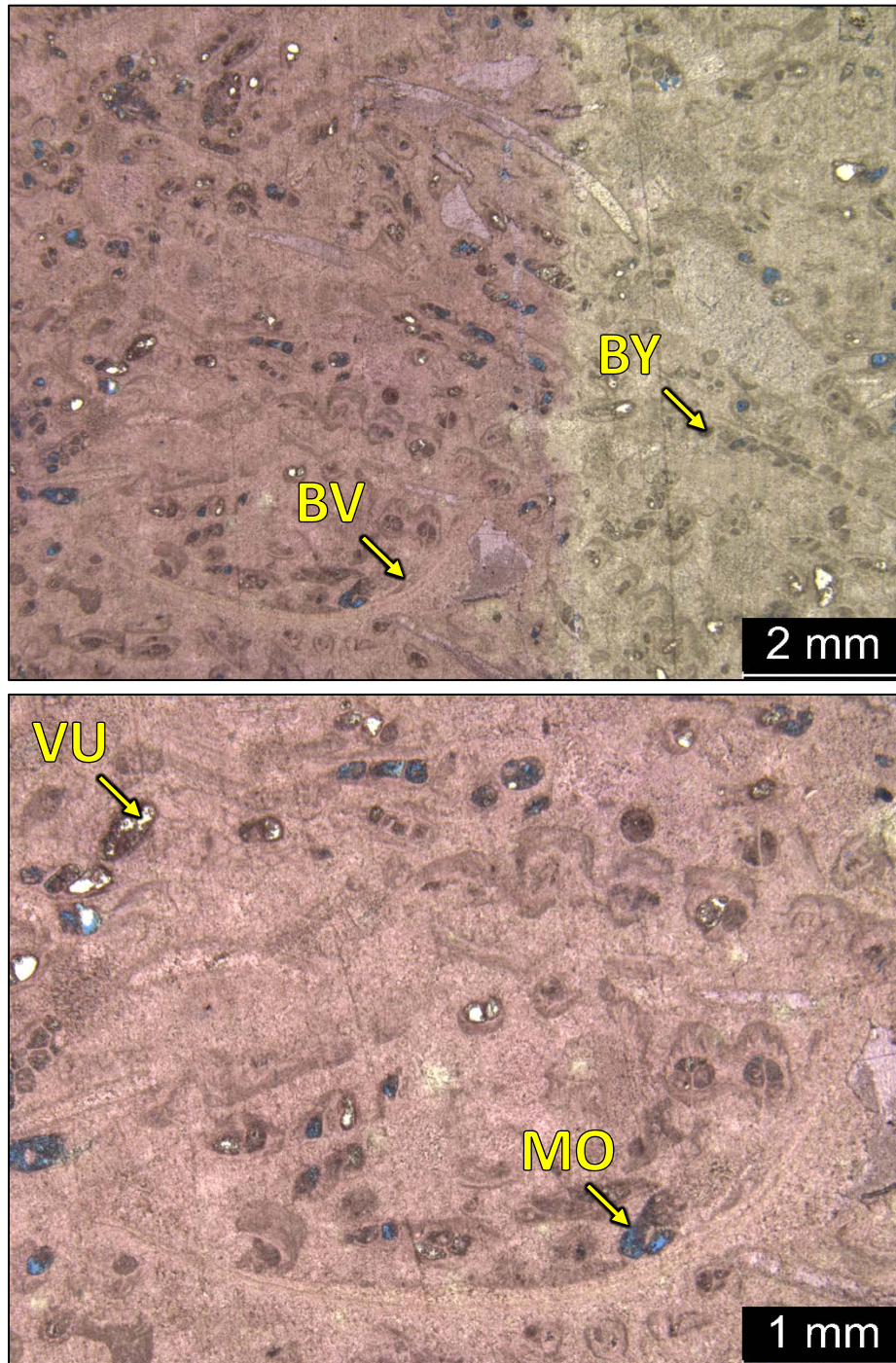
Facies 2



3 TF – 5400.78’: Bryozoan grain rich packstone to grainstone. Sample is alizarin red stained (half slide) and blue epoxy impregnated. Porosity (NCS): 1.6%. Permeability (Klinkenberg): 0.003 mD. XRD: 0.5% clay (kaolinite), 99.3% carbonate (calcite), and trace amounts of quartz. Sample contains bivalves (5%), brachiopods (1%), bryozoans

(40%), crinoid fragments (20%) and undifferentiated skeletal debris. Intraparticle, moldic and vuggy porosity observed.

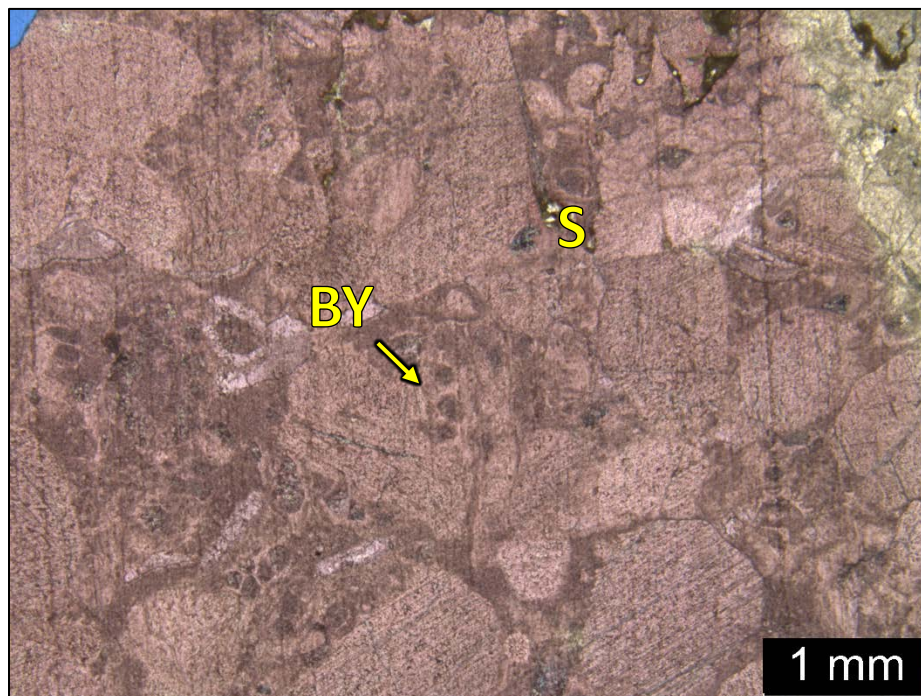
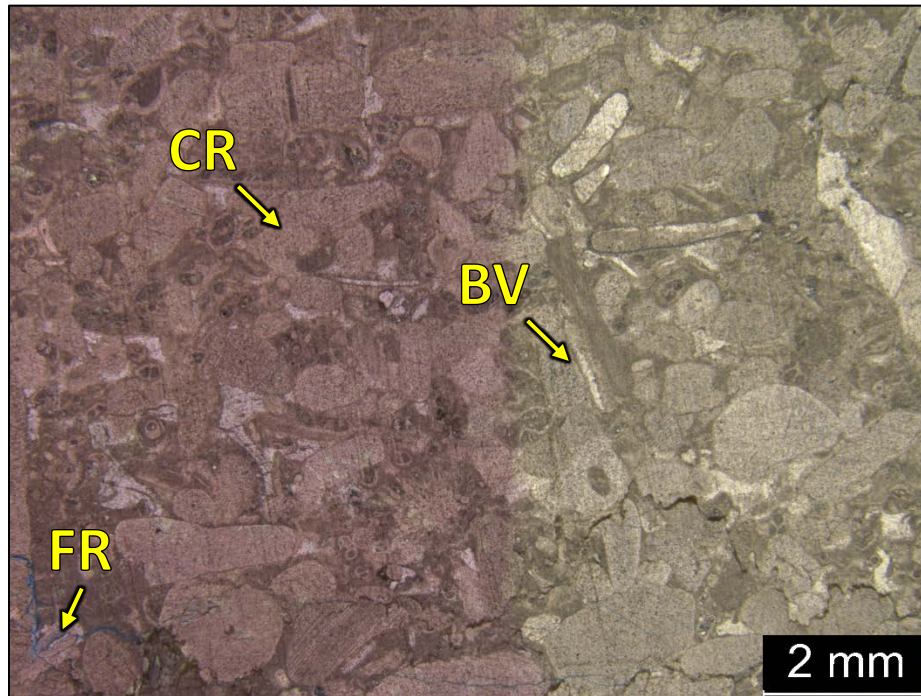
Facies 2



3 TF – 5398.26': Bryozoan grain rich packstone to grainstone. Sample is alizarin red stained (half slide) and blue epoxy impregnated. Porosity (NCS): 2.3%. Permeability (Klinkenberg): 0.119 mD. Visual estimation: 1% clays, 99% carbonates. Sample contains

bivalves (5%), brachiopods (1%), bryozoans (30%), crinoid fragments (10%) and undifferentiated skeletal debris. Intraparticle, moldic, and fracture porosity observed.

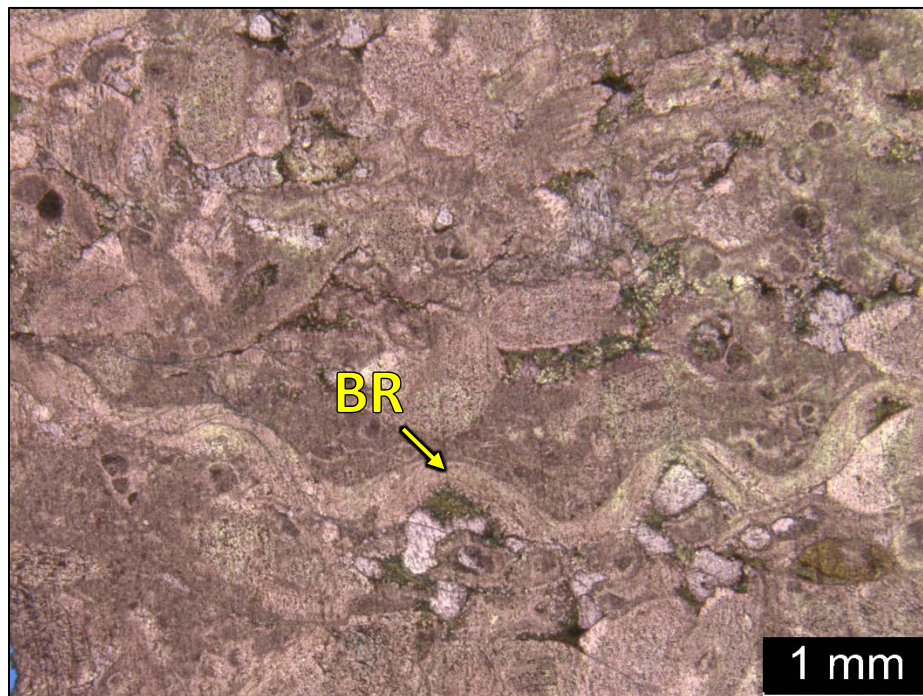
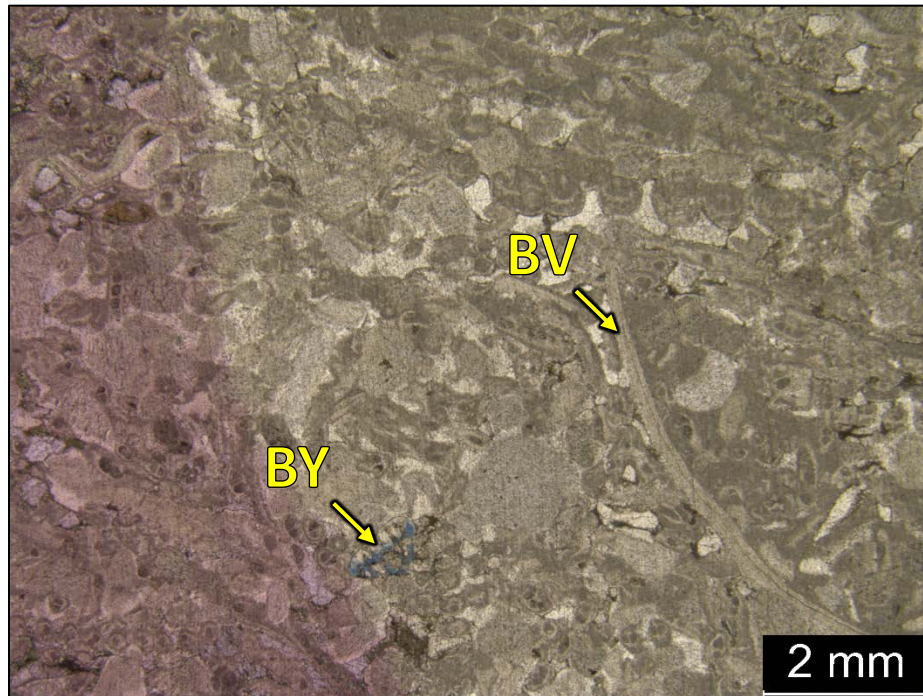
Facies 2



3 TF – 5395.70': Skeletal grain rich packstone to grainstone Sample is alizarin red stained (half slide) and blue epoxy impregnated. Porosity (NCS): 1.5%. Permeability (Klinkenberg): 0.0027 mD. XRD: 0.5% clay (kaolinite), 98.8% carbonate (calcite), and

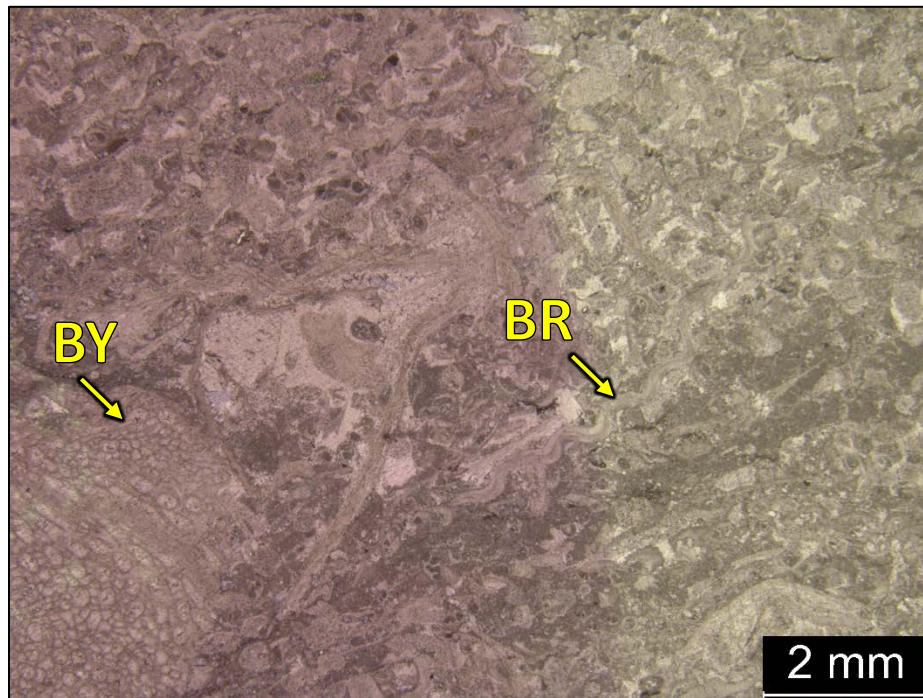
trace amounts of quartz and apatite. Sample contains bivalves (5%), bryozoans (20%), crinoid fragments (30%) and undifferentiated skeletal debris. Intraparticle, moldic, and fracture porosity observed.

Facies 2



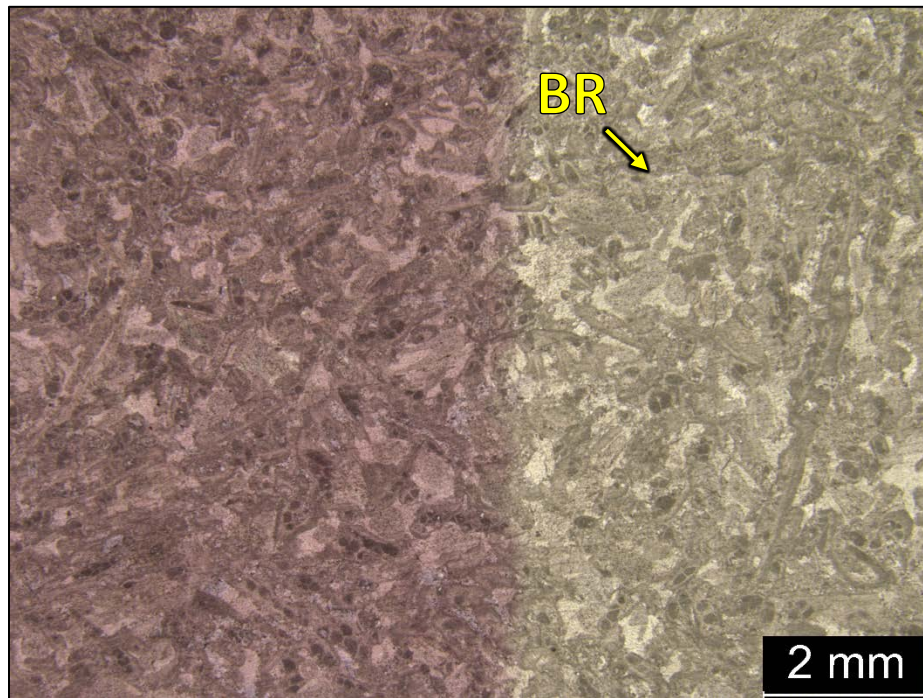
3 TF – 5386.76': Bryozoan grain rich packstone. Sample is alizarin red stained (half slide) and blue epoxy impregnated. Porosity (NCS): 1.5%. Permeability (Klinkenberg): 0.0009 mD. Visual estimation: 3% clays, 97% carbonates. Sample contains bivalves (5%), brachiopods (1%), bryozoans (25%), crinoid fragments (10%) and undifferentiated skeletal debris. Clay filled intraparticle, interparticle, open moldic, and fracture porosity observed.

Facies 2



3 TF – 5353.18’: Skeletal (bryozoan) grain rich packstone to grainstone. Sample is alizarin red stained (half slide) and blue epoxy impregnated. Porosity (NCS): 1.1%. Permeability (Klinkenberg): 0.0007 mD. XRD: 0.6% clay (kaolinite), 98.7% carbonate (calcite), and 0.7% quartz. Sample contains bivalves (10%) brachiopods (5%), bryozoans (30%), crinoid fragments (30%) and undifferentiated skeletal debris. Minor interparticle porosity observed.

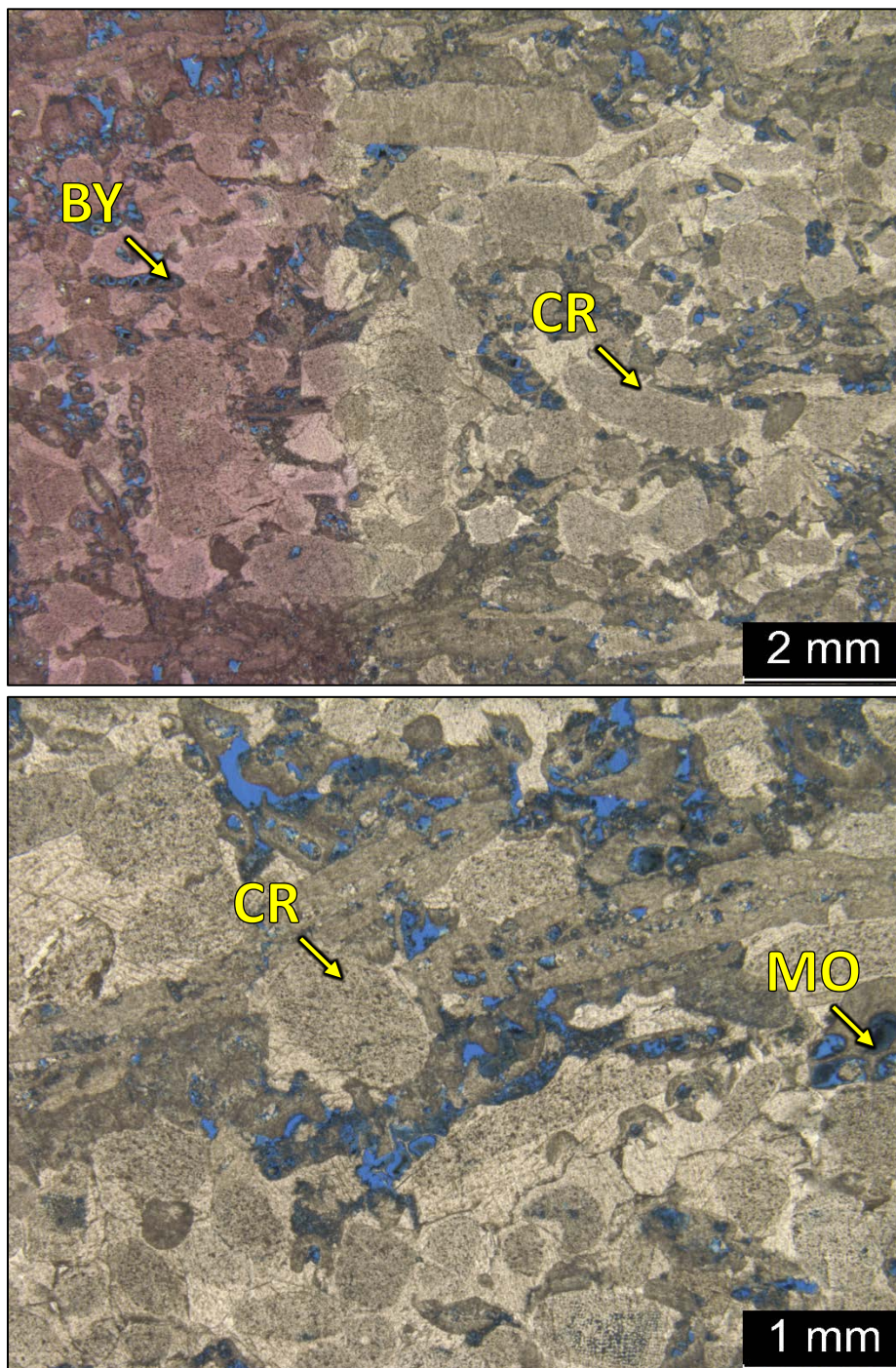
Facies 2





3 TF – 5347.5': Bryozoan grain rich packstone to grainstone. Sample is alizarin red stained (half slide) and blue epoxy impregnated. Porosity (NCS): 0.8%. Permeability (Klinkenberg): 0.0001 mD. Visual estimation: 2% clays, 98% carbonates. Sample contains bivalves (20%), brachiopods (2%), bryozoans (20%), crinoid fragments (15%) and undifferentiated skeletal debris. Slight intraparticle porosity observed.

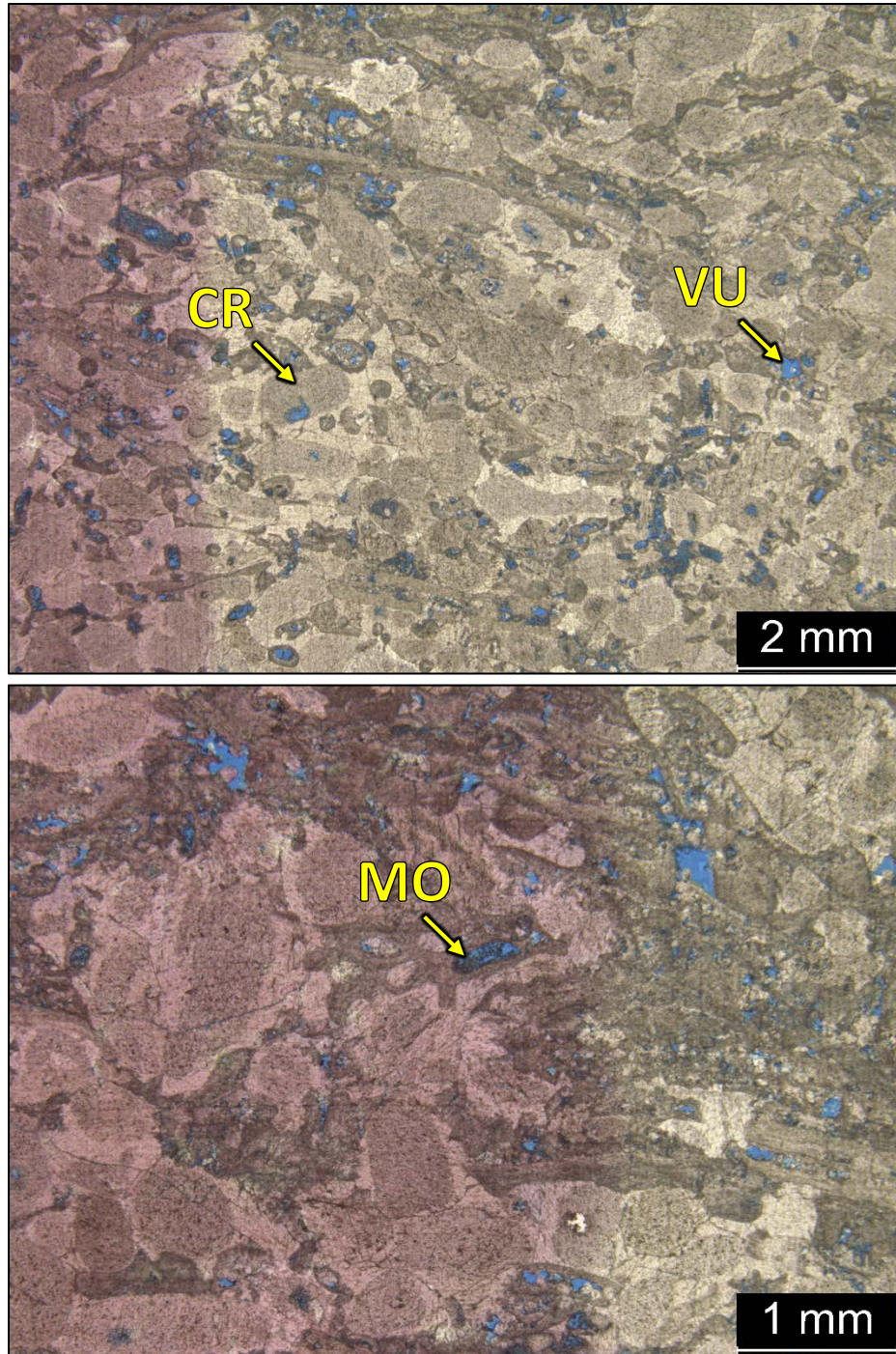
Facies 3



3 TF – 5435.36’: Crinoidal grainstone to grain rich packstone. Sample is alizarin red stained and blue epoxy impregnated. Porosity (NCS): 9%. Permeability (Klinkenberg): 1.01 mD. XRD: 1.9% clay (0.8% illite/mica, 1% kaolinite), 97.1% carbonate (94.3% calcite, 2.8% dolomite), and 1% other minerals (0.8% quartz and trace amounts of apatite). Sample contains bivalves (5%), bryozoans (8%), crinoid fragments (15%) and

undifferentiated skeletal debris. Abundant interparticle, intraparticle, moldic and vuggy porosity observed.

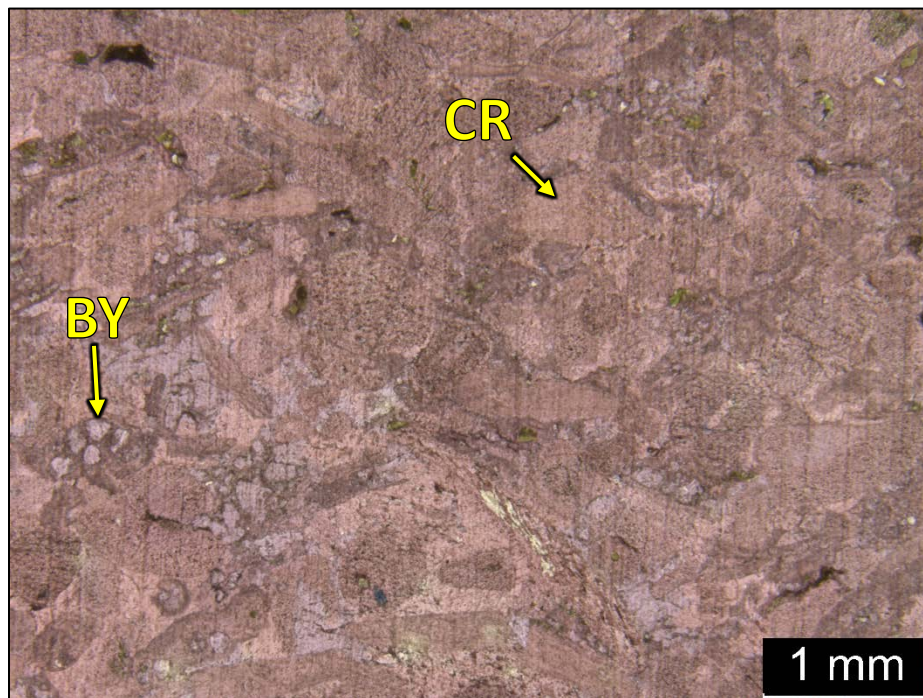
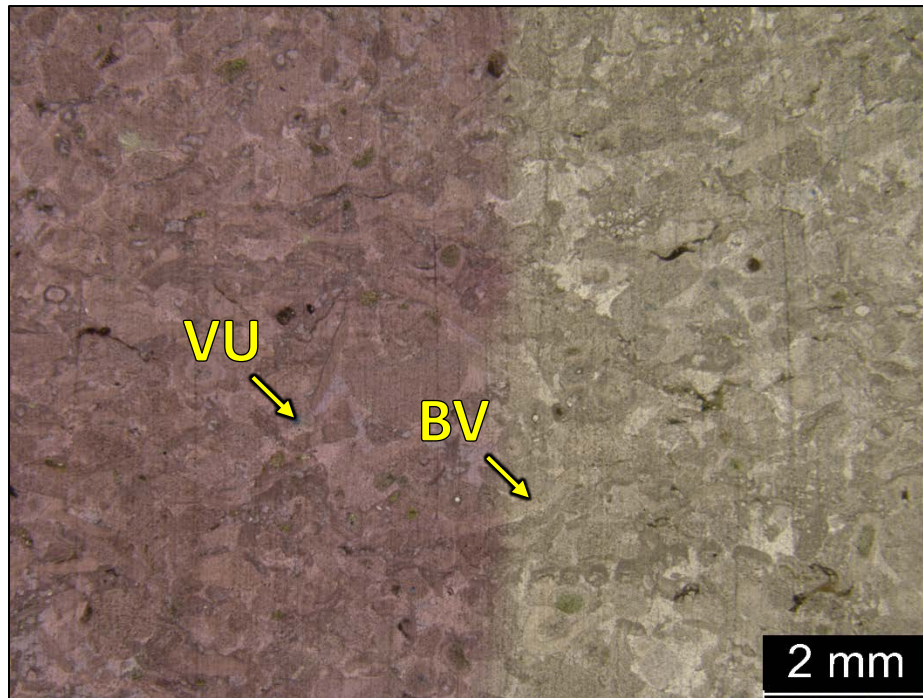
Facies 3



3 TF – 5434.34’: Crinoidal grain rich packstone to grainstone. Sample is alizarin red stained (half slide) and blue epoxy impregnated. Porosity (NCS): 5.5%. Permeability (Klinkenberg): 0.19 mD. XRD: 99.4% carbonate (calcite), and trace amounts of quartz and apatite. Sample contains brachiopods (3%), bivalves (10%), bryozoans (5%), crinoid

fragments (20%) and undifferentiated skeletal debris. Abundant interparticle, intraparticle, moldic and vuggy porosity observed.

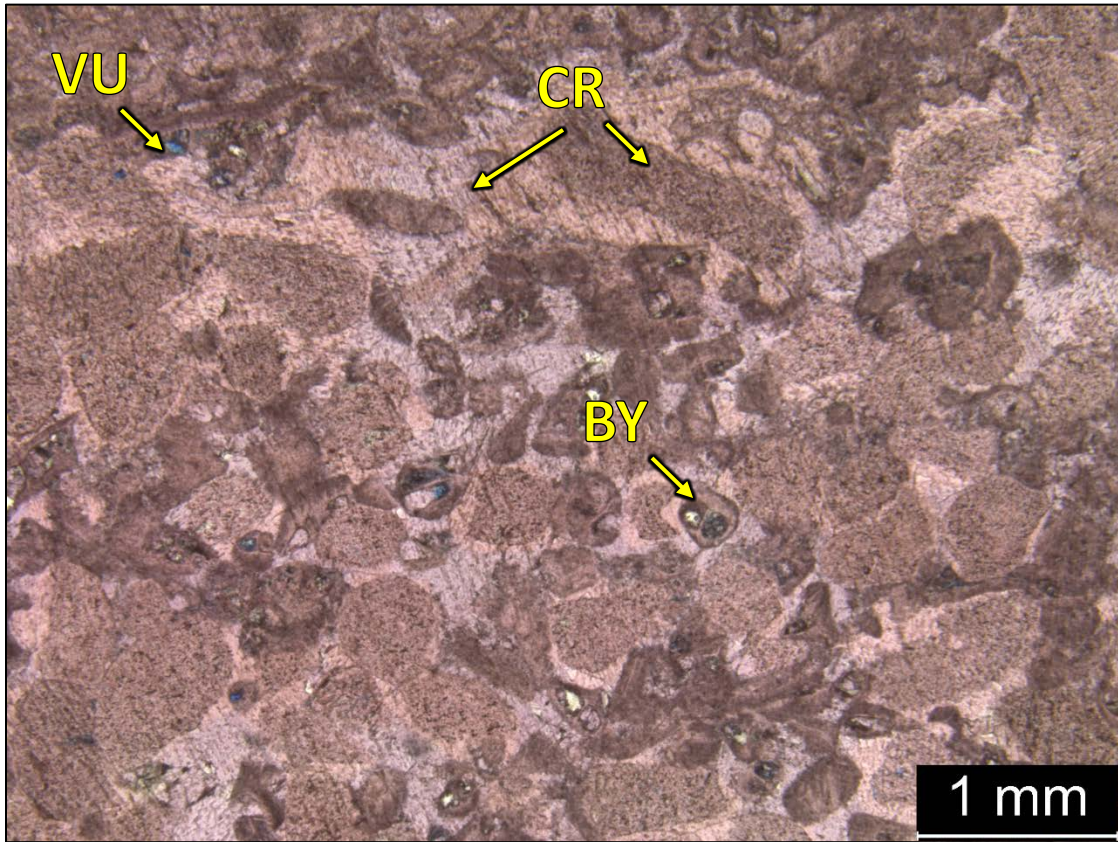
Facies 3



3 TF – 5375.04’: Skeletal grainstone to grain rich packstone. Sample is alizarin red stained (half slide) and blue epoxy impregnated. Porosity (NCS): 1.3%. Permeability (Klinkenberg): 0.0005 mD. XRD: 1.1% clay (illite/mica), 98.1% carbonate (calcite) and trace amounts of pyrite, quartz and apatite. Sample contains bivalves (10%), bryozoans

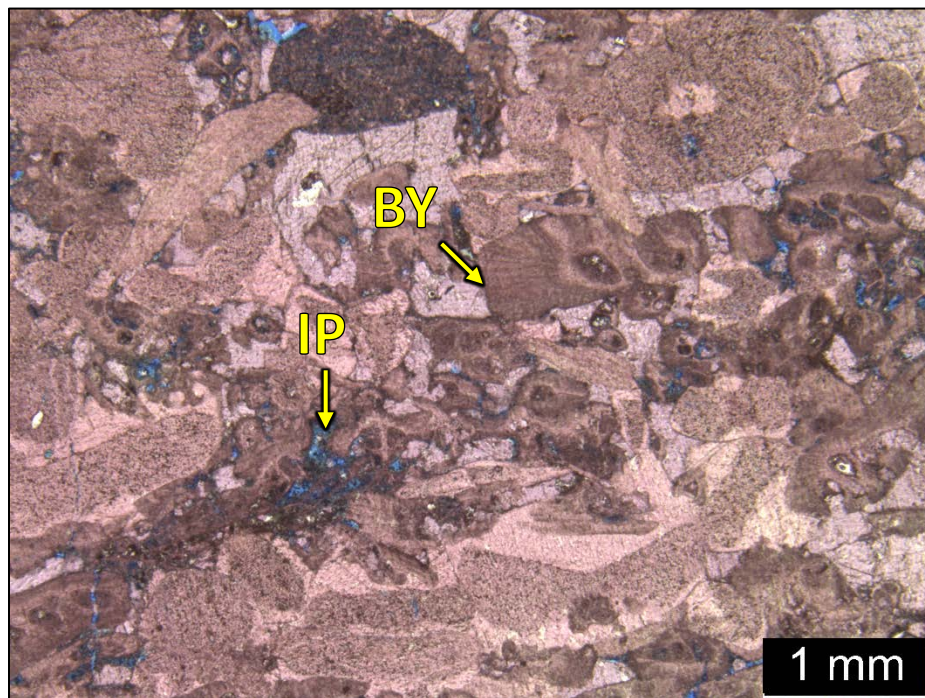
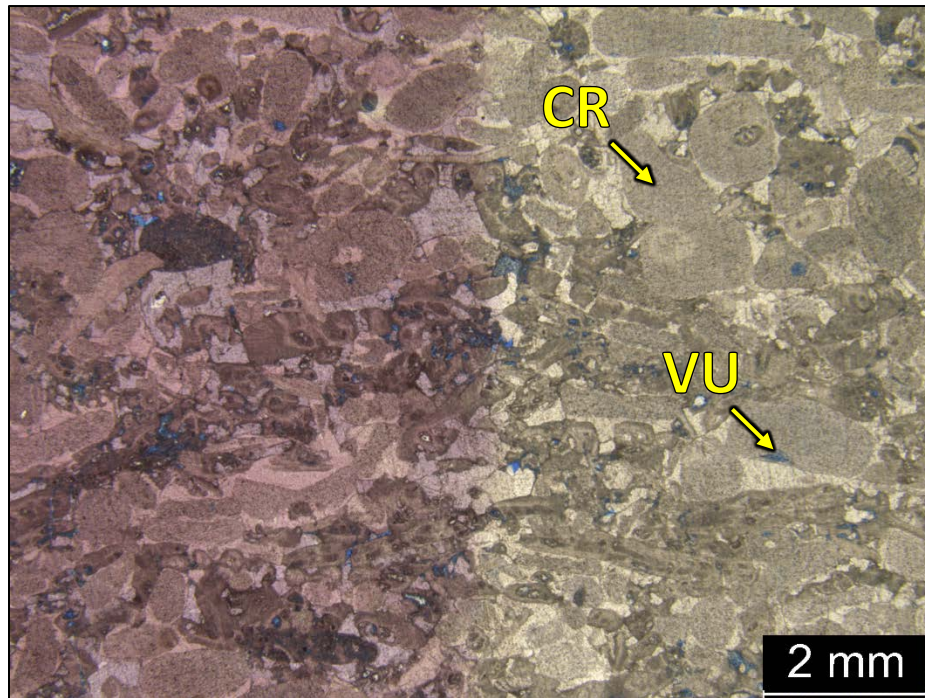
(10%), crinoid fragments (25%) and undifferentiated skeletal debris. Slight intraparticle, interparticle, vuggy, moldic and fracture porosity observed.

Facies 3



3 TF – 5358.98’: Crinoidal grain rich packstone to grainstone. Sample is alizarin red stained and blue epoxy impregnated. Porosity (NCS): 2%. Permeability (Klinkenberg): 0.0008 mD. Visual estimation: 1% clays, 99% carbonates. Sample contains bivalves (10%), bryozoans (20%), crinoid fragments (30%) and undifferentiated skeletal debris. Slight intraparticle, interparticle, moldic and vuggy porosity observed.

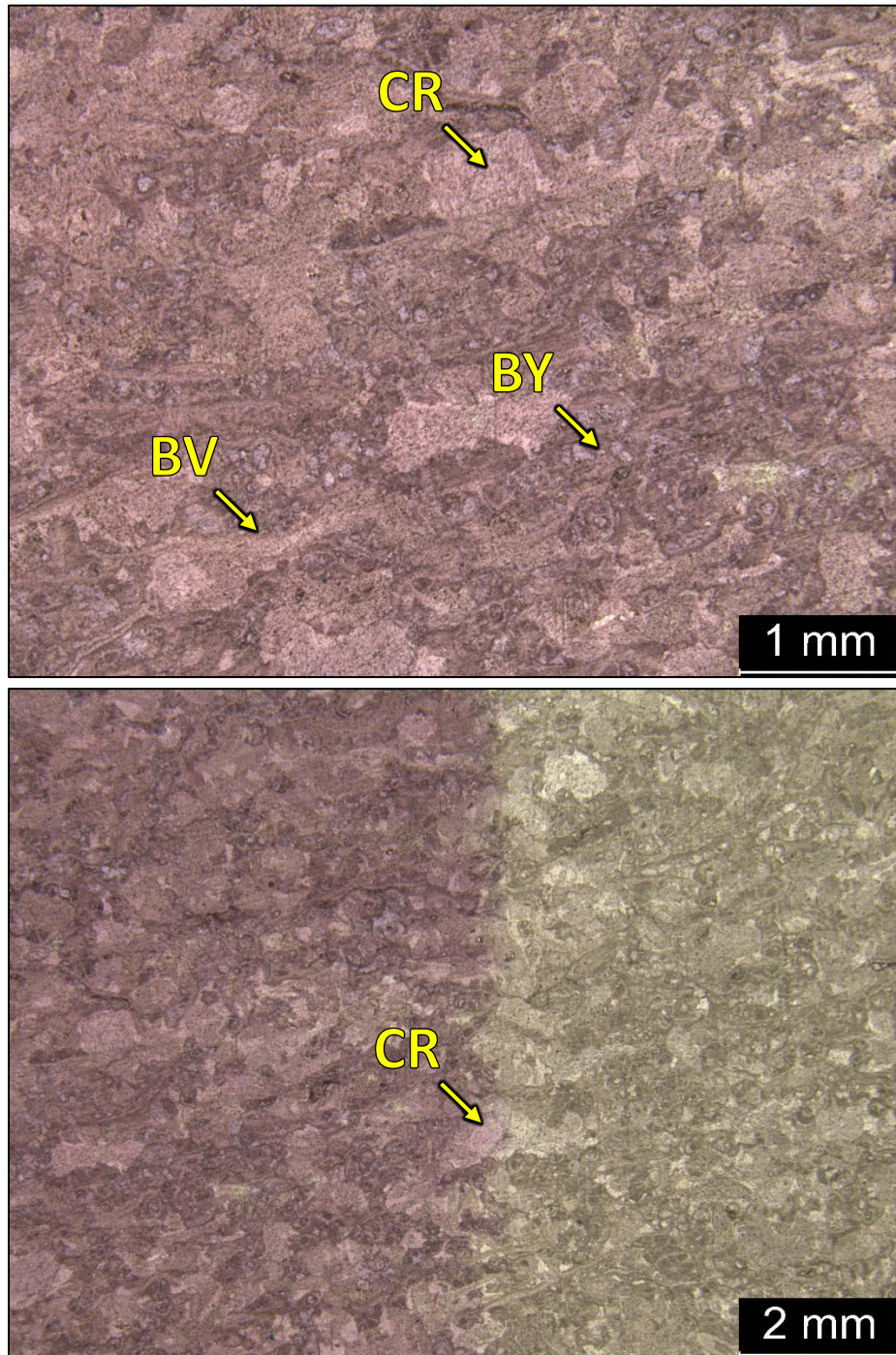
Facies 3



3 TF – 5351.08’: Crinoidal grain rich packstone. Sample is alizarin red stained and blue epoxy impregnated. Porosity (NCS): 2.6%. Permeability (Klinkenberg): 0.0005 mD. XRD: 0.8% clay (0.3% chlorite, 0.5% kaolinite), 98.6% carbonate (calcite), and 0.6% quartz. Sample contains bivalves (5%), bryozoans (25%), crinoid fragments (30%) and

undifferentiated skeletal debris. Slight intraparticle, interparticle, fracture, moldic and vuggy porosity observed.

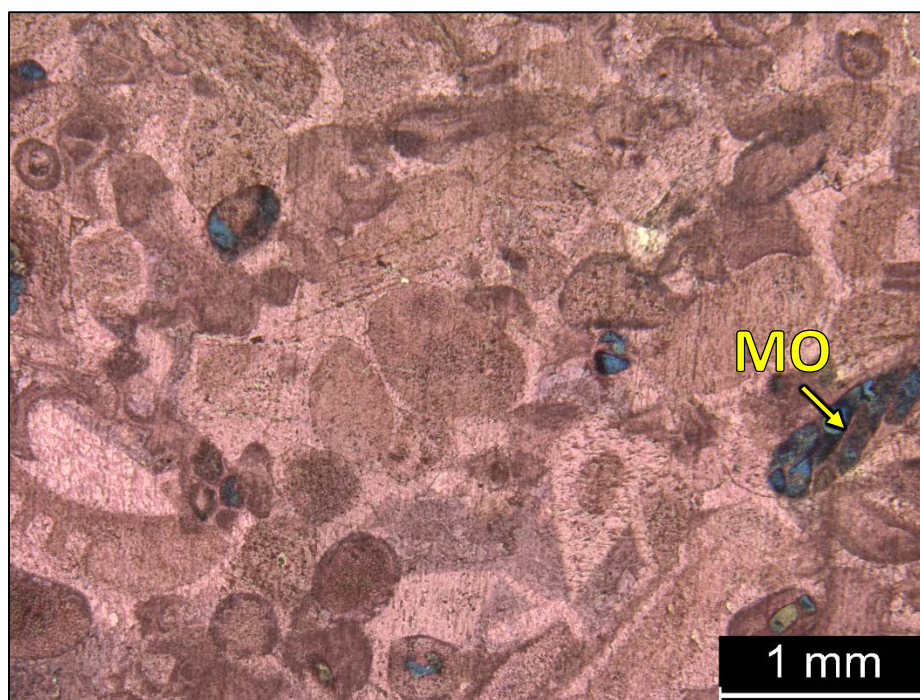
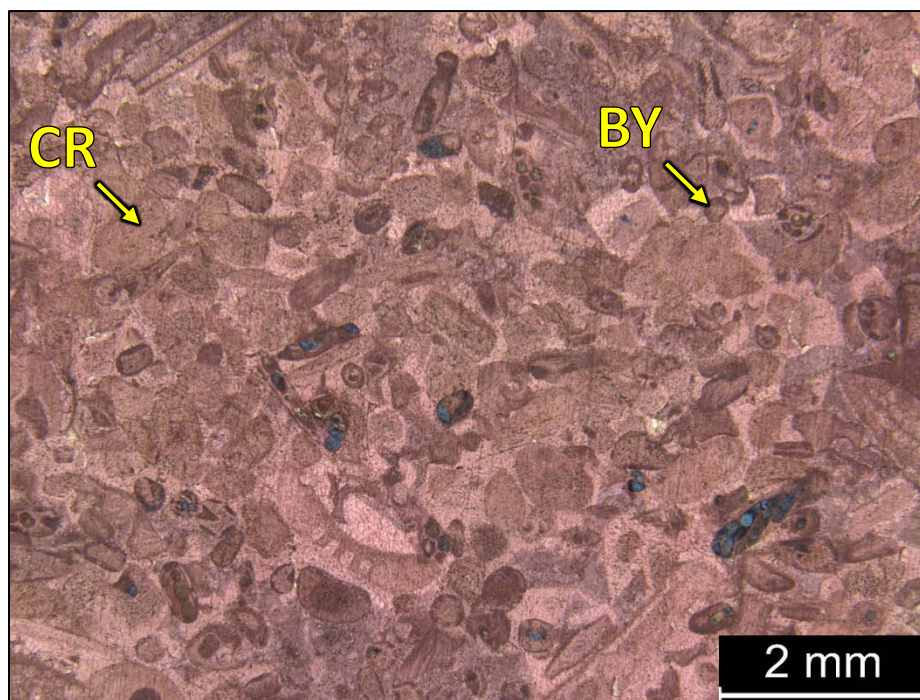
Facies 3



3 TF – 5343.12’: Crinoidal grain rich packstone to grainstone. Sample is alizarin red stained (half slide) and blue epoxy impregnated. Porosity (NCS): 2.1%. Permeability (Klinkenberg): 0.0022 mD. Visual estimation: 3% clays, 97% carbonates. Sample

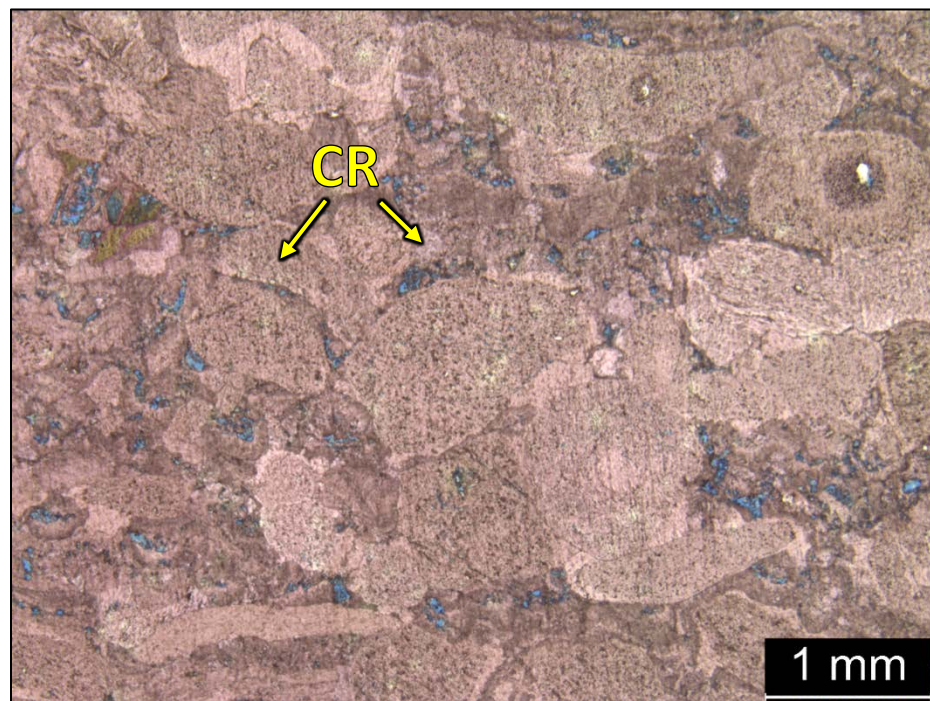
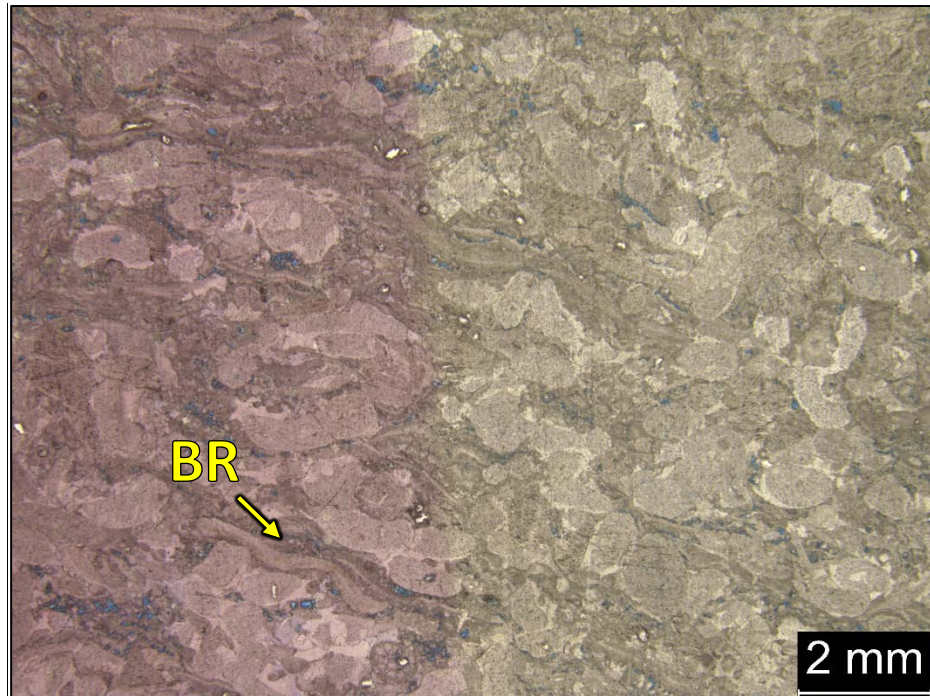
contains bivalves (15%), bryozoans (15%), crinoid fragments (30%) and undifferentiated skeletal debris. Slight intraparticle and interparticle porosity observed.

Facies 4



3 TF – 5449.6’: Skeletal grainstone. Sample is alizarin red stained and blue epoxy impregnated. Porosity (NCS): 1.5%. Permeability (Klinkenberg): 0.0001 mD. XRD: 0.6% clay (illite/mica), 98.7% carbonate (calcite), and trace amounts of other minerals (quartz and apatite). Sample contains bryozoans (15%), crinoid fragments (15%) and undifferentiated skeletal debris. Moldic, intraparticle and vuggy porosity observed.

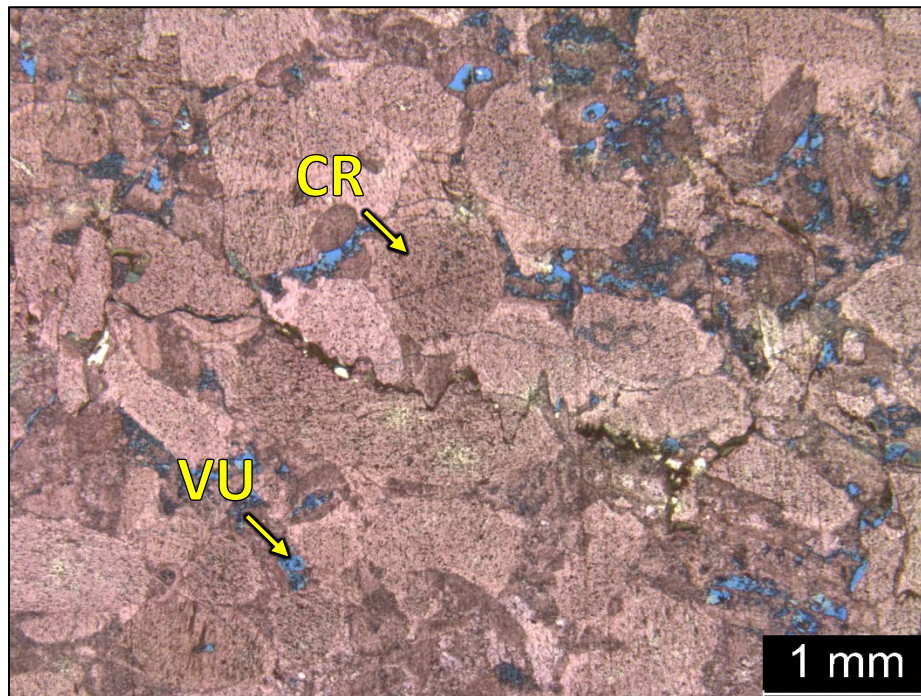
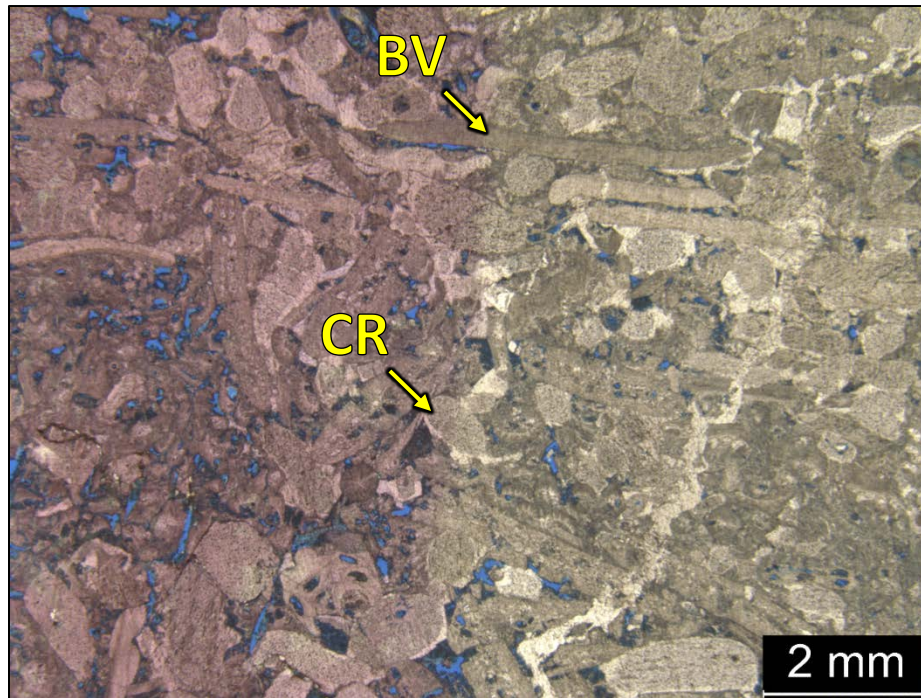
Facies 4



3 TF – 5442.3': Skeletal grain rich packstone to grainstone. Sample is alizarin red stained (half slide) and blue epoxy impregnated. Porosity (NCS): 4.3%. Permeability (Klinkenberg): 0.031 mD. Visual estimation: 1% clays, 99% carbonates. Sample contains brachiopods (5%), bivalves (1%), bryozoans (5%), crinoid fragments (25%) and

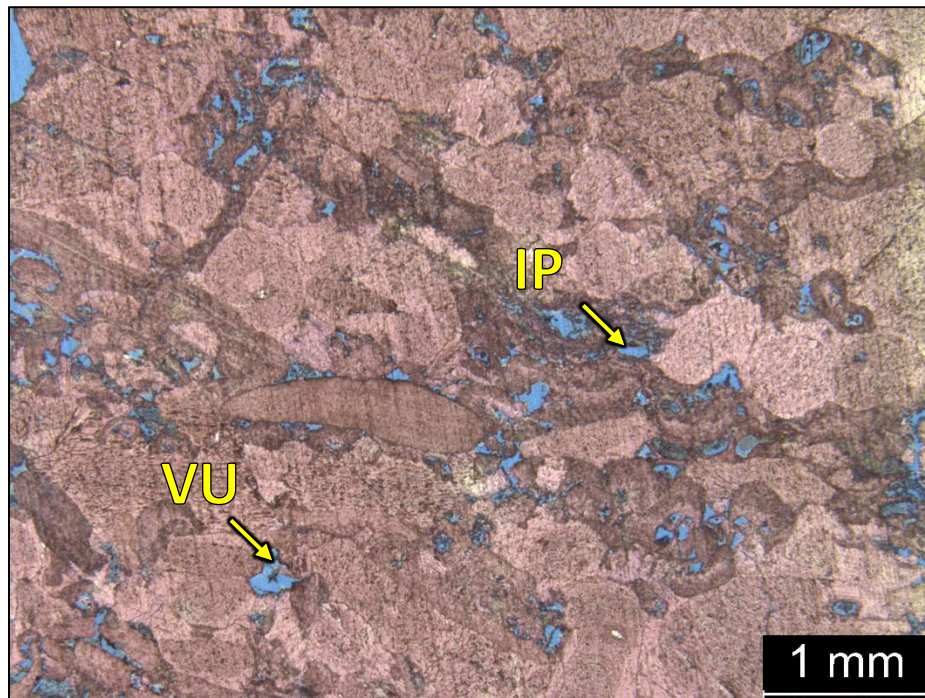
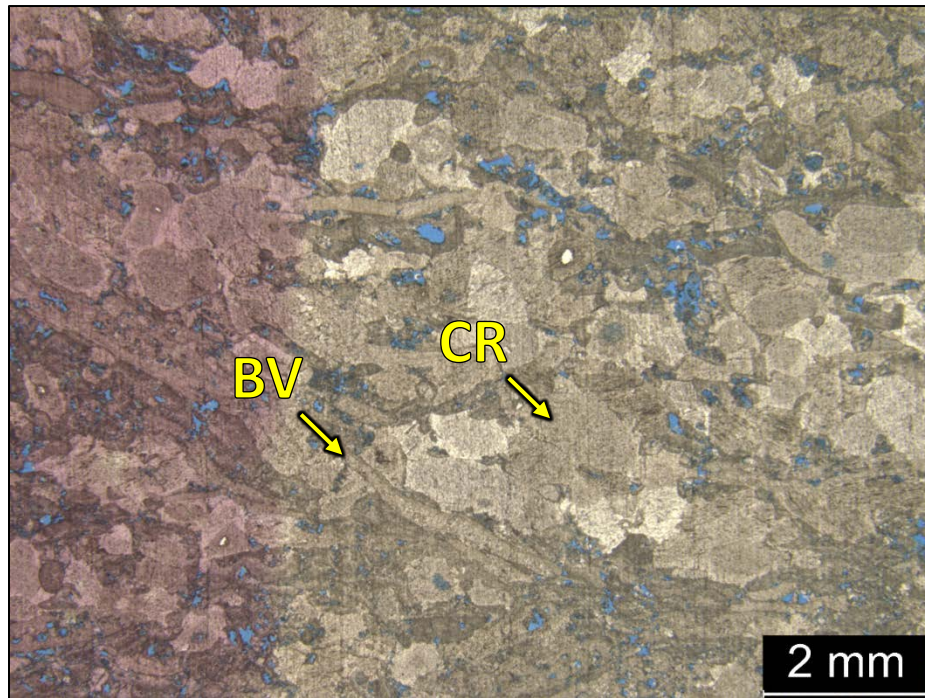
undifferentiated skeletal debris. Moldic, interparticle, intraparticle and vuggy porosity observed.

Facies 4



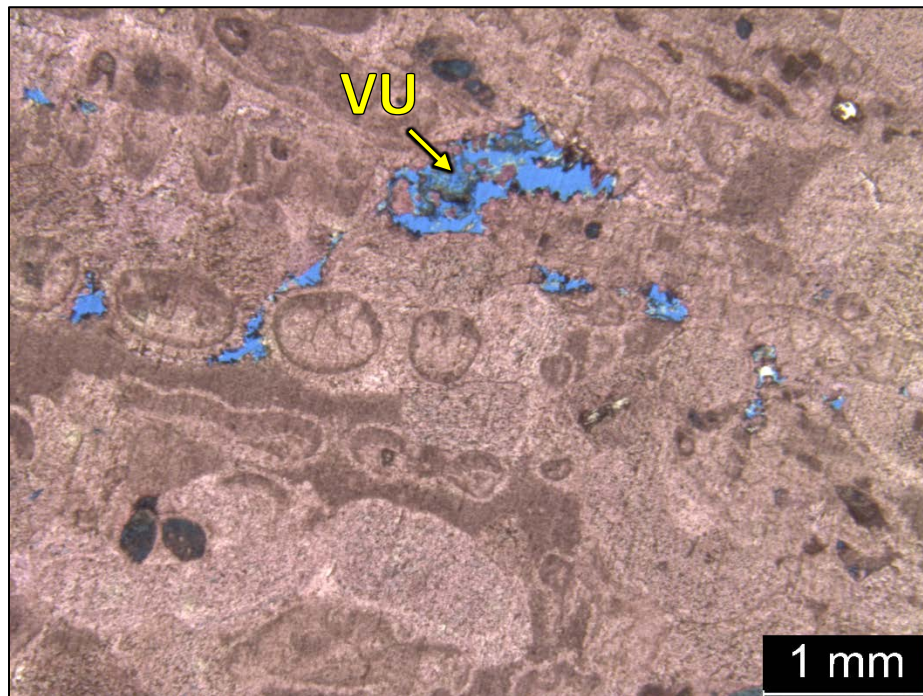
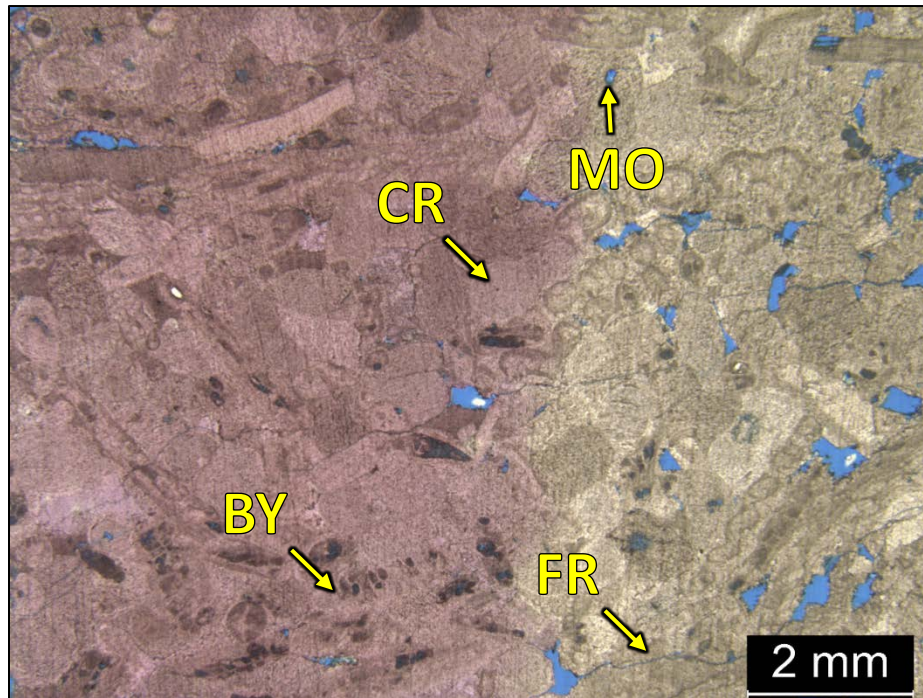
3 TF – 5436.32': Skeletal grainstone. Sample is alizarin red stained (half slide) and blue epoxy impregnated. Porosity (NCS): 3.7%. Permeability (Klinkenberg): 0.011 mD. Visual estimation: 1% clays, 99% carbonates. Sample contains brachiopods (8%), bivalves (6%), bryozoans (8%), crinoid fragments (15%) and undifferentiated skeletal debris. Interparticle, intraparticle, moldic and vuggy porosity observed.

Facies 4



3 TF – 5435.18³: Skeletal grainstone to grain rich packstone. Sample is alizarin red stained (half slide) and blue epoxy impregnated. Porosity (NCS): 7.3%. Permeability (Klinkenberg): 0.208 mD. Visual estimation: 2% clays, 98% carbonates. Sample contains bivalves (8%), brachiopods (3%), crinoid fragments (15%) and undifferentiated skeletal debris. Abundant interparticle, intraparticle, moldic and vuggy porosity observed.

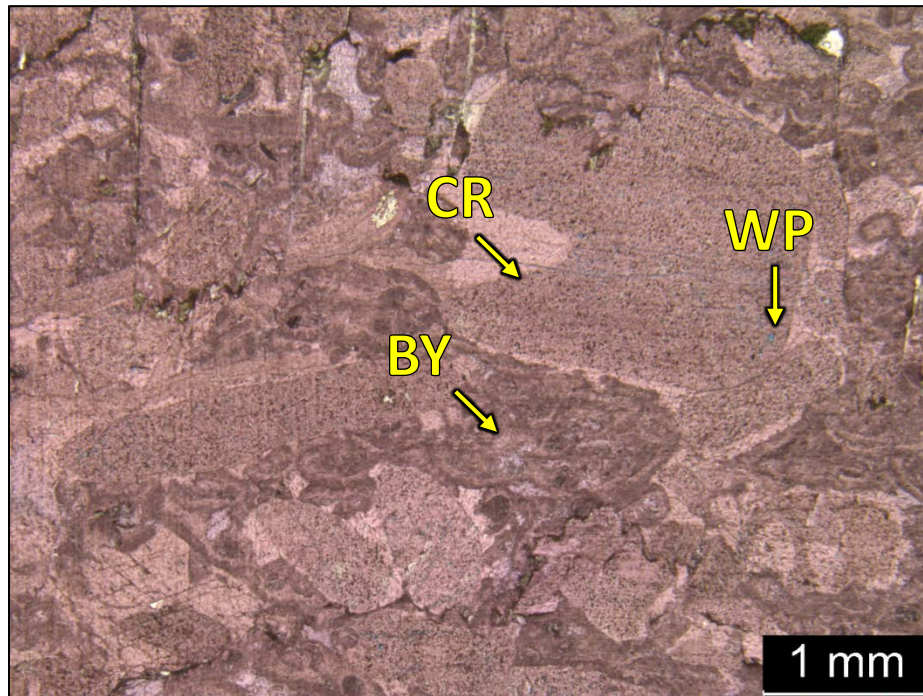
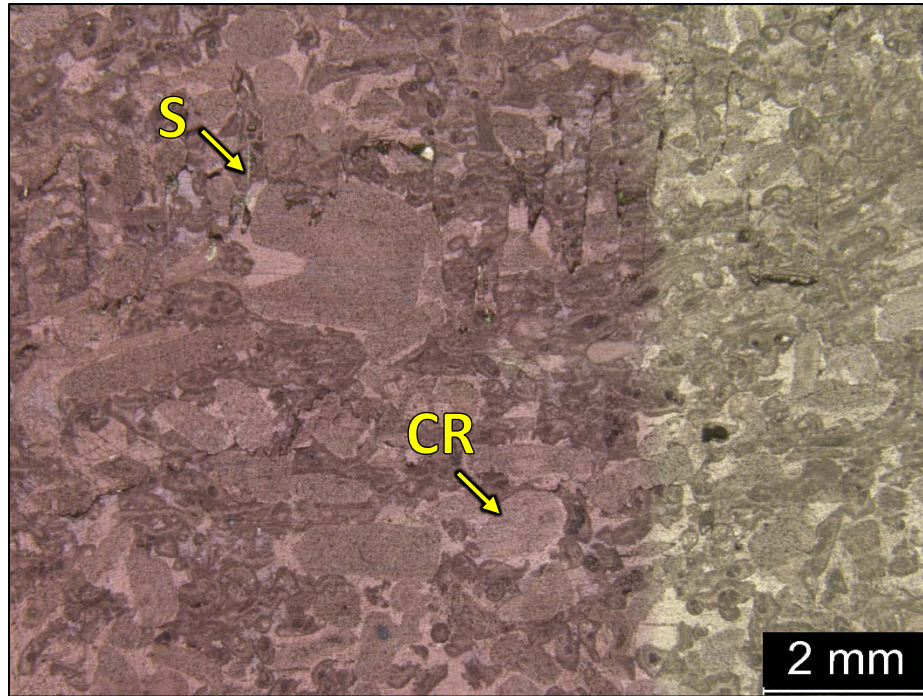
Facies 4



3 TF – 5430.12’: Skeletal grainstone. Sample is alizarin red stained (half slide) and blue epoxy impregnated. Porosity (NCS): 4.6%. Permeability (Klinkenberg): 0.619 mD. XRD: 1.8% clay (kaolinite), 97.5% carbonate (calcite), and trace amounts of quartz. Sample contains bryozoans (15%), bivalves (5%), brachiopods (2%), crinoid fragments (18%)

and undifferentiated skeletal debris. Moldic, fracture, interparticle, intraparticle and vuggy porosity observed.

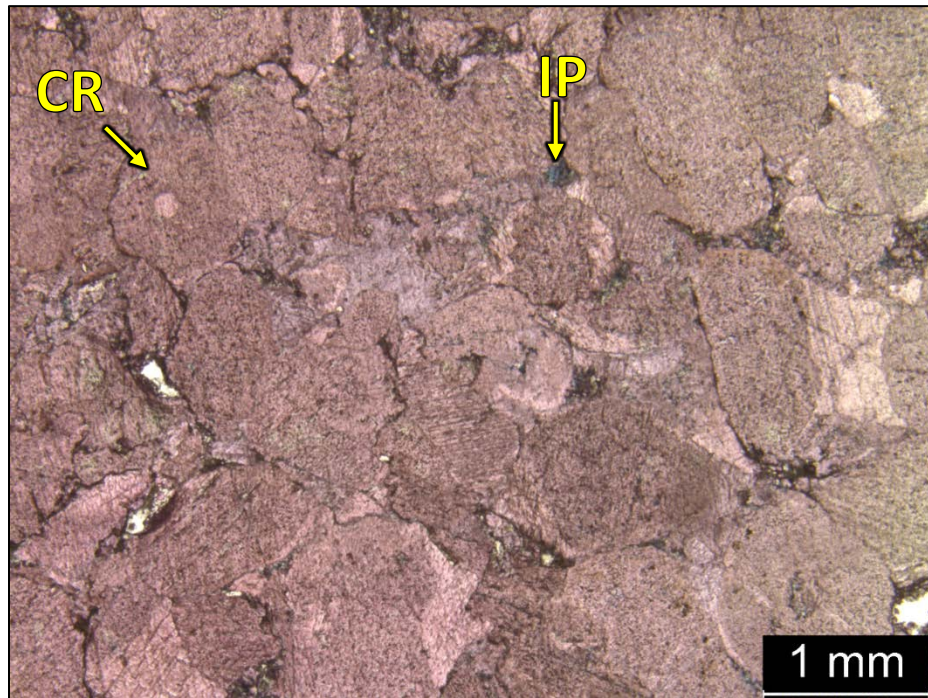
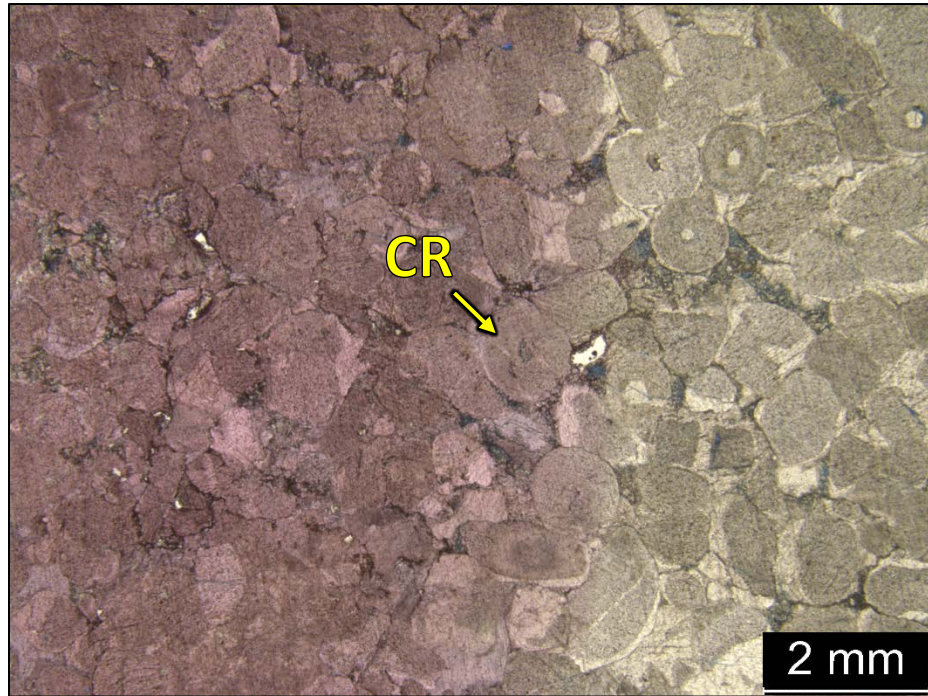
Facies 4



3 TF – 5419.2': Crinoidal grain rich packstone to grainstone. Sample is alizarin red stained (half slide) and blue epoxy impregnated. Porosity (NCS): 1.5%. Permeability (Klinkenberg): 0.0001 mD. XRD: 4.3% clay (2% illite/mica, 2.3% kaolinite), 92.6% carbonate (calcite), and 3.1% other minerals (2.7% quartz and trace amounts of apatite). Sample contains bivalves (5%), bryozoans (15%), crinoid fragments (20%) and

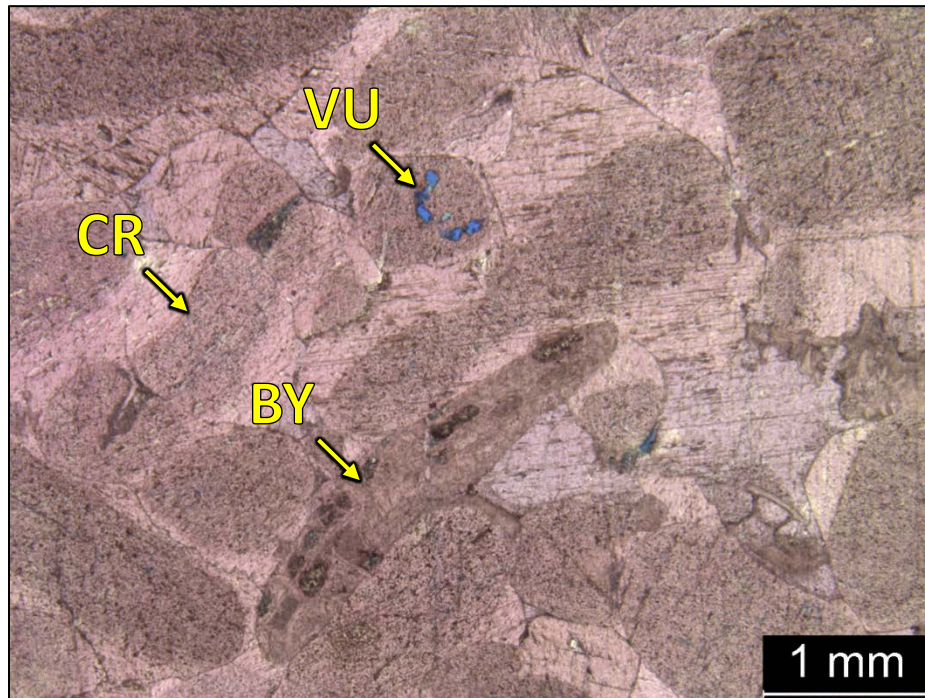
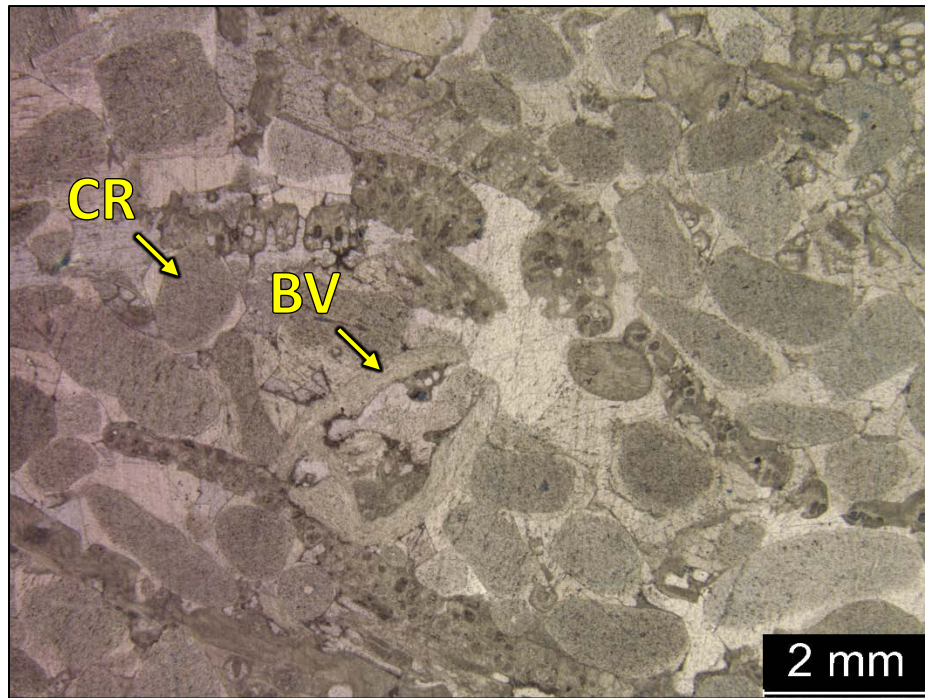
undifferentiated skeletal debris. Filled vuggy porosity observed, as well as open interparticle and intraparticle porosity.

Facies 4



3 TF – 5416.84': Crinoidal grainstone. Sample is alizarin red stained (half slide) and blue epoxy impregnated. Porosity (NCS): 1.5%. Permeability (Klinkenberg): 0.0006 mD. Visual estimation: 2% clays, 97% carbonates, 1% other minerals. Sample contains bivalves (2%), silt-sized quartz grains (1%), crinoid fragments (80%) and undifferentiated skeletal debris. Fracture, interparticle and interparticle porosity observed.

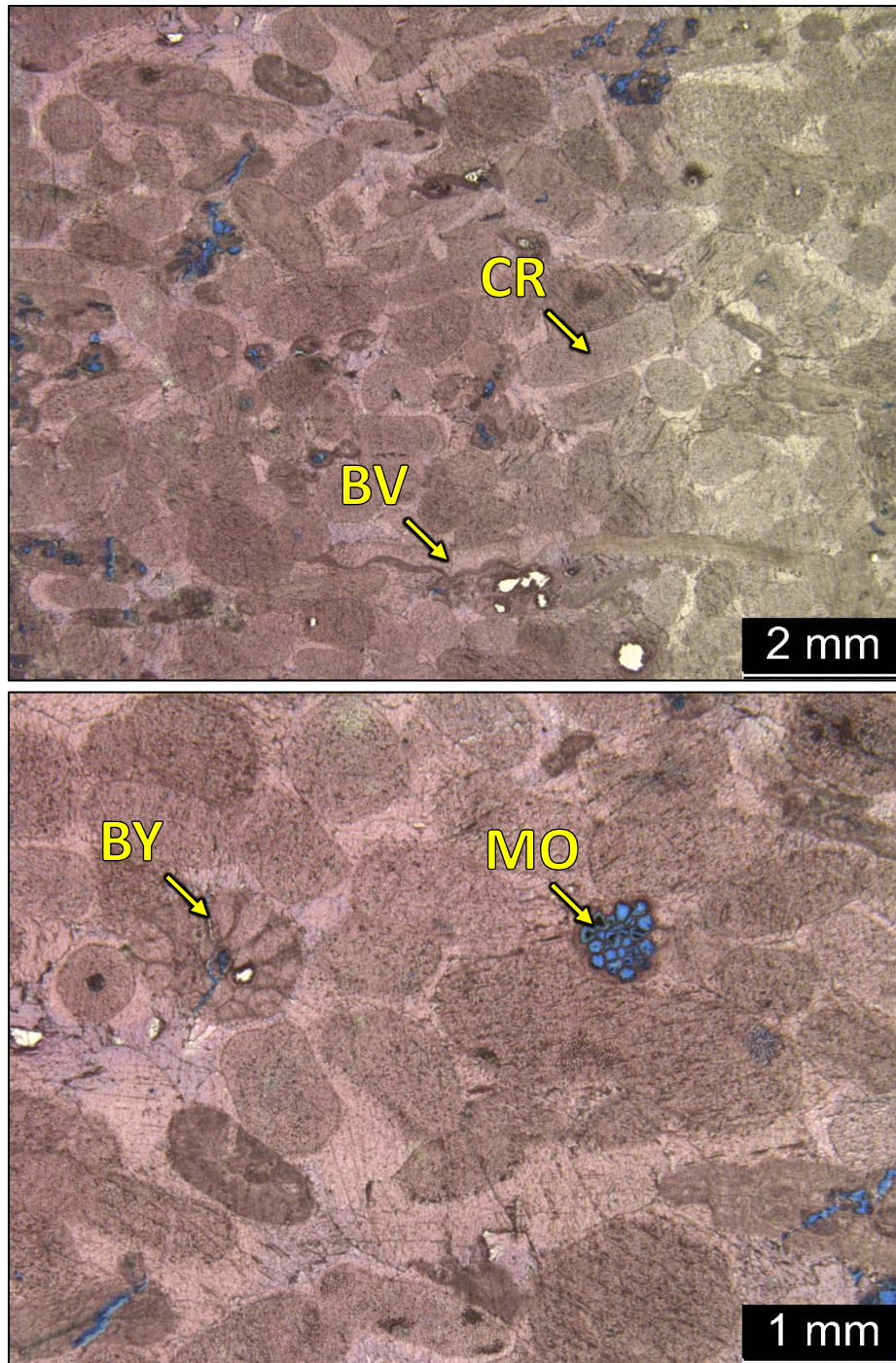
Facies 4



3 TF – 5411.46³: Crinoidal grainstone to grain rich packstone. Sample is alizarin red stained (half slide) and blue epoxy impregnated. Porosity (NCS): 1.3%. Permeability (Klinkenberg): 0.0003 mD. XRD: 99.5% carbonate (calcite), and trace amounts of quartz. Sample contains bryozoans (15%), bivalves (2%), crinoid fragments (35%) and

undifferentiated skeletal debris. Slight interparticle, intraparticle and vuggy porosity observed.

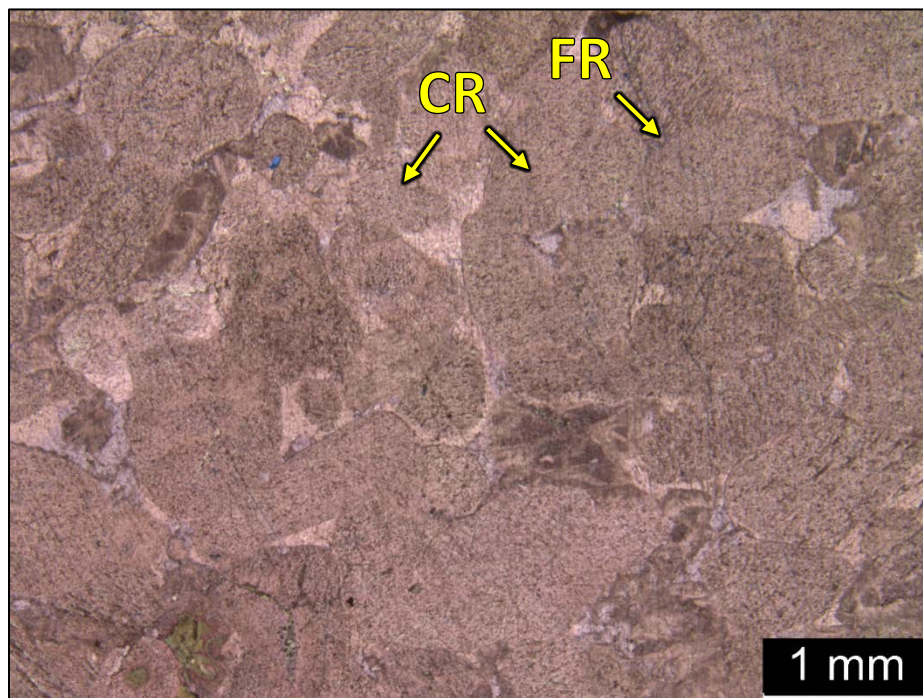
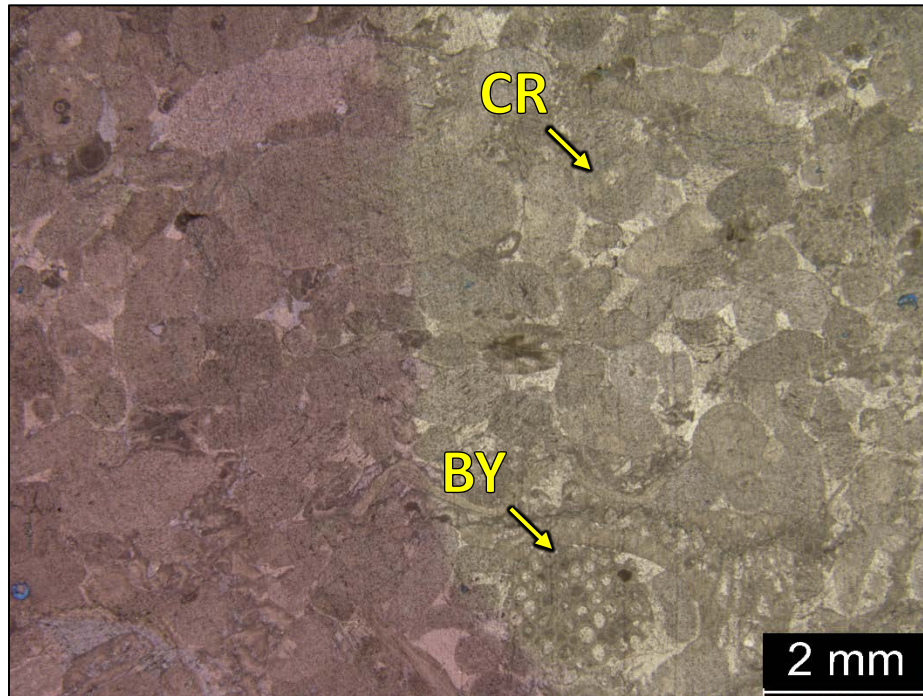
Facies 4



3 TF – 5407.84’: Crinoidal grainstone to grain rich packstone. Sample is alizarin red stained (half slide) and blue epoxy impregnated. Porosity (NCS): 2.2%. Permeability (Klinkenberg): 0.0015 mD. XRD: 99.4% carbonate (calcite) and trace amounts of quartz. Sample contains bivalves (3%), bryozoans (15%), crinoid fragments (35%) and

undifferentiated skeletal debris. Slight interparticle, intraparticle, moldic, fracture and vuggy porosity observed.

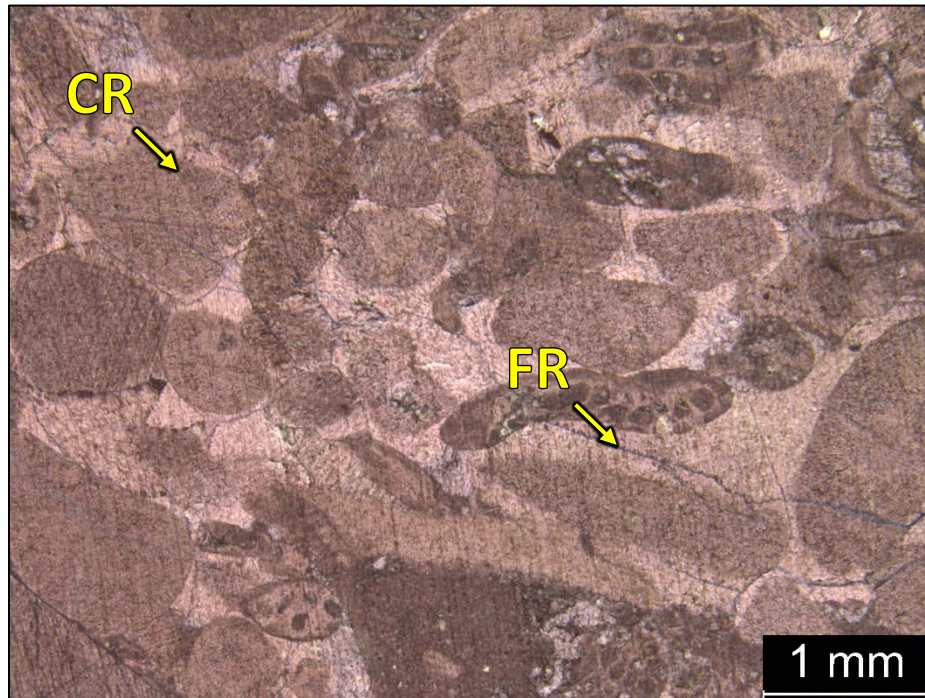
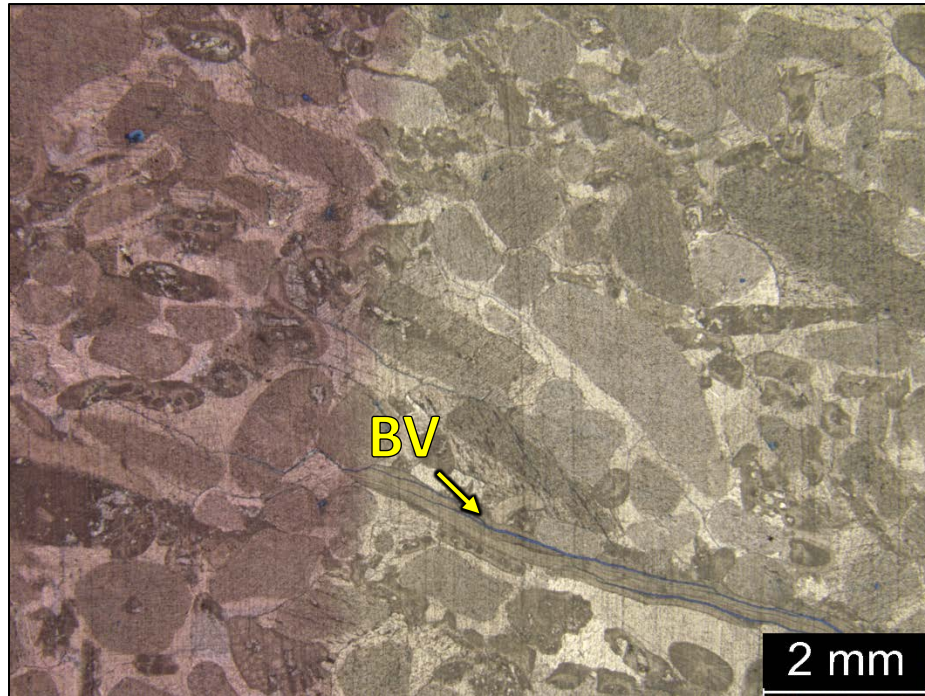
Facies 4



3 TF – 5382.6': Crinoidal grainstone to grain rich packstone. Sample is alizarin red stained (half slide) and blue epoxy impregnated. Porosity (NCS): 1.3%. Permeability

(Klinkenberg): 0.0022 mD. Visual estimation: 2% clays, 98% carbonates. Sample contains bivalves (2%), brachiopods (3%), bryozoans (10%), crinoid fragments (40%) and undifferentiated skeletal debris. Slight intraparticle (clay filled) and fracture porosity observed.

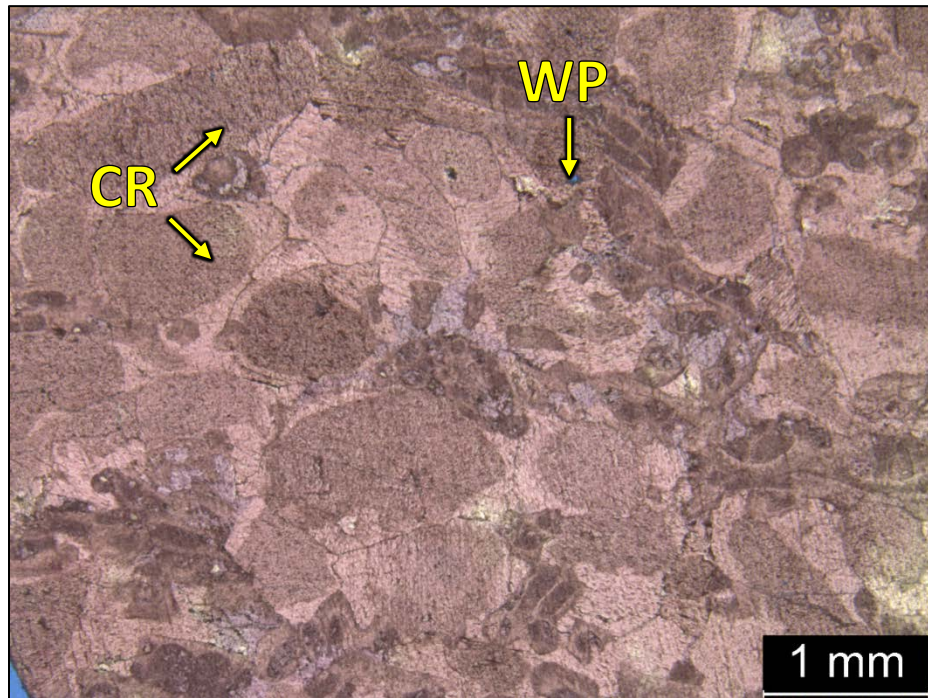
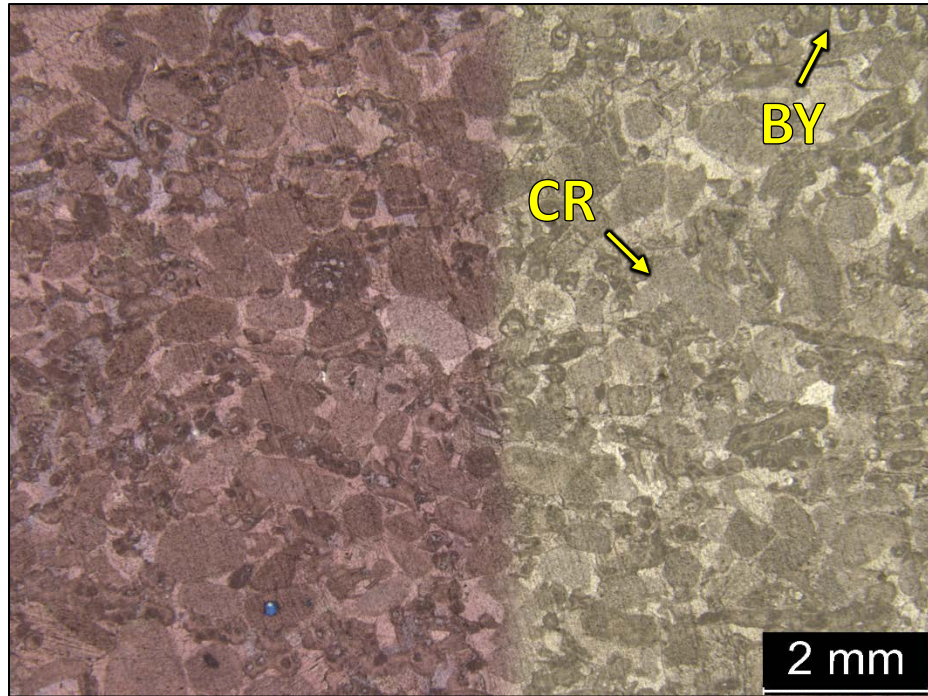
Facies 4



3 TF – 5378.14’: Skeletal (crinoidal) grainstone to grain rich packstone. Sample is alizarin red stained (half slide) and blue epoxy impregnated. Porosity (NCS): 1.2%. Permeability (Klinkenberg): 0.0006 mD. XRD: 99.7% carbonate (calcite) and trace amounts of quartz. Sample contains bivalves (2%), bryozoans (15%), crinoid fragments

(40%) and undifferentiated skeletal debris. Slight intraparticle, interparticle and fracture porosity observed.

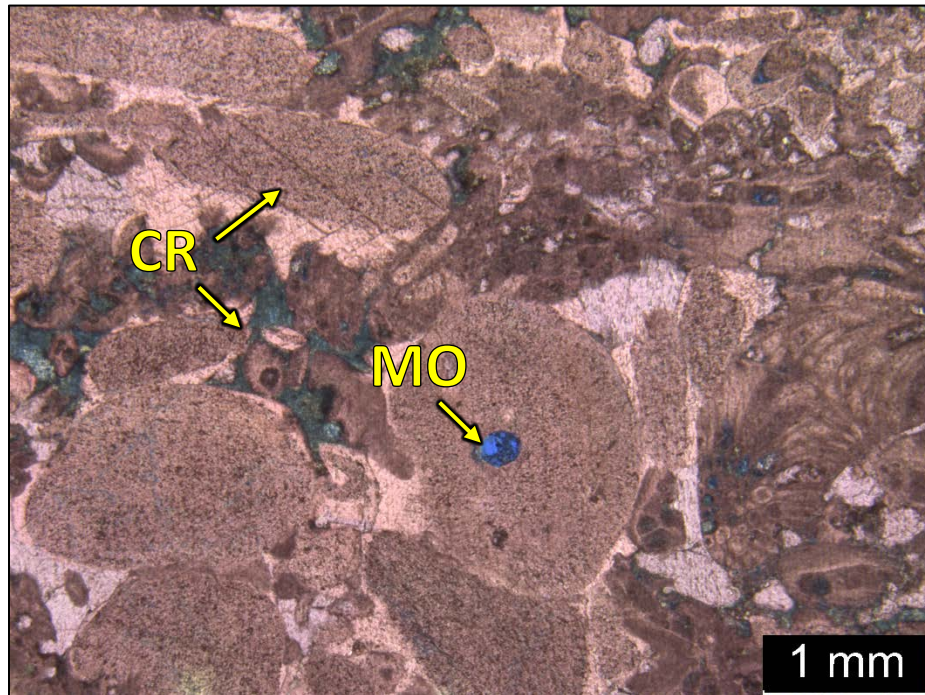
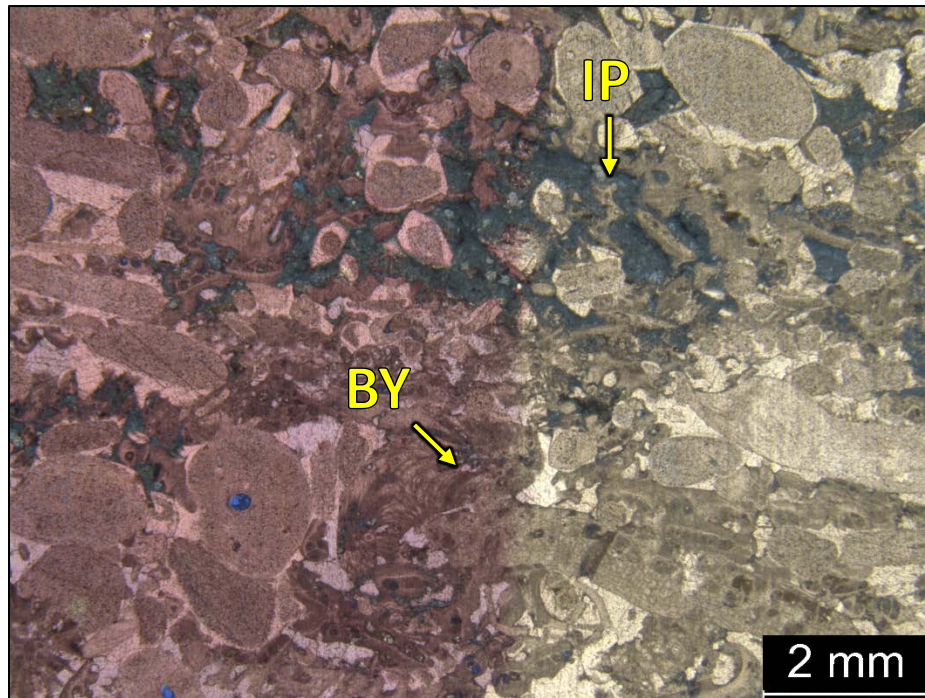
Facies 4



3 TF – 5376.26³: Skeletal (crinoidal) grainstone to grain rich packstone. Sample is alizarin red stained and blue epoxy impregnated. Porosity (NCS): 0.9%. Permeability (Klinkenberg): 0.0009 mD. Visual estimation: 1% clays, 99% carbonates. Sample

contains bivalves (2%), bryozoans (15%), crinoid fragments (30%) and undifferentiated skeletal debris. Slight intraparticle and fracture porosity observed.

Facies 4



3 TF – 5350.14’: Crinoidal grain rich packstone. Sample is alizarin red stained (half slide) and blue epoxy impregnated. Porosity (NCS): 3%. Permeability (Klinkenberg): 0.0012 mD. Visual estimation: 1% clays, 99% carbonates. Sample contains bivalves (5%), bryozoans (25%), crinoid fragments (35%) and undifferentiated skeletal debris. Slight intraparticle, interparticle, moldic and vuggy porosity observed.

VITA

Lara Jaeckel

Candidate for the Degree of

Master of Science

Thesis: HIGH-RESOLUTION SEQUENCE STRATIGRAPHY AND RESERVOIR CHARACTERIZATION OF MID-CONTINENT MISSISSIPPIAN CARBONATES IN NORTH-CENTRAL OKLAHOMA AND SOUTH CENTRAL KANSAS

Major Field: Geology

Biographical:

Education:

Completed the requirements for the Master of Science in Geology at Oklahoma State University, Stillwater, Oklahoma in July, 2016.

Completed the requirements for the Bachelor of Science in Geology at George Mason University, Fairfax, VA/USA in 2010.

Experience:

Began full-time position as a geologist at Chesapeake Energy in Oklahoma City, OK in 2016.

Geoscience intern at Chesapeake Energy in Oklahoma City, OK in 2015.

Senior Operations Support Center Production Technician at Chesapeake Energy in Oklahoma City, OK in 2014 – 2015.

Geosteered at Chesapeake Energy in 2012 – 2014 in Oklahoma City, OK.

Training Specialist at Nomac Services Geo and Horizon Well Logging, LLC in Oklahoma City and Tulsa, OK in 2011 – 2012.

Lead Mudlogger at Horizon Well Logging, LLC in Towanda, PA in 2011.

Interned at GeoConcepts Engineering, Inc. in Ashburn, VA in 2010.

Professional Memberships:

American Association of Petroleum Geologists